ISSN 0021-9673

VOL. 629 NO. 2 JANUARY 22, 1993

THIS ISSUE COMPLETES VOL. 629

JOURNAL OF CHROMATOGRAPHY

INCLUDING ELECTROPHORESIS AND OTHER SEPARATION METHODS

ELSEVIER

JOURNAL OF CHROMATOGRAPHY

INCLUDING ELECTROPHORESIS AND OTHER SEPARATION METHODS

Scope. The *Journal of Chromatography* publishes papers on all aspects of **chromatography, electrophoresis** and related methods. Contributions consist mainly of research papers dealing with chromatographic theory, instrumental developments and their applications. The section *Biomedical Applications*, which is under separate editorship, deals with the following aspects: developments in and applications of chromatographic and electrophoretic techniques related to clinical diagnosis or alterations during medical treatment; screening and profiling of body fluids or tissues related to the analysis of active substances and to metabolic disorders; drug level monitoring and pharmacokinetic studies; clinical toxicology; forensic medicine; veterinary medicine; occupational medicine; results from basic medical research with direct consequences in clinical practice. In *Symposium volumes*, which are under separate editorship, proceedings of symposia on chromatography, electrophoresis and related methods are published.

Submission of Papers. The preferred medium of submission is on disk with accompanying manuscript (see *Electronic manuscripts* in the Instructions to Authors, which can be obtained from the publisher, Elsevier Science Publishers B.V., P.O. Box 330, 1000 AH Amsterdam, Netherlands). Manuscripts (in English; *four* copies are required) should be submitted to: Editorial Office of *Journal of Chromatography*, P.O. Box 681, 1000 AR Amsterdam, Netherlands, Telefax (+31-20) 5862 304, or to: The Editor of *Journal of Chromatography, Biomedical Applications*, P.O. Box 681, 1000 AR Amsterdam, Netherlands. Review articles are invited or proposed in writing to the Editors who welcome suggestions for subjects. An outline of the proposed review should first be forwarded to the Editors for preliminary discussion prior to preparation. Submission of an article is understood to imply that the article is original and unpublished and is not being considered for publication elsewhere. For copyright regulations, see below.

Publication. The *Journal of Chromatography* (incl. *Biomedical Applications*) has 40 volumes in 1993. The subscription prices for 1993 are:

J. Chromatogr. (incl. *Cum. Indexes, Vols. 601–650*) + *Biomed. Appl.* (Vols. 612–651):
Dfl. 8520.00 plus Dfl. 1320.00 (p.p.h.) (total *ca.* US$ 5927.75)

J. Chromatogr. (incl. *Cum. Indexes, Vols. 601–650*) only (Vols. 623–651):
Dfl. 7047.00 plus Dfl. 957.00 (p.p.h.) (total *ca.* US$ 4821.75)

Biomed. Appl. only (Vols. 612–622):
Dfl. 2783.00 plus Dfl. 363.00 (p.p.h.) (total *ca.* US$ 1895.25).

Subscription Orders. The Dutch guilder price is definitive. The US$ price is subject to exchange-rate fluctuations and is given as a guide. Subscriptions are accepted on a prepaid basis only, unless different terms have been previously agreed upon. Subscriptions orders can be entered only by calender year (Jan.–Dec.) and should be sent to Elsevier Science Publishers, Journal Department, P.O. Box 211, 1000 AE Amsterdam, Netherlands, Tel. (+31-20) 5803 642, Telefax (+31-20) 5803 598, or to your usual subscription agent. Postage and handling charges include surface delivery except to the following countries where air delivery via SAL (Surface Air Lift) mail is ensured: Argentina, Australia, Brazil, Canada, China, Hong Kong, India, Israel, Japan*, Malaysia, Mexico, New Zealand, Pakistan, Singapore, South Africa, South Korea, Taiwan, Thailand, USA. *For Japan air delivery (SAL) requires 25% additional charge of the normal postage and handling charge. For all other countries airmail rates are available upon request. Claims for missing issues must be made within six months of our publication (mailing) date, otherwise such claims cannot be honoured free of charge. Back volumes of the *Journal of Chromatography* (Vols. 1–611) are available at Dfl. 230.00 (plus postage). Customers in the USA and Canada wishing information on this and other Elsevier journals, please contact Journal Information Center, Elsevier Science Publishing Co. Inc., 655 Avenue of the Americas, New York, NY 10010, USA, Tel. (+1-212) 633 3750, Telefax (+1-212) 633 3764.

Abstracts/Contents Lists published in Analytical Abstracts, Biochemical Abstracts, Biological Abstracts, Chemical Abstracts, Chemical Titles, Chromatography Abstracts, Clinical Chemistry Lookout, Current Awareness in Biological Sciences (CABS), Current Contents/Life Sciences, Current Contents/Physical, Chemical & Earth Sciences, Deep-Sea Research/Part B: Oceanographic Literature Review, Excerpta Medica, Index Medicus, Mass Spectrometry Bulletin, PASCAL-CNRS, Pharmaceutical Abstracts, Referativnyi Zhurnal, Research Alert, Science Citation Index and Trends in Biotechnology.

US Mailing Notice. *Journal of Chromatography* (ISSN 0021-9673) is published weekly (total 58 issues) by Elsevier Science Publishers (Sara Burgerhartstraat 25, P.O. Box 211, 1000 AE Amsterdam, Netherlands). Annual subscription price in the USA US$ 5927.75 (subject to change), including air speed delivery. Application to mail at second class postage rate is pending at Jamaica, NY 11431. **USA POSTMASTERS:** Send address changes to *Journal of Chromatography*, Publications Expediting, Inc., 200 Meacham Avenue, Elmont, NY 11003. Airfreight and mailing in the USA by Publication Expediting.

See inside back cover for Publication Schedule, Information for Authors and information on Advertisements.

0021-9673/93/$06.00

Printed in the Netherlands

CONTENTS

(Abstracts/Contents Lists published in Analytical Abstracts, Biochemical Abstracts, Biological Abstracts, Chemical Abstracts, Chemical Titles, Chromatography Abstracts, Current Awareness in Biological Sciences (CABS), Current Contents/Life Sciences, Current Contents/Physical, Chemical & Earth Sciences, Deep-Sea Research/Part B: Oceanographic Literature Review, Excerpta Medica, Index Medicus, Mass Spectrometry Bulletin, PASCAL-CNRS, Referativnyi Zhurnal, Research Alert and Science Citation Index)

Introduction to the series "Non-linear waves in chromatography"
by F. G. Helfferich (University Park, PA, USA) (Received October 27th, 1992) 95

REVIEW

Non-linear waves in chromatography. I. Waves, shocks, and shapes
by F. G. Helfferich (University Park, PA, USA) and P. W. Carr (Minneapolis, MN, USA) (Received October 27th, 1992) 97

REGULAR PAPERS

Column Liquid Chromatography

Reversed-phase high-performance liquid chromatography for evaluating the lipophilicity of pharmaceutical substances with ionization up to log P_{app} = 8
by K. Belsner, M. Pfeifer and B. Wilffert (Neuss, Germany) (Received September 25th, 1992) 123

Improved ultraviolet detection in high-temperature open-tubular liquid chromatography
by N. M. Djordjevic, D. Stegehuis, G. Liu and F. Erni (Basle, Switzerland) (Received September 21st, 1992) 135

High-performance liquid chromatography using continous on-line post-elution photoirradiation with subsequent diode-assay UV or thermospray mass spectrometry detection
by I. S. Lurie and D. A. Cooper (McLean, VA, USA) and I. S. Krull (Boston, MA, USA) (Received September 1st, 1992) 143

Chromatographic properties of chemically bonded bovine serum albumin working as a chiral selector in alkaline mobile phases
by Z. Šimek and R. Vespalec (Brno, Czechoslovakia) (Received September 7th, 1992) 153

Stability of immunoadsorbents comprising antibody fragments. Comparison of Fv fragments and single-chain Fv fragments
by M. J. Berry and J. J. Pierce (Sharnbrook, UK) (Received September 17th, 1992) 161

High-performance liquid chromatographic enantioseparation of glycyl di- and tripeptides on native cyclodextrin bonded phases. Mechanistic considerations
by J. Zukowski, M. Pawlowska, M. Nagatkina and D. W. Armstrong (Rolla, MO, USA) (Received September 1st, 1992) 169

Chemometrics in bioanalytical sample preparation. A fractionated combined mixture and factorial design for the modelling of the recovery of five tricyclic amines from plasma after liquid–liquid extraction prior to high-performance liquid chromatography
by J. Wieling (Zuidlaren and Groningen, Netherlands), H. Dijkstra, C. K. Mensink and J. H. G. Jonkman (Zuidlaren, Netherlands) and P. M. J. Coenegracht, C. A. A. Duineveld and D. A. Doornbos (Groningen, Netherlands) (Received September 25th, 1992) 181

Novel affinity separations based on perfluorocarbon emulsions. Development of a perfluorocarbon emulsion reactor for continuous affinity separations and its application in the purification of human serum albumin from blood plasma
by G. E. McCreath, H. A. Chase, D. R. Purvis and C. R. Lowe (Cambridge, UK) (Received September 29th, 1992) . 201

Enantiospecific drug analysis via the *ortho*-phthalaldehyde/homochiral thiol derivatization method
by D. M. Desai and J. Gal (Denver, CO, USA) (Received September 15th, 1992) 215

Multimycotoxin detection and clean-up method for aflatoxins, ochratoxin and zearalenone in animal feed ingredients using high-performance liquid chromatography and gel permeation chromatography
by C. Dunne, M. Meaney and M. Smyth (Dublin, Ireland) and L. G. M. Th. Tuinstra (Wageningen, Netherlands) (Received September 25th, 1992) 229

Correlation of reversed-phase high-performance liquid chromatography and gas–liquid chromatography for fatty acid compositions of some vegetable oils
by H. Konishi, W. E. Neff and T. L. Mounts (Peoria, IL, USA) (Received August 26th, 1992) 237

(Continued overleaf)

Contents (continued)

Chemical characterization of cellulose acetate by non-exclusion liquid chromatography
by T. R. Floyd (Kingsport, TN, USA) (Received September 24th, 1992) 243

Method for the determination of indole-3-acetic acid and related compounds of L-tryptophan catabolism in soils
by M. Lebuhn and A. Hartmann (Neuherberg, Germany) (Received September 25th, 1992) 255

High-performance liquid chromatography–thermospray mass spectrometry of ten sulfonamide antibodies. Analysis in milk at the ppb level
by J. Abián, M. I. Churchwell and W. A. Korfmacher (Jefferson, AR, USA) (Received August 5th, 1992) 267

Liquid chromatographic determination of amoxicillin preparations. Interlaboratory validation
by H.-C. Chung and M.-C. Hsu (Taipei, Taiwan) (Received October 6th, 1992) 277

Identification by particle-beam liquid chromatography–mass spectrometry of transformation products of the antioxidant Irganox 1330 in food-contact polymers subjected to electron-beam irradiation
by D. W. Allen, M. R. Clench, A. Crowson and D. A. Leathard (Sheffield, UK) (Received October 12th, 1992) . . . 283

Gas Chromatography

Improvement of continuous counter-current gas–liquid chromatography for practical use
by K. Sato (Tokyo, Japan), K. Watabe (Kyoto, Japan) and T. Ihara and T. Hobo (Tokyo, Japan) (Received July 16th, 1992) 291

Gas chromatographic analysis of alkanolamine solutions using capillary and packed columns
by O. F. Dawodu and A. Meisen (Vancouver, Canada) (Received September 18th, 1992) 297

Analysis of multi-component mixtures by high-resolution capillary gas chromatography and combined gas chromatography–mass spectrometry. II. Trace aromatics in an *n*-alkane matrix
by E. Matisová, Š. Vodný, S. Škrabáková and M. Onderová (Bratislava, Czechoslovakia) (Received July 30th, 1992) . 309

Determination of selected chlorinated benzenes in water by purging directly to a capillary column with whole column cryotrapping and electron-capture detection
by S. A. Rounds and J. F. Pankow (Beaverton, OR, USA) (Received September 24th, 1992) 321

Determination of coplanar polychlorobiphenyl congeners in biota samples
by M. D. Pastor, J. Sanchez, D. Barceló and J. Albaigés (Barcelona, Spain) (Received August 6th, 1992) 329

Gas chromatographic determination of trace nitrite after derivatization with ethyl 3-oxobutanoate
by T. Mitsuhashi (Kobe, Japan) (Received September 22nd, 1992) 339

Supercritical Fluid Chromatography

Influence of linear velocity and multigradient programming in supercritical fluid chromatography
by S. Küppers, M. Grosse-Ophoff and E. Klesper (Aachen, Germany) (Received September 21st, 1992) 345

Calibration of spectrophotometric detectors for supercritical fluid chromatography
by U. Meier and Ch. Trepp (Zurich, Switzerland) (Received October 2nd, 1992) 361

Electrophoresis

Effect of sample stacking on resolution, calibration graphs and pH in capillary zone electrophoresis
by J. L. Beckers and M. T. Ackermans (Eindhoven, Netherlands) (Received October 6th, 1992) 371

Analysis of anthraquinone sulphonates. Comparison of capillary electrophoresis with high-performance liquid chromatography
by S. J. Williams and D. M. Goodall (York, UK) and K. P. Evans (Manchester, UK) (Received September 29th, 1992) 379

SHORT COMMUNICATIONS

Column Liquid Chromatography

Enantiomer separations of secondary alkanols with little asymmetry by high-performance liquid chromatography on chiral columns
by T. Takagi, N. Aoyanagi, K. Nishimura, Y. Ando and T. Ota (Hakodate, Japan) (Received October 23rd, 1992) . . 385

Characterization of flavonoids by liquid chromatography–tandem mass spectrometry
by Y. Y. Lin (Staten Island, NY, USA), K. J. Ng (Bloomfield, NJ, USA) and S. Yang (Hangzhou, China) (Received October 28th, 1992) 389

Determination of volatile fatty acids in landfill leachates by high-performance liquid chromatography
by J.-F. Jen, C.-W. Lin, C.-J. Lin and C.-T. Yan (Taichung, Taiwan) (Received October 23rd, 1992) 394

Determination of N-hydroxysuccinimidyl-activated polyethylene glycol esters by gel permeation chromatography with post-column alkaline hydrolysis
by B. Shah and E. Watson (Thousand Oaks, CA, USA) (Received November 9th, 1992) 398

BOOK REVIEW

Advances in electrophoresis (edited by A. Chrambach, M. J. Dunn and B. J. Radola), reviewed by M. Bier (Tucson, AZ, USA) 401

AUTHOR INDEX 402

Journal of Chromatography, 629 (1993) 95–96
Elsevier Science Publishers B.V., Amsterdam

CHROM. 24 716

Introduction to the series "Non-linear waves in chromatography"

Friedrich G. Helfferich

Department of Chemical Engineering, Pennsylvania State University, University Park, PA 16802 (USA)

(First received April 13th, 1992; revised manuscript received October 27th, 1992)

ABSTRACT

The series of Reviews on "Non-linear waves in chromatography", to be published in this journal, is outlined.

We owe our very life to non-linearity. It is nature's non-linearity that makes all the complex phenomena possible that are needed to sustain a living organism, that has made our world what it is. The scientist and engineer of course know that, yet they love linear theories for the relative ease with which they lead to solutions and predictions. And once in a while an important field opens up in which the practitioner can indulge in the luxury of a linear theory without sacrificing essentials. Such a field has been analytical chromatography.

Non-linearity in chromatography arises from interactions between molecules of the same or different solutes. In analytical chromatography, the desire to work with smallest samples and attain highest separation efficiency has led to techniques working at extreme dilution and very low column loading. Solute molecules then rarely encounter one another, and so do not interact to any significant extent. Improvements in sorbents and stationary phases, in column design, and, most of all, in detector technology have made it possible to reduce sample size and column loading farther and farther, and so have kept moving analytical chromatography ever more deeply into the linear range. Only in the last few years has interest in chromatography as a *preparative* tool experienced a substantial revival. Here, the desire is for large througput and recovery at high concentrations, conditions under which solute interactions and thus non-linearity become prominent.

To be sure, there is nothing new about non-linear chromatography. From Tswett [1] to Tiselius [2] and Spedding [3], chromatography was used primarily for preparative separations. Only the enormous success of analytical liquid–liquid and gas–liquid chromatography in the 1950s changed that, making chromatography a method of chemical analysis almost by definition. In a way, we are now paying the price for the genius of A. J. P. Martin (see refs. 4 and 5), who conceived of analytical chromatography as we know it today and triggered the "gas chromatographic revolution" that made us forget much of the earlier work.

What the practical chromatographer today may wish to know about basic non-linear theory dates largely back to the years before 1970, a good deal of it to before 1955. However, this information is not easy to retrieve. One problem is that many of the bits and pieces do not seem quite to fit together as they stem from different fields of science, each of which had developed its own framework and viewpoints. Also, some of the essential work is highly mathematical, making it difficult to recognize the

Correspondence to: F. G. Helfferich, Department of Chemical Engineering, Pennsylvania State University, University Park, PA 16802, USA.

0021-9673/93/$06.00

underlying physical reality. Lastly, not only had each field developed its own terminology, but it kept changing it as time progressed. Therefore one should not be surprised to see old ideas reinvented, usually being given new names that add to the confusion.

I have been asked by one of the editors of this journal, Dr. Lloyd R. Snyder, to attempt presenting a review of basic non-linear theory aimed at the practitioner rather than the theoretician, with an emphasis on understanding of cause and effect, and with a minimum of mathematics. Not being a practicing chromatographer myself and no longer having followed all recent developments, I agreed only after I had succeeded in persuading Dr. Peter W. Carr to act as my guide, contribute the essential perspective and direction, provide the expertise in current practical chromatography, and join me in formulating the analysis of the various facets. Moreover, Lloyd Snyder kindly offered to give our series more than just the routine editorial attention. Any credit for the series will be owed to all three of us, any blame must be mine alone.

The topics we intend to cover are:

Part I. Waves, shocks and shapes: single-solute, non-linear chromatographic waves, their velocities, and their sharpening or spreading tendencies; shocks and shock layers and their profiles; constant and proportionate patterns; and shapes of single-solute peaks in elution and bands in displacement.

Part II. Wave interference and coherence: column response in multicomponent systems; wave patterns; interference of waves generated by successive injections; the coherence concept; composition paths and distance–time diagrams; vacancy chromatography; gradient elution; and linear chromatography as limiting case of solutes at trace level.

Part III. Multicomponent Langmuir systems: ideal chromatography in systems with competitive Langmuir isotherms; simple mathematics for such systems, based on the ω- or h-transformations; analogy to ion exchange with constant separation factors; and transients in displacement development.

Part IV. Arbitrary multicomponent systems: with synergism; effects of selectivity reversals; non-isothermal systems; methods for multicomponent isotherm determination.

This agenda is flexible, and additional or alternative topics might suggest themselves or be suggested to us as we proceed. Mathematics will remain restricted to a few simple equations needed to understand effects and to some techniques that can give approximate answers in complex cases with minimal effort. As much as possible, a framework will be provided in which standard theories have their logical places and can be compared with one another, and a dictionary of equivalent terms will be compiled. Emphasis will be on conceptual understanding and practical utility rather than on derivations or interpretation of observations. Also, as much as possible, the instalments will be kept independent so that each can be read without detailed study of the others, in order to allow the reader to pick and choose.

Lastly, we claim no original authorship for the material to be presented. Almost all of it will be from previous work, much of it by others, and the few exceptions will be relatively insignificant. However, there will be no attempt to cover prior theories exhaustively. Rather, those will be chosen which best prove or illustrate the points to be made, and often reviews rather than first publications will be cited. We apologize ahead of time to all whose worthy contributions may go without mention.

REFERENCES

1 M. Tswett, *Ber. Deutsche Botan. Gesellsch.*, 24 (1906) 316, 384.
2 A. Tiselius, *Ark. Kemi Mineral. Geol.*, A16, No. 18 (1943).
3 F. H. Spedding, *Discuss. Faraday Soc.*, 7 (1949) 214.
4 A. J. P. Martin and R. L. M. Synge, *Biochem J.*, 35 (1941) 1358.
5 A. T. James and A. J. P. Martin, *Analyst*, 77 (1952) 915.

Journal of Chromatography, 629 (1993) 97–122
Elsevier Science Publishers B.V., Amsterdam

CHROM. 24 717

Review

Non-linear waves in chromatography

I. Waves, shocks, and shapes

Friedrich G. Helfferich

Department of Chemical Engineering, Pennsylvania State University, University Park, PA 16802 (USA)

Peter W. Carr

Department of Chemistry, University of Minnesota, Minneapolis, MN 55455 (USA)

(First received April 13th, 1992; revised manuscript received October 27th, 1992)

ABSTRACT

Cause and effect in non-linear chromatography are examined from the point of view of wave theory. This first of four instalments is restricted to single-component systems and examines monotonic concentration variations and chromatographic peaks and bands. It uses the wave equation, which states the velocity at which a given concentration advances, to establish the properties of "waves," that is, monotonic concentration variations. Depending on the sense of curvature of the isotherm, a wave may be self-sharpening or non-sharpening. A self-sharpening wave remains, or sharpens to become, a shock layer; a nonsharpening wave spreads indefinitely, eventually in proportion to traveled distance. The concentration profile of a shock layer depends on the shape of the isotherm and on the dispersive effect of non-idealities, of which resistance to mass transfer usually is the most important. Mass-transfer resistance in the moving phase causes "fronting;" mass-transfer resistance within the stationary sorbent causes "tailing." It is therefore in general not possible to model shock layers with only a single, lumped mass-transfer parameter. The concentration profile of a nonsharpening wave depends almost exclusively on the shape of the isotherm.

The knowledge of wave behavior is used to examine peak shapes in elution under overload conditions and bands in displacement. The peak shape in elution is almost entirely determined by the degree of overload and the shape of the isotherm. Wave theory confirms a rule previously stated by Knox that, in columns exceeding a certain length, samples containing the same amount of solute give peaks of essentially the same shape under conditions of predominant concentration overload, predominant volume overload, or any combination of the two. In displacement development, the final pattern can be established by determination of the lengths of the bands of the individual components according to Tiselius and separate calculation of the shock-layer profiles.

CONTENTS

I.1. Definitions 98
I.2. Velocities 99
I.3. Linear waves 101
I.4. Self-sharpening waves, shocks, and shock layers 102

Correspondence to: F. G. Helfferich, Department of Chemical Engineering, Pennsylvania State University, University Park, PA 16802. USA.

0021-9673/93/$06.00

I.5. Nonsharpening waves . . . 104
I.6. Constant and proportionate patterns . . . 105
I.7. Terminology . . . 106
I.8. Shock-layer profiles . . . 107
I.8.1. Finite mass-transfer rate . . . 107
I.8.1.1. Linear driving-force approximations . . . 107
I.8.1.2. Other mass-transfer models . . . 110
I.8.2. Finite rate of attachment to sorbent ("reaction-rate control") . . . 110
I.8.3. Other non-idealities . . . 110
I.8.3.1. Axial diffusion . . . 110
I.8.3.2. Non-plug flow . . . 111
I.8.4. Other non-linear effects . . . 111
I.8.4.1. Axially non-uniform flow-rate . . . 111
I.8.4.2. Thermal effects and reactions . . . 111
I.8.5. Analytical solutions . . . 111
I.8.6. Summary of effects . . . 111
I.9. Profiles of nonsharpening waves . . . 112
I.10. Complex isotherms and composite waves . . . 112
I.11. Standard theories and models . . . 113
I.11.1. Equilibrium-stage models . . . 113
I.11.2. "Semi-ideal" models . . . 113
I.11.3. Thomas model ("reaction-kinetic model") . . . 114
I.11.4. Mass-transfer models . . . 114
I.11.5. General models . . . 114
I.12. Elution peaks . . . 114
I.13. Bands in displacement . . . 117
I.14. Symbols . . . 120
I.15. Acknowledgement . . . 121
I.16. Appendix . . . 121
References . . . 121

This first instalment of the series will examine the nature of non-linear waves and the implications for *single-component* non-linear chromatography, specifically, for the dependence of the shapes of waves, peaks, and bands on physical aspects such as isotherm shape and mass-transfer resistances. Multicomponent problems will be examined later in this series.

I.1. DEFINITIONS

For simplicity, the two phases between which a solute partitions will be called the *moving phase* and the *sorbent* (or sorbent phase). Thus, "sorbent" will refer to gel-type or porous sorbent beads, to the surfaces of impermeable adsorbent beads or column walls, or to a stationary liquid sorbent on or in a solid support which may be a particle or the column wall. "Moving phase" rather than "mobile phase" is used to make clear that the term refers exclusively to the fluid traveling through the column, not to a stationary liquid within or on a support.

In conformity with established usage, *linear chromatography* will be understood to refer to chromatography with no interaction between solute molecules of the same or different kinds (*i.e.*, linear sorption isotherms, no interactions through occupancy of moving-phase volume, axially uniform flow-rate). Linear chromatography thus does not exclude non-linear mass-transfer equations. Correspondingly, *non-linear chromatography* is taken to be chromatography with non-linear isotherms or other interactions between solute molecules.

The term *multicomponent chromatography* will be reserved for systems in which different solutes affect one another's behavior, specifically, systems in which the sorbent-phase concentration of a solute depends not only on the moving-phase concentration of that solute, but on those of all other solutes as well. Multicomponent systems thus are necessarily non-linear. This definition of multicomponent

chromatography is practical because the response in systems with independent solutes is easily constructed by additive superposition of single-solute responses and so requires no theory beyond that for single solutes.

Ideal chromatography, in some earlier work also called equilibrium theory, will be understood to imply the following simplifying premises: (1) local equilibrium between moving and sorbent phases, (2) ideal plug flow, (3) mass transfer in axial direction by convection only, (4) axially uniform volumetric flow-rate of bulk moving phase, (5) isobaric behavior, (6) isothermal behavior, and (7) absence of chemical reactions that transform solutes and thereby alter their sorption behavior. Except where specifically mentioned, assumptions 4–7 will also be taken as valid when non-ideal systems are discussed.

Non-linear chromatography is most easily understood as a phenomenon of *waves*, a term borrowed from physics of compressible fluids [1,2], where quite similar differential equations apply. A wave is defined as a variation of dependent variables; in chromatography, of solute concentrations and possibly of temperature [3,4]. (Usually, a wave moves; however, standing waves can arise under certain conditions, *e.g.*, in countercurrent operation). A typical chromatographic wave is the advancing "front" of a solute that is being injected into a column initially free of solutes. In contrast to waves in acoustics and optics, those in chromatography thus are not oscillations, are not characterized by frequencies. It will prove expedient to reserve the term wave to a *monotonic* variation. A typical chromatographic peak then consists of two waves: its front and its rear (*i.e.*, the parts downstream and upstream of the apex, respectively); similarly, a flat-top peak under overload conditions or a band in displacement consists of a plateau between two waves (see Fig. I.1). The behavior of peaks and bands is necessarily more complex than that of (monotonic) waves. Therefore, the properties of waves are discussed in detail before this knowledge is applied to peaks and bands.

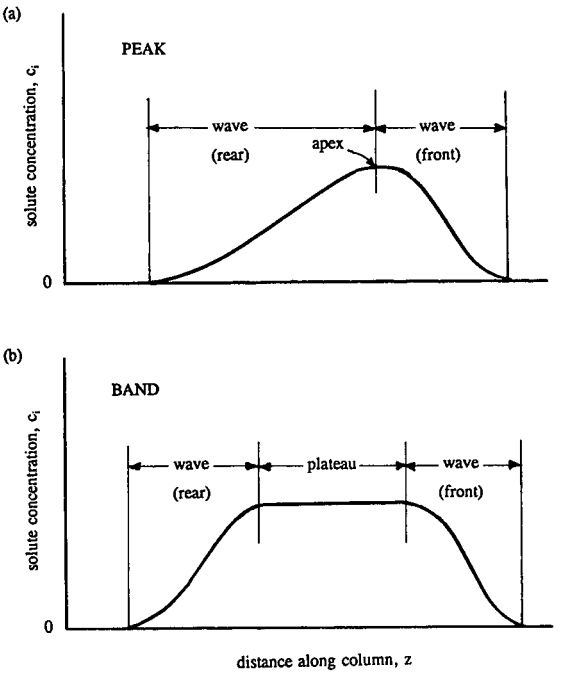

Fig. I.1. Wave terminology for (a) chromatographic peak, (b) chromatographic band or flat-top peak.

I.2. VELOCITIES

Most of the conventional literature on chromatography and fixed-bed adsorption is in terms of retention times or volumes [5–7] or other throughput-related parameters [8,9] rather than velocities. The latter [4,10–13], although less directly related to observable effluent concentration histories, are used here because they allow waves to be studied regardless of their origin and position in a column, and so make it easier to visualize their properties and behavior: A velocity is a *local* phenomenon, independent of conditions elsewhere and thus of the column size, elapsed time, injection history, etc.

With this focus on waves, the central question in the analysis of any chromatographic phenomenon becomes, "how fast does any given solute *concentration* advance in the direction of flow?" This, rather than the velocity of solutes molecules, is the starting point. By definition, the velocity v_{c_i} of a moving-phase concentration c_i of solute i is

$$v_{c_i} \equiv (\partial z/\partial t)_{c_i} \tag{I.1}$$

(z = linear distance in direction of flow, t = time). Granted the premises of ideal chromatography *except local equilibrium*, the equation for conservation

of mass of solute in a differential cross-section of the column is

$$\underbrace{\frac{\rho}{\varepsilon}\left(\frac{\partial q_i}{\partial t}\right)_z}_{\text{accumulation}} + \underbrace{\left(\frac{\partial c_i}{\partial t}\right)_z + v^0\left(\frac{\partial c_i}{\partial z}\right)_t}_{\text{outflow - inflow}} = 0 \qquad \text{(I.2)}$$

and gives the concentration velocity [11]

$$v_{c_i} = \frac{v^0}{1 + (\rho/\varepsilon)(\partial q_i/\partial c_i)_z} \qquad \text{(I.3)}$$

(v^0 = velocity of moving-phase flow; q_i = sorbent loading, ρ = bulk density of sorbent, ε = fractional void volume of bed; ρ/ε is constant under normal conditions; for exact definitions see Symbols section). This "wave equation" is the most important equation in non-linear chromatography. Characteristic of non-linear chromatography is that the wave velocity, even under ideal conditions, varies with the solute concentration.

In *ideal* chromatography, the phases are in local equilibrium, so that q_i can be expressed as a unique function of c_i alone, regardless of distance and time. Accordingly, the partial differential in eqn. I.3 can be replaced by the respective total differential, so that the wave equation becomes [4,11]

$$v_{c_i} = \frac{v^0}{1 + (\rho/\varepsilon)(\mathrm{d}q_i/\mathrm{d}c_i)} \qquad \text{(I.4)}$$

where $\mathrm{d}q_i/\mathrm{d}c_i$ is the slope of the equilibrium sorption isotherm of solute i (or of the tangent to the isotherm) at the respective concentration c_i (see Fig. I.2). This velocity, at which the concentration would travel if the phases were in equilibrium, will be called the "natural" wave velocity. *The steeper the isotherm, the lower is the natural wave velocity.*

In non-linear chromatography, the distinction between *particle velocities* and *wave velocities* is important [11,14]. In physics of fluids [1], a particle velocity is the (macroscopic and average) velocity of an identifiable *object*, say, a volume element of fluid; a wave velocity is the velocity of a given *value of a variable*. The two can be very different. For example, a hurricane with sustained winds of over a hundred miles an hour may advance at only, say, ten or twenty miles per hour and possibly in a quite different direction. The wind velocity (of volume elements of air) is a particle velocity, the velocity of the storm itself (the low-pressure system) is a wave

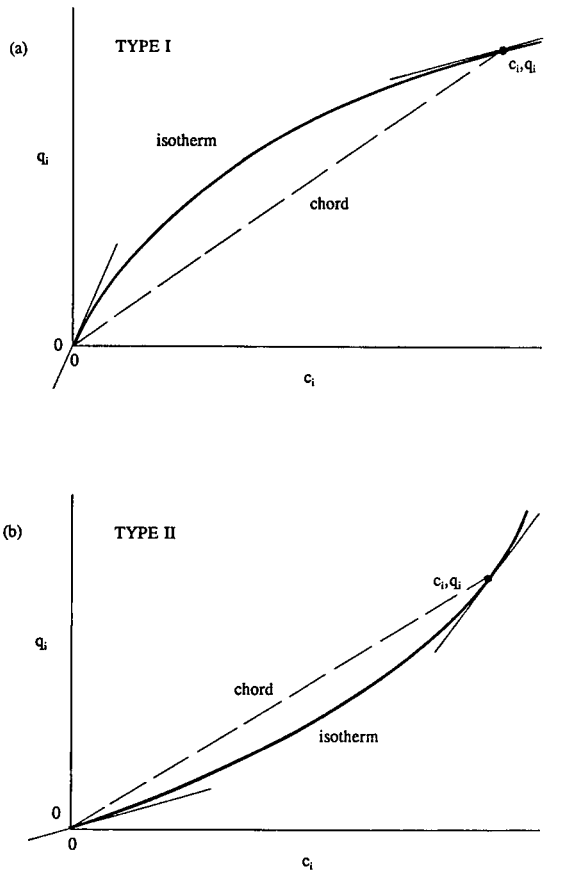

Fig. I.2. Isotherms with tangents $\mathrm{d}q_i/\mathrm{d}c_i$ at $c_i = 0$ and a point $c_i > 0$, and with chord of that point; (a) Type I; (b) Type II.

velocity. The concentration velocities in eqns. I.3 and I.4 above are wave velocities. The particle velocity v_i of a solute i at a given concentration is readily derived with the argument that molecules of i advance, at the velocity of moving-phase flow, only while they are in that phase, and not at all while they are at rest on or in the stationary sorbent. The fraction of solute that is moving is $\varepsilon c_i/(\varepsilon c_i + \rho q_i)$ or, rearranged, $1/[1 + (\rho/\varepsilon)q_i/c_i)]$, and the particle velocity accordingly is [11,14]

$$v_i = \frac{v^0}{1 + (\rho/\varepsilon)q_i/c_i} \qquad \text{(I.5)}$$

While the natural wave velocity depends on the slope of the *tangent* to the isotherm at the respective concentration, the particle velocity depends on the

ratio q_i/c_i, that is, on the slope of the *chord* of the isotherm point corresponding to that concentration (see Fig. I.2). Only in linear chromatography do waves (concentration variations) and particles (solute molecules) move at the same velocity.

To appreciate the difference between the two types of velocities, consider the advance of a pulse of incrementally higher moving-phase concentration of solute in a column whose sorbent, at the original, lower concentration, is already loaded to its maximum capacity. The sorbent cannot accommodate any more solute, so the pulse must advance at the velocity of moving-phase flow (the pulse velocity is a wave velocity); indeed, for zero isotherm slope, eqn. I.4 gives $v_{c_i} = v^0$. Meanwhile, the solute molecules that, at any given moment, constitute the pulse spend part of their time at rest on or in the sorbent and so advance at a lower average velocity (particle velocity) given by eqn. I.5; they are being overtaken by the pulse. A standard detector (measuring a spectral response, fluorescence, refractive index, conductivity, or any other property that is a measure of concentration) in the effluent registers the arrival of the *concentration pulse* that traveled at the *wave velocity*. In contrast, a radioactivity detector would register the arrival of a pulse of injected tagged molecules that traveled at the *particle velocity*. If the injected concentration pulse were to have contained radioactively tagged molecules, the concentration pulse and the radioactivity pulse would reach the column end at different times [14].

[The fact that a concentration perturbation (the concentration pulse) should outrun or lag behind the slug of molecules of which it consisted upon injection is not easy to accept. However, the underlying difference between wave velocities and particle velocities is one of the fundamental principles of physics and is absolutely essential for proper understanding of non-linear chromatography. A more easily visualized and somewhat analogous situation is that of a sonic boom, in which the wave (a pressure variation in this case) travels much faster than the molecules that generated the boom in the first place, as well as those being compressed by the boom at any given moment. Still another interesting example is that of a traffic jam, in which the congestion (a wave) is actually propagated *against* the direction of the flow of the cars (the particles). A reader who still has conceptual reservations may wish to study ref. 14 and section 3.III.B of ref. 11, where such matters are discussed in more detail.]

I.3. LINEAR WAVES

Waves in linear chromatography, thoroughly familiar to all practitioners, present a logical starting point for the application of the concepts and equations of wave theory.

In linear chromatography, the isotherm slope dq_i/dc_i is constant, independent of the moving-phase concentration, so that according to the wave equation I.4 all moving-phase concentrations of a given solute have the same natural velocity. In *ideal* linear chromatography, in which concentrations move with their natural velocities, any wave then travels "as is", that is, without sharpening or spreading (see Fig. I.4a and b); the same is, of course, also true for a peak. In *real* linear chromatography, the dispersive effects of non-idealities make the wave spread. In chromatography, the relevant effects are: (i) deviation from local equilibrium because of finite rate of equilibration between the moving and sorbent phases, (ii) axial diffusion, and (iii) deviation from plug flow.

If local equilibrium were to be maintained, the rate coefficients of all steps required for equilibration of the moving phase with the sorbent would have to be infinitely large. With coefficients of finite values, transfer of solute from one phase to the other to establish equilibrium can occur only if non-equilibrium provides a "driving force". Accordingly, the concentration variation in or on the sorbent always lags slightly behind that in the moving phase as a wave moves through a position in the column. The sharper the wave, the faster is the concentration variation in the moving phase at a position in the column as the wave passes through, and so the harder it is for the concentration variation in or on the sorbent to keep pace with that in the moving phase. Accordingly, the stronger is the dispersive effect of non-equilibrium.

The flux of axial diffusion is proportional to the axial concentration gradient (Fick's law). Thus, here, too, the dispersive effect is stronger if the wave is sharper.

The irregular packing of a real column causes deviations from plug flow even if the flow is laminar. Stream lines branch and rejoin, and travel times

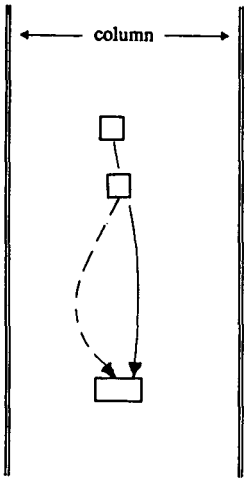

Fig. I.3. Branching and rejoining of stream lines with different residence times in an irregular packing. From ref. 15.

along such branches are not equal. This amounts to mixing, at the confluence of two stream lines (or at the column exit), two moving-phase volume elements that were previously at different distances from the column entry (see Fig. I.3). The sharper a wave, the greater is the concentration difference between two such volume elements, and the stronger is the dispersive effect. The same is obviously true for eddy mixing in turbulent flow, where once again volume elements previously at different distances from the column entry are mixed.

In all three cases —finite equilibration rate, axial diffusion and non-plug flow— the dispersive effect thus is seen to diminish as the wave spreads. The familiar result is that the wave spreads in proportion to the *square root* of traveled distance (or elapsed time), as is common in diffusion processes. In non-linear wave theory, such linear waves are also called *indifferent* [11], in distinction from self-sharpening, nonsharpening, and composite non-linear waves (see farther below, and Table I.1, in which the sharpening or spreading behavior of linear and non-linear waves is summarized).

I.4. SELF-SHARPENING WAVES, SHOCKS, AND SHOCK LAYERS

We turn now to non-linear waves, that is, monotonic concentration variations in systems with non-linear isotherms.

Imagine a moving phase containing solute at constant concentration c_i^0 entering a column that was initially free of sorbate, and the adsorption isotherm being of *Type I* (negative curvature, see Fig. I.2a). The advancing "front" of solute i is a non-linear wave. At the leading edge of this sorption wave, where the concentrations of i are still low, the isotherm is steep and, according to the wave equation I.4, the natural wave velocity is low. At the tail end of the wave, at high concentrations of i, the opposite is true. Since the trailing portions tend to advance more rapidly than the leading ones, the wave tends to sharpen if initially diffuse (see Fig. I.4c) [16]. The wave is said to be *self-sharpening* [17] (in physics of fluids it is called a compressive wave).

In *ideal* chromatography, in which concentrations travel at their natural velocities, such a wave sharpens to become, or remains, a concentration discontinuity (see Table I.1). Unlike an ocean wave rolling onto a beach, such a wave cannot "break", *i.e.*, higher concentrations from its rear cannot

TABLE I.1

SHARPENING AND SPREADING BEHAVIOR OF WAVES

Wave	Ideal chromatography	Real chromatography
Indifferent wave (linear wave)	Travels without change in profile	Spreads in proportion to square root of traveled distance
Self-sharpening wave	Sharpens into discontinuity (shock) then travels as such	Sharpens (or spreads) into shock layer of finite width, then travels without change in profile
Nonsharpening wave	Width increases linearly with traveled distance	

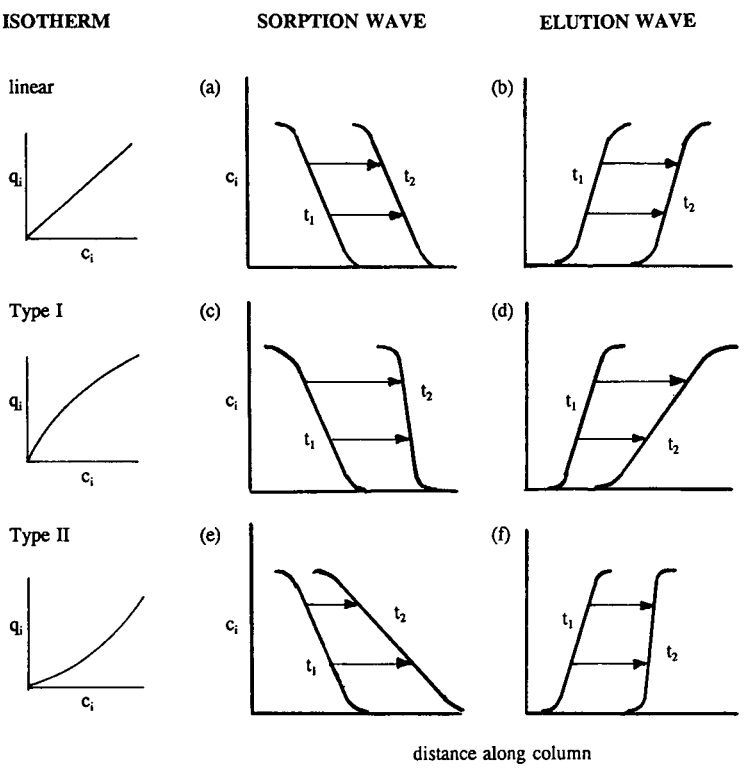

Fig. I.4. Sharpening behavior of sorption and desorption waves of ideal chromatography resulting from shape of isotherm: concentration profiles at successive times t_1 and $t_2 > t_1$ of waves diffuse at t_1 (schematic).

overtake lower ones ahead because this would lead to the physically impossible coexistence of three different concentrations of the same solute at the same location. Instead, the wave keeps traveling as a discontinuity [16]. In terms of mathematics, the physically realized solution of the differential mass balance (eqn. I.2) is a so-called weak solution, with two branches separated by a discontinuity [18,19]. The velocity $v\Delta_{c_i}$ at which the discontinuity advances is readily derived from a mass balance across it [4,11]:

$$v\Delta_{c_i} = \frac{v^0}{1 + (\rho/\varepsilon)\Delta q_i/\Delta c_i} \tag{I.6}$$

where Δ stands for the difference between the downstream and upstream sides of the wave. [Eqn. I.6 is equivalent to the Rankine–Hugoniot equation in physics of fluids.] The discontinuity is called a *shock*. An infinite number of weak solutions satisfy the differential mass balance (eqn. I.2) and the initial and input conditions since the position of the discontinuity remains unspecified, but eqn. I.6 uniquely identifies the appropriate one.

In our *real* world of compressible fluids or of chromatography, dispersive effects of non-idealities prevent a wave from sharpening into a discontinuity. As was shown for linear waves, the relevant dispersive effects of finite equilibration rate, axial diffusion, and deviation from plug flow all decrease in strength as the wave spreads (or increase as the wave sharpens). In contrast, the sharpening tendency of the wave resulting from the dependence of the natural velocity on concentration, given by the difference in isotherm slopes at its front and rear ends, is independent of the current sharpness of the wave. Therefore, at some finite width of the wave, the sharpening and spreading tendencies achieve a balance [9,17,20]. A shelf-sharpening wave sharpens if initially more diffuse, or spreads if initially sharper, until that balance is attained, and then continues its travel without further change in width or shape (see

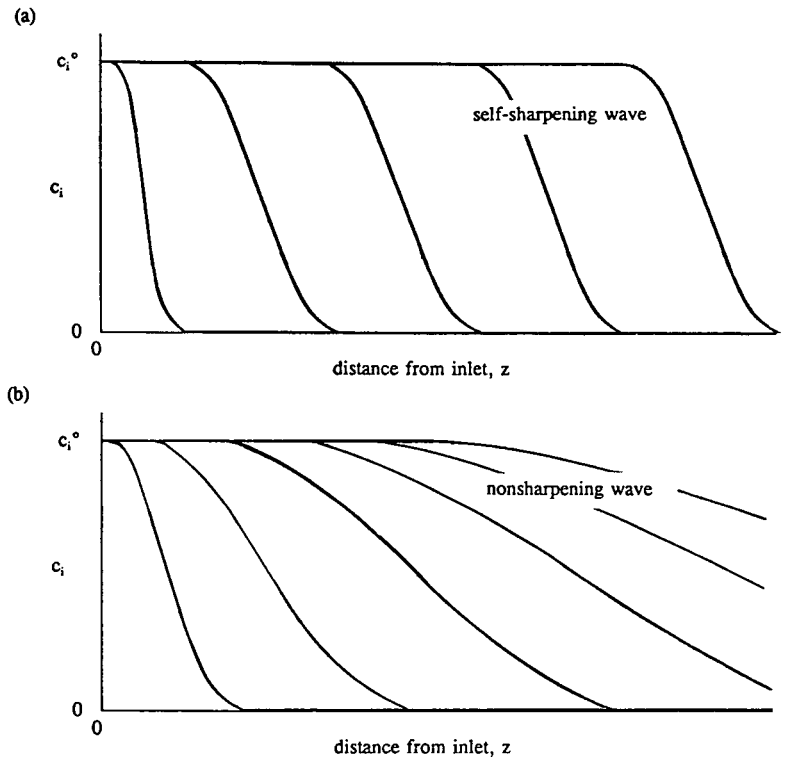

Fig. I.5. Concentration profiles in non-ideal chromatography at successive times for waves generated by step input; (a) self-sharpening wave; (b) nonsharpening wave.

Fig. I.5a and Table I.1). Such a wave with a steep, but continuous profile is often called a *shock layer* if attention is to be drawn to its not being a discontinuity. The shock velocity equation (eqn. I.6) remains valid for the shock layer [11].

A shock layer also results, for the same physical reasons, when a solute with an isotherm of Type II is eluted from the column by a solvent or carrier gas: In this case, the high solute concentrations are in the forward portion of the wave and are most strongly retarded because they have the steepest isotherm slopes (see Fig. I.2b), so that the wave sharpens if initially diffuse (see Fig. I.4f).

The terms shock and shock layer, adopted from physics of compressible fluids, are relatively new in chromatography and fixed-bed adsorption. However, the phenomena they describe have been familiar to chromatographers and adsorption engineers for almost half a century, if under different names. For a glossary of equivalent terms, see Table I.2.

I.5. NONSHARPENING WAVES

Consider the case in which the solute advancing in the initially sorbate-free column has an isotherm of *Type II* (positively curved, see Fig. I.2b). Here, the isotherm slope is less steep at the leading (low) concentrations than at the trailing (high) concentrations. According to the wave equation I.4, the forward portions now have higher natural velocities than those farther behind, so that the sorption wave tends to spread (see Fig. 1.4e) [16]. Non-idealities only add to that tendency. Soon, the wave becomes so diffuse that the dispersive effects of the non-idealities no longer matter. From then on, the width of the wave increases *linearly* with traveled distance or elapsed time (see Fig. I.5b and Table I.1) [9]. Such a wave is said to be *nonsharpening* [17] (dispersive wave or rarefaction wave in physics of fluids).

A nonsharpening wave also results when a solute with Type I isotherm is eluted from the column by a

TABLE I.2

EQUIVALENT TERMS IN WAVE MATHEMATICS, FIXED-BED ENGINEERING AND NON-LINEAR CHROMATOGRAPHY

Terms used here are shown in bold. The equivalence of terms is not exact, in part because problems other than with uniform initial and constant influent conditions have rarely been considered except by wave mathematicians. Terms used with more restrictive meanings are shown in parentheses.

Wave mathematics	Fixed-bed engineering	Chromatography (pre-1970)
Wave	Mass-transfer zone[a] [21], transition [9,12], front or wavefront [13]	Boundary [16,17,22], (front) [23]
Compressive wave		**Self-sharpening** boundary [17]
Shock, **shock layer**	Constant mass-transfer zone[a] [15], abrupt transition [9], **constant pattern** [8,9,12,24]	Steady form of boundary [22]
Rarefaction wave, dispersive wave (simple wave)	Gradual transition [9]	**Nonsharpening** boundary [17]
Centered wave (self-similar wave)	**Proportionate pattern** [8,9,12]	
Linear wave, contact discontinuity (if sharp)		**Indifferent** boundary [11]

[a] Originally called exchange zone (for binary ion exchange).

solvent or carrier gas. Here, the isotherm slope and thus the retardation are greater for the trailing, low concentrations than for leading, high concentrations of the elution wave (see Figs. I.2b and I.4d).

Since the dispersive effects of non-idealities fade as the wave spreads, ideal theory is usually quite satisfactory for nonsharpening waves.

[As is often pointed out, in the mathematics of ideal chromatography a weak solution satisfying the differential and overall mass balances also exists for a nonsharpening wave that starts as a discontinuity, allowing it to travel as such. The intermediate concentrations then never come into existence, so that the wave equation I.4 remains inapplicable because no gradients dq_i/dc_i can be defined. That this weak solution has no physical reality can be shown with a complex argument according to which the effect would be to decrease the entropy of the system, in violation of the second law of thermodynamics [18,25,26]. For practical purposes, however, if suffices to say that the slightest non-ideality of the real world causes the intermediate concentrations to become realized, so that the wave equation becomes applicable and produces proportionate spreading; this shows that, for a nonsharpening wave, the weak solution of ideal chromatography is not an asymptotic solution for vanishing non-idealities, and so is of no practical significance.]

I.6. CONSTANT AND PROPORTIONATE PATTERNS

A shock layer traveling without further sharpening or spreading is said to have attained a *constant pattern* [8,9,12,13,24]. A nonsharpening wave that spreads in proportion to traveled distance is said to have attained a *proportionate pattern* [8,9,12, 13]. Exactly constant or proportionate patterns are possible only in ideal chromatography, and proportionate ones only for waves starting as discontinuities. Like equilibrium and steady state, in the real world the patterns are only approached asymptotically.

The time or distance of travel required for approach to a constant or proportionate pattern (to within a specified margin) in non-ideal chromatography depends on the shape of the isotherm [8,9]. For any wave that enters the column as a discontinuity (step change in solute concentration of enter-

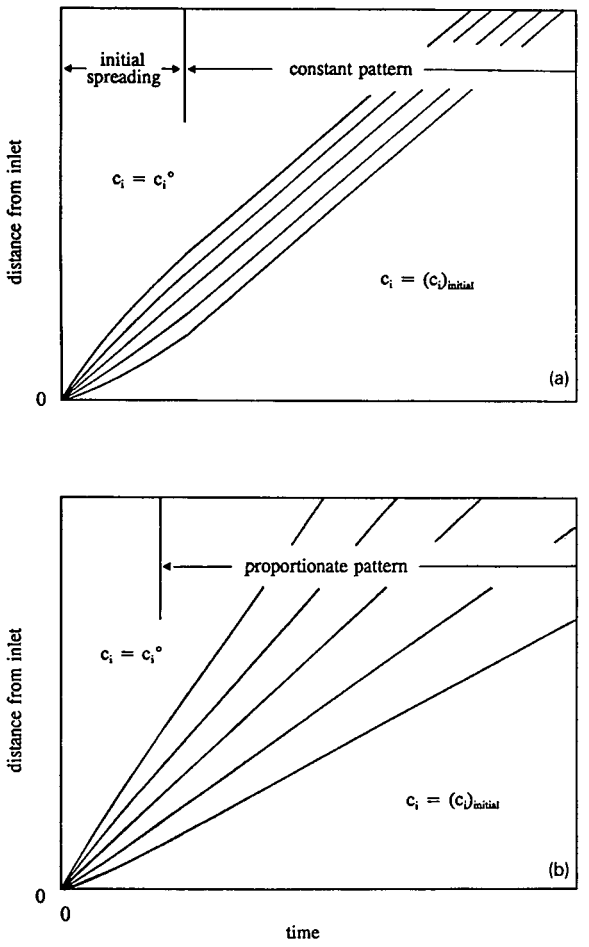

Fig. I.6. Concentration contours in distance–time diagrams in non-ideal chromatography, showing approach to final patterns of waves generated by step input; (a) constant pattern of self-sharpening wave; (b) proportionate pattern of nonsharpening wave. From ref. 15.

ing fluid), the dispersive effect of the non-idealities is overwhelming initially, making the wave spread at first in a square-root pattern regardless of its self-sharpening or nonsharpening nature (see Fig. I.6). If the isotherm is strongly curved, the final pattern is approached rapidly [*e.g.*, in passing through about 10 theoretical plates for a Langmuir isotherm $q_i/Q_i = Kc_i/(1 + Kc_i)$ with $K(c_i)_{max} = 4$]: In a self-sharpening wave, the sharpening tendency owing to the isotherm curvature then is so strong that the balance with the dispersive effects is closely approached when the wave has spread but a little; in a nonsharpening wave the spreading tendency then is so strong and spreading so fast that the dispersive effects of the non-idealities quickly become negligible compared with that of the isotherm curvature. On the other hand, if the isotherm is almost linear, the sharpening or spreading tendency resulting from the minute curvature is so weak that the dispersive effects of the non-idealities remain dominant for a long time; if so, the wave may leave the column before it has deviated much from square-root spreading. (For guidance concerning requirements for close approach to the final pattern, see Fig. 16-11 in Perry's Handbook [9]).

What matters in this context is the change in isotherm slope *within the isotherm segment over which the wave extends* or, in other words, the difference in isotherm slopes between the points corresponding to the concentrations upstream and downstream of the wave. Thus, for a given isotherm, the sharpening or spreading tendency is weaker, the smaller the concentration variation across the wave. In the extreme, very small waves or pulses are, as a rule, essentially indifferent and adequately described by linear theory, even if the isotherm spanning large variations is non-linear.

I.7. TERMINOLOGY

Use of a precise terminology can help to avoid confusion. Note the differences:

"*Sharp*" and "*diffuse*" describe current states of waves.

"*Self-sharpening*" and "*nonsharpening*" describe tendencies.

"*Sharpens*" or "*spreads*" describes what a wave currently does.

"*Shocks*" or "*shock layers*" are self-sharpening waves that have attained or closely approached their final patterns.

A self-sharpening wave may well be diffuse, for instance if it was recently generated by a gradual variation of the inlet concentration; likewise, a nonsharpening wave may still be sharp, not yet having had time to spread much from an initial, even sharper state. A self-sharpening wave may actually spread, namely, while it approaches its constant pattern after having started as a discontinuity, or if an increase in flow-rate makes it approach a new and less sharp constant pattern.

I.8. SHOCK-LAYER PROFILES

While non-idealities have little, if any, effect on a nonsharpening wave, they in combination with the isotherm curvature dictate the shape of the concentration profile in a shock layer. In *linear* chromatography, the lumping of all non-ideal effects into one parameter —a lumped dispersion coefficient, Peclet number, or height equivalent to a theoretical plate (HETP)— is customary [5,6,7,10,27]. However, *the classic doctrine of likeness and additivity of effects is not in general valid in non-linear chromatography*, as will be seen. (Even in linear chromatography it is valid only if linear driving force approximations are used for the equilibration rate; with more elaborate mass-transfer equations, distinct differences between non-ideal effects appear [28–30]).

Of the three principal non-idealities —finite equilibration rate, non-plug flow, and axial diffusion— the dispersive effect of the first increases with increasing flow-rate (faster wave), that of the second (branching and rejoining of stream lines) depends only weakly on flow-rate as long as the flow remains laminar, and that of the third increases with decreasing flow-rate (longer residence time gives more time for diffusion) [5–7,10,27]. Whereas the separation efficiency in analytical chromatography is best when the effects are comparable in magnitude [5–7,10,27], the desire for high throughput in preparative chromatography usually calls for flow-rates so high that local non-equilibrium caused by the finite equilibration rate is dominant and therefore must receive greatest attention.

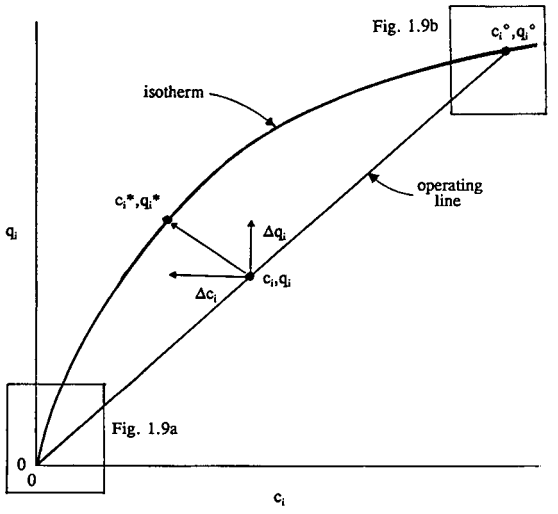

Fig. I.7. q_i *vs.* c_i diagram with isotherm, operating line, and driving force with its contributions; boxes in lower left and upper right indicate areas enlarged in Fig. I.9. From ref. 15.

I.8.1. Finite mass-transfer rate

To understand the effect of a finite mass-transfer rate on the profile of a shock, we must first establish how the sorbent loading q_i varies with the moving-phase concentration c_i within the constant-pattern shock layer. The concentrations are *not* in local equilibrium, as the shock would then be an ideal discontinuity. However, granted the effects of non-plug flow and axial diffusion are unimportant, the wave equation I.3 still holds since equilibrium was not postulated in its derivation. By definition, the wave in its constant pattern does not change its shape; this requires all concentrations to move at the same velocity. According to the wave equation, this is true only if the derivative $(\partial q_i/\partial c_i)_z$ has the same value at all concentrations. Therefore, the variation of q_i with c_i in a constant pattern must be *linear*! [9,17]. Fig. I.7 shows such a linear variation in the form of an "operating line" in a q_i *vs.* c_i diagram, together with the respective "equilibrium curve" (isotherm)[a], here of Type I. At any location within the constant-pattern shock layer, the bulk-phase concentrations correspond to a point (c_i,q_i) on the operating line, and the concentrations at the interface of sorbent and moving phase correspond to a point (c_i^*,q_i^*) on the isotherm (granted equilibrium at the interface).

I.8.1.1. Linear driving-force approximations

Many mathematical models for mass-transfer rates have been postulated, and depending on the type of sorbent one or the other may be more appropriate. The simplest model assumes equilibrium

[a] The terms *equilibrium curve* and *operating curve* (or operating line, if linear) are from chemical engineering usage in mass-transfer operations such as distillation, liquid extraction, gas absorption, etc. The operating curve shows the actual, non-equilibrium condition of the column, and its distance from the equilibrium curve is a quantitative measure of the distance from equilibrium and thus of the driving force for interphase mass-transfer.

at the interface between the moving and stationary phases and postulates linear driving-force approximations for both phases, implying that the rate in each is proportional to the distance from equilibrium:

$$(\rho/a)(\partial q_i/\partial t)_z = k_f(c_i - c_i^*) = k_s\rho(q_i^* - q_i) \quad (I.7)$$

where a is the specific surface area, k_f and k_g are the coefficients of mass transfer between bulk moving phase and interface and between interface and sorption sites, respectively, asterisks refer to the interface between sorbent and moving phase (see also Fig. I.8; the transfer rates in two phases are equal because the interface, being two-dimensional, has no capacity.) The overall driving force corresponds to an arrow from (c_i,q_i) to (c_i^*,q_i^*) in Fig. I.7, with components $\Delta c_i \equiv c_i - c_i^*$ and $\Delta q_i \equiv q_i^* - q_i$. As the distance from equilibrium, the length of the arrow is a measure for the magnitude of the driving force.

The mass-transfer resistance in the moving phase may dominate. This is true if at all concentrations the product of mass-transfer coefficient and maximum possible driving force is much smaller in the moving phase than in the sorbent; that is:

$$\text{rate control in moving phase if } k_f c_i/k_s\rho f(c_i) \ll 1 \quad (I.8)$$

where $f(c_i)$ is the sorbent loading q_i in equilibrium with c_i. If so, $q_i^* \approx q_i$ (no significant concentration gradient in the sorbent), and the driving-force arrow in the q_i *vs.* c_i diagram (Fig. I.7) then is practically *horizontal.* Similarly:

$$\text{rate control in sorbent phase if } k_f c_i/k_s\rho f(c_i) \gg 1 \quad (I.9)$$

Here, $c_i^* \approx c_i$, and the driving-force arrow then is practically *vertical.* [Even if the mass-transfer coefficient is smaller in the sorbent, as is usually the case because of obstruction in the sorbent, a highly favorable partitioning of the solute into the sorbent, $f(c_i)/c_i \gg 1$, most likely at low c_i, may overcompensate this effect.]

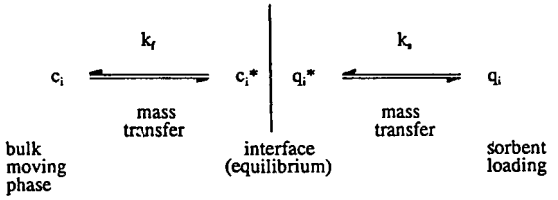

Fig. I.8. Model underlying driving-force approximations for mass transfer (sorbent loading q_i is averaged over bead and taken as bulk sorbent-phase concentration).

We consider first an adsorption shock with Type I, Langmuir-like isotherm of the solute. As can be seen in Fig. I.9, for ideal rate control in the moving phase the driving force (dashed arrows) is rather weak (short arrow) at low concentrations, and is still respectable even at quite high concentrations; reference to Fig. I.7 shows it to have its maximum (largest horizontal distance between operating line and isotherm) at concentrations well above the halfway point on the operating line. The opposite is seen to be true for rate control in the sorbent: Here, the driving force (solid arrows) is weak at high and still fairly strong at low concentrations, and has its maximum at well below the halfway point. The stronger the driving force, the faster are the concentration variations $(\partial q_i/\partial t)_z$ and $(\partial c_i/\partial t)_z$ in a sorbent layer (note that q_i varies linearly with c_i along the operating line). That is to say, the strength of the driving force translates directly into the steepness of the slope of the concentration history or profile at the respective concentration. Accordingly, for rate control in the moving phase, the profile or history of the sorption shock is less steep at the leading, low concentrations (weak driving force) than at the trailing, high concentrations (strong driving force); and for rate control in the sorbent the opposite is true. The profile and history are asymmetrical, depending on where the predominant mass-transfer resistance resides:

- *For rate control in the moving phase, the wave "fronts" and has a sharp tail; for rate control in the sorbent, the wave has a sharp front and "tails"* [9,22,31]

(see Fig. I.10; as used here, "fronting" of a wave implies a profile that is less steep in the forward than in the rear portion of the wave, and "tailing" implies the opposite). The effect is stronger, the stronger the isotherm is curved within the segment over which the wave extends, and is practically nonexistent if that segment is almost linear. Also, the profile is almost symmetrical if the two mass-transfer resistances are about equally important, that is, if $k_f c_i \approx k_s\rho f(c_i)$.

If the isotherm segment of interest is strongly curved, the driving-force ratio $\Delta c_i/\Delta q_i$ decreases sig-

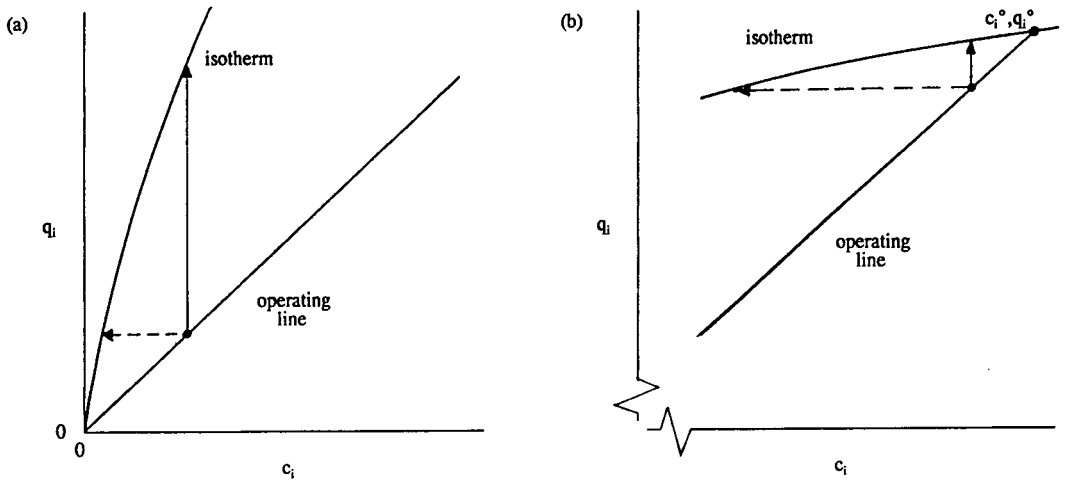

Fig. I.9. Driving forces for ideal moving-phase control (– – →) and ideal sorbent-phase control (→); (a) at low concentrations; (b) at high concentrations (enlarged portions of Fig. I.7). From ref. 15.

nificantly with decreasing concentration. As a result, the mass-transfer resistance in the moving phase is most serious at the very lowest concentrations and so causes some fronting even if it is negligible at higher concentrations [22]. This is very important in practice because fronting amounts to early breakthrough and so affects efficiency or purity.

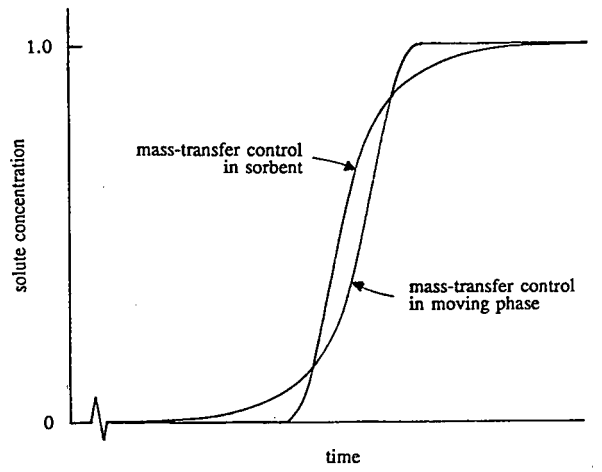

Fig. I.10. Concentration histories of shock layers for rate control by mass transfer in moving phase and in sorbent, exhibiting "fronting" and "tailing", respectively; calculated with linear driving-force approximations [17,21] for strongly curved Langmuir isotherm $q_i/Q_i = Kc_i/(1 + Kc_i)$ with $K(c_i)_{max} = 9$ (corresponds to binary ion exchange with separation factor $\alpha_{12} = 10$).

The discussion so far has assumed that the isotherm is reasonably Langmuir-like. Any deviation from such a shape also affects the shock-layer profile. As an illustration, Fig. I.11 shows a Type III isotherm with driving-force arrows corresponding to about equal importance of the resistances in the two phases. For this isotherm and under such mass-transfer conditions, the driving force is strong at low and weak at high concentrations, producing a wave with little fronting and fairly heavy tailing, an asymmetry in this case *not* attributable to a predominant mass-transfer resistance in the sorbent.

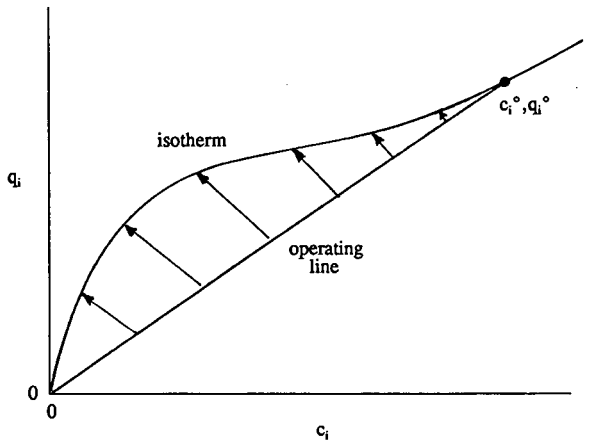

Fig. I.11. Type III isotherm, with operating line and driving-force arrows for shock layer.

In elution of a solute with Type II isotherm (Fig. I.2b), the driving-force arrows for sorbent-phase rate control tend to be long at the high (leading) and short at the low (trailing) concentrations, and for moving-phase rate control the opposite applies. Accordingly, the elution shock tends to tail in the former case and to front in the latter. The behavior thus is the same as for the Type I adsorption shock.

I.8.1.2. Other mass-transfer models

The linear driving-force relationships in eqn. I.7 are idealizations. For the moving phase the approximation is usually satisfactory; for the sorbent, much less so. In the first place, the structure of the sorbent phase may suggest a different mechanism, say, sorption by a stationary liquid in the pores of a support, followed by diffusion in that liquid and finally adsorption at the pore walls ("pore diffusion model") [32]. Even if the sorbent can be regarded as quasi-homogeneous, as is true for gel-type beads, the linear driving-force approximation is problematic: Strictly speaking, there is no "bulk-phase concentration" in the sorbent as the concentration at any time varies throughout the bead, so that the sorbent loading (amount of sorbate in bead, divided by sorbate-free bead mass) has to be used instead. Also, diffusion in such a bead obeys Fick's (see ref. 28) or Nernst–Planck's (see ref. 33) laws rather than a linear driving-force relationship. Moreover, because the rate under such conditions depends on the current shape of the concentration profile in the sorbent as well as on the loading, *no* equation in which the rate is a unique function of equilibrium, moving-phase concentration, and sorbent loading, regardless of its complexity, can fit actual behavior under all sets of possible initial and boundary conditions [33].

Chemical engineers have devised a great number of more realistic mass-transfer models, calculated the constant-pattern shock shapes they produce, and represented the results in various forms. The most complete collection, largely in form of dimensionless graphs, can be found in section 16 of Perry's Handbook [9]. The only justification for singling out the linear driving-force approximations here is because they are the simplest and easiest to visualize, and because the *qualitative* behavior of the other, more realistic models is the same, as a study of the information in the handbook section shows. In particular:

- *The more complex models give qualitatively the same fronting and tailing of shocks as do the linear driving-force approximations.*

This is not surprising since even in the more complex models the mass-transfer rate increases or decreases with the distance from equilibrium, though not in proportion to that distance as in the linear driving-force approximations.

I.8.2. Finite rate of attachment to sorbent ("reaction-rate control")

The equilibration rate may also be controlled by the rate of attachment to (or detachment from) active sites on the sorbent. This is sometimes called an adsorption "reaction", even if the solute undergoes no chemical transformation other than the attachment itself (*e.g.*, by hydrogen-bonding). Such behavior is fairly common in chromatography of large molecules, *e.g.*, peptides and proteins, on small or impenetrable sorbent particles. The most commonly used rate equation is that employed by Langmuir in the derivation of his famous isotherm [34]:

$$(\partial q_i/\partial t)_z = k_a c_i(Q_i - q_i) - k_d q_i \qquad \text{(I.10)}$$

[k_a = Langmuir adsorption rate coefficient, k_d = Langmuir desorption rate coefficient, $Q_i = f(c_i)$ at $c_i \rightarrow \infty$ = ultimate sorption capacity]. Eqn. I.10 is mathematically equivalent to the rate equation in the Thomas model (see Appendix) and implies a Langmuir isotherm. Applied to constant-pattern shock layers it produces concentration profiles with *symmetrical* S-shapes (see Appendix for proof).

I.8.3. Other non-idealities

I.8.3.1. Axial diffusion

Axial diffusion contributes an additional term to the basic material balance. Eqn. I.2 becomes [10,11]:

$$\frac{\rho}{\varepsilon}\left(\frac{\partial q_i}{\partial t}\right)_z + \left(\frac{\partial c_i}{\partial t}\right)_z + v^0\left(\frac{\partial c_i}{\partial z}\right)_t - \underbrace{D\left(\frac{\partial^2 c_i}{\partial z^2}\right)_t}_{\text{diffusion term}} = 0 \qquad \text{(I.11)}$$

(D = diffusion coefficient, assumed concentration-independent) and results in a more complex wave equation. Under conditions of local equilibrium and with a reasonably Langmuir-like isotherm, this produces a tailing profile not unlike that resulting from rate control by sorbent-phase mass transfer. This is evident from the mathematical solutions [9,35] and can be made plausible as follows: Solute that has diffused forward into volume elements ahead of the main wave is effectively picked up by the sorbent which, preequilibrated at a still lower concentration, is loaded to a significantly lesser extent (steep isotherm); behind the main wave, solute that diffused forward and so depleted the solution is not as readily replaced by desorption from a sorbent whose equilibrium loading is not much lower at the lower solution concentration (flat isotherm).

I.8.3.2. Non-plug flow

The effect of non-plug flow (see Fig. I.3) is essentially the same as that of diffusion. Usually, both are accounted for by use of eqn. I.11 with D as a lumped dispersion coefficient. A more detailed model includes channeling and transverse diffusion [36].

I.8.4. Other non-linear effects

I.8.4.1. Axially non-uniform flow-rate

In gas and supercritical-fluid chromatography, the flow-rate may be axially non-uniform. If the pressure drop is significant, volume elements of the gas phase expand as they travel through the column, so the volumetric flow-rate is higher at the front end of a wave than at its tail. This effect is very slight (small pressure drop across any one wave) and is of little interest because it increases the distances between waves by the same factor as it broadens the waves themselves. A more important effect is that, at high solute concentrations, the mass and volumetric flow-rates are significantly higher where solute molecules are present and thus must be moved in addition to those of the carrier gas. This so-called *sorption effect* tends to sharpen the front of a solute peak or band and to spread its rear [37–41]. In liquid-phase chromatography, the effect is negligible because the change in total volume upon mass transfer between two condensed phases is insignificant.

I.8.4.2. Thermal effects and reactions

The effects caused by non-isothermal behavior and chemical transformation of the solute are different in kind from those discussed above: Rather than having a dispersive effect on wave profiles, they produce entirely different chromatographic patterns. Therefore, their discussion is deferred for the time being.

I.8.5. Analytical solutions

Constant-pattern profiles of shock layers are relatively easy to calculate by use of a frame of reference that travels with the wave. Within this frame there is no change with time, so only an ordinary rather than partial differential equation has to be solved [17]. Explicit analytical solutions or approximations have been given for some isotherms, including especially Langmuir's, in combination with linear driving-force equations in the moving phase [21] and in the sorbent [17] and for axial diffusion or dispersion [35] (see section 16 of Perry's Handbook [9] for details).

I.8.6. Summary of effects

The various non-idealities are seen to produce effects that differ in kind, as shown in Table I.3. Therefore, unless one single non-ideality completely dominates:

- *Shock layers cannot in general be modeled with a single dispersion parameter.*

The exception is that the effects of mass-transfer resistance in the sorbent, axial diffusion, and non-plug flow are similar (although not strictly additive) and so can be lumped. However, such single-parameter modeling fails to account for the mass-transfer resistance in the moving phase, which tends to produce significant fronting of any shock layers even if it is negligible elsewhere.

The profile or effluent history of a shock layer are seen to depend on the isotherm shape as well as on the effects of the non-idealities. Therefore, the isotherm cannot be determined from effluent histories of shock layers unless the effects of the non-idealities are known in detail, nor can the latter effects be established without exact knowledge of the isotherm shape. Because so many different non-ideal-

TABLE I.3

EFFECTS OF NON-IDEALITIES OF SHOCK-LAYER PROFILE

Dominant non-ideality	Effect on shock-layer profile
Mass-transfer resistance in moving phase	Fronting
Mass-transfer resistance in sorbent	Tailing
Rate controlled by attachment to sorbent ("reaction control")	Symmetrical spreading
Axial diffusion	Tailing
Non-plug flow	Tailing
Axially non-uniform flow-rate (in gas chromatography)	Slight sharpening (if saturation wave), slight spreading (if elution wave)

ities may affect the effluent history of a shock, the most reliable approach is to determine the isotherm first point-by-point by batch or column equilibration. Tentative conclusions about non-idealities can then be drawn from the shapes of shock profiles at different inlet concentrations and flow-rates.

I.9. PROFILES OF NONSHARPENING WAVES

Nonsharpening waves were seen to be affected by non-idealities only as long as they are still relatively sharp. Ideal chromatography is therefore a good approximation, provided the column is reasonably long and the isotherm curvature is significant. Accordingly, the profile of a nonsharpening wave that starts out as a discontinuity depends almost exclusively on the shape of the isotherm. An approximate profile can be calculated from the isotherm by application of the wave equation I.4 to a number of concentrations, with dq_i/dc_i as the isotherm slopes at the respective concentrations. The wave velocity given by eqn. I.4 multiplied with the time t gives the distance which the concentration has advanced in the column. Similarly, for an approximate effluent history, the wave velocity divided by the column length gives the retention time of the concentration.

The procedure can be reversed in order to determine an isotherm from the effluent history of a nonsharpening wave [42] (an elution wave if the isotherm is of Type I). However, this procedure is not very accurate. One source of error is the difficulty of accounting correctly for the small but not negligible effect of non-idealities. Another is the fact that the technique yields isotherm *slopes* rather than points, so that the isotherm must be pieced together from the former, a procedure in which any error at a low concentration is propagated to all higher concentrations. Chromatographic techniques for isotherm determinations will be discussed in more detail in a later instalment.

I.10. COMPLEX ISOTHERMS AND COMPOSITE WAVES

Isotherms with inflection points may give rise to "composite waves" consisting of self-sharpening and nonsharpening portions. In the fully developed pattern resulting from a step input, shock portions have linear operating lines while nonsharpening portions have operating curves that coincide with the isotherm. Fig. I.12a shows a Type III isotherm and the operating curve for saturation of a column initially free of sorbate. For a given isotherm, the operating curve can be constructed with a rule based on the following argument. Concentrations (or shock portions) that have advanced farther must have higher velocities; according to the wave equations I.3 and I.6, the slope of the operating curve therefore must decrease monotonically from the point corresponding to the entering concentration (c_i^0, q_i^0) to that of the initial concentration ($c_i = q_i = 0$). As a result, the operating line of any shock portion is *tangential* to the isotherm [9,43,44]. One can envisage the operating curve as a rubber band stretched between the points of the initial and entering compositions and at most touching the isotherm but not intersecting it. For adsorption the operating curve is below the isotherm, for desorption it is above it. Among fixed-bed engineers this rule is known as the "Golden Rule" (named after Berkeley doctoral student F. M. Golden, quoted in section 16

of Perry's Handbook [9] but not separately published). The resulting saturation wave for the isotherm in Fig. I.12a consists of a leading shock in which the concentration rises to c_i', followed by a nonsharpening portion in which it rises from c_i' to the influent value, c_i^0, and is shown in Fig. I.12b. A convenient graphical procedure developed by Welge [45] for construction of wave profiles in two-phase flow in permeable media from fractional-flow curves and widely used in oil reservoir engineering can be adapted to the construction of concentration profiles of composite waves in chromatography from isotherms.

An inflection point on the isotherm does not necessarily produce a composite wave. For instance, the Type III isotherm in Fig. I.11 has an inflection point at a concentration below that of the entering solution, yet application of the Golden Rule shows the wave to be a pure shock (no line from the origin is tangential to the isotherm at any concentration below that of the entering solution).

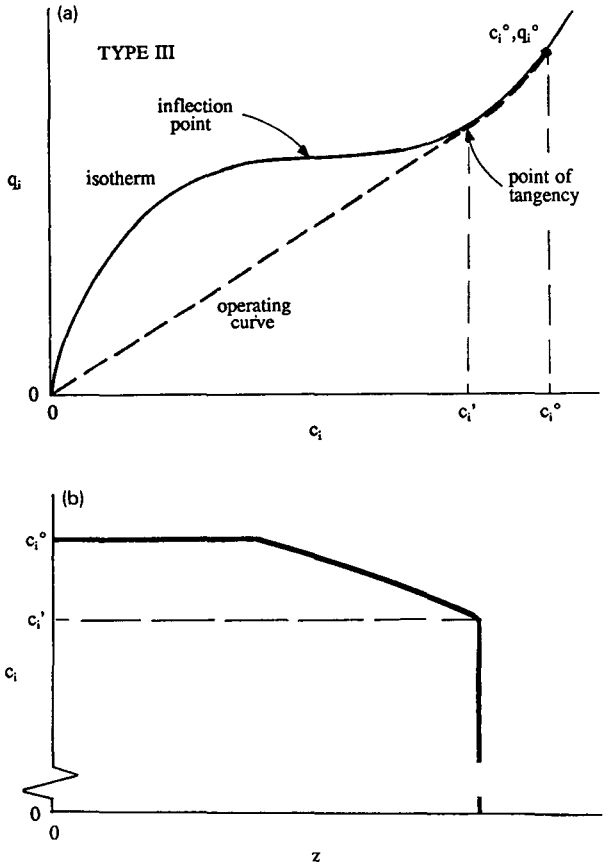

Fig. I.12. Composite wave resulting from Type III isotherm; (a) isotherm and operating curve; (b) concentration profile of composite wave produced by step input (ideal chromatography).

I.11. STANDARD THEORIES AND MODELS

The non-linear models most commonly referred to can now be put in context.

I.11.1. Equilibrium-stage models

The concept of equilibrium stages, with an HETP accounting for the effects of non-idealities, has also been used for numerical stage-by-stage calculations in non-linear chromatography [46]. This is possible although the familiar correlations between HETP and wave spreading are not in general valid under non-linear conditions. Inasmuch as a succession of equilibrium stages physically amounts to back-mixing in the column, the calculations actually model the effects of axial diffusion and non-plug flow. That is, for symmetrically shaped isotherms, calculated *shock layers tail.* Because of the similarity with the effect of non-equilibrium owing to mass-transfer resistance in the sorbent, the results are reasonable approximations, *provided the mass-transfer resistance in the moving phase is negligible even at the lowest concentrations.* As was seen earlier, the latter resistance produces fronting rather than tailing of shock layers, and so invalidates the model.

I.11.2. "Semi-ideal" models

So-called semi-ideal models [47] postulate that all non-ideal effects can be accounted for in a single, lumped dispersion coefficient [47,48]. They use the material balance equation I.11 with $q_i = f(c_i)$, that is, with q_i in equilibrium with c_i. Analytical solutions have been given for some special cases [48]. Because of the similarity of the effect of hydrodynamic dispersion with actual back-mixing in stages, semi-ideal models give essentially the same results as equilibrium-stage models. Specifically, they produce tailing shock-layer profiles if the isotherm shape resembles Langmuir's, and fail to show the shock-layer fronting that results from a significant mass-transfer resistance in the moving phase.

I.11.3. Thomas model ("reaction-kinetic model")

The model developed by Thomas [49,50] for binary ion exchange attributes local non-equilibrium to the finite rate of a second-order reversible exchange "reaction" and assumes ideal behavior in all other respects. The rate equation implies constancy of the separation factor (defined as $q_i c_j / q_j c_i$ at equilibrium of exchanging ions i and j). The model has also been used for single-component adsorption [51,52]. In this modification, the rate is given by eqn. I.10 and implies a Langmuir isotherm (the mathematics of binary ion exchange with constant separation factor and single-component Langmuir adsorption are formally identical). Analytical solutions in terms of a tabulated function [53] have been derived for input in form of a step [49,50] or pulse [52] and for arbitrary input [51]. The solution for step input is valid for both nonsharpening and self-sharpening waves and, for the latter, covers the transient approach to the constant pattern.

I.11.4. Mass-transfer models

The simplest models that account explicitly for local non-equilibrium owing to finite mass-transfer rates use linear driving-force approximations, as discussed previously. In some of these procedures an HETP [22] or a "number of mass-transfer units" [8,9] is obtained from the mass-transfer coefficient and then used to calculate the shock-layer profile. For situations in which the resistances in both phases are significant, Glueckauf [22] sums up the dispersions caused by each; this tends to overstate spreading but gives a smooth transition from a fronting to a tailing profile as the dominant resistance shifts from the moving phase to the sorbent. In contrast, Vermeulen and co-workers [8,9,54] calculate an "overall" mass-transfer coefficient with the principle of additivity of resistances in series, apply an approximate correction factor for the error in that principle, and then use the resulting coefficient in the driving-force equation for the phase in which the resistance is more serious. This procedure gives an abrupt transition from extreme fronting to extreme tailing at the point where both resistances are equally important. A procedure that avoids this unrealistic result by construction of driving-force arrows in the q_i *vs.* c_i diagram to obtain concentration-history slopes at a set of concentrations in the shock layer and then piecing the effluent history together from short segments has been suggested by Klein [55].

More elaborate mass-transfer models for the sorbent phase use non-linear driving-force approximations, Fick's law of diffusion for the particles (assumed to be spherical), or diffusion in pores with adsorption onto the pore walls ("pore diffusion model"). For more detail, see Table I.4, section 16 of Perry's Handbook [9], and a recent review by Lee *et al.* [56].

I.11.5. General models

Analytical solutions for non-ideal chromatography are possible only in a few special cases. Since execution time is usually not a problem on today's computers, it makes sense to turn to the most general and flexible computer models where numerical calculation is required anyway. At present, the most general, publicly available and reasonably "user-friendly" program is VERSE-LC [63]. Written in FORTRAN, it is for single- and multicomponent adsorption with arbitrary isotherms and arbitrary input conditions and allows for finite rates of mass transfer in the moving phase, diffusion in pores, adsorption on pore walls, and reactions in both the moving and sorbent phases. The LC in the title indicates that it is intended for liquid chromatography only. The program is available from the Purdue Research Foundation.

I.12. ELUTION PEAKS

With knowledge of the behavior of non-linear waves, the shapes of peaks and bands under non-linear conditions ("overload") can now be predicted. For this purpose, the injected sample is viewed as a concentration plateau between two initially discontinuous waves which interact with one another on their travel through the column.

The asymmetry of a single-component peak or slug (flat-top peak) in elution under overload conditions depends on the shape of the isotherm. With a Type I isotherm, the peak or slug has a shock front and nonsharpening rear, and tails accordingly. With a Type II isotherm, the opposite is true, that is, the peak or slug fronts. Isotherms with inflection

TABLE I.4

COMMON MODELS OF NON-LINEAR, NON-IDEAL CHROMATOGRAPHY

Explanations: Axial dispersion = axial diffusion and dispersion from non-ideal flow; LDF = linear driving-force approximation; intraparticle diffusion = Fick's law or approximation; IEX constant α = ion exchange with constant separation factor (mathematically equivalent to Langmuir adsorption isotherm).

Features	Isotherm	Input	Solution method	Author(s)
Axial dispersion	IEX constant α	Step	Analytical	Acrivos [35]
	Parabolic	Pulse	Analytical approximation	Houghton [57]
	Arbitrary	Arbitrary	Finite difference	Smit *et al.* [58]
Axial dispersion and fluid-phase LDF	IEX constant α	Step	Numerical	Acrivos [35], Ruthven [12]
Lumped dispersion (semi-ideal model)	Parabolic	Pulse	Analytical	Haarhoff and Van der Linde [48]
	Langmuir, S-shaped	Pulse	Finite difference	Guiochon *et al.* [47]
	Langmuir	Pulse	Analytical approximation	Knox and Pyper [59]
Attachment to site (Thomas model)	IEX constant α	Step	Analytical	Thomas [49,50]
	IEX constant α and Langmuir	Arbitrary	Analytical	Goldstein [51]
	Langmuir	Pulse	Analytical	Wade *et al.* [52]
Moving-phase LDF	IEX constant α	Step	Analytical	Michaels [21]
Sorbent-phase LDF	IEX constant α	Step	Analytical	Glueckauf and Coates [17]
Both phases LDF	IEX constant α	Step	Analytical approximation	Glueckauf [22]
	IEX constant α, Langmuir	Step	Analytical approximation	Hiester *et al.* [54] Vermeulen *et al.* [8,9]
		Step	Semi-graphical	Klein [55]
Intraparticle difussion	Langmuir	Step	Numerical Method of moments	Weber and Chakravorti [60] Radeke *et al.* [61]
Pore diffusion	IEX constant α, Langmuir	Step	Numerical	Hall *et al.* [62]
Moving-phase LDF, pore diffusion, dispersion and reactions	Arbitrary	Arbitrary	Orthogonal collocation	Berninger *et al.* [63] (VERSE-LC)
Non-uniform flow	Linear (pressure-dependent partition)	Arbitrary	Method of characteristics	Guiochon and Jacob [40]
Non-uniform flow and axial dispersion	BET	Step	Numerical	LeVan *et al.* [41]

points produce more complex asymmetries and shapes that also depend on how much the peak has already flattened.

The overload can be primarily a concentration overload (concentrated small sample) or a volume overload (dilute large sample) or some compromise between these two. Absolutely "pure" concentration or volume overloads are not possible: since the injected concentration cannot be infinite, the sample volume must be finite; and since the isotherm is curved over its entire range, strictly linear chromatography would require the dilution and thus the sample volume to be infinite. Fig. I.13 shows for comparison how the peak shape evolves from predominant concentration overload and predominant volume overload, granted a Type I isotherm and

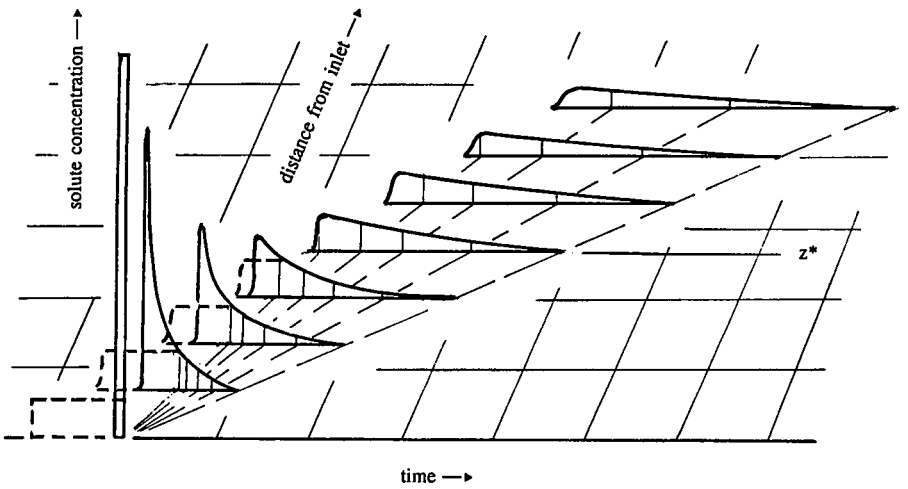

Fig. I.13. Concentration histories on distance-time field for elution of single solute under conditions of concentration overload (solid curves) and volume overload (dashed curves where different); histories are superimposed on one another for better comparison; z^* = survival distance of plateau in volume overload; also shown are concentration contours common to both overloads (thin dashed lines, originating from end of injection).

with the same amount of same solute injected into the same column.

Let us examine a peak or slug with Type I isotherm more closely. The nonsharpening rear travels practically in a proportionate pattern since the small, initial dispersive effect of non-idealities soon becomes negligible. For the shock front, $\Delta q_i \equiv (q_i)_{max}$ and $(\Delta c_i) \equiv (c_i)_{max}$, where the index max refers to the apex or, as long as it exists, to the plateau. Thus, according to eqn. I.6, the shock velocity at any time is

$$v_{\Delta c_i} = \frac{v^0}{1 + (\rho/\varepsilon)(q_i/c_i)_{max}} \qquad \text{(I.12)}$$

For concentration overload, the shock travels rather rapidly at first, but slows down as the effect of isotherm curvature causes the peak to spread and its apex concentration to decrease (lower concentrations on the isotherm give steeper chord slopes q_i/c_i, resulting in stronger retardation; see Fig. I.1a). For volume overload, the shock is relatively slow to start with and travels at constant velocity until the plateau has eroded. In both cases, the nonsharpening rear of the peak or slug produces a fan of concentration contours in the distance–time plane; the difference is that for concentration overload the high-concentration contours are soon "eaten up" by the shock as the apex concentration diminishes, whereas for volume overload these contours, of concentrations higher than injected, do not exist in the first place. The contours of concentrations lower than those of volume-overload injection are practically the same in both cases (except for a slightly greater effect of non-idealities in the earliest stages of concentration overload because of the higher apex concentration), being traced by the same concentrations under identical conditions. Granted that overload is so heavy that the peak remains far from symmetrical, the profile of the nonsharpening rear of the peak depends almost exclusively on the shape of the isotherm; the exact profile of the self-sharpening front depends on both the isotherm and the non-idealities, but contributes little to the total peak width, fades as the peak attenuates, and so is not of much interest. A detailed knowledge of mass-transfer resistances etc. therefore is usually not needed:

- *Except for possible fronting caused by mass-transfer resistance in the moving phase, the peak shape and width depend almost exclusively on the shape of the isotherm.*

Since the contours of the concentrations lower than that of volume-overload injection are essentially the same in both cases, and since the area under the concentration history must also be the same

(same amount injected), the histories resulting from concentration overload and volume overload are practically the same once the pleateau of the slug in volume overload has disappeared (at distance z^* in Fig. I.12). In other words:

• *Beyond a certain column length, there is no significant difference between peak shapes from predominant concentration overload, predominant volume overload, or any combination of the two.*

An essentially equivalent rule, in terms of profiles and eluent volume rather than histories and column length, has been derived by Knox and Pyper [59] with some simplifying assumptions. However, it is necessary to specify that, for the effluent histories to be equal, the retention times must be measured from the *end* of injection, not from its start.

The rule of equal concentration histories for concentration overload and volume overload beyond some distance of travel holds even though the peak front is not an ideal discontinuity and, in fact, gradually loses sharpness as the apex concentration decreases [the self-sharpening tendency weakens as the isotherm slope at $(c_i)_{max}$ becomes more similar to that at $c_i = 0$]. This is because the width of the shock layer is essentially quasi-stationary, and so is the same in both cases at the same apex concentration, independent of prior events.

Other immediately apparent conclusions are that overload speeds up the apex, and that the extreme tail of the peak from any overload moves at the same velocity as does the peak of an infinitesimally small amount of solute.

If the isotherm is of Type II —resulting in a peak with diffuse front and sharp rear— any overload delays the apex, and the leading, lowest concentrations move at the velocity of a peak of infinitesimal size. The Knox rule of essentially equal effluent histories from concentration and volume overload also holds, but now with retention times counted from the *start* of injection. The behavior of isotherms with inflection points is more complex because the development may involve shock portions that are present only at higher concentrations and disappear with attenuation [47].

It is interesting to see that Knox and Pyper [59] employed the HETP concept of linear chromatography —additive HETP contributions that are independent of one another and of column length and produce square-root spreading—a concept they verified empirically by comparison with numerical results. A "kinetic" contribution is said to stem from non-idealities; an additional "thermodynamic" one, from the isotherm curvature. At first glance, this seems paradoxical because isotherm curvature sharpens rather than spreads the peak front and produces a proportionate rather than square-root spreading pattern of the peak rear, and the non-idealities help to turn the peak front into a shock layer and have no significant effect on the peak rear. However, closer inspection resolves the paradox. Firstly, provided the peak is *triangular*, as Knox and Pyper postulate, and the concentrations of its nonsharpening rear fan out in a proportionate pattern (straight-line contours), the base width must indeed increase in proportion to the square root of traveled distance because the constancy of peak area (amount of solute) requires the apex concentration to decrease —*i.e.*, the higher concentrations "get lost" (see Fig. I.14). Secondly, the non-idealities do contribute a little to peak spreading, approximately in proportion to the square root of traveled distance: while they have no effect to speak of on the nonsharpening flank of the peak, the shock flank loses sharpness as the sharpening effect of isotherm curvature fades with decreasing apex concentration.

Unfortunately, the concept of an HETP composed of additive, independent, and constant thermodynamic and kinetic contributions that make waves spread indefinitely in a square-root pattern is not in general applicable to non-linear chromatography. For instance, in displacement development, where the band of a solute travels between two shock layers, isotherm curvature sharpens rather than spreads the waves at *both* front and rear; moreover, after having traveled a finite distance, the entire sample slug attains a constant pattern that remains unchanged upon further travel.

I.13. BANDS IN DISPLACEMENT

In displacement development, massive overload is intentional. A large amount of mixture is injected and then displaced by an agent whose affinity for the sorbent is higher than that of any species of the mixture. Given competitive isotherms (*e.g.*, Langmuir-type), the mixture advances through the col-

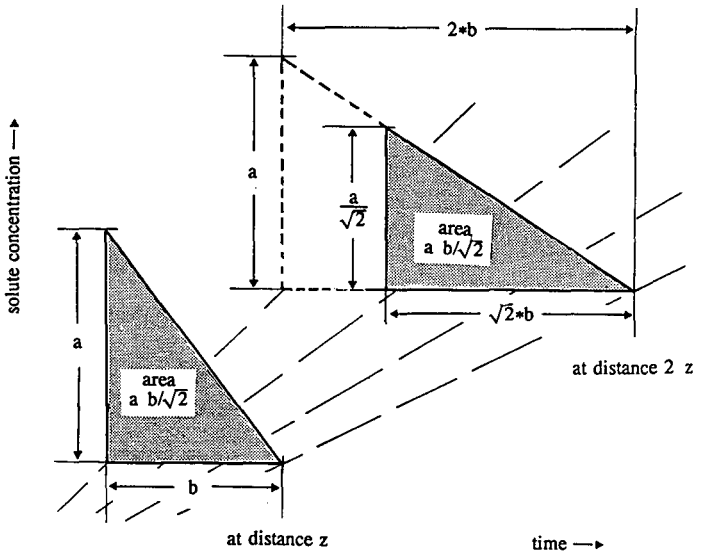

Fig. I.14. Spreading of triangular peak with proportionate pattern of diffuse flank; proportionate spreading of entire peak would double its area when distance of travel is doubled; reduction by linear factor $\sqrt{2}$ is required to keep area to original size (a = peak height at distance z; b = peak width at distance z).

umn in a piston-like fashion between two shocks. In the presence of one another, the particle velocities of the components of lower affinities for the sorbent are higher (lower values of q_i/c_i, see eqn. I.5). Accordingly, the components sort themselves out in the sequence of their affinities. The final, constant pattern has a shock between each two adjacent components in addition to the shocks at the front and the rear of the sample slug (see Fig. I.15).

The calculation of resolution distances in displacement development is a complex problem of multicomponent chromatography, to be discussed later in this series. However, the final pattern is relatively easy to predict with a knowledge of the single-component isotherms, as shown by Tiselius [64]. At each shock, the component present on one side is absent from the other, so that the shock wave equation I.6 reduces once again to eqn. I.12, here with q_i

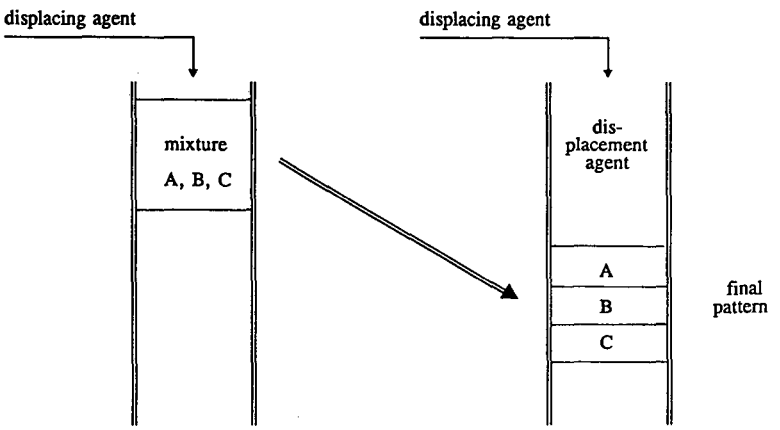

Fig. I.15. Principle of displacement development.

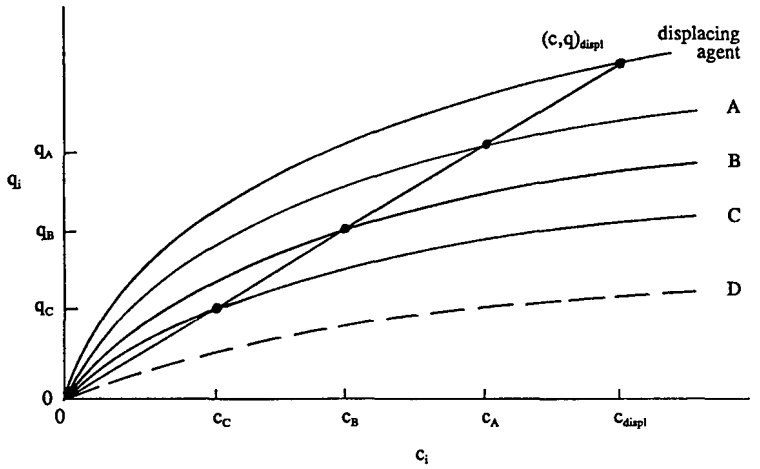

Fig. I.16. Tiselius method [64] for determining concentrations of solutes in their bands in final pattern of displacement development (Solute D runs ahead of displacement pattern).

and c_i as the concentrations in the respective adjacent bands. In the final constant pattern, material balance and constant amounts of all solutes of the mixture require all shocks move at the *same* velocity, so that q_i/c_i in eqn. I.12 must have the same value for all solutes, including the displacing agent. (It is interesting to see that, once the solutes have separated, the entire wave pattern and all solutes travel at one common particle velocity; see eqn. I.5.). The concentrations of the solutes in their bands can now be determined with a graphical procedure illustrated in Fig. I.16: The concentration c_{displ} of the displacing agent is known and identifies a point $(c,q)_{displ}$ on the isotherm of the latter, and the chord of that point intersects the isotherms of the other solutes at their concentrations c_i and q_i. The isotherms in this construction are the *single-component* isotherms, the mixture having been resolved into its components. If algebraic equations for the isotherms are available, all that is needed is to equate the partition coefficient q_i/c_i of the respective solute to that of the displacing agent at its concentration c_{displ} and solve for c_i. With all solute concentrations in both phases known, the band width of each solute of the mixture in the composition profile or history can be obtained from the injected amount of that solute by a material balance. This completes the quantitative prediction of the final pattern under ideal conditions. If more accuracy is required, the shock-layer profiles must be calculated. Since each shock in the final pattern is between two single-component bands, this can be done in much the same way as discussed previously.

If the concentration of the development agent is not high enough, not all isotherms may be intersected by the chord of $(c,q)_{displ}$. An example is the (dashed) isotherm of solute D in Fig. I.16. Any such solute breaks away from the displacement pattern, running ahead as an attenuating peak.

As can be seen from Fig. I.16, the concentrations in the individual bands of the final pattern are dictated by that of the displacing agent; often, they can be made much higher than those in the injected sample: *displacement development permits solutes to be concentrated while they are separated.* Also, large overload is beneficial: The higher the concentrations, the stronger are the self-sharpening tendencies of the shock layers (greater differences in isotherm slopes between front and rear ends of the shock layers); and the larger the amounts of solutes at given concentrations, the longer are the individual bands and, therefore, the smaller is the fractional overlap that results from the less than ideal sharpness of each shock layer. In short, overload, a detriment to be contended with in elution, is put to work for a good purpose in displacement.

I.14. SYMBOLS

a	specific surface area (area of interface sorbent/moving phase, per unit volume of column)	cm^{-1}
c_i	concentration of solute i in moving phase (per unit volume of moving phase)	mmol cm^{-3}
c_i^0	concentration c_i upstream of wave (or in entering fluid)	mmol cm^{-3}
c_i^*	concentration c_i at interface with sorbent (in equilibrium with q_i^*)	mmol cm^{-3}
D	axial diffusion or dispersion coefficient	$cm^2\ s^{-1}$
$f(c_i)$	sorbent loading q_i in equilibrium with c_i	mmol g^{-1}
k_a	Langmuir adsorption rate coefficient	$mmol^{-1}\ cm^3\ s^{-1}$
k_d	Langmuir desorption rate coefficient	s^{-1}
k_f	mass-transfer coefficient in moving phase	cm s^{-1}
k_s	mass-transfer coefficient in sorbent	cm s^{-1}
k_1, k_2	rate coefficients in Thomas law	s^{-1}
K	constant in Langmuir isotherm $q_i/Q_i = Kc_i/(1 + Kc_i)$	$mmol^{-1}\ cm^3$
q_i	sorbent loading with solute i: amount of i in sorbent (averaged over bead) per unit mass of sorbate-free sorbent	mmol g^{-1}
q_i^0	sorbent loading q_i upstream of wave (in equilibrium with c_i^0)	mmol g^{-1}
q_i^*	sorbent loading q_i at interface with moving phase (in equilibrium with c_i^*)	mmol g^{-1}
Q_i	ultimate sorbent loading: $f(c_i)$ for $c_i \to \infty$	mmol g^{-1}
t	time	s
v^0	linear velocity of moving-phase flow	cm s^{-1}
v_i	linear particle velocity of solute i	cm s^{-1}
v_{c_i}	linear wave velocity of concentration c_i	cm s^{-1}
$v_{\Delta c_i}$	linear wave velocity of shock Δc_i	cm s^{-1}
x_i	equivalent fraction of counterion i in moving phase	dimensionless
y_i	equivalent fraction of counterion i in ion exchanger	dimensionless
z	linear distance from column inlet (inlet end of packing)	cm
z^*	survival distance of flat top of peak from volume overload	cm
α_{ij}	separation factor of counterions i and j ($\equiv q_i c_j / q_j c_i$)	dimensionless
Δ	difference across shock, or difference in driving force approximation	operator
ε	fractional volume of moving phase in column	dimensionless
ρ	bulk density of sorbent: mass of sorbate-free sorbent per unit volume of column	g cm^{-3}

Special subscripts: effl = effluent; initial = state before passage of wave; max = apex of peak, or plateau of flat-top band, or maximum at respective wave; displ = displacing agent in displacement development.

Comments

For ease of perception it is obviously convenient to have the value of z at a point in the column correspond to the linear distance from the inlet (and z at the column end, to the column length). The corresponding velocities $\partial z/\partial t$ are the *linear* velocities [volume of moving phase per unit time and unit (average) cross-sectional area of column void]. Any other self-consistent set of variables equivalent to distance, time, and velocity could be chosen instead; *e.g.*, cumulative effluent volume instead of time, column volume upstream of a point instead of distance from column inlet, and the corresponding dimensionless equivalent of velocity.

Any other self-consistent set of concentrations and mass-transfer coefficients can be substituted for those used here. For mathematics, concentrations per unit volume of *column* are most convenient in that they obviate the factor ρ/ε in the wave equations [11]; also, the factor ρ then disappears from eqn. I.7 and condition I.8 and I.9.

I.15. ACKNOWLEDGEMENT

We are indebted to Lloyd R. Snyder, Editor, for his encouragement and for arranging for the publication of this series.

I.16 APPENDIX

That the Thomas model gives shock-layer profiles or histories with symmetrical S-shape is easiest to show with the original version of the model, for binary ion exchange converting the exchanger completely from the A to the B form [49,50]. In terms of counterion fractions x_i in the solution (moving phase) and y_i in the exchanger, the rate law is

$$(\partial y_A/\partial t)_z = k_1 x_A y_B - k_2 y_A x_B$$

For binary ion exchange:

$$x_B = 1 - x_A \text{ and } y_B = 1 - y_A$$

The concentrations are those in the bulk phases, so that pairs (x_A,y_A) correspond to points on the operating line, on which $y_A = x_A$ (diagonal in x–y diagram for complete conversion). With these substitutions the rate is

$$(\partial y_A/\partial t)_z = (k_1 - k_2)x_A(1 - x_A)$$

The rate is seen to be zero at $x_A = 0$ and $x_A = 1$, have its maximum at $x_A = 1/2$ (halfway point on operating line), and have the same value for any x_A as for the corresponding $1 - x_A$. This translates into a symmetrical S shape with equal fronting and tailing. (For the shock layer to form, the separation factor α_{AB} must be larger than unity; since $\alpha_{AB} = k_1/k_2$, this requires $k_1 > k_2$ and ensures a positive rate.)

REFERENCES

1 L. D. Landau and E. M. Lifshitz, *Fluid Mechanics*, Pergamon, London, 1959.
2 G. B. Whitham, *Linear and Non-Linear Waves*, Wiley, New York, 1974.
3 R. Aris and N. R. Amundson, *Mathematical Methods in Chemical Engineering, Vol. 2, First-Order Partial Differential Equations*, Prentice-Hall, New York, 1973, Ch. 8.
4 D. Tondeur, *Chem. Eng. Proc.*, 21 (1987) 167.
5 A. B. Littlewood, *Gas Chromatography: Principles, Techniques and Applications*, Academic Press, New York, 2nd ed., 1970.
6 C. F. Poole and S. K. Poole, *Chromatography Today*, Elsevier, Amsterdam, 1991.
7 L. R. Snyder, in E. Heftmann (Editor), *Chromatography, Part A: Fundamentals and Techniques*, Elsevier, Amsterdam, 5th ed., 1992, Ch. 1.
8 T. Vermeulen, *Adv. Chem. Eng.*, 2 (1958) 147.
9 T. Vermeulen, M. D. LeVan, N. K. Hiester and G. Klein, in R. H. Perry, D. W. Green and J. O. Maloney (Editors), *Perry's Chemical Engineers' Handbook*, McGraw-Hill, New York, 6th ed., 1984, section 16.
10 J. C. Giddings, *Dynamics of Chromatography*, Marcel Dekker, New York, 1965.
11 F. Helfferich and G. Klein, *Multicomponent Chromatography*, Marcel Dekker, New York, 1970 (out of print, available from University Microfilms International, Ann Arbor, MI).
12 D. M. Ruthven, *Principles of Adsorption and Adsorption Processes*, Wiley, New York, 1984.
13 R. T. Yang, *Gas Separation by Adsorption Processes*, Butterworths, Boston, 1987.
14 F. Helfferich, *J. Chem. Educ.*, 41 (1964) 410.
15 F. G. Helfferich and R. L. Albright, *Ion Exchange: Theory and Practice*, AIChE Continuing Education Course Notes, Am. Inst. Chem. Engns., New York, 2nd ed., 1992.
16 D. DeVault, *J. Am. Chem. Soc.*, 65 (1943) 532.
17 E. Glueckauf and J. I. Coates, *J. Chem. Soc.*, (1947) 1315.
18 R. Courant and K. O. Friedrichs, *Supersonic Flow and Shock Waves*, Wiley, New York, 1948.
19 P. D. Lax, *Comm. Pure Appl. Math.*, 10 (1957) 537.
20 D. O. Cooney and E. N. Lightfoot, *Ind. Eng. Chem. Fundam.*, 4 (1965) 233.
21 A. J. Michaels, *Ind. Eng. Chem.*, 44 (1955) 1922.
22 E. Glueckauf, *Ion Exchange and its Applications*, Society of Chemical Industry, London, 1954, p. 34.
23 A. Tiselius, *Ark. Kemi Mineral. Geol.*, B14 (1940) No. 22.
24 N. K. Hiester and T. Vermeulen, *Chem. Eng. Progr.*, 48 (1952) 505.
25 H.-K. Rhee, B. F. Bodin and N. R. Amundson, *Chem. Eng. Sci.*, 26 (1971) 1571.
26 D. D. Frey, *J. Chromatogr.*, 409 (1987) 1.
27 J. J. van Deemter, F. J. Zuiderweg and A. Klinkenberg, *Chem. Eng. Sci.*, 5 (1956) 271.
28 J. B. Rosen, *J. Chem. Phys.*, 20 (1952) 387.
29 J. T. Hsu and T.-L. Chen, *J. Chromatogr.*, 404 (1987) 1.
30 J. Starek, *J. Chromatogr.*, 591 (1992) 1083.
31 T. Vermeulen, *Ind. Eng. Chem.*, 45 (1953) 1664.
32 T. Vermeulen and R. E. Quilici, *Ind. Eng. Chem. Fundam.*, 5 (1970) 179.
33 F. Helfferich, *Ion Exchange*, McGraw-Hill, New York, 1962, Ch. 6 (out of print, available from University Microfilms International, Ann Arbor, MI).
34 I. Langmuir, *J. Am. Chem. Soc.*, 38 (1916) 2221.
35 A. Acrivos, *Chem. Eng. Sci.*, 13 (1960) 1.
36 E. N. Rudisill and M. D. LeVan, *Ind. Eng. Chem. Res.*, 30 (1991) 1054.
37 C. H. Bosanquet and G. O. Morgan, in D. H. Desty (Editor), *Vapor Phase Chromatography*, Academic Press, New York, 1957, p. 35.
38 M. J. E. Golay, *Nature*, 202 (1964) 489.
39 D. L. Peterson and F. Helfferich, *J. Phys. Chem.*, 69 (1965) 1283.
40 G. Guiochon and L. Jacob, *Chromatogr. Rev.*, 14 (1971) 77.
41 M. D. LeVan, A. A. Costa, A. E. Rodrigues, A. Bossy and D. Tondeur, *AIChE J.*, 34 (1988) 1633.

42 E. Glückauf, *Nature*, 156 (1945) 748.
43 E. Glückauf, *J. Chem. Soc.*, 1947, 1302.
44 A. P. Tudge, *Can. J. Phys.*, 39 (1961) 1600 and 1611.
45 H. J. Welge, *Trans. AIME*, 195 (1952) 91.
46 E. Eble, R. L. Grob, P. E. Antle and L. R. Snyder, *J. Chromatogr.*, 384 (1987) 25.
47 G. Guiochon, S. Golshan-Shirazi and A. Jaulmes, *Anal. Chem.*, 60 (1988) 1856.
48 P. C. Haarhoff and H. J. van der Linde, *Anal. Chem.*, 38 (1966) 573.
49 H. C. Thomas, *J. Am. Chem. Soc.*, 66 (1944) 1664.
50 H. C. Thomas, *Ann. New York Acad. Sci.*, 49 (1948) 601.
51 S. Goldstein, *Proc. Roy. Soc.*, A219 (1953) 151, 171.
52 J. L. Wade, A. F. Bergold and P. W. Carr, *Anal. Chem.*, 59 (1987) 1286.
53 A. Opler and N. K. Hiester, *Tables for Predicting the Performance of Fixed-Bed Ion Exchange and Similar Mass Transfer Processes*, Report, Stanford Research Institute, Stanford, CA, 1954.
54 N. K. Hiester, S. B. Radding, R. L. Nelson, Jr. and T. Vermeulen, *AIChE J.*, 2 (1956) 404.
55 G. Klein, *AIChE Symp. Ser.*, 81 No. 242 (1985) 28.
56 C. K. Lee, Q. Yu, S. U. Kim and N.-H. L. Wang, *J. Chromatogr.*, 484 (1989) 29.
57 G. Houghton, *J. Phys. Chem.*, 67 (1963) 84.
58 J. C. Smit, H. C. Smit and E. M. de Jaeger, *Anal. Chim. Acta*, 122 (1980) 1.
59 J. H. Knox and H. M. Pyper, *J. Chromatogr.*, 363 (1986) 1.
60 T. W. Weber and R. K. Chakravorti, *AIChE J.*, 20 (1974) 228.
61 K.-H. Radeke, H.-J. Ortlieb and D. Gelbin, *Chem. Eng. Sci.*, 36 (1981) 11.
62 K. R. Hall, L. C. Eagleton, A. Acrivos and T. Vermeulen, *I&EC Fundam.*, 5 (1966) 212.
63 J. A. Berninger, R. D. Whitley, X. Zhang and N.-H. L. Wang, *Computers Chem. Eng.*, 15 (1991) 749.
64 A. Tiselius, *Ark. Kemi Mineral. Geol.*, A16 (1943) No. 18.

Journal of Chromatography, 629 (1993) 123–134
Elsevier Science Publishers B.V., Amsterdam

CHROM. 24 651

Reversed-phase high-performance liquid chromatography for evaluating the lipophilicity of pharmaceutical substances with ionization up to log $P_{app} = 8$

Klaus Belsner, Martina Pfeifer and Bob Wilffert

Janssen Research Foundation, Institut für Experimentelle Medizin, D(W)-4040 Neuss 21 (Germany)

(First received June 25th, 1992; revised manuscript received September 25th, 1992)

ABSTRACT

The RP-HPLC determination of drug lipophilicity was evaluated for its potency as a substitute for the determination of log P_{Oct-W} values. The relation of log k_w to log P_{app} (= log P_{Oct-W} at pH 7.4) is linear for a testset including protonable nitrogen bases. The method is reproducible on different columns (with the same brand and type of the stationary phases) and needs no recalibration then. Three series of substituted benzene homologues (one hydrogen bond acceptor and two weak donor groups) demonstrate structure–retention effects.

INTRODUCTION

Drug lipophilicity is an interesting molecular property, because in many instances it is correlated with the biological activity of a drug. A good measure of lipophilicity is the octanol–water partition coefficient, but its determination is prone to errors [1] and numerous alternative techniques have been suggested, as reviewed by Kaliszan [2].

Usually chromatographic data for similar organic compounds correlate fairly well with the logarithm of the octanol–water partition coefficient, log $P_{Oct/W}$. The problems associated with the interpretation of the reversal of elution order that sometimes occurs at different contents of organic solvent can be avoided by the so-called "polycratic" elution. Minick and co-workers [3,4] have described this technique and extended it to non-congeners by minimization of solute–silanol interaction. The addition of decylamine and octanol (to mimic the octanol hydrogen bonding activity) to the mobile phase in RP-HPLC resulted in a correlation coefficient of $r = 0.9951$ ($n = 24$) for log $P_{Oct/W}$ versus log k_W. Log k_W is the log k' value extrapolated to zero organic modifier content in the mobile phase. An evaluation of this method seemed reasonable because it offered several interesting advantages: (i) rapid and accurate determination of lipophilicity; (ii) data concerning the hydrogen bonding ability of a drug; and (iii) the influence of partial protonation on the retention of protonable molecules. Additionally, the chromatographic data obtained are useful as a database for the future development of chromatographic methods.

The set of compounds studied included a group of phenones, a group of 4-alkylanilines and a group of alkylbenzenes, to obtain a well characterized control set with different hydrogen bonding properties. With the same intention and to cover a broader range of polarity, a number of non-congeners were taken from the set published by Minick *et al.* [3]. Minick's group [3,4] limited their investigations to relatively simply structured and almost exclusively uncharged molecules in aqueous solution at neutral

Correspondence to: K. Belsner, Janssen Research Foundation, Institut für Experimentelle Medizin, D(W)-4040 Neuss 21, Germany.

0021-9673/93/$06.00

and acidic pH, compatible with silica-based RP-HPLC stationary phases. Although this approach can be extended to alkaline environments using polymer-based supports, with respect to comparability and instrumental requirements it is favourable to use a single column for organic bases and non-protonated compounds. The pH stability of silica supports allows the determination of the exact partition behaviour over the physiological range of pH, which is of major interest in pharmaceutical research. Further, the investigation of some drug molecules with known pK_a and log $P_{Oct/W}$ values should allow a more generalized validation of more complex structure and charge effects. If the results of the reversed-phase HPLC method with a silica-based support are in good agreement with the ion-corrected octanol–water partition coefficients, the problems associated with the use of different columns at different pH values of the eluents can be abolished.

EXPERIMENTAL

Instrumentation and materials

Two Beckmann M114 pumps connected to a system controller were used for solvent delivery and blending of the desired methanol concentration. A 25 mm × 4 mm I.D. cartridge filled with octyl-derivatized silica mounted between the static mixer (Lee Microsystems) and the injection valve served as a presaturator and to prevent column contamination by fines. Samples were injected by a Gilson autoinjector equipped with a Rheodyne Model 7010 injection valve with a 100-μl injection loop. The injection volumes were varied from 1 to 5 μl. A Perkin-Elmer diode-array detector was utilized for solute detection and to obtain low-resolution UV spectra for peak identification. A back-pressure regulator (Altex) was connected to the detector outlet to circumvent bubble formation in the detector cell. A 125 mm × 4 mm I.D. cartridge refilled with Hypersil 3 μm MOS (monooctylsilane) by CS-Chromatographie Service served as the chromatographic column. The autoinjector provided control over the whole chromatographic system via connections to the Beckmann controller and to a Spectra-Physics Model 4270 integrator. Temperature was maintained at 20°C by a laboratory-built Peltier-type column oven connected to a laboratory-built proportional integral differential (PID) regulator.

Methanol (MeOH) of HPLC grade was obtained from Merck (Darmstadt, Germany), octanol and diethylamine of analytical-reagent grade from Baker (Deventer, Netherlands), decylamine of analytical-reagent grade from Fluka (Neu-Ulm, Germany), drug substances (see formulae) from Janssen (Beerse, Belgium) and 3-morpholinopropanesulphonic acid (MOPS) from Sigma (Munich, Germany). The water for HPLC was purified using a Milli-Q water-purification system (Millipore). Mobile phases were filtered through a Millipore Type FH filter (0.5 μm pore size) and vacuum degassed during sonication in a Transsonic TS 540 sonicator (Elma). All other chemicals were of analytical-reagent grade and used as delivered.

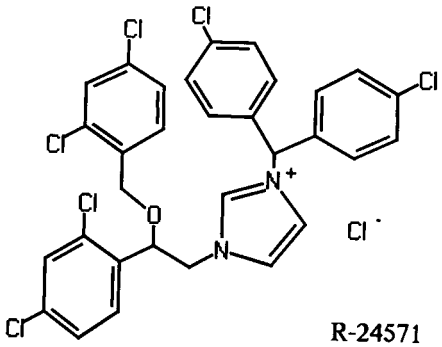

R-24571

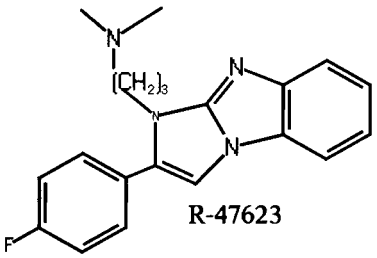

R-47623

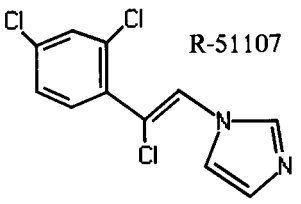

R-51107

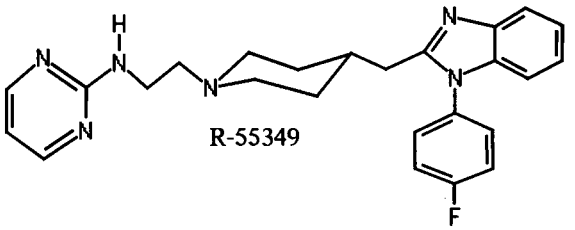

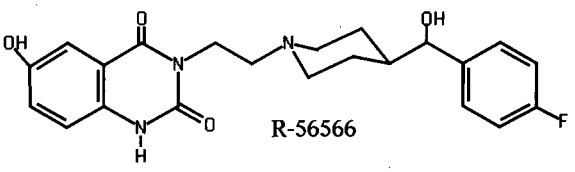

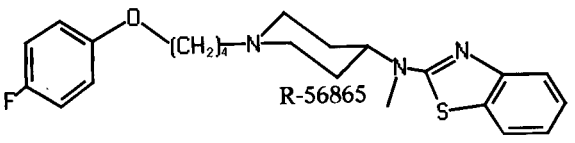

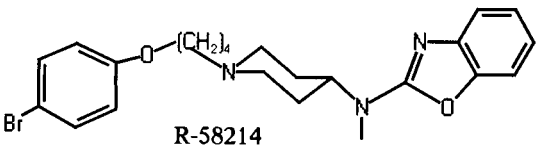

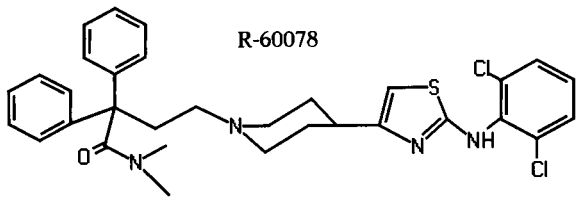

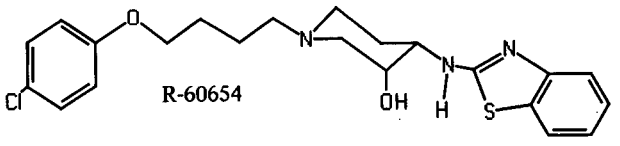

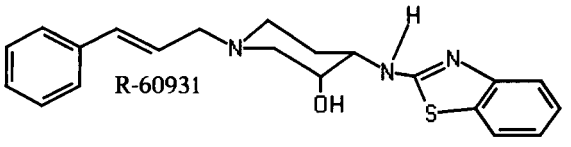

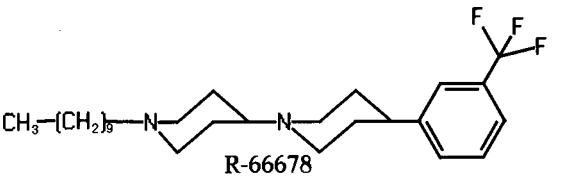

Methods

The mobile phases were a slightly modified version of those described by Minick *et al.* [3]: (A) 20 m*M* MOPS buffer in water, containing 0.15% (v/v) *n*-decylamine, pH 7.4 (adjusted with 1 *M* NaOH); (B) 94.75% (v/v) MeOH–5% (v/v) diethylamine stock solution, containing 3% (v/v) diethylamine in water, pH 7.4 adjusted with acetic acid–0.25% (v/v) *n*-octanol.

The solutes were eluted isocratically with several different mobile phase compositions and the corresponding retention indices were determined. A regression was calculated on the basis of a linear dependence of log k' on the methanol content of the mobile phase, φ_{MeOH}. The log k' values were extrapolated to a mobile phase without methanol. The resulting abscissa is log k_W and the slope is S. This procedure is "polycratic" elution as outlined by Minick *et al.* [3].

After some initial experiments the following conditions were formulated. A sufficient set of data had to contain at least four different concentrations of methanol and one k' value larger than 12. An exception was made only for adenine, with $k' < 12$ at 20% B. The concentration of methanol ranged from 92.5% (95% B) to 18% (v/v) (20% B). The concentration steps were 95%, 92.5%, 90% and then 10% increments of B.

At each methanol concentration a large set of compounds were chromatographed, thereby reducing the time for equilibration. Every injection was repeated twice. The flow-rate was 1.0 ml/min in all experiments. During elution the eluents were gently purged with helium to prevent redissolution of gases.

The void volumes of the columns were determined by injection of urea or deuterated water at each eluent composition and monitored at 205 nm. All regression calculations were performed using the natural logarithms of the k' values.

Calculation of apparent partition coefficients, log P_{app}

To correlate the lipophilicity parameter log k_W achieved by HPLC at pH 7.4 with the corresponding octanol–water partition coefficient of the neutral molecule, the apparent octanol–water distribution coefficients at pH 7.4 were calculated [5] on the basis of published ion-corrected water–octanol partition coefficients [5–12]:

$$\log P_{app} = \log P_{Oct/W} - \log (1 - 10\ pK_a - pH) \quad (1)$$

Eqn. 1 is the relationship between the pK_a of a monoprotic base and pH after introduction of the Henderson–Hasselbach equation into the distribution equilibrium to calculate the free base concentration. It is valid with the assumption that despite the fact that the distribution of a protonatable molecule is the sum of the distributions of the charged and the neutral species, the partition coefficient of the neutral molecule is orders of magnitude greater than that of the charged molecules. Diprotic bases can be treated similarly by consideration of their second pK_a.

Even higher protonation numbers can be handled in the same way, with correction terms for the resulting polyvalent ions. For completion additional terms to overcome the limits of the underlying Arrhenius law can be introduced. Concentrations can be replaced with activities (which decrease with increasing ionic charge) involving the influence of the ionic strength I according to Davies (see ref. 13).

$$\log f = KZ^2\left(0.2I - \frac{\sqrt{I}}{1 + \sqrt{I}}\right) \quad (2)$$

$$a(BH_i) = f(BH_i)[BH_i] \quad (3)$$

where a_i is the activity of the ion i and $K \approx 0.5$ for water at 25°C. This can be the starting point for a thorough calculation of concentration corrections as published by Poncelet *et al.* [14]. A calculation without ion strength refinement was applied to R-55349, a base with three potential protonation sites (pK_a = 2.00, 4.85, 8.32). The result is log P_{app} = 3.02 at pH 7.4, if all protonation steps are included in the correction. The calculation using eqn. 1 and treating R-55349 as a monoprotic base with pK_a = 8.32 gives log P_{app} = 3.00 (see Table III). Hence for polyprotic bases some simplifications are applicable: (a) pK_a values lower than 2 units below the pH of the aqueous phase contribute less than 1% to the distribution coefficient and can be neglected; and (b) in dilute solutions with low ionic strength as used in our method the activity coefficient nearly equals 1.

The P_{app} values of all solutes with more than one basic nitrogen were calculated with these simplifications. For weak acids such as catechol or amphoteric molecules such as ketanserin with a weak acidic group with a $pK_a > 9.4$ the contribution to the octanol–water distribution at pH 7.4 was also neglected.

Hydrogen bonding characteristics

As published by Minick *et al.* [4], the slope of the regression of log k' over φ_{MeOH}, S, was analysed for its hydrogen bonding dependence.

RESULTS

The investigations were started using the same eluents as described by Minick *et al.* [3]. These were prepared without diethylamine (DEA) in eluent B. At high percentages of B ($\geq$90%) the long-chain 4-alkylanilines eluted as broad peaks. In this concentration range the effective concentration of *n*-decylamine is <0.015%. Unfortunately, this long-chain alkylamine is not suficiently soluble in water to prepare a concentrated solution at pH 7.4 which could then be added instead of DEA to the organic phase. A high concentration of the amine stock solution is necessary to keep the content of water in B as low as possible. The addition of DEA effectively reduced the polar surface interactions of 4-alkylanilines at percentages of B $\geq$90% and led to reasonable peak shapes for these compounds. The linear increase in log k' with decreasing φ_{MeOH} for tetradecylaniline and decylaniline (r = 0.9996 and 0.9998), which were chromatographed at methanol concentrations ranging from 78.4 to 90.25% in five steps, and those for propylaniline (r = 0.9997) or acetophenone (r = 0.997) with seven or nine steps down to a methanol concentration of 68.9% indicates the absence or at least the indepence of silanol–solute interactions over that methanol concentration range.

The correct determination of the void volume of the column is essential for the linear correlation of log k' values with the methanol content of the mo-

TABLE I

CALIBRATION SETS

Compounds of the homologous series used for structure–retention investigation and the calibration set used for the regression calculation wit values of log k_W, $-S$ and log $P_{Oct/W}$. Ion-corrected value for the free base calculated according to ref. 5. Log $P_{Oct/w}$ from ref. 6 unless stated otherwise.

Substance	Log k_W	$-S$	Log $P_{Oct/W}$	Substance	Log k_W	$-S$	Log $P_{Oct/W}$
Alkylbenzenes				*Others*			
Methyl-	5.42	6.84	2.73	Pyrazole[a]	−0.07	2.14	0.26
Ethyl-	6.56	7.87	3.15	Diltiazem	5.65	7.13	2.8 [8]
n-Propyl-	7.79	8.96	3.68	Verapamil	4.30	5.72	3.27 [9]
n-Butyl	9.06	10.09	4.26	Propranolol[a]	1.52	2.62	3.56
n-Pentyl-	10.15	11.02		Lidoflazine	11.09	12.83	5.60 [7]
n-Hexyl	11.36	12.08	5.52	Flunarizine[a]	12.44	13.62	5.78 [7]
n-Heptyl	12.76	13.36		Lidocaine	3.07	4.00	2.26
sec.-Butyl-	8.70	9.76		Anthracene	8.72	9.94	4.45
tert.-Butyl-	8.35	9.45	4.11	Quinoline[a]	3.40	5.29	2.03
Phenones				Adenine[a]	−1.30	1.30[b]	2.27
Aceto-	2.59	4.40	1.73	4-Acetylpyridine[a]	0.15	2.06	0.54
Propio-	3.73	5.38	2.19	9-Anthracene carbaldehyde	8.07	9.85	
Butyro-	5.12	6.75		Benzothiazole	3.24	5.07	2.01
Valero-	6.44	7.97		Phenol	1.98	3.72	1.46
Hexano-	7.71	9.10		Resorcinol	0.99	4.56	0.80
Octano-	10.27	11.40		Hydroquinone	−0.06	3.42	0.55
Decano-	12.63	13.49		Acridine	5.87	7.72	3.40
Lauro-[a]	14.91	15.46		Sabeluzole	8.31	9.98	4.61 [7]
Myristo-[a]	17.46	17.76		R-56865	8.86	9.84	5.37 [7]
4-Alkylanilines				Cinnarizine	11.27	12.25	5.77 [7]
Methyl-	2.49	4.49	1.39	Mioflazine	11.24	13.64	5.26 [7]
Ethyl-	3.790	5.66		9-Anthracenemethanol	6.44	8.33	
Propyl-	5.24	7.03					
Butyl-	6.59	8.29					
Pentyl-[a]	7.895	9.45					
Heptyl-	10.28	11.55					
Octyl-	11.26	12.34					
Decyl-	13.67	14.50					
Tetradecyl-[a]	18.36	18.63					

[a] See Conclusions.
[b] See also Table II.

bile phase. The misinterpretation of a peak of a very polar solute instead of the refractive index as the "void volume peak" leads to a curve rather than a straight line of the graph of log k' *versus* φ_{MeOH}. The deviation from linearity can be exponential if this contaminant itself elutes without additional ionic interaction or more complex if ion-pair formation or exclusion are effective. Therefore, it is desirable to obtain void volumes independent of the marker. With urea and deuterated water this was achieved after analysis of the spectra of the void volume peaks with the diode-array spectrophotometer. Urea and deuterated water are only detectable with a UV spectrophotometer by the refractivity change of the solvent and therefore a UV spectrum registered at the maximum of the resulting peak in the chromatogram only reflects the wavelength dependence of the refractive index, a monotonic decline with increasing wavelength, in contrast to peaks of polar contaminants washed out behind the urea or D_2O peak with UV maxima between 220 and 260 nm. These peaks are higher than than the refractiv-

ity peak and their retention is dependent on φ_{MeOH} (volume percentage of methanol in the mobile phase), but can be discriminated by this qualitative analysis.

Table I lists the set of compounds that were chosen to obtain a representative group for the comparison of lipophilicity measured by HPLC with the corresponding apparent octanol–water data. In Table II the log k_W and the calculated apparent log $P_{Oct/W}$ ($\equiv$ log P_{app}) values [5] at pH 7.4 are given together with their pK_a values.

The result of the regression calculation for the values of log k_W and log P_{app} is shown in Fig. 1. For substances without a protonable nitrogen log $P_{Oct/W}$ is identical with log P_{app}.

$$\log P_{app} = 0.4197 \ln k_W + 0.5136 \quad (4)$$
(n = 29; r = 0.988)
(S.D.: coefficient = 0.0124, intercept = 0.266)

Verification

A comparison of the the apparent log P_{app} calculated from the reported log $P_{Oct/W}$ and the values of

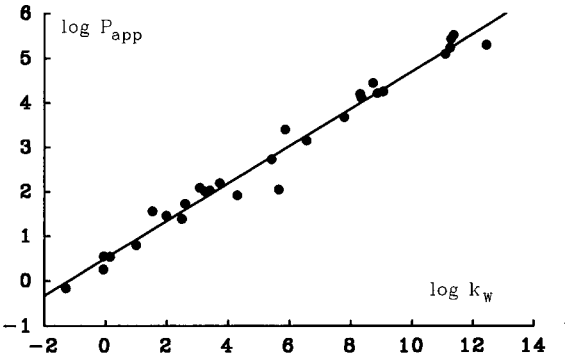

Fig. 1. Relationship between measured log $P_{Oct/W}$ or calculated log P_{app} and log k_W determined by HPLC for a series of non-congeners without separation into groups of high or low hydrophobicity.

log P_{calc} derived from the HPLC data using eqn. 4 further exemplifies the usefulness of the reported method. The group of substances selected for this purpose combines drugs and some other commonly available chemicals with known pK_a values and octanol–partition coefficients are listed in Table III. The means of the corresponding log P_{app} and log P_{calc} were calculated (abcissa in Fig. 2) and plotted together with the deviation from this mean value. The averaged absolute deviation from the mean was 0.13 (n = 28). The systematic deviation (bias) was 0.059 and can be neglected. The standard deviation (S.D.) from the log P_{app} to log P_{calc} group is 0.26, which is corresponds to the S.D. of the calibration set. This demonstrates the applicability of the regression results of the control group for the substances in Table III.

The differences in the retentions of reference compounds after 2000 injections caused by column ageing were in the range of the usual chromatographic inaccuracy. Thereafter the column was routinely exchanged to prevent a sudden loss of performance. Temperature-dependent variations of the retention times were successfully counteracted by the thermostating Peltier unit attached to the column. The measured temperature fluctuations in the column compartment were <0.1 K.

Structure–retention correlation

The parameter S of a solute, which is the slope of the line obtained by the linear least-squares fit of the

TABLE II

APPARENT LOG $P_{Oct/W}$ AND LOG k_W OF THE CALIBRATION SET

Log k_W *versus* the apparent log $P_{Oct/W}$ at pH 7.4 $\equiv$ log P_{app} of members of the calibration set with protonatable nitrogen atoms. All calculations as described in ref. 5.

Substance	Log k_w	Log P_{App}	pK_a
4-Acetylpyridine	0.15	0.54	4.96
Acridine	5.87	3.40	5.58
Adenine	−1.30	−0.16	4.12, 9.83[a]
Hydroquinone	−0.06	0.55	10.35
Lidocaine	3.07	2.09	7.90
Propranolol	1.52	1.56	9,32
Phenol	1.98	1.46	9.89
Quinoline	3.40	2.03	4.90
Resorcinol	0.99	0.80	9.81
p-Toluidine	2.49	1.39	5.08
Flunarizine	12.44	5.30	7.71
Verapamil	4.30	1.92	8.73
Diltiazem	5.65	2.05	8.06
Cinnarizine	11.27	5.43	3.50, 7.47
Lidoflazine	11.09	5.10	2.60, 7.74
Mioflazine	11.24	5.24	4.25, 6.10
R-56865	8.86	4.22	3.33, 8.52
Sabeluzole	8.31	4.20	3.40, 7.60

[a] The value for log $P_{Oct/W}$ published in ref. 4 was measured at pH 7.4 and taken.

TABLE III

VERIFICATION WITH A TEST SET

Results of the calculation of log P_{calc} derived from log k_W data using eqn. 4 and comparison with the log P_{app} values at pH 7.4 derived from log $P_{Oct/W}$ using eqn. 1 (n = 28).

Substance	Log k_W	Log P_{calc}	Log P_{app}	Log $P_{Oct/W}$	pK_a
Alprenolol	1.45	1.12	0.79[a]		9.50
Anisaldehyde	2.52	1.57	1.76	1.76	
Anisole	3.80	2.11	2.08	2.08	
Azobenzene	8.14	3.93	3.82	3.82	
Bemoridan	1.17	1.00	2.39	2.39	
Benzene	3.94	2.17	2.15	2.15	
Benzyl acohol	1.54	1.16	1.15	1.15	
Catechol	1.41	1.11	1.01[a]		9.85
Diazepam	5.94	3.01	2.86	2.86	3.30
Imipramine	3.87	2.14	2.52	4.62	9.50
Ketanserine	5.57	2.85	2.88	3.29	10.80
					7.60
Loperamide	5.23	2.71	3.66	5.13	8.86
Lorcainide	3.21	1.86	2.12	4.16	9.44
Naphthalene	6.41	3.20	3.37	3.37	
Nebivolol	5.47	2.81	2.91	4.04	8.50
Nebivolol (*SRR*)	5.51	2.83	3.01	4.05	8.40
Nebivolol (*RSS*)	5.5	2.82	3.092	4.06	8.40
Nimodipine	7.67	3.73	4.43	4.43	2.00
Nortryptyline	2.8	1.69	1.71[a]		9.70
Pimobendan	5.05	2.63	2.39	2.39	
Promethazine	6.35	3.18	3.02	4.73	9.10
Quinidine	2.47	1.55	1.11	3.71	5.40
					10.00
Quinine	2.74	1.66	1.41	3.71	5.07
					9.70
Ritanserine	8.74	4.18	4.34	5.20	0.90
					8.20
R-24571	11.98	5.54	5.37	5.37	
R-51107	7.97	3.86	4.07	4.07	5.13
R-55349	4.92	2.58	3.00	3.97	2.00
					4.85
					8.32
R-56566	3.39	1.94	1.92	2.62	8.00
					9.00

[a] The published value was determined at pH 7.4.

respective log k' *versus* φ_{MeOH}, is linearly correlated with log k_W in the three series of homologues in this study. Figure 3 presents the plots of S and log k_W for these groups. S is discussed as a lipophilicity measure and at least partially as a hydrogen bond activity indicator [3].

The results of the statistical evaluation are shown in Table IV. The slopes for phenones and alkylbenzenes are each outside their counterparts' 95% confidence intervals [15]. The slope calculated for the 4-alkylanilines compared with the phenones is also outside the 95% confidence interval. In comparison with the alkylbenzenes, the slope for the 4-alkylanilines is clearly inside the 95% confidence interval. The intercepts of the phenones and alkylbenzenes group are inside of each others' 95% confidence region but with respect to this parameter the 4-alkylaniline group is clearly outside the 95% interval. Hence all three regression lines are different with respect to their 95% confidence intervals. The lines

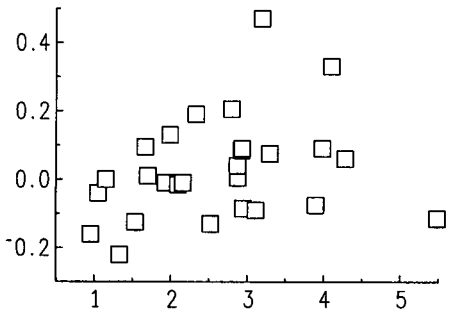

Fig. 2. Statistical evaluation of the test group (Table III). On the abscissa the mean of the corresponding log P_{app} and log P_{calc} and on the ordinate the deviation from this mean value are plotted. The averaged absolute deviation from the mean value of corresponding pairs was 0.130 (n = 28). The systematic deviation (bias) was 0.059. The most prominent deviations are found for nimodipine and loperamide.

for phenones have different slopes to those for benzenes and anilines. The lines for the anilines and the benzenes are nearly parallel but have different intercepts. The regression yielded nearly identical intercepts for the benzenes and phenones.

To answer the question of whether S or log k_W is the better choice for lipophilicity determinations, nineteen substances were randomly chosen and chromatographed on two columns containing different batches of the same stationary phase (Table V). Both columns were routinely refilled one time by the same supplier. The criteria for the choice of the eluent composition were the same as for the group of analytes in the reference group, so at the extreme positions acetylpyridine, hydroquinone and adenine were chromatographed in buffer A with 20% B and flunarizine with a maximum content of 95%B ≡ 92.5% methanol. The resulting S (Fig. 4) and log k_W values (Fig. 5) for both columns

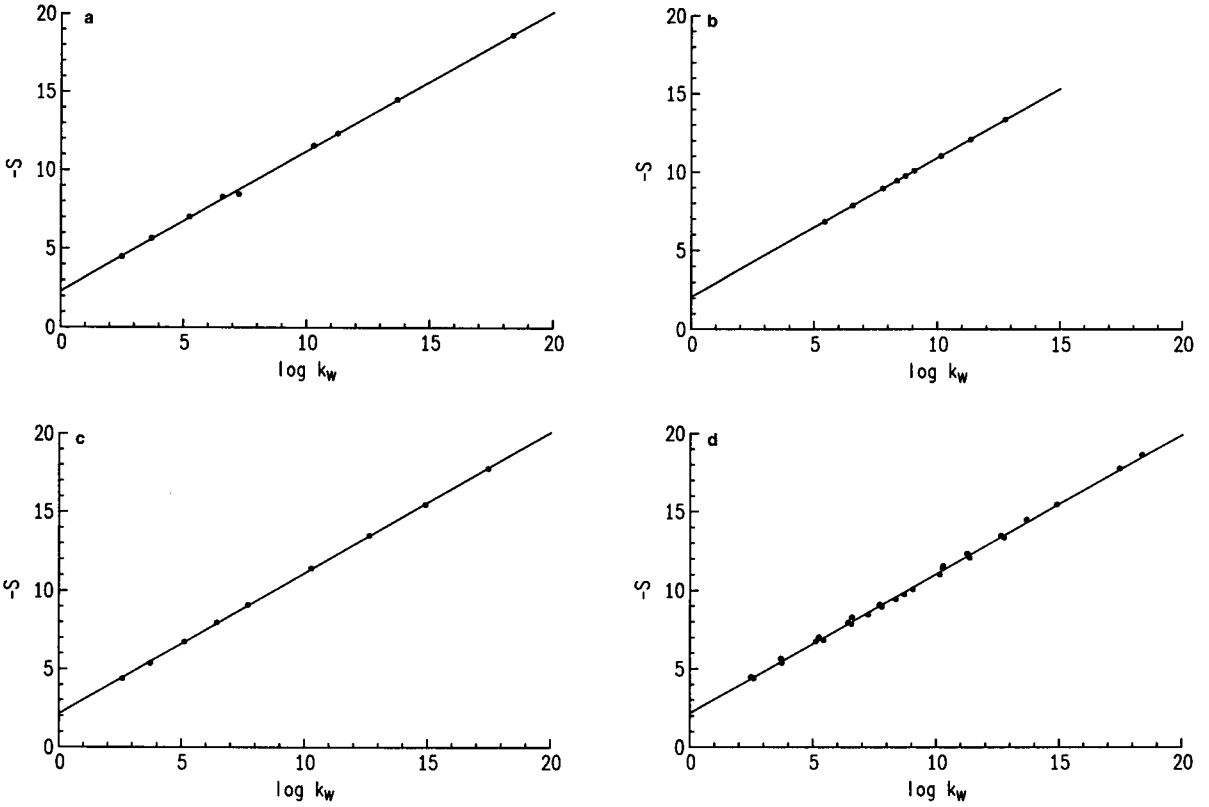

Fig. 3. Structure–retention relationship of three homologous series in the plot of log k_W *versus* $\Delta \log k_W/\Delta\varphi_{MeOH} \equiv S$. (a) 4-*n*-Alkylanilines; (b) alkylbenzenes; (c) phenones; (d) a plot of all three groups to illustrate the linearity and close resemblance of the regression results despite their significant differences (Table IV).

TABLE IV

STRUCTURE AND RETENTION

Statistical evaluation of the regression of log k_W and $-S$ for three series of substituted benzenes for structure–retention elucidation.

Class	Slope with 95% confidence	Abscissa with 95% confidence	
Alkylbenzenes	0.884	2.061	0.9999
	0.876–0.892	1.989–2.134	(5)[a]
4-Alkylanilines	0.887	2.385	0.9999
	0.876–0.898	2.278–2.493	(6)[a]
Phenones	0.898	2.124	0.9999
	0.888–0.908	2.022–2.226	(7)[a]
Combined	0.891	2.191	0.9992
			(8)[a]

[a] Numbers in parentheses are the numbers of the regression equations.

were statistically analysed. A linear regression yielded $r = 0.979$, intercept 0.249 and slope = 0.9625 for S and $r = 0.996$, intercept 0.182 and slope = 0.980 for the log k_W values. The difference from unity of the slope is greater for the S than for the log k_W values and the same is observed for the corresponding intercepts. The mean difference between the two series is -0.0797 for log k_W and 0.05 for S. The corresponding S.D. values are 0.38 and 0.68. Hence 95% of all measured log k_W values will tend to appear in the region of two standard deviation ± 0.76 on the log k_W scale of the mean value of two determinations with different columns, hence use of log k_W is favored in measuring lipophilicity by RP-HPLC.

The time consumption for the determination of log k_W and $-S$ values depends to some extent on the problems associated with the solubility of the compounds of interest in organic solvents. For simplicity dissolving the sample in methanol was tried, thereafter another solvent was chosen that does not interfere with the chromatographic process. With the equipment described under Experimental one person can easily measure the HPLC data of 20–30 new substances in one week.

CONCLUSIONS

Every HPLC method based on the use of retention indices is sensitive to errors in the determination of the column void volume. Care must be taken not to detect polar and UV-absorbing contaminants as the void volume peak, otherwise the interpretation of the alteration of log k' with the methanol content may be complicated by artificial non-linearities. Contaminant peaks co-eluting with the void volume at high methanol concentrations can be misinterpreted as an increase in void volume when the methanol content is decreased and the contaminants are slightly retained. The use of a diode-array detector to identify the contaminants was helpful in this instance. Hence our results are independent of the void volume test compound.

The test set used in this investigation covers a broad range of lipophilicity from log $P_{Oct/W} = -0.16$ to far above 6. The observed high correlation of log $P_{Oct/W}$ and log k_W found in these experiments (eqn. 4) confirms the results and conclusions presented by Minick and co-workers [3,4]. The addition of diethylamine to the mobile phase effectively extends the upper range of lipophilicity to a log P_{app} of *ca.* 8.3 (see tetradecylaniline, Table I), if a linear extrapolation to this region is allowed. This offers the possibility of avoiding the manual determination of partition coefficients of such highly lipophilic substances in a water–octanol solvent system. Especially for these compounds the log $P_{Oct/W}$ determination is prone to errors. Although the test sets chosen by Minick and co-workers [3,4] cover a broad range of polarity, they are mainly restricted to relatively simply structured and small molecules. For use in pharmaceutical drug research, the method had to be improved to accommodate molecules as large as flunarizine or larger and containing at least partially protonated nitrogen atoms. In Table III some examples with known pK_a and log $P_{Oct/W}$

TABLE V

COLUMN TO COLUMN COMPARABILITY

A test set of nineteen different substances measured with two different columns (1 and 2) containing the same stationary phase (see Experimental). The linear regression coefficients (r) for log k' over φ_{MeOH} are given.

Compound	Column	Log k_W	$-S$	r
Acetylpyridine	1	0.0953	2.0634	−0.9903
	2	0.1538	2.0634	−0.9996
Acridine	1	4.7136	6.1018	−0.9920
	2	5.8706	7.7216	−0.9999
Adenine	1	−0.9204	2.8303	−0.9732
	2	−1.2934	1.2996	−0.9283
Acetophenone	1	2.4268	4.1200	−0.9910
	2	2.5930	4.3976	−0.9977
Anthracene	1	8.5610	9.8772	−0.9992
	2	8.7721	9.9431	0.9997
9-Anthracenemethanol	1	5.9545	7.9085	−0.9972
	2	6.4421	8.3274	−0.9996
9-Anthracenecarbaldehyde	1	8.0584	10.0452	−0.9999
	2	8.0656	9.8516	−0.9999
Flunarizine	1	12.4954	13.8210	−0.9997
	2	12.4364	13.6210	−0.9998
Hydroquinone	1	−0.3587	2.5703	−0.9501
	2	−0.0663	3.4241	−0.9999
Nebivolol	1	5.2604	7.0185	−0.9899
	2	5.5104	7.2056	−0.9961
Phenol	1	2.1297	4.3362	−0.9929
	2	1.9817	3.7273	−0.9999
Quinoline	1	3.4570	5.7043	−0.9976
	2	3.3971	5.2897	−0.999
Resorcinol	1	0.7201	3.7864	−0.9850
	2	0.9938	4.5588	−0.999
R-47623	1	3.8262	4.5694	−0.9959
	2	3.8858	4.6099	−0.9959
R-58214	1	10.5948	11.7092	−0.9909
	2	9.8161	10.6899	0.9990
R-60078	1	6.9630	8.6186	−0.9972
	2	6.8968	8.3050	−0.9956
R-60654	1	7.34	8.6543	−0.9981
	2	7.2653	8.7267	−0.9948
R-60931	1	6.5418	8.2845	−0.9973
	2	6.6194	8.2337	−0.9963
R-66678	1	11.3287	11.6564	−0.9971
	2	11.2134	11.3988	−0.9996

values demonstrate the applicability of the method to this group of substances. When the apparent partition coefficient for the octanol–water system, log P_{app}, is taken into account, the data for organic bases correlate well with the retention log k_W or log P_{calc}, which can be calculated from log k_W using eqn. 4. The small deviations of the log P_{app} values from their counterparts' log P_{calc} in Table III indicate that the retention in this experimental set-up is favourably due to the relative amount of the free base or of the ion with the lowest positive charge, as for R-24571 with its quaternary nitrogen. Acidic compounds suffer from ion-pairing effects (data not shown), but can be chromatographed with mobile phases without basic modifiers.

For further use, one must remember that without an exact value for pK_a, the results of HPLC experiments only reflect the partition coefficient of a substance in an environment with the pH of the mobile phase. The good correlation of log P_{app}, derived

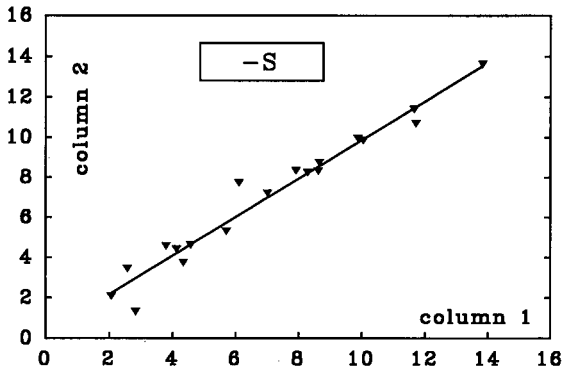

Fig. 4. Reproducibility of the chromatographic retention parameter S on two columns refilled with the same stationary phase but manufactured from diffent batch numbers of the latter.

from log $P_{Oct/W}$ for the actual pH, with the corresponding log P_{calc}, calculated from log k_W, seems to justify the application of the latter as a lipophilicity parameter. It will be easy to model closely the dependence of the partition and the pH over the (patho)physiological range when additional measurements at various pH values are performed.

The close correlation of log P_{calc} and log P_{app} strengthens the evidence for the similarity between the factors governing the retention mechanism in this HPLC environment and the factors of the octanol–water equilibrium. In dilute solution these are mainly hydrophobicity, hydration effects, charge distribution and hydrogen bond affinity. This is reflected by the results in Tables II and III. A differentiation according to hydrogen bonding and other structure effects of molecules seems possible and will be part of future work.

In Table III nimodipine and loperamide are obviously far less retarded in HPLC than could be expected from their log $P_{Oct/W}$ values. Both seem to be examples for the influence of steric effects. These molecules have a stiff central region and polar substituents at the molecular periphery, which can be covered by water molecules. Hence their central lipophilic parts are shielded and cannot not interact with hydrocarbon chains, which are fixed to the support surface, in contrast to liquid–liquid partition where neither of the bulk phases is ordered.

The analysis of the data found for the three different butylbenzenes shows a decrease in log $P_{Oct/W}$ from *n*-butylbenzene to *tert.*-butylbenzene corresponding to the decrease in log k_W. Interestingly, the change in log k_W is proportional to the change in S (Fig. 3). A plot of log k_W against the side-chain carbon number reveals as expected that *sec.*- and *tert.*-butylbenzene are not members of the *n*-alkyl series. On the other hand, the three straight-chain homologues (Fig. 6) show a step-width in log k_W for each chain increment of 1.22 (S.D. = 0.01).

The responsibility of proton donor or acceptor effects for the position relative to similar compounds in the log k_W *versus* S plot [3] can only be interpreted qualitatively. Each series of homologues represents a single straight line. The weak hydrogen bond donors (alkylbenzenes, alkylanilines) are found on parallel lines and the line for acceptors (alkylphenones) has the same S for log k_W = 0 as

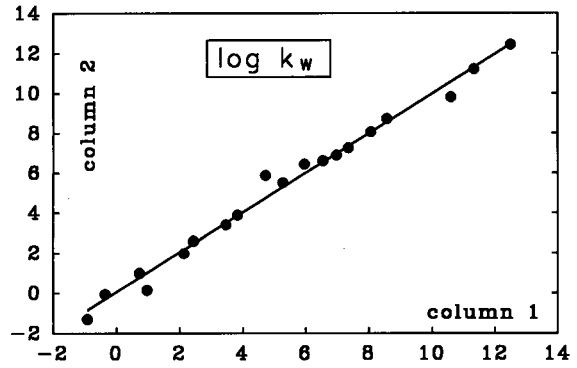

Fig. 5. Reproducibility of the chromatographic retention parameter log k_W on two columns with the same stationary phase but manufactured from diffent batch numbers of the latter.

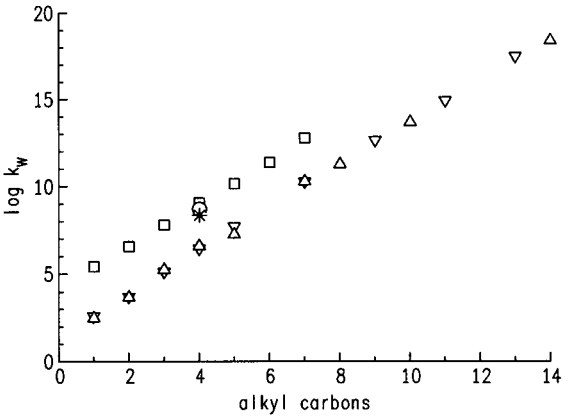

Fig. 6. Relationship between log k_W and carbon chain length and structure of (□) *n*-alkylbenzenes, (○) *sec.*-butylbenzene, (*) *tert.*-butylbenzene, (▽) phenonès and (△) 4-*n*-alkylanilines.

the other monosubstituted phenyl derivatives but a different slope. The variations of both the intercept and slope between these groups are significant but small. Additional data sets containing more donor and acceptor series are needed for quantitative calculations. For example, the S values can be calculated using eqn. 5 and the log k_W and the difference of the calculated value to the measured S can be used to construct a ΔS scale as a parameter in structure–activity investigations or as a measure for hydrogen bonding affinity [3]. Therefore, the proposal of Braumann *et al.* [16] to use chromatographic data in QSAR studies gains further support. Possibly this will give access to protein binding constants [4,17].

The question of whether log k_W or S is the better choice for the comparison of data from different columns (with the same stationary phase) without recalibration is answered in favour of log k_W. The reproducibility of log k_W on different columns (with the same stationary phase) allows the calculation of log P_{calc} with deviations smaller than or equal to those found for octanol–water partition coefficient data in the literature and which can be qualified as "reliable" [deviations lower than 0.3 in compliance with good laboratory practice (GLP) guidelines]. The control group mentioned above can serve to minimize the differences and as a quality assurance.

Small structure effects can be substantiated by chromatography of binary mixtures of solutes in the described manner. This is possible with shake-flask techniques only, when an additional chromatographic step is added [18] or if molecules labelled with two different isotopes are synthesized.

Therefore we would like to recommend chromatography as a substitute for the log $P_{Oct/W}$ determination. For routine use a reduced set of compounds for calibration is sufficient, containing some of the polar, lipophilic and intermediate members of the current test set. In order not to lose the effects of more complex molecular structures, solutes such as the dihydropyridines can be included. A possible set of compounds are marked *a* in Table I. This will reduce the inevitable standardization overhead. A conversion to the octanol–water scale to establish comparability with literature data can easily be done at any time.

Another prospect is chromatography at different pH values to model more closely the behaviour of the solutes under (patho)physiological conditions and to obtain information concerning the approximate pK_a data for basic organic molecules, especially because the aproximate elution times can be roughly proposed using a first-guess pK_a. Interlaboratory comparability of the data is possible if the same packing material and the same control group are used.

Questions concerning the correlation of the results obtained with different stationary phases will be the subject of a future publication.

REFERENCES

1 A. Brändström, *Acta Pharm. Suec.*, 19 (1982) 175–198.
2 R. Kaliszan, *Quant. Struct.–Act. Relat.*, 9 (1990) 83–87.
3 D. J. Minick, D. A. Brent and J. Frenz, *J. Chromatogr.*, 461 (1989) 177–191.
4 D. J. Minick, J. Frenz and D. A. Brent, *J. Med. Chem.*, 31 (1988) 1923–1933.
5 R. Mannhold, W. Voigt and K. Dross, *Cell Biol. Int. Rep.*, 14 (1990) 361–368.
6 C. Hansch and A. Leo (Editors), *Substituent Constants for Correlation Analysis in Chemistry and Biology*, Wiley-Interscience, New York, 1980.
7 M. Lauwers, Janssen Pharmaceutica, Beerse, Belgium, personal communications.
8 Goedecke, Freiburg, product information.
9 D. C. Pang and N. Sperelakis, *Biochem. Pharmacol.*, 33 (1984) 821–826.
10 R. C. Weast (Editor), *CRC Handbook of Chemical and Physics*, CRC Press, Boca Raton, FL, 67th ed., 1987, pp. D159–D163.
11 J. E. F. Reynolds (Editor), *Martindale, The Extra Pharmacopeia*, Pharmaceutical Press, London, 29th ed., 1989, p. XXVI.
12 R. Rodenkirchen, R. Bayer and R. Mannhold, *Prog. Pharmacol.*, 5 (1982) 16.
13 W. Stumm and J. J. Morgan, *Aquatic Chemistry*, Wiley, New York, 1981.
14 D. Poncelet, A. Pauss, H. Naveau, J.-M. Frere and E.-J. Nyns, *Anal. Biochem.*, 150 (1985) 421–428.
15 L. Sachs (Editor), *Angewandte Statistik, Anwendung Statistischer Methoden*, Springer, Berlin, 6th ed., 1982, pp. 342–343.
16 T. Braumann, H.-G. Genieser, C. Lüllmann and B. Jastorf, *Chromatographia*, 24 (1987) 777–782.
17 J. Ganansia, G. Bianchetti and J. P. Thénot, *J. Chromatogr.*, 421 (1987) 83–90.
18 P. Hairsine, *Lab. Pract.*, 38 (1989) 73–75.

Journal of Chromatography, 629 (1993) 135–141
Elsevier Science Publishers B.V., Amsterdam

CHROM. 24 642

Improved ultraviolet detection in high-temperature open-tubular liquid chromatography

Nebojsa M. Djordjevic, Desiree Stegehuis, Guanghui Liu and Fritz Erni

Analytical Research and Development, Sandoz Pharma, Basle CH-4002 (Switzerland)

(First received June 30th, 1992; revised manuscript received September 21st, 1992)

ABSTRACT

Different ways to increase the sensitivity of UV detection in high-temperature open-tubular liquid chromatography are addressed. A micro flow (Z-shaped) cell was evaluated for the possibility of enhancing the signal-to-noise ratio in high-temperature open-tubular liquid chromatography. For the same chromatographic technique, a novel approach was taken with on-column detection. Optical fibre bundles were employed, yielding a significant increase in sensitivity with only a small decrease in efficiency. This approach is also feasible for other micro-separation techniques, *e.g.*, capillary electrophoresis. Sample preconcentration and a gradient elution are also shown to be a powerful means of increasing detection limits in high-temperature open-tubular liquid chromatography.

INTRODUCTION

High-temperature open-tubular liquid chromatography (HT-OT-LC) suffers from the same problems as all the other micro-separation techniques *viz.*, a lack of sensitivity owing to reduced column loadability and limited light path length when on-column UV detection is employed. Although, fluorescence and electrochemical detection are feasible detection modes in OT-LC [1–4], UV detection is still preferred.

Whenever high efficiency is required, on-column UV detection is used [5–7]. On-column detection reduces the contribution of the detector cell volume to the peak band broadening. However, owing to the limited light path length, with capillary columns with I.D. $< 75\ \mu m$, the sensitivity of on-column UV detection is poor. The development of the small-volume Z-shaped micro flow cell [8–10] was a significant contribution to UV detection in micro separation techniques. In HT-OT-LC, detection has to be performed at the same temperature as the separation in order to avoid the cold spots, which have an adverse effect on the chromatographic efficiency [7,11] and may cause sample precipitation. This problem can be solved by placing the detector cell together with optical fibres in the column oven. On-column UV detection using either a single optical fibre or a bundle of optical fibres, was assessed for its usefulness in HT-OT-LC. Further, the Z-shaped micro flow cell was also tested for its applicability in HT-OT-LC. A sample focusing technique and gradient elution were tried as means of increasing detection in HT-OT-LC.

Correspondence to: N. M. Djordjevic, Analytical Research and Development, Sandoz Pharma, Basle CH-4002, Switzerland.

EXPERIMENTAL

The instrumental set-up is shown in Fig. 1. A high-temperature liquid chromatograph (consisting of two Model 420 pumps, a Model 460 autosampler and a Model 450 PC/AT data station was obtained from Kontron (Zurich, Switzerland). To generate a micro flow through the capillary column, a split T-piece [Valco, 1/16 in. × 0.01 in. bore (1 in. = 2.54 cm)] was used in combination with a relief valve (R3A series; Swagelok, Willoughby, OH, USA). Open-tubular capillary columns were obtained

0021-9673/93/$06.00

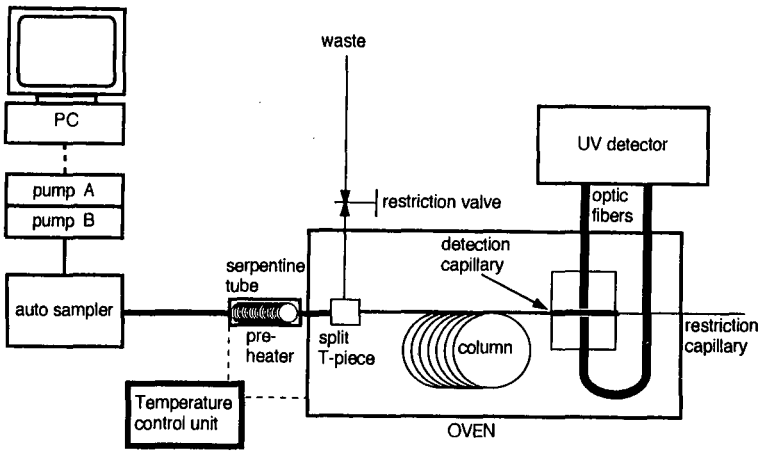

Fig. 1. High-temperature chromatograph.

from Lee Scientific (Salt Lake City, UT, USA) and Macherey–Nagel (Oensingen, Switzerland). A serpentine tube (400 mm × 0.2 mm I.D.) from Scientific Systems (State College, PA, USA) was fitted between the injection valve and the T-splitter in a separate heating body. The preheating temperature was usually set 5–10°C higher than the column temperature, enabling eluents to reach the column temperature before entering the separation column. To maintain the mobile phase in the liquid state, for temperatures above the boiling point of the eluent, a pressure restriction was necessary. The pressure restriction at the end of the analytical column was achieved by using a fused-silica tube (2 m × 18.5 μm I.D.). The split T-piece, the capillary column and the detector cell were placed in an oven. The oven and the solvent preheating unit were controlled by a temperature regulator from Zahner Electronic (Kaltbrunn, Switzerland). A Spectroflow 783 UV detector (Kratos, Ramsey, NJ, USA) was modified to allow the use of optical fibres and thus could provide on-column detection in the column oven itself. The original detector flow cell was removed from the detector. One end of the optical fibre (or the round end with the bundle of fibres) was placed in front of the monochromator to direct the light to the capillary, which was placed in the holder depicted in Fig. 2. The equivalent fibre was placed across the capillary to collect light transmitted through the capillary and guide the light to the photomultiplier. The bundles of fibres, with a round-end I.D. of 1.57 mm and a line-end bundle length and width of 8.8 and 0.23 mm, respectively, were obtained from Luxmatic (Baar, Switzerland). A schematic diagram of the detection set-up, with the bundle of fibres, is shown in Fig. 2. The single optical fibres, with core size 200 μm, were also from Luxmatic. The Z-shaped flow cell (10 mm × 25 μm) was purchased from LC Packings (Amsterdam, Netherlands) and was installed in a Model 432 UV detector (Kontron), between the column outlet and the flow restriction fused-silica tube.

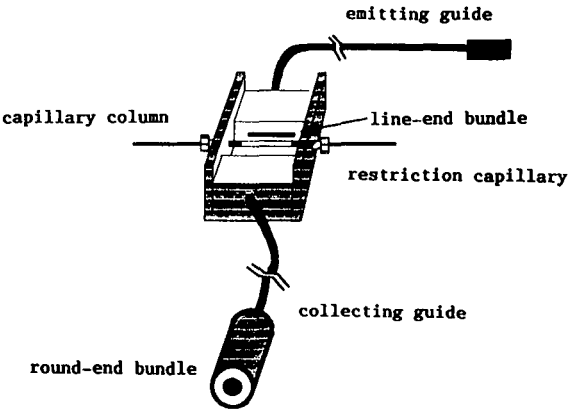

Fig. 2. Set-up for on-column detection with the bundle of optical fibres.

All solvents were of HPLC grade from Rathburn (Walkerburn, UK). Cyclosporin A was obtained from Sandoz Pharma (Basle, Switzerland). All other chemicals were from Fluka (Buchs, Switzerland).

RESULTS AND DISCUSSION

Sample focusing and gradient elution

Various methods were tested in order to find the most suitable way to increase detectability and at the same time maintain a high system efficiency. One way to improve the detection limit of a minor sample component, without losing efficiency, is to focus the sample on the top of the column. This can be done according to the same principle as in conventional reversed-phase column liquid chromatography. Sample injection (sample loading) is performed with a weak mobile phase, so that the sample is strongly retarded on the top of the column. When this procedure is followed by a gradient elution, a significant improvement in detectability can be accomplished.

Generally, cyclosporins (cyclic peptides) lack a chromophore that yields a low signal in the UV absorption range. In order to overcome this problem, the amount of substance injected has to be increased. To minimize the contribution of the injection volume to the total peak broadening, especially for the early-eluting peaks [7], and thus maintain a high system efficiency, the sample focusing technique is preferred to the injection of the large volume in one stroke. A solution of cyclosporin A in methanol (1.25 mg/ml) was prepared. The sample solution was injected (injection volume 80 μl) and split (splitting ratio = 1:750) before entering the analytical column. Because cyclosporins have a pronounced hydrophobic character, sample loading of cyclosporin A (several consecutive injections) was performed utilizing a mobile phase that had a low solvent strength. When the injections were completed, the solute was eluted under gradient conditions. Signals generated with on-column detection, using single optical fibres, for (A) ten and (B) five consecutive injections per minute are presented in Fig. 3. Sample loading was performed under isocratic conditions [acetonitrile–water (15:85)] followed by the gradient run (from 15% to 50% acetonitrile in water in 14 min). Doubling the peak area counts was accomplished without a decrease in efficiency.

A solvent gradient is a useful method for optimizing the resolution and analysis time and at the same time achieve a higher relative peak sensitivity (reciprocal of peak width) in liquid chromatography. An increase in the mobile phase strength during the separation greatly decreases the retention time and increases the relative peak sensitivity. There are several mechanisms responsible for sample retention in reversed-phase HPLC (hydrophobic interactions, adsorption with residual silanols and solute solubility in the mobile phase) [12]. The equilibria of the processes indicated are altered when the gradient run is performed. Further, solute mass transfer in the mobile and stationary phases (kinetic processes) is also changed in the gradient mode. Combined thermodynamic and kinetic effects in the gradient

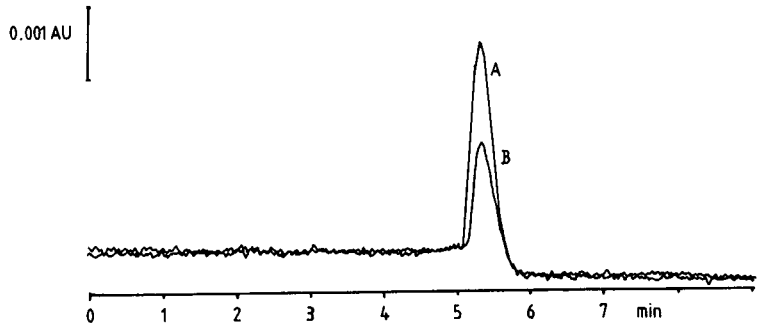

Fig. 3. Chromatogram of cyclosporin A (1.25 mg/ml). Injection volume, 80 μl with a splitting ratio of 1:750. Sample loading was done with (A) ten and (B) five consecutive injections per minute with acetonitrile in water (15:85). Elution was done with a gradient from 15% to 50% acetonitrile in water in 14 min. Analytical column, SB-Methyl-100 (1.5 m × 50 μm I.D.), film thickness 0.25 μm; column temperature, 100°C; flow-rate, 1.5 μl/min.

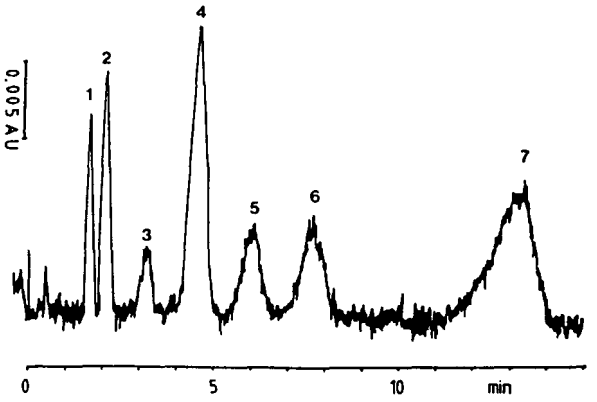

Fig. 4. On-column detection with single optical fibres. Separation column, SB-Methyl-100 (1.5 m × 50 μm I.D.), film thickness 0.25 μm; column temperature, 150°C; mobile phase, methanol–water (50:50); flow-rate, 1.5 μl/min; injection volume, 50 μl with a splitting ratio of 1:670. Peaks: 1 = tropolone; 2 = benzene; 3 = chlorobenzene; 4 = 1,4-dichlorobenzene; 5 = 1,3,5-trichlorobenzene; 6 = 1,2,4,5-tetrachlorobenzene; 7 = pentachlorobenzene.

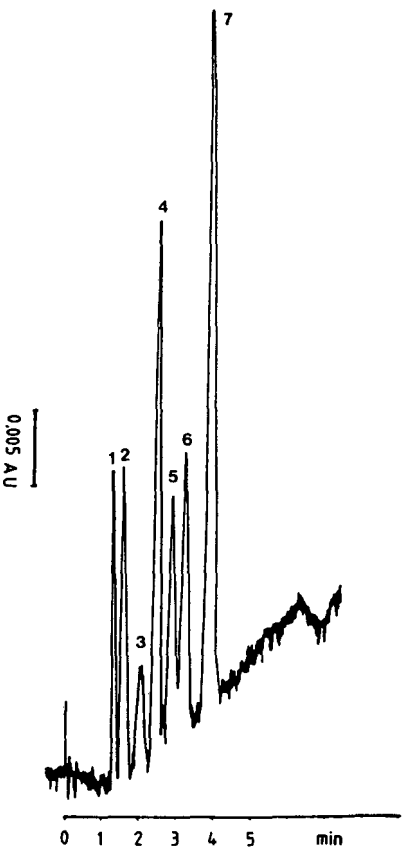

Fig. 5. Gradient elution separation with column and temperature as in Fig. 4. Mobile phase: A = methanol and B = water with a gradient from 30 to 60% B in 5 min; flow-rate, 1.5 μl/min; injection volume, 50 μl with a splitting ratio of 1:670. Peak identification as in Fig. 4.

mode lead to peak compression. The concept of the gradient separation in HT-OT-LC is the same as the gradient strategy for column liquid chromatography. The usual shortcoming with a mobile phase gradient is mobile phase mixing. In our experimental set-up, static mixing was utilized together with thermal mixing. Thermal mixing was induced by preheating the mobile phase before it entered the analytical column. A temperature increase leads to an increase in the kinetic energy of the molecules in the mixtures, resulting in rapid mixing. This was an additional benefit, apart from higher efficiency, of working at higher temperatures. Signals obtained with on-column detection employing single optical fibres with isocratic and gradient elution are shown in Figs. 4 and 5, respectively. There was a significant improvement in the relative peak sensitivity in the gradient mode compared with isocratic elution.

On-column detection

On-column detection is usually performed to minimize the peak broadening cause by the detector cell volume. Single optical fibres are commonly used for on-column detection in micro separation techniques. We investigated the use of round to line-end bundle optical fibres in on-column detection. A segment (15 mm) of the polyimide coating was burned off the analytical column to make a window for UV detection. The window was placed in the specially made cell holder, between the line-ends of the bundles, as depicted in Fig. 2. The length of the optical window is determined by the length of the line-end of the bundle (8.8 mm), while its width was limited by the diameter of a single fibre in the bundle (0.23 mm). The detection window for on-column detection utilizing a single optical fibre is limited by the fibre diameter (0.20 mm). The light path length in on-column detection is equal by the capillary column I.D. (50 μm). The separation of chlorobenzenes on a biphenyl column was studied with the single and bundle optical fibres and is shown in Figs. 6 and 7, respectively. The bun-

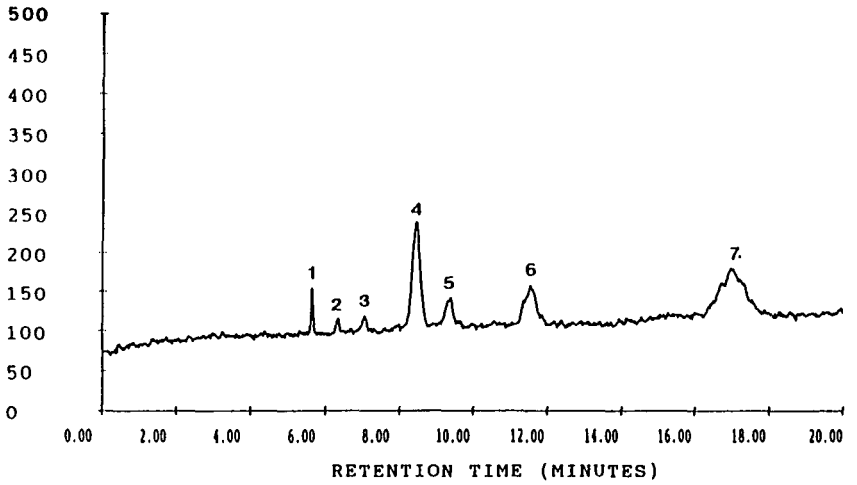

Fig. 6. On-column detection with single optical fibres. Separation column, biphenyl (10 m × 50 μm I.D.), film thickness 0.25 μm; mobile phase, acetonitrile–water (40:60); flow-rate, 4 μl/min; injection volume, 10 μl with a splitting ratio of 1:900. Peak identification as in Fig. 4. *y*-Axis is detector response (10 μV).

dled fibres provided a tenfold increase in signal-to-noise ratio (*S/N*) compared with single fibres. With the bundle of fibres a *ca.* 15% decrease in efficiency was observed owing to the large detection window. This decrease in efficiency is tolerable in most routine separations.

A study of two different detection modes, on-column detection with the single optical fibres and the Z-shaped micro flow cell, was also performed. The separation of chlorobenzenes was done at 100°C utilizing a SB-Methyl-100 capillary column (19.5 m × 5 μm I.D.) with acetonitrile–water (50:50) as the mobile phase. A very long column was used in order to minimize the contribution of the cell volume to the overall band broadening [7]. The length of the column outlet section (outside the oven) was 4 cm

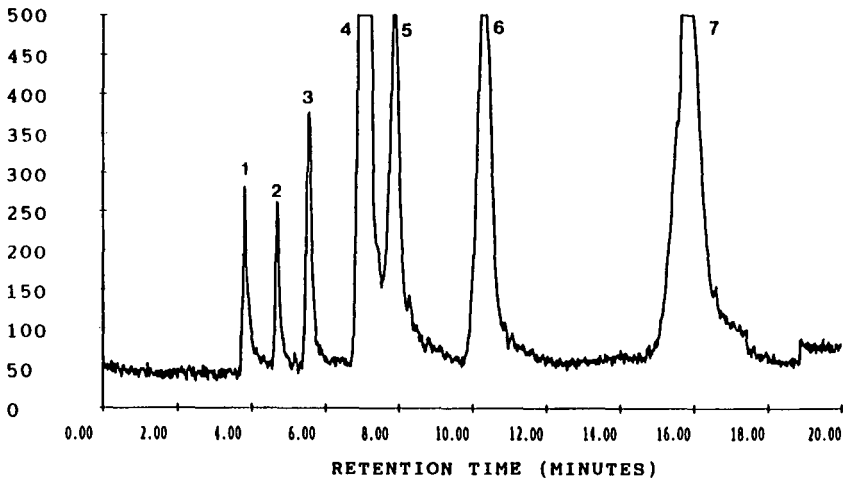

Fig. 7. On-column detection with the bundle of optical fibres. Separation conditions (except flow-rate, 5 μl/min) and peak identification as in Fig. 6. *y*-Axis is detector response (10 μV).

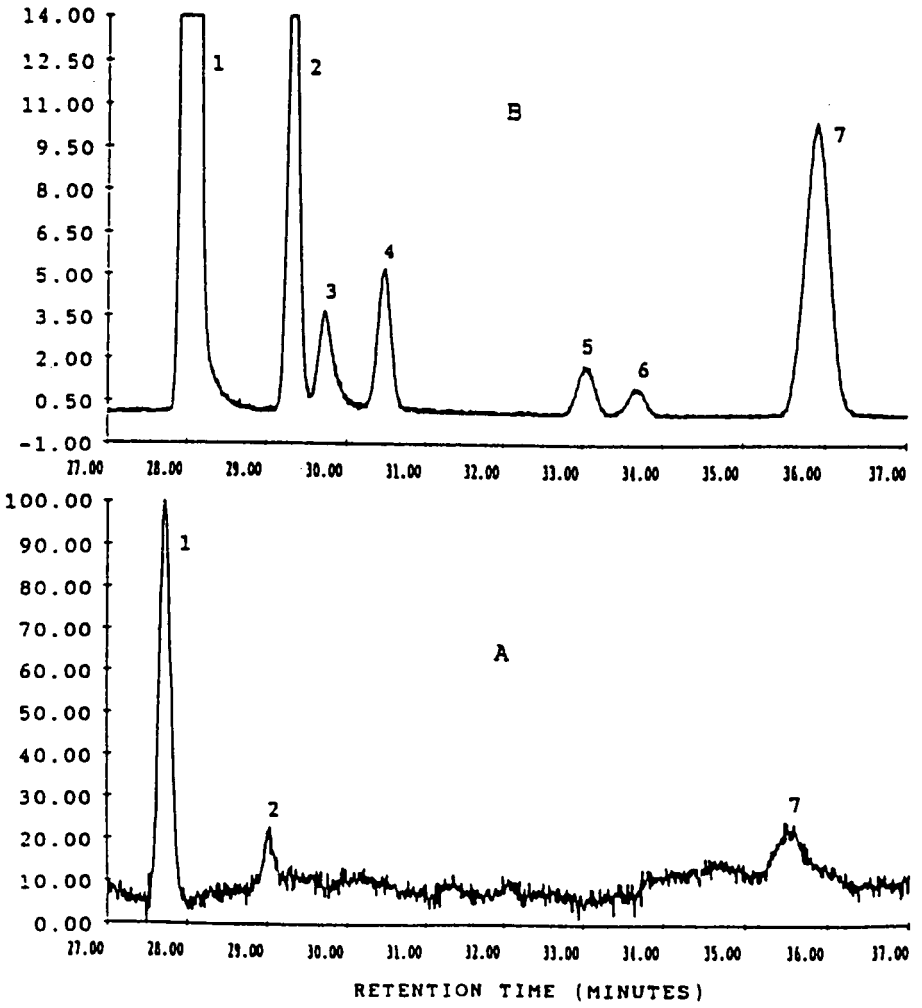

Fig. 8 (A) On-column detection with the single optical fibres. Detector wavelength, 250 nm; separation column, SB-Methyl-100 (19.5 m × 50 μm I.D.), film thickness 0.25 μm; column temperature, 100°C; mobile phase, acetonitrile–water (50:50); flow-rate, 1 μl/min; injection volume, 10 μl with a splitting ratio of 1:900. Peak identification as in Fig. 4. Signals are normalized to the highest signal. (B) Detection with the Z-shaped cell. Separation conditions as in (A). Peak identification as in Fig. 4. The *y*-axes represent detector responses: (A) 10 μV and (B) %.

and that of the cell inlet section was 40 cm. The cell and its holder were placed in the detector, which was outside the column oven at room temperature. Chromatograms obtained with on-column detection with a single optical fibre and the Z-shaped micro flow cell are shown in Fig. 8A and B, respectively. The *S/N* with the Z-shaped cell is twenty times higher than with single fibre on-column detection. As the outlet section of the analytical column was at a lower temperature, the decrease in efficiency of more retained solutes was expected to be greater at elevated column temperatures owing to the "cold spot" effect [7]. The decrease in efficiency for pentachlorobenzene becomes significant with increase of the column temperature. This obviously results from the additional retardation of the more retained solute on the cold stationary phase at the outlet section. If the Z-shaped cell is to be used in HT-OT-LC, the connection between the column and the cell should be as short as possible and, if possible, heated. In addition to the "cold spot", the detector cell volume (5.0 nl) can also lead to an inferior efficiency.

CONCLUSION

Gradient elution could be easily and successfully performed with the HT-OT-LC system. Indeed, the sample focusing provided by this method may prove to be very important when improved detection limits are required. When seeking the optimum efficiency, one should also take into consideration the detection sensitivity. The sensitivity gain with the Z-shaped flow cell is impressive. The Z-shaped micro flow cell should be applied for separations in which detection is the first priority and problems associated with some decrease in efficiency due to the "cold spot" and a prolonged analysis time (long column) could be tolerated. Use of an optical fibre bundle also significantly enhanced the detection limit of the system. This is a very promising mode for on-column detection which can be applied to some other micro separation techniques. The bundled fibres give the best compromise between increased sensitivity, decreased efficiency and speed of analysis, and therefore are the best choice for detection in HT-OT-LC.

ACKNOWLEDGEMENTS

The authors are grateful to Mr. J. P. Chervet for helpful discussions and to LC Packings for providing the Z-shaped flow cell.

REFERENCES

1 O. van Berkel, H. Poppe and J. C. Kraak, *Chromatographia*, 24 (1987) 739.
2 P. P. H. Tock, G. Stegeman, R. Peerboom, H. Poppe, J. C. Kraak and K. K. Unger, *Chromatographia*, 24 (1987) 617.
3 S. R. Mueller, W. Simon, H. M Widmer, K. Grolimund, G. Schomburg and P. Kolla, *Anal. Chem.*, 61 (1989) 2747.
4 N. D. Pfeffer and E. S. Yeung, *Anal. Chem.*, 62 (1990) 2178.
5 F. J. Yang, *J. High Resolut. Chromatogr. Chromatogr. Commun.*, 4 (1981) 83.
6 C. K. Kientz and A. Verweij, *J. High Resolut. Chromatogr. Chromatogr. Commun.*, 11 (1988) 294.
7 G. Liu, N. Djordjevic and F. Erni, *J. Chromatogr.*, 592 (1992) 239.
8 M. Janecek, V. Kahle and M. Krejci, *J. Chromatogr.*, 438 (1988) 409.
9 J. P. Chervet, R. E. J. Van Soest and M. Ursem, *J. Chromatogr.*, 543 (1991) 439.
10 J. P. Chervet, M. Ursem, J. P. Salzmann and R. W. Vannoort, *J. High Resolut. Chromatogr.*, 12 (1989) 278.
11 C. N. Renn and R. E. Synovec, *Anal. Chem.*, 63 (1991) 568.
12 R. E. Majors, *Analusis*, 3 (1975) 549.

Journal of Chromatography, 629 (1993) 143–151
Elsevier Science Publishers B.V., Amsterdam

CHROM. 24 596

High-performance liquid chromatography using continuous on-line post-elution photoirradiation with subsequent diode-array UV or thermospray mass spectrometry detection

Ira S. Lurie and Donald A. Cooper

Drug Enforcement Administration, Special Testing and Research Laboratory, 7704 Old Springhouse Road, McLean, VA 22102-3494 (USA)

Ira S. Krull

Department of Chemistry and the Barnett Institute of Chemical Analysis, 341 Mugar Building, Northeastern University, 360 Huntington Avenue, Boston, MA 02115 (USA)

(First received April 7th, 1992; revised manuscript received September 1st, 1992)

ABSTRACT

The use of HPLC with continuous on-line post-elution photoirradiation followed by either diode-array UV or thermospray mass spectrometric detection is presented. These tandem techniques can greatly increase specificity of analysis, as demonstrated by select compounds whose UV or thermospray mass spectra are highly similar under lamp off conditions but significantly different after photoirradiation. The utility of the above approach for various compounds of forensic interest is presented.

INTRODUCTION

For HPLC analysis, retention data alone lack selectivity. As a result, additional on-line detectors are commonly used to increase specificity by providing complementary information [1,2]. Typical on-line detection modes include UV, MS, fluorescence and electrochemical. This approach is particularly useful in forensic drug analysis, where trace level analyses and establishment of peak identity and purity are very important [1,2].

Use of diode-array UV detectors can greatly increase selectivity by providing UV spectra; however, the spectra themselves are generally not unique. Similarly, thermospray (TSP) MS can also greatly increase selectivity by providing molecular weight information; however, usually little or no additional information beyond molecular weight is obtained. Furthermore, certain compounds do not give any detectable ion current at all using TSP-MS.

Continuous on-line post-elution photoirradiation has been previously employed as a means of converting an eluting compound into one or more photoproduct(s) prior to ether variable-wavelength UV [3,4], fluorescence [5–13] or electrochemical detection [14–23]. Photoirradiation of photosensitive solutes frequently results in formation of photoproducts with enhanced detectability. HPLC–photoirradiation followed by fluorescence or electrochemical detection has been previously reported for determination of drugs of forensic interest [5–8,14–17], herbicides [9,18], pesticides [13], sulfonamide

Correspondence to: I. S. Lurie, Drug Enforcement Administration, Special Testing and Research Laboratory, 7704 Old Springhouse Road, McLean, VA 22102-3494, USA.

diuretics [10], stilbene derivatives [11], vitamin K homologues [12], penicillins [19], explosives and related nitro compounds [20], foods [21], inorganic anions [22] and amino acids and proteins [23].

In this paper, the applicability of continuous on-line post-elution photoirradiation to increase the selectivity of diode-array UV and TSP-MS detection is described. The utility of this technique for the determination of various drugs of forensic interest is discussed.

EXPERIMENTAL

Equipment

Two HPLC systems were employed in this study. For diode-array UV detection, a Series 4 liquid chromatograph (Perkin-Elmer, Norwalk, CT, USA) fitted with an ISS autosampler (Perkin-Elmer), a Partisil-5 ODS-3 cartridge system (11.0 cm × 4.7 mm I.D., 5 μm, column) (Whatman, Clifton, NJ, USA) and a 1040M diode-array UV detection system (Hewlett-Packard, Waldbronn, Germany) were employed. For TSP-MS detection, a Series 4 liquid chromatograph fitted with a Model 7125 valve injector (Rheodyne, Cotati, CA, USA) and a Model 701C thermospray interface (Vestec, Houston, TX, USA) fitted to a 4530 quadrupole mass spectrometer (Finnigan-MAT, San Jose, CA, USA) were employed. For both systems, a "Phred" photochemical reactor (Aura Industries, Staten Island, NY, USA) fitted with a KRC 10-50 knitted open tube (KOT) reactor coil (10 m × 500 μm I.D.) and a low-pressure 8-W mercury lamp with a strong 254-nm line (Aura Industries) were employed prior to the detection system.

Materials

Acetonitrile and ammonium acetate were HPLC grade. Water was obtained from a Milli-Q system (Millipore, Milford, MA, USA). All other chemicals were reagent grade or better. Drug standards were obtained from the Reference Standards Collection of the Drug Enforcement Administration's Special Testing and Research Laboratory.

The HPLC mobile phase was internally mixed from two individual solvent reservoirs containing acetonitrile and 0.1 *M* ammonium acetate buffer, respectively.

Procedures

For flow injection analysis, 1 mg of standard was dissolved in 50.0 ml mobile phase prior to a 50- or 100-μl injection onto the liquid chromatograph. For the TSP-MS flow-rate optimization study, 1 mg of each standard was dissolved in 25.0 ml mobile phase prior to a 50-μl injection onto the liquid chromatograph. The mobile phase for both flow injection and HPLC with post-column analysis consisted of 0.1 *M* ammonium acetate–acetonitrile (60:40, v/v).

TSP conditions were optimized at a flow-rate of 1.0 ml/min (see below). The vaporizer had a tip orifice of 125 μm and was operated at 238–259°C with the source block temperature held at 266–282°C. The repeller was set at approximately 28 + V d.c. Data acquisition was from *m/z* 100 to 500 at 3 s/scan.

RESULTS AND DISCUSSION

Determination of the optimum photochemical reaction time (i.e., flow-rate)

It was of interest to determine whether the optimum flow-rate for TSP-MS analysis (*i.e.*, approximately 1.0 ml/min) also represented the optimum exposure time for photochemical reaction. Six representative compounds of forensic interest (acetaminophen, heroin, noscapine, pentobarbital, methapyrilene and diphenhydramine) were subjected to photoirradiation at several different flow-rates (effectively giving different photochemical reaction times). Following diode-array UV detection, peak heights were measured at wavelengths where the photoproduct(s) have significantly higher absorbances than the parent compounds. Acetaminophen was measured at 380 nm, heroin and noscapine at 340 nm and pentobarbital, methapyrilene and diphenhydramine at 270 nm. As shown in Fig. 1, comparison of peak height response *vs.* flow-rate indicates unchanged or only slightly reduced sensitivity levels (compared with the maximum response) when the optimum TSP-MS flow-rate of 1.0 ml/min is used for acetaminophen, heroin, pentobarbital and methapyrilene, with greater reductions for noscapine and diphenhydramine. However, there are still significant and sufficient photoinduced reactions occurring at 1.0 ml/min for each of the photosensitive substrates examined, and this flow-rate was therefore utilized for all studies.

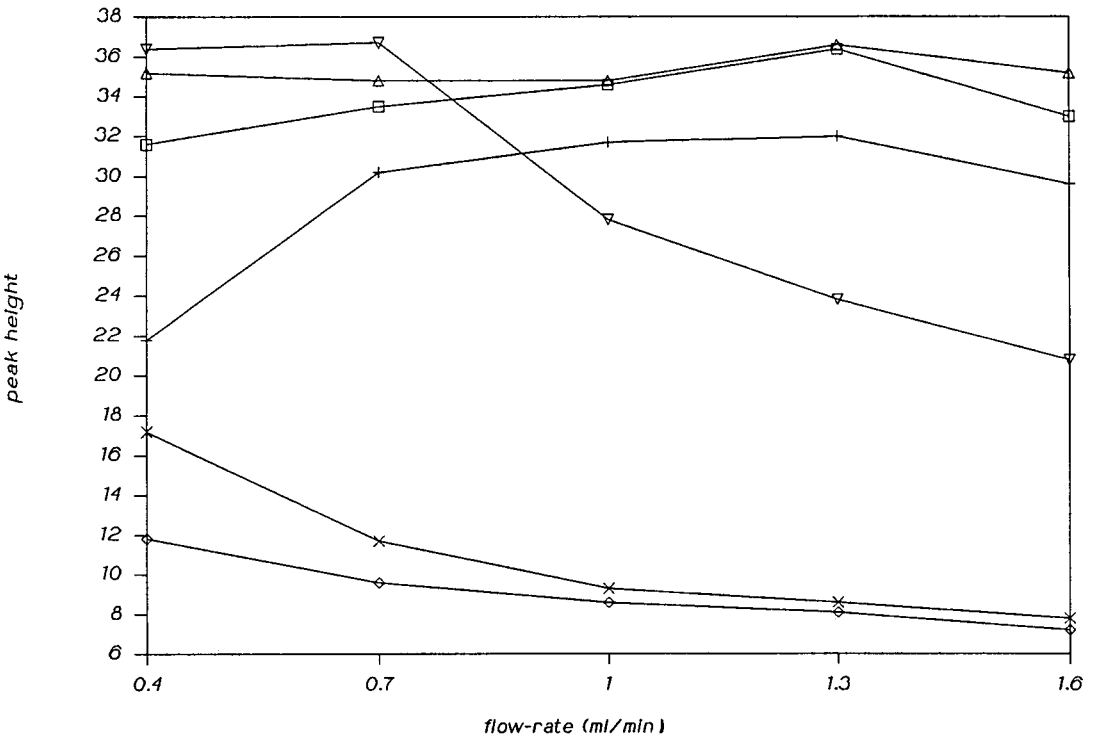

Fig. 1. Peak height response *versus* flow-rate for pentobarbital (+), heroin (◇), methapyrilene (△), diphenhydramine (×), acetaminophen (□) and noscapine (▽) after post-column photochemical reaction and diode-array detection.

Photoirridiation with subsequent diode-array UV detection

The utility of photoirradiation–diode-array UV detection is demonstrated by select compounds whose UV spectra are highly similar under lamp off conditions but which exhibit quite different spectra after photoirradiation. In this vein, it is particularly illustrative to compare structurally closely related compounds, *e.g.*, butalbital *vs.* talbutal, O6-monoacetylmorphine (O6-MAM) *vs.* morphine and 3,4-methylenedioxyamphetamine (MDA) *vs.* 3,4-methylenedioxymethamphetamine (MDMA). As shown in Figs. 2–4, these pairs display similar spectra under lamp off conditions but significantly different spectra following photoirradiation. Butalbital and talbutal display no discernible UV maxima under lamp off conditions; following photoirradiation, however, both compounds displayed distinct UV maxima at 265 nm, with talbutal undergoing the significantly more pronounced hyperchromic effect (Fig. 2). Similarly, both O6-MAM and morphine gave slight blue shifts (286 → 284 nm) following photoirradiation, with morphine undergoing the greater hyperchromic effect (Fig. 3). Finally, both MDA and MDMA developed a shoulder at 318 nm following photoirradiation, with MDMA undergoing the more pronounced hyperchromic effect at 318 nm and more pronounced hypochromic effect at 286 nm.

Molecular consequences of photoirradiation on UV spectra

UV absorption and photochemical reaction both involve excitation of photosensitive substrates via photoirradiation. However, the former process involves only a fully reversible absorption of energy raising a specific chromophore from its ground level to a low lying excited electronic energy level. The resulting excited state quickly returns to the ground state via various intra- and intermolecular vibra-

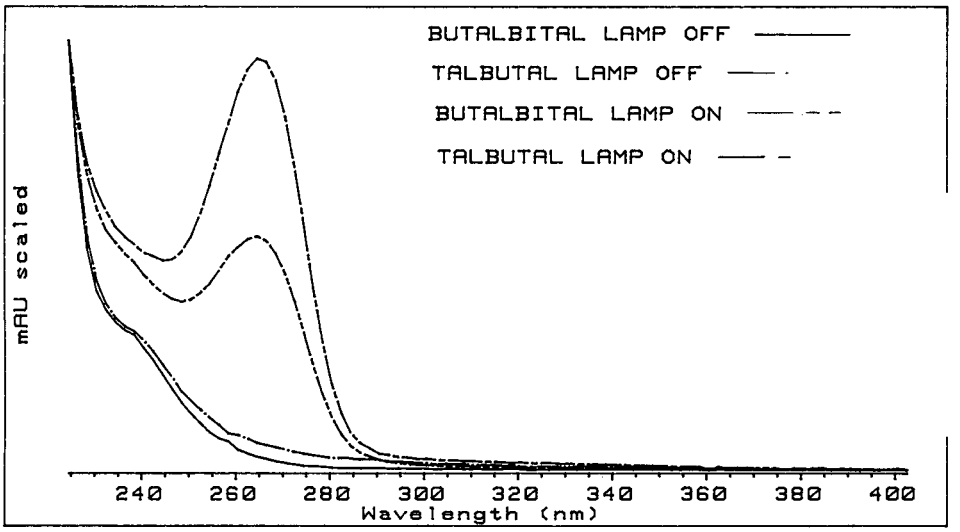

Fig. 2. UV spectra of butalbital and talbutal before and after photoirradiation.

tional and rotational interactions (thereby end-resulting only in simple heating of the solution). In contrast, the latter process involves absorption of very high energy photons raising a specific chromophore from its ground level to an upper excited electronic energy level. As with standard UV absorption, the resulting photoexcited molecule *may* return to the ground state via vibrational–rotational interactions, but can alternately act as a high energy transition state to a new molecule (or molecules) via (usually) intra- or (rarely) intermolecular reactions. The resulting photoproducts, whose formation and structure(s) can be highly dependent on the presence of nearby functional groups and/or stereochemistry, can have different chromophores (and therefore dramatically different UV spectra)

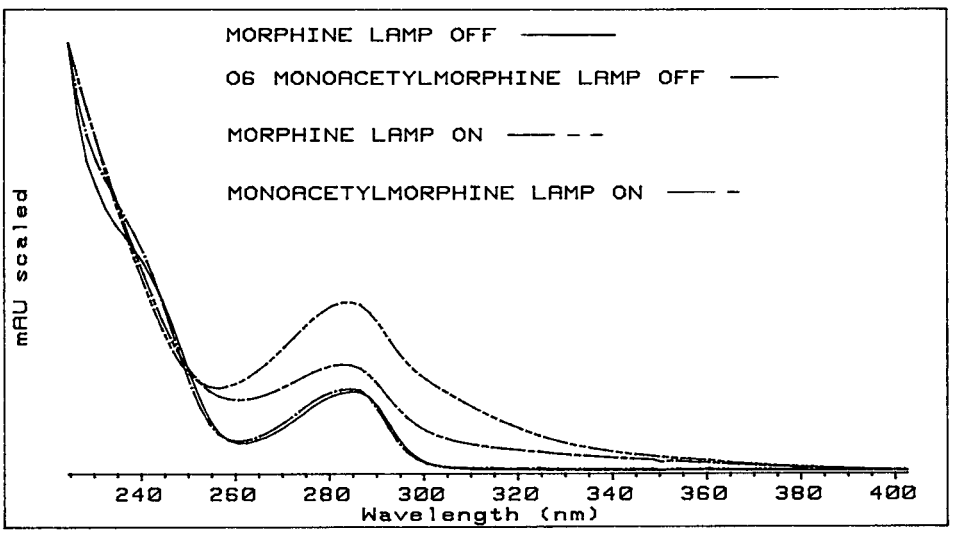

Fig. 3. UV spectra of morphine and O6-monoacetylmorphine before and after photoirradiation.

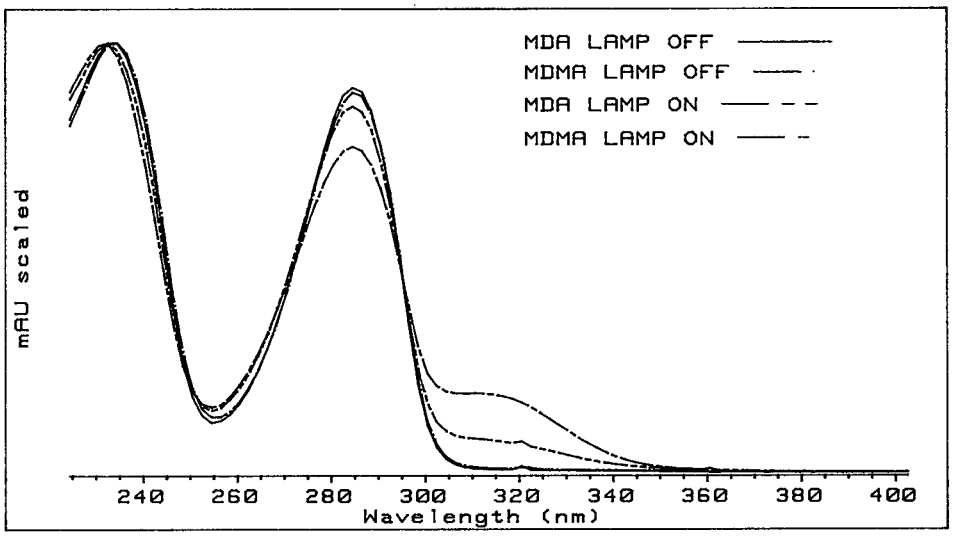

Fig. 4. UV spectra of MDA and MDMA before and after photoirradiation.

vs. the original substrate. As the examples detailed above illustrate, even minor structural and/or stereochemical differences can lead to significant changes in UV spectra.

Photoirradiation with subsequent TSP-MS detection

As is the case for diode-array detection, photoirradiation frequently increases specificity of pure TSP-MS analyses. For compounds having the same molecular mass, pure TSP mass spectra are frequently the same, however, as shown in Table I. For example, O3- and O6-MAM, both of which give only *m/z* 328 ions (MH^+) under lamp-off conditions, give significantly different spectra containing multiple ions under lamp-on conditions which formally can be interpreted. O3-MAM has an intense *m/z* 345 ion (probably $[M + NH_3]H^+$) and a weak *m/z* 314 and *m/z* 304 (probably $[M - CH_2CO + H_2O]H^+$) ion; in contrast, O6-MAM has strong *m/z* 346 (probably $[M + H_2O]H^+$), *m/z* 302 and *m/z* 300, 284, 270, 268, 257 and 256 ions. Both compounds retain very intense *m/z* 328 ions (which almost certainly represent the unreacted parent compound MH^+'s) and also display common *m/z* 286 (most probably $[M - CH_2CO]H^+$) ions.

In another pertinent example, cannabidiol and Δ^9-tetrahydrocannabinol (Δ^9-THC) also give identical TSP mass spectra under lamp off conditions but different spectra after photoirradiation. Under lamp-off conditions, both compounds exhibit *m/z* 315 ions (MH^+). After photoirradiation, cannabidiol gives only the *m/z* 315 ion (Note, however, that the absolute intensity of the UV spectrum was significantly higher, suggesting that at least some photoproducts were produced); in contrast, Δ9-THC gives three ions {an intense *m/z* 315 (= MH^+) and smaller *m/z* 373 and 333 (probably $[M + H_2O]H^+$) ions}.

TABLE I

MASS SPECTRA (THERMOSPRAY IONIZATION) OF COMPOUNDS OF FORENSIC INTEREST BEFORE AND AFTER PHOTOCHEMICAL REACTION

Compound	*m/z* (relative abundance)	
	Lamp off	Lamp on
O3-Monoacetylmorphine	328(100)	345(34), 328(100), 314 (3), 304(3), 286(51)
O6-Monoacetylmorphine	328(100)	346(36), 328(70), 302 (10), 300(8), 286(40), 284(40), 270(18), 268(12), 257(100), 256(12)
Cannabidiol	315(100)	315(100)
Δ^9-THC	315(100)	373(6), 333(12), 315 (100)

TABLE II

MASS SPECTRA (THERMOSPRAY IONIZATION) OF BARBITURATES BEFORE AND AFTER PHOTOCHEMICAL REACTION

Compound	*m/z* (relative abundance)	
	Lamp off	Lamp on[a]
Pentobarbital	–	261(12)^{B2b}, 244(100)^{B2a,B1b}, 227(4)^{B1a} 218(4)^{Cb}, 201(25)^{Ca}, 157(14)^{AaR1}
Butalbital	–	242(49)^{B2a,B1b}, 225(6)^{B1a}, 207(100)^{Da} 199(15)^{Ca}
Barbital	–	219(24)^{B2b}, 202(100)^{B2a,B1b}, 185(4)^{B1a} 159(8)^{Ca}
Talbutal	–	259(8)^{B2b}, 242(37)^{B2a,B1b}, 207(100)^{Da} 199(20)^{Ca}, 155(12), 143(10)
Allobarbital	–	243(6)^{B2b}, 232(5), 226(16)^{B2a,B1b} 209(4)^{B1a}, 201(4), 191(100)^{Da}
Amobarbital	–	261(15)^{B2b}, 244(100)^{B2a,B1b}, 227(8)^{B1a} 218(4)^{Cb}, 201(20)^{Ca}
Secobarbital	–	256(68)^{B2a,B1b}, 239(8)^{B1a}, 221(100)^{Da} 213(45)^{Ca}, 169(19)^{AaR1}
Phenobarbital	–	250(96)^{B2a,B1b}, 233(100)^{B1a}, 207(56)^{Ca} 204(8), 164(4)

[a] A, B1, B2 and C: see Fig. 5 and refs. 25–27 for postulated structures; D: see Fig. 6 for postulated mechanism and structure; lower case a and b denotes H^+ and NH_4^+ ion adducts respectively; Rx references the C-5 substituent lost to form ion A.

Finally, in contrast to the findings of Heeremans *et al.* [24] for heptabarbital, most barbiturates give *no* detectable TSP mass spectra at all under lamp off conditions, but (as detailed for eight typical barbiturates in Table II) numerous ions after photoirradiation. These results were expected in light of previously reported photoproducts for secobarbital, pentobarbital and barbital [25–27]. All eight barbiturates displayed an intense $[M + NH_3]H^+$ ion (consistent with the previously postulated protonated photoproduct B2 shown in Fig. 5). In addition, a previously unreported photoproduct (designated photoproduct D) was observed at M − 17 for all barbiturates having a 5-allyl subsituent; D appears to be the end result of a combined photo-Fries rearrangement–dehydration reaction mechanism (Fig. 6) and represents a highly specific and convenient marker for identification of 5-allyl barbituric acids [28].

Molecular consequences of photoirradiation on TSP mass spectra

Under pure TSP-MS conditions, the ions which are typically observed represent combinations of proton, ammonium and solvent adducts; the formation of these adducts essentially depends on the ability of a compound to act as a Bronsted base. As shown earlier, any compounds with the same molecular mass and closely similar structures will typically have similar Bronsted base properties and therefore essentially identical TSP mass spectra.

As previously discussed, photoirradiation can result in the formation of new photoproducts, which will result in clear differences in TSP mass spectra *if* those new compounds have different molecular masses and/or altered Bronsted base properties. In addition, dramatically increased fragmentation may be observed, even with photoproducts of identical molecular mass and Bronsted base properties, if those compounds are (as expected) thermodynamically less stable than the original substrate (thermodynamically unstable photoproducts are more susceptible to fragmentation under standard TSP-MS conditions). As the examples detailed above again illustrate, even minor structural and/or stereochemical differences can result in significant changes in TSP mass spectra.

Determination of psilocybin in hallucinogenic mushrooms

The use of diode-array UV and TSP-MS detection under lamp-off/lamp-on conditions provides for both the identification of psilocybin and its differentiation from psilocin. The UV spectra of psilocybin and psilocin are quite similar under lamp off conditions, with UV maxima at 265 nm (Fig. 7). After photoirradiation, both compounds exhibit pronounced hyperchromic effects throughout the entire UV spectra 220–400 nm; however, psilocybin displays no discernible UV maxima, while psilocin displays a new maxima at 233 nm. The TSP mass spectra of psilocybin displays only an abundant *m/z* 285 MH^+ ion and a more intense *m/z* 205 ion (the latter almost certainly representing the MH^+ ion for psilocin) under lamp off conditions (Table III).

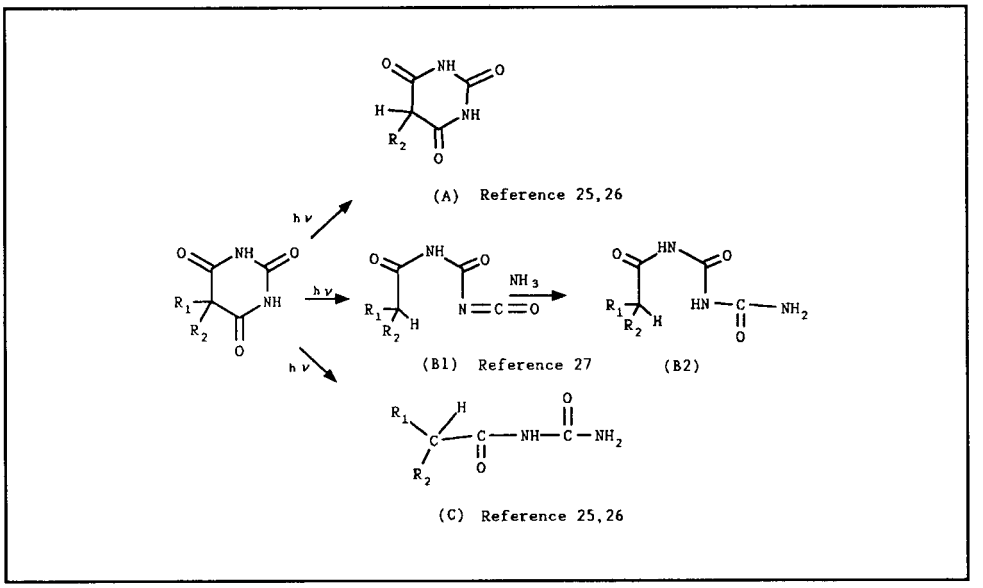

pentobarbital	R_1- $CH_3CH_2CH_2CH(CH_3)$	R_2- C_2H_5
butalbital	R_1- $(CH_3)_2CHCH_2$	R_2- $CH_2{=}CHCH_2$
barbital	R_1- C_2H_5	R_2- C_2H_5
talbutal	R_1- $CH_3CH_2CH(CH_3)$	R_2- $CH_2{=}CHCH_2$
allobarbital	R_1- $CH_2{=}CHCH_2$	R_2- $CH_2{=}CHCH_2$
amobarbital	R_1- $(CH_3)_2CHCH_2CH_2$	R_2- C_2H_5
secobarbital	R_1- $CH_3CH_2CH_2CH(CH_3)$	R_2- $CH_2{=}CHCH_2$
phenobarbital	R_1- C_6H_5	R_2- C_2H_5

Fig. 5. Correlation of 5,5-disubstituted barbituric acid photoproducts [25–27].

After photoirradiation, however, a highly complex TSP mass spectra is obtained containing 27 ions; the spectrum is vastly different than that obtained for the structurally similar psilocin under identical conditions. The new base peak for psilocybin is *m/z* 221, while for psilocin is *m/z* 219. In all, there are 22 unique ions in the photoirradiated–TSP mass spectra of psilocybin (*vs.* psilocin), including intense ions at *m/z* 164, 162, 128 and 118. The intense *m/z* 205 ion present in both spectra is consistent with the MH^+ ion for psilocin. Finally, since the ion of *m/z* = 285 (representing the MH^+ for psilocybin) is *not* present after photoirradiation, the aquisition of preliminary lamp off TSP mass spectra further increases the specificity of analysis.

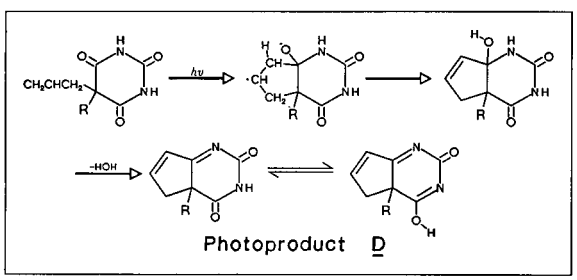

Fig. 6. Postulated mechanism for photoproduct D.

For actual sample analysis the chromatographic system reported by Borner and Brenneisen [29] appears to be viable. The reversed-phase gradient system which was used (containing ammonium acetate buffer and methanol) would be expected to be compatible with photoirradiation and diode-array UV and TSP-MS detection. Borner and Brenneisen [29] showed the homogeneity of the psilocybin peak from a mushroom sample by overlaying upslope,

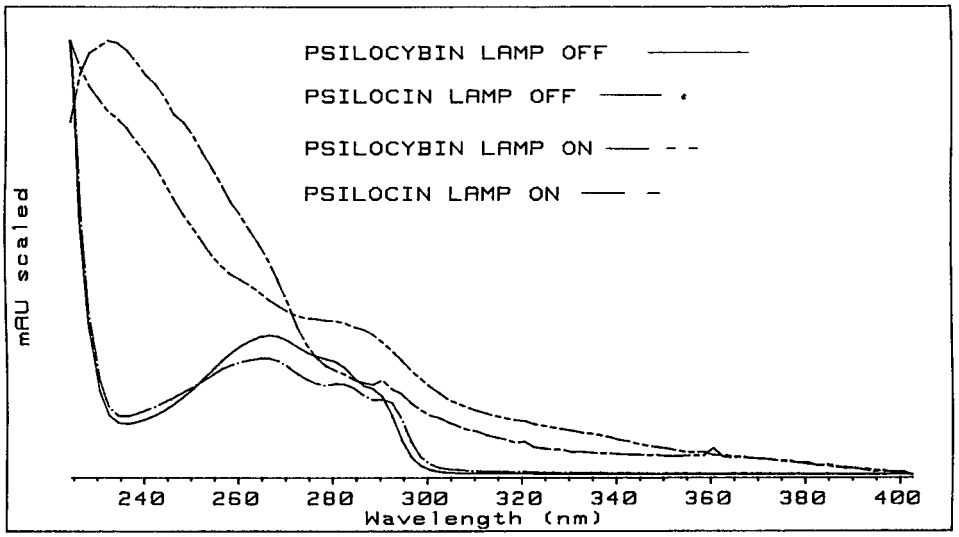

Fig. 7. UV spectra of psilocybin and psilocin before and after photoirradiation.

apex and downslope spectra obtained using a diode array UV detector.

Limitations of photoirradiation

The two reactor coils used in this study lasted for 150 and 80 injections, respectively, before developing leaks (approximately equal injections for each detector). It has been previously reported that fluoride liberated from PTFE (polytetrafluoroethylene) tubing during UV irradiation causes the tubing to turn brittle and eventually rupture [30,31]. This problem might be alleviated if ice-bath cooling is provided for the lamp and the KOT assembly [31]. Another possible factor contributing to coil rupture may be the back pressure generated by the TSP apparatus (4.4–6.1 MPa), since the PTFE tubing used in this study is only rated for 3.4 MPa. Working at lower flow-rates (e.g., 0.7 ml/min) would significantly lower back pressure —although at the expense of TSP detector sensitivity (approximately 2× loss). However (as shown in Fig. 1), there would still be sufficient generation of photoproducts for routine analytical analyses even at this lower flow-rate. Alternately, use of different lengths and/or internal diameters of PTFE tubing for the KOT assembly could maintain or increase sensitivity even at lower flow-rates.

TABLE III

MASS SPECTRA (THERMOSPRAY IONIZATION) OF PSILOCYBIN AND PSILOCIN BEFORE AND AFTER PHOTOCHEMICAL REACTION

Compound	*m/z* (relative abundance)	
	Lamp off	Lamp on
Psilocybin	205(100) 285(18)	391(4), 348(3), 301(3) 300(3), 283(4), 240(4) 237(3), 221(100), 219(17) 217(4), 212(11), 205(30) 203(39), 192(5), 191(9) 190(3), 178(5), 177(5) 167(5), 164(14), 162(26) 128(36), 126(6), 125(3) 118(12), 116(4), 114(8)
Psilocin	205(100)	266(13), 247(8), 235(5) 221(31), 219(100), 217(5) 212(3), 205(39)

CONCLUSIONS

Continuous on-line post-elution photoirradiation followed by diode-array UV or TSP-MS detection is a readily performed technique which results in significantly increased specificity of analysis. Although flow injection analysis was primarily used to acquire data for this study, the approach presented is applicable to HPLC with post-column analysis.

The UV and TSP-MS data obtained are highly complementary. In addition, the possibility exists for the direct coupling of the diode-array UV and/or TSP-MS detectors with a high-pressure-rated UV flow cell.

Additional drugs of forensic interest which undergo changes in either their TSP-mass spectra and or UV after photoirradiation include morphine, codeine, acetylcodeine, heroin, lysergic acid diethylamide, phencyclidine, N-hydroxy-MDA, fentanyl, noscapine, quinine, diphenhydramine, phenacetin, acetaminophen, antipyrene, methapyrilene and nicotinamide. Further applications can be reasonably expected for analysis of, *e.g.*, penicillin, sulfonamide diuretics, herbicides, stilbene derivatives, vitamin K homologues, explosives, foods, inorganic anions, amino acids and proteins; in all of the latter examples, photoproducts have been previously reported using either fluorescence or electrochemical detectors (see above). Ballard and Grinberg [32] are presently investigating the use of flow injection–photoirradiation–TSP-MS for analyses of benzophenone, heptylphysotigmine (used for the treatment of Alzheimer's disease) and the immuno-suppressant drug FK-520. Finally, diode-array UV and/or TSP-MS detection may be used for continuous on-line monitoring of photochemical reactions.

ACKNOWLEDGEMENTS

The authors thank Henry Joshua (Merck, Sharp and Dohme Research Laboratories, Rahway, NJ, USA) and Dr. Robert F. X. Klein (Special Testing and Research Laboratory) for valuable discussions.

REFERENCES

1 I. S. Krull and I. S. Lurie, in G. Davies (Editor), *Forensic Science*, American Chemical Society, Washington, DC, 2nd ed., 1986, p. 153.
2 I. S. Lurie, *LC · GC*, 8 (1990).
3 R. W. Schmid and C. Wolf, *J. Chromatogr.*, 478 (1989) 369.
4 C. Wolf and R. W. Schmid, *J. Liq. Chromatogr.*, 13 (1990) 2207.
5 P. J. Twitchett, P. L. Williams and A. C. Moffat, *J. Chromatogr.*, 149 (1978) 683.
6 A. H. M. T. Scholten and R. W. Frei, *J. Chromatogr.*, 176 (1979) 349.
7 A. H. M. T. Scholten, P. L. M. Welling, U. A. Th. Brinkman and R. W. Frei, *J. Chromatogr.*, 199 (1980) 239.
8 U. A. Th. Brinkman, P. L. M. Welling, G. de Vries, A. H. M. T. Scholten and R. W. Frei, *J. Chromatogr.*, 217 (1981) 463.
9 C. J. Miles and H. A. Moye, *Chromatographia*, 24 (1987) 628.
10 J. T. Stewart and W. J. Bachman, *Trends Anal. Chem.*, 7 (1988) 106.
11 P. J. Harman, G. L. Blackman and G. Phillipou, *J. Chromatogr.*, 225 (1981) 131.
12 M. F. Lefevere, R. W. Frei, A. H. M. T. Scholten and U. A. Th. Brinkman, *Chromatographia*, 15 (1982) 459.
13 B. M. Patel, H. A. Moye and R. Weinberger, *Talanta*, 38 (1991) 913.
14 C. M. Selavka, I. S. Krull and I. S. Lurie, *J. Chromatogr. Sci.*, 23 (1985) 499.
15 C. M. Selavka, I. S. Krull and I. S. Lurie, *Forensic Sci. Int.*, 31 (1986) 103.
16 C. M. Selavka and I. S. Krull, *J. Liq. Chromatogr.*, 10 (1987) 345.
17 C. M. Selavka and I. S. Krull, in H. Ho (Editor), *Analytical Methods in Forensic Chemistry*, Ellis Horwood, Chichester, 1990, p. 195.
18 X. D. Ding and I. S. Krull, *J. Agric. Food Chem.*, 32 (1984) 622.
19 C. M. Selavka, I. S. Krull and K. Bratin, *J. Pharm. Biomed. Anal.*, 4 (1986) 83.
20 I. S. Krull, C. Selavka, X. D. Ding, K. Bratin and G. Forcier, *J. Forensic Sci.*, 29 (1984) 449.
21 W. R. LaCourse and I. S. Krull, *Anal. Chem.*, 59 (1987) 49.
22 L. Dou and I. S. Krull, *J. Chromatogr.*, 499 (1990) 685.
23 L. Dou, J. Mazzeo, and I. S. Krull, *BioChromatography*, 5 (1990) 74.
24 C. E. M. Heeremans, A. M. Stijnen, R. A. M. van der Hoeven, W. M. A. Niessen, M. Danhof and J. van der Greef, *J. Chromatogr.*, 554 (1991) 205.
25 H. Barton, J. Mokrosz, J. Bojarski and M. Klimczak, *Pharmazie*, 35 (1980) 155.
26 H. Barton and J. Bojarski, *Pharmazie*, 38 (1983) 630.
27 H. Barton, J. Bojarski and J. Mokrosz, *Tetrahedron Lett.*, 23 (1982) 2133.
28 M. R. Sandner, E. Hedays, and D. J. Trecker, *J. Am. Chem. Soc.*, 90 (1968) 7249.
29 S. Borner and R. Brenneisen, *J. Chromatogr.*, 408 (1987) 402.
30 G. E. Batley, *Anal. Chem.*, 56 (1984) 2261.
31 M. Selavka, K. S. Jiao and I. S. Krull, *Anal. Chem.*, 59 (1987) 2221.
32 J. M. Ballard and N. Grinberg, presented at the *40th ASMS Conference on Mass Spectrometry, 1992, Washington, DC, May 31–June 5, 1990*, Wednesday post No. 103.

Journal of Chromatography, 629 (1993) 153–160
Elsevier Science Publishers B.V., Amsterdam

CHROM. 24 613

Chromatographic properties of chemically bonded bovine serum albumin working as a chiral selector in alkaline mobile phases

Zdeněk Šimek* and Radim Vespalec

Institute of Analytical Chemistry, Czechoslovak Academy of Science, Veveří 97, 611 42 Brno (Czechoslovakia)

(First received March 3rd, 1992; revised manuscript received September 7th, 1992)

ABSTRACT

By chemical bonding of bovine serum albumin to a hydrolytically stable Separon HEMA matrix, a sorbent with an excellent lifetime in mobile phases with pH $\leqslant$ 11 is obtained. Maximum retentions of amino acids and separation selectivity of amino acids and monocarboxylic and dicarboxylic acids on chemically bonded albumin are attained around pH 9. By prolonged action of slightly alkaline mobile phases of pH $<$ 10 to bonded albumin, the separation selectivity of the compounds with one carboxylic group (amino acids and monocarboxylic acids) decreases whereas that of dicarboxylic acids increases. The initial selectivity of albumin can be restored by methanol. At a given pH the rate of the changes can be increased by 1-propanol or caprylic acid. It was demonstrated that lowering of the efficiency of the column packed with Separon HEMA–BSA with respect to that packed with the matrix and the dependence of the solute retention on the injected amount of the solute are due to the bonded albumin.

INTRODUCTION

Systems with chemically bonded proteins belong to widely studied separation systems in liquid chromatography for the separation of chiral compounds. Compared with specially synthesized chiral stationary phases, protein stationary phases have two advantages: they are perfectly chirally stable and with a suitable selection of the protein they can be considerably cheaper.

Bovine serum albumin (BSA) is produced in large amounts, with sufficient purity and relatively cheaply. Moreover, albumin [1] interacts more specifically with many enantiomers than, *e.g.*, synthetic chiral stationary phases of Pirkle's type [1]. The enantioselective properties of BSA as a chromatographic chiral selector have been studied almost exclusively after bonding of albumin to silica gel. The unsatisfactory hydrolytic stability of currently available silica gels permits the application only of acidic and neutral mobile phases. Therefore, the properties of chemically bonded albumin acting as a chromatographic chiral selector are not known and have not been exploited over the whole range of pH were high selectivity of chemically bonded albumin may be reached [2,3].

High hydrolytic stability typical of porous organic sorbents is often observed with packings derived from them. For the wide-pore hydroxyethylmethacrylate polymer Separon HEMA the manufacturer guarantees perfect hydrolytic stability at pH 2–12 [4]. Investigations of the influence of temperature on the enantioselectivity of the sorbent obtained by bonding BSA to the matrix Separon HEMA [5] revealed perfect stability of the sorbent Separon HEMA–BSA at high temperatures in mobile phases up to pH 7.5. Hence the stability of this sorbent is

Correspondence to: R. Vespalec, Institute of Analytical Chemistry, Czechoslovak Academy of Sciences, Veveří 97, 611 42 Brno, Czechoslovakia.

* Present address: Department of Chemistry, Technical University, Gorkého 7, 662 38 Brno, Czechoslovakia.

0021-9673/93/$06.00

also assumed to be sufficient for alkaline mobile phases.

This study attention mainly concerned the enantioselectivity of the sorbent Separon HEMA–BSA at pH > 7. The sorption capacity of the sorbent and the lifetime and efficiency of columns filled with the sorbent were also investigated. Experiments were performed in order to be able to differentiate the contribution of the matrix from that of bonded BSA.

EXPERIMENTAL

Two sorbents were used: Separon HEMA 1000–BSA (HEMA–BSA) and Separon HEMA 1000-BIO–BSA (HEMA BIO–BSA) (Tessek, Prague, Czechoslovakia). The sorbents were packed in stainless-steel columns (200 × 4 mm I.D.) and in glass CGC columns (150 × 3.3 mm I.D.) using techniques recommended by the manufacturer for unmodified matrices of Separon HEMA 1000 and Separon HEMA 1000 BIO. For comparative measurements with BSA bonded to the silica gel matrix, a commercial column (150 × 4 mm I.D.) containing the chiral stationary phase Resolvosil was used (Macherey–Nagel, Düren, Germany).

Mobile phase was supplied by an HPP 4001 syringe pump (Laboratory Instruments, Prague, Czechoslovakia). The samples were injected with a Hamilton (Reno, NV, USA) Model 1801 microsyringe or by the sampling valve. A PU 4021 diode-array spectrophotometer (Pye Unicam, Cambridge, UK) or an LCD 254 photometer (Laboratory Instruments) was used for detection. Between measurements (overnight) the columns were protected by a flow of mobile phase (0.1 ml/min) or stored in a refrigerator at 5°C. If the work was interrupted for a longer period, the columns were washed with phosphate buffer (pH 7.45) containing 0.1% (w/v) sodium azide.

Methanol (analytical-reagent grade) for regeneration of the enantioselectivity was distilled. Phosphate buffers of pH 2.2–11.5, at a concentration of 50 mmol/l, occasionally with addition of 3% 1-propanol, were prepared from boiled distilled water. The solutes from various sources and the chemicals employed for preparation of the mobile phase were of analytical-reagent grade. The D- or L-enantiomers of the solutes being separated were identified by injecting the pure D- or L-form.

In all measurements the retention time of the peak maximum was considered as the retention time of the solute peak. The retention volume of water was regarded as the column dead volume.

RESULTS AND DISCUSSION

Selectivity

The selectivity of separation on chemically bonded BSA depends substantially on the pH of the environment. The buffer concentration and low-concentration mobile phase constituents (1-propanol, caprylic acid) especially influence retentions [6]. Therefore, the mobile phase pH was used as the main means for tuning the selectivity. Strong increases in both retention and separation selectivity for tryptophan enantiomers in weakly alkaline mobile phases with increasing pH have been reported [2]. At pH ⩽ 7 dissolved albumin very effectively retains solutes with negative charge [7,8]. For these reasons, we chose D,L-tryptophan, two of its analogues and several representatives of monocarboxylic and dicarboxylic acids as solutes.

The pH dependences of the retention and separation selectivity of D,L-tryptophan and its amphoteric analogues, D,L-hydroxytryptophan and D,L-kynurenine, on HEMA–BSA in the pH range 2–11 are summarized in Fig. 1. The marked increase in retention of the more retained form with respect to that of the less retained form in the neighbourhood of pH 9 is in agreement with the increase in the retention of D,L-tryptophan on a sorbent obtained by binding BSA to agarose [2]. This agreement, together with comparison of the retentions of D,L-tryptophan on the sorbent HEMA–BSA and D,L-tryptophan on the matrix HEMA (Fig. 2), indicates that both the course of the pH dependence of the retention and the separation selectivity of D- and L-enantiomers of tryptophan can be unequivocally ascribed to the bonded albumin. Addition of 1-propanol to the mobile phase reduced the retentions of both D- and L-tryptophan and the enantioselectivity of their separations. The pronounced difference in the retentions of D,L-tryptophan and its hydroxy derivative agrees with the earlier observation that even a relatively small change in the solute molecule can dramatically affect the retention of solutes or even their separation selectivity [9].

The highest separation selectivities in the neigh-

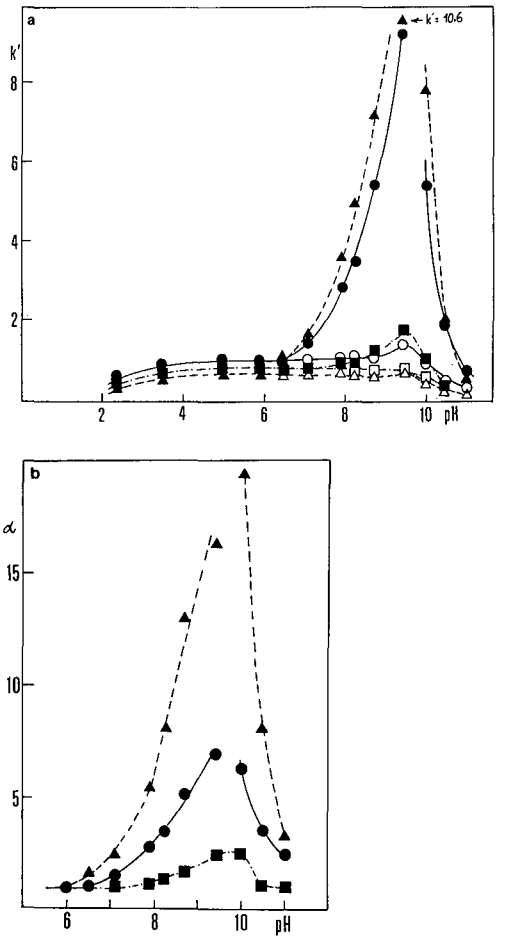

Fig. 1. pH dependence of (a) retention and (b) selectivities of amino acids. (a) ○ = D-Tryptophan; ● = L-tryptophan; △ = D-kynurenine; ▲ = L-kynurenine; □ = D-hydroxytryptophan; ■ = L-hydroxytryptophan. (b) ● = D,L-Tryptophan; ▲ = D,L-kynurenine; ■ = D,L-hydroxytryptophan. Column, Separon HEMA 1000–BSA (200 × 4 mm I.D.); mobile phase, 0.05 mol/l phosphate buffer; flow-rate, F_m = 1 ml/min; amount injected, 5 μl (0.96 mmol/l).

bourhood of pH 9 were found also for the dicarboxylic compounds N-2,4-dinitrophenyl-D,L-glutamic, dansyl-D,L-glutamic and 3-dibenzoyl-D,L-tartaric acids and for the N-benzoyl derivative of D,L-phenylalanine carrying one carboxy group. Only the monocarboxylic D,L-3-indolelactic acid had a sufficient separation selectivity in the neutral and slightly acidic mobile phases also (Figs. 3 and 4).

In measurements requiring slightly alkaline mobile phases (7 < pH < 10) and lasting as long as several weeks, a decrease in the enantioselectivity of

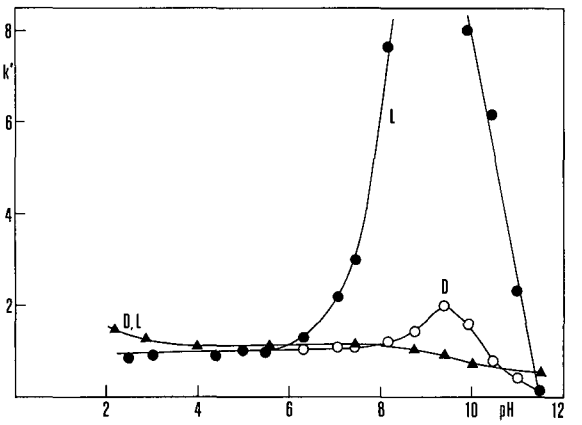

Fig. 2. Comparison of the dependence of the retention of D,L-tryptophan on the mobile phase pH for the sorbents (○, ●) Separon HEMA 1000–BSA and (▲) Separon HEMA 1000. Column, 200 × 4 mm I.D.; mobile phase, 0.05 mol/l phosphate buffer; flow-rate, F_m = 1 ml/min; amount injected, 5 μl (0.96 mmol/l).

D,L-tryptophan separation was observed. The rate of the decrease is strongly pH dependent. At pH 7.0–7.5 the enantioselectivity changed markedly only after several months, whereas at pH 9.5 it decreased

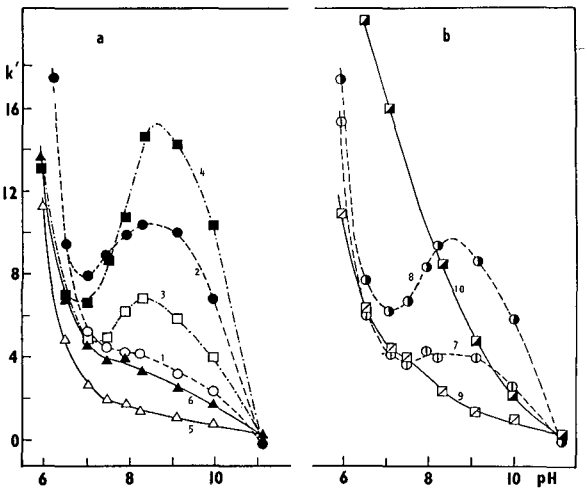

Fig. 3. Dependence of retentions of carboxylic acids on the pH of the mobile phase. Column, Separon HEMA 1000-BIO–BSA, CGC (150 × 3.3 mm I.D.); mobile phase, 0.05 mol/l phosphate buffer + 3% (v/v) 1-propanol. (a) 1, 2 = N-2,4-DNP-D,L-glutamic acid; 3, 4 = 2,3-dibenzoyl-D,L-tartaric acid; 5, 6 = N-benzoyl-D,L-phenylalanine. (b) 7, 8 = Dansyl-D,L-glutamic acid; 9, 10 = D,L-3-indolelactic acid.

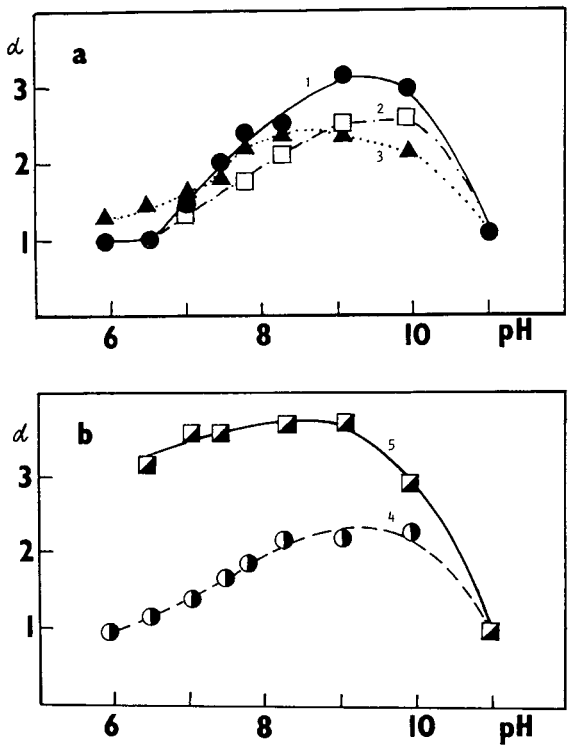

Fig. 4. Dependence of separation selectivity of carboxylic acids. (a) 1 = N-2,4-DNP-D,L-glutamic acid; 2 = 2,3-dibenzoyl-D,L-tartaric acid; 3 = N-benzoyl-D,L-phenylalanine. (b) 4 = Dansyl-D,L-glutamic acid; 5 = D,L-3-indolelactic acid.

markedly after 4 days (Fig. 5). Subsequent washing of the column exposed to pH 9 with mobile phase of pH 7.45 did not improve the enantioselectivity even after 5 days. Treatment with mobile phases of pH < 7 was also ineffective. The decreased enantioselectivity of the bonded albumin for D,L-tryptophan caused by the alkaline mobile phase was restored by washing the column with methanol for 24 h. Methanol acted similarly in restoring the decrease in the enantioselectivity of BSA for tryptophan caused by increased temperature [5].

Immediately after washing of the column with methanol, the enantioselectivity of the bonded BSA for D,L-tryptophan was higher than that of the bonded BSA tested after delivery of the column by the manufacturer (new column). During the separation of D,L-tryptophan in the mobile phase of pH 7.45 on the column treated with methanol, its retention and separation selectivity decreased markedly during the first 24 h. The rate of the decrease of both characteristics decreased with the time of action of the mobile phase pH 7.45. After 4 days the decrease in retention and selectivities caused by 24 h of action was comparable to the measurement error. The retention and selectivity were higher in this "stable" state than those of a new column.

The pH range in which the enantioselectivity of

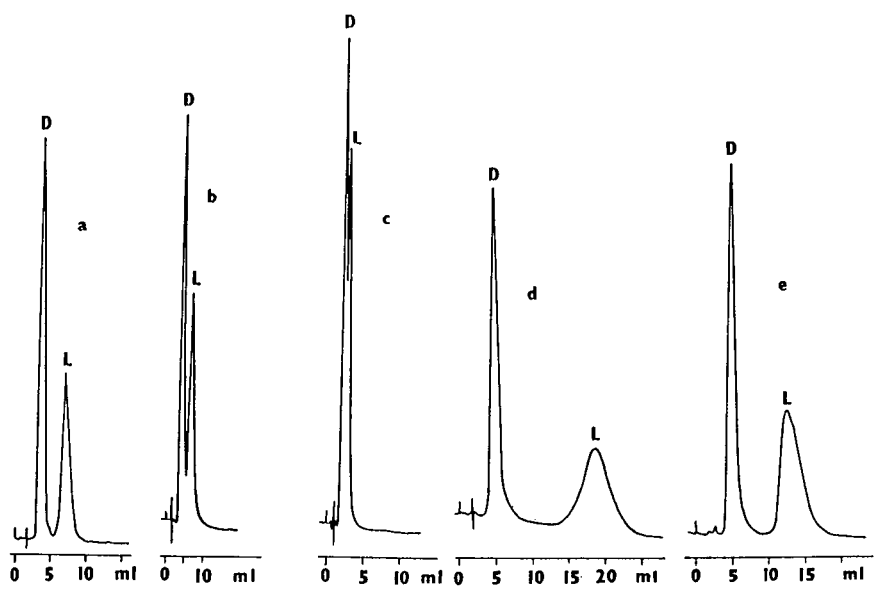

Fig. 5. Decrease in the enantioselectivity of D,L-tryptophan separation caused by pH of the mobile phase > 7 and its regeneration with methanol. Column, Separon HEMA 1000–BSA (250 × 4 mm I.D.); mobile phase, 0.05 mol/l phosphate buffer (pH 7.45); flow-rate, F_m = 1 ml/min; amount injected, 5 μl (0.96 mmol/l). (a) Fresh column; (b) after 6 months in mobile phase of pH 7–8; (c) after 4 days in mobile phase of pH 9.5; (d) immediately after regeneration with methanol; (e) 4 days after methanol-induced regeneration, washed out with mobile phase of pH 7.45.

the column with bonded BSA for D,L-tryptophan separation decreases is identical with that in which albumin in aqueous solution creates a special covalently stabilized conformation labelled the A (aged) form [10,11]. Under the assumption that the chemical binding of albumin to a support does not fully rule out a capability of the bonded molecules to respond to alterations in the liquid environment by changes in spatial arrangement (conformation), one can explain the observed change in the enantioselectivity of D,L-tryptophan separation by the formation of a conformation of the bonded BSA analogous to the A form ("ageing").

For control of the retentions of some types of solutes, 1-propanol and caprylic ions are used. Their influence on the ageing of bonded BSA were tested at pH 8.22 and it was found that 3% (v/v) of 1-propanol accelerates the ageing about twofold. If caprylic acid at a concentration of 5 mmol/l is added to a mobile phase of pH 8.22 containing 3% (v/v) of 1-propanol, after treatment with this mobile phase for 8 days the chemically bonded BSA completely loses its ability to separate D,L-tryptophan. In the same mobile phase without caprylic anions $R_s = 4$ after 8 days. Caprylic anions, therefore, act similarly to 1-propanol or even they exhibit a synergic effect. Such an influence of caprylic anions is surprising as caprylic acid is generally used as an additive stabilizing albumin against changes induced by increased temperature [12–14].

The enantioselectivity of bonded BSA decreased by mobile phase containing 1-propanol or 1-propanol and caprylic anions may be restored by methanol. Similarly to the effect of phosphate buffers of $7 < pH < 10$, these cycles, even if repeated, did not induce irreversible changes or the permanent loss of the enantioselectivity of the sorbent. From the chromatographic point of view, bonded BSA always returned to the same state.

The "ageing" of bonded BSA in alkaline medium and subsequent treatment of the column with methanol did not have the same effect on the separation selectivity of all the solutes applied. The separation selectivity of dicarboxylic acids increased owing to the "ageing", whereas the separation selectivity of monocarboxylic acids decreased (Table I). Because of the action of methanol, the separation selectivity increased for the monocarboxylic acids (similarly as for D,L-tryptophan), whereas it decreased below the initial value for the dicarboxylic acids. No separation at all took place with dibenzoyltartaric acid after the treatment with methanol. When, however, the mobile phase of pH 7.45 was used for conditioning of the column treated with methanol, the enantioselectivity became gradually re-established (Fig. 6).

The experiments on the effect of bonded albumin "ageing" and regeneration of its selectivity by methanol show that in addition to the regulation of the separation enantioselectivity by changing the

TABLE I

EFFECT OF "AGEING" OF THE SORBENT SEPARON HEMA 1000-BIO–BSA IN PHOSPHATE BUFFER (pH 8.22) CONTAINING 3% (v/v) 1-PROPANOL AND ITS REGENERATION WITH METHANOL ON RETENTIONS AND SELECTIVITIES

Column, Separon HEMA 1000-BIO–BSA (150 × 3.3 mm I.D.). Mobile phase, 0.05 mol/l phosphate buffer (pH 7.45) + 3% (v/v) 1-propanol.

Acid	Fresh column		"Aged" column		Regenerated column	
	k'_1	α	k'_1	α	k'_1	α
N-2,4-DNP-D,L-glutamic	4.09	2.00	4.28	2.69	4.33	1.62
Dansyl-D,L-glutamic	3.69	1.80	3.07	2.19	3.92	1.53
2,3-Dibenzoyl-D,L-tartaric	4.94	1.77	3.80	3.35	6.36	1.00
D,L-Indolelactic	3.84	4.19	0.98	2.58	6.55	4.50
N-Benzoyl-D,L-phenylalanine	2.00	1.93	1.70	1.61	2.58	2.20
D,L-Tryptophan[a]	0.78	8.03	0.54	4.59	0.86	9.65

[a] Mobile phase without 1-propanol, pH 7.39.

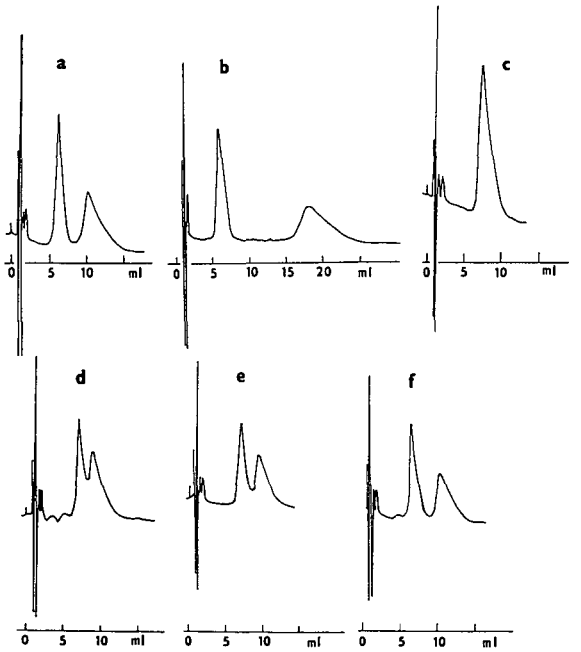

Fig. 6. Separation of 2,3-dibenzoyl-D,L-tartaric acid in 0.05 mol/l phosphate buffer (pH 7.45) with addition of 3% (v/v) of 1-propanol. (a) Fresh column; (b) after "ageing" of the column in mobile phase of pH 8.22 + 3% (v/v) of 1-propanol; (c) 48 h after regeneration of the column; (d) 72 h after regeneration of the column; (e) 96 h after regeneration of the column; (f) 192 h after regeneration of the column. Column, Separon HEMA 1000-BIO–BSA CGC (150 × 3.3 mm I.D.).

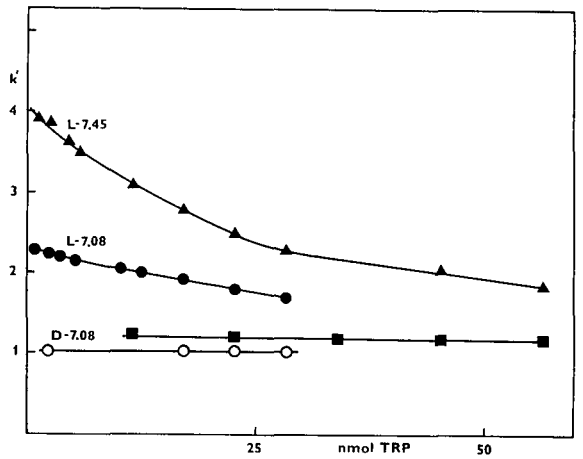

Fig. 7. Dependence of capacity factors on the amount of D,L-tryptophan injected. Sorbent, ■ = Separon HEMA 1000 (pH 7.4); ○, ● = Separon HEMA 1000–BSA (pH 7.08); ▲ = Separon HEMA 1000–BSA (pH 7.45). Mobile phase, 0.05 mol/l phosphate buffer with pH as indicated. ○ = D-Tryptophan; ● = L-tryptophan.

albumin charge by means of the pH of the environment, there exists an additional possibility, probably the influence of the bonded albumin conformation. Our ideas on the role of BSA charge and conformation, permitting a consistent qualitative explanation of the effects and dependences reported here, will be the subject of a separate paper.

Sorption capacity and efficiency

A characteristic feature of analyses on sorbents prepared by binding BSA to a silica gel support is the dependence of the retention volume of the peak maximum and the asymmetry of the peak on the amount injected [1,2]. Similar behaviour was observed using D,L-tryptophan as a solute chromatographed on columns packed with sorbents with BSA bonded to the hydroxyethylmethacrylate matrix (Fig. 7). As can be seen from the comparison with dependences measured on the matrices HEMA and HEMA BIO, the non-linearity and the increase in the non-linearity of the L-isomer with increasing retention must be ascribed to the interactions between the L-isomer and the bonded albumin.

The binding of BSA to the silica gel matrix reduces the efficiency of the silica gel-based columns [15]. Our measurements show a significant decrease in column efficiency caused by the binding of BSA to the HEMA matrix also (Fig. 8). The column efficiency is low also when the linear velocity of the mobile phase is very close to that representing the optimum linear velocity for silica gel-based sorbents. A comparison with Resolvosil (BSA–silica) shows that the efficiency of the silica gel-based sorbent is substantially higher. With a reduced linear velocity below 5, the efficiency of the Resolvosil column for the D-isomer is even better than the efficiency of columns packed with HEMA or HEMA-BIO supports. The efficiency of columns packed with HEMA-BIO–BSA and HEMA–BSA did not differ within the limits of accuracy of the measurements.

The dependences of H/d_p on the reduced linear velocity of the mobile phase for D-tryptophan measured on the Resolvosil and HEMA-BIO–BSA are parallel (Fig. 8). The same holds for the depen-

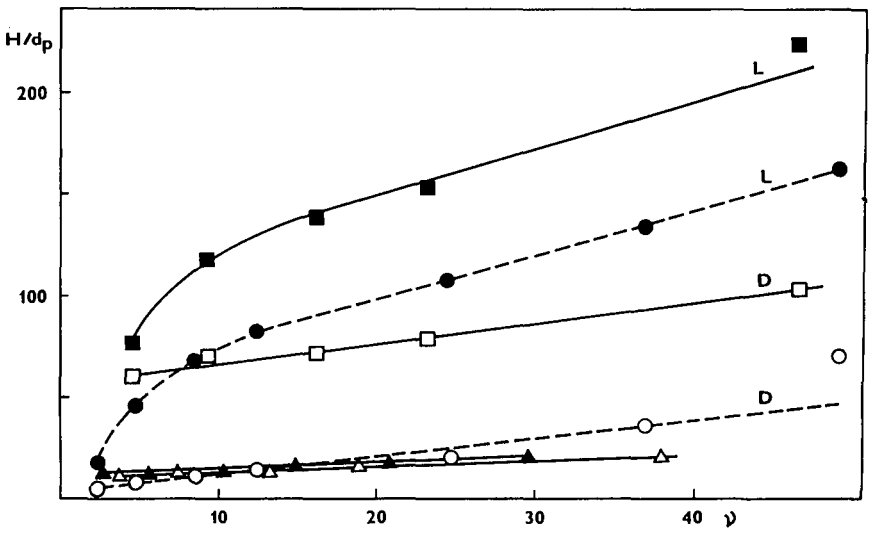

Fig. 8. Dependence of efficiency of D,L-tryptophan separation on the reduced linear flow-rate of the mobile phase. Mobile phase, 0.05 mol/l phosphate buffer (pH 7.45). Column, △ = Separon HEMA 1000; ▲ = Separon HEMA 1000-BIO; □, ■ = Separon HEMA 1000-BIO–BSA; ○, ● = Resolvosil.

dences of L-isomer at reduced velocity $v > 18$. In this range, (for any $v > 18$) AH/d_p measured on the sorbents Resolvosil and HEMA-BIO–BSA for the L-isomer also agrees with AH/d_p for the D-isomer found on the same sorbents. This indicates that the matrix HEMA contributes to the low efficiency of the columns. During efficiency measurements the optimum linear mobile phase velocity for HEMA-based columns was never approached. This suggests that the reduced optimum linear mobile phase velocity of the HEMA matrix may be well below that of the silica gel.

The matrix HEMA gives a sorbent of high hydrolytic stability and lifetime. During running of one of the columns for 18 months no loss of enantioselectivity was found. The pH of the mobile phase varied in the range 2–11 and as much as 5% of 1-propanol was added to the mobile phase. The decreased enantioselectivity was repeatedly restored by washing with methanol. The efficiency of the column decreased by about 30% in the course of this period.

CONCLUSIONS

Comparison of the enantioselectivity, efficiency and sorption capacity of columns packed with sorbents prepared by bonding of BSA to the organic polymeric matrix with those measured on columns packed with the matrix, demonstrated on the example of D,L-trytophan, enabled the influence of bonded BSA and the matrix on the measured dependences and characteristics to be resolved. It has been demonstrated that bonded BSA has a high selectivity for D,L-tryptophan in alkaline medium and that with bonded BSA a high enantioselectivity can be obtained not only for some other amino acids but also for monocarboxylic and dicarboxylic acids. The shape of the pH dependences of the retentions and the separation enantioselectivity was characteristic for each group of compounds. This indicates the dominant influence of ionized functional groups on the enantioselective retention of the solutes.

Changes in separation enantioselectivity induced by long-term action of slightly alkaline mobile phases showed that the influence of pH on the enantioselective properties of chemically bonded albumin is complex. Rapid (immediate) changes are undoubtedly caused by the influence of the pH of the medium on the albumin charge. Slow changes can be explained only as consequences of conformational changes having the same course as with dissolved albumin [11], but probably with a lower rate. The influence of methanol and the following slow changes in both the retentions of different types of compounds and the enantioselectivity of albumin

for these compounds in mobile phases with pH > 7 can be considered to be a consequence of conformational changes also. Experiments explicable only if conformational changes of bonded albumin are considered demonstrate the importance of the conformation of albumin for its action as a chiral selector. There is no reason to presume that conformation will be important only for the enantioselectivity of BSA. On the contrary, it must be assumed that the conformation and conformational variability of any biomacromolecule will be important properties in any analytical applications.

For 1-propanol and caprylic anions as minor components of the mobile phase, it is impossible to establish on the basis of the described experiments whether they affect only the rate of conformational changes or if they have any further influence. However, it has been demonstrated that the dependence of the retentions of solutes on the volume injected and the low efficiency of the columns are inseparably connected with bonded BSA.

There are three possibilities for the construction of the BSA-bonded sorbents having both an efficiency comparable to that of present-day silica gel sorbents and acceptable durability up to pH 10: (i) to improve the mass transport in the particles of the matrix HEMA, (ii) to select a more suitable organic matrix than HEMA and (iii) to test the durability of sorbents prepared by bonding BSA on the matrix from high-purity silica gel; such a matrix provides reversed-phase sorbents of remarkable stability in mobile phases up to pH 9 [16]. An interesting alternative is particles of alumina protected by a cross-linked polymer [17].

REFERENCES

1 J. Vindevogel, J. van Dijck and M. Verzele, *J. Chromatogr.*, 447 (1988) 297.
2 K. K. Stewart and R. F. Doherty, *Proc. Natl. Acad. Sci. U.S.A.*, 70 (1973) 2850.
3 S. Allenmark and B. Bomgren, *J. Chromatogr.*, 237 (1982) 473.
4 *Catalogue of Sorbents for LC*, Tessek, Prague, 1987.
5 Z. Šimek and R. Vespalec, *J. Chromatogr.*, 543 (1991) 475.
6 S. Andersson and S. Allenmark, *J. Liq. Chromatogr.*, 12 (1989) 345.
7 S. Allenmark and S. Andersson, *J. Chromatogr.*, 351 (1986) 231.
8 S. Allenmark, B. Bomgren and H. Borén, *J. Chromatogr.*, 316 (1984) 617.
9 J. Hermansson and G. Schill, in M. Zief and L. J. Crane (Editors), *Chromatographic Chiral Separations*, Marcel Dekker, New York, 1988, pp. 259–265.
10 S. Tormod, *Acta Univ. Ups.*, No. 21 (1985) 58.
11 J. F. Foster, in V. Rosenoer, M. Oratz and M. Rothshild (Editors), *Albumin Structure, Function and Uses*, Pergamon Press, New York, 1977, pp. 53–84.
12 H. Hock and A. Chamunin, *Arch. Biochem. Biophys.*, 51 (1954) 271.
13 W. Schneider, H. Leferre, H. Friedler and L. J. McCarty, *Blut*, 30 (1975) 121.
14 M. W. Yu and J. S. Finlayson, *Vox Sang.*, 47 (1984) 28.
15 W. Lindner and C. Pettersson, in I. W. Wainer (Editor), *LC in Pharmaceutical Development*, Aster, Springfield, OR, 1985, p. 99.
16 *Prospect Inertsil, Packed Columns for HPLC*, GL Science, Tokyo, 1992.
17 R. E. Majors, *LC · GC Int.*, 4, No. 4 (1992) 12.

Journal of Chromatography, 629 (1993) 161–168
Elsevier Science Publishers B.V., Amsterdam

CHROM. 24 631

Stability of immunoadsorbents comprising antibody fragments

Comparison of Fv fragments and single-chain Fv fragments

M. J. Berry and J. J. Pierce

Immunology Department, Unilever Research, Colworth House, Sharnbrook, Bedfordshire MK44 1LQ (UK)

(First received July 10th, 1992; revised manuscript received September 17th, 1992)

ABSTRACT

Immunoadsorbents comprising Fv fragments specific for hen egg lysozyme were used to recover the enzyme from a 20-fold excess of bovine albumin. We designed automatic equipment to run this model purification system for 100 cycles non-stop and monitored the deterioration of the immunoadsorbents during the cycling procedure. Only minor losses (approximately 25%) in the immunoadsorbents' capacity were detected; this correlated well with ligand loss (measured by enzyme-linked immunosorbent assay) which was approximately 0.2% per cycle. A surprising finding was that the use of "single-chain" Fv fragments conferred only a minor advantage with respect to stability of the immunoadsorbents.

INTRODUCTION

A new generation of antibody fragments has brought an exciting opportunity to the technique of immunoaffinity chromatography. We have recently reported the use of Fv fragments as ligands [1,2]; these reagents are readily produced as recombinant proteins in *E. coli* [3,4]. Another group has reported the use of even smaller immunoreagents or "mini-antibodies" [5,6]; these reagents may be produced completely chemically by solid-phase peptide synthesis. The advantages of these antibody fragments compared with conventional monoclonal antibodies include: lower production costs, higher capacity for antigen on a weight for weight basis, better penetration in small-bore separation media. We have discussed these advantages in more detail elsewhere [1,2]; we have also discussed the relative merits of the different antibody fragments currently available [2]. We believe that the general availability of these new antibody fragments will broaden the use of immunoaffinity chromatography, particularly in industrial processes. However, to achieve this wider acceptability, affinity media comprising antibody fragments will need to be sufficiently stable to retain activity and specificity over many purification cycles.

The deterioration of affinity adsorbents during prolonged use may be caused by inactivation of the ligand, fouling, or ligand leakage. This deterioration has often been modelled by investigating one of these component causes in isolation; most work has been done on ligand leakage [7–10]. However, it is not always clear which of these route causes will contribute most to the deterioration of a particular adsorbent. Therefore, we took the view that the

Correspondence to: M. J. Berry, Immunology Department, Unilever Research, Colworth House, Sharnbrook, Bedfordshire MK44 1LQ, UK.

0021-9673/93/$06.00

most convincing evaluation of our Fv immunoadsorbents would be to measure their stability directly by monitoring changes in performance after repeated cycles of recovering target analyte from feedstock. Previous reporting of this type of data for the stability of affinity adsorbents has often been anecdotal [11–14]. In this study, we set out to evaluate the stability of affinity media comprising 4% agarose and Fv fragments specific for hen-egg lysozyme by monitoring the deterioration in the performance of these immunoadsorbents after being subjected to 100 cycles of a model purification system: the recovery of hen-egg lysozyme from a 20-fold excess of bovine albumin. The performance of the immunoadsorbents was measured against three criteria: capacity for target antigen, the sharpness of breakthrough upon reaching capacity, and the purity of product (*i.e.*, lysozyme) recovered. We also determined ligand leakage (*i.e.*, the presence of Fv in washings) by enzyme-linked immunosorbent assay (ELISA) and correlated these results with observed changes in capacity for antigen. This would allow us to estimate the relative contribution made by ligand leakage to the deterioration of immunoadsorbent performance and therefore also (by inference) the relative contribution made by inactivation of ligand.

A particular objective of this study was to compare and contrast the re-use potential of Fv antibody fragments with that of "single-chain" antibody fragments, or scFv. [In Fv fragments, the two component chains of Fv (V_H and V_L) are held together, non-covalently, by three pairs of hydrophobic patches [15]; whereas in scFv fragments, V_H and V_L are also covalently linked by a short hydrophilic peptide chain [16,17]. For a fuller description of Fv structure and terminology see refs. 1 and 2]. Since Fv fragments are non-covalently associated, they may be expected to have poor re-use potential, especially after treatment with the harsh elution buffers typically used in immunoaffinity chromatography. These buffers are, of course, designed to disrupt the non-covalent interactions between antibodies and antigens and therefore they may also disrupt the, not dissimilar, non-covalent interaction between V_H and V_L. However, with scFv, even if V_H and V_L are temporarily dissociated on treatment with elution buffer, the linker peptide should keep V_H and V_L in close proximity thereby enabling reassembly when the column is re-equilibrated in a mild buffer (such as physiological strength saline, pH 7).

EXPERIMENTAL

Production of antibody fragments

A vector encoding the Fv fragment of a parent antibody specific for hen-egg lysozyme (the "D.1.3" antibody [18]) and tagged at the C-terminus of its V_L with the *myc* peptide [19] was obtained from Dr. G. Winter (MRC, Cambridge, UK [20]). A vector encoding an analogous scFv fragment with a peptide linker sequence of $(Gly–Gly–Gly–Gly–Ser)_3$ [17] and tagged at the C-terminus of its V_L with the *myc* peptide was also obtained from Dr. G. Winter. (We have previously found that the *myc* peptide serves as a useful linking group for covalently coupling antibody fragments to solid phases without loosing their binding activity [21,22].

The vectors were transformed into *E.coli* (strain JM109) and grown in cultured medium according to the method of Ward *et al.* [20]. Secreted Fv fragments were recovered from the medium by affinity chromatography on lysozyme–Sepharose [20]. Hen-egg lysozyme was obtained from Sigma (Poole, UK) and Sepharose from Pharmacia (Uppsala, Sweden).

Preparation of immunoadsorbents

An homogeneous preparation of antibody fragment (*ca.* 4 mg) at a concentration of 0.5 mg/ml was dialysed into coupling buffer [0.1 *M* $NaHCO_3$ (BDH, Poole, UK)–0.5 *M* NaCl (BDH) (pH 8.3)] and immobilised on *ca.* 1 g of cyanogen bromide-activated Sepharose 4B (Pharmacia) according to that manufacturer's instructions. One immunoadsorbent was made with Fv anti-lysozyme and one with scFv anti-lysozyme. Unreacted cyanogen bromide groups were blocked by washing overnight in 1 *M* ethanolamine pH 8 at 4°C according to manufacturer's instructions. The efficiency of ligand coupling was determined by measuring the absorbance of the ligand solution at 280 nm before and after coupling. [The orientation of the ligands was checked by estimating the specific activity of the immobilized Fv (*i.e.*, the % of Fv molecules in an active orientation/conformation). This was done by estimating the capacity of the immunoadsorbents for antigen and comparing with the amount of im-

mobilised Fv on a molar basis.] A "blank" column was also prepared in parallel for use as a negative control. This was 1 g of the same batch of activated Sepharose 4B which was subjected to the same coupling protocol but to which no immunoligand (*i.e.*, Fv) was added.

Model purification system

A 1-g amount of each immunoadsorbent was conditioned in PBSA (0.01 *M* Na_2HPO_4/NaH_2PO_4–0.15 *M* NaCl, pH 7 with 0.1% sodium azide as a bacteriostat) and then packed in a glass column (Pharmacia C16). Each column was loaded with a feedstock of 1 mg/ml bovine albumin (Sigma) and 50 μg/ml hen-egg lysozyme made up in PBSA. (A 50 μg/ml solution of this lysozyme preparation had an activity of approximately 2550 I.U./ml) This feedstock was loaded until a stable breakthrough was reached; the columns were then washed back to baseline with PBSA. Flow-rates were kept at 150 ml/h throughout the experiments. Bound protein was recovered by eluting with desorption buffer (4 *M* $MgCl_2$) and dialysing the peak into PBSA. The columns were then re-equilibrated in PBSA. Chromatograms were drawn by monitoring A_{280} on-line using a Uvicord monitor linked to a chart recorder (Pharmacia).

Testing of model purification system

Lysozyme activity was monitored across the chromatogram profile by assaying fractions using a suspension of Micrococcus (Sigma) according to that manufacturer's instructions. The 4 *M* $MgCl_2$ fraction recovered from the immunoadsorbents was analysed by sodium dodecyl sulphate-polyacrylamide gel electrophoresis (SDS-PAGE) using a Pharmacia homogeneous 20 Phastgel. (For a fuller description see ref. 2.)

We tested the specificity of our purification model by three control experiments. Firstly, a feedstock of 50 μg/ml lysozyme only was loaded onto the immunoadsorbents and eluted as above. Secondly, the albumin/lysozyme feedstock was loaded onto the blank column and eluted as above. Thirdly, a feedstock of 1 mg/ml bovine albumin and 50 μg/ml cytochrome *c* (Sigma) was loaded onto the immunoadsorbents and eluted as above.

Continuous cycling of purification model

We designed automated equipment to run our model purification system for 100 cycles non-stop. The automated equipment was custom-built by a local subsidiary of Lee Products (Westbrook, CT, USA). In brief, the feedstock and elution buffer (4 *M* $MgCl_2$) were pumped onto the column from reservoirs as controlled by two miniature solenoid valves with zero dead volumes (Lee LFYA). These valves were placed on-line between the reservoir containing running buffer (PBSA) and the peristaltic pump so that when neither valve was activated PBSA pumped through the system. The timings of valve activation were pre-set by a controller comprising a microprocessor. At the end of a complete purification cycle another identical purification cycle was started automatically. Sufficient stocks of PBSA, feedstock and elution buffer were made up to last for 100 purification cycles. These were degassed and sterile filtered (Gelman 0.2 μm); all glassware had been sterilised by autoclaving.

A toal of 100 purification cycles using the albumin/lysozyme feedstock was carried out on each immunoadsorbent and the blank column. The whole procedure was repeated for both Fv and scFv using freshly prepared immunoadsorbents. A total of 100 purification cycles using the albumin/cytochrome *c* feedstock was also carried out on the immunoadsorbents.

Analysis of immunoadsorbent deterioration

Chromatograms were drawn for all 100 purification cycles; these were compared for evidence of gradual changes in peak height or breakthrough shape. For cycle 1 and cycle 100, lysozyme activity was monitored across the chromatogram; these profiles were compared for evidence of immunoadsorbent deterioration. For cycle 1 and cycle 100, the purity of the lysozyme fraction recovered from the immunoadsorbents was analysed by SDS-PAGE. The findings were examined for evidence in immunoadsorbent deterioration.

Measuring ligand leakage

Ligand leakage (*i.e.*, the presence of Fv or scFv in washings) was determined by ELISA. The solid phase used in the ELISA system was a specially designed nylon peg [23] which dipped into the wells of standard microtitre plates. Pegs were sensitised with

lysozyme at 50 μg/ml by coupling with glutaraldehyde [24]. Samples of washings from columns (200 μl) were added to the wells of a microtitre plate and wells plus pegs were incubated for 1 h at room temperature. The pegs were removed and washed with distilled water, then incubated for a further hour with 200 μl of a 1:5000 dilution of a rabbit serum specific for Fv anti-lysozyme [2]. The pegs were washed again and then incubated for 1 h with 200 μl of a 1:4000 dilution of conjugate [alkaline phosphatase-labelled goat anti-rabbit (Sigma)]. The pegs were washed again and then incubated with 200 μl of substrate solution (*p*-nitrophenyl phosphate, 2 mg/ml, in 1.0 *M* diethanolamine, pH 9.8) for approximately 30 min at room temperature. The pegs were then removed from the solution, and the optical density (at 410 nm) of the solutions was measured with an ELISA reader (Dynatech).

The assay for Fv and scFv was calibrated each time by drawing a standard curve with a carefully prepared and characterised set of Fv anti-lysozyme standards. Fv and scFv gave an equally strong signal in the assay. The assay was sensitive down to a level of 0.01 μg/ml (results not shown).

Since the assay works by capturing Fv with immobilised lysozyme, free lysozyme in solution interferes with the assay. Consequently, the assay could not be used directly to measure the presence of Fv across chromatogram profiles. Instead, we eluted immunoadsorbents in turn with each of the two buffers used in this study (PBSA and 4 *M* $MgCl_2$) in the absence of lysozyme and assayed the washings for Fv (in the case of 4 *M* $MgCl_2$ this was after dialysis into PBSA). We did this analysis immediately after cycle 1 and cycle 100 for both immunoadsorbents and then superimposed the data on the chromatogram profile: the assumption being that leakage during the previous cycle will have been similar.

RESULTS

Preparation of immunoadsorbents

The efficiency of ligand coupling was found to be between 80% and 90%. The specific activity of the immobilised ligand was found to be between 50% and 60%. Full details are given in Table I.

TABLE I

SPECIFIC ACTIVITY OF IMMOBILISED LIGANDS

The orientation of immobilised ligand was checked by determining the specific activity of Fv. This was done by comparing the immunoadsorbents' capacity for antigen with the amount of immobilised Fv on a molar basis (assuming molecular weights of 25 kilodalton for Fv and 14.4 kilodalton for lysozyme). The capacity for antigen was estimated from the position of breakthrough in Fig. 1 (for example, the capacity of the Fv-immunoadsorbent at cycle 1 was approximately 24 ml × 50 μg/ml = 1.2 mg). The amount of ligand immobilised was determined by measuring the absorbance of the ligand solution at 280 nm before and after coupling.

Parameters	Fv	scFv
Ligand used	4 mg	4 mg
Ligand immobilised	3.6 mg	3.2 mg
Antigen capacity	1.2 mg	1.0 mg
Specific activity	58%	55%

Testing of model purification system

When the albumin/lysozyme feedstock was loaded onto the immunoadsorbents, a breakthrough curve developed after about 20–25 ml which correlated with the first appearance of lysozyme activity in washings (Fig. 1A and C). The 4 *M* $MgCl_2$ peaks recovered from the immunoadsorbents were found to be homogeneous lysozyme (by analysis with SDS-PAGE). The peak recovered from the immunoadsorbent comprising Fv is shown in Fig. 2.

When the lysozyme (only) feedstock was loaded onto the immunoadsorbents, a breakthrough curve developed in the same position and the same amount of protein was recovered on elution with 4 *M* $MgCl_2$ (chromatogram not shown).

When the albumin/lysozyme feedstock was loaded onto the "blank" column, a breakthrough curve did not develop; no protein was eluted with 4 *M* $MgCl_2$ (see Fig. 1E).

When the albumin/cytochrome *c* feedstock was loaded onto the immunoadsorbents, a breakthrough curve did not develop; no protein was eluted with 4 *M* $MgCl_2$ (chromatogram not shown).

Changes in capacity/activity of immunoadsorbents over 100 purification cycles

The immunoadsorbent comprising Fv developed a slightly shallower and earlier breakthrough as the cycling procedure progressed. Also, the peak eluted

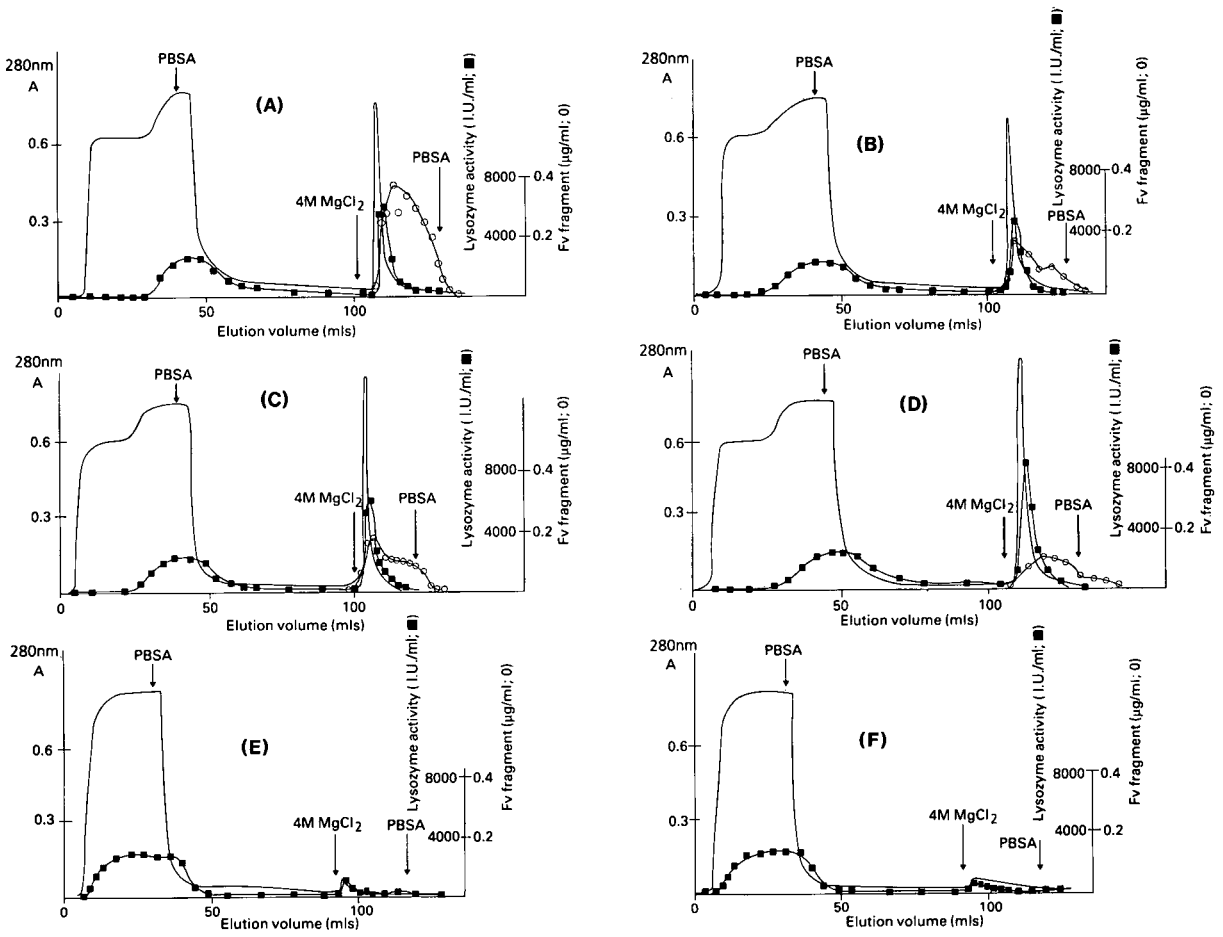

Fig. 1. Changes in immunoadsorbents' performance after repeated recovery of lysozyme from a 20-fold excess of albumin: comparison of chromatograms. (A) Fv Sepharose after 1 cycle. (B) Fv Sepharose after 100 cycles. (C) scFv Sepharose after 1 cycle (D) scFv Sepharose after 100 cycles. (E) "Blank" Sepharose (*i.e.*, no immunoligand coupled) after 1 cycle. (F) Blank Sepharose after 100 cycles. Absorbance at 280 nm (———) was measured on line; (■) lysozyme activity and (○) ligand (*i.e.*, Fv or scFv) leakage were monitored by assaying fractions.

with 4 *M* $MgCl_2$ was about 25% smaller by cycle 100 (see Fig. 1A and B). For the immunoadsorbent comprising scFv, the breakthrough curve did not become shallower during the cycling procedure. Furthermore, the peak eluted with 4 *M* $MgCl_2$ was about 25% larger for cycle 100 than cycle 1 (see Fig. 1C and D). Table II details the capacity and recovery efficiency of each column at cycle 1 and cycle 100.

Results from the repeat experiments were essentially the same in all respects.

Changes in specificity of immunoadsorbents over 100 purification cycles

There was not a significant contamination of albumin in the lysozyme recovered from the immunoadsorbents even after 100 cycles (see Fig. 2). There was not a significant binding of protein from the albumin/lysozyme feedstock to the blank column even after 100 cycles (see Fig. 1F). There was not a significant binding of protein from the albumin/cytochrome *c* feedstock to the immunoadsorbents even after 100 cycles (results not shown).

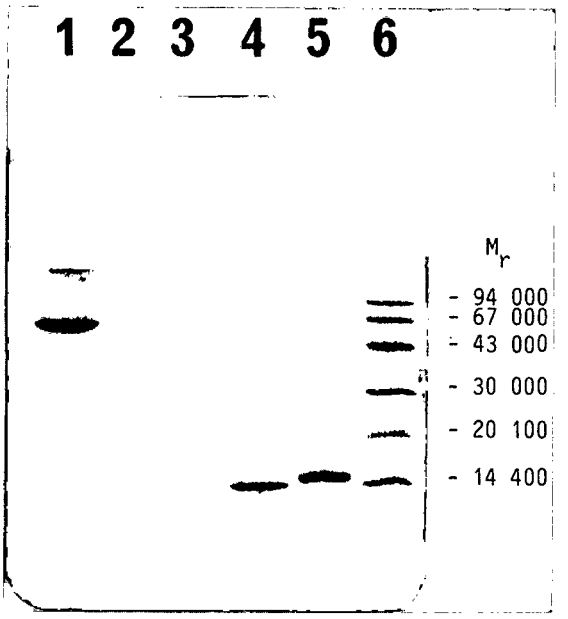

Fig. 2. SDS-PAGE analysis of separation achieved with Fv Sepharose immunoadsorbent. Lanes: 1 = albumin/lysozyme feedstock; 2 = lysozyme recovered after 100 cycles; 3 = lysozyme recovered after 1 cycle; 4 = Fv*myc* anti-lysozyme marker; 5 = lysozyme marker; 6 = Pharmacia low-molecular-weight standards (94 000, 67 000, 43 000, 30 000, 20 100, 14 400 dalton). (Fv*myc* anti-lysozyme migrates to a single band due to the near identical molecular weights of its two component chains, V_H and V_L *myc*. The presence of both V_H and V_L*myc* was confirmed by Western blot analysis with V_H-specific and *myc*-specific immunoreagents. Furthermore, *myc* can be selectively removed from Fv*myc* by protease-activitiy with the result that 2 bands are detected by SDS-PAGE [27])

Ligand leakage

Fv fragments were not detectable in washings when the immunoadsorbents were eluted with PBSA. In contrast, Fv was detectable in washings when the immunoadsorbents were eluted with 4 *M* $MgCl_2$. Ligand leakage was highest as the $MgCl_2$ front passed through the immunoadsorbents and continued at measurable levels while $MgCl_2$ was being eluted. Ligand leakage returned to baseline when $MgCl_2$ was cleared from the immunoadsorbents by elution with PBSA (see Fig. 1A–D).

Ligand leakage was approximately twice as high from immunoadsorbents comprising Fv compared with immunoadsorbents comprising scFv. For both immunoadsorbents, ligand leakage had reduced significantly by cycle 100 (about two-fold) but was still readily detectable by the ELISA (see Fig. 1A–D).

In general ligand leakage was very low. The highest level of ligand detected in washings throughout the study was 0.4 μg/ml (for cycle 1 of the immunoadsorbent comprising Fv, see Fig. 1A). The lysozyme peak fraction from this cycle contained lysozyme at approximately 100 μg/ml; therefore leaked ligand in this fraction represents a contamination of 0.4%. At the other end of the spectrum, the lowest level of ligand leakage detected throughout the study was 0.1 μg/ml (for cycle 100 of the immunoadsorbent comprising scFv). In this case, leaked ligand represents a contamination of about 0.1% in the lysozyme peak fraction.

DISCUSSION

In this study, we used a model system of recovering hen lysozyme from a 20-fold excess of bovine albumin using immunoadsorbents comprising 4% agarose and Fv fragments specific for hen-egg lysozyme. We confirmed that binding of lysozyme to the

TABLE II

CAPACITY AND RECOVERY EFFICIENCY OF IMMUNOADSORBENTS

The amount of lysozyme bound was estimated from the position of breakthrough in Fig. 1 (for example the amount of lysozyme which bound the Fv immunoadsorbent during cycle 1 was approximately 24 ml × 2550 I.U./ml = 61 000 I.U.). The amount of lysozyme which eluted with 4 *M* $MgCl_2$ was determined by direct measurement of activity in this fraction after dialysis. (All results are expressed as I.U. · 1000). The recovery efficiency for each column was calculated as a% of these two figures.

Ligand	Cycle	Lysozyme bound	Lysozyme eluted	Recovery efficiency (%)
Fv	1	61	37	61
Fv	100	46	27	59
scFv	1	51	39	76
scFv	100	64	49	76

immunoadsorbents required specific interaction between Fv and its antigen by three control experiments. Firstly, lysozyme bound to the immunoadsorbents regardless of whether albumin was present or not. Secondly, lysozyme did not bind to a blank column (*i.e.* agarose with no Fv attached). Thirdly, cytochrome *c* (a protein of similar size and charge to lysozyme) did not bind the immunoadsorbents. Having validated our model, we used it as a tool for investigating the stability of the immunoadsorbents during repeated cycles of loading feedstock and eluting product.

We have found that immunoadsorbents comprising scFv can be re-used for 100 cycles without a significant loss of capacity for target antigen; in fact the scFv immunoadsorbent in our model system appeared to have an increased capacity (*ca.* 25%) for antigen after 100 cycles compared with the first cycle. This seemingly anomalous result may be explained as follows: we have previously measured the recovery of lysozyme protein from an Fv immunoadsorbent during a single purification cycle to be 75–80% [1]; therefore if the residual 20–25% of lysozyme protein were to accumulate on the immunoadsorbent cycle upon cycle, the immunoadsorbent would be irreversibly saturated after 5 cycles. However, since we have found that immunoadsorbents continue to bind and elute target antigen, even after 100 cycles, it is clear that this cumulative binding does not occur. Moreover, it is our opinion that during repeated cycling, there was a degree of randomness in the precise amount of lysozyme that was eluted at the end of each cycle and that a small proportion of the lysozyme eluted may have bound the column one or more cycles previously.

We also made the surprising finding that immunoadsorbents comprising "conventional" Fv ligands (*i.e.*, with non-covalently associated V_H and V_L chains) are also remarkably stable to repeated cycling; the Fv immunoadsorbent in our model system did show a detectable capacity loss over 100 cycles but only about 25%. There may be several reasons for this unexpected stability. Firstly, the Fv derived from D.1.3 is known to have a very high binding constant (approximately $10^{10}/M$) for association of its two component polypeptide chains, V_H and V_L [25]. This is significantly higher than for many other Fv fragments [25]. Secondly, the major mechanism for V_H and V_L association is the mutual attraction of three pairs of hydrophobic patches on the two chains [15]. Therefore, an elution buffer with high ionic strength (such as 4 *M* $MgCl_2$) would be expected to promote association. Thirdly, Fv association may be stabilised by immobilisation, on agarose, possibly because of multi-site attachment. Whatever the reason, Fv remains intact over 100 cycles in our model system without the need for a peptide linker between V_H and V_L.

The amount of ligand leakage determined by ELISA correlated well with the observed loss of the immunoadsorbents' capacity over 100 cycles. For example, the Fv immunoadsorbent was found to leak ligand at a concentration of 0.4 μg/ml on elution with 4 *M* $MgCl_2$ during cycle 1; therefore an elution volume of 20 ml would remove 8 μg of Fv from the column (this represents 0.2% of the total Fv on the column). By cycle 100, ligand leakage had dropped to 0.2 μg/ml; therefore about 0.1% of the total Fv would be lost. Taking an average of these results, 100 cycles would be expected to result in a capacity loss of about 15% which would account for a large proportion of the 25% capacity loss measured experimentally. Another correlation between loss of immunoadsorbent capacity and ligand leakage was presented by the finding that Fv immunoadsorbents had a significantly higher capacity loss than scFv immunoadsorbents and that they were also found to leak more ligand by independent experiment. Taking these two correlations together, we conclude that ligand leakage made a major contribution to immunoadsorbent deterioration in this study.

A disappointing finding was that the efficiency of recovering active lysozyme from the Fv immunoadsorbents was in the order of 60%. Furthermore, it is unclear why this was lower than the recovery efficiency of the scFv immunoadsorbents which was in the order of 75%. However, we do not think that these results detract from our key findings about the stability of immobilised Fv and scFv.

Once the production of Fv fragments has been optimised in *E. coli*, they may be available from about US$ 30/g, a cost which has been achieved for other recombinant proteins in this organism. Since immunoadsorbents comprising Fv can be used for (at least) 100 cycles, the contributory cost of Fv fragments towards producing 1 g of target antigen would be in the order of 60 cents (assuming a target

antigen of similar molecular weight and a specific activity of 50% for immobilised Fv). This cost is very minor compared with labour costs and buffer costs [26]. Consequently, we conclude that the cost of immunoligand, often cited as a reason for not using immunoaffinity chromatography at process-scale, is no longer restrictive.

REFERENCES

1 M. J. Berry, J. Davies, C. G. Smith and I. Smith, *J. Chromatogr.*, 587 (1991) 161.
2 M. J. Berry and J. Davies, *J. Chromatogr*, 597 (1992) 239.
3 A. Skerra and A. Pluckthun, *Science (Washington, D.C.)*, 240 (1988) 1038.
4 A. Skerra, I. Pfitzinger and A. Pluckthun, *Biotechnology*, 9 (1991) 273.
5 G. W. Welling, T. Geurts, J. van Gorkum, R. A. Damhof, J. W. Drijfhout, W. Bloemhoff and S. Welling-Wester, *J. Chromatogr.*, 512 (1990) 337.
6 G. W. Welling, J. van Gorkum, R. A. Damhof, J. W. Drijfhout, W. Bloemhoff and S. Welling-Wester, *J. Chromatogr.*, 548 (1991) 235.
7 G. W. Jack and H. E. Wade, *TibTech*, 5 (1987) 91.
8 J. Tharakan, D. Strickland, W. Burgess, W. N. Drohanand D. B. Clark, *Vox Sang*, 58 (1990) 21.
9 J.-C. Janson, *TibTech*, 2 (1984) 31.
10 J. W. Goding, *J. Immunol. Methods*, 20 (1978) 241.
11 G. I. Tesser, H.-U. Fisch and R. Schwyzer, *FEBS Lett.*, 23 (1972) 56.
12 M. Wilchek, *FEBS Lett.*, 33 (1973) 70.
13 A. Lihme, C. Schafer-Nielson, K. P. Larson and K. G. Midler, *J. Chromatogr*, 376 (1986) 299.
14 K. Jones, *LC·GC Int.*, 4 (1991) 32.
15 C. Chothia, J. Novotny, R. Bruccoleri and M. Karplus, *J. Mol Biol.*, 186 (1985) 651.
16 R. E. Bird, K. D. Hardman, J. W. Jacobson, S. Johnson, M. Kaufman, S. M. Lee, T. Lee, S. H. Pope, G. S. Riordam and M. Whitlow, *Science (Washington, D.C.)*, 242 (1988) 424.
17 R. Glockshuber, M. Malia, I. Pfitzinger and A. Pluckthun, *Biochemistry*, 29 (1990) 1362.
18 A. G. Amit, R. A. Mariuzza, S. E. Phillipos and R. J. Poljak, *Science (Washington, D.C.)*, 233 (1986) 747.
19 S. Munro and H. Pelham, *Cell*, 46 (1986) 291.
20 E. S. Ward, D. Gussow, A. D. Griffiths, P. T. Jones and G. Winter, *Nature (London)*, 341 (1989) 544.
21 M. J. Berry, P. J. Davis, M. E. Verhoeyen and R. F. J. de Winter, *Eur. Pat. Appl.*, PN 0 434 317 A1 (1990).
22 P. J. Davis, M. E. Verhoeyen and R. F. J. de Winter, *Internat. Pat. Appl.*, PN WO 91/08482 (1991).
23 P. J. Davis, M. J. Doherty and P. Porter, *Protides Biol. Fluids*, 30th (1983) 543.
24 D. J. Inman and W. E. Hornby, *Biochem. J.*, 129 (1972) 255.
25 G. Winter, *Personal Communication*, 1992.
26 J. E. Porterand M. R. Ladish, *Biotech. Bioeng.*, 39 (1992) 717.
27 M. J. Berry, S. Eida and J. J. Pierce, unpublished results.

Journal of Chromatography, 629 (1993) 169–179
Elsevier Science Publishers B.V., Amsterdam

CHROM. 24 638

High-performance liquid chromatographic enantioseparation of glycyl di- and tripeptides on native cyclodextrin bonded phases

Mechanistic considerations

J. Zukowski, M. Pawlowska, M. Nagatkina and D. W. Armstrong

Department of Chemistry, University of Missouri-Rolla, 142 Schrenk Hall, Rolla, MO 65401-0249 (USA)

(First received July 16th, 1992; revised manuscript received September 1st, 1992)

ABSTRACT

Di- and tripeptides containing at least one glycine moiety were separated into enantiomers on α-, β- and γ-cyclodextrin bonded phases after their precolumn derivatization with 9-fluorenylmethyl chloroformate (FMOC-Cl). It is shown that the choice of a suitable cyclodextrin bonded phase used with a nonaqueous polar mobile phase offers a wide range of possibilities to optimize enantioselectivity. Use of the FMOC derivative greatly enhances sensitivity, stability and enantioselectivity.

It is postulated that under reversed-phase conditions the inclusion complex formation between the hydrophobic aromatic part of the FMOC-functionalized peptides and non-polar cyclodextrin cavity interior is the major factor contributing to retention. However, under these conditions there seems to be insufficient interaction between the hydrophilic peptide chain and cyclodextrin hydroxyls. Hence no chiral recognition and enantiomeric separation is observed. In systems operating with polar organic mobile phases the inclusion complex is suppressed as the cyclodextrin cavity is largely occupied by the mobile phase. The enantioselectivity observed is caused by hydrogen bonding between peptide chain and the hydroxyl groups at the mouth of the cyclodextrin. The stereospecific interactions depend very strongly on the cyclodextrin size, the length of the peptide chain and the mobile phase composition.

INTRODUCTION

As an extension of prior work [1], we report the separation of enantiomeric peptides having a glycine moiety in their structures. Several small peptides are known to show significant biological activity. Many of them are used as substrates in the study of transport, hydrolysis and other processes connected with absorption of protein digestion products [2,3]. Others may be precursors in the synthesis of larger peptides. All of these small peptides (except those bearing only glycine moieties) are optically active. Therefore, a technique for the easy and sensitive determination of enantiomeric purity of peptides can be useful.

Previously, several studies concerning the resolution of enantiomeric dipeptides using HPLC have been reported [4–6]. Amino acids and small peptides are not easy compounds to detect and elute. Often, these polar compounds require non-traditional mobile phases and detection techniques [7,8]. Frequently amino acids and peptides are derivatized in order to make them more suitable for chromatographic separation and/or detection. Generally the derivatizing group is a highly absorbant or fluorescent moiety. Fluorimetry is a well-known analytical

Correspondence to: D. W. Armstrong, Department of Chemistry, University of Missouri-Rolla, 142 Schrenk Hall, Rolla, MO 65401-0249, USA.

0021-9673/93/$06.00

method with high selectivity and sensitivity which enables the detection of small quantities of many important compounds.

Recently we reported the facile determination of trace enantiomeric impurities of imino acids after 9-fluorenylmethyl chloroformate (FMOC-Cl) derivatization [1]. The current work shows the result of enantiomeric resolution of glycine di- and tripeptides on native α-, β- and γ-cyclodextrin bonded phases after their precolumn derivatization with FMOC reagent. Furthermore, these results provide an opportunity to examine the separation mechanism of chiral peptides on cyclodextrin bonded stationary phases.

EXPERIMENTAL

Apparatus

The HPLC system consisted of two pumps (LC-6A, Shimadzu, Kyoto, Japan), a system controller (SCL-6B, Shimadzu), Chromatopac (CR 601, Shimadzu), fluorescence detector (RF-535, Shimadzu) operated with λ_{ex} = 266 nm and λ_{em} = 315 nm and 0.2-μl injector valve (Valco, Houston, TX, USA). The columns were 250 × 4.6 mm I.D. and were packed with α-, β- and γ-cyclodextrin bonded to 5-μm spherical silica gel (Astec, Whippany, NJ, USA).

TABLE I

SEPARATION DATA FOR A NUMBER OF FMOC-DIPEPTIDES ON THREE DIFFERENT CYCLODEXTRIN BONDED PHASES

The mobile phase used with the γ- and β-cyclodextrin columns was (by volume): acetonitrile–triethylamine–acetic acid (1000:12:3). The mobile phase used with the α-cyclodextrin column was (by volume): acetonitrile–methanol–triethylamine–acetic acid (850:150:12:3). The methanol was used to shorten the long retention times. The flow-rate was 1 ml/min. All compounds were resolved as racemates or nearly racemic D,L-mixtures. When available the pure enantiomer was also run in order to determine the retention order.

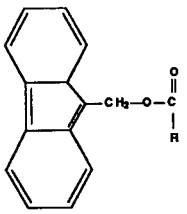

Dipeptide	γ-Cyclodextrin column			β-Cyclodextrin column			α-Cyclodextrin column		
	First eluted enantiomer	k'^a	α^b	First eluted enantiomer	k'^a	α^b	First eluted enantiomer	k'^a	α^b
Gly–Abu	L	2.23	1.07		2.48	1.00		2.56	1.00
Gly–Ser	L	2.07	1.08		2.76	1.00	D	2.73	1.00
Gly–Thr	L	1.30	1.07		1.61	1.00	D	2.38	1.00
Gly–Leu	L	2.29	1.15	D	4.79	1.06	L	2.77	1.10
Gly–Phe	D	2.33	1.09	D	4.27	1.29	L	2.20	1.14
Gly–Asn	L	6.04	1.18	L	7.54	1.04	D	5.48	1.03
Gly–Met	L	1.74	1.19		2.71	1.00	L	2.72	1.03
Gly–Ala	L	2.41	1.07		3.35	1.00		2.27	1.00
Gly–Asp		10.33	1.00	D	11.75	1.22	D[c]	21.0[c]	1.05[c]
Gly–Val		2.15	1.00	D	2.81	1.05		2.25	1.00
Gly–Nva	L	2.17	1.08		2.77	1.00	L	3.79	1.17
Gly–Nle	L	2.07	1.08	D	3.41	1.05	L	4.16	1.24
Ala–Gly	D	2.60	1.06		2.87	1.00		2.12	1.00
Leu–Gly	L	2.22	1.12		2.58	1.00		1.83	1.00

[a] The capacity factors shown designate the first eluted enantiomer.
[b] α-Values of 1.00 mean that no separation of enantiomers occurred.
[c] Acetonitrile–methanol–triethylamine–acetic acid (850:150:14:1).

Chemicals

Amino acids di- and tripeptides were purchased from different sources (ICN, Irvine, CA, USA), (Sigma, St. Louis, MO, USA), and (Novobiochem, La Jolla, CA, USA). Acetonitrile, methanol, acetic acid and triethylamine were of OmniSolv grade and supplied from EM Science (Gibbstown, NJ, USA).

Procedure

The derivatizing agent, FMOC-Cl, was purchased from Sigma (St. Louis, MO, USA). Derivatization was performed according to ref. 9. FMOC-glycine chloride (FMOC-Gly-Cl) was prepared according to ref. 10 and was used for derivatization of amino acids and dipeptides. The derivatization procedure was performed in 0.2 *M* boric acid buffer–acetonitrile solution (1:1, pH 7.7). After derivatization samples were acidified with a 50% acetic acid solution to stabilize the FMOC group. Following acidification, the samples were diluted 10–50 times with acetonitrile prior to injection.

RESULTS AND DISCUSSION

Selectivity

Table I gives retention data for a number of glycine dipeptides that were resolved on α-, β- and γ-cyclodextrin bonded phase columns. As indicated, two standard eluents containing acetonitrile with the same amount of triethylamine and acetic acid were used for the enantioseparation of the 15 racemates listed in Table I. In the case of β- and γ-cyclodextrin bonded stationary phases, the use of neat acetonitrile proved to be an optimal eluent for the enantioseparation of a number of FMOC-imino acids [1]. Under the same mobile phase conditions, most of the FMOC-dipeptides investigated in this study elute in reasonable amount of time. In general the retention times obtained on the β-cyclodextrin column were slightly higher than those found on the γ-cyclodextrin column. For glycyl aspartic acid (Gly–Asp) and glycyl aspargine (Gly–Asn) which contain, respectively, carboxylic acid and amide groups in their side chains, the analysis times were significantly longer. At equivalent mobile phase compositions, the α-cyclodextrin column retained peptides longer than the β- and γ-cyclodextrin columns. In this case, the addition of a small percentage of methanol to the acetonitrile mobile phase decreases the analysis time to practical levels. It is apparent from this data (Table I) that retardation and enantioselectivity are closely related to cyclodextrin size.

In general, the γ-cyclodextrin column was the most selective stationary phase since it resolved 13 of the 15 investigated racemic mixtures. The only two exceptions were glycyl valine (Gly–Val) and Gly–Asp. Surprisingly these racemates are resolved on the β-cyclodextrin column, which exhibited rather limited enantioselectivity towards the other analytes investigated. Fig. 1 shows the base line resolution of glycyl norvaline (Gly–Nva) on an α-cyclodextrin column and Gly–Asp on a β-cyclodextrin column.

The data in Table I shows a selection of suitable cyclodextrin bonded phases which, in many cases, enables one to choose the elution order for a given pair of enantiomers. This is also illustrated in Fig. 2, where the enantiomers of glycyl phenylalanine (Gly–Phe) are shown to have a reversal in elution order on the α-cyclodextrin and β-cyclodextrin columns. This is of great practical importance in the trace analysis of enantiomers since the detectability and accuracy of the determination is much better when the minor component is eluted first [1,11]. Thus the choice of a suitable cyclodextrin stationary phase offers a wide range of possibilities to optimize enantioselectivity.

Previously reported chromatographic separations in analogous systems exhibiting enantioselectivity are optimized by changing two independent factors:

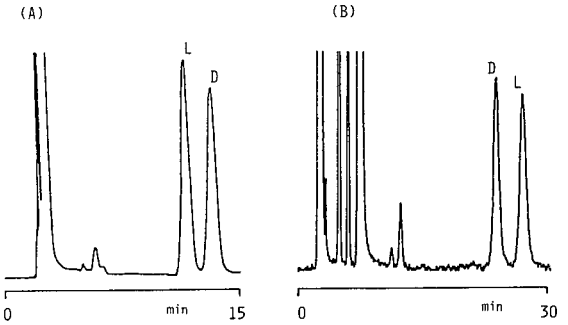

Fig. 1. Enantiomeric resolution of glycyl dipeptides on cyclodextrin bonded phases under optimal experimental conditions. (A) FMOC-Gly–Nva. Stationary phase: α-cyclodextrin bonded phase. Eluent: acetonitrile–methanol–triethylamine–acetic acid (850:150:12:3, v/v). (B) FMOC-Gly–Asp. Stationary phase: β-cyclodextrin bonded phase. Eluent: acetonitrile–methanol–triethylamine–acetic acid (900:100:6:1.5, v/v). Flow-rate: 1 ml/min.

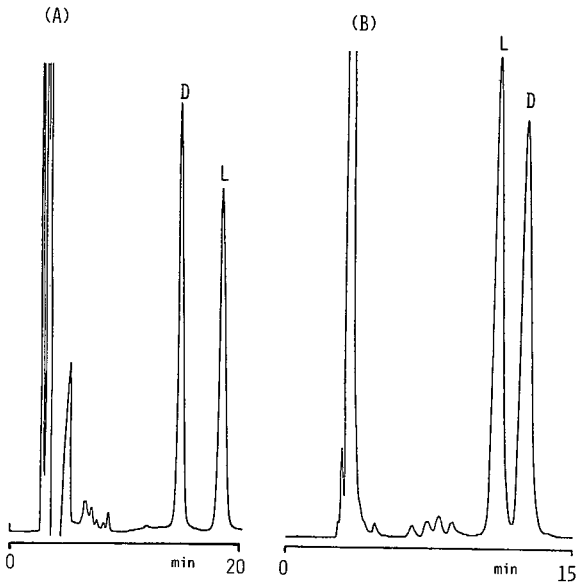

Fig. 2. Change of elution order for FMOC-Gly–Phe enantiomers obtained on β- and α-cyclodextrin bonded phases. (A) Stationary phase: β-cyclodextrin bonded phase. Eluent: acetonitrile–triethylamine–acetic acid (1000:12:3, v/v/v). (B) Stationary phase: α-cyclodextrin bonded phase. Eluent: acetonitrile–methanol–triethylamine–acetic acid (850:150:14:1, v/v). Flow-rate: 1 ml/min.

the composition of the polar organic solvents used in mobile phases and/or the relative ratio of triethylamine and acetic acid used [1]. Fig. 3 shows how the triethylamine and acetic acid concentration influence the resolution of Gly–Asn enantiomers. This behavior was also used to optimize enantioseparation of Gly–Phe (see Fig. 2B). The ratio of 14:1 of triethylamine to acetic acid improves enantioseparation ($\alpha = 118$) whereas utilizing the conditions in Table I slightly decreases resolution ($\alpha = 1.14$) without significantly effecting the retention time.

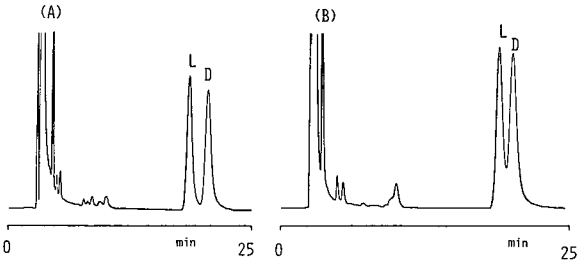

Fig. 3. Effect of relative amounts of triethylamine and acetic acid in the eluent consisting of neat acetonitrile on the resolution of FMOC-Gly–Asn enantiomers. Stationary phase: γ-cyclodextrin bonded phase. Eluent: acetonitrile–triethylamine–acetic acid; (A) 1000:9:6 (v/v/v); (B) 1000:6:9 (v/v/v).

Neat acetonitrile has proved to be an optimal solvent for many analogous separations [1,12]. However, some separations (as mentioned above for the α-cyclodextrin column) require the addition of methanol to decrease retention times. The separation of Gly–Asp on the β-cyclodextrin column, which exhibits a very long analysis time under the conditions listed in Table I, was optimized by changing the concentration of polar organic solvents as well as the amount of amine and acid modifiers (see Fig. 1B). Note that the experimental conditions in Fig. 1B have been optimized to provide the best analytical separation. These conditions are different from those in Table I which summarizes data generated

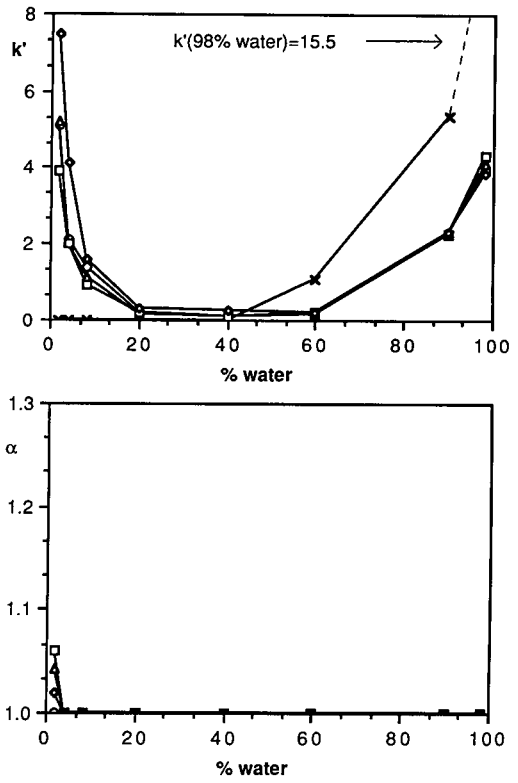

Fig. 4. Influence of water concentration in the mobile phase on the retention characteristics of selected FMOC-derivatized dipeptides and fluorene obtained on α-cyclodextrin bonded phase. Eluent: acetonitrile–water–1.2% triethylamine–0.3% acetic acid (v/v). Test compounds: × = fluorene; ○ = FMOC-Gly–Abu; △ = FMOC-Gly–Leu; □ = FMOC-Gly–Phe, ◇ = FMOC-Gly–Asn. Flow-rate: 1 ml/min.

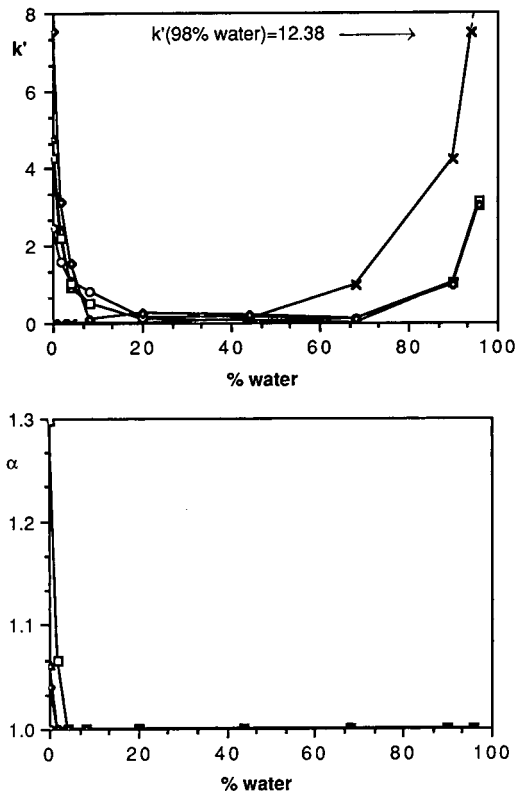

Fig. 5. Influence of water concentration in the mobile phase on the retention characteristics of selected FMOC-derivatized dipeptides and fluorene obtained on β-cyclodextrin bonded phase. Other conditions as in Fig. 4.

under identical conditions so that valid comparisons could be made.

Chiral recognition mechanism

It has been reported that the chiral recognition mechanism for a number of FMOC-derivatized imino acids on *R*(−)-1-(1-naphthyl)ethylcarbamoylated-β-cyclodextrin bonded phase is dependent on the mobile phase composition [1]. The retardation and selectivity of the system were found to be very sensitive to the water content of the eluent. Similar behavior was observed in this study for native α-, β- and γ-cyclodextrin bonded phases.

Figs. 4–6 show the change in retention characteristics for selected glycyl dipeptides obtained on cyclodextrin bonded phases. The eluents consisted of acetonitrile–water mixtures and included small amounts of triethylamine and glacial acetic acid. The chromatographic sorption on the native cyclodextrin bonded phases as well as carbamoylated-β-cyclodextrin bonded phases, occur under two operating conditions (*i.e.*, in the reversed-phase mode with water-rich eluents and under unconventional conditions using non-aqueous polar organic mobile phases). However, in contrast to the carbamoylated-β-cyclodextrin bonded phase, the native α-, β- and γ-cyclodextrin columns exhibit enantioselectivity towards FMOC-derivatized dipeptides *only* when operated with non-aqueous polar organic solvents.

Aqueous systems

In the reversed-phase mode, the separation mechanism on native cyclodextrins phases is thought to be the result of the inclusion complex formation between the hydrophobic moiety of the analyte and the relatively non-polar interior of the cyclodextrin

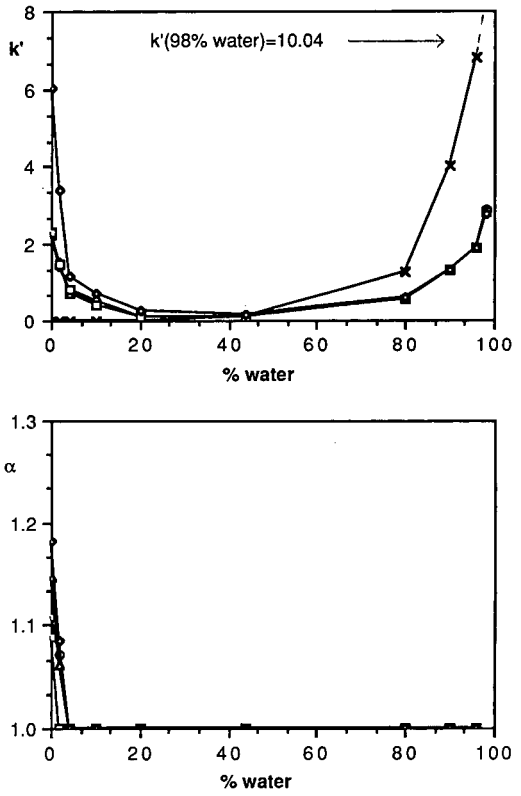

Fig. 6. Influence of water concentration in the mobile phase on the retention characteristics of selected FMOC-derivatized dipeptides and fluorene obtained on γ-cyclodextrin bonded phase. Other conditions as in Fig. 4.

cavity [13,14]. The retention behavior of FMOC functionalized glycyl dipeptides and the fluorene probe molecule shown in Figs. 4–6 confirm this behavior. The plots obtained on α-, β- and γ-cyclodextrin stationary phases are essentially identical with respect to retardation and selectivity. For eluents containing more then 50% (v/v) water, all stationary phases exhibit affinity not only towards FMOC-derivatized dipeptides but also toward the fluorene molecule (Figs. 4–6). Also note that only the fluorene probe molecule is not retarded in water poor systems. Moreover, no enantioselectivity is observed under reversed-phase conditions for all stationary phases investigated. The lack of enantioselectivity in the reversed-phase mode could be due to the FMOC-dipeptide totally interacting with the achiral linkage chain which connects the cyclodextrin to the silica gel. This could result in retention without enantiomeric selectivity. However, this particular scenario is not likely to occur. In fact it is apparent that the retardation of analytes depends very strongly on cyclodextrin cavity size. The larger size of the β-cyclodextrin and γ-cyclodextrin cavity result in inefficient binding due to the loose nature between the arene and cyclodextrin. This, in turn, reduces the retention time of the analytes compared to those obtained on the α-cyclodextrin column. It is most likely that the fluorene group is included in the cyclodextrin cavity and the dipeptide chain is located outside the cavity and is solvated by the hydrophilic mobile phase.

It should be mentioned that the data on inclusion complex formation between cyclodextrin and polyaromatic hydrocarbons of different sizes are not consistent and often diverse. Some literature reports that the naphthalene molecule is too large to be included into the α-cyclodextrin cavity [15,16] as are anthracene molecules for the β-cyclodextrin cavity [15]. On the other hand, an induced circular dichroism study [17] has provided evidence that β-cyclodextrin accommodates one pyrene molecule with axial inclusion while γ-cyclodextrin includes two pyrene molecules of "S" helicity. This study has been confirmed by comparative spectroscopic binding studies (absorption spectral characteristics, circular dichroism and fluorescence evidence), where benz[*a*]pyrene was shown to form an inclusion complex of 1:1 host–analyte ratio with the β-cyclodextrin and a 1:2 host–analyte ratio with γ-cyclodextrin [18]. Additionally there are several chromatographic studies reporting the retardation of large polyaromatic hydrocarbon molecules (pyrene, chrysene) on β- and γ-cyclodextrin [19,20] and more recently on α-cyclodextrin columns [21]. Moreover, NMR study [22], conformational (optical rotation) analysis [23] and X-ray crystallographic data [24] provide evidence that the bonds of α-cyclodextrin are relatively weaker than β- and γ-cyclodextrins. These can lead to induced fits of larger molecules into the α-cyclodextrin cavity by deformation of its structure under high aqueous buffer conditions.

The results of the present study indicate that the fluorene molecule can penetrate into all cyclodextrin cavities and that the inclusion complex formation between the hydrophobic aromatic part of the analytes and apolar cyclodextrin cavity is the major factor contributing to the retention of FMOC-functionalized dipeptides under reversed-phase conditions. The hydrophilic part of the guest molecule remains outside the cavity. The most striking conformation of this picture is the finding that the retention of different types of FMOC-dipeptides is nearly identical (on a given column) and always lower than retention of the fluorene molecule. The fact that no enantioselectivity is observed in any of these cases would seem to indicate that the simultaneous, optimum interaction of the fluorene moiety with the cyclodextrin cavity and between the peptide moieties and the cyclodextrin hydroxyls does not occur with these analytes.

The model postulated for the retention mechanism based on inclusion complex formation is further supported by the kinetic study presented below. Fig. 7 shows the dependence of the plate height, H, on the linear flow velocity, u, for the fluorene molecule and different FMOC-derivatized glycyl dipeptides obtained on γ- and β-cyclodextrin columns. The dashed line represents H values obtained for fluorene on cyclodextrin columns operated with neat acetonitrile. No retardation of fluorene was observed in this system and therefore the dashed line can be considered the limit for column efficiency due to the packing quality and extra column effects. As can be seen in Fig. 7 the characteristics presented are very similar for γ- and β-cyclodextrin column, which enables teh comparison of the results obtained on these two columns.

According to the general non-equilibrium theory

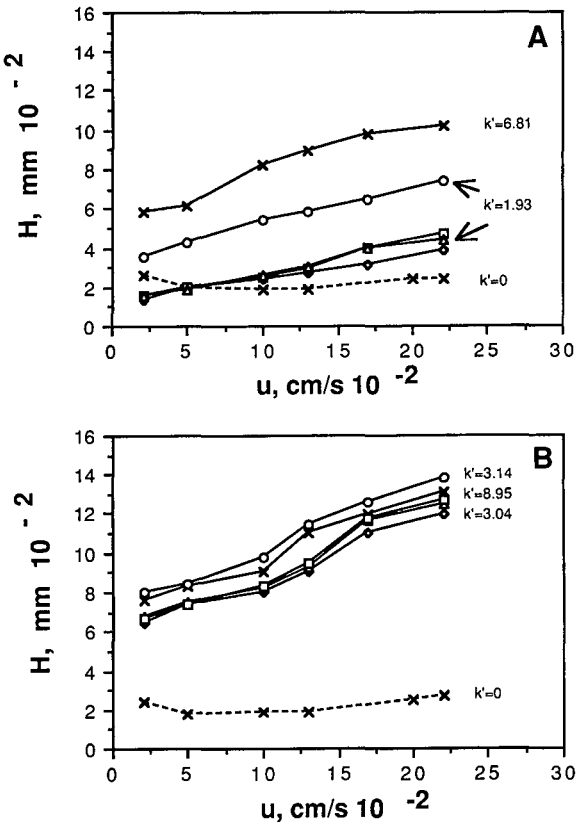

Fig. 7. The dependence of height equivalent to a theoretical plate (HETP) values on linear velocity for fluorene and selected FMOC-derivatized dipeptides in aqueous systems. Eluent: water–acetonitrile–triethylamine–acetic acid (960:40:12:3, v/v). Test compounds: × = fluorene, ◇ = Asn, △ = Abu, □ = Leu, ○ = Phe. Stationary phase: (A) γ-cyclodextrin bonded to 5-μm spherical silica gel, (B) β-cyclodextrin bonded to 5-μm spherical silica gel. The dashed line represents HETP values obtained for fluorene in systems operated with neat acetonitrile as the mobile phase.

developed by Giddings [25] the plate height, H, results from three independent contributions: flow pattern effects (A), longitudinal diffusion (B) and mass transfer effects (C).

$$H = B/u + C_k u + \sum 1/(1/A + 1/C_m u) \quad (1)$$

where the terms C_k and C_m indicate adsorption–desorption kinetics and diffusion controlled kinetics originating in the stationary and mobile phase, respectively.

The equation in the coupling form represents the major sources of zone spreading in practical liquid chromatography (LC) for a very broad range of the flow velocities. The terms in eqn. 1 have a different dependence on the flow velocity. Ordinary molecular diffusion in the flow direction is inversely proportional to flow velocity and contributes significantly only at very low flow velocities. The sorption–desorption kinetics provides a term proportional to flow velocity. The coupling terms arise from inequalities of flow velocity in the mobile phase. Over the limited flow range used in LC some of these terms (A) are believed to be constant and some proportional to velocity (C_m).

As shown in Fig. 7, the dependence of the plate height on the flow-rate of all analytes investigated is approximately linear within the range of flow-rates applied. This indicates that the zone spreading is mainly caused by mass transfer effects in the stationary phase. Moreover, although linear velocities as low as $2 \cdot 10^{-2}$ cm/s were used, no minimum of H, u_{min}, was found (although the minimum of H for the unretained analyte on the same column was observed at $u > 5 \cdot 10^{-2}$ cm/s). Generally the values of u_{min} and H_{min} depend on the magnitude of the C_k term and therefore can differ between different solutes. Extremely high contribution of C_k shifts the minimum in H to very small values of u.

Since the mass transfer effect can be expressed as:

$$C_k = \frac{2q}{k_d} \cdot \frac{k'}{(1 + k')^2} \quad (2)$$

were: q is the geometrical parameter and k_d is the desorption rate constant; the two findings discussed above indicate that the overall plate height of a solute is determined by the sorption–desorption kinetics in the stationary phase.

It can be concluded from plots in Fig. 7 that the rate of the adsorption–desorption process for functionalized dipeptides is usually higher than for fluorene molecule (the only possible exception would be Phe on the β-cyclodextrin column). The kinetic data presented provide strong support for the postulated model. The strength of the interaction between the solute and the stationary phase (*i.e.*, retention and to some extent sorption–desorption kinetics) are a result of the inclusion complexation process. The presence of the hydrophilic chain of FMOC-derivatized dipeptides results in shorter retention times and faster mass transfer effects compared with values found for the fluorene molecule itself. The

differences observed in adsorption–desorption rate between fluorene and FMOC-derivatized dipeptides are especially significant for processes on the γ-cyclodextrin stationary phase, which owing to the large cavity, forms relatively loose complexes with the analytes. For the β-cyclodextrin column the sorption–desorption processes are significantly slower for all analytes investigated compared with the values obtained on γ-cyclodextrin phase that is undoubtedly due to the stronger interactions between the smaller cyclodextrin cavity and the aromatic part of the molecule.

The different magnitudes of band spreading processes for the different dipeptide chains can be explained by taking into account additional factors, *e.g.*, the structure of the side chains. The side chains as shown in Figs. 4–6 do not influence the retention in the reversed-phase mode. However, they can contribute to the band broadening in two ways: (1) by changing the individual diffusion velocity of the solute in the mobile phase, which would contribute to C_m term ($C_m = wd_p^2/D_m$, where: w is dimensionless constant, d_p particle size, D_m diffusion coefficient) and (2) by affecting the degree of solvation of the analyte in the bulk mobile phase (*i.e.*, increasing or decreasing the rate of mass transfer effect between stationary and mobile phases).

As can be seen in Fig. 7, the H values for Leucine (Leu) and α-aminobutyric acid (Abu), having aliphatic side chains, are almost identical for the same column. In case of Gly–Asn the presence of the hydrophilic side chain increases the rate of mass transfer of the solute between cyclodextrin stationary phase and hydrophilic mobile phase resulting in slightly lower H values. The hydrophobic aromatic group in Gly–Phe increases the tendency of the analyte to be excluded from the water rich eluent to the vicinity of cyclocdextrin moiety. This results in significantly slower kinetics for both columns investigated as well as a slightly higher retention time for FMOC-Gly–Phe on β-cyclodextrin column.

It should be pointed out that the analytes investigated form symmetrical peaks in the reversed-phase mode. Only Gly–Phe shows a slightly leading peak (fronting) suggesting a slight concave form of its adsorption isotherm, which might result from a second layer (or multi layer) adsorption of other molecules onto the adsorbed aromatic ring of the side chain.

Non-aqueous systems

It is evident from retention characteristics shown in Figs. 4–6 that a different retention mechanism is involved for systems operating with polar organic mobile phases. This is in direct contrast to the traditional reversed-phase mode. First, the fluorene molecule is not retarded on any native cyclodextrin columns. Apparently there is no inclusion complex formation between cyclodextrin and hydrophobic part of the analyte in acetonitrile. It is also highly unlikely that the hydrophilic peptide chain would penetrate into apolar cyclodextrin cavity. Moreover, it has been reported previously that acetonitrile exhibits an appreciable affinity for the cyclodextrin cavity [26,27] and in polar organic solvents (above 80% acetonitrile) the formation of a conventional inclusion complex is not likely since the cyclodextrin cavity is occupied by the mobile phase [28]. This is in a good agreement with results presented in this study and leads to the assumption that the enantioselectivity observed is caused by hydrogen bonding between the analyte and the hydroxyl groups at the mouth of the cyclodextrin.

The results in Table I demonstrate how the retardation of the peptides are closely related to the size of cyclodextrin. The k' values of dipeptides increase when the molecular size of cyclodextrin used is decreased. In the case of α-cyclodextrin, the addition of 15% (by volume) of methanol is needed to decrease the retardation time to a practical level. In order to compare the data in a meaningful way, the results shown in Figs. 4–6 were obtained using the same mobile phase for all cyclodextrin stationary phases. Because of the long retention times ($k' > 15$) the data for α-cyclodextrin operated in conjunction with neat acetonitrile are not included.

Table II and Fig. 8 show dependence of k' values and selectivities on the length of the peptide chain. In general, with the exception of leucine, the native cyclodextrins exhibit no enantioselectivity towards FMOC-functionalized amino acids in spite of the presence of the functional (carboamide and carboxylic) groups available for hydrogen bonding. This could be due either to steric hindrance of the adjacent, bulky fluorene moiety which may effectively prevent the access of hydroxyl groups of cyclodextrin molecule to the appropriate functional groups of the analyte, or it could result from the inability of the FMOC-deactivated nitrogen to form

strong hydrogen bonds. Extending the chain length and introducing new hydrogen bonding groups enables stereoselective interaction between the peptide "tail" and the hydroxyl groups of the cyclodextrin moiety and results in an increase in retention and enantioselectivity. The dependence demonstrated in Tables I and II and Figs. 4–6 is strong evidence that hydrogen bonding formation between hydrophilic chain of the FMOC-functionalized peptides and the external part of cyclodextrin molecules (outer sphere complex) is the major factor contributing to the chiral recognition on native cyclodextrin phases operated with polar organic mobile phases. Proper geometric conditions must be met for stereoselective interaction between the analyte and the hydroxyls at the mouth of the cyclodextrin moiety. The "small" diameter of α-cyclodextrin properly match the length of the di- and tripeptide chain. Carboamide and carboxylic groups in the solute can interact with several hydroxyl groups on the both sides of the cyclodextrin mouth which results in large increases in retention time compared with the results obtained on β- and γ-cyclodextrins.

Fig. 9 presents the kinetic data for L-enantiomers of selected FMOC-functionalized amino acids, dipeptides and tripeptides obtained on the most selective γ-cyclodextrin column, operated with the non-aqueous eluent. Unlike the kinetic behavior found for the reversed-phase model (*i.e.*, inclusion complex formation), the plate height with polar organic mobile phases is simply correlated with the capacity factors of the analytes [29,30]; the stronger the interaction between the stationary phase and the solute (which results in the strong retardation) the slower the mass transfer is between stationary and mobile phases. The strength of interaction and the kinetic behavior depends on the structure of the analyte. The presence of the polar carboamide group in the Asn molecule significantly increases the retention and decreases the rate of sorption–desorption process. Extending the peptide chain and thereby introducing additional sites for hydrogen bonding causes a similar effect; the retardation tends to increase and the adsorption–desorption rate decreases. No significant differences were found in the sorptiona–desorption kinetics for enantiomers. The mass transfer was always slightly slower for the longer retained stereoisomer. The peak shapes for all analytes investigated were found to be highly symmetrical. This indicates that the adsorption sites are

TABLE II

A COMPARISON OF SEPARATION DATA FOR RELATED FMOC-AMINO ACIDS, DIPEPTIDES AND TRIPEPTIDES

The mobile phase composition and the flow-rate of these columns are identical to that in Table I.

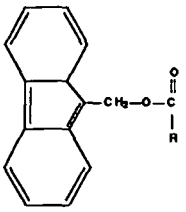

Compound	α-Cyclodextrin column			β-Cyclodextrin column			γ-Cyclodextrin column		
	First eluted enantiomer	k'^a	α	First eluted enantiomer	k'^a	α	First eluted enantiomer	k'^a	α
Ala		1.11	1.00		1.45	1.00		1.42	1.00
Gly–Ala		2.27	1.00		3.35	1.00	L	2.41	1.07
Gly–Gly–Ala	L	3.27	1.05		7.61	1.00	L	7.29	1.06
Leu		1.16	1.00	D	1.03	1.07		1.03	1.00
Gly–Leu	L	2.77	1.10	D	4.79	1.06	L	2.29	1.15
Gly–Gly–Leu	L	5.12	1.14	D	14.10	1.31	L	7.54	1.14

[a] The capacity factors shown designate the first eluted enantiomer.

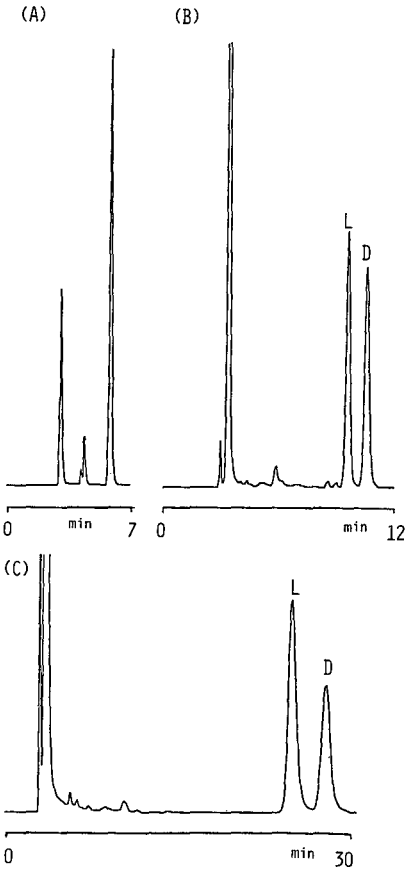

Fig. 8. Influence of the length of peptide chain on retention and enantioselectivity obtained on γ-cyclodextrin bonded phase. Eluent: acetonitrile–triethylamine–acetic acid (100:12:3, v/v/v). (A) FMOC-Leu; (B) FMOC-Gly–Leu; (C) FMOC-Gly–Gly–Leu. Flow-rate: 1 ml/min.

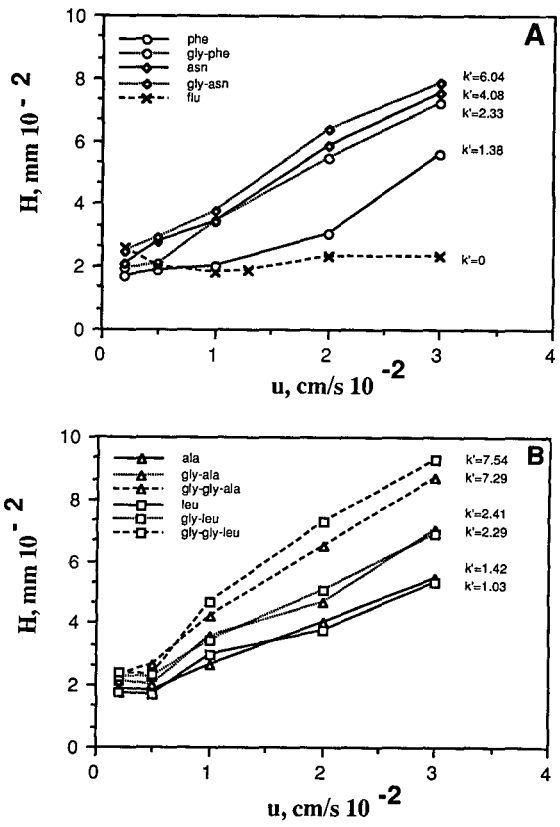

Fig. 9. The dependence of HETP values on linear velocity for fluorene and selected FMOC-derivatized amino acids, di- and tripeptides in non-aqueous system. Eluent: acetonitrile–triethylamine–acetic acid (1000:12:3, v/v/v). Stationary phase: γ-cyclodextrin.

essentially of a single type, *e.g.*, homogeneous in adsorption energies [25,31]. Therefore the type and strength of the interaction between the sites and the analytes depend mainly on the analyte structure and configuration. These data provide consistent support for the model of external adsorption on the hydroxyl groups at the mouth of cyclodextrin cavity as proposed for these non-aqueous systems.

It is clear that several other factors contribute to the retention behavior observed in this study. It has been reported [32,33] that the peptide bond has the ability to enhance the acidity of neighboring groups due to an inductive effect. Thus, considering this effect, it is apparent that the N-terminal peptide bond of the tripeptide will exhibit an N–H bond of substantially enhanced acidity compared with the dipeptide, which can significantly change the interaction between the cyclodextrin and the analyte. It is also possible that the interaction of the analyte with cyclodextrin can significantly alter the structure of the peptide chain in cases where strong hydrogen bonding is involved. This can also lead to a better "fit" of the extended chain with the relatively static structure of the cyclodextrin molecule. Moreover, short peptide chains and even cyclic peptides in certain solvents from definite structures [34]. The nature of the solvent has a great influence on the strength of non-covalent interactions. This could explain the very narrow range of mobile phase compositions where the enantioselectivity towards

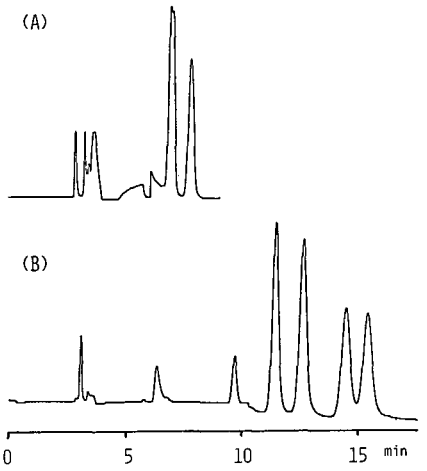

Fig. 10. Stereoisomeric resolution of Ala–Val on γ-cyclodextrin bonded phase. (A) Derivatization with FMOC-Cl; (B) derivatization with FMOC-Gly-Cl. Eluent: acetonitrile–triethylamine–acetic acid (1000:12:3, v/v/v). It is apparent that both pairs of enantiomers are resolved in chromatogram "B", whereas there is only slight resolution in chromatogram "A".

small peptides is observed. Clearly the addition of small amounts of water to the system can totally destroy enatioselectivity. This must be the result of the solvation of the peptide chain and cyclodextrin as well as any induced structural changes caused by the water solvation.

The dependence of enantioselectivity on peptide chain length shown in this study for glycyl di- and tripeptides seems to be a general trend for enantioseparations on native cyclodextrin phases. Fig. 10 shows the chromatographiv behavior of FMOC-derivatized dipeptides having two chiral centers in the peptide chain; the addition of glycyl residue significantly improves the enantioselectivity. Further study on this subject is in progress.

ACKNOWLEDGEMENT

Support of this work by the National Institute of General Medical Science (BMT 2R01 GM36292-04) is gratefully acknowledged.

REFERENCES

1 J. Zukowski, M. Pawlowska and D. W. Armstrong, *J. Chromatogr.*, 623 (1992) 33.
2 K. Yasumoto and K. Sugiyama, *Agric. Biol. Chem.*, 44 (1980) 1339.
3 D. A. Priestman and J. Butterworth, *Biochem. J.*, 231 (1985) 689.
4 M. H. Hyun, I. K. Baik and W. H. Pirkle, *J. Liq. Chromatogr.*, 11 (1988) 1249.
5 M. Katoh, T. Ishida, Y. Baba and H. Kiniwa, *J. Chromatogr.*, 473 (1989) 241.
6 J. Florance and Z. Konteatis, *J. Chromatogr.*, 543 (1991) 299.
7 I. Molnar and Cs. Horváth, *J. Chromatogr.*, 142 (1977) 623.
8 T. Shibo, T. Yamaguchi, K. Nishimura and M. Sugiura, *J. Chromatogr.*, 405 (1987) 145.
9 S. Einarsson, B. Josefsson and S. Lagerkvist, *J. Chromatogr.*, 382 (1983) 609.
10 L. A. Carpino, B. J. Cohen, K. E. Stephens, Jr., S. Y. Sadat-Aalaee, J. H. Tien and D. C. Langridge, *J. Org. Chem.*, 51 (1986) 3734.
11 J. A. Perry, J. D. Rateike and T. J. Szczerba, *J. Chromatogr.*, 389 (1987) 57.
12 D. W. Armstrong, S. Chen, C. Chang and S. Chang, *J. Liq. Chromatogr.*, 15 (1992) 545.
13 D. W. Armstrong, W. DeMond and B. P. Czech, *Anal. Chem.*, 57 (1985) 481.
14 D. W. Armstrong, *J. Liq. Chromatogr.*, 7 (1984) 353.
15 J. Szejtli, *Cyclodextrins and Their Inclusion Complexes*, Akademiai Kiado, Budapest, 1982.
16 J. Emest, D. Kodali and R. Catena, *J. Chem. Soc. Chem. Commun.*, (1981) 758.
17 N. Kobayashi, R. Saito, Y. Hino, A Veno and T. Osa, *J. Chem. Soc. Chem. Commun.*, (1982) 706.
18 R. Woodberry, S. Ranson and V. Fu-Ming, *Anal. Chem.*, 60 (1988) 2621.
19 D. W. Armstrong, A. Alak, W. DeMond, W. L. Hinze and T. E. Riehl, *J. Liq. Chromatogr.*, 8 (1985) 261.
20 M. Olsson, L. E. Sander and S. A. Wise, *J. Chromatogr.*, 477 (1989) 277.
21 *Cyclobond™ Handbook*, ASTEC, Whippany, NJ, 1992.
22 D. J. Wood, F. E. Hruska and W. Saenger, *J. Am. Chem. Soc.*, 99 (1977) 1735.
23 D. A. Ress, *J. Chem. Soc. B.*, (1970) 877.
24 K. Harata and H. Uedaiva, *Nature (London)*, 253 (1975) 190.
25 J. C. Giddings, *Dynamics of Chromatography*, Dekker, New York, 1965.
26 L. T. Ward and D. W. Armstrong, *J. Liq. Chromatogr.*, 9 (1986) 407.
27 S. M. Han and D. W. Armstrong, *J. Chromatogr.*, 389 (1987) 257.
28 P. R. Fielden and A. J. Packhann, *J. Chromatogr.*, 516 (1991) 355.
29 Cs. Horváth and H. J. Lin, *J. Chromatogr.*, 149 (1978) 43.
30 E. Katz, K. L. Ogan and P. W. Scott, *J. Chromatogr.*, 270 (1983) 51.
31 A. M. Rizzi, *J. Chromatogr.*, 478 (1989) 71.
32 S. A. Bernhard, A. Berger, J. H. Carter, E. Katchalski, M. Sela and Y. Shalitin, *J. Am. Chem. Soc.*, 84 (1962) 2421.
33 P. DeMontigny, C. M. Riley, L. A. Sternson and J. F. Stobaugh, *J. Pharm. Biomed. Anal.*, 8 (1990) 419.
34 H. D. Jakubke and H. Jeschkait, *Amino Acids, Peptides and Proteins*, Wiley, New York, 1977, p. 68.

Journal of Chromatography, 629 (1993) 181–199
Elsevier Science Publishers B.V., Amsterdam

CHROM. 24 646

Chemometrics in bioanalytical sample preparation

A fractionated combined mixture and factorial design for the modelling of the recovery of five tricyclic amines from plasma after liquid–liquid extraction prior to high-performance liquid chromatography

J. Wieling

Pharma Bio-Research International BV, P.O. Box 200, Science Park, NL-9470 AE Zuidlaren (Netherlands) and Chemometrics Research Group, University Centre for Pharmacy, University of Groningen, Antonius Deusinglaan 2, NL-9713 AW Groningen (Netherlands)

H. Dijkstra, C. K. Mensink and J. H. G. Jonkman

Pharma Bio-Research International BV, P.O. Box 200, Science Park, NL-9470 AE Zuidlaren (Netherlands)

P. M. J. Coenegracht, C. A. A. Duineveld and D. A. Doornbos

Chemometrics Research Group, University Centre for Pharmacy, University of Groningen, Antonius Deusinglaan 2, NL-9713 AW Groningen (Netherlands)

(First received June 26th, 1992; revised manuscript received September 25th, 1992)

ABSTRACT

A general systematic approach is described for the chemometric modelling of liquid–liquid extraction data of drugs from biological fluids. Extraction solvents were selected from Snyder's solvent selectivity triangle: methyl *tert.*-butyl ether, methylene chloride and chloroform. The composition of a mixture of the three extraction solvents was varied and the extraction yield (recovery) of a group of tricyclic amines was measured at all compositions selected. Two process variables, the extraction time and the extraction intensity, were varied simultaneously with the mixture variables to study their influence and their interaction with the mixture composition. The combined mixture and factorial design statistical techniques obtained in this way enabled the recovery to be modelled as a function of both the composition of the extraction liquid and the process variables. The models were assessed with regard to both descriptive and predictive capacities. The results showed that structurally related compounds may demonstrate different partitioning behaviour with regard to both mixture variables and process variables. It was concluded that mixtures of solvents result in higher extraction efficiencies for the amines. A positive effect on the extraction efficiency was demonstrated by the extraction intensity process variable and extraction time. A positive effect on the extraction efficiency was demonstrated by an interaction between extraction intensity and time. Mixture models in which process variables were introduced were recognized as being very suitable for modelling liquid–liquid extraction systems.

Correspondence to: J. Wieling, Institute of Environmental Sciences TNO, Department of Analytical Chemistry, P.O. Box 6011, 2600 JA Delft, Netherlands (present address).

0021-9673/93/$06.00

INTRODUCTION

Liquid–liquid extraction is often part of bioanalytical assay methods prior to chromatographic analysis. Although this sample preparation stage is very important from an analytical point of view, less attention has been paid until now to the systematic optimization of liquid–liquid extraction. For method development involving liquid–liquid extraction prior to high-performance liquid chromatography (HPLC), great effort is often spent on the development of a proper sample preparation procedure. Choices have to be made with respect to the extraction solvent or mixture of solvents used, what buffer solution will be used, etc. The choice of all these parameters depends on the matrix that has to be analysed, the equipment available, the method of determination that is used and the amount of labour and time spent. The use of systematic methods for the development of sample preparation procedures may decrease the method development time.

In liquid–liquid extraction, the partition coefficient of individual solutes may be influenced by a number of factors. First, the influence of the pH is an important factor [1–4]. Adjusting the pH to a suitable value converts acidic or basic drugs into non-ionized species, which are more soluble in a non-polar solvent. Second, the ionic strength of the biological sample influences the partition coefficient. The addition of highly water-soluble ionized salts decreases the solubility of drugs in the aqueous phase, followed by an increase in the solubility of the drug in the organic phase. This phenomenon is called the "salting out effect" and is caused by diminished availability of water molecules acting as a solvent for the drug [5,6]. The influence of the ratio of the volume of the organic phase, V_{org}, to the volume of the aqueous phase, V_{aq}, is also known. There is no influence of the ratio of V_{org} to V_{aq} on the magnitude of the partition coefficient. However, it does influence the fraction of the drug extracted into the organic phase (recovery). Of course, V_{org} should not be too high, for economical and practical reasons. The temperature of an extraction system has a minor effect on the partition coefficients. Extractions are generally performed at room temperature. Small fluctuations of room temperature have insignificant effects on partitioning. Also important for the extraction of drugs from body fluids is the sample matrix. However, this is an uncontrollable factor. Finally, a very important factor influencing the partitioning of drugs between two phases is the choice of the organic solvent [4,7]. Specific solvents can be selected with regard to their physical properties. Intuitively, one may have an idea about the extraction behaviour of the analyte in developing new analytical assay methods using liquid–liquid extraction. However, it is difficult to select a proper extraction solvent with a first guess. Contingent selection of a mixture of different solvents is even more difficult. Extraction solvents are often selected by trial and error, and improvement of extraction yields is not considered as long as they are satisfactory, even if they are not optimum or if the reproducibility of the extraction could be improved. Implementation of chemometric optimization procedures in sample preparation procedures using liquid–liquid extraction may be useful for the selection of optimum extraction conditions.

Two general systematic optimization procedures are the simultaneous and sequential methods. In sequential methods (*e.g.*, simplex optimization), results of previously performed experiments are used to calculate conditions for new experiments to be carried out. In this manner, the response surface is sequentially tracked until an optimum has been located, which is not, however, *a priori* a global optimum. Another disadvantage of this located optimum is that it may be dependent on the initial variable settings. Finally, a very important restriction of a sequential simplex optimization may be the complexity of the optimization function. This function is a predefined function, which may be composed of several criteria. Such a composite criterion leads to ambigious results [8]. Other important disadvantages of a simplex optimization method are that often local optima are determined and that the number of experiments needed is not known beforehand.

Simultaneous optimization methods do not suffer from these problems. Experiments to be carried out are previously planned, according to some experimental design within the factor space. The experimental results are collected and then any response criterion desired can be modelled. Simultaneous methods may provide the global optimum. The experimental designs are used to obtain maximum information out of a series of carefully selected experiments.

Applications of simultaneous methods in chromatography have been described by Glajch *et al.* [9] and Weyland *et al.* [10] and more recently by Mulholland and Waterhouse [11–13] and Coenegracht *et al.* [14].

Applications of systematic optimization of extraction liquid composition in biomedical analysis using sequential or simultaneous methods in liquid–liquid extraction have not been reported. In liquid–liquid extraction, the selective interactions of the extraction solvent and the matrix components to be extracted influence the magnitude of extraction [15]. The extraction liquid composition should be chosen such that there is high selectivity for the matrix component(s) to be extracted. The polarity of the extraction solvent used is very important for the recovery. However, the selective interactions between solvent and solute are also very important. Therefore, the selectivity of the solvent should be adjusted such that interaction between the solvent and solute is optimum. In this way, extraction yields can be maximized. Here, we propose a new method for the systematic optimization of the extraction liquid in liquid–liquid extraction, in which several theories have been incorporated. The solvent selectivity theory developed by Rohrschneider [16] and Snyder [17] was used to select three solvents representing different types of selective interactions. Tricyclic amines were extracted with different mixtures of three extraction solvents according to a mixture experimental design in combination with a factorial design for two extraction process variables. The efficiency of the extraction (recovery) was modelled. The final objective of this investigation was to study the applicability of combined fractional experimental designs for the simultaneous optimum choice of extraction liquid composition (the mixture design part), extraction time and extraction intensity (the factorial design part). The optimization criterion was to maximize tha extraction efficiency of the extraction system and to minimize the time needed for a single extraction. The latter criterion was introduced for future application of a laboratory robot with serialized sample processing. Moreover, the ruggedness of the extraction system was evaluated for pairs of amines.

THEORY

Several studies have attempted to relate the partition coefficient of a solute in a liquid chromatographic system between two phases, one of which has a varying composition [16,18–20]. Schoenmakers and co-workers [21,22] derived a relationship for a binary mobile phase in reversed-phase HPLC from the solubility parameter theory of Hildebrand *et al.* [23]. Similarly, a relationship can be derived for liquid–liquid extraction with extraction liquids composed of three components:

$$\ln P = A\varphi_1^2 + B\varphi_2^2 + C\varphi_3^2 + D\varphi_1\varphi_2 + E\varphi_1\varphi_3 + F\varphi_2\varphi_3 + G\varphi_1 + H\varphi_2 + I\varphi_3 + J \quad (1)$$

where A–J are functions of the solubility parameters of the extraction liquid components and φ_1, φ_2 and φ_3 are the fractions of mixture components 1, 2 and 3, respectively. This equation is a reduced form of a more complex equation with three mixture variables, but this complex equation has been simplified because in mixture designs the sum of the fractions of the extraction liquid components equals 1 ($\varphi_3 = 1 - \varphi_1 - \varphi_2$). Eqn. 1 provides considerable insight into the partitioning of a solute between the aqueous and the organic phase in liquid–liquid extraction. Quadratic effects of fractions and interaction effects between two fractions are indicated. This factorial design-like model can be transformed into a quadratic mixture model when the constraint that the sum of the fractions equals 1 ($\varphi_1 + \varphi_2 + \varphi_3 = 1$) is substituted. The mixture variables (the fractions of the components in the extraction liquid) are now represented by x_i:

$$\ln P = \beta_1 x_1 + \beta_2 x_2 + \beta_3 x_3 + \beta_{12} x_1 x_2 + \beta_{13} x_1 x_3 + \beta_{23} x_2 x_3 + \varepsilon \quad (2)$$

This transformation of a physico-chemical model into a chemometric model was also discussed by Weyland *et al.* [9]. A ternary non-linear blending term is often added to improve the descriptive power of eqn. 2. Then, a special cubic mixture model (eqn. 3) is obtained:

$$\ln P = \beta_1 x_1 + \beta_2 x_2 + \beta_3 x_3 + \beta_{12} x_1 x_2 + \beta_{13} x_1 x_3 + \beta_{23} x_2 x_3 + \beta_{123} x_1 x_2 x_3 + \varepsilon \quad (3)$$

where β_1–β_{123} are the regression coefficients to be estimated after the experimental part and ε is the residual error to be estimated. For estimation of the regression coefficients and the residual error, at least

as many experiments have to be performed as the number of model coefficients plus one. In a mixture design experiment, the response to a mixture of q components depends only on the fractions of mixture components and does not depend on the total amount of the mixture.

Eqn. 3 describes the relationship between the composition of an extraction liquid and the partition coefficient. However, liquid–liquid extraction is often quantified by the recovery R, *i.e.*, the fraction of the total amount of analyte transferred from the aqueous phase into the organic phase ($R = \Phi_{org}$):

$$R = \Phi_{org} = \frac{P\left(\frac{V_{org}}{V_{aq}}\right)}{P\left(\frac{V_{org}}{V_{aq}}\right) + 1} \quad (4)$$

where V_{aq} and V_{org} are the volumes of the aqueous and organic phase, respectively, and P is the partition coefficient of a given analyte under certain conditions (pH, ionic strength, extraction liquid, temperature, sample matrix). This relationship can be transformed into the following:

$$P = \frac{R}{(1-R)} \cdot \frac{V_{aq}}{V_{org}}$$

With a constant ratio of the phase volumes through all the experiments:

$$P \propto \frac{R}{1-R}$$

Thus, when recoveries of analytes are measured, these recoveries can be related to the extraction liquid composition by writing eqns. 2 and 3 as follows:

$$\ln\left(\frac{R}{1-R}\right) = \beta_1 x_1 + \beta_2 x_2 + \beta_3 x_3 + \beta_{12} x_1 x_2 + \beta_{13} x_1 x_3 + \beta_{23} x_2 x_3 \; (+ \beta_{123} x_1 x_2 x_3) + \varepsilon \quad (5)$$

Summarizing, to optimize the partition coefficient P of a solute i and consequently R_i, P_i and R_i should be maximized by mixing three solvents in the correct proportions. The use of mixture design statistical techniques with the natural logarithm of the partition coefficient as response criterion is a valid way to achieve this.

Introduction of process variables in mixture models

For the selection of factors that influence extraction one has to select as few variables as possible, to avoid models with large numbers of coefficient and, consequently, large numbers of experiments. Factors that influence liquid–liquid extraction are the following: the pH of the aqueous phase of the extraction system; the ionic strength of the aqueous phase; the ratio of the volumes of the organic phase and the aqueous phase, V_{org} and V_{aq}; the temperature of the extraction system; the matrix in which the solute is dissolved; the choice of the solvent; the time in which the extraction is performed (extraction time); and the intensity with which the extraction takes place (extraction intensity) ≡ the rotations per minute of a tumble mixer.

The first six factors were discussed in the Introduction. Arguments for the introduction of the last two factors (extraction intensity and extraction time) are discussed below.

Liquid–liquid extraction is based on partitioning equilibrium of a solute over the two phases. Important factors for this phenomenon may be the time of extraction and the intensity of extraction. The influence of these factors is generally not known. For extraction solvents with different compositions, equilibria may possibly adjust differently. Thus, when different solvents (or mixtures of solvents) are used, different adjustment parameters (process variables) are probably needed. They may be different for several solutes [24]. Often, an extraction equilibrium is obtained rapidly. Extraction times are often too long [25], which was also acknowledged by Campbell [26]. However, Lagerström *et al.* [27] found a time-dependent extraction from plasma. They investigated the influence of extraction time on the extraction yield of hydrophobic tertiary amines in diethyl ether, hexane–propanol (95:5) and methylene chloride. They suggested that the amines investigated were probably occluded in protein precipitates and that diffusion out of that environment was very time consuming. Schill *et al.* [28] showed the effect of dilution in protein precipitation: extraction yields of two sulphonamides increased strongly after dilution of plasma with water.

A survey of a number of recent issues of *Journal of Chromatography* (*Biomedical Applications*) showed that a small number of publications describing liquid–liquid extraction prior to determination did

not report the extraction time. However, most of the publications in these issues did not report the extraction intensity or even the method of shaking. This indicates that the significance of the physical conditions during an extraction is often disregarded and is not considered as being important. However, investigation of the extraction conditions other than pH or solvent used may be interesting, as demonstrated by the examples reported above [24–26].

Of course, neither factor influences partition coefficients, but they may help to accelerate the adjustment of extraction equilibria. Arguments can be put forward to optimize both factors. In most routine laboratories samples to be analysed are prepared simultaneously; the actual shaking of all samples does not last longer than the time needed to extract one sample. In automated liquid–liquid extraction processes (robots), however, in which samples ar processed consecutive [29–31], time is an important variable; the shorter the time of extraction, the higher is the throughput of samples. On the other hand, equilibria may adjust slowly and long periods of extraction may be necessary. Optimization of the extraction time may be required. Higher extraction intensities decrease the size of the droplets of the organic and the aqueous phase in the extraction container. This results in a larger contact surface between the two phases and may influence extraction positively. Vigorous shaking may reduce the extraction time needed. In other words, there may be interaction between extraction time and extraction intensity. Disadvantages of thorough mixing may be the formation of emulsions, which may be difficult to separate in a centrifuge. A disadvantage of both long periods of extraction and high extraction intensities may be the amount of contamination extracted. Also, drawbacks of extended extraction may be irreversible adsorption of associated drug molecules to plasma proteins. Hence for many reasons it is important to select proper values of the process variables.

Three variables were selected: the composition of the extraction liquid (which may be divided into a number of sub-variables, the number of mixture components), the extraction time and the extraction intensity. The extraction liquid components are called mixture variables. Extraction time and extraction intensity are called process variables or factors and their influence can be studied with factorial designs. It is not irrational to presume interaction(s) between mixture and process variables: equilibrium may be achieved faster using a given extraction solvent A than using a given extraction solvent B or a mixture of A and B.

Optimization strategy

Mixture designs. A wide variety of applications of mixture experimental designs were summarized by Cornell [32]. For the optimization of the liquid–liquid extraction of drugs from biological matrices, the use of mixture components as variables seems very reasonable, as discussed previously. The logarithm of the partition coefficient of the analyte is the response to be optimized and the fractions of the different mixture components in the extraction solvent are the control variables. Particularly when more solutes with different structures have to be extracted from a sample, a mixture of solvents may give a better response than a single solvent.

Aspects of mixture designs have been described in detail by Scheffé [33], Snee [34] and Gorman and Hinman [35]. Influences of pure components cannot be investigated in mixture designs, as a change in the fraction of one mixture component always causes a change in the fraction of another component: variables cannot be varied independently. The quadratic and cubic terms in eqns. 2 and 3 are therefore not called interaction terms, but non-linear blending terms.

By mixing more solvents into one extraction solvent, the multivariate solubility parameter δ [22,23] of the extraction liquid can be adjusted to an optimum value.

Factorial designs. Factorial designs are often applied to study the influence of process variables (factors) or to optimize the settings of factors. The application, use and characteristics of factorial designs have been discussed in detail by Box *et al.* [36].

Combined designs. When both mixture and process variables are observed in one design, interaction between these variables can be investigated. Therefore, a combined experimental design has to be selected, which may become large unless efficient fractionation can be accomplished. There are numerous examples in the literature of combined mixture and factorial designs [37–43]. Fractionation may often be necessary: the experimental effort may

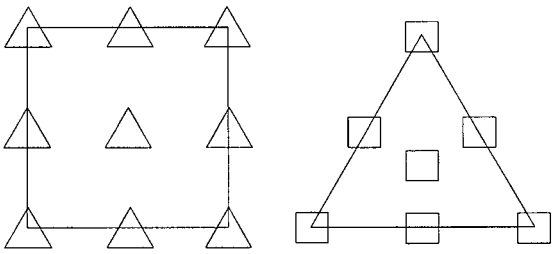

Fig. 1. Two representations of full combined mixture and factorial designs for three mixture variables and two factorial variables at three levels.

increase considerably without fractionation. In our problem, where we have two factors at three levels (3^2 = nine experiments) and three mixture variables with a special cubic mixture model (eqn. 3: seven experiments), $7 \cdot 9 = 63$ model coefficients plus an error term would have to be estimated. Therefore, 64 experiments should be performed according to the designs in Fig. 1, which represents (1) the performance of a mixture design with every combination of process variable settings of the factorial design and (2) the performance of a factorial design with all compositions of the mixture. In fact, these representations correspond to the same experiments. Doornbos *et al.* [42] developed fractionated combined mixture-factorial designs with a concomitant hierarchy of polynomial models. Optimality of the designs was judged with G, V and D optimality criteria. By rotation and contraction they selected a combination design for a 2^{5-1} design (Fig. 2).

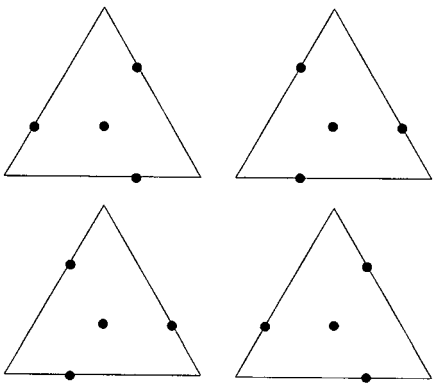

Fig. 2. A fractionated 2^{5-1} combined design after rotation and contraction [42].

EXPERIMENTAL

Selection of extraction solvents

The composition of the extraction liquid is very important for the magnitude of the partition coefficient of a solute. Several quantities have been studied to describe solvent properties [16–18,22,44–46]. Snyder [17,18] grouped the relative selectivities of solvents into solvent selectivity classification groups, each group being characterized by its proton-donating, proton-accepting and dipole interaction properties.

Solvents used here for a general liquid–liquid extraction method were selected from Snyder's solvent selectivity triangle. The goal was to select three solvents that represent a wide variety of selective interactions, so that extraction liquids composed of mixtures of these solvents may enter into maximum interaction with the analyte. Additionally, the solvents should be sufficiently polar to ensure quantitative extraction. In addition to selectivity and polarity requirements, the solvents should also meet a few other criteria, mainly for practical reasons: they should not be miscible with water, have low boiling points (for relatively fast evaporation procedures) and have densities sufficiently different from the density of water, for pure solvents and for selected binary or ternary mixtures of solvents.

The solvents selected were similar to those which Glajch *et al.* [9] used for normal-phase liquid chromatography. Methyl *tert.*-butyl ether (a proton acceptor) was selected instead of diethyl ether, as the former is less volatile. The other two solvents selected were methylene chloride (dipole interactions) and chloroform (proton donor). These three solvents meet all practical requirements. The polarities P' [17] of the solvents are 2.5, 3.1 and 4.1, respectively. The solvents were used in pure form: no supporting solvent was used.

Process variables

The extraction process variable adjustments were a rotating speed of 20, 40 and 60 rotations per minute (rpm) during 5, 15 and 25 min of shaking.

Three levels of a process variable justify investigation of quadratic effects of this process variable. Also, interaction between mixture variables (fractions of solvents in the extraction liquid) and both process variables can be examined.

Regression models and experimental design

The fractions of the three solvents in the extraction liquid are mixture variables. Details of mixture variables were given by Cornell [47]. The process variables extraction intensity and extraction time have to be optimized using a factorial design. Here we propose a combined design for the simultaneous optimization of mixture and process variables, which reduces the number of experiments needed. All variable interactions are given in Fig. 3.

Previous experiments led to the choice of a special cubic model for mixture and process variables (eqn. 6). To estimate the 22 coefficients and the error term at least 23 experiments are required.

variable	1	t	v	t*t	v*v	t*v
x_1	■	■	■	■	■	■
x_2	■	■	■	■	■	■
x_3	■	■	■	■	■	■
x_1x_2	■					
x_1x_3	■					
x_2x_3	■					
$x_1x_2x_3$	■					

Fig. 3. Schematic representation of interaction terms in eqn. 6 (t = extraction time; v = extraction intensity; x_i = mixture variables).

$$E(y) = \beta_1x_1 + \beta_2x_2 + \beta_3x_3 + \beta_{12}x_1x_2 + \beta_{13}x_1x_3 + \beta_{23}x_2x_3 + \beta_{123}x_1x_2x_3 + \gamma_1^1x_1t + \gamma_2^1x_2t + \gamma_3^1x_3t + \gamma_1^{11}x_1t^2 + \gamma_2^{11}x_2t^2 + \gamma_3^{11}x_3t^2 + \gamma_1^2x_1v + \gamma_2^2x_2v + \gamma_3^2x_3v + \gamma_1^{22}x_1v^2 + \gamma_2^{22}x_2v^2 + \gamma_3^{22}x_3v^2 + \gamma_1^{12}x_1tv + \gamma_2^{12}x_2tv + \gamma_3^{12}x_3tv + \varepsilon \quad (6)$$

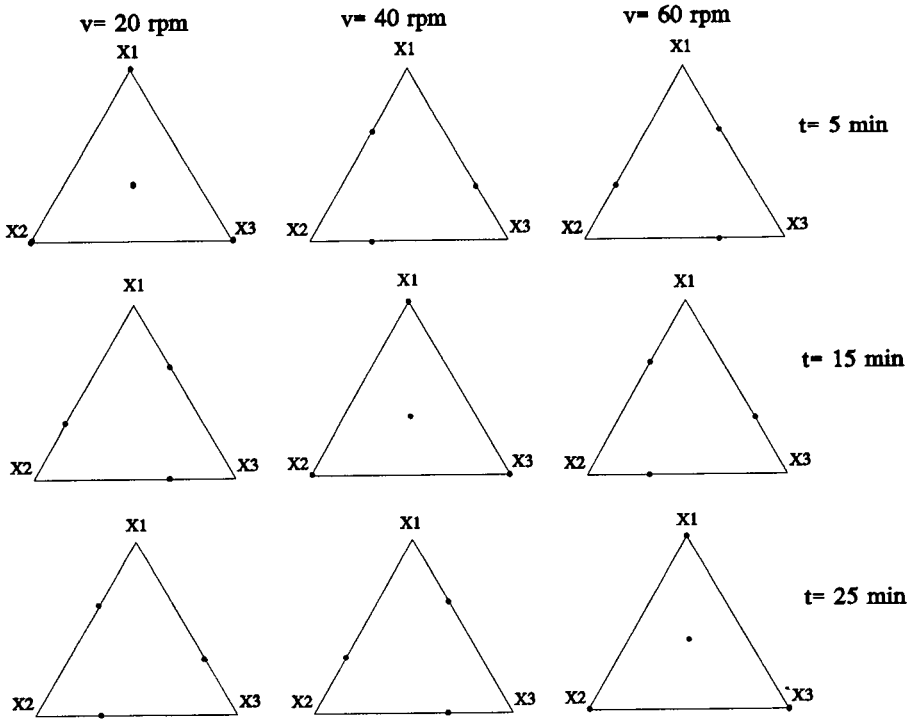

Fig. 4. Experimental design for the extraction of tricyclic amines.

Eqn. 6 is a special cubic mixture model expanded with combinations of mixture variables with linear and squared process variables and with an interaction term between the two process variables with one mixture variable; t is the extraction time and v is the extraction intensity. The β-terms are parameters of the mixture models included. The γ-terms are the parameters for the interaction terms between mixture and process variables. Superscripts in the parameters refer to the process variable(s) involved and subscripts in the parameters refer to mixture variables involved.

Each of the three solvents selected (the mixture variables x_i) is located at a vertex of a triangle, here called factor space. Each point within the factor space is a combination of the fractions of the solvents in the extraction liquid. Several mixture triangles are plotted which symbolize the levels of the process variable(s). Experiments selected should be well distributed over the factor space. With the method described here, no restrictions were made to maximum or minimum fractions of mixture components. The entire factor space (the mixture triangle) is used for design of experiments. In total, 30 experiments were selected, which is seven more than needed for the model (eqn. 6). The extra experiments were used for statistical evaluation of the model. Fig. 4 depicts the factor space and the experiments in the fractional experimental design selected for the amines. Corresponding values of the fractions of methyl *tert.*-butyl ether, chloroform and methylene chloride and the process variables t (extraction time) and v (extraction intensity) are given in Table I.

The criterion modelled in this study was the extraction efficiency (recovery, R). Owing to the introduction of the two process variables the physico-chemical model of the partition coefficient introduced in the theory section was of less value.

Instruments and instrumental conditions

Analyses were performed with an HPLC system consisting of a Waters (Milford, MA, USA) Model 45 HPLC pump used at a flow-rate of 1.2 ml min^{-1} and a Kratos (Ramsey, NJ, USA) Model 757 UV detector (wavelength 250 nm, range 0.01 a.u.f.s., rise time 1 s). Injections of extracts into a Zymark (Hopkinton, MA, USA) Z 310 HPLC injection station, equipped with an electrically controlled Rheodyne valve with a 10-μl sample loop, were performed by a Zymate II robot system. The Zymark Z 310 analytical instrument interface was used to control the HPLC injection station. Data analysis was performed by means of a Spectra-Physics SP4270 computing integrator. The analytical column was a Chrompack (100 × 3.0 mm I.D.) Spherisorb, 5-μm CN cartridge system, which was maintained at 35°C by a thermostatic bath. The injection volume was 10 μl. Mixing was performed on a vortex mixer type FV2 (Janke und Kunkel, Staufen, Germany), shaking of the extraction container was performed on a Heidolph (Kelheim, Germany) Reax-2s shaker for tumble mixing and a Heraeus (Osterrode am

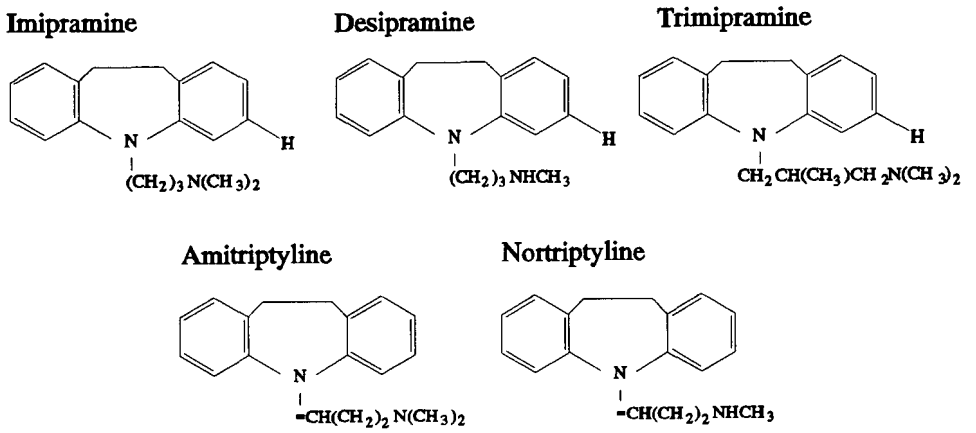

Fig. 5. Structures of the tricyclic amines.

Harz, Germany) Labofuge GL was used for centrifuging.

Chemicals and reagents

The tricyclic amines imipramine (IMI), amitriptyline (AMI), nortriptyline (NOR), desipramine (DES) and trimipramine (TRI) (Fig. 5) were supplied by Sigma (St. Louis, MO, USA). These amines were used because Lagerström *et al.* [27] found a time-dependent recovery for these compounds in several extraction solvents. Acetonitrile (ACN), methylene chloride (DCM) and methanol (MeOH) were supplied by Labscan (Dublin, Ireland) and were of HPLC grade. Chloroform (Clf) was of analytical-reagent grade and supplied by Malinckrodt (Promochem, Wesel, Germany). Phosphoric acid (85%), sodium hydroxide (NaOH), disodium phosphate ($Na_2HPO_4 \cdot 2H_2O$) were all of analytical-reagent grade and supplied by Merck (Darmstadt, Germany). Methyl *tert.*-butyl ether (Uvasol) (tBME) was also supplied by Merck. Water was purified by using a Milli-RO-4 and a Milli-Q water purification system (Millipore, Bedford, MA, USA). Unless stated otherwise, Milli-Q quality water was used throughout. All blank plasma samples used in this study were obtained from a single pool of blank plasma. This was done in order to eliminate the effect that may be present through the use of different plasma samples.

A phosphate buffer (pH 6.5) was prepared by dissolving 450 mg of $Na_2HPO_4 \cdot 2H_2O$ in 500 ml of water. pH adjustment was performed using concentrated phosphoric acid. The mobile phase was prepared by mixing 200 ml of phosphate buffer, 600 ml of ACN and 200 ml of MeOH. NaOH solution (0.03 *M*; pH 12.5) was prepared by dissolving 1.20 g of NaOH in 1 l of water. Stock solutions of the tricyclic amines were prepared by dissolving 100 mg of the compounds in 50 ml of water. These solutions were stored at 4°C and were used to prepare a standard solution of 2 mg l^{-1} of all amines in water. This standard solution contained all five amines and was used for the extraction studies and stored at 4°C.

Analytical procedure

A 250-μl aliquot of plasma to be analysed and 250 μl of the standard solution were pipetted into a 11.5-ml glass tube, then 250 μl of NaOH solution (pH 12.5) were added and mixed for 10 s on a vortex mixer. A 9-ml volume of extraction liquid was added and the tubes were extracted on a Heidolph tumble mixer according to the experimental design in Fig. 4 and Table I. A potential problem arises if the solvents used are mixed in different compositions: a composition can possibly be selected that has a density equal to the density of the aqueous layer, which may give rise to problems with the phase separation.

After centrifugation at 4000 rpm (2755 *g*) for 10 min, the organic layer was transferred into another glass tube of 11.5 ml and evaporated to dryness under a gentle stream of nitrogen at 55°C. The residue was reconstituted in 1 ml of MeOH; 10 μl of the solution were injected into the HPLC system.

For the determination of the absolute analytical recovery ($R = \Phi_{org}$), the peak heights of the prepared samples were compared with the mean peak height of seven direct injections of the standard solution into the HPLC system.

For the correct determination of the recoveries and the partition coefficients (for use in future studies), each tube was weighed separately before and after the extraction solvent dispensing step (to give w_{in}) and before and after phase separation (to give w_{out}). The volume of the extraction liquid used for extraction, V_{in}, was calculated from w_{in} and the density of the extraction liquid considered. In this way the exact volumes used could be measured, which were used to calculate the recoveries and the partition coefficients:

$$\Phi_{org} = R = \frac{\text{peak height extractions}}{\text{peak height direct injection}} \cdot \frac{w_{in}}{w_{out}}$$

$$P = \frac{R}{1-R} \cdot \frac{0.75}{V_{in}}$$

where 0.75 is the volume of the aqueous layer (ml), V_{in} is the volume of the organic phase (*ca.* 9 ml) used for extraction ($V_{in} = w_{in}/\rho_i$; ρ_i is the density of the extraction liquid involved).

As the volumes of both the organic and the aqueous phase influence the recovery of a solute, experiments were done to study if there was an effect of mixing on the volume of the resulting extraction liquid: volumes of 10 ml of methyl *tert.*-butyl ether, chloroform and methylene chloride were mixed to give binary and ternary solvents. These experiments

TABLE I

RECOVERIES OF THE TRICYCLIC AMINES AFTER EXTRACTION ACCORDING TO THE EXPERIMENTAL DESIGN IN FIG. 3

Experimental design					Recovery				
x_{DCM}	x_{Clf}	x_{iBME}	t^a	v^b	TRI	AMI	IMI	NOR	DES
1.0000	0.0000	0.0000	0.0000	0.0000	0.1462	0.2260	0.2726	0.4377	0.5216
0.0000	1.0000	0.0000	0.0000	0.0000	0.1111	0.1897	0.2669	0.4730	0.5780
0.0000	0.0000	1.0000	0.0000	0.0000	0.2875	0.3541	0.4267	0.6428	0.7709
0.3333	0.3333	0.3333	0.0000	0.0000	0.1780	0.2640	0.3370	0.5300	0.6400
0.6667	0.3333	0.0000	0.0000	0.5000	0.2225	0.3151	0.3976	0.6230	0.7294
0.3333	0.0000	0.6667	0.0000	0.5000	0.3732	0.4575	0.5418	0.7950	0.9123
0.0000	0.6667	0.3333	0.0000	0.5000	0.3063	0.4098	0.5227	0.7985	0.9383
0.3333	0.6667	0.0000	0.0000	1.0000	0.2262	0.3191	0.4162	0.6638	0.7943
0.6667	0.0000	0.3333	0.0000	1.0000	0.3487	0.4847	0.5981	0.8195	0.9463
0.0000	0.3333	0.6667	0.0000	1.0000	0.4723	0.5626	0.6695	0.8646	0.9649
0.3333	0.6667	0.0000	0.5000	0.0000	0.1244	0.2367	0.2980	0.4184	0.5670
0.6667	0.0000	0.3333	0.5000	0.0000	0.2323	0.3320	0.4140	0.7193	0.8502
0.0000	0.3333	0.6667	0.5000	0.0000	0.3012	0.3828	0.4665	0.6984	0.8076
1.0000	0.0000	0.0000	0.5000	0.5000	0.2262	0.3318	0.4372	0.7074	0.7811
0.0000	1.0000	0.0000	0.5000	0.5000	0.1551	0.2559	0.3859	0.6897	0.8021
0.0000	0.0000	1.0000	0.5000	0.5000	0.3854	0.4596	0.5621	0.7595	0.8319
0.3333	0.3333	0.3333	0.5000	0.5000	0.2744	0.3930	0.5125	0.7170	0.8090
0.6667	0.3333	0.0000	0.5000	1.0000	0.1928	0.3034	0.4203	0.6944	0.7793
0.3333	0.0000	0.6667	0.5000	1.0000	0.3774	0.4673	0.5742	0.7725	0.8606
0.0000	0.6667	0.3333	0.5000	1.0000	0.2696	0.3971	0.5335	0.7395	0.8189
0.6667	0.3333	0.0000	1.0000	0.0000	0.1907	0.3047	0.4346	0.7587	0.8844
0.3333	0.0000	0.6667	1.0000	0.0000	0.3525	0.4462	0.5653	0.7993	0.9484
0.0000	0.6667	0.3333	1.0000	0.0000	0.2889	0.4188	0.5635	0.7871	0.9055
0.3333	0.6667	0.0000	1.0000	0.5000	0.1782	0.2975	0.4641	0.8630	1.0093
0.6667	0.0000	0.3333	1.0000	0.5000	0.2937	0.4269	0.5859	0.8792	0.9724
0.0000	0.3333	0.6667	1.0000	0.5000	0.4262	0.5341	0.6836	0.9292	1.0206
1.0000	0.0000	0.0000	1.0000	1.0000	0.2660	0.4010	0.5190	0.9074	1.0173
0.0000	1.0000	0.0000	1.0000	1.0000	0.1822	0.3145	0.4850	0.9244	1.0404
0.0000	0.0000	1.0000	1.0000	1.0000	0.4645	0.5485	0.6836	0.9444	1.0143
0.3333	0.3333	0.3333	1.0000	1.0000	0.3485	0.4918	0.6562	0.9538	1.0570

[a] Extraction time: 0.0 = 5 min, 0.5 = 15 min and 1.0 = 25 min.
[b] Extraction intensity: 0.0 = 20 rpm, 0.5 = 40 rpm and 1.0 = 60 rpm.

were done prior to the actual extraction experiments. The densities and volumes of the outcoming liquids were measured to investigate the effect of mixing on the density and volume of the outcoming liquid.

Models of the recoveries were calculated with multiple ordinary least-squares regression for each amine on an IBM PS/2 Model 60 computer using the laboratory-made software package SOLEX (systematic optimization of liquid extraction) written in Pascal.

RESULTS AND DISCUSSION

Effect of mixing on the density and volume

The mixture compositions in Table I did not give rise to any problems with phase separation due to equal densities of the organic and the aqueous layers; all compositions used could be separated from the aqueous layer.

The density and volume measurements after mixing different solvents showed that there was no influence of mixing on the density and volume of the

outcoming liquid. The outcoming volume (V_o) of the mixed liquid was equal to the sum of the individual volumes of the different extraction solvents. For a liquid composed of arbitrary volumes of methylene chloride (V_{DCM}), chloroform (V_{Clf}) and methyl *tert.*-butyl ether (V_{tBME}),

$$V_o = V_{DCM} + V_{Clf} + V_{tBME}$$

A linear relationship ($r = 0.9999$) was found to describe the density of the outcoming (ρ_o) liquid as a function of the particular densities (ρ_i) and fractions of the different solvents in the liquid (x_i). For a liquid composed of n extraction solvents:

$$\rho_o = \sum_{i=1}^{n} x_i \rho_i \quad \left(0 \leqslant x_i \leqslant 1; \sum_{i=1}^{n} x_i = 1\right)$$

Owing to the linearity of these properties it was unnecessary to correct for mixing effects on density and volume.

Extraction of tricyclic amines

No difficulties in any of the settings of the variables in Table I were observed with respect to emulsion formation due to vigorously shaking the extraction container. The recoveries of the five tricyclic amines were measured with the extraction

TABLE II

CALCULATED REGRESSION COEFFICIENTS AND MODEL VALIDATION CRITERIA OF THE COMBINED SPECIAL CUBIC MIXTURE MODEL AND THE QUADRATIC FACTORIAL MODEL (EQN. 6) WITH THE RESULT OF ALL EXPERIMENTS FOR THE AMINES

Models fitted with relative values of extraction time (5 min = 0; 15 min = 0.5; 25 min = 1) and extraction intensity (20 rpm = 0; 40 rpm = 0.5; 60 rpm = 1).

Parameter	Solute				
	TRI	AMI	IMI	NOR	DES
β_1	0.154210	0.234054	0.274570	0.459544	0.549154
β_2	0.113260	0.193460	0.264623	0.473312	0.588316
β_3	0.290544	0.351359	0.420103	0.675951	0.808063
β_{12}	−0.033326	−0.070526	−0.129337	−0.250048	−0.156492
β_{13}	−0.016629	0.044897	0.067622	0.115694	0.234026
β_{23}	0.195647	0.291028	0.337651	0.318056	0.309693
β_{123}	0.099205	0.300874	0.608050	−0.200810	−0.678243
γ_1^1	0.027051	0.034034	0.084671	0.257396	0.258674
γ_2^1	−0.121329	−0.031847	−0.038799	−0.425237	−0.484925
γ_3^1	−0.066026	−0.107685	−0.108416	−0.152534	−0.242696
γ_1^2	0.152585	0.206947	0.341010	0.334618	0.230069
γ_2^2	0.192261	0.162094	0.293614	0.772193	0.865737
γ_3^2	0.304983	0.346528	0.387500	0.237280	0.148014
γ_1^{11}	0.026032	0.070831	0.125472	0.152000	0.168939
γ_2^{11}	0.166929	0.127651	0.206621	0.648396	0.721530
γ_3^{11}	0.213938	0.248285	0.280305	0.230019	0.311115
γ_1^{22}	−0.034391	−0.028792	−0.086476	−0.008965	0.090038
γ_2^{22}	−0.101252	−0.063534	−0.151102	−0.557608	−0.653206
γ_3^{22}	−0.062259	−0.104108	−0.128425	−0.093811	−0.032648
γ_1^{12}	−0.067718	−0.124277	−0.218690	−0.298908	−0.300969
γ_2^{12}	−0.073636	−0.078822	−0.087763	0.009673	−0.006080
γ_3^{12}	−0.214948	−0.183735	−0.162549	0.018651	−0.011766
r	0.9900	0.9888	0.9940	0.9835	0.9783
r^2	0.9802	0.9778	0.9880	0.9673	0.9571
RSD	0.005	0.006	0.006	0.007	0.007
SEP	0.047	0.041	0.036	0.103	0.115
SEP-adj	0.047	0.045	0.038	0.088	0.094
mPRESS	0.002	0.002	0.001	0.010	0.013
mPRESS-adj	0.002	0.002	0.001	0.007	0.008

liquid compositions, extraction times and extraction intensities in Table I, which also gives the results. For adequate sensitivity of detection and analytical reproducibility, it is essential that extraction recovery of the analyte is at least 50%. Desipramine and nortriptyline have recoveries higher than 50% for all extraction liquid compositions using all process variables. The other amines, trimipramine, amitriptyline and imipramine, show relatively low recoveries. These recoveries can be improved by selecting another composition and/or another value for the process variables, as can be seen in Table I.

For desipramine, the recovery in some cases exceeds 100%, which is mainly a result of small variations in the HPLC analysis and the evaporation step (1.5–4%). However, the variation of the recovery of one analyte relative to another is smaller, as variations in HPLC analysis and evaporation affect all compounds similarly.

Polynomial regression was performed on the data in Table I using eqn. 6. Regression models and descriptive capacities of the combined regression models in accordance with eqn. 6 are given in Table II.

Generally, it can be concluded that the recovery of the tricyclic amines is best in methyl *tert.*-butyl ether and worst in chloroform. Hence the recovery increases with decreasing solvent polarity. This is unexpected, as it is often assumed that the more polar the extraction solvent, the higher is the recovery of the analytes in the solvent. It seems appropriate to assume an important role of the selectivity of the extraction liquid in the extraction. Methyl *tert.*-butyl ether is capable of having stronger interactions with the amines than chloroform or methylene chloride, probably because of its proton-accepting properties.

The model presented in eqn. 6 describes well the results obtained according to the experimental design in Fig. 4. Correlation coefficients vary from 0.978 for desipramine to 0.994 for imipramine, values which correspond to explained variance percentages of 95.7–98.8. The standard deviation of the residuals (RSD) after the regression analysis was very small, 0.0053 for trimipramine to 0.0070 for imipramine. The predictive power of the regression models can be judged by two criteria. First, the mean predictive error sum of squares (mPRESS):

$$\text{mPRESS} = \frac{1}{n} \sum_{i=1}^{n} (y_i - \hat{y}_i)^2$$

where y_i is the experimental value for the recovery

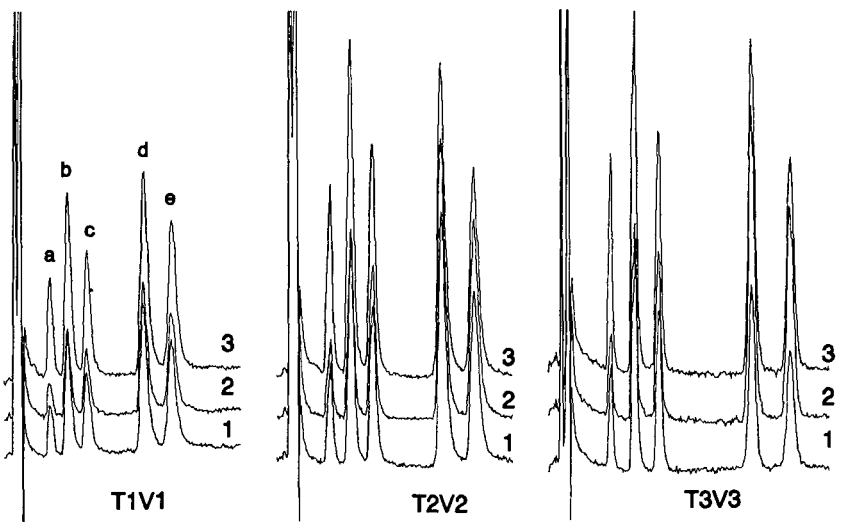

Fig. 6. Chromatograms of the five tricyclic amines after liquid–liquid extraction with pure methylene chloride (1), chloroform (2) and methyl *tert.*-butyl ether (3). Three settings of the process variables were used: T1V1, $t = 5$ min, $v = 20$ rpm; T2V2, $t = 15$ min, $v = 40$ rpm; T3V3, $t = 25$ min, $v = 60$ rpm.

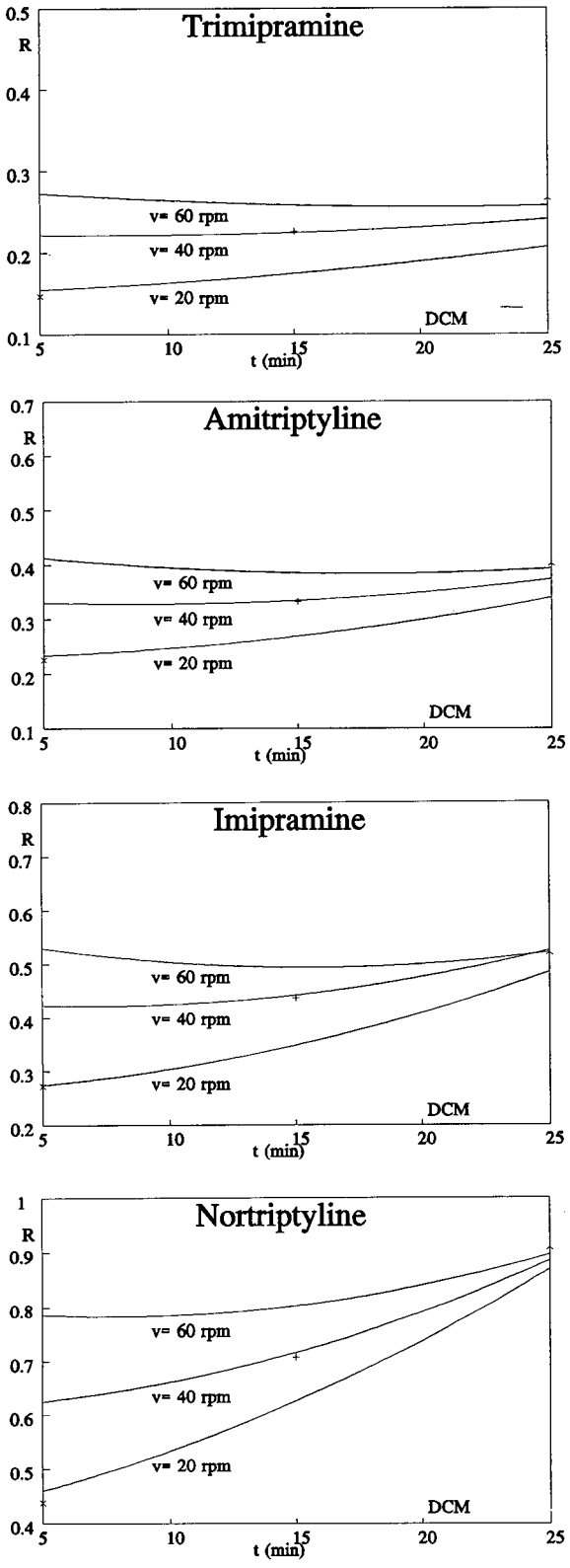

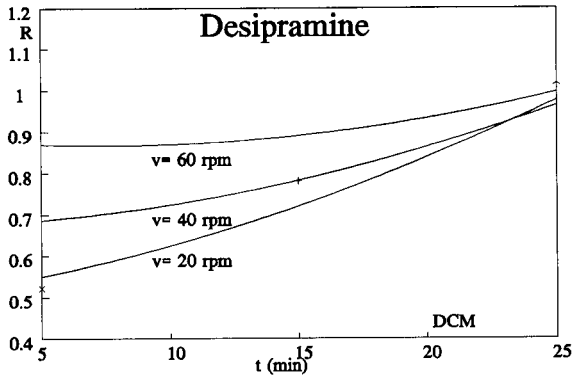

Fig. 7. Recoveries of five tricyclic amines in pure methylene chloride *vs.* extraction time t for three extraction intensities (20, 40 and 60 rpm).

and $\hat{y}_i$ is the value predicted by the regression model, in which experiment i was not incorporated. The mPRESS value is very good for trimipramine, amitriptyline and imipramine and acceptable for nortriptyline and desipramine. Second, the standard error of prediction (SEP) was calculated:

$$\text{SEP} = \sqrt{\frac{\sum_{i=1}^{n} (d_i - \bar{d})^2}{n-1}}$$

where d_i is the predicted error calculated from y_i (the experimental value) and $\hat{y}_i$ (the value predicted by the regression model, in which experiment i was not incorporated), $d_i = y_i - \hat{y}_i$; $\bar{d}$ is the mean of d_i. The SEP value shows the same characteristics for the amines as the mPRESS criterion, *i.e.*, good for trimipramine, amitriptyline and imipramine and acceptable for nortriptyline and desipramine. However, the adjusted value for PRESS and SEP, which are the values calculated without the use of extrapolated design points in the cross-validation, are significantly better for nortriptyline and desipramine.

Fig. 6 shows nine chromatograms of the five amines using three different extraction liquids [(1) DCM, (2) Clf and (3) tBME] with three different settings of the process variables (T1V1, $t = 5$ min, $v = 20$ rpm; T2V2, $t = 15$ min, $v = 40$ rpm; T3V3, $t = 25$ min, $v = 60$ rpm). It can be seen from these chromatograms that the peak heights of the amines increase considerably from T1V1 to T2V2 owing to an increase in the recovery and that there is also a small increase from T2V2 to T3V3. From these

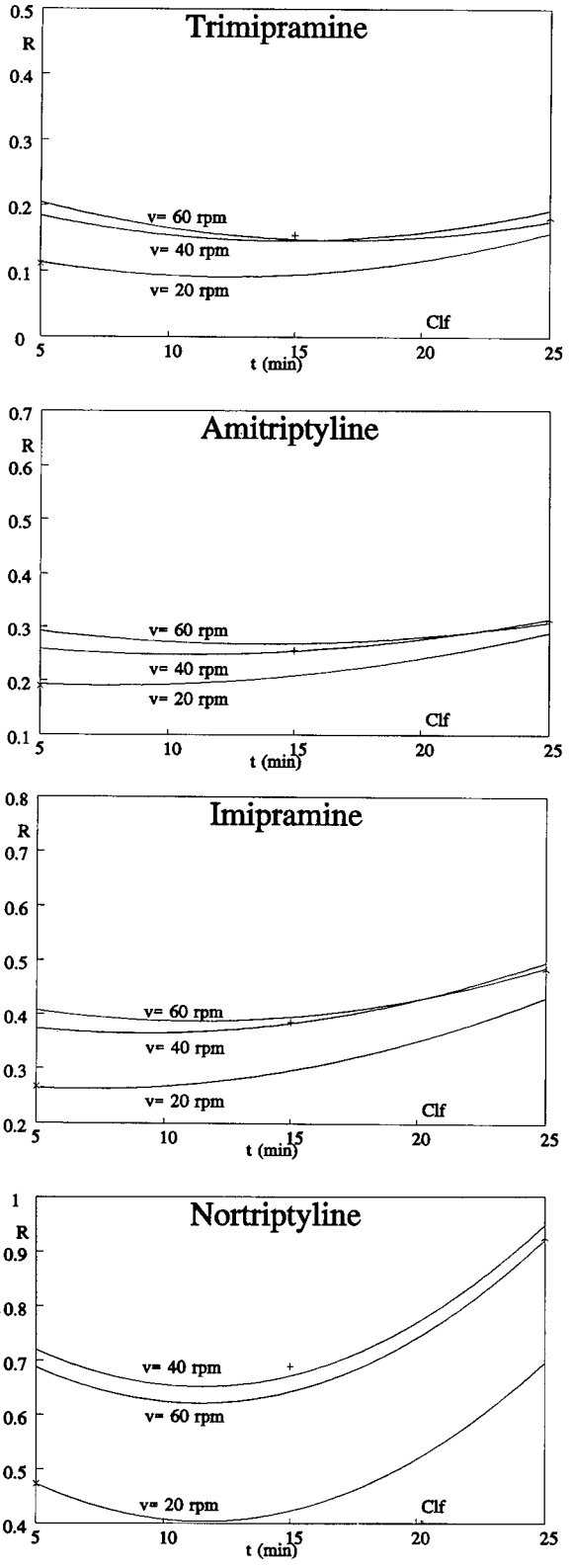

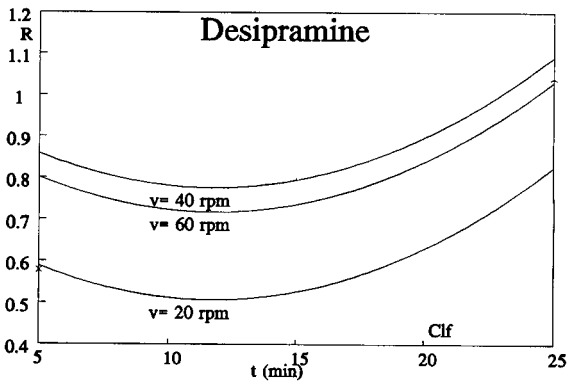

Fig. 8. Recoveries of five tricyclic amines in pure chloroform *vs.* extraction time t for three extraction intensities (20, 40 and 60 rpm).

chromatograms the selectivity of the different extraction liquids used can also be seen: the ratio of the peak heights of each combination of two peaks varies with the extraction liquid used.

The plots of the extraction efficiency *versus* the extraction time of the extraction system in Figs. 7, 8 and 9 (DCM, Clf and tBME, respectively) demonstrate an obvious effect of both extraction intensity and extraction time. The importance of the extraction time decreases if the extraction intensity increases. This is especially demonstrated by the recovery of nortriptyline in methylene chloride (Fig. 7), which increases from less than 60% at 20 rpm to almost 90% at 60 rpm using an extraction time of 5 min. The latter is almost the same as the recovery at 20 rpm for 25 min. This is important information for extraction performed by laboratory robotic systems. Such systems often are programmed for scheduled sample preparation (*i.e.*, processing samples sequentially; within the procedure several samples may be processed in different modules at the same time [29–31]). A significant decrease in the duration of the often time-consuming extraction phase in sample preparation may dramatically decrease the total duration of the analysis of a series of samples or may dramatically increase sample throughput (productivity) in the laboratory.

The initial decrease in recovery as a function of extraction time is not significant. This is a result of small variations in recovery due to HPLC variations and variations in evaporation. Fig. 10 shows the contour plots of the recovery of nortriptyline for

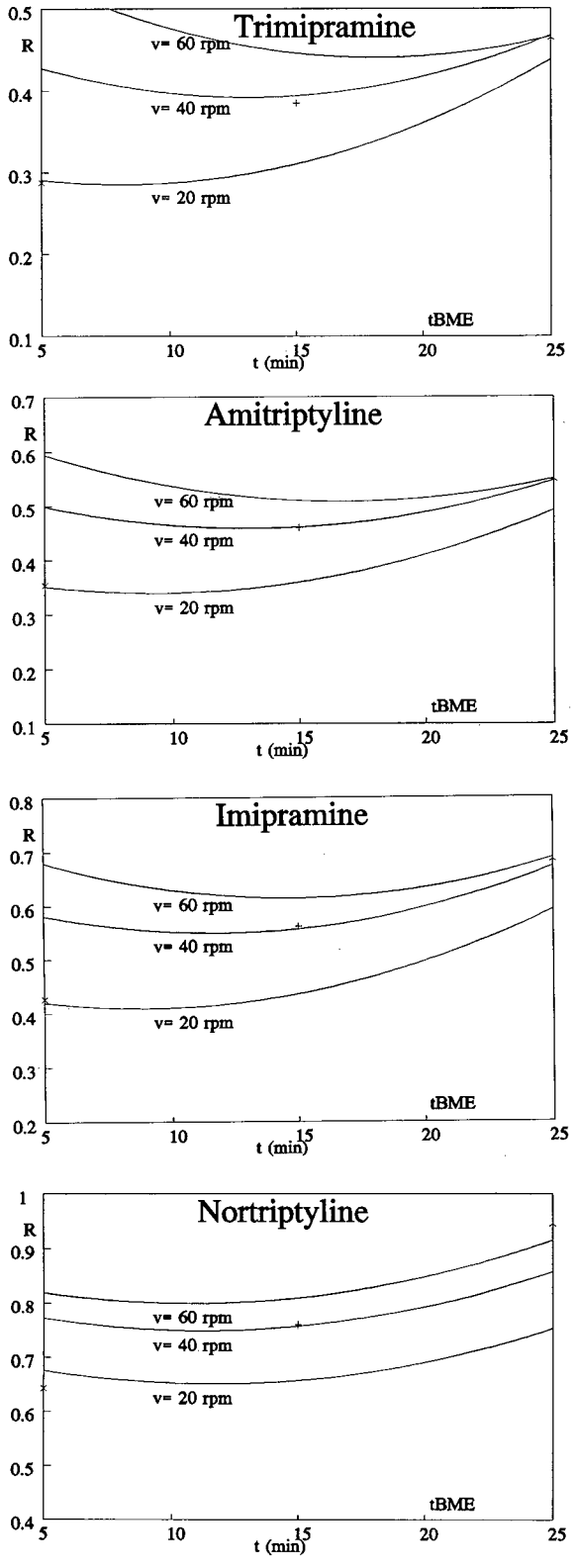

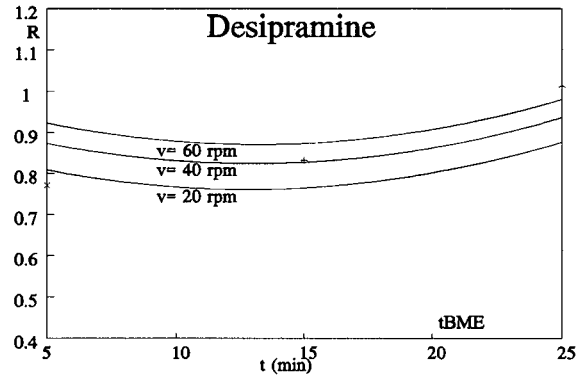

Fig. 9. Recoveries of five tricyclic amines in pure methyl *tert.*-butyl ether *vs.* extraction time *t* for three extraction intensities *v* (20, 40 and 60 rpm).

three different settings of the process variables. It demonstrates a change in the extraction behaviour with respect to the composition of the extraction liquid when the settings of the process variables are altered: the optimum moves from 18% Clf in tBME (T1V1) to 51% Clf in tBME (T3V3). The conclusion for nortriptyline from Fig. 10 may be the following: the optimum selectivity of the extraction liquid within the experimental design applied here may be reached by mixing chloroform and methyl *tert.*-butyl ether. However, the partitioning equilibrium may adjust more slowly with such a mixture as compared with a extraction liquid consisting of pure methyl *tert.*-butyl ether. Methyl *tert.*-butyl ether has a lower partition coefficient but the equilibrium is reached faster.

Figs. 11 and 12 show the ratio of the recovery of trimipramine to those of amitriptyline, imipramine, nortriptyline and desipramine after extraction with methylene chloride, chloroform and methyl *tert.*-butyl ether with varying extraction time (Fig. 11) and extraction intensity (Fig. 12). It can be seen that the extraction time and the extraction intensity can be optimized in a proper extraction liquid composition with respect to the ratio of the recoveries. The ratios can be optimized towards unity or the robustness of the extraction conditions can be optimized to the best values. For the extraction of compounds it is important to have high recoveries; the higher the recovery, the better is the precision. In analyses where two or more solutes have to be extracted simultaneously (*e.g.*, compounds with an internal

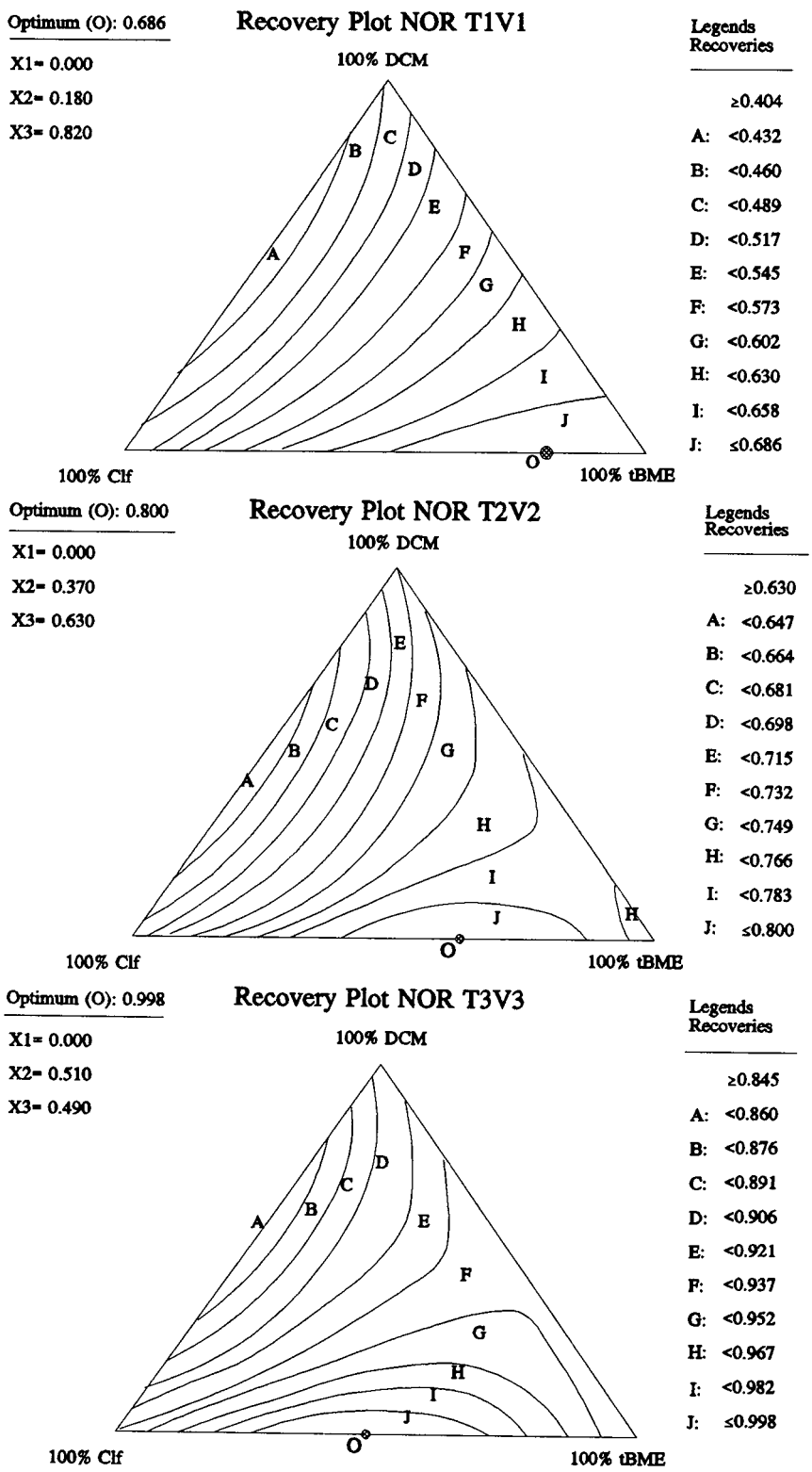

Fig. 10. Contour plots of the recovery of nortriptyline made with three settings of the process variables: T1V1, $t = 5$ min, $v = 20$ rpm; T2V2, $t = 15$ min, $v = 40$ rpm; T3V3, $t = 25$ min, $v = 60$ rpm.

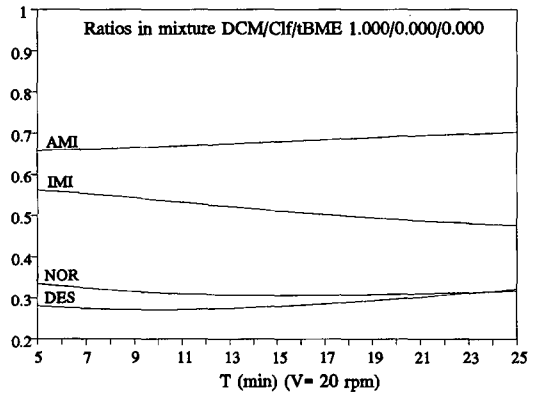

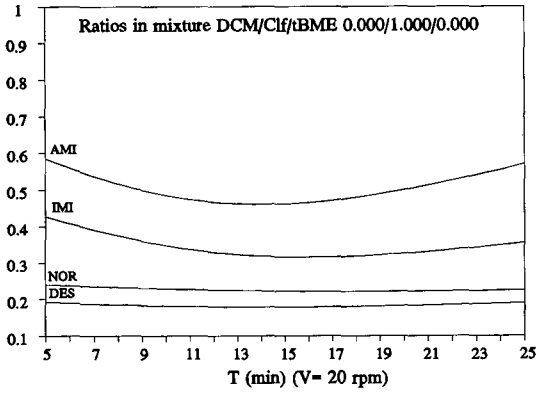

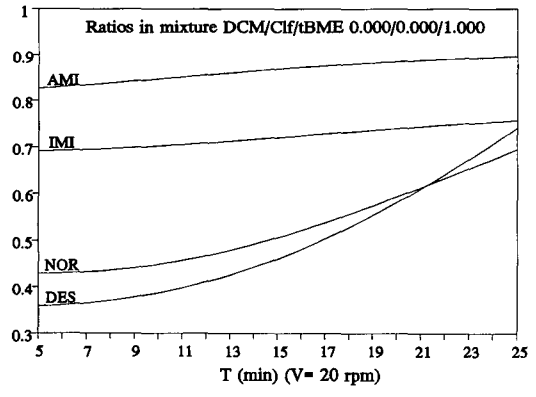

Fig. 11. Ratios of the recovery of trimipramine to the recoveries of amipramine, imipramine, nortriptyline and desipramine after extraction with methylene chloride (DCM), chloroform (Clf) and methyl *tert.*-butyl ether (tBME) *versus* the extraction time *T*.

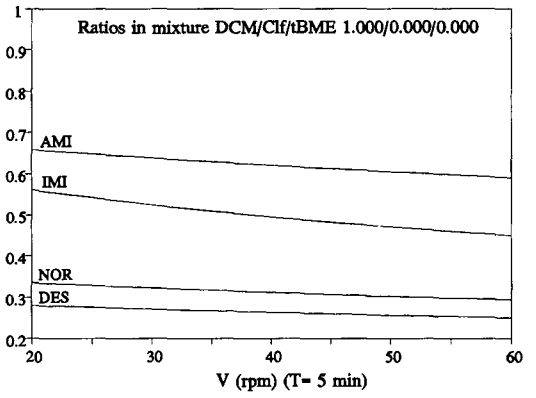

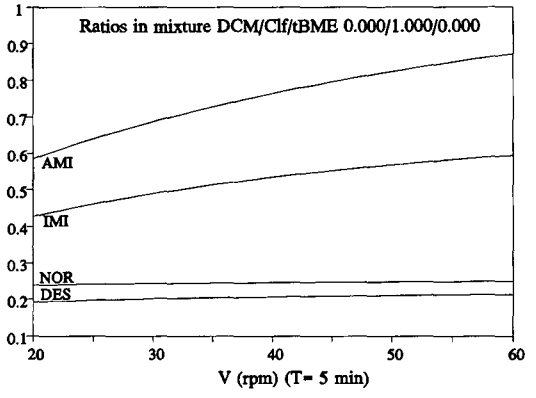

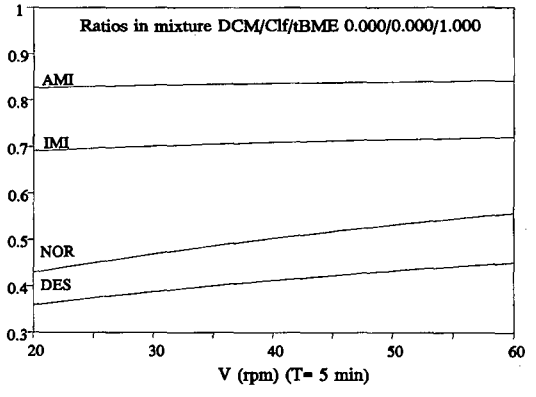

Fig. 12. Ratios of the recovery of trimipramine to the recoveries of amipramine, imipramine, nortriptyline and desipramine after extraction with methylene chloride (DCM), chloroform (Clf) and methyl *tert.*-butyl ether (tBME) *versus* the extraction intensity *V*.

standard), it is also important to have an equal affinity of the extraction liquid for all compounds to be extracted ($R_i/R_j = 1$) and robust extraction ratios: small variations in the extraction conditions (extraction liquid composition, extraction time, extraction intensity) should therefore not affect the

ratio of the recoveries of two compounds. Conditions should be selected where the variation in the ratio, due to variation in the conditions, is small, *i.e.*, the ratio is robust. The robustness criterion can be used to select values of the extraction intensity and the extraction time where the conditions are robust to small variances. This robustness is very important in routine analysis [48].

A typical case is the extraction of trimipramine and desipramine in tBME with varying extraction time (Fig. 11): the extraction ratio of these analytes is optimum (0.75) using an extraction time of 25 min. However, using this extraction time, the robustness of these conditions for the ratio is not very good. The best extraction time for this pair of analytes with respect to the robustness of the extraction conditions for the ratio is 5 min. However, using this extraction time, the ratio is worse (0.28).

Generally, it can be seen from the results in this paper that interactions between extraction liquid composition and process variables do not equally affect the recovery of all amines; small differences can be seen. Therefore, even when the differences between compounds to be extracted are very small, as in this instance, a significant difference in extraction behaviour can be seen. This observation may lead to new extraction experiments where compounds are used that have larger differences. Then the differences in extraction behaviour may be even more dramatic.

CONCLUSIONS

Mixtures of preselected organic solvents result in higher recoveries of the tricyclic amines than pure solvents. The application of a factorial design incorporated in a mixture experimental design in the optimization liquid–liquid extraction of drugs from biological matrices gives good results for the extraction of a number of tricyclic amines from plasma. Optimization of recoveries is reasonable by mixing three solvents with different selective interactions. The introduction of two process variables and the simultaneous variation of these variables with the mixture variables makes possible the simultaneous modelling of combined experimental designs. A preselected limited number of design points permits the use of fractional designs for the optimization of liquid–liquid extraction of drugs from biological matrices; the applicability of combined fractional experimental designs for the simultaneous optimization of extraction liquid composition, extraction time and extraction intensity has been demonstrated. For a group of tricyclic amines there is interaction between the two process variables (extraction intensity and extraction time): a higher extraction intensity justifies a shorter extraction time. For future research, using optimization of liquid–liquid extraction of drug with a laboratory robot and subsequent use of the optimized extraction liquid composition and process variable adjustment under routine conditions may result in a distinct decrease in the time needed for an analytical run.

An interaction exists between the composition of the extraction liquid and the process variables: the extraction behaviour changes when these variables are varied simultaneously. Structurally related compounds demonstrate different extraction behaviours in a ternary liquid–liquid extraction system composed of methylene chloride, chloroform and methyl *tert.*-butyl ether. In investigations for finding proper internal standards, one should take into account the extraction liquid used for extraction of both analyte and internal standard.

ACKNOWLEDGEMENT

The authors thank the Dutch Technology Foundation (Stichting voor de Technische Wetenschappen, STW) for their support of this project.

REFERENCES

1 J. Chamberlain, *Analysis of Drugs in Biological Fluids*, CRC Press, Boca Raton, FL, 1985, pp. 152–154.
2 R. Whelpton and S. H. Curry, in E. Reid (Editor), *Assay of Drugs and Other Trace Compounds in Biological Fluids*, North-Holland, Amsterdam, 1976, pp. 115–120.
3 P. Bouis, G. Taccard and U. A. Boelsterli, *J. Chromatogr.*, 526 (1990) 447–459.
4 O. Y.-P. Hu, S.-P. Chang, Y.-B. Song, K.-Y. Chen and C.-K. Law, *J. Chromatogr.*, 532 (1990) 337–350.
5 D. Westerlund and A. Theodorsen, *Acta Pharm. Suec.*, 12 (1975) 127–148.
6 M. Aravagiri, S. R. Marder and Th. van Putten, *J. Chromatogr.*, 525 (1990) 419–425.
7 R. Modin and G. Schill, *Talanta*, 22 (1975) 1017–1022.
8 J. W. Weyland, C. H. P. Bruins, H. J. G. Debets, B. L. Bajema and D. A. Doornbos, *Anal. Chim. Acta*, 153 (1983) 93–101.
9 J. L. Glajch, J. J. Kirkland, K. M. Squire and J. M. Minor, *J. Chromatogr.*, 199 (1980) 57.

10 J. W. Weyland, C. H. P. Bruins and D. A. Doornbos, *J. Chromatogr. Sci.*, 22 (1984) 31.
11 M. Mulholland and J. Waterhouse, *J. Chromatogr.*, 395 (1987) 539–551.
12 M. Mulholland and J. Waterhouse, *Chromatographia*, 25 (1988) 769–774.
13 M. Mulholland and J. Waterhouse, *Chemom. Intell. Lab. Syst.*, 5 (1988) 263.
14 P. M. J. Coenegracht, A. K. Smilde, H. J. Metting and D. A. Doornbos, *J. Chromatogr.*, 485 (1989) 195–217.
15 J. Wieling, J. Hempenius, P. M. J. Coenegracht, J. H. G. Jonkman, C. K. Mensink and D. A. Doornbos, *Pharm. Weekbl., Sci. Ed.*, 11 (1989) N11.
16 L. Rohrschneider, *Anal. Chem.*, 45 (1973) 1241.
17 L. R. Snyder, *J. Chromatogr. Sci.*, 16 (1978) 223–234.
18 L. R. Snyder, *J. Chromatogr.*, 92 (1974) 223–230.
19 Cs. Horváth, W. Melander and I. Molnár, *J. Chromatogr.*, 125 (1976) 129.
20 Cs. Horváth, W. Melander and I. Molnár, *Anal. Chem.*, 49 (1977) 142.
21 R. Tijssen, H. A. H. Billiet and P. J. Schoenmakers, *J. Chromatogr.*, 122 (1976) 185.
22 P. H. J. Schoenmakers, *Ph. D. Thesis*, Technical University, Delft, 1981.
23 J. H. Hildebrand, J. M. Prausnitz and J. M. M. Scott, *Regular and Related Solutions*, Van Nostrand Reinhold, New York, 1970.
24 J. Wieling, P. M. J. Coenegracht, C. A. A. Duineveld, J. H. G. Jonkman and D. A. Doornbos, presented at the *COBAC V Session of Euroanalysis VII, Vienna, 1990.*
25 Trevor, M. Rowland and E. L. Way, in B. N. La Du, H. G. Mandel and E. L. Way (Editors), *Fundamentals of Drug Metabolism and Drug Disposition*, Williams & Wilkins, Baltimore, 1972, p. 369.
26 D. B. Campbell, in E. Reid (Editor), *Assay of Drugs and Other Trace Compounds in Biological Fluids*, North-Holland, Amsterdam, 1976, p. 105.
27 P.-O. Lagerström, I. Marle and B.-A. Persson, *J. Chromatogr.*, 273 (1983) 151.
28 G. Schill, H. Ehrsson, J. Vessman and D. Westerlund, *Separation Methods for Drugs and Related Organic Compounds*, Swedish Pharmaceutical Press, Stockholm, 1983, pp. 129–130.
29 J. Hempenius, J. Wieling, J. H. G. Jonkman, O. E. de Noord, P. M. J. Coenegracht and D. A. Doornbos, *J. Pharm. Biomed. Anal.*, 8 (1990) 313–320.
30 J. Wieling, J. P. de Kleijn, J. H. G. Jonkman and C. K. Mensink, in J. Klaessens (Editor), *Computers in de Chemie —J. Toepassingen in de Analytische Laboratoria*, SCME/KNCV, Den Haag, 1991.
31 J. Wieling, J. Hempenius, H. J. Jeuring, J. H. G. Jonkman, P. M. J. Coenegracht and D. A. Doornbos, *J. Pharm. Biomed. Anal.*, 8 (1990) 577–582.
32 J. A. Cornell, *Technometrics*, 21 (1979) 95–106.
33 H. Scheffé, *J. R. Stat. Soc., Ser. B*, 20 (1958) 344–360.
34 R. D. Snee, *Chemtech*, (1979) 702–710.
35 J. W. Gorman and J. E. Hinman, *Technometrics*, 4 (1962) 463–487.
36 G. E. P. Box, W. G. Hunter and J. S. Hunter, *Statistics for Experimenters*, Wiley, New York, 1978.
37 J. A. Cornell, *J. Am. Stat. Assoc., Ser. A*, 66 (1971) 42–48.
38 L. B. Hare, *Technometrics*, 21 (1979) 159–173.
39 I. N. Vuchkov, D. L. Damgaliev and Ch. A. Yontchev, *Technometrics*, 23 (1981) 233–238.
40 J. W. Gorman and J. A. Cornell, *Technometrics*, 24 (1982) 243–247.
41 V. Czitrom, *Commun. Stat. Theory*, 17 (1988) 105–121.
42 D. A. Doornbos, A. K. Smilde, J. H. de Boer and C. A. A. Duineveld, in E. J. Karjalainen (Editor), *Scientific Computing and Automation (Europe) 1990, Proceedings of the Scientific Computing and Automation (Europe) Conference, 12–15 June, 1990, Maastricht, The Netherlands*, Elsevier, Amsterdam, 1990, pp. 85–95.
43 C. A. A. Duineveld, *Chemom. Intell. Lab. Syst.*, in press.
44 Cs. Horváth, W. Melander and I. Molnár, *J. Chromatogr.*, 125 (1976) 129.
45 Cs. Horváth, W. Melander and I. Molnár, *Anal. Chem.*, 49 (1977) 142.
46 L. R. Snyder, *J. Chromatogr. Sci.*, 16 (1978) 223.
47 J. A. Cornell, *Experiments with Mixtures*, Wiley, New York, 2nd ed., 1990.
48 J. Wieling, P. M. J. Coenegracht, C. K. Mensink, J. H. G. Jonkman and D. A. Doornbos, *J. Chromatogr.*, 594 (1992) 45–64.

Journal of Chromatography, 629 (1993) 201–213
Elsevier Science Publishers B.V., Amsterdam

CHROM. 24 652

Novel affinity separations based on perfluorocarbon emulsions

Development of a perfluorocarbon emulsion reactor for continuous affinity separations and its application in the purification of human serum albumin from blood plasma

Graham E. McCreath and Howard A. Chase

Department of Chemical Engineering, University of Cambridge, Pembroke Street, Cambridge CB2 3RA (UK)

Duncan R. Purvis and Christopher R. Lowe

Institute of Biotechnology, University of Cambridge, Tennis Court Road, Cambridge CB2 1QT (UK)

(First received August 13th, 1992; revised manuscript received September 29th, 1992)

ABSTRACT

Perfluorocarbon affinity emulsions are generated by the homogenisation of a perfluorocarbon oil with a polymeric fluorosurfactant previously derivatised with an affinity ligand and subsequently cross-linked *in situ*. This procedure gives rise to a novel liquid affinity adsorbent that can be used for continuous protein purification. Discrete emulsion droplets were found to be unstable when pumped for prolonged periods; however, when flocculated, the emulsion floccules with diameters of around 125 μm, were very stable and sedimented faster. A four-stage reactor unit (perfluorocarbon emulsion reactor for continuous affinity separations, PERCAS) was designed and constructed to carry out continuous separations, and exploited the unusual properties of the adsorbent, *i.e.* liquid nature and high density. Each of the four stages of PERCAS consisted of a mixing tank, for contacting between emulsion phase and aqueous phase, adjacent to a settling tank for the subsequent separation of emulsion from the aqueous phase. Using PERCAS adsorption, washing, elution and re-equilibration of the emulsion could be carried out continuously with emulsion recycle. Using single-component adsorption of human serum albumin to a perfluorocarbon affinity emulsion derivatised with the triazine dye C.I. Reactive Blue 2, PERCAS was optimised with respect to flow-rates and input concentrations. The work was then extended to the continuous purification of essentially homogeneous human serum albumin from blood plasma.

INTRODUCTION

Affinity chromatography, based on biological recognition, offers a powerful technique for analytical and process scale bioseparation. However, its usual column mode of operation imposes some limitations on its practicality when moving from analytical to process scale. One of the limitations is the inherent cyclic batch mode of operation (*i.e.* load, wash, elute and re-equilibrate), which means that purified product is only being recovered at one stage of the operation. Furthermore, operational problems are also encountered, e.g. the difficulty of scaling up, column occlusion by particulates neces-

Correspondence to: G. E. McCreath, Department of Chemical Engineering, University of Cambridge, Pembroke Street, Cambridge CB2 3RA, UK.

0021-9673/93/$06.00

sitating the incorporation of a filtration or centrifugation step, attainable throughputs etc. Some of these problems have been tackled by changing the contacting stage from a column to some other contactor. Notable examples include continuous affinity-recycle extraction (CARE) [1], in which solid–liquid contacting is carried out in well-mixed reactors (continuous operation is achieved by recirculation of adsorbent between two or more contactors) and expanded bed adsorption which can work in the presence of particulates [2]. By expanding a bed of adsorbent by flowing a solution upwards through the bed, particulates can pass unhindered through spaces generated between the adsorbent particles. Other systems change the physical nature of the adsorbent or use reverse micelles [3], membrane encapsulated ligands [4] and affinity partitioning using two-phase aqueous polymer solutions [5]. All the above processes are amenable to both scale up and continuous operation and have met with some degree of success.

A novel approach to continuous affinity separations is the use of perfluorocarbon affinity emulsions. Perfluorocarbons are a class of synthetic molecules derived from hydrocarbons in which all the hydrogen atoms have been replaced with fluorine atoms and are characterised as being chemically and biologically inert, have low solubility in aqueous and organic solvents and have densities in the region 1.6–2.0 g/ml. In separation science, perfluorocarbons have been used as packings for HPLC [6] and as stationary phases in gas–liquid chromatography [7]. Conceptually, a solid perfluorocarbon would make an ideal chromatographic support because of its stability and mechanical strength, allowing it to be used at high flow-rates and under harsh conditions. However, the inertness and hydrophobic character of perfluorocarbon surfaces has precluded their use in affinity chromatography where hydrophilicity and ease of derivatisation are deemed desirable. Recently, chemistries have been developed that allow for modification of the perfluorocarbon surface with subsequent ease of ligand immobilisation [8]. Perfluorocarbon surfaces are only wetted, in water, in the presence of surfactants that adsorb to their surface. Kobos *et al.* [9] described the technique of perfluoroalkylating enzymes in order to promote their adsorption to fluorocarbon surfaces. This was exploited in the development of a urea electrode by immobilising perfluoroalkylated urease onto the surface of a gas-permeable fluorocarbon membrane of an ammonia sensor. Further work led to the development of immobilisation procedures for a variety of biomolecules ranging from enzymes to affinity ligands on both solid and liquid perfluorocarbon surfaces [10]. More recently, the technique of perfluoroalylation has been used to generate perfluorocarbon based affinity supports based on triazine dyes [11]. Consequently, C.I. Reactive Blue 4 was substituted with perfluoroalkyl groups and used to purify rabbit muscle lactate dehydrogenase on both solid and liquid perfluorocarbons. These affinity supports were found to be quite stable under a range of harsh conditions; however, ligand leakage was detected in certain aprotic solvents and in the presence of albumin solutions. A new range of perfluorocarbon supports were then developed which utilised the coating of the perfluorocarbon surface with a hydrophilic polymer layer [12]: poly(vinyl alcohol) (PVA) was derivatised with perfluoroalkyl groups and was found to adsorb strongly, and essentially irreversibly, to perfluorocarbon surfaces. This approach and subsequent approaches, gave rise to generic chromatographic supports which could be substituted with a range of ligands such as triazine dyes [12], metal chelating groups [13] and Protein A [13].

We have concentrated on the development of liquid perfluorocarbon chromatographic supports using techniques similar to those outlined above. Perfluorocarbon affinity emulsions are generated by homogenisation of a perfluorocarbon oil with a polymeric surfactant previously derivatised with an affinity ligand and subsequently cross-linked *in situ*. Perfluorocarbon emulsions are interesting, in a biochemical engineering sense, because they open up possibilities for continuous affinity separations. We have previously shown [14] that perfluorocarbon emulsions incorporating affinity ligands could be generated which could bind human serum albumin (HSA) and lysozyme. We later showed how an affinity emulsion incorporating the affinity ligand C.I. Reactive Blue 4 could be used in an expanded bed for the semi-continuous purification of HSA from blood plasma [15]. However, these operations were restricted to the use of the emulsions in expanded beds and in order that the emulsions be used for continuous separations, the emulsion phase would

have to be transported. Although the emulsions were stable when used in expanded beds, it was found that when pumped, for prolonged periods of time, the droplets began to coalesce. The stability of the emulsions was found to be dependent on both the molecular mass of the polymeric surfactant used and the degree of substitution of the ligand [16]. In order to make the emulsions more stable a technique of chemically inducing flocculation between discrete emulsion droplets was developed. This was carried out by increasing the molar ratio of the cross-linker used and by maintaining excess polymeric surfactant in solution when cross-linking. A mol/mol ratio of 141:1 (glutaraldehyde:PVA) was found to give a very stable floccule of a predictable size and gave a high recovery of bound protein [17]. Flocculation (20–60 drops/floccule) also increased the sedimentation rate of the emulsion and facilitated collection from the aqueous phase.

Perfluorocarbon affinity emulsions possess unique features not commonly found in conventional affinity supports. Both the high density of the core perfluorocarbon oil (1.92 g/ml), which generates rapid sedimentation times in aqueous solutions, and the inherent transportability of liquid emulsions are features which can be used in continuous affinity separations. In order to perform continuous separations, we have designed and constructed a four-stage mixer settler unit, PERCAS (an acronym for perfluorocarbon emulsion reactor for continuous affinity separations). And in this paper we describe the use of PERCAS for the continuous separation of HSA from blood plasma.

EXPERIMENTAL

Materials

PVA (M_r 115 000, 100% hydrolysed) was purchased from Aldrich (Gillingham, UK) as was sodium thiocyanate. Perfluorodecalin (Flutec PP6) was obtained from ISC Chemicals (Avonmouth, Bristol, UK). Sodium acetate (anhydrous) was purchased from Fisons (Loughborough, UK). The diagnostic reagent kit for serum albumin determination was purchased from Sigma (Poole, UK) as were the chemicals sodium dihydrogenphosphate, disodium hydrogenphosphate, 2-mercaptoethanol and glutaraldehyde (25%, w/v). Pure human serum albumin was also purchased from Sigma while human plasma was obtained from a known donor at the National Blood Transfusion Centre (Nottingham, UK) and tested negative for HIV III, HBS antigen and syphilis. C.I. Reactive Blue 2 was purchased from Polysciences. All other chemicals were purchased from BDH (Dagenham, UK). Masterflex peristaltic pumps (Cole-Palmer, UK) were partly used for delivery to the PERCAS unit, the remaining delivery pumps were a Pharmacia P-1 (Pharmacia Biotechnology, Milton Keynes, UK) and a Minipuls II (Gilson, France).

Synthesis of polymeric fluorosurfactant–dye conjugate

The polymeric fluorosurfactant–dye conjugate was synthesised essentially as described previously [15]. Hence, PVA (M_r 115 000, 100% hydrolysed, 10 g) was dissolved in distilled water (200 ml) by heating to 80–90°C for 30–40 min. The solution was cooled and the triazine dye C.I. Reactive Blue 2 (5 g) added and the solution stirred for 30 min at room temperature. The reaction mixture was heated to 70°C with the addition of sodium chloride (5 g) and sodium carbonate (5 g) and refluxed for 3 h. Sodium hydroxide was added (5 g) and refluxing continued for a further 5 h. Dyed polymeric fluorosurfactant was purified and characterised as described previously [15].

Generation of perfluorocarbon affinity emulsions

Perfluorodecalin (95 g) was homogenised with a solution of dyed polymeric fluorosurfactant (200 ml, 25 mg/ml) in a cylindrical glass vessel. Homogenisation was carried out for 2 min using an Ultra-Turrax T-25 homogeniser (Sartorius, Surrey, UK) (full speed). The resulting emulsion was then cross-linked and flocculated.

Cross-linking and flocculation

Perfluorocarbon affinity emulsion (60 ml) was added to a solution of free dyed polymeric fluorosurfactant in distilled water (100 ml, 10 mg/ml, pH 7.0). To this stirred solution was added glutaraldehyde to a final molar ratio of 141:1 (glutaraldehyde:PVA). After 10 min, HCl (5 *M*) was added to give a final concentration of 0.1 *M*. Cross-linking and flocculation was carried out for 1.5 h and terminated by the addition of sodium hydroxide to 0.5 *M*. The emulsion was allowed to settle and the

aqueous phase discarded and replaced with 60 ml distilled water and mixed. This solution (emulsion and water) was transferred to a buchner flask and vigorously degassed for 2 h. The settled emulsion was collected and washed with 20 m*M* sodium phosphate buffer, pH 5.0 until washings were clear of free dyed polymer as determined spectrophotometrically at peak absorbance of the ligand (620 nm). A sample of the emulsions was then analysed for floccule size distributions using a Mastersizer M6.02 (Malvern Instruments).

Protein determination and assay

Protein determination was carried out routinely using the Pierce Coomassie protein assay reagent. Protein concentrations in stock solutions were initially determined by absorbance at 280 nm using an extinction coefficient of 0.53 ml mg^{-1} cm^{-1} for HSA [18] and 0.66 ml mg^{-1} cm^{-1} for bovine serum albumin [19]. Spectrophotometry was carried out using a Shimadzu UV-160A spectrophotometer (VA Howe, UK). Serial dilutions of stock solutions (20 μl) were incubated with assay reagent (1 ml) by mixing for 10 min at room temperature. The absorbance was then read at 595 nm against a buffer blank to prepare standard curves.

Serum albumin content in plasma was determined using the bromocresol green assay [20]. A standard curve was prepared by taking serial dilutions of stock HSA (200 μl) and adding assay reagent (1 ml). The absorbance was read at 628 nm after 10 min incubation. Plasma was centrifuged (8800 *g*, 5 min) and then filtered (0.45 μm). Diluted (1 in 50) samples were assayed for total protein. Dilutions (1 in 10) were assayed specifically for HSA.

Equilibrium adsorption isotherms for HSA

The equilibrium adsorption isotherm for HSA was determined using the procedures outlined by Chase [21]. An emulsion slurry (1 ml of a 1:1 emulsion:buffer) (20 m*M* sodium phosphate buffer, pH 5.0) was pipetted into each of a series of Eppendorf micro test tubes. The emulsion phase was allowed to settle and the supernatant discarded. To each of these tubes was added HSA (1 ml) in 20 m*M* sodium phosphate buffer, pH 5.0 to give a range of concentrations up to 5 mg/ml. The test tubes were rotary mixed for 2 h at room temperature before the emulsion was settled and the aqueous phase assayed for remaining protein. The amount bound to the emulsion can be calculated from a knowledge of the equilibrium concentration and the starting concentration.

In order to determine the recovery of bound HSA, the supernatant was removed and the emulsion washed (× 3) with 20 m*M* sodium phosphate buffer, pH 5.0 (1 ml), HSA was eluted with sodium thiocyanate (0.5 *M*) in 20 m*M* sodium phosphate buffer, pH 8.0 (1 ml) and all fractions were assayed for protein. The recovery of bound HSA could be determined by constructing a simple mass balance.

Single stage batch adsorption of HSA using PERCAS

PERCAS (containing 30 ml of settled emulsion) was equilibrated with the appropriate buffers (stages 1, 2 and 4, 20 m*M* sodium acetate, pH 5.0; stage 3, 0.5 *M* sodium thiocyanate in 100 m*M* sodium phosphate, pH 8.0) at the flow-rates shown in Fig. 3a. Once a steady state had been reached (1 h) where the levels of emulsion in the settling chambers were equal, the buffer input into stage 1 was changed to HSA (500 μg/ml). The experiment was continued for 3 h with aliquots (200 μl) being taken from the top phase of settling chambers 1 and 3 every 15 min. The flow over from each stage was also collected throughout the experiment. All samples were assayed for HSA and the flow over was also monitored for change in pH.

Continuous purification of HSA from plasma using PERCAS

PERCAS was equilibrated as described above using the flow-rates shown in Fig. 3b. Again, once a steady state was achieved the buffer input into stage 1 was changed to plasma (0.75 mg/ml). Samples were again collected every 15 min for 4 h, the flow over was also collected. All samples were assayed for total protein and specifically for HSA. Samples were taken for analysis by sodium dodecyl sulphate–polyacrylamide gel electrophoresis (SDS-PAGE).

SDS-PAGE

SDS-PAGE was carried out essentially as described by Laemmli [22] using a Pharmacia Phast-System horizontal electrophoresis unit. Gels used

were PhastGel Homogeneous 12.5 (13 mm stacking gel zone, 32 mm separation gel zone), used in conjunction with PhastGel SDS Buffer strips (0.55%, w/v, SDS). To the samples was added SDS to 2.5% (w/v) and 2-mercaptoethanol to 5% (v/v). The samples were than heated to 100°C for 5 min and bromophenol blue added to approximately 0.01% (w/v). Protein samples (4 μl) were loaded and the gels stained with PhastGel Blue R (Coomassie R 350). Gels were stored in a preserving solution containing 10% (v/v) glycerol and 10% (v/v) acetic acid in distilled water.

RESULTS AND DISCUSSION

Qualitative aspects of PERCAS design

Fig. 1 presents a diagramatic representation of PERCAS. The unit was made entirely from Perspex to allow ease of construction and to enable visualisation of the process. Mixing was induced in the four chambers by use of a small rectangular impeller connected via a stainless-steel shaft to a belt and pulley system. The impellers were rotated using a simple variable speed a.c. motor. The settling chamber was designed to ensure that emulsion phase

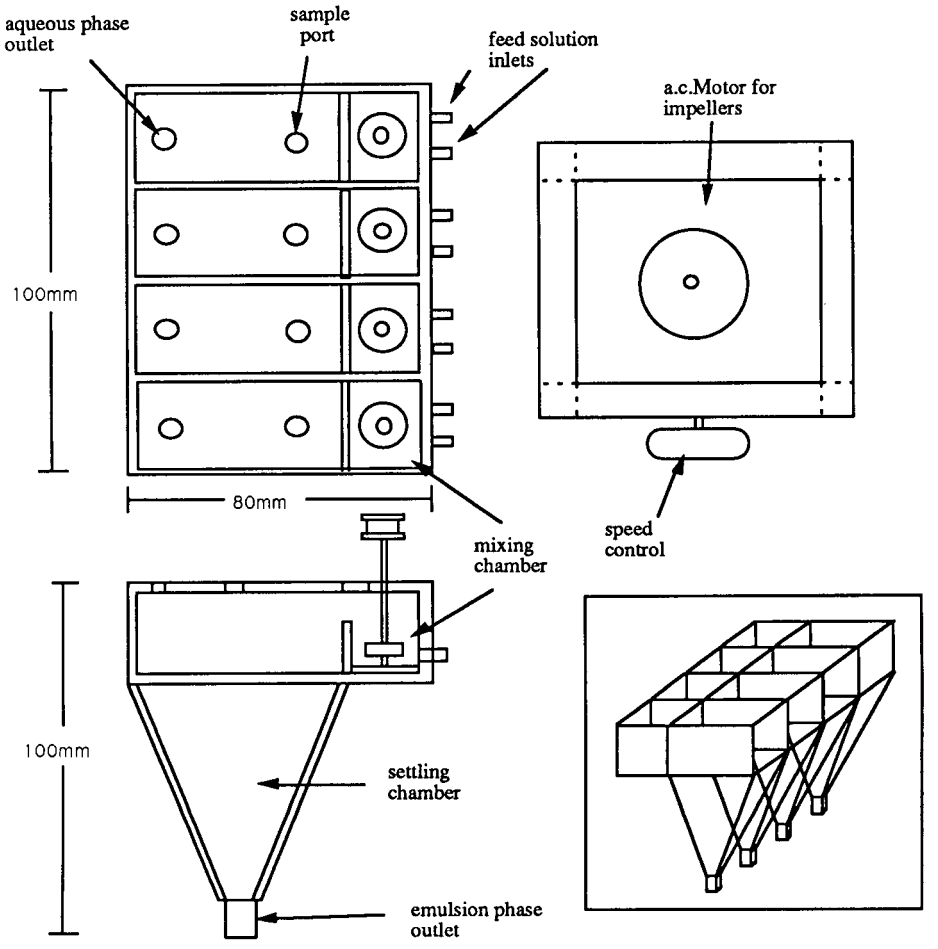

Fig. 1. Plan view and side elevation of the PERCAS unit. Insert box, schematic representation of complete PERCAS unit minus the drive unit and support stand.

contamination of the upper aqueous phase was kept to a minimum. The upper aqueous (or non-perfluorocarbon phase) was actively pumped out of the settling chamber which also includes a sample port for sampling of the aqueous phase. Fig. 2 shows the operational principle behind continuous affinity separations using perfluorocarbon affinity emulsions. Emulsion and aqueous protein phase are pumped into the first mixing chamber where adsorption takes place between the affinity emulsion and the target protein. After a predetermined residence time, which is governed by the flow-rates, the contents begin to spill over a weir into the adjacent settling tank. Here, because of the high density, separation of the emulsion phase from the aqueous phase occurs rapidly. The aqueous phase containing non-adsorbed components is pumped out and the emulsion phase is pumped into the second mixing chamber. A flow of wash buffer into this second chamber removes any contaminants entrapped within the loaded emulsion phase. Again, the contents spill over into a settling tank where phase separation takes place. The washed emulsion is then pumped into the eluting stage where the eluent flow-rate is controlled so as to maximise the concentration of protein eluted into the aqueous product. The emulsion phase is then pumped into the fourth mixing chamber where the emulsion is washed free of entrapped eluent with loading buffer. After settling, the emulsion is recycled back to the first stage. The flow-rate of the emulsion phase throughout the unit is kept constant while the flow-rates of the various aqueous phase constituents can be varied. By using PERCAS it is possible to process large volumes of protein containing solutions by using a relatively small volume of emulsion because the emulsion is continuously recycled.

Fig. 3a and b present, diagramatically, the vari-

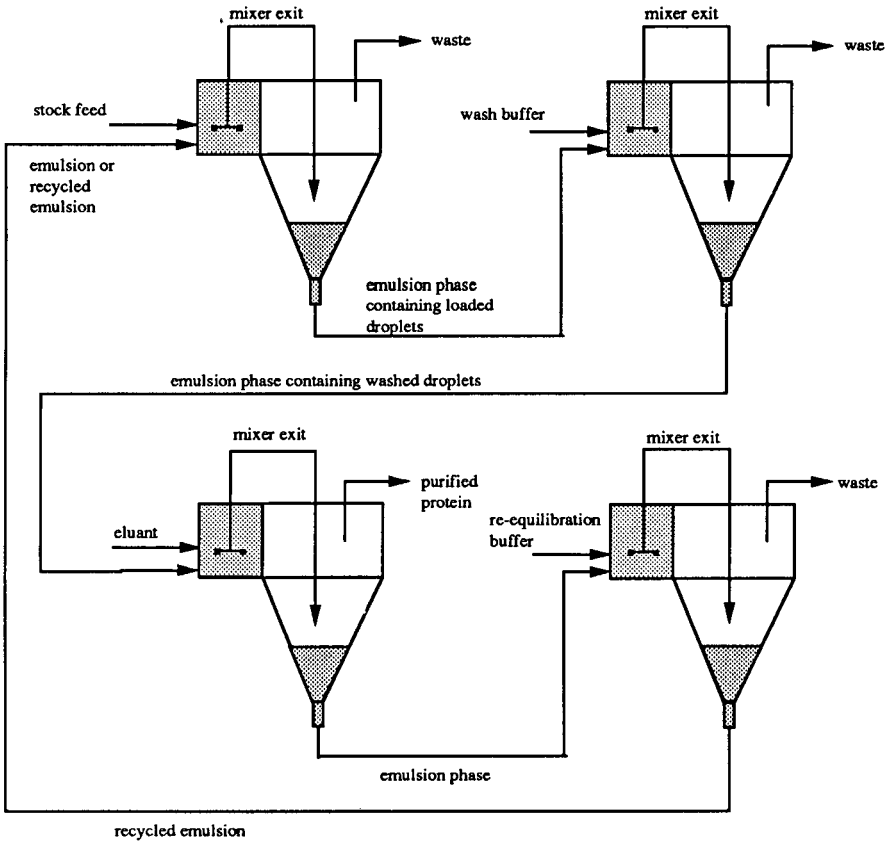

Fig. 2. Operating principle of continuous affinity separations using PERCAS as described in introduction.

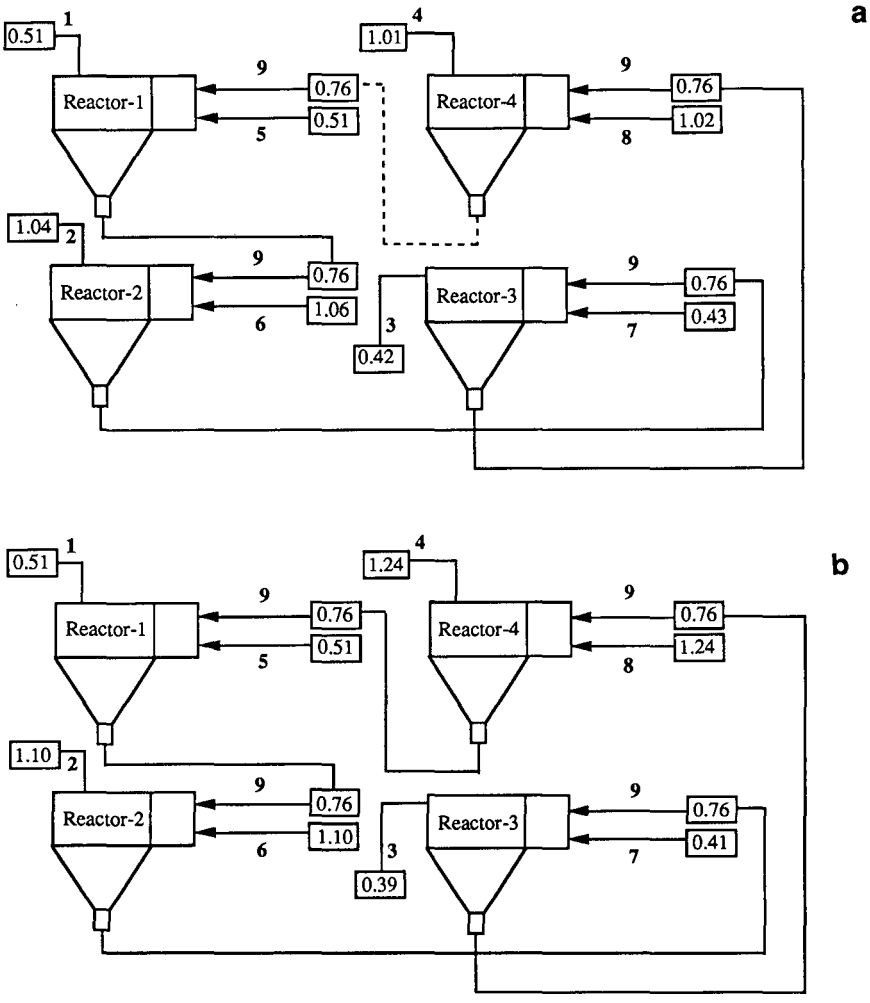

Stream	Description
1	Flow out of settler 1
2	Flow out of settler 2
3	Flow out of settler 3
4	Flow out of settler 4
5	Protein feed solution
6	Wash buffer
7	Eluate
8	Re-equilibration buffer
9	Emulsion (recycled)

Fig. 3. Diagramatic representation of operational set-up of PERCAS using flocculated C.I. Reactive Blue 2 perfluorocarbon affinity emulsion showing a description of all flow streams. (a) Flow-rates for the single component adsorption test for HSA; (b) flow-rates used for the continuous purification of HSA from plasma. All flow-rates quoted are in ml/min.

ous pump positions and descriptions of feed compositions for the PERCAS unit. Streams 1, 2, 3 and 4 are pumped using a single multichannel pump; which could have been omitted if each settling chamber had a weir. Stream 9 (*i.e.* the emulsion phase stream from each settler) also used a multichannel pump. The remaining streams 5, 6, 7 and 8 all used single-channel pumps, which makes the total inventory of pumps 6. This inventory could be reduced to 2 if a series of weirs replaced the single multichannel pump used for streams 1, 2, 3 and 4 and a multichannel pump replaced the single channel pumps used for streams 5, 6, 7 and 8.

Emulsion preparation

The degree of ligand substitution on the PVA (M_r 115 000, 100% hydrolysed) was estimated to be 0.98:1 (dye:PVA molar ratio) and is similar to that we have reported previously [14]. Homogenisation (20%, v/v, perfluorodecalin) produced emulsion

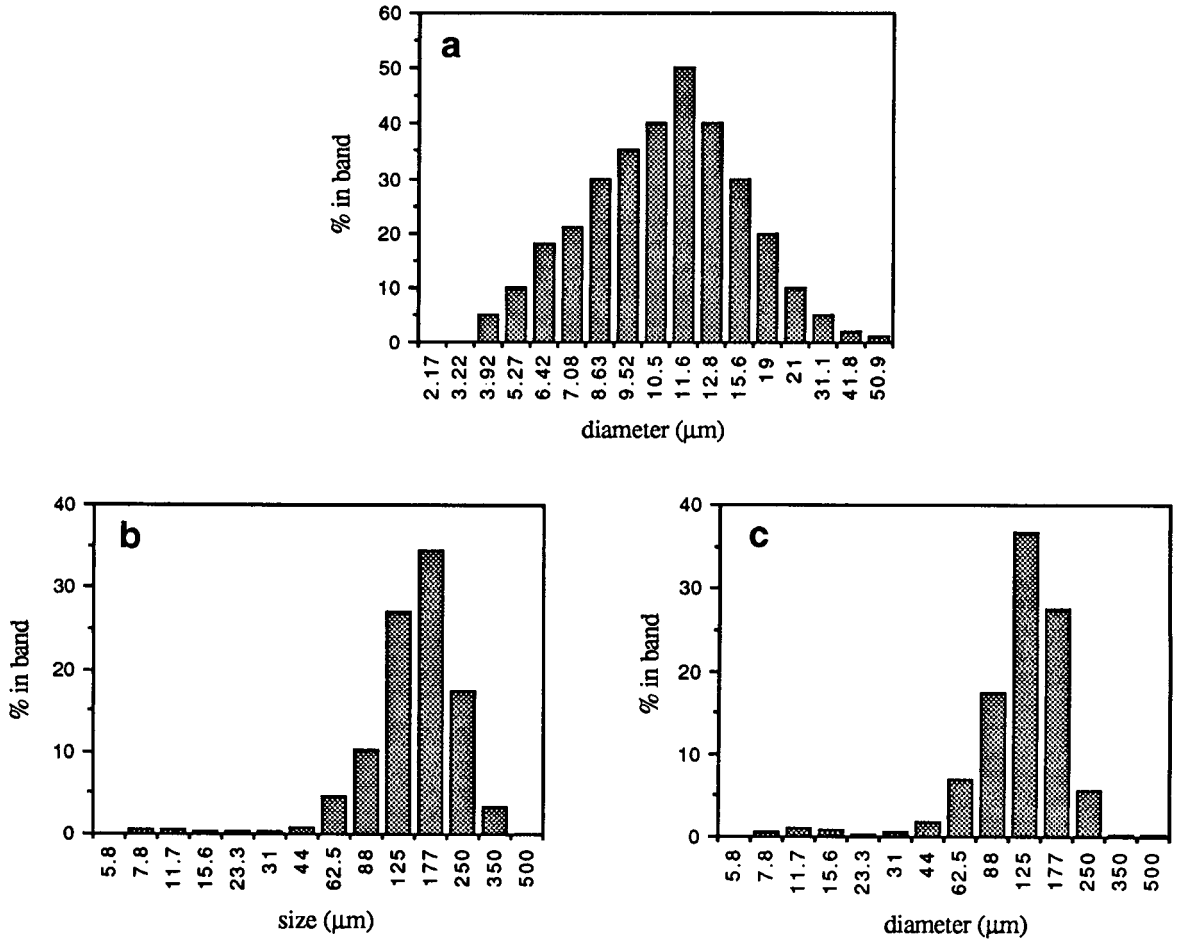

Fig. 4. Size distribution curves for the generation of C.I. Reactive Blue 2 perfluorocarbon affinity emulsion floccules. Perfluorodecalin (95 g) was homogenised with dyed polymeric fluorosurfactant (200 ml, 25 mg/ml) for 2 min using an Ultra-Turrax T-25 homogeniser (full speed). Resulting emulsion was cross-linked and flocculated by the addition of settled emulsion (60 ml) to a solution of dyed polymeric fluorosurfactant (10 mg/ml) in distilled water (100 ml, pH 7.0). Glutaraldehyde was added to a mol/mol ratio of 141:1 (glutaraldehyde:PVA) and HCl (5 *M*) added to a final concentration of 0.1 *M*. Cross-linking and flocculation was carried out for 1.5 h when it was terminated by the addition of NaOH to 0.5 *M*. Flocculated emulsion was then degassed for 2 h. (a) Size distribution of perfluorocarbon affinity emulsion after homogenisation; (b) flocculated perfluorocarbon affinity emulsion before degassing; (c) after degassing.

droplets with an average diameter of 12.5 μm and a size range of 4–40 μm (Fig. 4a). The surface area (a parameter determined by the Malvern Particle Sizer) was 0.6 m^2/ml settled emulsion. Cross-linking of the emulsion was instigated by the addition of glutaraldehyde with HCl as a catalyst [23]. As excess glutaraldehyde and PVA were used, cross-linking occurs between adsorbed PVA molecules on the surface of the droplet and between free PVA in solution, between adsorbed PVA molecules and also between PVA molecules on separate droplets. This inter- and intra-cross-linking effectively builds up a floccule of discrete emulsion droplets whose growth (for a given concentration of PVA and cross-linker) is dependent on the time of cross-linking. Following cross-linking, the emulsion floccules are vigourously degassed. We believe that degassing leads to a condensation of the PVA on the emulsion floccule and an overall tightening up of the floccule. This is evidenced by a change in the floccule size distribution. Fig. 4b shows the size distribution of a flocculated emulsion before degassing while Fig. 4c shows the same emulsion once degassing has been completed. The mean floccule diameter drops from 177 μm to 125 μm on degassing. A microscopic examination of the supernatant after degassing reveals no evidence either of the floccule breaking up, or of the emulsion breaking down. We believe that on degassing, the outermost PVA layer is pulled to the surface bringing with it bound droplets, if present. Once on the surface, the PVA may react with remaining free aldehyde groups. Therefore, in using these procedures dense emulsion floccules are produced which show superior stability yet still retain the inherent transportability of the discrete emulsion.

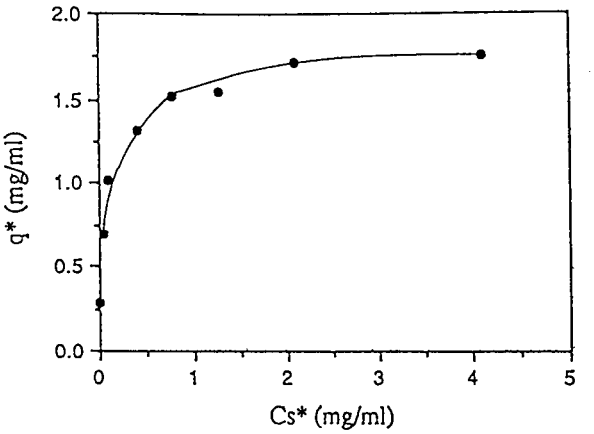

Fig. 5. Equilibrium adsorption isotherm for HSA on flocculated C.I. Reactive Blue 2 perfluorocarbon affinity emulsion. Emulsion (1:1 in 20 m*M* sodium acetate buffer, pH 5.0) was added to a series of micro test tubes, allowed to settle and the aqueous phase removed and replaced with HSA (in 20 m*M* sodium acetate buffer, pH 5.0) in a concentration range up to 5 mg/ml (1 ml). Incubation was carried out by rotary tumbling for 2 h at room temperature, the emulsion was allowed to settle and aqueous phase assayed for the disappearance of HSA.

HSA adsorption

The equilibrium adsorption isotherm for HSA (Fig. 5) was found to fit a Langmuir isotherm of the form:

$$q^* = \frac{q_m C_s^*}{(K_d + C_s^*)}$$

which describes the equilibrium capacity of the emulsion (q^*) as a function of the equilibrium concentration of protein in the soluble phase (C_s^*) [21]

TABLE I

RECOVERY OF BOUND SERUM ALBUMIN

Samples of emulsion with adsorbed HSA were washed (× 3) with 20 m*M* sodium acetate buffer, pH 5.0, bound HSA was eluted by the addition of 0.5 *M* sodium thiocyanate in 100 m*M* sodium phosphate buffer, pH 8.0 (1 ml). Washings and elutions were collected and assayed as described under Experimental.

Experiment number	1	2	3	4	5	6	7	8
HSA added (mg)	0.19	0.38	0.57	0.95	1.43	1.90	2.85	4.76
HSA recovered (mg)	0.17	0.37	0.58	0.84	1.40	1.85	2.86	4.63
Recovery (%)	89	98	101	88	98	97	100	97

where K_d is the dissociation constant. The maximum capacity of the flocculated emulsion (q_m) for HSA was found to be 1.81 mg/ml settled emulsion with (K_d) = 0.12 mg/ml. The q_m of the flocculated emulsion (1.81 mg/ml) is higher than that quoted for a previous discrete emulsion incorporating the same affinity ligand (0.37 mg/ml) [14]. This is to be expected since the flocculated affinity emulsion contains not only emulsion droplets but also bridging dyed PVA molecules which would result in an increase in the surface area compared to a non-porous particle with the same diameter. (K_d) is approximately the same as described previously (0.12 mg/ml as opposed to 0.10 mg/ml [14]). It is desirable to have the K_d as low as possible as this will determine, in part, the residence time required in the adsorption stage of the PERCAS unit.

The possibility of irreversible non-specific adsorption of HSA onto the emulsion floccule was tested by washing and elution of HSA from the emulsion following the isotherm determination. These results are depicted in Table I and show that the average recovery of HSA was 96%. The absence of irreversible adsorption demonstrates that the PVA was effectively wetting the surface of the perfluorocarbon and that there was limited exposure of free aldehyde groups. Consequently, the cross-linked emulsion did not require capping with ethanolamine.

Continuous adsorption and elution of HSA

PERCAS, with the flocculated emulsion, was tested for its ability to bind and elute HSA on a continuous basis. In stage 1 contact between the HSA and the affinity emulsion takes place. After settling, the loaded emulsion is transported to stage 2. Any HSA that has not been adsorbed to the emulsion remains in the aqueous phase and is pumped out of the settling chamber (referred to as the flow through). Thus, a concentration profile for non-adsorbed HSA appears as shown in Fig. 6. This is analogous to a breakthrough curve as obtained in column chromatography. The elution of bound HSA from the affinity emulsion takes place in stage 3. Again the concentration of eluted HSA builds up in the settling chamber as seen in Fig. 6 until a steady state is reached. The concentration of HSA used was 500 μg/ml. The emulsion flow-rate (0.76 ml/min) and the HSA solution flow-rate (0.51 ml/min) gave an average residence time in the mixer unit of 8 min. An analysis of the results is presented in Table II. By multiplying the volumetric flow-rate by the concentration the data can be used to calculate the yield in each stage of the reactor. The input

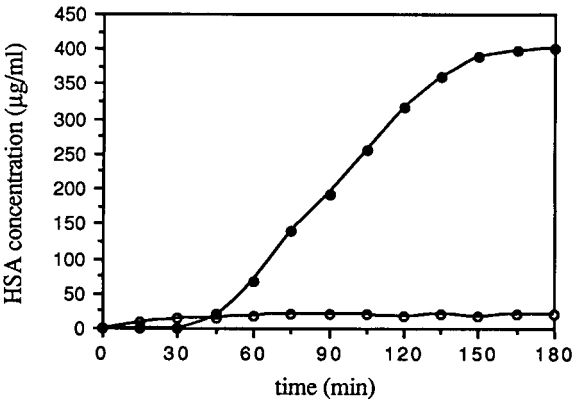

Fig. 6. Single-component adsorption test of HSA on flocculated C.I. Reactive Blue 2 perfluorocarbon affinity emulsion. The PERCAS unit was equilibrated at the flow-rates and buffer compositions shown in Fig. 3. HSA (500 μg/ml in 20 m*M* sodium acetate buffer, pH 5.0) was pumped into the PERCAS unit at 0.508 ml/min. HSA was recovered from stage 3 after elution of the emulsion with 0.5 *M* sodium thiocyanate in 100 m*M* sodium phosphate buffer, pH 8.0 at a flow-rate of 0.42 ml/min. Assays performed as described under Experimental. ○ = Flow through; ● = eluted.

TABLE II

DETERMINATION OF HSA YIELD FROM CONTINUOUS ADSORPTION AND ELUTION OF HSA

HSA (500 μg/ml) was pumped into the PERCAS unit at a volumetric flow-rate of 0.51 ml/min (0.255 mg/min). Bound HSA was eluted in stage 3 with 0.5 *M* sodium thiocyanate in 100 m*M* sodium phosphate buffer, pH 8.0. HSA detected by Pierce Coomasie reagent kit as described under Experimental. The stream numbers refer to Fig. 3.

Stream	Flow-rate (ml/min)	Protein concentration (mg/ml)	Protein flow-rate (mg/min)
(HSA) 5 – in	0.508	0.50	0.254
1 — out	0.51	0.025	0.013
2 — out	1.04	0.008	0.008
3 — out	0.42	0.40	0.168
4 — out	1.01	0.020	0.020

of HSA into PERCAS was 0.255 mg/min, the sum of the outputs of HSA from each stage equalled 0.21 mg/min which gave the process an overall yield of 82%. Fig. 6 clearly demonstrates that PERCAS is capable of binding and eluting HSA on a continuous basis. The versatility of the system enables residence times, wash rates and product concentration to be controlled by changing the appropriate flow-rates.

Continuous purification of HSA from plasma

Fig. 7 presents the results for the continuous purification of HSA from human plasma using a flocculated perfluorocarbon affinity emulsion and PERCAS over a 4-h period. The graph is plotted as total protein concentration against time for the out flow from stages 1 and 3. The experiment was run for 3 h to reach a steady state and then for a further 1 h. Aliquots from the steady state region were collected and used to prepare the data in Table III which shows PERCAS performance in steady state conditions. The input flow-rate of plasma was 0.51 ml/min and the eluted HSA flow-rate was 0.39 ml/min. In both wash streams (stages 2 and 4) the flow-rates were increased from those previously used to 1.10 and 1.24 ml/min, respectively. This was to ensure that contamination of the eluted stream was kept to a minimum and that re-equilibration of the emulsion occured. Consideration of the levels of total protein in all the aqueous streams indicated that

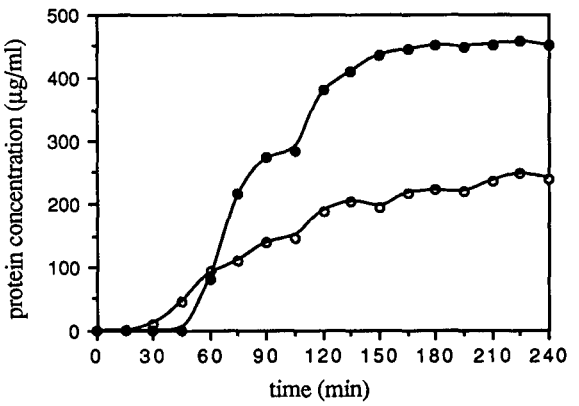

Fig. 7. Continuous purification of HSA from plasma using flocculated C.I. Reactive Blue 2 perfluorocarbon affinity emulsion and PERCAS. Plasma (diluted 1 in 100 with 20 m*M* sodium acetate buffer, pH 5.0) was pumped into PERCAS stage 1 at 0.508 ml/min. Purified HSA was collected from stage 3 after elution of the emulsion with 0.5 *M* sodium thiocyanate in 100 m*M* sodium phosphate buffer, pH 8.0 at a flow-rate of 0.39 ml/min. Assays performed as described under Experimental. ○ = Flow through; ● = eluted.

recovery of total protein was 89% with the recovery of HSA at 81%. The overall yield for the process was calculated by dividing the eluted HSA rate by the input HSA rate and gave 71%. Table III shows that HSA was recovered at 91% purity which corresponded to a purification factor of 1.52 (theoretical maximum purification fold in the sample used is

TABLE III

CONTINUOUS PURIFICATION OF SERUM ALBUMIN FROM PLASMA USING FLOCCULATED C.I. REACTIVE BLUE 2 PERFLUOROCARBON AFFINITY EMULSION

Albumin was purified from dilute plasma (1 in 100) in a continuous fashion using the PERCAS unit and flocculated C.I. Reactive Blue 2 perfluorocarbon affinity emulsion. Settled emulsion volume in PERCAS, 30 ml; running and washing buffer (in stages 1, 2 and 4), 20 m*M* sodium acetate, pH 5.0; eluting buffer (stage 3), 0.5 *M* sodium thiocyanate in 100 m*M* sodium phosphate buffer, pH 8.0. Flow-rate of applied plasma stream, 0.508 ml/min, flow-rate of product stream, 0.39 ml/min. Protein measured by Pierce Coomasie assay, albumin detected by the bromocresol green assay.

Stream	Flow-rate (ml/min)	Protein concentration (mg/ml)	Protein flow-rate (mg/min)	HSA concentration (mg/ml)	HSA flow-rate (mg/min)	Albumin content (%)	Yield (%)	Purification (fold)
5 — in (Plasma)	0.508	0.75	0.381	0.457	0.232	61	(100)	(1)
1 — out	0.510	0.24	0.122	0.036	0.018	–	–	
2 — out	1.10	0.021	0.023	< 0.005	< 0.005	–	–	
3 — out	0.39	0.45	0.175	0.42	0.164	91	70	1.52
4 — out	1.24	0.015	0.018	0.01	0.018	–	–	

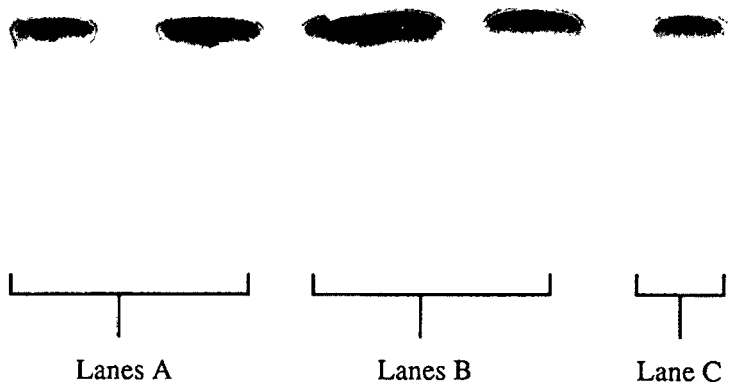

Fig. 8. SDS-PAGE analysis of the continuous purification of serum albumin from blood plasma using a four-stage mixer-settler. Lanes: A = crude human plasma; B = purified stream, flocculated C.I. Reactive Blue 2 perfluorocarbon affinity emulsion; C = pure human serum albumin, fraction V, Sigma.

1.64). Fig. 8 shows the SDS-PAGE analysis of the purification and clearly demonstrates the high purity of HSA in the eluted stream (B) compared to a commercially available pure HSA sample (C).

CONCLUSIONS

The importance of downstream processing in biotechnology has been evident now for a number of years. General downstream processing flowsheets ultimately contain a cascade of fractionation techniques of varying selectivity. The final yield of purified product depends heavily on the number of steps required for purification, as does its selling price. In order to reduce the number of steps required for purification, the inclusion of a high resolution technique as early on in the flowsheet as possible is desirable. Ideally, this high resolution technique should be able to operate efficiently in the presence of cells, cell debris, cell culture constituents etc. If this process were also able to work continuously then the process economics would be more favourable. Continuous processes are better suited to scale up and optimisation than batch processes and are more easily integrated into a production that is itself run continuously. The inventory of bioseparation processes that fit into this ideal category is, at present, somewhat limited. Expanded bed adsorption [2] has the advantage that crude feedstocks can be processed efficiently; however, its mode of operation is not continuous since washing, elution and regeneration of the bed has to be carried out before another cycle of adsorption can take place. CARE [1] is a relatively new concept that uses standard adsorbent particles in continuous stirred tank reactors. Contacting between adsorbents and solu-

tions is carried out in continuous stirred tank reactors which permits the processing of particulate containing streams. The adsorbent is pumped as a slurry from stage to stage and is kept within the unit by use of a macroporous filter. The operating principle of PERCAS is very similar to that of CARE; however, the use of deformable emulsion floccules ensures that no attrition is encountered as could be observed with solid particles leading to breakup and loss of ligand. The separation principle behind PERCAS relies solely on gravity settling, therefore forgoing the need for filters to retain the adsorbent; these may become blocked with extended use.

This report demonstrates the feasibility of a truly continuous bioseparation procedure using novel perfluorocarbon affinity emulsions and a simple four stage mixer-settler reactor. The relative instability of discrete emulsions has been increased by flocculation, which not only, imparts greater stability, but also faster settling rates and greater capacity. Experiments carried out consisting of recirculating the affinity emulsions through a peristaltic pump at flow-rates of 10 ml/min for 24 h have shown that the emulsion is very stable with no coalescence being observed. Indeed, in the course of our experiments we have not witnesed any emulsion breakdown after many cycles of repeated use and the emulsion can be readily autoclaved. We are now extending our work to direct broth extraction of enzymes from *Saccharomyces cerevisiae* homogenates. The rapid settling times of the adsorbent compared to cells and cell debris should ensure that clarification, as well as purification, of the enzyme takes place.

ACKNOWLEDGEMENTS

G.E.McC. gratefully acknowledges the Biotechnology Directorate of the Science and Engineering Research Council (UK) for the provision of a research studentship.

REFERENCES

1 N. F. Gordon and C. L. Cooney, in M. R. Ladisch, R. C. Wilson, C.-D.C. Painton and S. E. Builder (Editors), *Protein Purification, From Molecular Mechanisms to Large-Scale Processes, (ACS Symposium Series,* No. 427), American Chemical Society, Washington, DC, 1990, p. 118.
2 H. A. Chase and N. M. Draeger, *J. Chromatogr.*, 597 (1992) 129.
3 M. Delzher, R. Hilhurst and C. Laane, *Anal. Biochem.*, 178 (1989) 217.
4 A. Sakoda, S. C. Nigan and H. Y. Wang, *Enzyme Microb. Technol.*, 12 (1990) 349.
5 S. P. Foaden, *Ph.D. Thesis*, University of Cambridge, Cambridge, 1990.
6 N. D. Danielson, L. G. Beaver and J. Wangso, *J. Chromatogr.*, 544 (1991) 187.
7 J. J. Kirkland, *Anal. Chem.*, 35 (1963) 2003.
8 J. W. Eveleigh, presented at the *7th International Conference on Affinity Chromatography, Oberammergau, August 17–21, 1987.*
9 R. K. Kobos, J. W. Eveleigh, M. L. Stepler, B. J. Haley and S. L. Papa, *Anal. Chem.*, 60 (1988) 1996.
10 R. K. Kobos, J. W. Eveleigh and R. Arentzen, *Trends Biotechnol.*, 7 (1989) 101.
11 D. J. Stewart, P. Hughes and C. R. Lowe, *J. Biotechnol.*, 11 (1989) 13.
12 D. J. Stewart, D. R. Purvis and C. R. Lowe, *J. Chromatogr.*, 510 (1990) 177.
13 I. D. Pitfield, D. R. Purvis, D. J. Stewart and C. R. Lowe, in preparation.
14 G. E. McCreath, H. A. Chase, D. R. Purvis and C. R. Lowe, *proceedings from I. Chem. E. Res. Event*, Queens College, Cambridge, January 9–10, 1991, p. 67.
15 G. E. McCreath, H. A. Chase, D. R. Purvis and C. R. Lowe, *J. Chromatogr.*, 597 (1992) 189.
16 G. E. McCreath, H. A. Chase, D. R. Purvis and C. R. Lowe, presented at *NATO ASI, Theoretical Advancement in Chromatography and Related Separation Techniques, Ferrara, August 18–30, 1991.*
17 G. E. McCreath, H. A. Chase, D. R. Purvis and C. R. Lowe, presented at the *9th International Symposium on Affinity Chromatography and Biological Recognition, Yokohama, September 24–28, 1991.*
18 T. Peters, Jr., *The Plasma Proteins*, Academic Press, New York, 1975, p. 133.
19 D. M. Kirschenbaum, *Handbook of Biochemistry and Molecular Biology*, Vol. 2, CRC Press, Cleveland, OH, 3rd ed., 1976, p. 54.
20 B. Doumas, W. Watson and H. Higgs, *Clin. Chim. Acta*, 31 (1971) 87.
21 H. A. Chase, *J. Chromatogr.*, 159 (1984) 179.
22 U. K. Laemmli, *Nature*, 227 (1970) 680.
23 A. Higuchi and T. Iijima, *Polymer*, 26 (1985) 1207.

Journal of Chromatography, 629 (1993) 215–228
Elsevier Science Publishers B.V., Amsterdam

CHROM. 24 624

Enantiospecific drug analysis via the *ortho*-phthalaldehyde/homochiral thiol derivatization method☆

Daksha M. Desai☆☆ and Joseph Gal

Division of Clinical Pharmacology, School of Medicine, University of Colorado Health Sciences Center C 237, 4200 E. 9th Avenue, Denver, CO 80262 (USA)

(First received July 1st, 1992; revised manuscript received September 15th, 1992)

ABSTRACT

Pre-column derivatization with *o*-phthaldialdehyde and an optically active thiol has hitherto been used mainly for liquid-chromatographic chiral separation of amino acids. Chiral separation of non-amino-acid primary amines, especially of *pharmaceuticals*, via this approach has been largely ignored. We have therefore examined the applicability of the method to the chiral resolution of several pharmaceutical amines. *o*-Phthaldialdehyde and four commercially available homochiral thiols were used to study the separation of the enantiomers of amphetamine, *p*-hydroxyamphetamine, *p*-chloroamphetamine, 3-amino-1-phenylbutane, 3-amino-1-(4-hydroxyphenyl)-butane, mexiletine, tocainide, tranylcypromine and rimantidine. The resulting highly fluorescent isoindole derivatives were resolved on a Waters Nova-Pak C_{18} column using mobile phases consisting of mixtures of methanol, a sodium acetate buffer and acetonitrile, and the column effluent was monitored using fluorescence or UV detection. In some cases the fluorescence and/or the UV absorbance of the two diastereomers were unequal. It was found that the resolution of most of the amines could be optimized by varying the homochiral thiol in the derivatization step. This method of chiral separation may have wide applicability in enantiospecific drug analysis of non-amino-acid primary amines due to its simplicity and the high sensitivity it provides.

INTRODUCTION

In 1971 Roth [1] described a sensitive analytical method for amino acids based on their reaction with *o*-phthaldialdehyde (OPA) and a thiol, 2-mercaptoethanol. The reaction produces an intensely fluorescent isoindole derivative of the amino acid and is specific for the primary amino group [2,3]. Early applications of this method used an amino acid analyzer in conjunction with postcolumn derivatization [1,4], but subsequently precolumn derivatization combined with high-performance liquid chromatography (HPLC) gained popularity [5–8].

More recently, the OPA method was extended to the enantiospecific liquid-chromatographic analysis of amino acids by substituting a homochiral (single enantiomer) thiol for 2-mercaptoethanol in the derivatization reaction [9–14]. This results in the formation of two diastereomeric isoindoles derived from the enantiomeric amino acids, respectively, and the derivatives are then separated on conventional (non-chiral) HPLC columns. This approach to enantiospecific chromatographic analysis, *i.e.*, derivatization with a homochiral reagent to form diastereomers prior to chromatography, is often termed the indirect approach because the enantiomers are not separated as such but as dia-

Correspondence to: J. Gal, Division of Clinical Pharmacology, School of Medicine, University of Colorado Health Sciences Center C 237, 4200 E. 9th Avenue, Denver, CO 80262, USA.

☆ A preliminary account of this work has been presented at the *13th International Symposium on Column Liquid Chromatography, Stockholm, June 1989*, paper WE20. The majority of the papers presented at this symposium were published in *J. Chromatogr.*, Vols. 506 and 507 (1990).

☆☆ Present address: R. W. Johnson Pharmaceutical Research Institute, Drug Metabolism R-256, Welsh and McKean Roads, Spring House, PA 19477-0776, USA.

0021-9673/93/$06.00

stereomeric derivatives [15]. The ratio of the diastereomers formed can be used to obtain the enantiomeric ratio of the starting analyte mixture, provided that care is taken to avoid the pitfalls inherent in the indirect method [15].

Many drugs, intermediates in drug synthesis, and metabolites of drugs are primary amines, and thus sensitive enantiospecific analytical methods for compounds containing this functional group are of considerable importance. It is surprising, therefore, that the applicability of the enantiospecific OPA method to non-amino-acid primary amines in general and to drug analysis in particular, has been nearly completely ignored. Indeed, it appears in this regard that the enantiospecific OPA method has been nearly exclusively limited to amino acid analysis; the few exceptions to this generalization involve the application of the method to amino acid derivatives such as dipeptides and an amino acid ester [16] (poor resolution was obtained in the latter case), amino acid amides [17], and to amino alcohols mostly derived from α-amino acids [11,18]. It is indeed noteworthy in this regard that the only published attempt to resolve a chiral aliphatic amine failed [11].

Many primary amines of pharmacological interest are neither amino acids nor amino alcohols, and it is clear therefore that a broader applicability of the OPA/homochiral thiol method beyond the analysis of amino acids or their derivatives would be of considerable interest. Since the OPA derivatives are usually intensely fluorescent and are therefore detectable with high sensitivity, this method would be valuable in enantiospecific drug analysis in general, provided that the diastereomeric derivatives of drugs could be separated chromatographically. We therefore undertook to study the applicability of the enantiospecific OPA method to a variety of primary-amine drugs.

EXPERIMENTAL

Chemicals

o-Pthaldialdehyde, 1-thio-β-D-glucose (TG) sodium salt and N-acetyl-L-cysteine (NAC) were obtained from Sigma (St. Louis, MO, USA); N-acetyl-D-penicillamine (NAP) was obtained from Fluka (Buchs, Switzerland); (±)-*p*-chloroamphetamine, (±)-1-methyl-3-phenylpropylamine (3-amino-1-phenylbutane), 2,3,4,6-tetra-O-acetyl-1-thio-β-D-glucopyranoside (TATG), quinine sulfate, 9-anthraldehyde and ACS-grade sodium hydroxide were obtained from Aldrich (Milwaukee, WI, USA); (±)-tocainide was obtained from Astra Pharmaceutical (Worcester, MA, USA); (±)-, (+)- and (−)-mexiletine (MEX) were provided by Boehringer Ingelheim (Ingelheim, Germany); (±)-amphetamine, (−)-amphetamine and (±)-*p*-hydroxyamphetamine were obtained from Smith, Kline and French Labs. (Philadelphia, PA, USA); tranylcypromine was purchased from Regis (Chicago, IL, USA); rimantadine (RIM) was provided by Hoffmann-La Roche (Nutley, NJ, USA); HPLC-grade methanol and acetonitrile, and sodium borate decahydrate were from J. T. Baker (Phillipsburg, NJ, USA); ACS-grade glacial acetic acid was obtained from Fisher Scientific (Pittsburgh, PA, USA).

The synthesis of 3-amino-1-(4-hydroxyphenyl)-butane was described earlier by Gal *et al.* [19].

Drug, reagent and buffer solutions

The derivatization solutions were prepared as follows: OPA (13.40 mg) and an equimolar amount of one of the four thiols were placed in a conical tube and dissolved in 1 ml methanol. The quantities of the thiols were: NAC: 16.3 mg; NAP: 19.1 mg; TG: 21.8 mg; TATG: 36.4 mg. The tubes were capped, protected from light and kept on ice. The solutions were kept refrigerated when not in use. Fresh solutions were prepared every other day.

The amine to be derivatized, in salt or free base form, was dissolved in 0.10 *M* hydrochloric acid solution to obtain a concentration of 0.25 mg of the amine as free base in 50 μl of solution.

A 0.1 *M* sodium borate buffer was prepared and the pH adjusted to 9.50 with a 2.0 *M* solution of sodium hydroxide. For the HPLC mobile phase, a sodium acetate buffer was prepared by diluting 3.0 ml glacial acetic acid to 1 liter with water and adjusting the pH of the buffer to 7.20 with a 2.0 *M* solution of sodium hydroxide. The buffers were vacuum filtered prior to use.

Derivatization procedure

A 50-μl aliquot of the amine solution was placed in a conical centrifuge tube and was treated successively with 50 μl of the borate buffer and 100 μl of

the derivatization solution. The contents of the tube were swirl-mixed for one minute and the tubes were then placed on ice and protected from light. After a derivatization period of exactly 5 min the contents of the tube were diluted with 2 ml of mobile phase and aliquots of 5 μl were injected into the LC system. The tubes were continued to be kept on ice and protected from light.

Determination of enantiomeric purity

The enantiomeric purity of (+)-norephedrine was determined using the homochiral isothiocyanate 2,3,4,6-tetra-O-acetyl-β-D-glucopyranosyl isothiocyanate (TAGIT) of high enantiomeric purity (> 99.90%) [20]. (+)-Norephedrine free base (1 mg) was placed in a conical tube. To the tube was added 3 mg TAGIT in 100 μl acetonitrile. The contents of the tube were swirl-mixed and derivatization was allowed to take place at room temperature for 30 min. The reaction mixture was diluted with 900 μl mobile phase (methanol–water, 47:53, v/v) and aliquots of 10 μl were injected into the LC system. The derivatives were monitored by UV detection at 254 nm.

(+)-Norephedrine was derivatized with OPA/NAC and analyzed as described above. The mobile phase employed consisted of methanol–HPLC buffer–acetonitrile mixed in the ratio of 40:60:1 (v/v/v), and the flow-rate was 1 ml/min. The eluent was monitored at 254 nm with UV detection.

Studies on the formation and stability of MEX/NAC

(±)-MEX HCl (1 mg) in 400 μl methanol was placed in a Reacti-Vial, and was treated successively with 400 μl borate buffer and 200 μl of the NAC derivatization solution. The derivatization was carried out as described above, and after a derivatization period of exactly 5 min, the external standard solution, containing 5 mg quinine sulfate in 200 μl of a 1:1 (v/v) solution of acetonitrile and ethanol, was added to the vial, the contents of the vial swirl-mixed and placed on ice in the dark. Aliquots of 100 μl were withdrawn from the Reacti-Vial at 5, 10, 15, 30, 60, 180 and 360 min, and immediately diluted with 2 ml of mobile phase. Aliquots of 10 μl of the diluted samples were injected into the LC system.

Studies on the formation and stability of MEX/TATG

(±)-MEX hydrochloride (1 mg) in 400 μl methanol was placed in a Reacti-Vial and derivatized with OPA/TATG as described in the preceding section. After the 5-min reaction time 100 μl of the external standard solution containing 9-anthraldehyde at a concentration of 1 mg in 10 ml acetonitrile was added to the vial, the contents of the vial swirl-mixed and placed on ice in the dark. Aliquots of 100 μl were withdrawn from the Reacti-Vial at 5, 10, 15, 30, 60, 180 and 360 min, and immediately diluted with 2 ml mobile phase. Aliquots of 50 μl were injected into the LC system.

Chromatography

The HPLC system consisted of a Waters Associates (Milford, MA, USA) Model U6K injector, a Model 6000A solvent delivery system and a Model 420 fluorescence detector equipped with a 338-nm excitation filter (band pass ± 6 nm) and a 425-nm long-pass emission filter. In some cases the fluorescence detector used was a Hitachi–Perkin-Elmer Model 204 A. The determination of the excitation and emission maxima of the RIM/TATG derivatives was carried out on a Waters Model 470 fluorescence detector. UV monitoring of the HPLC effluent was performed at 254 nm with a Waters Model 440 or a model Lambda-Max Model 480 detector.

The separations were carried out on a Waters Nova-Pak C_{18} column, 150 mm x 3.9 mm, with 4 μm particle size. The mobile phases used for the separation of the amines (Table I) were prepared by

TABLE I

COMPOSITION OF MOBILE PHASES EMPLOYED FOR THE RESOLUTION OF PRIMARY-AMINE DRUGS

MP[a]	Ratio[b]	MP[a]	Ratio[b]	MP[a]	Ratio[b]
A	85:15:0	G	60:40:1.5	M	50:50:2.5
B	75:25:0	H	60:40:0	N	50:50:2.0
C	70:30:0	I	55:45:2.5	O	50:50:0.5
D	67:33:0	J	55:45:2.0	P	40:60:5.0
E	66:34:0	K	53:47:2.5	Q	40:60:2.0
F	65:35:0	L	50:50:5.0	R	30:50:20

[a] Mobile phase code for Table II.

[b] The ratio methanol–sodium acetate buffer, pH 7.20–acetonitrile, mixed v/v/v.

first vacuum filtering the individual components and then mixing them in the appropriate ratio. The buffer used was 50 m*M* sodium acetate, pH 7.20. The mobile phases were delivered at 1.0 ml/min, and the effluent was monitored with a fluorescence or a UV detector.

RESULTS AND DISCUSSION

Nine primary amines of pharmacological interest were studied (first name given is that from Chemical Abstracts Service): α-methylbenzeneethanamine (amphetamine, AMP), 4-chloro-α-methylbenzeneethanamine (*p*-chloroamphetamine, PCA), 4-(2-aminopropyl)phenol (hydroxyamphetamine, HAM), α-methylbenzenepropanamine (3-amino-1-phenylbutane, APB), 4-(3-aminobutyl)phenol [3-amino-1-(4-hydroxyphenyl)butane, AHB], *trans*-2-phenylcyclopropanamine (tranylcypromine, TCP), 2-amino-N-(2,6-dimethylphenyl)propanamide (tocainide, TOC), 1-(2,6-dimethylphenoxy)-2-propanamine (mexiletine, MEX) and α-methyltricyclo [3.3.1.1^{3,7}]-decane-1-methanamine (rimantadine, RIM) (Fig. 1).

RIM is a simple aliphatic amine with a bulky alkyl group near the primary amine moiety. AMP, TCP and APB are simple arylalkylamines without any heteroatoms in their structure; HAM and AHB are the *p*-hydroxy derivatives corresponding to AMP and APB, respectively; it is noteworthy that

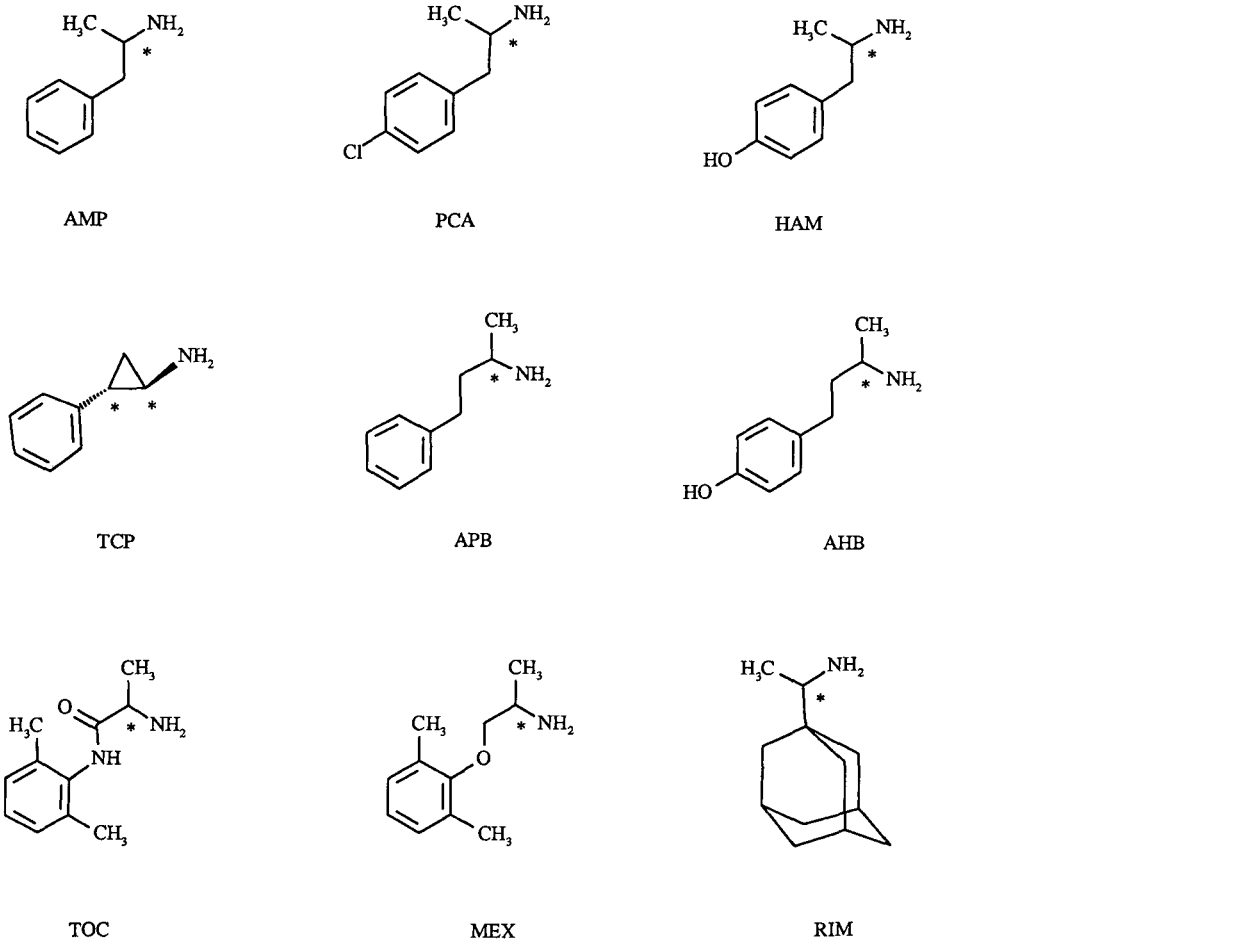

Fig. 1. The chemical structures of the drugs used in the derivatizations; the asterisk indicates the stereogenic center(s). The stereochemical bonds in the structure of TCP denote only relative (*trans*) configuration.

the hydroxyl group in these phenols is in a position remote from the primary amino group, unlike the hydroxyl group in the β-amino alcohols previously studied [11,18]. In PCA a *p*-chloro group is added to the basic structure of AMP. MEX contains an ether linkage between the aromatic ring and the side chain with the primary amino group, while TOC contains a carboxamide moiety between the aromatic ring and the primary amino functionality in the side chain. In all of the drugs the primary amino group is at the stereogenic center (in TCP, at one of the two stereogenic centers), and all but one (TCP) of the drugs have a methyl group at the stereogenic center which also bears the amino group; this is representative of many chiral drugs, inasmuch as a review of the *USAN and USP Dictionary of Drug Names* [45] indicates that the vast majority of chiral primary amines that are not amino acids or derivatives thereof have such an arrangement at the stereogenic center.

From the pharmacological standpoint, the drugs selected represent a variety of classes. AMP, PCA and HAM are based on the 1-phenyl-2-aminopropane (amphetamine) structure; such drugs display a variety of pharmacological activities [21–23] depending on structural details, and stereochemistry plays an important role in the actions and biological disposition of such drugs [24–26]. HAM is not only a drug in its own right but is also a metabolite of AMP in some species [27]. APB is a sympathomimetic amine, and both APB and AHB are metabolites of the antihypertensive drug labetalol [19]. Furthermore, we have found that the metabolism of labetalol to APB is stereoselective [28]. It is also noteworthy that the basic skeleton of APB and AHB —the 3-amino-1-phenylbutane moiety— is present in a number of drugs in addition to labetalol, *e.g.*, bufeniode, butopamine, dobutamine, medroxalol, sulfinalol, etc. In analogy with labetalol, some of these drugs may be metabolized by N-dealkylation, a common biotransformation, to the primary amine APB, AHB, or a derivative thereof, and thus the chromatographic resolution of the enantiomers of these compounds is of interest. TCP is an inhibitor of the enzyme monoamine oxidase (MAO), and is used as an antidepressant drug. The two enantiomers of TCP differ in their biological effects [29]. TOC and MEX are cardiac antiarrhythmic drugs that display enantiomeric differences in their actions [30] and disposition [31–33]. RIM is an antiviral agent used clinically as the racemate; preliminary evidence was recently published suggesting that the drug may undergo stereoselective metabolic conjugation [34].

Four chiral thiols were used in the derivatizations: N-acetyl-L-cysteine (NAC), N-acetyl-D-penicillamine (NAP), 2,3,4,6,-tetra-O-acetyl-1-thio-β-D-glucopyranoside (TATG), and 1-thio-β-D-glucose (TG) (Fig. 2). NAC and NAP are α-amino-acid derivatives, while TATG and TG are derivatives of glucose. All four reagents are commercially available in the homochiral form.

In general, it is often observed that homochiral reagents that are natural products or derivatives thereof, are available in high enantiomeric purity. It is noteworthy in this regard that all four reagents used in the present work are based on natural products. The enantiomeric purity of a sample of TATG obtained from Sigma has been previously determined [12] using homochiral tyrosine to be 99.9%. Our sample of TATG was also from Sigma, and we did not examine in detail its enantiomeric purity; however, derivatization of homochiral samples of AMP and MEX with TATG followed by chromatographic analysis of the derivatives showed that the reagent was at least 99.0% enantiomerically pure, as 1.0% of enantiomeric contamination would have been detectable under our chromatographic conditions.

The enantiomeric purity of NAP obtained from Fluka has been previously determined using homochiral amino acids and has been found to be 99.9% [11]. Our sample of NAP was also from Fluka, and analysis of AMP and TOC with the reagent showed that it was at least 99.0% enantiomerically pure.

In order to determine the enantiomeric purity of NAC, the reagent was reacted with OPA and (+)-norephedrine of known enantiomeric purity, and the product mixture was analyzed by chromatography. The enantiomeric purity of the norephedrine sample was determined via derivatization of norephedrine with the homochiral isothiocyanate TAGIT [20]; this reagent is based on D-glucose and is enantiomerically pure within experimental determination. Using this method the enantiomeric purity of NAC was found to be >99.0%.

The enantiomeric purity of TG used previously in the HPLC resolution of amino acids [35] or amino

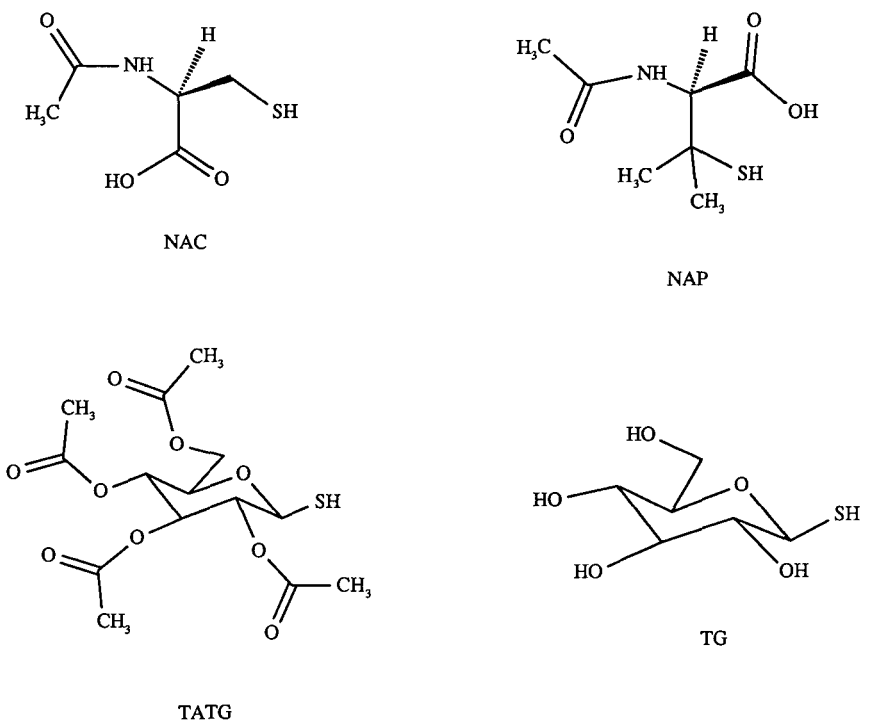

Fig. 2. The chemical structures of the homochiral thiols used as derivatizing agents.

alcohols [18] was not specified. We also did not examine the enantiomeric purity of TG, but it was clear from the analysis of the single-enantiomeric forms of AMP that the reagent was at least 99.0%.

The reaction of a racemic primary amine with OPA and an optically active thiol produces two diastereoisomeric isoindoles; this reaction is known to be rapid, and is complete in a few minutes or less [11,14]. The chemistry of the reaction of OPA and NAP with (±)-AHB is shown in Fig. 3. We examined the time course of the reaction of NAC and of TATG with (±)-MEX. After 5 min, the first time point, there was no further product formation; the derivatives were found to be stable over a period of 6 h while kept in ice in the dark (Fig. 4).

A great deal of data in the literature shows that the OPA derivatives of amino acids and related primary amines with thiols are generally highly fluorescent, and excitation and emission wavelengths in the ranges of *ca.* 330–350 and 400–480 nm, respectively, are typically monitored during the analysis of OPA derivatives, the exact values in each case depending on the identity of the thiol, the amine, and the solution medium. We determined the excitation and emission maxima of the TATG derivatives of RIM to be 338 nm and 420 nm, respectively, values very similar to 342 and 410 nm, respectively, found for the TATG derivatives of amino acids [12].

The resolution of the nine drugs with the four reagents is summarized in Table II. The separations were achieved on Waters Nova-Pak octadecylsilane HPLC columns, and other brands were not evaluated. The thiols varied in their ability to resolve the nine drugs (see below), but it was found that for all but one amine (TCP) at least one homochiral reagent provided suitable resolution, *i.e.*, baseline separation (resolution factor $R_s \geqslant 1.50$ [37]) within a reasonably short run time (Table II). For TCP, a near-baseline value of 1.30 was obtained for the resolution factor R_s with NAC at retention times of *ca.* 25 min. Representative examples of separations are shown in Fig. 5.

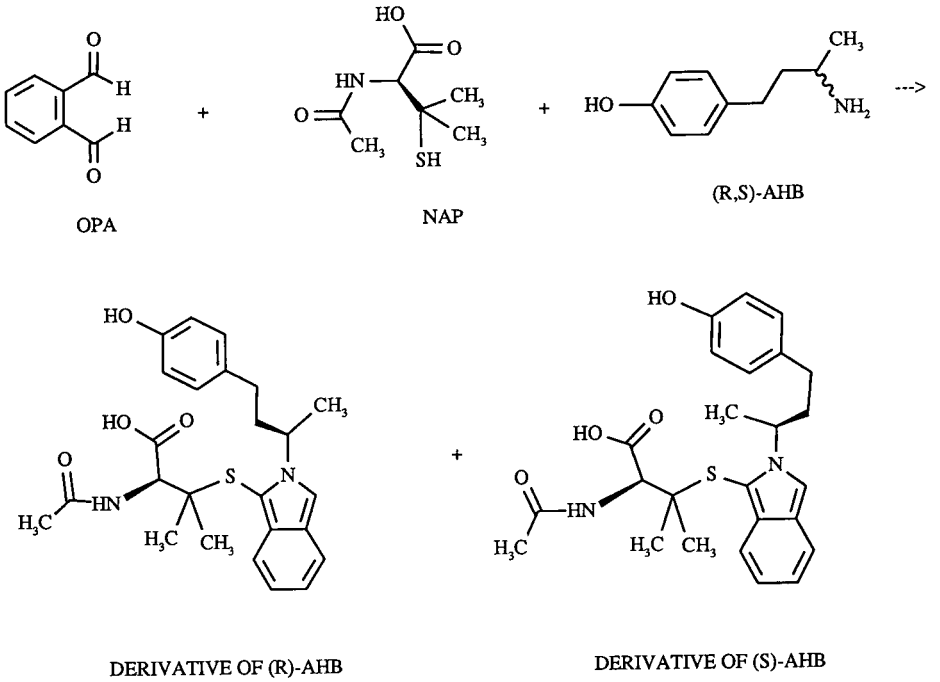

Fig. 3. The reaction of racemic AHB with OPA and NAP to produce the two diastereomeric isoindole derivatives.

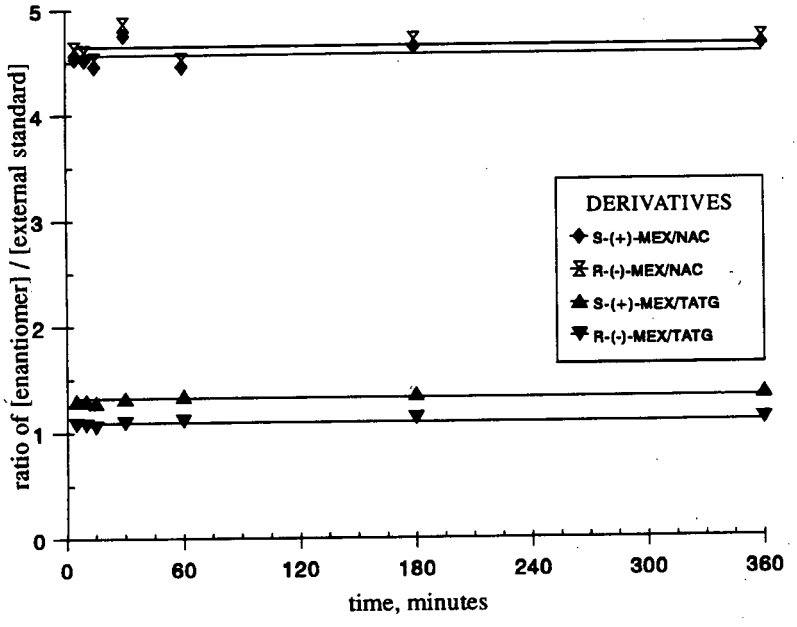

Fig. 4. The formation and stability of the MEX/NAC and the MEX/TATG derivatives; each point is the mean of duplicate determinations.

TABLE II

SEPARATION OF ENANTIOMERIC PRIMARY-AMINE DRUGS AS THEIR ISOINDOLE DERIVATIVES ON A WATERS C_{18} COLUMN

Drug	Thiols											
	NAC			NAP			TATG			TG		
	α^a	R_s^b	t_R^c	α^a	R_s^b	t_R^c	α^a	R_s^b	t_R^c	α^a	R_s^b	t_R^c
AMP	1.17[M]	2.58	16.98 *R*-(−)	1.12[I]	1.61	15.41 *S*-(+)	1.35[B]	4.33	6.48 *R*-(−)	1.15[J]	2.19	12.37 *R*-(−)
HAM	1.22[M]	2.67	6.11 *S*-(+)	1.10[M]	1.31	11.24 *R*-(−)	1.07[G]	1.17	25.66 *R*-(−)	1.14[N]	1.80	8.84 *S*-(+)
PCA	1.15[G]	2.09	8.57	1.15[J]	1.97	22.83	1.47[O]	6.10	7.95	1.14[G]	2.10	12.31
APB	NR[d,H,R]	NR	8.00	1.07[R]	1.50	24.43	NR[H]	NR	12.00 NR	NR[J]	NR	28.70
AHB	1.25[I]	2.56	4.63	1.11[K]	1.64	10.94	1.07[G]	1.32	36.27	1.17[N]	2.32	12.69
MEX	1.11[G]	1.71	12.38 *S*-(+)	1.08[J]	1.08	25.73 *R*-(−)	1.19[B]	3.00	14.69 *S*-(+)	NR[G]	NR	22.94
TOC	1.11[Q]	1.78	20.32 *S*-(+)	1.13[O]	2.00	12.75 *R*-(−)	NR[C]	NR	5.84(NR)	1.10[P]	1.64	22.12 *S*-(+)
TCP	1.13[N]	1.30	25.81	1.07[L]	1.10	30.11	1.07[D]	1.31	30.02	1.06[J]	1.02	25.42
RIM	1.03[F]	0.34	23.87	1.10[E]	1.35	17.78	1.24[A]	2.61	5.88	NR[C]	NR	15.01

[a] Separation factor, see ref. 36; capital letter in superscript indicates mobile phase composition given in Table I.

[b] Peak resolution, see ref. 37.

[c] Retention time of first eluting peak; if known, configuration of corresponding enantiomer is indicated; if no resolution, retention time of single peak.

[d] NR = No resolution.

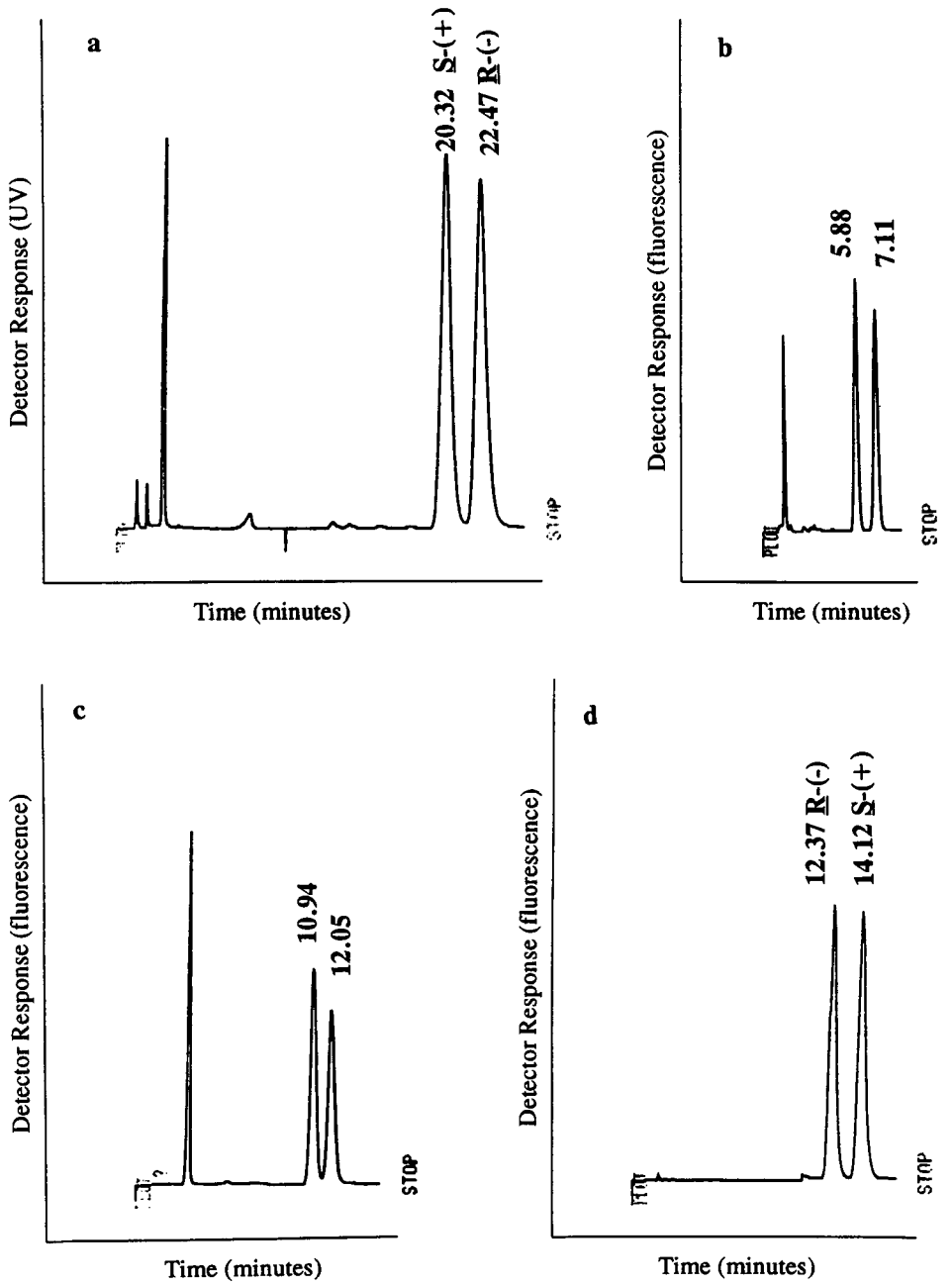

Fig. 5. The resolutions of (a) TOC with NAC; (b) RIM with TATG; (c) AHB with NAP; (d) AMP with TG. Retention times in minutes are shown, and the order of elution of the derivatives is also given when known. For chromatographic conditions see Experimental and Table I.

In general, good peak shapes were obtained using mixtures of a sodium acetate buffer pH 7.2, methanol, and acetonitrile. The composition of mobile phase is important, as we found that other mobile phases, *e.g.* a 0.02 *M* ammonium phosphate buffer, pH 4.50, gave broad and poor chromatographic

TABLE III

DIASTEREOMERIC ISOINDOLE DERIVATIVES WITH UNEQUAL FLUORESCENCE AND/OR UV DETECTOR RESPONSES

Drug/thiol	% Relative size[a,b] of smaller peak	
	Fluorescence	UV
AMP/NAC	[c]	95.14 ± 0.30
AMP/NAP	80.25 ± 0.45	[c]
AMP/TATG	88.27 ± 1.36	97.37 ± 0.91
AMP/TG	92.48 ± 0.63	[c]
HAM/NAC	[c]	95.67 ± 1.01
HAM/TG	95.77 ± 0.33	95.13 ± 2.02
PCA/NAC	[c]	90.87 ± 0.32
PCA/NAP	[d]	97.02 ± 0.31
PCA/TATG	90.59 ± 0.92	[c]
PCA/TG	93.07 ± 0.18	[c]
APB/NAP	92.07 ± 0.67	[d]
AHB/NAC	95.00 ± 0.42	95.24 ± 0.50
AHB/NAP	91.98 ± 0.37	97.80 ± 0.50
AHB/TG	97.40 ± 0.53	[c]
MEX/NAC	[c]	94.27 ± 0.58
MEX/TATG	81.58 ± 1.22	93.49 ± 1.09
TOC/NAC	62.67 ± 1.26	91.91 ± 0.23
TOC/NAP	80.83 ± 0.65	95.37 ± 0.65
TOC/TG	68.46 ± 0.30	81.75 ± 1.30
RIM/TATG	[c]	70.71 ± 0.96

[a] Defined by setting larger diastereomeric peak area = 100% and calculating relative size of the other diastereomeric peak.
[b] Mean ± S.D., n ⩾ 3. No determination of the relative peak sizes could be made if the peaks were not completely resolved.
[c] Value ⩾ 98%, considered not significantly different from 100% peak.
[d] Not evaluated.

peak shapes. Furthermore, it has also been reported that the fluorescence intensity and stability of some OPA derivatives are dependent on the nature and pH of the medium [38]. We observed that the presence of acetonitrile in the mobile phase improved the peak shapes, but in a few cases (Table I) acetonitrile was found to be unnecessary because good peak shapes were obtained using only mixtures of the buffer and methanol.

Individual enantiomers were available for AMP, HAM, TOC, and MEX, and were used to determine the order of elution of the diastereomeric derivatives (Table II). All four of these drugs have the *S*-(+)/*R*-(−) absolute configuration. The NAC-derivative of the (+)-enantiomer of HAM, MEX and TOC eluted before the derivative of the corresponding (−)-enantiomer, while the reverse order was seen for AMP (Table II). For all four amines the order of elution of the derivatives was reversed when NAP was the derivatizing agent, a reversal that is not surprising since NAP and NAC have opposite configurations, NAC being the L enantiomer while NAP is the D isomer. The levorotatory enantiomer of AMP eluted first after derivatization with TATG or with TG. Interestingly, however, there was a reversal of the order of elution of the HAM derivatives between TATG and TG. Our data obtained with the individual enantiomers also indicated that no racemization of the starting materials (*i.e.* the thiol and the drug) or epimerization of the derivatives occurred, since a single peak was obtained in every case where a single enantiomer was derivatized. Detailed studies of the mechanisms of the chromatographic diastereoselectivity will have to be carried out before we can predict the order of elution of the diastereomers.

It was observed in several cases that the two diastereomeric derivatives exhibited unequal fluorescence intensities (Table III). Among the potential causes of this phenomenon are unequal rates of formation of the two derivatives (kinetic resolution), unequal rates of decomposition of the formed derivatives, and an unequal response by the detector employed. The derivatizing reagents are used in excess with respect to the amine, and the reaction is known to be rapid, usually complete in a few minutes [11,14]. It is clear, therefore, that unequal formation rates could not account for the unequal fluorescence intensities. This conclusion is confirmed by the data presented in Fig. 4. Furthermore, Fig. 4 also indicates that diastereoselective decomposition of the derivatives also does not occur and thus cannot explain the differences observed. These considerations and results suggest therefore that unequal peak areas were the result of unequal response by the fluorescence detector, *i.e.*, the diastereomers differ in their fluorescence properties. This conclusion is further supported by similar observations reported for some amino acid OPA derivatives [9,11,13]. When UV absorption at 254 nm was used to monitor the column effluent, it was found that the difference between the diastereomeric responses were considerably smaller in most cases, and for several amines reverted to the 1:1 ratio (Table III). Interestingly, however, in several cases fluorescence detec-

tion gave equal-area peaks for the diastereomers, while UV detection gave unequal peak areas (Table III). It is also to be noted that for all of the drugs except TOC, APB and AHB, at least one of the derivatizing agents produced diastereomers that exhibited equal fluorescence.

Unequal detector response to diastereomeric derivatives, when it occurs, is a significant disadvantage of the indirect approach to chiral separations. It is indeed undeniable that an equal response to the derivatives is highly preferable, and this is one of the factors that make the *direct* approach to enantiospecific analysis (*i.e.* homochiral stationary or mobile phase) superior in principle to the indirect method. It should be noted, however, that an unequal detector response does not necessarily render an indirect separation useless in many applications, because in quantitative enantiospecific drugs analysis it is usually necessary to base the quantification individual calibration curves for the enantiomers, a procedure that accounts for unequal detector response. The occurrence of unequal detector response by a given pair of diastereomeric derivatives can be determined without difficulty by derivatizing the racemate and ruling out other potential sources of unequal peak heights, as we did in the present study (see above).

It was observed qualitatively that the NAC derivatives appeared considerably more fluorescent than those of the other reagents. This phenomenon was not examined quantitatively, but similar observations have also been reported for amino acids. Euerby *et al.* [39], for example, found that the NAC derivatives of some amino acids were more intensely fluorescent than the corresponding NAP derivatives. Such differences may be important in maximizing the sensitivity of the method, and therefore deserve further study.

The minimum detectable amount was 120 pg for each enantiomer of MEX/NAC derivative at a signal-to-noise ratio of 3:1 when the Waters Model 420 detector was used. With a more sensitive fluorescence detector equipped with a xenon lamp (Hitachi–Perkin-Elmer) the minimum amount detectable was 75 pg per enantiomer. The minimum amount of RIM/TATG derivatives detectable using UV absorption at 254 nm was 6 ng per enantiomer with a signal-to-noise ratio of 3:1.

The purpose of our study was to explore the applicability of the enantiospecific OPA method to non-amino-acid drugs and to establish suitable conditions for such analyses, and a systematic investigation of the structure–resolution relationships of the method remains to be carried out. Nevertheless, our data allow several observations about the influence of structural elements on the resolution. In general, the amphetamine derivatives (AMP, PCA, HAM) were well resolved with all of the reagents, with the exception of HAM, which was not well resolved with TATG and only slightly better with NAP (Table II). In HAM the *para*-substituent on the phenyl ring is electron-donating (OH) and in PCA it is electron-withdrawing (Cl) with respect to the unsubstituted analogue AMP, but a uniform relationship between diastereoselectivity (α in Table II) and the electronic properties of the substituents was not discernible. AMP differs structurally from APB in that in the latter an additional methylene group separates the chiral center (and the amino group) from the phenyl ring (Fig. 1). As seen in Table II, in every case better selectivity (α) was obtained for AMP than for APB. Indeed, APB was poorly or not at all resolved with three of the four reagents, while good to excellent resolution was achieved for AMP with all four reagents. These observations indicate an important role for the phenyl ring of the analyte in the separation, and show that its distance from the chiral center or from the amino group is important for the separation of the diastereomers. It has been suggested [40] that diastereomer separations depend on intramolecular interactions (*e.g.*, via hydrogen bonding, hydrophobic forces, dipole interactions, etc) that result in a reduction of the conformational mobility of the molecule, which may in turn result in increased physicochemical differences between the diastereomers. Such differences are, of course, responsible for the chromatographic separation. Clearly, the ability of the phenyl ring to participate in intramolecular interactions (*e.g.* via its π-electron system) is dependent on its particular position in the molecule, and our data show that the phenyl ring is better disposed in AMP than in APB to enhance the separation.

That the situation is rather complex, however, is shown by an analogous comparison of the diastereomeric separations of the derivatives of HAM and AHB, *i.e.*, the *p*-hydroxy analogues of AMP

and APB, respectively. As seen in Table II, in one case (TATG derivatives) the α values for the two drugs were identical, and for each of the remaining three reagents the α value of the AHB derivatives was always greater than that of the HAM derivatives. Thus, in a reversal of the findings for the AMP/APB pair, the *p*-hydroxyphenyl ring in AHB is in general better able to influence the separation —possibly through some diastereoselective intramolecular interaction— than the *p*-hydroxyphenyl ring of HAM. Also relevant in this regard is the observation (Table II) that the derivatives of AHB were always better separated (as judged by the α values) than those of APB, suggesting that the introduction of the *p*-hydroxy group either diastereoselectively enhanced the particular intramolecular interaction involved, or in fact caused the predominance of an entirely different interaction. When the AMP/HAM pair is similarly examined (Table II), however, it is seen that the introduction of the *p*-hydroxy group into the amphetamine structure caused a *decrease* in the α value in three of the four cases, suggesting that the potential intramolecular interaction(s) involved may be significantly different from those operating in the APB/AHB case. Furthermore, introduction of the *p*-hydroxy group into the amphetamine structure also caused the reversal of the order of elution of the derivatives for three of the four homochiral derivatizing agents (Table II), suggesting a change in the nature of the predominant interaction(s).

It is also instructive to compare the resolutions of TCP with those of AMP. The former compound, *trans*-phenylcyclopropylamine (Fig. 1), may be considered a rigid analogue of AMP. An inspection of the relevant α values (Table II) shows that in all cases AMP was better resolved than TCP, suggesting that the conformational requirements for the resolution of AMP are not well mimicked by the rigid analogue TCP. Clearly, further detailed studies will have to be carried out to explain fully the role of physicochemical and structural factors in the above separations.

It is also interesting to consider the role of the chemical structure of the homochiral thiols in the resolutions. The two amino acid derivatives NAC and NAP are closely related, the latter being the β,β-dimethyl analogue of the former (Fig. 2). The two sugar derivatives are also related, TATG being the tetraacetylated analogue of TG (Fig. 2). TATG is clearly less polar and more hydrophobic than TG. To obtain a rough index of resolving ability for the reagents, we calculated the mean α value for each thiol, using $\alpha = 1.00$ when no resolution was obtained. The results were: TG mean $\alpha = 1.08$, NAP 1.10, NAC 1.13, TATG 1.16. Thus, by this standard, the best reagent was TATG, *i.e.* a molecule with a bulky hydrophobic group attached to the thiol moiety, in agreement with suggestions that such groups can maximize physicochemical differences between the diastereoisomers [40]. It is interesting in this context that TG, probably the most hydrophilic molecule among our reagents, proved to be the poorest reagent in our separations, raising the question of the role of lipophilicity of the reagent in the resolutions. However, that lipophilicity may not be an overriding factor is indicated by the comparison between NAP and NAC: the former compound, being a dimethyl derivative of the latter, is more hydrophobic than the latter, but exhibits a lower mean α value. Our limited data do not, however, allow detailed conclusions about the role of the structure of the thiol in the resolutions. It should be emphasized also that the mean α value for a reagent is only an average index of resolving power that does not predict the separation achieved for any specific racemate. Consider, for example, the case of APB: this compound could only be resolved with NAP. It is noteworthy in this context that several other homochiral thiols have been employed in separations of enantiomeric amino acids, *e.g.*, a series of N-acylcysteines [41]. While some of these reagents produced good resolutions of some amino acid enantiomers, they suffer from the major disadvantage that they are not commercially available.

As mentioned earlier, a previous attempt [11] to resolve a chiral aliphatic amine failed, prompting the authors to speculate that the hydroxyl or carboxyl group of an amino alcohol or amino acid, respectively, is required to separate the diastereomeric OPA derivatives of chiral amines. Such suggestions are incompatible with our results, as our data clearly show that the OPA/homochiral thiol method is applicable to a variety of primary amines, including alkyl- and arylalkylamines.

It is also clear from the above discussion that in applying the enantiospecific OPA method to a given compound the analyst should adopt a flexible and

empirical approach. Thus, a given racemate may be resolved with several thiols, but the resolution should be optimized with regard to extent of separation, detector response, analysis time, etc., by the judicious selection of the homochiral reagent.

Pre-column derivatization of primary amines with OPA-homochiral thiols offers several advantages: commercially available reagents and chromatographic columns are used; the reaction is simple and rapid, specific to primary amines, and is applicable to a variety of primary-amine drugs; the derivatives are generally highly fluorescent and the reagents are non-fluorescent, providing for sensitive and specific detection, and the procedure can be readily automated [11]. Furthermore, the OPA–isoindole derivatives have also been shown to be electrochemically active [42,43], thus widening the scope of this approach. A significant disadvantage of the method is the possibility of unequal detector response. This was observed for some of the diastereomeric pairs in this study, and both fluorescence and UV detection suffered from such differences, the former more frequently and to a greater extent than the latter. It is important to emphasize, however, that for a majority of the amines at least one thiol provided diastereomers with equal detector response. Furthermore, even when unequal detector response is unavoidable, suitable calibration curves readily allow quantification of the enantiomers.

There are many therapeutic agents that are primary amines. Furthermore, many non-primary-amine drugs are metabolized to metabolites that are primary amines, via such biotransformations as N-dealkylation, amide hydrolysis, reduction of azo, nitro, nitroso and hydroxylamino groups, etc. It is reasonable to expect, therefore, that this method will be valuable in the area of enantiospecific pharmaceutical analysis and in drug metabolism and pharmacokinetic studies. It is interesting to note here that a preliminary attempt to apply the OPA/homochiral thiol to the enantiospecific analysis of a drug —baclofen, a γ-amino acid— was described [44] several years ago; while the procedure appeared promising, difficulties in the derivatization reaction were encountered that could not be explained [44]. Nevertheless, our results suggest that the OPA method should be further investigated in enantiospecific drug analysis.

In summary, then, the OPA/homochiral thiol method of enantiospecific analysis is applicable to a variety of primary-amine drugs representing a variety of pharmacological classes. We are currently investigating applications of the method to problems of stereoselective drug disposition.

ACKNOWLEDGEMENTS

This work was supported by US Public Health Service grant HL 34789. The authors are grateful to Dr. W. Garland for a sample of racemic rimantadine and to Boehringer Ingelheim for samples of (±)-, (+)- and (−)-mexiletine.

REFERENCES

1 M. Roth, *Anal. Chem.*, 43 (1971) 880–882.
2 S. S. Simons Jr. and D. F. Jonnson, *J. Org. Chem.*, 43 (1978) 2886–2891.
3 R. C. Simpson, J. E. Spriggle and H. Veening, *J. Chromatogr.*, 261 (1983) 407–414.
4 J. R. Benson and P. E. Hare, *Proc. Nat. Acad. Sci. U.S.A.*, 72 (1975) 619–622.
5 S. Lam and G. Malikin, *J. Chromatogr.*, 368 (1986) 413–422.
6 T. P. Davis, C. W. Gehrke, C. W. Gehrke Jr., T. D. Cunningham, K. C. Kuo, K. O. Gerhardt, H. D. Johnson and C. H. Williams, *J. Chromatogr.*, 162 (1979) 293–310.
7 P. Lindroth and K. Mopper, *Anal. Chem.*, 51 (1979) 1667–1674.
8 D. Hill, F. Walters, T. Wilson and J. Stuart, *Anal. Chem.*, 51 (1979) 1338–1341.
9 D. W. Aswad, *Anal. Biochem.*, 137 (1984) 405–409.
10 R. H. Buck and K. Krummen, *J. Chromatogr.*, 315 (1984) 279–285.
11 R. H. Buck and K. Krummen, *J. Chromatogr.*, 387 (1987) 255–265.
12 S. Einarsson, S. Folestad and B. Josefsson, *J. Liq. Chromatogr.*, 10 (1987) 1589–1601.
13 M. R. Euerby, L. Z. Partridge and P. B. Nunn, *J. Chromatogr.*, 469 (1989) 412–419.
14 N. Nimura, K. Iwaki and T. Kinoshita, *J. Chromatogr.*, 402 (1987) 387–391.
15 J. Gal, in I. W. Wainer and D. E. Drayer (Editors), *Drug Stereochemistry: Analytical Methods and Pharmacology*, Marcel Dekker, New York, 1988, pp. 77–112.
16 J. Florance, A. Galdes, Z. Konteatis, Z. Kosarych, K. Langer and C. Martucci, *J. Chromatogr.*, 414 (1987) 313–322.
17 A. Duchateau, M. Crombach, J. Kamphuis, W. H. J. Boesten, H. E. Schoemaker and E. M. Meijer, *J. Chromatogr.*, 471 (1989) 263–270.
18 A. Jegorov, T. Trnka and J. Stuchlik, *J. Chromatogr.*, 558 (1991) 311–317.
19 J. Gal, J. A. Zirrolli and P. S. Lichtenstein, *Res. Commun. Chem. Pathol. Pharmacol.*, 62 (1988) 3–17.
20 J. Gal, *J. Chromatogr.*, 307 (1984) 220–223.

21 B. B. Hoffman and R. J. Lefkowitz, in A. G. Gilman, T. W. Rall, A. S. Nies, and P. Taylor (Editors), *Catecholamines and Sympathomimetic Drugs, The Pharmacological Basis of Therapeutics*, Pergamon Press, New York 8th ed., 1985, pp. 187–220.
22 R. W. Fuller, *Neurochem. Res.*, 17 (1992) 449–456.
23 A. Shulgin and A. Shulgin, *PIHKAL—A Chemical Love Story*, Transform Press, Berkeley, CA, (1991).
24 M. B. Nichols and R. P. Maickel, *Pharmacol. Biochem. Behavior*, 33 (1989) 181–188.
25 R. A. Harris, D. Snell and H. H. Loh, *Pharmacol. Biochem. Behavior*, 7 (1977) 307–310.
26 J. Wright, A. K. Cho and J. Gal, *Xenobiotica*, 7 (1977) 257–266.
27 J. A. Jonsson, *Biochem. Pharmacol.*, 23 (1977) 3191–3197.
28 A. Changchit, J. A. Zirrolli and J. Gal, *Biol. Mass Spectrom.*, 20 (1991) 751–758.
29 D. F. Smith, *Pharmacol. Toxicol.*, 65 (1989) 321–331.
30 R. J. Hill, H. J. Duff and R. S. Sheldon, *Mol. Pharmacol.*, 34 (1988) 659–663.
31 L. Igwemezie, C. R. Derr and K. M. McErlane, *Xenobiotica*, 19 (1989) 677–682.
32 O. Grech-Belanger, J. Turgeon and M. Gilbert, *Br. J. Clin. Pharmacol.*, 21 (1986) 481–487.
33 J. Gal, T. A. French, T. Zysset and P. E. Haroldsen, *Drug Metab. Disp.*, 10 (1982) 399–404.
34 B. J. Miwa, N. Choma, S. Y. Brown, N. Keigher, W. A. Garland and E. K. Fukuda, *J. Chromatogr.*, 431 (1988) 343–352.
35 A. Jegorov, J. Triska, T. Trnka and M. Cerny, *J. Chromatogr.*, 434 (1988) 417–422.
36 L. R. Snyder and J. J. Kirkland, *Introduction to Modern Liquid Chromatography*, Wiley, New York, 2nd ed., 1979, p. 35.
37 L. R. Snyder and J. J. Kirkland, *Introduction to Modern Liquid Chromatography*, Wiley, New York, 2nd ed., 1979, p. 34.
38 S. S. Simons and D. F. Johnson, *Anal. Biochem.*, 90 (1978) 705–725.
39 M. R. Euerby, P. B. Nunn and L. Z. Partridge, *J. Chromatogr.*, 466 (1989) 407–414.
40 W. Lindner and C. Petterson, in I. W. Wainer (Editor), *Liquid Chromatography in Pharmaceutical Development—An Introduction*, Aster, Springfield, OR, 1985, pp. 75–77.
41 H. Bruckner, R. Wittner and H. Godel, *J. Chromatogr.*, 476 (1989) 73–82.
42 M. Joseph and P. Davies, *J. Chromatogr.*, 277 (1983) 125–136.
43 S. Murai, H. Nagahama, H. Saito, H. Miyate, Y. Masuda and T. Itoh, *J. Pharmacol. Methods*, 21 (1989) 115–121.
44 E. W. Wuis, E. W. J. Beneken Kolmer, L. E. C. Van Beijsterveldt, R. C. M. Burgers, T. B. Vree and E. van der Kleyn, *J. Chromatogr.* 415 (1987) 419–422.
45 *USAN and USP Dictionary of Drug Names*, US Pharmacopeial Convention, Rockville, MD, 1992.

Journal of Chromatography, 629 (1993) 229–235
Elsevier Science Publishers B.V., Amsterdam

CHROM. 24 649

Multimycotoxin detection and clean-up method for aflatoxins, ochratoxin and zearalenone in animal feed ingredients using high-performance liquid chromatography and gel permeation chromatography

Catherine Dunne, Mary Meaney and Malcolm Smyth

School of Chemical Sciences, Dublin City University, Glasnevin, Dublin 9 (Ireland)

Louis G. M. Th. Tuinstra

State Institute for Quality Control of Agricultural Products, Bornsesteeg 45, 6708 PD Wageningen (Netherlands)

(First received July 24th, 1992; revised manuscript received September 25th, 1992)

ABSTRACT

A sensitive and reliable method is described for the determination of aflatoxins B_1, B_2, G_1 and G_2, ochratoxin A and zearalenone in animal feed ingredients. A multi-toxin extraction and clean-up procedure is used, with dichloromethane–1 *M* hydrochloric acid (10:1) being used for the extraction and gel permeation chromatography being used for the clean-up. The liquid chromatographic method developed for the separation of the six mycotoxins involves gradient elution with a reversed-phase C_{18} column and fluorescence detection. Recoveries, repeatability and reproducibility have been determined on maize, palm and wheat. The detection limits varied depending on the type of feed.

INTRODUCTION

The presence of mycotoxins in animal feeds has been of major concern for many years. A tolerance level of aflotoxin B_1, in groundnut, copra, palm-kernal, cotton seed, babassu, maize and products derived from the processing thereof is 20 μg/kg in the European Communities Regulations 1991. Many analytical procedures have been developed for their determination [1–5]. The majority of these are based on single extraction and single determinations. In more recent publications there is widespread interest in the developement of multi-toxin clean-up and determination to achieve a rapid, sensitive and more economical analysis. Hetmanski and Scudamore [6] used gel permeation chromatography (GPC) for clean-up of extracts prior to separation by reversed-phase HPLC for the analysis of aflatoxins B_1, B_2, G_1 and G_2. Langseth *et al.* [7] determined zearalenone and ochratoxin A in cereals and feed using one extraction step. The clean-up step used silica solid-phase extraction columns and the mycotoxins were eluted separately with different solvent mixtures. They were injected separately into a HPLC system under similar conditions. Hunt *et al.* [8] determined aflatoxins and ochratoxin A in food. The extract was purified using grooved thin-layer chromatography plates coated with silica gel. After chromatography any fluorescent bands were removed and examined by HPLC.

In this paper an extraction and clean-up method developed by Scudamore and Hetmanski [9] was

Correspondence to: L. G. M. Th. Tuinstra, State Institute for Quality Control of Agricultural Products, Bornesteeg 45, 6708 PD Wageningen, Netherlands.

0021-9673/93/$06.00

used with slight modifications. Dichloromethane–1 *M* hydrochloric acid (10:1) was used for the extraction. GPC was used for the clean-up. The HPLC method developed here, for the determination of the six mycotoxins, used gradient elution with two mobile phases: (A) water–methanol–acetonitrile (130:70:40) plus 1 m*M* nitric acid plus 1 m*M* potassium bromide; (B) 0.01 *M* phosphoric acid–acetonitrile (50:50).

Post-column derivatization with bromine was used to enhance the sensitivity of aflatoxin B_1 and G_1 in conjuction with fluorescence detection with pre-programmed wavelength change. Kok *et al.* [10] showed that the fluorescence intensity of aflatoxin B_1 and G_1 increased after the addition of bromine solution. The reaction is believed to be the bromination of the 8,9 double bond. Aflatoxin B_2 and G_2 do not react with bromine owing to the absence of the double bond. The fluorescent signal enhancement of the aflatoxin may be carried out by derivatization with on-line, electrochemically generated bromine. Bromine can be produced from bromide present in the mobile phase in an electrochemical cell after the column. The derivatization with bromine decreased the sensitivity of zearalenone. It was therefore necessary to inject the extract again without derivatization in order to determine zearalenone.

In brief the method described here allows the determination of aflatoxins B_1, B_2, G_1 and G_2, ochratoxin A and zearalenone in animal feed using a multi-toxin extraction and clean-up and gradient elution with HPLC for the determination. Maize, palm and wheat were used for recovery, reproducibility and repeatability studies.

EXPERIMENTAL

Reagents

Aflatoxin B_1 and ochratoxin A were obtained from Calbiochem (San Diego, CA, USA). Aflatoxins B_2, G_1 and G_2 were obtained from Makor Chemicals (Jerusalem, Israel). Zearalenone was obtained from Carl Roth (KG 1975 Karlsruhe 21, Germany). All solvents were of analytical-reagent grade and were purchased from Merck (Darmstadt, Germany), Water was obtained from a Milli-Q system (Millipore, Bedford, MA, USA).

The following stock solutions were prepared: (a) aflatoxin B_1, 1 μg/ml in chloroform, (b) aflatoxin B_2, 1 μg/l in chloroform, (c) aflatoxin G_1, 1 μg/ml in chloroform, (d) aflatoxin G_2, 1 μg/ml in chloroform, (e) ochratoxin A_1, 1 μg/ml in methanol, (f) zearalenone, 100 μg/ml in methanol.

Equipment

The GPC equipment consisted of a 60 mm × 6 mm I.D. glass column (Spectrum Medical Industries, Los Angeles, CA, USA) fitted with a 40–60 μm porous bed support and adjustable plunger packed with Bio-Beads SX-3 gel (Bio-Rad, Watford, UK). The gel was suspended in a mixture of dichloromethane–ethylacetate–formic acid (49.9:49.9:0.2) for one day before loading onto the glass column. The height of the column was 55 mm. A Waters (Milford, MA, USA) M-45 pump was used and a Waters WISP 710B automatic injector. A Gilson (Villiers-le-Bel, France) 202 fraction collector and 201-202 fraction controller were used for collecting fractions.

The HPLC equipment included a Gilson 305 and 302 pump, a Gilson 505 manometric module, Gilson 511B dynamic mixer, chromsphere RP-C_{18} column (Chrompack, Middelburg, Netherlands), KOBRA device (Lamers & Pleuger, Den Bosch, Netherlands) for generating bromine for the post-column derivatisation and a Perkin-Elmer LS4 fluorescence detector (Perkin-Elmer, Norwalk, CT, USA). An automatic Gilson 231 sample injector with a Gilson 401 dilutor was also used.

Other equipment included a Desaga flask shaker (Heidelburg, Germany) and a Büchi rotary evaporator (Switzerland).

Extraction

A 25-g portion of well mixed, finely ground sample was weighed into a 250-ml erlenmeyer flask. A 12.5-g amount of Celite (Johns-Manville, Denver, CO, USA), 12.5 ml 1 *M* hydrochloric acid and 125 ml dichloromethane were added. The flask was stoppered and shaken for 30 min before filtering the sample through a Whatman No. 1 filter paper into a 250-ml round-bottom flask. The residue in the filter paper was rinsed with 3 × 25 ml portions of dichloromethane. The combined filtrate and washings were evaporated to near dryness (*ca.* 0.5 ml) by rotary evaporation at 30°C. The residue in the flask was transferred to a 10-ml volumetric flask with at

least four rinses of dichloromethane, approximately 1 ml each time. A 5-ml volume of ethyl acetate and 0.02 ml formic acid were added and the solution was made up to the mark with dichloromethane.

Clean-up

Approximately 1 ml of the sample extract was filtered through a disposable 0.45-μm organic filter (Acrodisc CR PTFE; Gelman, Ann Arbor, MI, USA). A 200-μl volume of the filtrate was injected onto the GPC column using a WISP 710 B automatic injector. Dichloromethane–ethyl acetate–formic acid (49.9:49.9:0.20) mixture was passed through the column at 0.3 ml/min. One fraction from 25–45 min was collected. A 2-ml volume of water was added to the fraction which was stoppered and well shaken. The lower organic layer was passed through anhydrous sodium sulphate. The sodium sulphate was rinsed with 5 ml dichloromethane. The combined filtrate and washings were evaporated to near dryness (*ca.* 0.5 ml). The residue was taken up in water–acetone (85:15). This was well shaken and sonicated for 5 min and then filtered through a disposable organic filter before HPLC determination.

High-performance liquid chromatography

A gradient solvent system was used. The initial percentage of A was 100%. This was maintained for 8 min after injection. Over the next 5 min the percentage A was reduced to 30% and the percentage of B increased from 0% to 70% linearly. These were maintained at these levels for the following 14 min. The percentage A was then increased to 100% and the percentage B decreased to 0% linearly over the next 5 min and maintained for 8 min at which point the next injection could be made. The wavelengths of excitation and emission were changed as follows:

	Ex/Em
0–20.0 min	= 369/422 nm
20.0–24.0 min	= 335/500 nm
24.0–26.2 min	= 310/470 nm
26.2–38.9 min	= 335/500 nm
38.9–40.0 min	= 369/422 nm

RESULTS AND DISCUSSION

The extraction and clean-up method used was developed by Scudamore and Hetmanski [9]. Some minor modifications were made. Before the GPC injection, extracts were filtered through a 0.45-μm disposable filter in order to remove any suspended particles. The GPC column and injection volume were smaller than that used by Scudamore and Hetmanski [9]; however, these were reduced porportionally in our work. The flow-rate was also reduced porportionally. The solvent consumption is reduced due to the smaller injection volume and lower flow-rate, thus making the analysis more economical. Water–acetone was used to dissolve the mycotoxins for HPLC analysis as it had been used previously by Kok *et al.* [10] to determine aflatoxins in cattle feed. The dissolved mycotoxins were filtered through a 0.45-μm disposable filter in order to remove residue drops which did not dissolve. Residue drops were also present if acetonitrile–water (1:1) was used. This was the solvent used by Scudamore and Hetmanski [9]. The filtration did not affect recovery. It also ensured that a clean sample was injected onto the HPLC column.

The fraction in which the mycotoxins eluted from

TABLE I

RECOVERY OF MYCOTOXIN STANDARDS

Levels of mycotoxins used were 0.2 ng aflatoxins B_1, G_1 and G_2, 0.1 ng aflatoxin B_2, 1 ng ochratoxin A and 20 ng zearalenone. The analysis was repeated three times.

	Recovery (%)					
	B_1	B_2	G_1	G_2	Ochratoxin A	Zearalenone
Mean	99.1	96.5	100.5	98.5	74.0	87.3
S.D.	5.8	4.0	13.7	11.2	10.4	5.9
R.S.D. (%)	5.8	4.1	13.6	11.4	14.1	6.7

GPC was determined by monitoring the output, using fluorescence detection at appropriate wavelengths of excitation and emission, for each mycotoxin. Mycotoxins with a higher molecular mass eluted earlier, as expected. However, collecting from 25 to 45 min ensured that all mycotoxins of interest were included in the fraction.

Kok *et al.* [10] used a mobile phase of water–methanol–acetonitrile (130:70:40) plus 1 m*M* nitric acid and 1 m*M* potassium bromide to separate aflatoxins B_1, B_2, G_1 and G_2. By using a mobile phase of 180:70:40 water–methanol–acetonitrile, better separation of aflatoxins was achieved. In order to elute ochratoxin A and zearalenone the polarity of the mobile phase had to be decreased. The elution of ochratoxin A containing a carboxylic acid group also requires and acidic mobile phase [7]. The second mobile phase in the gradient elution system was 0.01 *M* phosphoric acid–acetonitrile (50:50). A similar mobile phase had been used by Howell and Taylor [11] for the determination of zearalenone and ochratoxin A.

Standard solutions containing known amounts of aflatoxins B_1, B_2, G_1 and G_2, ochratoxin A and zearalenone, made up in the GPC mobile phase, were injected onto the GPC column, collected and determined by the HPLC method. Table I shows the recoveries obtained.

Typical chromatograms of samples spiked to contain aflatoxins B_1, B_2, G_1 and G_2, ochratoxin A and zearalenone are shown in Figs. 1 and 2. The peak identified as zearalenone in the blank sample in Fig. 2 has the same retention time as that of the spiked zearalenone sample. The zearalenone peak also disappears when post-column derivatization is used as indicated in Fig. 1a, thus confirming the peak is zearalenone. Any change in baseline at 20, 24 and 26.2 min is due to a wavelength change. Although the post-column derivatization with bromine enhances aflatoxin B_1 and G_1, the zearalenone peak disappears under these conditions. This, however, can be used as a useful confirmation test for zearalenone, in particular with samples that contain interferences that coelute with zearalenone and give false positive results [12]. In order to determine zearalenone the extract must be re-injected without derivatization. To avoid this re-injection a second detector, set for the detection of zearalenone, may be placed after the column and before derivatization. The KOBRA cell also continues to influence the chromatogram for some time, *i.e.* a few hours, after it is switched off. In the setup used it is therefore not

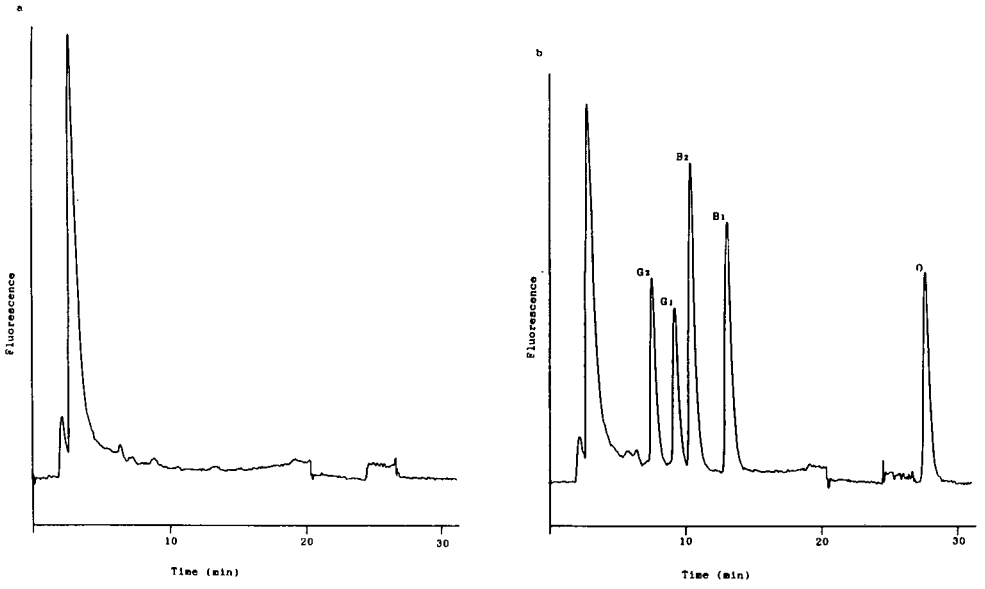

Fig. 1. Chromatograms of (a) maize samples and (b) maize sample spiked to contain 3.2 μg/kg aflatoxin B_1, G_1 and G_2, 1.6 μg/kg aflatoxin B_2, 16 μg/kg ochratoxin A and 320 μg/kg zearalenone with post-column derivatization. No zearalenone detected due to post-column derivatization.

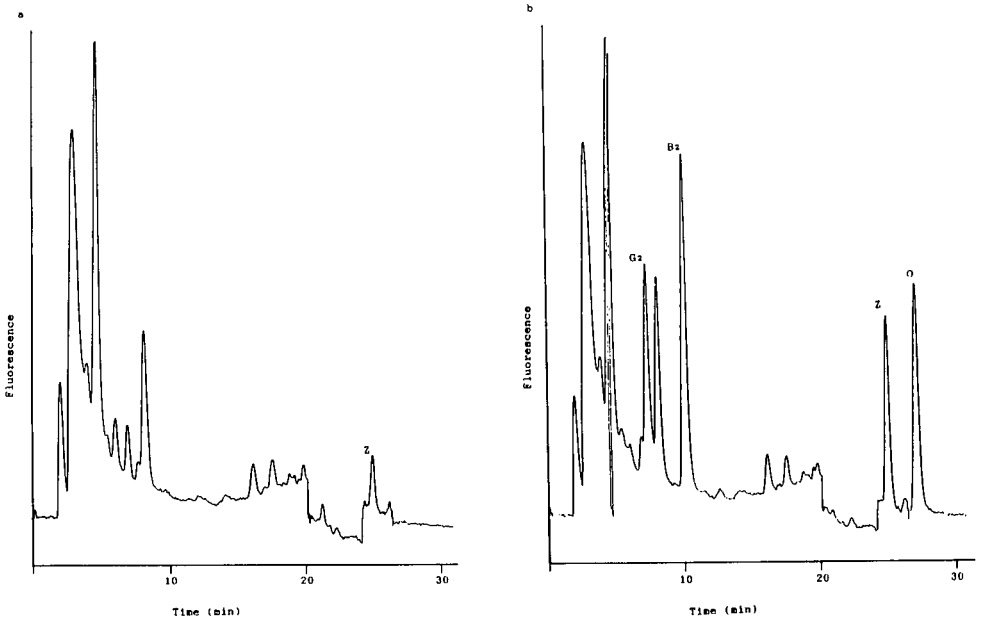

Fig. 2. Chromatograms (a) and (b) as in Fig. 1 without post-column derivatization.

possible to determine zearalenone immediately. The zearalenone should be determined first, before derivatization is carried out for the determination of the other mycotoxins, on the other hand the KOBRA cell may be bypassed. Post-column derivatization with bromine not only enhances the fluorescence intensity of aflatoxins B_1 and G_1 but also reduces, and in some cases completely diminishes, the fluorescence intensity of many interfering components.

Recoveries for spiked extracts of maize, palm and wheat are shown in Table II. Known amounts of standard mycotoxin solutions were added to extracts of maize, palm and wheat. Recoveries for zearalenone in maize and palm were low.

The reproducibility of the method was checked using different types of feed. Three feed ingredients were analyzed three times each for aflatoxins B_1, B_2, G_1 and G_2, ochratoxin A and zearalenone, which were spiked onto the feed ingredient. The results are shown in Table III. The aflatoxin recoveries are greater than 73% for all feeds. The aflatoxin recoveries obtained for wheat had a tendancy to be higher than those obtained by Scudamore and Hetmanski [9], the ochratoxin A recoveries compare favourably and the zearalenone recoveries are

TABLE II

RECOVERY OF MYCOTOXINS FROM SPIKED EXTRACT

Levels of mycotoxins used the same as in Table I. N.D. = Not determined.

	Recovery (%)					
	B_1	B_2	G_1	G_2	Ochratoxin A	Zearalenone
Maize	93.4	102.4	97.3	97.9	N.D.	49.7
Palm	81.4	99.6	93.1	90.2	N.D.	17.2
Wheat	90.9	102.2	103.9	103.0	N.D.	71.6

TABLE III

REPRODUCIBILITY TEST ON THREE DIFFERENT SPIKED FEEDS

Levels of mycotoxins used were 3.2 μg/kg aflatoxins B_1, G_1, and G_2, 1.6 μg/kg aflatoxins B_2, 16 μg/kg ochratoxin A and 320 μg/kg zearalenone.

	Recovery (%)					
	B_1	B_2	G_1	G_2	Ochratoxin A	Zearalenone
Maize mean	96.3	101.0	102.6	102.6	77.6	24.6
S.D.	5.1	7.1	9.6	9.5	2.4	1.7
Palm mean	73.1	82.0	87.5	76.7	12.5	12.9
S.D.	7.3	5.5	10.5	10.3	3.7	0.9
Wheat mean	75.9	84.6	96.7	88.7	59.4	38.8
S.D.	5.6	2.6	7.3	12.2	12.6	9.0

much less than those obtained by Scudamore and Hetmanski [9]. The recoveries for palm are lower than other feed ingredients analysed, but this is due to the higher background interference especially in the case of aflatoxin B_2, G_1 and G_2 (refer to Fig. 3).

Repeatability of the method was checked using maize. Ten portions of feed ingredient from the same batch were spiked with aflatoxins, ochratoxin A and zearalenone. The results are shown in Table IV.

Detection limits for each mycotoxin are shown in Table V. These are based on the noise × 3 and are in ng levels. Taking the original feed ingredient and recovery into account the detection limits are quoted in μg/kg. This detection limit depends on the type of feed being analysed as the recovery varies from feed to feed. Therefore a range of values are included which take into account the different types of feed ingredient being analysed.

The detection limits are good, despite the poor

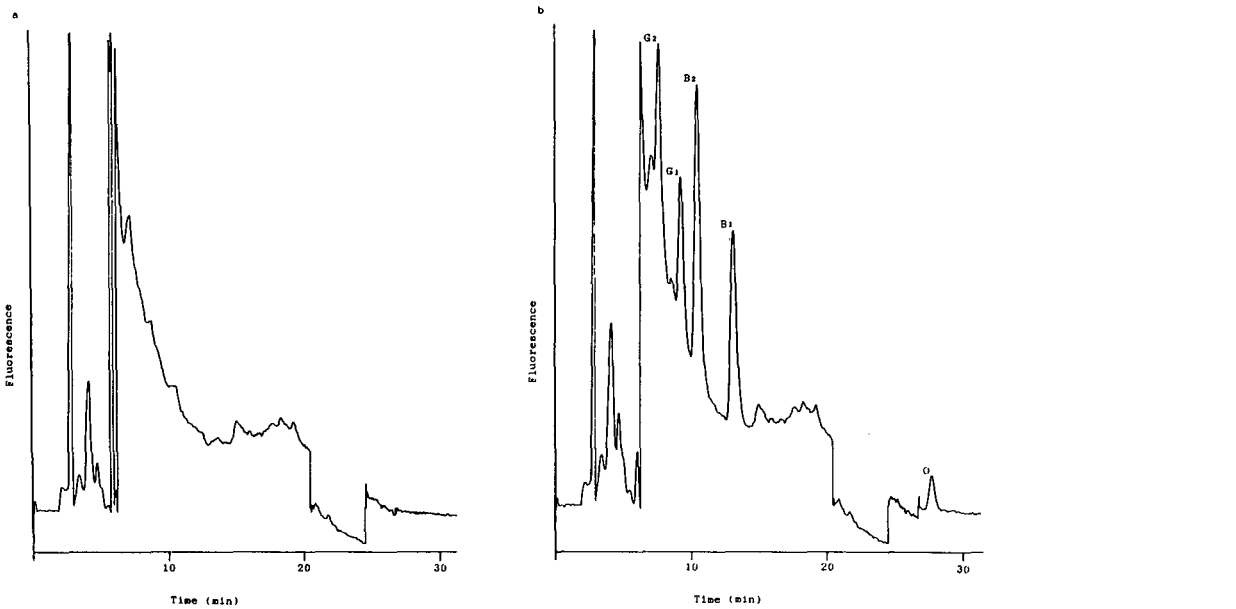

Fig. 3. Chromatograms of (a) palm sample and (b) palm sample, spiked to contain 3.2 μg/kg aflatoxin B_1, G_1 and G_2. 1.6 μg/kg aflatoxin B_2, 16 μg/kg ochratoxin A, with post-column derivatization.

TABLE IV

REPEATABILITY TEST ON MAIZE (n = 10)

Levels of mycotoxins used the same as in Table III. N.D. = Not determined.

	Recovery (%)					
	B_1	B_2	G_1	G_2	Ochratoxin A	Zearalenone
Mean	102.7	105.6	108.2	106.5	73.1	N.D.
S.D.	4.1	4.9	5.8	4.6	3.8	N.D.
R.S.D. (%)	4.0	4.6	5.4	4.3	5.2	N.D.

TABLE V

LIMITS OF DETECTION

Mycotoxin	Detection limit	
	ng	μg/kg
B_1	0.009	0.144–0.197
B_2	0.003	0.048–0.058
G_1	0.016	0.256–0.334
G_2	0.013	0.208–0.271
Ochratoxin A	0.050	1.031–6.349
Zearalenone	0.619	25.525–76.775

recoveries in some cases for ochratoxin and zearalenone.

CONCLUSIONS

The HPLC method developed is fast, sensitive and economical. It allows the determination of six mycotoxins using one HPLC set up and gradient elution. The method is readily adaptable to automation. The clean-up procedure involving GPC lends itself to partial automation. Due to the low recoveries of zearalenone and improved or separate clean-up method is required. The reproducibility and detection limits of the overall method are good.

ACKNOWLEDGEMENTS

The authors thank the Commission of the European Communities for granting a research bursary, under the framework of the FLAIR programme, to enable this research project to be carried out at the State Institute for Quality Control of Agricultural Products (RIKILT)-DLO, Wageningen, Netherlands.

REFERENCES

1 W. E. Paulisch, E. A. Sizoo and H. P. van Egmond, *J. Assoc. Off. Anal. Chem.*, 71 (1988) 957.
2 M. R. Smyth, D. W. Lawellin and J. Osteryoung, *Analyst*, 104 (1979) 73.
3 H. Cohen and M. LaPointe, *J. Assoc. Off. Anal Chem.*, 69 (1986) 957.
4 E. Josefsson and T. Möller, *J. Assoc. Off. Anal. Chem.*, 62 (1979) 1165.
5 P. M. Scott, T. Panalaks, S. Kanhere and W. F. Miles, *J. Assoc. Off. Anal. Chem.*, 61 (1978) 593.
6 M. T. Hetmanski and K. A. Scudamore, *Food Addit. Contam.*, 6 (1989) 35.
7 W. Langseth, Y. Ellingson, U. Nymoen and E. M. Økland, *J. Chromatogr.*, 478 (1989) 269.
8 D. C. Hunt, A. T. Bourden, P. J. Wild and W. T. Croby, *J. Sci. Food Agric.*, 29 (1978) 234.
9 K. A. Scudamore and M. T. Hetmanski, *Mycotoxin Res.*, in press.
10 W. Th. Kok, Th. C. H. van Neer, W. A. Traag and L. G. M. Th. Tuinstra, *J. Chromatogr.*, 367 (1986) 231.
11 M. V. Howell and P.W. Taylor, *J. Assoc. Off. Anal.Chem.*, 64 (1981) 1356.
12 N. Chamkasem, W. Y. Cobb, G. W. Latimer, C. Salmas and B. A. Clement, *J. Assoc. Off. Anal. Chem.*, 72 (1989) 336.

Journal of Chromatography, 629 (1993) 237–241
Elsevier Science Publishers B.V., Amsterdam

CHROM. 24 590

Correlation of reversed-phase high-performance liquid chromatography and gas–liquid chromatography for fatty acid compositions of some vegetable oils

Hiroaki Konishi*, William E. Neff and Timothy L. Mounts

Food Quality and Safety Research, National Center for Agricultural Utilization Research, Agricultural Research Service, US Department of Agriculture, 1815 N. University Street, Peoria, IL 61604 (USA)

(First received May 5th, 1992; revised manuscript received August 26th, 1992)

ABSTRACT

The triacylglycerol compositions of six genetically modified soybean oils, and commercial soybean, corn, safflower and sunflower oils were determined by reversed-phase high-performance liquid chromatography with flame ionization detection. Triacylglycerol molecular species were identified based on theoretical carbon numbers. Fatty acid compositions of the above soybean oils were estimated from concentrations of the triacylglycerol molecular species. Fatty acid composition was calculated by multiplying the concentration of each triacylglycerol by the percent of each fatty acid species in the triacylglycerol molecule. The fatty acid composition calculated from triacylglycerol analysis was compared with the composition determined by gas–liquid chromatography. There was good agreement between the fatty acid composition as calculated from the high-performance liquid chromatographic data and as determined by gas–liquid chromatography. These results support the findings that triacylglycerol molecular species could be identified based on theoretical carbon numbers and that fatty acid composition of soybean oil can be obtained from the data of reversed-phase high-performance liquid chromatography with flame ionization detection. The triacylglycerol composition for soybean oil obtained by this procedure required no response factors for quantitation.

INTRODUCTION

The quantitative measurement of triacylglycerol (TAG) and fatty acid composition of lipids is required in many biological research areas, like food, medicine and agriculture. Studies of genetic control of fatty acid distribution in TAG of vegetable oil depend firmly upon knowledge of TAG molecular species. Likewise, TAG molecular species analysis is necessary for the studies regarding natural and synthetic fats like cocoa butter and its substitutes, and for the nutritional evaluation of edible oil [1–4]. Several reports have been published on the separation and identification of TAG by using high-performance liquid chromatography (HPLC). In the studies by El Hamdy and Perkins [5,6], reversed-phase HPLC (RP-HPLC) was used and demonstrated improved TAG separation. Phillips and coworkers [7,8] adopted flame ionization detection (FID) connected to RP-HPLC for quantitative analysis of TAG. Nurmela and Satama [9] reported that FID showed a more quantitative response than that obtained by ultraviolet (UV) and refractive index (RI) detection. Christie [10] reported that FID had a good linear response to sample size and gave satisfactory results with microgram amounts of sample. Also, FID did not show baseline drift during gradient elution because the volatile solvent was vaporized and removed before the nonvolatile sol-

Correspondence to: W. E. Neff, Food Quality and Safety Research, National Center for Agricultural Utilization Research, Agricultural Research Service, US Department of Agriculture, 1815 N. University Street, Peoria, IL 61604, USA.

* Visiting Scientist from Technical Research Institute, Snow Brand Milk Co., Ltd., Saitama, Japan.

utes were carried into the flames of the detector for combustion [10]. Christie [11,12] concluded that the best and ideal detection system available currently for TAG molecular species analysis by HPLC was based on the FID principle which allowed a wide use of solvents and gave quantitative response. We have previously used RP-HPLC–FID to determine the TAG composition for oxidative studies [13] and studies of the interesterification of blends of vegetable oils with hydrogenated soybean oil [14].

The retention times or elution volumes of TAG molecular species are best predicted by theoretical carbon number (TCN) [11,13,14] which considers other elution factors determined experimentally in addition to the numbers of total carbon and carbon–carbon double bond, associated with the previously adopted equivalent carbon number (ECN).

In order to confirm that TAG molecular species can be identified based on TCN, the correlation of RP-HPLC–FID and gas–liquid chromatography (GLC) methods to obtain fatty acid composition of vegetable oils is reported here.

EXPERIMENTAL

Materials

Soybeans were commercial cultivars obtained from Randall L. Nelson, Curator, US Department of Agriculture, Germplasm Collection (University of Illinois, Urbana, IL, USA), and included plant introductions selected on the basis of fatty acid composition. Experimental lines were provided by Walter R. Fehr (Iowa State University, Ames, IA, USA). Soybean, corn, safflower and sunflower oils were obtained from a commercial source. The solid-phase extraction (SPE) columns (6.5 ml volume, loaded 2000 mg silica) used for purification of TAG were purchased from Baxter Health Care (Muskegon, MI, USA). All organic solvents used in this research were HPLC grade. TAG reference mixtures used for identification and quantitation were obtained from NuChek Prep (Elysian, MN, USA), and Sigma (St. Louis, MO, USA).

Methods

Crude oil (1.4–2.6 g) was obtained from genetically modified soybeans by hexane extraction of 15 g of soybean [11]. The beans were ground in a Varco coffee bean grinder (Type 228; Mouli Manufacturing, Belleville, NJ, USA) and soaked in 30 ml hexane at room temperature for 10 min. Oil was extracted by sonication for 5 min with an ultrasonic homogenizer Model 4710 sonicator (Cole Parmer, Chicago, IL, USA) with outlet setting at 7. After sonication, the hexane–bean mixture was cooled in ice to room temperature. This mixture was filtered over 0.6 g Celite filter aid and 1.2 g activated carbon, and the filter cake was rinsed five times with 80 ml hexane. The filtrate was dried with 4 g sodium sulfate and then filtered through folded filter paper (2V). Hexane was removed in 45 min on a roto-evaporator with water bath at 27°C.

The vegetable oils were stripped of non-TAG components by SPE chromatography with a hexane–diethyl ether gradient elution of each oil (1.2 g) mixed with 0.485 g activated carbon [11].

Purity and identification of TAG were determined by thin layer chromatography developed by diethyl ether–hexane (20:80, v/v), visualized by iodine and ultraviolet radiation.

TAGs (0.5 mg/5–10 μl hexane) were resolved by RP-HPLC [8,11,12] equipped with two Zorbax C_{18} columns (25 cm × 0.49 cm I.D., 5 μm particles, DuPont, Wilmington, DE, USA) in series, with linear gradient elution program [0.8 ml/min, acetonitrile–methylene chloride (70:30 to 60:40, v/v) over 120 min], followed by column clean up with 100% methylene chloride. The detection of eluents was done by FID, Tracor Model 945 HPLC detector (Austin, TX, USA) [9], block temperature: 180°C; detector and cleaning flame gas flow-rates: 140 and 160 ml/min hydrogen, respectively, and 300 ml/min oxygen. The noise filter was set high and baseline correction was used. The quantification of TAG molecular species by FID was checked with standard mixtures of trilinolenin, trilinolein, triolein, tristearin and tripalmitin.

Fatty acid methyl esters (FAMEs) of oils were prepared by potassium hydroxide-catalyzed transmethylation [13] and analyzed with a Hewlett-Packard (Avondale, PA, USA) Model 5710 A gas chromatograph equipped with a flame ionization detector. The glass column (180 cm × 0.31 cm I.D.) packed with 10% SP 2330 on 100–120-mesh Chromosorb W, AW, obtained from Supelco (Bellefonte, PA, USA), was operated at 160°C with a helium carrier gas flow-rate of 20 ml/min. The injection port and detector were held at 250°C. Methyl esters

TABLE I

FATTY ACID COMPOSITION OF SOYBEAN OILS

P = Palmitic; S = stearic; O = oleic; L = linoleic; Ln = linolenic acid. Quantitation was confirmed with NuChek. Prep standard 15 A.

Sample	Composition (%)				
	P	S	O	L	Ln
1	9.9	4.6	30.2	51.7	3.6
2	12.2	4.2	16.6	55.3	11.7
3	9.0	3.3	50.5	34.4	2.8
4	12.9	3.7	15.5	55.7	12.2
5	10.9	4.4	28.1	50.2	6.4
6	10.2	3.7	24.5	53.6	8.0
Commercial	9.7	3.1	22.0	56.6	8.6

were identified and their quantitation was calibrated with the NuChek Prep soybean methyl ester standard 15A (methyl palmitate, 6.0%; methyl stearate, 3.0%; methyl oleate, 35.0%; methyl linoleate, 50%; methyl linolenate, 3.0%; methyl arachidate, 3.0%).

RESULTS AND DISCUSSION

The fatty acid compositions of the soybean oils as determined by GLC–FID are presented in Table I.

The TAG molecular species (TAGMSs) were identified by matching calculated and experimental TCN values [5,8,14] to those of known TAGs in reference mixtures. Retention times and TCNs were linearly correlated, as reported previously [14].

TABLE II

TRIACYLGLYCEROL MOLECULAR SPECIES ANALYSIS OF A GENETICALLY MODIFIED SOYBEAN OIL BY RP-HPLC–FID, CALCULATION FOR FATTY ACID COMPOSITION AND THOSE DETERMINED BY GLC–FID

Ln, L, O, S, P are linolenic, linoleic, oleic, stearic and palmitic acids, respectively.

Molecular species	RP-HPLC (%)	Calculated fatty acid concentration (%)[a]				
		P	S	O	L	Ln
LnLnL	0.2	–	–	–	0.07	0.13
LnLL	3.1	–	–	–	2.07	1.03
LnLnO	0.3	–	–	0.10	–	0.20
LLL	16.3	–	–	–	16.30	–
LnLO	3.2	–	–	1.07	1.07	1.07
LnLP	1.1	0.37	–	–	0.37	0.37
LLO	19.6	–	–	6.53	13.06	–
LnOO	1.1	–	–	0.73	–	0.37
LLP	10.3	3.43	–	–	6.86	–
LNOP	0.7	0.23	–	0.23	–	0.23
LOO	12.7	–	–	8.47	4.23	–
LLS	3.7	–	1.23	–	2.47	–
LOP	10.0	3.33	–	3.33	3.33	–
PLP	1.5	1.0	–	–	0.50	–
OOO	4.9	–	–	4.90	–	–
LOS	4.2	–	1.40	1.40	1.40	–
POO	3.5	1.17	–	2.33	–	–
SLP	1.1	0.37	0.37	–	0.37	–
POP	0.4	0.27	–	0.13	–	–
SOO	1.3	–	0.43	0.87	–	–
SLS	0.3	–	0.20	–	0.10	–
SOP	0.5	0.17	0.17	0.17	–	–
	100.0					
Fatty acid composition, HPLC[b]		10.34	3.80	30.26	52.20	3.40
Fatty acid, composition, GLC		9.86	4.61	30.16	51.74	3.63

[a] Concentration calculated from RP-HPLC–FID data.

[b] Quantitation was confirmed with NuChek Prep standard 15 A.

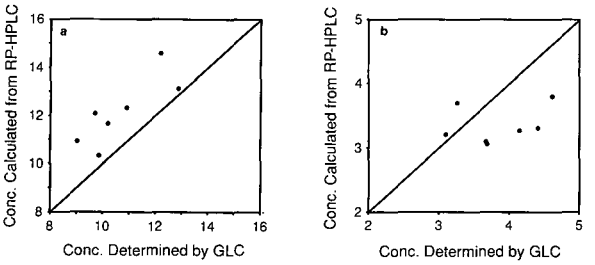

Fig. 1. Plot of palmitic (a) and stearic acid (b) concentrations in soybean oils determined by GLC–FID *versus* values of these acids calculated from RP-HPLC–FID.

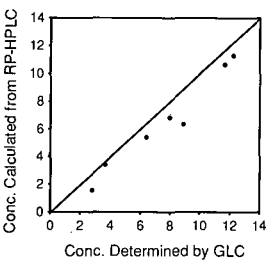

Fig. 3. Plot of linolenic concentrations in soybean oils determined by GLC–FID *versus* values of this acid calculated from RP-HPLC–FID.

TAGMS concentrations were calculated from their peak areas which correspond to the concentrations based on mass without requirement of correlation factors, as reported previously [14]. Fatty acid compositions were calculated from concentrations of TAGMSs by summation of the values calculated by multiplying the concentration of each TAGMS by the percent of the specific fatty acid in that TAGMS. As an example, the calculated fatty acid composition of a genetically modified soybean oil is presented in Table II. Close agreement was observed between calculated fatty acid composition obtained from TAG analysis by RP-HPLC–FID and fatty acid composition determined by GLC–FID (Table II).

Each fatty acid concentration, in oils from different soybean varieties, calculated from RP-HPLC–FID data was compared with the concentration determined by GLC–FID. Correlation coefficients between the concentrations of soybean oils determined using the two methods for five fatty acids (Figs. 1–3) were: palmitic, 0.982, stearic, 0.932, oleic, 0.998, linoleic, 0.999 and linolenic acids 0.986. Palmitic acid concentrations calculated from RP-HPLC–FID were slightly higher than those determined by GLC–FID (Fig. 1a); while linolenic acid concentrations calculated from RP-HPLC–FID tended to be slightly lower than those determined by GLC–FID (Fig. 3).

Fatty acid compositions of corn, safflower and sunflower oils as determined by the two methods were in good agreement and did not show the variation of palmitic acid and linolenic acid concentrations as found with soybean oils (Table III).

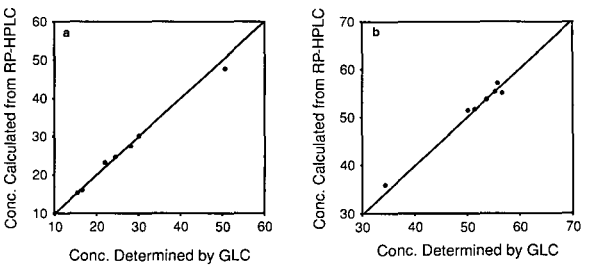

Fig. 2. Plot of oleic (a) and linoleic acid (b) concentrations in soybean oils determined by GLC–FID *versus* values of these acids calculated from RP-HPLC–FID.

CONCLUSIONS

The high correlation obtained between fatty acid composition calculated from RP-HPLC–FID TAG

TABLE III

COMPARISON OF FATTY ACID COMPOSITIONS CALCULATED FROM RP-HPLC–FID AND THOSE DETERMINED BY GLC–FID

Fatty acid	Composition (%)					
	Corn oil		Safflower oil		Sunflower oil	
	HPLC	GLC	HPLC	GLC	HPLC	GLC
Palmitic	11.0	11.3	6.8	6.8	6.9	7.0
Stearic	1.7	1.7	1.8	2.4	3.8	4.5
Oleic	24.2	26.1	13.9	14.9	17.9	17.8
Linoleic	62.3	59.8	77.4	75.4	71.1	70.2
Linolenic	0.7	1.1	0.7	0.5	0.1	0.5

analysis and the composition determined by GLC–FID FAME analysis indicates that TAG molecular species can be identified based on TCNs. RP-HPLC–FID analysis of soybean oil TAG can be quantitated without response factors. Fatty acid compositions of vegetable oils can be obtained by calculation from the results of RP-HPLC–FID.

ACKNOWLEDGEMENT

Wilma M. Rinsch, National Center for Agricultural Utilization Research, Peoria, IL 61604, USA, provided experimental support.

REFERENCES

1 C. Merritt, Jr., M. Vajdi, S. G. Kayser, J. W. Halliday and M. L. Bazinet, *J. Am. Oil Chem. Soc.*, 59 (1982) 422.
2 T. R. Davis and P. S. Dimick, *J. Am. Oil Chem. Soc.*, 66 (1989) 1494.
3 S. Chaiseri and P. S. Dimick, *J. Am. Oil Chem. Soc.*, 66 (1989) 1771.
4 W. M. N. Ratnakaya, D. G. Matthews and R. G. Ackman, *J. Am. Oil Chem. Soc.*, 66 (1989) 966.
5 A. H. El Hamdy and E. G. Perkins, *J. Am. Oil Chem. Soc.*, 58 (1981) 868.
6 A. H. El Hamdy and E. G. Perkins, *J. Am. Oil Chem. Soc.*, 58 (1981) 49.
7 F. C. Phillips, W. L. Erdahl, J. D. Nadenicek, L. J. Nutter, J. A. Schmit and O. S. Privett, *Lipids*, 19 (1984) 142.
8 F. C. Phillips, W. L. Erdahl, J. A. Schmit and O. S. Privett, *Lipids*, 19 (1984) 880.
9 K. V. V. Nurmela and L. T. Satama, *J. Chromatogr.*, 435 (1988) 139.
10 W. W. Christie, *High-Performance Liquid Chromatography and Lipids*, Pergamon Press, Oxford, 1987, p. 25.
11 W. W. Christie, *Gas Chromatography and Lipids*, The Oily Press, Glasgow, 1989, p. 242.
12 W. W. Christie, *High-Performance Liquid Chromatography and Lipids*, Pergamon Press, Oxford, 1987, p. 186.
13 W. E. Neff, E. Selke, T. L. Mounts, W. Rinsch, E. N. Frankel and M. A. M. Zeitoun, *J. Am. Oil Chem. Soc.*, 69 (1992) 111.
14 M. A. M. Zeitoun, W. E. Neff, E. Selke and T. L. Mounts, *J. Liq. Chromatogr.*, 14 (1991) 2685.

Journal of Chromatography, 629 (1993) 243–254
Elsevier Science Publishers B.V., Amsterdam

CHROM. 24 644

Chemical characterization of cellulose acetate by non-exclusion liquid chromatography

Thomas R. Floyd

Eastman Chemicals Co., P.O. Box 1972, Kingsport, TN 37663 (USA)

(First received November 22nd, 1991; revised manuscript received September 24th, 1992)

ABSTRACT

The physical properties of cellulose acetate polymers are not governed solely by their average chemical properties, but are also dependent upon molecular mass and acetyl distributions. Currently, most analytical techniques that are routinely used to characterize cellulose esters, provide only a mean value of the property that is measured. Non-exclusion liquid chromatography was investigated as a means of analyzing cellulose acetate polymers over a compositional range from 37–43% (w/w) acetyl. Under optimum conditions this technique was highly selective for the chemical composition of these polymers, providing information on both mean acetyl composition and acetyl distribution. The purpose of this paper is to describe chromatographic variables required to successfully characterize cellulose acetate.

INTRODUCTION

Because heterogeneous polymers (or heteropolymers) possess both molecular mass and chemical composition distributions, they are a difficult class of polymers to characterize. To measure any distribution of a polymer, *e.g.*, molecular mass or chemical composition, requires the implementation of some separation method. When measuring a single distribution of a heteropolymer, a separation is required which either is dependent predominantly upon this one distribution variable or provides a means of readily extracting from the raw data information on this variable.

Gel permeation chromatography (GPC) is the most common separation method used to characterize the molecular mass distribution of homopolymers. The application of GPC for heteropolymers has been limited since a polymer's molecular volume is dependent on both molecular mass and chemical composition. Because of this shortcoming, alternative separation techniques, such as non-exclusion liquid chromatography separations, have become increasingly invaluable when characterizing heteropolymers.

To date, several polymers have been analyzed by non-exclusion liquid chromatography. They include poly(styrene methacrylate) [1–3], poly(styrene acrylate) [4,5], poly(styrene acrylonitrile) [6,7], and poly(styrene–vinyl acetate) [8]. Specific separation factors should be known when assessing the usefulness of liquid chromatography for heteropolymer characterization. Polymer separations routinely require mobile phase gradients. Changes in the mobile phase may alter the underlying retention mechanism for a polymer. This is most pronounced when polymer solubility is effected, since it will influence the predominance of either an adsorption or a phase separation mechanism [9]. Mobile phase and stationary phase conditions will also affect the dependence of elution upon either the polymer's molecular mass and/or chemical composition [10–12].

In this work liquid chromatography was used to determine the acetyl composition of cellulose acetate

Correspondence to: T. R. Floyd, Eastman Chemicals Co., P.O. Box 1972, Kingsport, TN 37663, USA.

polymers. This was performed on a conventional high-performance liquid chromatograph using reversed-phase separation conditions. The eluted polymer was detected using an evaporative light scattering detector. As opposed to previous chromatographic work on cellulose acetate, neither prederivatization or off-line detection was necessary using this unique detector [12–17]. The observed separation of cellulose acetate was strongly dependent upon mass percent acetyl composition. Under reversed-phase HPLC conditions cellulose acetate was retained on the column primarily due to adsorption.

In the context of this paper acetyl distribution or "acetyl spread" is defined as both the distribution of acetyl groups along the cellulose backbone and the distribution due to intermolecular mixing of dissimilar cellulose acetate molecules. Cellulose ester chemists have theorized that many physical properties of cellulose acetate may be attributed to its acetyl distribution. This theory has been difficult to validate since all historical analytical methods have relied on tedious and irreproducible separation techniques. It is agreed that much is to be gained in the development of an accurate and automated means of characterizing the chemical composition of this polymer.

CELLULOSE ACETATE FRACTIONATION

Cellulose esters form a unique class of synthetic polymers. Unlike either polyolefins or polyesters, cellulose esters are synthesized from a natural polymer. Cellulose acetate is synthesized by the complete acetylation of cellulose followed by a controlled back hydrolysis to a desired degree of acetyl substitution. As shown in Fig. 1, acetylation can take place along the cellulose chain at three available hydroxyl groups per glucose monomer. Cellulose acetate can have an acetyl content from >0% to 44.8% (w/w). As the acetyl content of cellulose acetate is increased, it changes from a hydrophilic to a hydrophobic polymer. Completely acetylated cellulose is referred to as cellulose triacetate. Polymer solubility is highly dependent on both the degree of acetyl substitution (DS) and degree of polymerization (DP) [10,18–26]. From a manufacturing standpoint, the extent and consistency of both composition and molecular mass are important

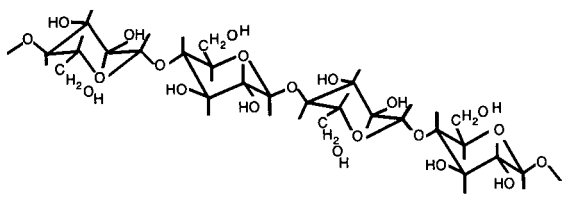

Fig. 1. Structure of α-cellulose.

variables that should be measured when controlling cellulose acetate reactions.

Four primary techniques historically used in the separation of cellulose acetate have been solutional fractionation, precipitative fractionation, thin-layer chromatography, and column chromatography. Solutional fractionation involves taking a solid polymer and extracting the polymer with a successively stronger solvent. The solvent is chosen so that it dissolves a select fraction of the polymer. Precipitative fractionation involves dissolving a polymer in a good solvent, and then decreasing the solubility and precipitating out a desired polymer fraction by either successively adding a controlled volume of poor solvent or changing the temperature. Comparisons between these two bulk separation techniques, used for cellulose ester fractionation, have been previously reported [18,19]. The terms "good" solvent and "poor" solvent will be used throughout this paper to describe the strength of solvent for a polymer in relation to either solubility or chromatographic elution.

The first reported fractionation of cellulose acetate was by Mardles in 1923 [20]. Fractionation was performed by precipitation with acetone and water as the respective "good" and "poor" solvent pair. The fractionation order was strongly dependent upon molecular mass. The effect of temperature on solutional fractionation of cellulose diacetate was studied by Sookne and co-workers [21,22] and by Morey and Tamblyn [23]. As expected, solubility increased for a given solvent fraction as temperature was increased. Fractionation was found to proceed primarily as a function of molecular mass.

Howlett and Urquhart [24] performed an extensive study on solvent–non-solvent pairs in fractionating cellulose diacetate. While performing precipitative fractionation they found that it was desirable

to use a pair of solvents where the change in polymer solubility was small relative to non-solvent addition. Rosenthal and White [10] were the first to use solubility parameter information in choosing "good"/"poor" solvent pairs in the precipitative fractionation of cellulose acetate. They demonstrated that the choice of "poor" solvent can influence the dependence of intrinsic viscosity and weight percent acetyl on fractionation.

Most polymers exhibit a low and high critical solution temperature, the points where precipitation begins. Cowie and co-workers [25,26] determined that the upper critical solution temperature for cellulose acetate increased as a function of acetyl content. Kamide and co-workers [13,27] evaluated the use of thin-layer chromatography for the fractionation of cellulose acetate. Silica gel was used as the stationary phase. A binary mobile phase solvent system of methanol–methylene chloride was used. The migration of cellulose acetate polymers of varying acetyl composition ranging from 39% to 44% acetyl were influenced by changes in the mobile phase volume ratio. Under these conditions polymer migration was found to be independent of molecular mass. A binary solvent system of methylene chloride–butanol was also useful in fractionating by composition. Interesting enough, while both of these binary mobile phases fractionated by composition, the fraction of polymer that migrated (*i.e.*, either high or low acetyl fraction) was different. Apparently this difference resulted from two opposing separation mechanisms; either phase separation or adsorption. This was controlled by the alcohol–methylene chloride volume ratio.

Mark and Saito [12] were the first to use a chromatographic support to separate cellulose acetate. A number of supports, including calcium carbonate, alumina, starch and carbon, were investigated. Polymer adsorption was studied using both acetone and dioxane. In all cases the fraction of adsorbed polymer was less when dioxane was used instead of acetone. Tarakanov and Okunev [14,15] used column chromatography for the fractionation of cellulose triacetate. Using a binary mobile phase gradient of methylene chloride and heptane, the separation was shown to be directly dependent upon polymer viscosity.

Tung [16] used column chromatography to fractionate cellulose esters. Both solvent and thermal gradient conditions were investigated. This work focused on fractionating various cellulose esters based upon molecular mass. Whether the separation mechanism was due either to phase-separation (precipitation) or adsorption determined the significance of the stationary phase in the separation process.

EXPERIMENTAL

Liquid chromatography was performed on a Perkin-Elmer (Norwalk, CT, USA) Model 410 gradient pumping system with a Perkin-Elmer LC-600 autosampler and a 20-μl injection loop. All exploratory separation experiments were done at ambient temperature, nominally 25°C. Statistical and long-term precision studies were performed using a Waters TCM column heater set at 30°C for cellulose diacetates. Data storage and analysis were performed using the PE/Nelson Access-Chrom software, version 1.6, on a 8600 VAX mainframe computer. The statistical plates programme was used to determine peak controid (M1) and peak variance (M2). The Foley–Dorsey plates programme was also used to generate width at one tenth height and number of theoretical plates (N). Column dead volume was estimated by injecting a 500 mg/l solution of acetone, while detecting the eluted peak with a Waters Model 481 variable-wavelength detector set at 300 nm. Gradient delay volume was estimated by tracking the rising baseline of a binary gradient using acetone in the "B" solvent reservoir.

Several HPLC columns were evaluated during this study. These columns are listed in Table I. Spherisorb ODS2, Spherisorb Si, and Spherisorb Al were purchased from Keystone Scientific (Bellefonte, PA, USA). Hamilton PRP-1 column was purchased from Hamilton (Reno, NV, USA) and the Polymer Lab. PLRP-S columns were purchased from Polymer Lab. (Amherst, MA, USA) (all of these columns had a diameter of 4.6 mm). Methanol, n-propanol, ethanol, tetrahydrofuran and acetone were purchased from Burdick & Jackson (Muskegon, MI, USA). Distilled/de-ionized water was produced in-house.

A Varex Mark II evaporative light scattering detector was used to detect the cellulose acetate polymer. The detector settings were as follows: attenuation range, 5; evaporator tube temperature, 105°C;

TABLE I

HPLC COLUMNS USED IN COMPOSITIONAL ANALYSIS OF CELLULOSE ACETATE

Column type	Particle size (μm)	Mean pore diameter (nm)	Column length (cm)
Spherisorb Si	5	8	15
Spherisorb Al	5	13	15
Spherisorb ODS2	5	8	15
Hamilton PRP-1	10	10	15
Polymer Lab. PLRP-S	10	10	15
Polymer Lab. PLRP-S	10	10	5
Polymer Lab. PLRP-S	10	30	5
Polymer Lab. PLRP-S	10	100	5

nitrogen pressure, 20 p.s.i. (1 p.s.i. = 6894.76 Pa); time constant, 5 s.

Mean acetyl composition of cellulose acetate was determined either by saponification followed by an acid titration or by ^{1}H NMR. Inherent viscosity was determined using acetone. These analytical methods are described in detail elsewhere [28,29].

GPC was performed with both a 100 Å and a mixed-bed columns in series. These columns were purchased from Polymer Lab. Tetrahydrofuran was used as the mobile phase when performing GPC on cellulose diacetate polymers (<42.5%Ac). Polymer samples were made up in mobile phase at a concentration of 1000 mg/l. Polystyrene standards were used to calibrate for number average and mass average molecular mass. Analytical information for all cellulose acetate polymers studied during this work are listed in Table II. When performing non-exclusion liquid chromatography, the cellulose diacetate (samples A–K in Table II) polymer solutions were made up to a concentration of approximately 2000 mg/l using acetone. All cellulose acetate samples were supplied by Tennessee Eastman (Kingsport, TN, USA).

RESULTS AND DISCUSSION

Chromatographic conditions used in the analysis of cellulose acetate

Cellulose acetate polymers were separated by reversed-phase liquid chromatography. Chromatograms of a series of cellulose acetate polymers, ranging in acetyl substitution (or mean mass percent acetyl) from 38.3% to 42.6%, are shown in Fig. 2. As the degree of acetyl substitution increased, the samples elution time increased. These polymers were chromatographed on a Hamilton PRP-1 (150 × 4.6 mm, 10 μm) column under a mobile phase condition of acetone–water–methanol (4:3:1) to 100% acetone in 15 min at a flow-rate of 0.8 ml/min. A strong linear correlation existed between mean mass percent acetyl and the polymer elution time. This is shown in Fig. 3. The slope, intercept, and correlation coefficient were determined to be 2.01, 21.0 and 0.993, respectively, over a acetyl range from 37.9% to 43.5%. In generating the retention time data peak centroid, the first statistical moment, was chosen instead of peak maximum. This was used because the eluting polymer peak would rarely conformed to a gaussian profile and because there was no reason to assume *a priori* that the polymer peak would be gaussian.

During development of this HPLC method a number of solvent conditions were evaluated. Factors such as detector response, polymer solubility and column back pressure restricted the number of potential mobile phase choices. Since this analysis required a mobile phase gradient, both "good" and "poor" solvents were required [30]. In the past,

TABLE II

CELLULOSE ACETATE ANALYTICAL DATA

M_n = Number-average molecular mass; M_w = mass-average molecular mass.

Sample	Acetyl (%, w/w)	Inherent viscosity (dl/g)	M_n	M_w
A	37.9	1.34	64 000	130 000
B	38.3	1.26	52 000	129 000
C	38.8	1.30	53 000	139 000
D	39.3	1.43	58 000	173 000
E	39.9	1.30	69 000	158 000
F	40.3	1.35	51 000	165 000
G	41.0	1.32	78 000	170 000
H	39.8	1.05	52 000	111 000
I	39.9	1.37	72 000	164 000
J	41.5	1.20		
K	42.6	1.09	52 000	106 000

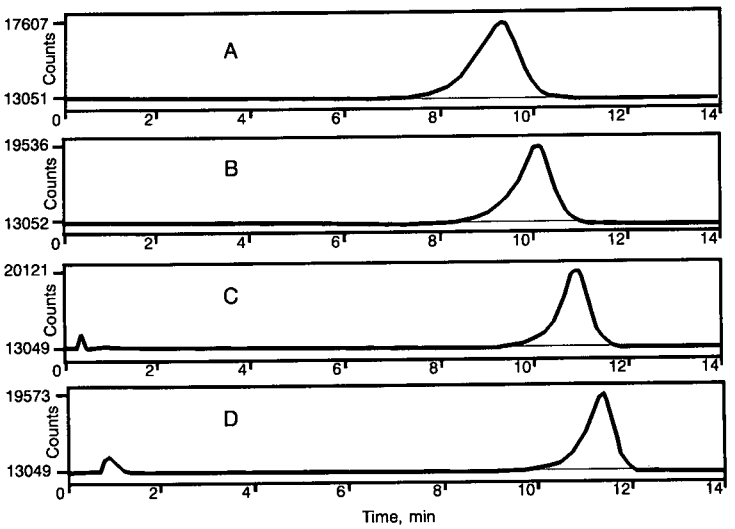

Fig. 2. Superimposed chromatograms of four cellulose acetate samples; A = 37.9%, B = 39.9%, C = 41.5% and D = 42.6% (w/w) acetyl. A 15-min linear gradient from acetone–water–methanol (4:3:1) to 100% acetone at a flow-rate of 0.8 ml/min was used.

"good" solvents that have been used for solubilizing cellulose acetate have included; acetone, tetrahydrofuran, ethyl acetate, dimethyl sulphoxide, and a binary solvent system of methylene chloride–methanol. Dimethyl sulphoxide was eliminated due to its high viscosity, which would have created problems both due to high back pressure and high detector background noise [31]. In this study ethyl acetate and methylene chloride–methanol were rejected due to their immiscibility in water. Acetone and tetrahydrofuran were the only "good" solvents that fulfilled all initial requirements.

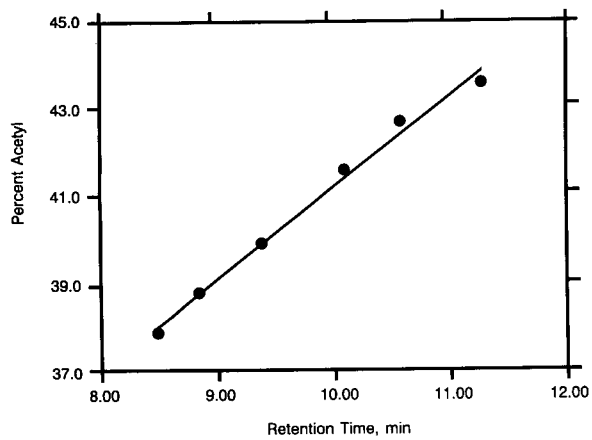

Fig. 3. Graph of retention time in minutes *versus* mass percent acetyl. Linear least squares fit provided a slope of 2.01, an intercept of 21.0 and a correlation coefficient of 0.993.

In choosing the most appropriate "poor" solvent, several conditions were also required. First, the initial mobile phase should not precipitate the polymer at the head of the column. Second, the initial solvent should not allow the polymer to be excluded through the HPLC packing. Third, the initial solvent should not produce an excessively high back pressure on the system. Methanol and water, as well as binary solvents of methanol–water, methanol–acetone, water–acetone and water–tetrahydrofuran failed at least one of these initial three criteria. Ternary solvent mixtures were then investigated as a possible "poor" mobile phase. A number of suitable solvent combinations were ultimately identified. They are listed in Table III.

These five solvent systems were further evaluated. Chromatographic selectivity toward acetyl composition relative to molecular mass was chosen as the final criteria. This was measured using three different cellulose acetate polymers. Both mass percent acetyl (%Ac) and inherent viscosity (IV) are listed in Table I for these three polymers. One sample pair had a comparable acetyl substitution (39.9% *vs.*

TABLE III

EFFECT OF MOBILE PHASE ON CHROMATOGRAPHIC SELECTIVITY OF CELLULOSE ACETATES

%Ac = Acetyl (%, w/w); IV = inherent viscosity.

No.	Mobile phase	Retention time (min)			Δ%Ac I – A	ΔIV I – H	|Δ%Ac/ΔIV|
		Sample I	Sample A	Sample H			
1	Water–methanol–tetrahydrofuran (2:1:1) to 100% tetrahydrofuran	9.67	9.01	9.82	0.66	−0.15	4.4
2	Water–ethanol–tetrahydrofuran (2:1:1) to 100% tetrahydrofuran	8.81	8.46	8.94	0.35	−0.13	2.7
3	Water–isopropanol–tetrahydrofuran (2:1:1) to 100% tetrahydrofuran	8.95	7.08	9.41	1.87	−0.46	4.1
4	Acetone–water–methanol (4:3:1) to 100% acetone	9.40	8.48	9.31	0.92	0.09	10.2
5	Acetone–water–methanol (3:4:1) to 100% acetone	12.22	11.41	12.34	0.93	−0.12	7.8

39.8%Ac) but a different IV (1.37 *vs.* 1.05). The second pair had a comparable IV (1.34 *vs.* 1.37), but a different acetyl substitution (37.9% *vs.* 39.9%Ac). In evaluating different mobile phase conditions a relative selectivity index was devised by determining the absolute ratio of the change in retention due to %Ac at a constant IV, relative to the change in retention time due to the change in IV at a constant %Ac. This has been abbreviated as $|\Delta\%Ac/\Delta IV|$ and is listed in Table III for the five different mobile phase conditions.

Solvent systems 1–3 used tetrahydrofuran as the "good" solvent. The "poor" solvent in these first three mobile phase systems consisted of water–alcohol–tetrahydrofuran (2:1:1, v/v/v) where the alcohol was either methanol, ethanol or isopropanol. No advantage in selectivity was observed in replacing methanol with the other two alcohols. Substituting acetone instead of tetrahydrofuran in solvent systems 4 and 5 produced a significant improvement in compositional selectivity. Weakening the "poor" solvent's composition from 4:3:1 to 3:4:1 acetone–water–methanol did not improve acetyl selectivity. Conversely when the volume fraction of water was decreased further, partial exclusion of the lower acetyl (*i.e.*, <38%Ac) polymeric fraction occurred.

Five HPLC columns were compared using the same three cellulose acetate samples previously discussed. Initially, care was taken to choose stationary phases of narrow pore diameter. This was done

TABLE IV

EFFECT OF COLUMN TYPE ON CHROMATOGRAPHIC SELECTIVITY OF CELLULOSE ACETATES

No.	Column type	Retention time (min)			Δ%Ac I – A	ΔIV I – H	|Δ%Ac/ΔIV|
		Sample I	Sample A	Sample H			
1	Polymer Lab.	11.76	10.93	11.89	0.83	−0.13	6.4
2	Spherisorb ODS2	11.16	10.33	11.29	0.83	−0.13	6.4
3	Hamilton PRP-1	12.22	11.41	12.34	0.93	−0.12	7.8
4	Spherisorb Al	11.98	NR	12.79	–	−0.81	–
5	Spherisorb Si	NR[a]	NR	NR	–	–	–

[a] NR = polymer not retained.

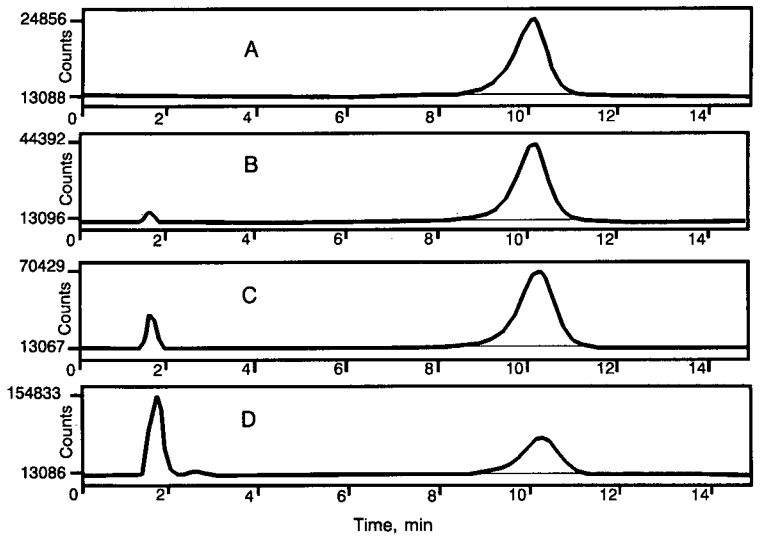

Fig. 4. Effect of injection volume on polymer exclusion. A single polymer (39.9%Ac) was injected using three different injection volumes; A = 20-, B = 50-, C = 100- and D = 200-μl loops. Chromatographic conditions as in Fig. 2.

in order to minimize molecular mass discrimination due to preferential migration of lower-molecular-mass subpopulations into more accessible pores. The column types, particle sizes, and pore sizes for these four columns are listed in Table I. A mobile phase gradient of acetone–water–methanol (3:4:1) to 100% acetone in 15 min at 0.8 ml/min was used for this study. The results from this study are shown in Table IV. No difference in the $|\Delta\%Ac/\Delta IV|$ selectivity between the Polymer Lab. PLRP-S (styrene–divinylbenzene based) and Spherisorb ODS2 (octadecylsilane bonded silica gel) columns was observed. The selectivity index was slightly better using the Hamilton PRP-1 column (styrene–divinylbenzene based). Cellulose acetate was retained longer on the polystyrene–divinylbenzene based supports. The Spherisorb Al (alumina) column provided no retention (NR) for the 37.9%Ac/1.37 IV cellulose acetate polymer. At a constant acetyl substitution, the Spherisorb Al column had a significantly longer retention for the lower IV polymer. Presently no reasons are known to explain this observed selectivity profile. The Spherisorb Si (silica gel) column failed to retain any of the cellulose acetate samples. This result was consistent with earlier work reported by Mark and Saito [12].

The effects of both injection volume and polymer concentration were studied. Previous work had shown that polymer exclusion will occur at high injection volumes [2]. This effect was studied in order to avoid injection discrimination. Fig. 4 illustrates the effect of injection volume on polymer exclusion. At both 100 and 200 μl, a large fraction of the cellulose acetate sample was excluded from the column. When collected this excluded polymer was found to have the same acetyl composition and inherent viscosity of the non-excluded polymer fraction. Lochmüller *et al.* [32] have shown under isocratic conditions that polymer exclusion can be influenced by the strength of the injection solvent. This has been shown to be due to poor equilibrium of the polymer with the mobile phase prior to introduction onto the column. This effect is dependent upon injection volume and solvent strength. In this work initial conditions were weak enough that at an injection volume of 20 μl polymer exclusion was not evident. As a result of this study, injection volumes were kept at 20 μl.

Separation mechanism for a polymer can primarily result from either phase separation or stationary phase adsorption. One way of determining the presence of phase separation (polymer precipitation) is by studying the dependence of polymer concentration on retention [30]. In Fig. 5, a cellulose

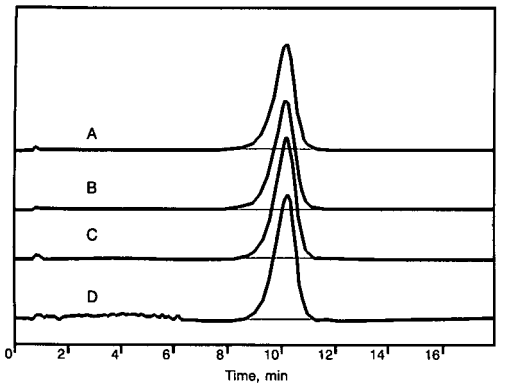

Fig. 5. Effect of cellulose acetate concentration on chromatographic retention. A single polymer (39.9%Ac) was injected at four different concentrations; A = 10 000, B = 8000, C = 3000 and D = 1000 ppm. Chromatographic conditions as in Fig. 2.

acetate polymer at four different concentrations was chromatographed using the standard conditions described earlier. No dependence of polymer concentration on retention was observed, both with regards to peak centroid retention time and peak dispersion, measured as peak variance.

The evaporative light scattering detector's response is non-linear and known to be dependent on a number of variables [31]. In chromatographing cellulose acetate, it was important to know if the detector's response was dependent upon the degree of acetyl substitution. A series of cellulose acetate samples of differing acetyl substitution and similar molecular mass were chromatographed using the conditions listed for Fig. 2. Normalized area counts were compared within this series and are listed in Table V. Detector response (normalized area counts) was observed to be slightly dependent on %Ac over this acetyl series. Approximately a 30% increase in area was observed in going from a cellulose acetate polymer of 38% to 41.5%Ac. In conjunction a 30% decrease in peak width was also observed over this same range. Since the response of the evaporative light scattering detector is non-linear, it is believed that the increase in area counts is mostly due to the decrease in peak width than due to the polymer's compositional changes.

The comparison of these detector responses would be more accurate if they were run under identical isocratic conditions. This study was designed to measure the potential response differences under the working range of the mobile phase. This experiment was set-up using conditions which the polymers would typically elute under. Over the 2–3-min window by which most of these polymers eluted solvent composition did not significantly change, for instance water composition decreased from 28 to 20%, methanol decreased from 9 to 7% and acetone increased from 63 to 73%.

Polymer peak dispersion

An important aspect of the liquid chromatography method is the ability to determine acetyl spread by measuring peak dispersion. Due to the novelty of using chromatographic peak dispersion to measure compositional distribution in polymers, it was necessary to evaluate several dispersion descriptors in

TABLE V

RETENTION TIME, NORMALIZED PEAK AREA, AND PEAK DESCRIPTORS OF VARIOUS CELLULOSE ACETATE POLYMERS

The values in parentheses are the respective standard deviations of 9 replicates.

Sample	Acetyl (%, w/w)	Retention time (min)	Normalized area counts	Plate efficiency (N)	1/10 Peak width (s)	1/2 Peak width (s)
A	37.9	8.30 (0.00)	93 077 (3200)	555 (18)	96.9 (1.7)	47.1 (0.5)
C	38.8	8.80 (0.01)	105 650 (7600)	583 (14)	103.1 (1.1)	47.6 (0.4)
D	39.3	9.10 (0.01)	117 148 (2500)	729 (13)	95.7 (0.7)	44.2 (0.6)
E	39.9	9.32 (0.02)	121 024 (1400)	757 (10)	97.5 (1.1)	43.3 (0.4)
F	40.3	9.53 (0.01)	127 474 (2500)	963 (14)	89.2 (0.6)	39.4 (0.5)
K	41.5	10.17 (0.01)	123 521 (1000)	1279 (30)	84.4 (0.8)	35.1 (0.7)

order to arrive at the most accurate and precise one. Three original peak dispersion descriptors are listed in Table V. They are (1) plate efficiency, (2) width at 1/10 height and (3) width at 1/2 height. Both plate efficiency and width at 1/10 height were determined using the Foley–Dorsey calculations in the PE Nelson Access-Chrom software, while the width at 1/2 height was calculated by hand. Plate efficiency was found to be less precise than the others. In addition the Foley–Dorsey calculations for plate efficiency assume a modified gaussian peak which the polymer peaks usually did not resemble [33]. These two factors led us to immediately abandon its consideration as a descriptor. The coefficients of variance for both the width at 1/2 height and the width at 1/10 height were between 1 and 2%. Since the width at 1/10 height was more sensitive to peak asymmetry arising from skewed peaks, it was the preferred choice.

Statistical moments were also evaluated as peak descriptors. Fundamentally the second statistical moment or peak variance (M2) would be a sound descriptor of peak dispersion. Skew (M3) and excess (M4) would in addition be valuable descriptors of non-gaussian behavior, which is believed to result from over or under hydrolyzed sub-populations of cellulose esters. In comparing several cellulose acetate polymers the square root of peak variance (σ), was found to be slightly less precise than the width at 1/10 height: 3% *vs.* 1%. Skew and excess exhibited even greater variability. Since statistical moments are more influenced by the selection of peak start and stop points they are generally excepted to be less precise [34].

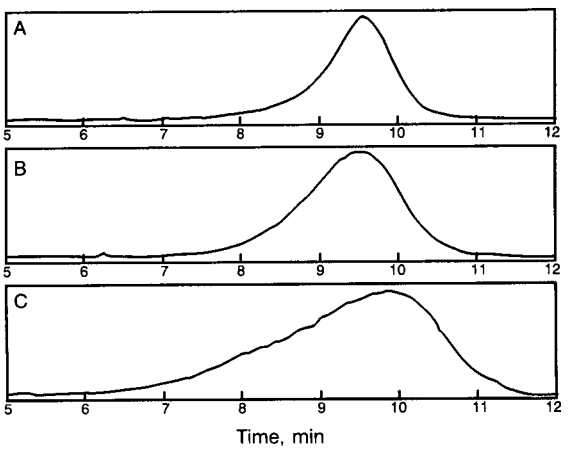

Fig. 6. Comparison of three cellulose acetate polymers, having a mean mass percent acetyl of 39.9% and a comparable molecular mass. Chromatographic conditions as in Fig. 2.

In practice there is no clear preference between width at 1/10 height and second statistical moment. Both have been valuable in helping to characterize the chemical composition of various cellulose acetates. In Fig. 6 there is a comparison of three cellulose acetates. All three polymers have comparable molecular mass and a nominal mass percent acetyl of 39.3%; however, both peak variance ($A = 910\ s^2$, $B = 1400\ s^2$ and $C = 4300\ s^2$) and width at 1/10 height ($A = 122$ s, $B = 159$ s and $C = 261$ s) varied significantly. From these results it was not surprising to learn that sample C exhibited significant haze when dissolved in acetone while samples B and A did not.

There are a number of factors that could potentially contribute to peak dispersion. These contributions include gradient profile, normal column variance, acetyl distribution and molecular mass. The gradient profile was an important factor when understanding external dispersion effects. All polymer samples should see the same gradient change over time. The system dead volume and gradient delay time were calculated in order to better understand this method's working range. Even though the gradient started at injection, the gradient did not reach the head of the column until 2.4 min and the detector for 4.1 min. Since the lower acetyl polymers did not elute until after 7 min, all polymers experienced a constant gradient change.

External and internal column variance will contribute to the total peak dispersion. Since external variance would be constant for all polymer samples, it was simply ignored. It should be noted that without compensating for this contribution, acetyl spread values constitute a relative measurement.

While over the range of 37 to 43% acetyl polymer mean retention time behaved linearly, further proof was required to show that peak dispersion did not change relative to mean acetyl. To study this effect a 38.8% cellulose acetate polymer was fractionated in 0.3-min slices and re-chromatographed. The chromatograms of the original polymer along with six successive fractions (peaks 6–10) are shown in Fig. 7. It is evident from this figure that the original polymer separation could be reconstructed from the individual fractions and that peak dispersion was negligible. In reviewing the results of this experiment in Table VI, 50–60% of the polymer was re-chro-

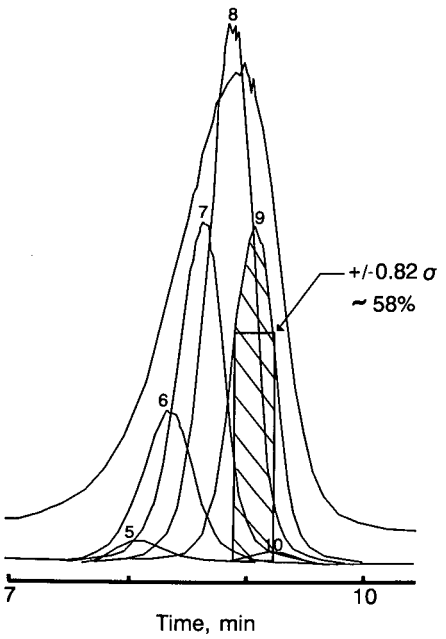

Fig. 7. Superimposed chromatograms of a single polymer (38.8%Ac) before and after fractionation. Chromatographic conditions as in Fig. 2.

matographed within the fractionated time period. When closely examining the width at 1/10 height and the area percent within the original fraction period, there was a slight dependence between the peak dispersion (measured as both width at 1/10 height and peak variance) and retention time (%Ac). The peak width of fraction 5 may be called into question because of the low signal-to-noise ratio for this fraction. This may have made it difficult to accurately measure peak dispersion for this fraction. By ignoring this fraction one could contend that no bias exists, while including this fraction one could postulate that an approximate 15% chromatographic bias exists over a range from 37 to 40% acetyl.

TABLE VI

PEAK DESCRIPTORS OF FRACTIONATED CELLULOSE ACETATE

Fraction No.	Peak centroid (min)	Peak variance (s^2)	Width at 1/10 height (s)	Area percent within 0.3 min fraction window (%)
5	8.10	356	72	46
6	8.35	235	63	50
7	8.62	186	56	54
8	8.86	166	53	57
9	9.07	159	52	59
10	9.25	163	55	55
Original	8.74	903	121	–

To validate the usefulness of this liquid chromatography method, it was important that the effect of cellulose acetate molecular mass on elution time be minimal or altogether absent. A careful study was undertaken to verify this condition. Again, the 38.8% cellulose acetate sample was fractionated, however, this time by GPC. A 20 × 300 mm I.D. mixed-bed Polymer Lab. GPC column was used. This polymer was fractionated using 0.3-min time slices. Six fractions were collected and reanalyzed by GPC to determine M_w, M_n and polydispersity. These data are listed in Table VII. M_n covered a range from 30 000 to 200 000 u and the polydispersity was generally between 1.2–1.3. Mean retention times varied approximately 6 s over this molecular mass range, while peak dispersion increased about 30–40%. As shown in Table VII, several fractions over the molecular mass range were analyzed by ^1H NMR for mean mass percent acetyl. This analysis confirmed that the mean acetyl composition of this cellulose ester did not vary over the molecular mass range. It was concluded from these results that the change in peak dispersion is a reflection of increased "acetyl spread" at lower molecular mass.

Effect of stationary phase pore diameter

A pore diameter study was conducted using a series of Polymer Lab. PLRP-S columns having pore diameters of 10, 30 and 100 nm. These stationary phases were packed into 50 mm × 4. 6 mm columns. The 10 nm pore diameter stationary phase was also evaluated in a 150 mm long column format. Peak variance and retention time were measured for these supports. A cellulose acetate polymer series varying in acetyl composition from 38.3–40.3% acetyl was studied. The results for the chemical composition series is listed in Table VIII. The column temperature for the chemical composition series was 30°C. Butyl octyl phthalate was used as a low-molecular-mass control to determine total system variance under an ideal case.

In Table VIII no significant changes in retention time or peak variance for any of the cellulose diacetate polymers were observed for the pore diameters studied. Even though the total surface

TABLE VII

ANALYTICAL RESULTS FROM CELLULOSE ACETATE POLYMER FRACTIONATED BY GEL PERMEATION CHROMATOGRAPHY

Fraction No.	GPC data			HPLC acetyl data			Acetyl (%, w/w) by ^{1}H NMR
	M_n (u)	M_w (u)	Poly-dispersity	Retention time (min)	Width at 1/2 height (min)	Width at 1/10 height (min)	
4	$1.81 \cdot 10^5$	$2.21 \cdot 10^5$	1.23	8.74	0.751	1.79	–
6	$1.10 \cdot 10^5$	$1.32 \cdot 10^5$	1.20	8.71	0.699	1.44	38.6
8	$7.46 \cdot 10^4$	$9.44 \cdot 10^4$	1.27	8.72	0.813	1.69	–
10	$4.97 \cdot 10^4$	$6.71 \cdot 10^4$	1.35	8.69	1.05	2.02	38.8
12	$3.34 \cdot 10^4$	$4.28 \cdot 10^4$	1.28	8.63	1.22	2.20	–
14	$3.48 \cdot 10^4$	$8.96 \cdot 10^4$	1.35	8.73	1.09	2.37	38.8

area decreased 65% from 410 to 270 m^2/g, no difference in effective surface area was observed for this series of polymers. As expected butyl octyl phthalate, which would be able to penetrate smaller pore diameters and thus accessible to more surface area, showed a greater dependence between retention time and pore diameter.

It has been well reported in the literature that in precipitation liquid chromatography peak efficiency of macromolecules is not dependent upon column length [35]. This theory was tested by comparing the 10 nm pore diameter stationary phase packed in both 5 and 15 cm long columns. The results for these two columns are shown in Table VIII. In all cases the retention time difference between the 15- and 5-cm columns was 1.5 min which at a flow-rate of 0.8 ml/min would correspond to an observed volume for these polymers of 1.2 ml for the last 10 cm of column. The dead volume for the 15-cm column was previously determined to be 1.36 ml for cellulose diacetate using a mobile phase of 100% acetone. Over a length of 10 cm this dead volume would relate to 0.91 ml. Since the dead volume is significantly lower than the observed volume, this would suggest that the polymer is retained even beyond 5 cm.

In Table VIII a significant difference in peak variance was also revealed between the 15 and 5 cm long columns. Column efficiency (N) is both directly dependent upon column length and inversely dependent upon peak variance. In comparing the inverse peak variance for butyl octyl phthalate for the two column lengths, the 15-cm column is three times as efficient as the 5-cm column. This nicely follows fundamental chromatographic theory for a small molecule. For the cellulose acetate polymers the inverse variance difference for the 15-cm column was 1.3–1.7 times as efficient as the 5-cm column. Clearly this increase in efficiency supports an ad-

TABLE VIII

STUDY OF PORE DIAMETER FOR CELLULOSE ACETATE

Sample	Acetyl (%, w/w)	Retention time (min)				Peak variance (s^2)			
		10 nm, 15 cm	10 nm, 5 cm	30 nm, 5 cm	100 nm, 5 cm	10 nm, 15 cm	10 nm, 5 cm	30 nm, 5 cm	100 nm, 5 cm
B	38.3	9.53	7.97	7.82	7.86	980	1360	1310	1380
C	38.8	9.75	8.22	8.06	8.09	890	1200	1220	1270
D	39.3	10.06	8.55	8.41	8.43	790	1140	1120	1220
E	39.9	10.27	8.77	8.61	8.64	820	1200	1130	1140
F	40.3	10.52	9.00	8.85	8.89	670	1140	1090	1070
Butyl octyl phthalate	–	15.83	11.75	11.43	9.30	30	110	110	250

sorption rather than a precipitation retention mechanism. While there is some advantage to a longer column in chromatographing cellulose acetate polymers, the advantage is less than what is observed for smaller solutes.

CONCLUSIONS

A new analytical method for determining the composition of cellulose acetate polymers, that differ in degree of acetate substitution, has been developed. This method is performed on a conventional HPLC instrument under reversed-phase conditions. Chromatographic peak shape and retention time of cellulose acetate samples can be used to distinguish samples of various acetyl substitution and the extent of acetyl spread.

Chromatographic conditions were optimized to selectively separate cellulose acetate as a function of acetyl content. Polymer retention was independent of molecular mass over an M_n range from 33 000 to 180 000. Cellulose acetate was found to elute under adsorption rather than precipitation chromatography conditions. Polymer exclusion was avoided by the judicious choice of the initial mobile phase conditions and injection volume.

Peak width descriptors were found to be useful as a means of quantifying acetyl spread. Acetyl spread is a relative measure of compositional variability since it is inclusive of all contributors to peak variance. Changes in pore diameter over a range from 100 to 1000 Å had little effect upon polymer peak variance. A 15% bias in peak width was observed over a compositional range from 37–40% acetyl. This measurement provided information about cellulose acetate substitution which is more detailed than any other contemporary analysis.

ACKNOWLEDGEMENTS

The author is grateful to Pryor Lambdin and Susan Lindamood for their assistance in this work. The author would also like to thank Dr. Steven A. Wilson for his invaluable suggestions during the early stages of this research.

REFERENCES

1 S. Mori, *Anal. Chem.*, 60 (1988) 1125.
2 G. Glöckner, *Chromatographia*, 23 (1987) 517.
3 M. Augenstein and M. Mueller, *Makromol. Chem.*, 91 (1990) 2151.
4 S. Mori, *J. Liq. Chromatogr.*, 13 (1990) 3039.
5 T. Mourey, *J. Chromatogr.*, 357 (1986) 101.
6 G. Glöckner, J. van den Berg, N. Meijerink, T. Scholte and R. Koningsveld, *Macromolecules*, 17 (1984) 962.
7 M. Danielewicz, M. Kubin and S. Vozka, *J. Appl. Polymer Sci.*, 27 (1982) 3629.
8 S. Mori, *J. Chromatogr.*, 503 (1990) 411.
9 R. Schultz and H. Engelhardt, *Chromatographia*, 29 (1990) 205.
10 A. J. Rosenthal and B. B. White, *Ind. Eng. Chem.*, 44 (1952) 2693.
11 G. Glöckner, D. Wolf and H. Engelhardt, *Chromatographia*, 23 (1991) 107.
12 H. Mark and G. Saito, *Monatsh. Chemie*, 68 (1936) 237.
13 K. Kamide, T. Matsui, K. Okajima and S. Manabe, *Cellulose Chem. Technol.*, 16 (1982) 601.
14 O. Tarakanov and P. Okunev, *Vysokomol. Soedin.*, 4 (1962) 683.
15 P. Okunev and O. Tarakanov, *Khim. Volokna*, 6 (1963) 44.
16 L. Tung, *Fractionation of Synthetic Polymers*, Marcel Dekker, New York, 1977.
17 T. Nevell and S. Zeronian, *Cellulose Chemistry and Its Applications*, Wiley, New York, 1985.
18 K. Kamide, Y. Miyazaki and T. Abe, *Br. Polym. J.*, 13 (1981) 168.
19 J. G. McNally and A. P. Godbout, *J. Am. Chem. Soc.*, 51 (1929) 3095.
20 E. Mardles, *J. Chem. Soc.*, 123 (1923) 1951.
21 A. M. Sookne, H. A. Rutherford, N. Mark and M. Harris, *J. Res. Natl. Bur. Standards*, 29 (1942) 123.
22 A. M. Sookne and M. Harris, *Ind. Eng. Chem.*, 37 (1945) 475.
23 D. R. Morey and J. W. Tamblyn, *J. Appl. Phys.*, 16 (1945) 419.
24 F. Howlett and A. Urquhart, *J. Textile Inst.*, 37 (1946) T89.
25 J. Cowie and R. Ranson, *Makromol. Chem.*, 143 (1971) 105.
26 J. Cowie, A. Macconnachie and R. Ranson, *Macromolecules*, 4 (1971) 57.
27 K. Kamide, S. Manabe and E. Osafune, *Makromol. Chem.*, 168 (1973) 173.
28 *Annual Book of ASTM Standards, Section 6.02, Standard Methods of Testing Cellulose Acetate*, American Society for Testing and Materials, Philadelphia, PA, 1991, ASTM methods D871–872, pp. 162–172.
29 C. Buchanan, J. Hyatt and D. Lowman, *Carbohydrate Res.*, 177 (1988) 228.
30 G. Glöckner, *Polymer Characterization by Liquid Chromatography (Journal of Chromatography Library*, Vol. 34), Elsevier, Amsterdam, 1987.
31 G. Guiochon, A. Moysan and C. Holley, *J. Liq. Chromatogr.*, 11 (1988) 2547.
32 C. Lochmüller and M. McGranaghan, *Anal. Chem.*, 61 (1989) 2449.
33 J. Foley and J. Dorsey, *Anal. Chem.*, 55 (1983) 730.
34 J. Foley, *Anal. Chem.*, 59 (1987) 1984.
35 K. Bui, D. Armstrong and R. Boehm, *J. Chromatogr.*, 295 (1984) 15.

Journal of Chromatography, 629 (1993) 255–266
Elsevier Science Publishers B.V., Amsterdam

CHROM. 24 645

Method for the determination of indole-3-acetic acid and related compounds of L-tryptophan catabolism in soils

Michael Lebuhn and Anton Hartmann

GSF–Forschungszentrum für Umwelt und Gesundheit GmbH, Institut für Bodenökologie, Ingolstädter Landstrasse 1, W-8042 Neuherberg (Germany)

(First received July 16th, 1992; revised manuscript received September 25th, 1992)

ABSTRACT

An optimized method for the determination of substances occurring in auxin metabolism and L-tryptophan (TRP) catabolism was developed. It is based on solid-phase extraction (SPE), two isocratic reversed-phase high-performance liquid chromatographic (HPLC) separations at different liquid phase conditions and the simultaneous detection of fluorescence and UV absorbance at different wavelengths. Advantages of the proposed method are: the solvent (ethanol) and liquid phase (containing 2-propanol) provide optimum stability and selectivity; almost no toxic wastes are produced; no time-consuming liquid–liquid extractions (LLE), derivatization procedures or column re-equilibration (obligatory for gradient systems) are necessary, no need for antioxidants, ion-pair or derivatization reagents; recovery rates of the SPE system are superior to LLE efficiencies; high sensitivity, selectivity and identification capacity are provided by the proposed HPLC and detection system. By measuring various chromatographic and spectral parameters simultaneously, the determination reliability is improved. The characteristic chromatographic and spectral data for selected indole derivatives and TRP catabolites are presented. In samples from two different soils that were tested with the proposed method, the actual contents of TRP were 1.4 and 5.8 μg/g dry soil. In addition, traces of indole-3-acetic acid (IAA) could be detected. When TRP was added, IAA was the predominant catabolite in both soils, and reached values of 2.9 and 8.0 μg/g dry soil. In addition to IAA, indole-3-ethanol, indole-3-aldehyde, indole-3-carboxylic acid, indole-3-lactic acid, anthranilic acid and traces of indole-3-acetamide were identified and determined.

INTRODUCTION

Indole-3-acetic acid (IAA) and other indole derivatives with auxin-like phytohormone activity are synthesized by plants and many soil microorganisms. Originating from the central auxin precursor L-tryptophan (TRP), different pathways of microbial auxin biosynthesis have been described: the tryptamine (TAM) [1,2], the indole-3-pyruvic acid (IPA) [1–3], the indole-3-acetamide (IAM) [1,2,4] and the tryptophan side-chain oxidase (TSO) [5] pathways. Many plant growth promoting rhizobacteria [3,5–9] seem to catabolize TRP via the IPA pathway. The occurrence of indole-3-lactic acid (ILA), a side product of the unstable intermediate IPA, points to the IPA pathway of IAA biosynthesis. IAM, the characteristic intermediate of the IAM pathway, has been detected in several plant pathogens [4,10–12].

Enzymatic IAA catabolism and autoxidative auxin degradation can result in many different products [2,13]. Indole-3-methanol (IM), indole-3-aldehyde (IAld) and indole-3-carboxylic acid (ICA), products of decarboxylative IAA degradation by "IAA oxidase" catalysis, have often been detected [2,7,13].

In addition to auxin biosynthesis, TRP can be catabolized via the "aromatic pathway" [14] with anthranilic acid (AnthrA) as an intermediate.

Although many soil microorganisms have been tested for IAA biosynthesis, very few reports have dealt with auxin metabolism in soil. Actual auxin

Correspondence to: M. Lebuhn, GSF–Forschungszentrum für Umwelt und Gesundheit GmbH, Institut für Bodenökologie, Ingolstädter Landstrasse 1, W-8042 Neuherberg, Germany.

0021-9673/93/$06.00

contents seem to be very low in soil, but microbial auxin production is greatly enhanced by adding TRP (potential for auxin biosynthesis) [1].

The preparation of samples containing different indole derivatives is usually performed by partition techniques that require several liquid–liquid extraction (LLE) steps [1,2,15–17]. LLE methods, however, are very time consuming, and produce considerable amounts of toxic organic wastes. Compared with LLE procedures, solid-phase extraction (SPE) provides several advantages: SPE produces less toxic organic waste, is less time consuming and can be applied easily to routine assays. For the purification and concentration of several plant hormones, Amberlite SPE resins have already been used successfully and provided excellent recoveries [18,19].

Immunoassays (*e.g.*, enzyme-linked immunosorbent assay, radioimmunoassay) [2] with highly specific antibodies provide the most sensitive methods to measure single phytohormones. However, if an unknown spectrum of various phytohormone derivatives in a sample is to be analysed, immunological methods cannot be applied. Derivatization procedures that focus on selected targets [16,17] are also of no use.

For the separation of several phytohormones and their derivatives, reversed-phase high-performance liquid chromatography (RP-HPLC) is a practical method [2,13]. The chromatographic process can be influenced by ion-pair reagents. Ion-pair RP-HPLC with gradient elution has been employed to determine the potency for auxin biosynthesis in TRP-spiked soil samples [1]. Many ion-pair reagents, however, are expensive and toxic. Additionally, as the chromatographic behaviour of standard, investigated and unknown substances is modified at the same time, ion-pair reagents can impede identification and quantification. Therefore, chromatography should be performed with the original substances, as far as possible.

Most of the proposed HPLC methods for the separation of indole derivatives use gradient systems and a mixture of methanol, water and acetic acid as the mobile phase [1,7–9]. Gradient elution, however, requires time- and solvent-consuming column re-equilibration after each run. This can be avoided by an optimized isocratic system and present advantages for routine analyses. According to our results, methanol neither provides optimum selectivity as an organic modifier in RP-HPLC for indole derivatives, nor prevents unstable indoles (*e.g.*, IPA) from autoxidative breakdown.

To reduce the breakdown of indole derivatives, the use of antioxidants has been proposed [2,13]. In our experience, they give rise to interfering peaks when they are present in the sample. As components of the liquid phase, they cause a high background noise.

Fluorescence monitors can detect as little as 1 pg of IAA, whereas UV absorbance monitors are less sensitive, with detection limits in the low nanogram range [2]. Concerning sensitivity and specificity, both are superior to spectrophotometric methods [15] and biotests used for auxin determination. In spite of its lower sensitivity, UV absorbance monitoring is necessary in addition to fluorimetry because some important indoles, such as IAld, IPA, indole-3-acetaldehyde (IAAld), indole-3-acrylic acid (IAcrA) and indole-3-glyoxylic acid (IGA), show no fluorescence [2]. The combination of a fluorimeter and a UV absorbance monitor has been used to determine indole derivatives excreted by bacteria [9].

An improved alternative system for the extraction, separation and simultaneous determination of different indole derivatives was still needed. We developed a simple, reliable, highly specific and sensitive routine method for the simultaneous determination of characteristic substances occurring in the different proposed pathways of TRP catabolism, auxin biosynthesis and IAA catabolism. This method combines the advantages of SPE, isocratic RP-HPLC, UV absorbance and fluorimetry. It was optimized to prevent indole derivatives from decomposing and to provide a high resolving power. The method was tested with soil samples, but it can also be applied to microorganisms. We determined actual concentrations of TRP and TRP catabolites and the potency for auxin biosynthesis and TRP catabolism in two different fallow agricultural fields.

EXPERIMENTAL

Chemicals and materials

As standard substances we tested L-tryptophan (TRP), 5-OH-tryptophan (5-OH-TRP), indole-3-acetic acid (IAA), indole-3-acetamide (IAM), in-

dole-3-pyruvic acid (IPA), indole-3-lactic acid (ILA), indole-3-ethanol (TOL, tryptophol), tryptamine (TAM), 5-OH-tryptamine (5-OH-TAM, serotonine), indole-3-glyoxylic acid (IGA), indole-3-acrylic acid (IAcrA), indole-3-butyric acid (IBA), indole-3-propionic acid (IPropA), indole-3-aldehyde (IAld), indole-3-acetaldehyde (hydrogensulphite compound, IAAld), indole-3-carboxylic acid (ICA), indole-3-methanol (IM), anthranilic acid (AnthrA), 3-OH-anthranilic acid (3-OH-AnthrA), kynurenine (Kynur), 3-OH-kynurenine (3-OH-Kynur), kynurenic acid (KynurA), phenylalanine (PAla), phenylacetic acid (PAA), phenyllactic acid (PLA), phenylacetamide (PAM), phenylpyruvic acid (PPA) and phenylethanol (POL). These compounds and sodium diethyldithiocarbamic acid (all of analytical-reagent grade) were purchased from Sigma.

The remaining chemicals (all of analytical-reagent grade), 2-propanol and ethanol (both of HPLC grade) were obtained from Merck or Sigma. Standard buffers (pH 2.00, 4.005 and 6.865) came from Ingold Messtechnik (Steinbach, Germany), and pH 523 pH meter and E 56 electrode from WTW (Weilheim, Germany).

Water for HPLC purposes and reference standard solutions was distilled twice. Contact of hot doubly distilled water with plastic materials was avoided.

Preparation of soil samples and extraction of indole derivatives and other TRP catabolites

Soil samples were taken early in March from the A_p horizons (5–20 cm) of two fallow agricultural wheat fields (Scheyern, Bavaria, Germany, sandy loam, water content 23%, total carbon 1.23%, total nitrogen 0.12%, $n = 3$, and Neumarkt, Bavaria, Germany, loamy sand, water content 13%, total carbon 0.78%, total nitrogen 0.07%, $n = 3$).

To determine the potency for auxin biosynthesis and TRP catabolism in soils, we modified the method of Frankenberger and Brunner [1] to incubate soil samples for 24 h with TRP. The actual contents of TRP and TRP catabolites were determined without TRP addition.

The sieved (<2 mm) soils were adjusted to 50% of the maximum water-holding capacity and equilibrated for at least 3 days at 22°C. A 3-g amount of equilibrated soil was incubated with 10 mg of TRP [dissolved freshly in 1 ml of a 0.1 *M* NaH_2PO_4–Na_2HPO_4 buffer (pH 7.0)] in 50-ml polypropylene centrifugation vials (Falcon 2070; Becton Dickinson, Heidelberg, Germany). The soil aggregates were stirred well and disrupted by ultrasonication for 20 s (Sonorex RK 100 ultrasonication bath , HF power 80/160 W; Bandelin, Berlin, Germany). This allows the endogenous microflora to effect a better contact with the applied TRP. Control experiments showed that this ultrasonication treatment slightly enhanced TRP catabolism.

After incubation for 24 h at 22°C in the dark, the soil samples were suspended in 4 ml of phosphate buffer (pH 7.0), stirred well and sonicated for 1 min. Ultrasonication after the incubation caused a higher extraction efficiency. This is probably due to a better desorption from clay, humic substances and other organic material.

The soil suspension was centrifuged in a swing-out rotor for 30 min at 5800 *g* (Heraeus Sepatech Omnifuge 2.0 RS, Model 3360 rotor). The supernatant was carefully removed and filtered (SM 16315 filtration equipment and 11106-25-N cellulose acetate filters, pore size 0.45 μm, from Sartorius). The pellet surfaces and filtration equipment were washed twice with 1 ml of phosphate buffer (pH 7.0).

The filtrate (including the filtered washing solutions) was adjusted to pH 2.0–2.5 with H_3PO_4 to protonate and enhance the lipophilicity of carboxyl groups. This solution was applied under partial vacuum to SPE columns (fixed on a Supelco Visiprep SPE 50730 vacuum manifold) prefilled with Amberlite XAD-2 (Bio-Rad SM2 Bio-Beads 731-6315, 200–400 mesh). The SPE columns had been equilibrated for at least 1 h with 0.1 *M* NaH_2PO_4–Na_2HPO_4 buffer, adjusted to pH 2.25 with H_3PO_4. The filtrate glass vial was washed twice with 1 ml of phosphate buffer (pH 2.25) and the washing solution was passed through the SPE columns. Until the elution step, the columns were not allowed to run dry.

For the solvent exchange, the columns were run dry under partial vacuum. The adsorbed purified TRP catabolites were eluted with 5 ml of ethanol and measured immediately or stored at −30°C in the dark.

Instead of the phosphate buffers (pH 7.0 and 2.25), 0.1 *M* Tris–HCl buffers (adjusted to the same pH values) can be used.

Determination of indole derivatives and TRP catabolites

For HPLC, a 5-μm Hyperchrome Spherisorb ODS II C_{18} column (250 × 4 mm I.D.) with a 20 mm precolumn, obtained from Bischoff Chromatography (Leonberg, Germany), was used. Two reversed-phase separations with different mobile phases were carried out for every sample. The first separation was performed with 2-propanol–doubly distilled water (13:87), with 1.80 m*M* citrate added, pH 4.20–4.30 adjusted with 32% NaOH, and the second with 2-propanol–doubly distilled water (14:86), containing 5.0 m*M* NaH_2PO_4, pH 2.15–2.35 adjusted with 85% H_3PO_4. The mobile phases were degassed under partial vacuum by ultrasonication for 5 min.

Volumes of 20 μl of the ethanolic SPE eluates were injected under isocratic [1.1 ml/min, Model 300 B high-precision pump from Gynkotek (Germering, Germany)] and isothermal conditions (22°C).

The UV absorption at 233 (or 280) nm and 316 nm and fluorescence emission at 360 (408) nm after excitation at 280 (340) nm were measured with a Pharmacia-LKB VWM 2141 variable-wavelength monitor and a Shimadzu RF-535 fluorescence monitor simultaneously by connecting the monitors in series. Data were processed with a Merck Hitachi D-2500 chromato-integrator (with two-channel option) and a Hewlett-Packard 3390A integrator.

For the calculation of actual contents of TRP and TRP catabolites and the potency for auxin biosynthesis in a soil, the data from the soil samples were corrected for the non-extractable part of the respective references. A defined mixture of indole derivatives and TRP catabolites was incubated for 11 min with the tested soil and stirred well. Sonication, extraction and determination were carried out as described above for the soil samples. The concentrations of the reference substances were about 50% higher than those present in the soil extract after the incubation with TRP. The extracted references represented the extractable part of the indole derivatives and TRP catabolites which were produced in the tested soil. The data for the soil samples were determined relative to these references.

For the determination of the potential for microbial auxin biosynthesis, the results from the TRP-spiked soil samples had to be corrected for the products that resulted from the autoxidation of TRP. The peak integrals of the extractable TRP breakdown products that were formed during 24 h of incubation of TRP in sterile filtered phosphate buffer (pH 7.0) (Sartorius Minisart NML sterile filtration equipment, SM 16534, pore size 0.2 μm) were determined as described above for the extractable references. The peak areas that resulted from TRP autoxidation were taken as the background for the microbial TRP catabolism in the soil samples.

A scheme of the important experimental steps for the determination of auxin biosynthesis and TRP catabolism in soils is presented in Fig. 1.

Heating the TRP, contamination of sterile TRP and sterile soil with microorganisms and exposure of indole derivatives to daylight were avoided. Samples containing indole derivatives must not come into contact with polystyrene.

RESULTS

Stability of the indole derivatives in different solvents

Different aqueous buffers, methanol, ethanol, 1-propanol, 2-propanol, butanol, acetonitrile and ethyl acetate were tested as solvents. Every tested indole derivative and TRP catabolite could be dissolved only in aqueous solutions, methanol and ethanol. Ethanol showed remarkable antioxidative effects.

When dissolved in aqueous solutions, indole-3-pyruvic acid (IPA) decomposed spontaneously. Different peaks with shifting UV absorbance maxima, depending on the pH and age of the sample, were observed. IAA and IAld were always present as breakdown products. In contrast, IPA was stable in ethanol and in the mobile phase at pH values below 2.75. Indole-3-methanol (IM) did not break down in ethanol and in the mobile phase at pH values higher than pH 4.0. Because of its rapid autoxidation, IAAld could only be determined as the hydrogensulphite adduct in the presence of excess of antioxidant ($Na_2S_2O_5$) in the liquid phase at low pH values when it was dissolved in ethanol. Samples of the standard compounds dissolved in ethanol could be stored as liquids at −30°C in the dark for more than 6 months without obvious degradation.

We tested $Na_2S_2O_5$, sodium diethyldithiocar-

SOIL SAMPLE (sieved < 2 mm, 3 g wet weight);

INCUBATION without and with **TRP**
(10 mg / ml 0.1 M phosphate buffer, pH 7.0)
24 h at 22°C in the dark, after 20 s ultrasonication;

suspend samples in phosphate buffer, pH 7.0,
1 min ultrasonication;

CENTRIFUGATION 30 min at 5800 g,
FILTRATION of the supernatant (0.45 μm),
adjust filtrate to **pH 2.0 - 2.5** with H_3PO_4;

SOLID PHASE EXTRACTION (Amberlite XAD-2, elution with **ethanol**);

ISOCRATIC REVERSED-PHASE HPLC
1) pH 4.2 - 4.3,
2) COO -suppressive conditions (pH 2.15 - 3.50);

DETECTION (simultaneous)
1) Fluorescence 280/360 nm (340/408 nm),
2) UV absorbance 233 or 280 nm, and 316 nm (340 nm);

Fig. 1. Scheme for the determination of auxin biosynthesis and TRP catabolism in soils.

bamic acid and 2,6-di-*tert.*-butyl-4-methylphenol as antioxidants. They had no significant preventive effect on the breakdown of IPA at high and of IM at low pH values of the mobile phase during HPLC, when IPA and IM had been dissolved in ethanol. However, the antioxidants impeded the chromatography. When present in the sample, they gave rise to peaks (partially negative). Being part of the mobile phase, the antioxidants modified the chromatographic conditions by enhancing the ionic strength and caused an increased background noise. Therefore, their use was avoided.

If IPA, IAAld or IM was to be determined, the composition of the solvent and the pH of the mobile phase have to be considered. For the detection of IAAld, excess of $Na_2S_2O_5$ should be present in each experimental step.

HPLC separation conditions

The best separations were obtained with 2-propanol–water as mobile phase and the Hyperchrome column. With a 5-μm LiChrospher 60 RP-select B column (250 × 4 mm I.D.) from Merck, the results were not as good as with the Hyperchrome column

(data not shown). We carried out two isocratic HPLC runs under different mobile phase conditions using the fact that the investigated compounds reacted differently in their chromatographic behaviour to changes in pH and ionic strength of the mobile phase (see Table I and Figs. 2 and 3). To ensure the identity of the sample peaks, their spectral properties and their chromatographic behaviour were compared with those of the mixed standard substances under both chromatographic conditions.

The first run was performed at pH 4.23 (adjusted with NaOH) of the mobile phase 2-propanol–water (13:87), with 1.80 m*M* citrate added, which provided the best separation conditions. The second run was carried out at a lower pH of the mobile phase [*e.g.*, 2-propanol–water (14:86) containing 5.0 m*M* NaH_2PO_4, pH 2.31 adjusted with H_3PO_4]. Ionic strength and pH were chosen specifically to resolve remaining doubts on peak identities and to verify the results from the first run.

The higher H^+ concentration in the second mobile phase changed the retention times by suppressing carboxyl ions and by enhancing the ionic character of amino groups. Compounds with a carboxyl group became more lipophilic, and were retarded by the reversed-phase column. Substances with an amino group became more ionic and were eluted faster by the hydrophilic liquid phase (Table I, Figs. 2 and 3). The retention times of amino compounds became shorter on raising the ionic strength in the mobile phase. A higher concentration of 2-propanol accelerated the passage of all the tested substances, with slight differences according to their lipophilicity (data not shown). For reproducible results, the pH and ionic strength of the mobile phase must be adjusted precisely because several compounds react very sensitively to these parameters.

TABLE I

SPECTRAL AND CHROMATOGRAPHIC CHARACTERISTICS OF TRP CATABOLITES AND INDOLE DERIVATIVES

Symbols: +, strong; (+), weak; and −, no fluorescence or UV absorbance. The compositions of the pH 4.23 and pH 2.31 mobile phases are described in under *HPLC separation conditions*.

Substance	Fluorescence (excitation/emission)		UV absorbance		Retention time (min) in the mobile phase at	
	280/360 nm	340/408 nm	280 nm	316 nm	pH 4.23	pH 2.31
Kynurenic acid	−	+	(+)	+	2.10	4.54 (slight decomposition)
3-Hydroxykynurenine	−	−	(+)	+	2.65	2.61
Kynurenine	−	−	(+)	+	2.75	2.90
5-Hydroxytryptophan	+	−	+	−	2.80	2.88
Indole-3-glyoxylic acid	−	−	+	+	2.80	8.82
L-Tryptophan	+	−	+	−	3.50	4.31
3-Hydroxyanthranilic acid	−	+	(+)	+	3.96	3.48
Indole-3-lactic acid	+	−	+	−	5.35	9.27
Indole-3-acetamide	+	−	+	−	6.96	6.60
5-Hydroxytryptamine	+	−	+	−	7.26	2.61
Indole-3-methanol	+	−	+	−	7.93	Decomposition
Anthranilic acid	−	+	(+)	+	8.50	5.71
Indole-3-acetic acid	+	−	+	−	12.80	13.92
Indole-3-ethanol	+	−	+	−	16.16	13.92
Indole-3-aldehyde	−	−	+	+	18.70	16.35
Indole-3-carboxylic acid	(+)	−	+	−	18.84	16.59
Tryptamine	+	−	+	−	23.06	5.16
Indole-3-puruvic acid	−	−	+	+	Decomposition	40.59
Indole-3-propionic aicd	+	−	+	−	27.34	29.03
Indole-3-acrylic acid	−	−	+	+	45.50	46.16
Indole-3-butyric acid	+	−	+	−	55.51	53.32

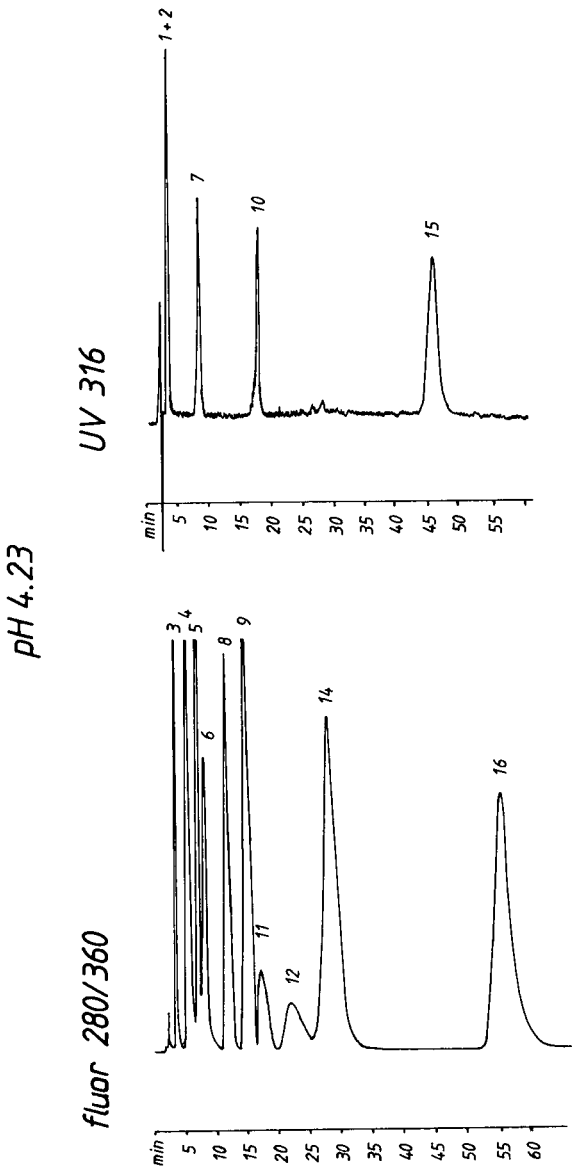

Fig. 2. Chromatogram of sixteen indole derivatives and TRP catabolites with the pH 4.23 mobile phase (for composition see *HPLC separation conditions*). Fluorescence was measured at 280 nm excitation and 360 nm emission (fluor 280/360) and UV absorbance at 316 nm (UV 316). Peaks: 1 = kynurenine; 2 = indole-3-glyoxylic acid; 3 = L-tryptophan; 4 = indole-3-lactic acid; 5 = indole-3-acetamide; 6 = indole-3-methanol; 7 = anthranilic acid; 8 = indole-3-acetic acid; 9 = indole-3-ethanol; 10 = indole-3-aldehyde; 11 = indole-3-carboxylic acid; 12 = tryptamine; 13 = indole-3-pyruvic acid; 14 = indole-3-propionic acid; 15 = indole-3-acrylic acid; 16 = indole-3-butyric acid.

Spectral characteristics and chromatographic behaviour of the indole derivatives and TRP catabolites

In spite of the much higher sensitivity of fluorescence detection, UV absorbance monitoring of two wavelengths was necessary, because several compounds showed no or only weak fluorescence and differed in their UV absorbance spectra. Table I summarizes the spectral characteristics and the retention times in the mobile phase of pH 4.23 and 2.31 which are relevant for the determination of the indole derivatives and TRP catabolites.

Figs. 2 and 3 show typical chromatograms of sixteen selected standard substances of indole derivatives and TRP catabolites which may be important

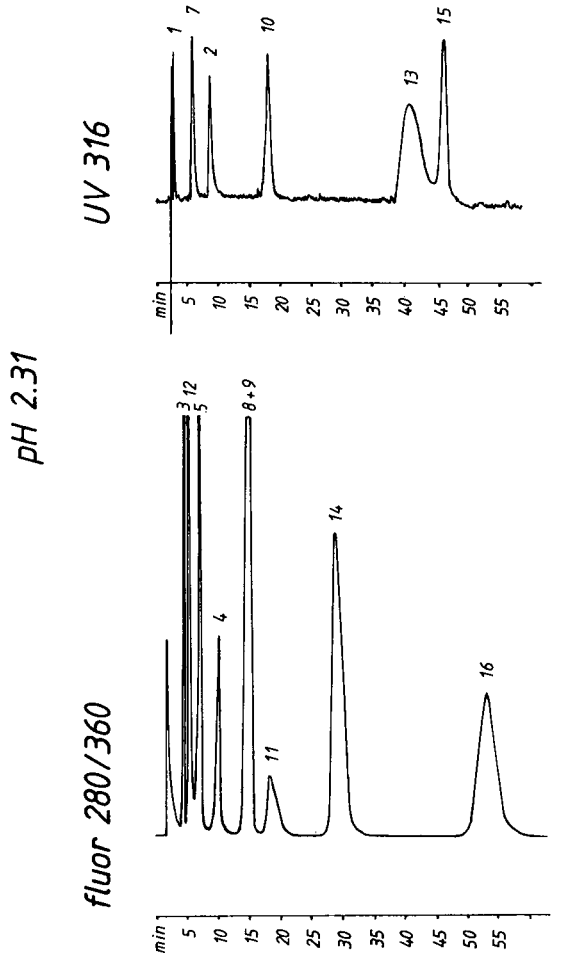

Fig. 3. As Fig. 2 with the pH 2.31 mobile phase. Peak numbers as in Fig. 2.

in the microbial turnover of TRP and auxin metabolism.

IAld and ICA co-chromatographed at all the chosen pH values. Their relative contributions to the total peak area at 233 (or 280) nm could be calculated, because IAld absorbs at 233, 280 and 316 nm and ICA absorbs at 233 and 280 nm but not at 316 nm (Table I, Figs. 2 and 3). Therefore, the factor IAld peak area at 316 nm divided by IAld peak area at 233 (or 280) nm was measured with an IAld standard sample. This allowed the ICA to be determined by difference calculation: IAld peak area measured at 316 nm × factor 1.26 resulted in the calculated IAld peak area at 233 nm. The difference between the total IAld plus ICA peak area measured at 233 nm and the calculated IAld peak area at 233 nm represented the ICA peak area at 233 nm. This calculation was supported by the data from the fluorescence determination of ICA. Similar calculations can be applied to other co-eluted substances, if they differ in their spectral properties. The spontaneous decomposition of IPA in the pH 4.23 mobile phase gave rise to IAA and two further peaks. The minor peak eluted at 12.7 min, and the major peak at 18.7 min. Both substances absorbed 316-nm UV radiation and were not fluorescent. The second peak represented IAld. The identity of the first peak could not be confirmed. IPA could be determined without decomposition at mobile phase pH values below 2.75. IM, which is unstable at pH values below 4.0, was completely destroyed in the pH 2.31 mobile phase and could not be detected.

Using the proposed combined chromatographic and spectral approach, it was possible to identify and determine simultaneously each tested compound of TRP catabolism. The identifications were confirmed by additional spiking experiments.

Recoveries provided by solid-phase extraction (SPE)

For the determination of the SPE efficiency, a mixture of standard compounds was dissolved in the incubation media used for soils [0.1 *M* phosphate buffer (pH 7.0) and 0.1 *M* Tris–HCl (pH 7.0)]. The concentrations of the references were in the range of the concentrations of the respective TRP catabolites which were detected in the experiments with soil. Titration to pH 2.25 and extraction of the standard substances at pH 2.25 were carried out as described for soil samples.

The highest recoveries were obtained with Amberlite XAD-2 (Bio-Rad SM2 Bio-Beads 731-6315, 200–400 mesh). They were higher than 90% (TAM and IAld 85%) for each tested standard compound. Compared with the LLE efficiencies [2] of indole derivatives, SPE with Amberlite XAD-2 provided better recoveries (data not shown). Particularly the aminoindoles TRP and TAM were recovered by XAD-2 with much higher efficiencies. C_{18} columns (Supelcoclean LC18 SPE columns 5-7012) yielded comparable results for carboxylic indoles, but they were less efficient for indoles with an amino group (TRP 90% and TAM only 40%). The recoveries with Amberlite XAD-7 material (SM7 Bio-Beads 731-6335, 200–400 mesh) were generally about 5–10% lower than those obtained with XAD-2. Amberlite XAD-4 (SM4 Bio-Beads 731-6244, 100–200 mesh), a more lipophilic resin, retained the aminoindoles only very poorly.

If IPA was present in aqueous samples at pH 7.0, only the breakdown products could be extracted and determined. IM decayed when the sample was acidified to pH 2.2–2.3. Therefore, the acidification step must be omitted if the presence of IM is to be investigated. Without the acidification, however, the SM2 SPE recovery rates were generally about 5–15% less than at pH 2.25. For our purposes, IM was not an important substance, being an intermediate in IAA oxidation [2,13]. As it left no interfering decay products, IM was disregarded.

The SPE recoveries with 0.1 *M* Tris–HCl (pH 7.0 and 2.25) were the same as with the respective 0.1 *M* phosphate buffers.

Binding of indole derivatives and other TRP catabolites to soil constituents

For the determination of the binding capacity of soils to indole derivatives and TRP catabolites, we added one part of a mixture of standard substances to soil and left the other without soil contact. After SPE extraction and HPLC, the peak areas were compared. The results are summarized in Table II.

The individual reference compounds were bound to soil constituents to different extents. Some of them could be extracted only partially. The losses due to adsorption to soil were generally greater in the soil from Scheyern (Table II). The total C and total N contents were higher in the sandy loam from Scheyern than in the loamy sand from Neumarkt

TABLE II

BINDING OF INDOLE DERIVATIVES AND TRP CATABOLITES TO DIFFERENT SOILS

Soil	Mean recoveries (n = 2) of indole derivatives and TRP catabolites (%)								
	TRP	ILA	IAM	IAA	TOL	IAld	ICA	TAM	AnthrA
Neumarkt	82.0	83.5	80.4	84.2	76.1	57.0	85.8	51.0	90.4
Scheyern	64.9	71.1	60.2	63.9	38.9	44.1	92.3	33.5	91.3

(see Experimental). This suggested that the non-extractable amount of the standard substances depended on soil structure and composition, probably mainly on the content of organic material. Compared with substances with a carboxyl group (*e.g.*, IAA, ICA, AnthrA and ILA), more lipophilic compounds (*e.g.*, TAM, TOL, and IAld) were adsorbed very efficiently, and could hardly be extracted from soil (Table II).

The capacity of the tested soils to bind indole derivatives and other TRP catabolites was checked separately in each soil experiment, obtaining the extractable and non-extractable fractions. The actual contents of TRP and TRP catabolites and the potential for TRP catabolism and auxin biosynthesis were calculated by correcting the data from the soil samples for the losses due to soil contact.

Autoxidation of TRP in aqueous solutions

Sterile aqueous solutions of TRP (Sartorius minisart NML sterile filtration equipment, SM 16534, pore size 0.2 μm), showed autoxidation. The pattern of the breakdown products depended on the incubation conditions and their amount increased with increasing incubation time.

In 24 h of incubation at 22°C in the dark, the breakdown of 10 mg of TRP, dissolved in phosphate buffer (pH 7.0) created 0.12 ± 0.03 μg of IAA, 0.10 ± 0.05 μg of TOL and traces of ILA. In addition, two substances were detected. In the pH 4.23 mobile phase, the first was strongly fluorescent and co-eluted with ILA at 5.35 min. The second was weakly fluorescent and eluted separately between ILA and IAM at 6.1 min. Spectrally, neither was different from ILA and IAM. At pH 2.31 of the mobile phase, the unknown substances eluted well separated prior to ILA. After exposure of the TRP decay products for 1 min to soil (as described above for the standard substances), only traces of IAA and TOL could be extracted, but the peak eluting at 5.35 min in the pH 4.23 mobile phase was still strong. Therefore, authentic ILA in TRP-treated samples was determined at liquid phase pH values below pH 2.75.

The peak areas that were due to TRP autoxidation were corrected for the losses due to binding to soil as described above, obtaining the extractable and non-extractable peak areas of TRP autoxidation. These corrected peak areas were taken as the background for the enzymatic TRP degradation by subtracting them from the areas of the corresponding soil sample peaks.

Determination of indole derivatives and TRP catabolites extracted from TRP-treated soil samples (potency for auxin biosynthesis) and actual contents of TRP and TRP catabolites

In the soils that were not treated with TRP, TRP was predominant. The actual TRP contents (corrected for the loss due to binding to soil) were 5.8 ± 0.2 μg/g dry soil from Scheyern and 1.4 ± 0.3 μg/g dry soil from Neumarkt. Without TRP addition, only traces of IAA could be detected in both soils.

Table III shows the potential for auxin biosynthesis and TRP catabolism in the soil samples from Neumarkt and Scheyern. The data were corrected for the non-extractable contents due to binding to soil constituents and for the amount of TRP autoxidation. They represent the total microbial substrate-induced biosynthesis.

The identification of the detected peaks was confirmed as described by performing two HPLC runs

TABLE III

POTENTIAL FOR AUXIN BIOSYNTHESIS AND TRP CATABOLISM IN DIFFERENT SOILS

Compound	Concentration (μg/g)[a]	
	Scheyern soil	Neumarkt soil
Indole-3-lactic acid	1.8 ± 0.5	1.0 ± 0.4
Indole-3-acetamide	0	Traces
Indole-3-acetic acid	8.0 ± 1.1	2.9 ± 0.2
Indole-3-ethanol	1.0 ± 0.4	Traces
Indole-3-aldehyde	1.3 ± 0.3	1.2 ± 0.4
Indole-3-carboxylic acid	2.4 ± 0.6	2.8 ± 0.3
Anthranilic acid	1.4 ± 0.2	1.7 ± 0.1

[a] Data are expressed in μg / g dry soil ± S.D. (n = 3) after 24 h of incubation with 10 mg of TRP per 3 g of fresh soil at 22°C.

at different mobile phase pH velues and by spiking the soil samples with the corresponding standard substances.

Both soils were autoclaved and/or irradiated (22 h at 35.1 Gy) and spiked with sterile TRP. No TRP conversion apart from TRP autoxidation could be monitored after 24 h of incubation. Without TRP addition, however, the actual contents of TRP were enhanced in the sterilized soils, indicating lysis of the endogenous microflora (data not presented).

DISCUSSION

The proposed method of SPE, isocratic HPLC separation and detection by combined fluorescence spectrometry and UV absorbance was developed for the simultaneous determination of the different indole auxins and related derivatives, central intermediates and side products of their different biosynthetic pathways [1–5,13], characteristic IAA catabolites [2,7,13] and TRP catabolites of the "aromatic pathway" [14]. It was tested with a mixture of the standard compounds and with samples from two different agricultural soils.

Two different mobile phase conditions in the HPLC separation were used in order to confirm the results that were obtained from the simultaneous measurements of UV absorbance and fluorescence emission at different characteristic wavelengths. The best separation conditions existed at pH 4.2–4.3 of the mobile phase. For the second run, pH values below 2.75 (COO^--suppressive conditions) were chosen which changed the retention times (see Results).

According to their different UV absorbance spectra and fluorescence properties, the investigated substances were simultaneously detected by their UV absorbance at 233 (280) and 316 nm, and their fluorescence at 360 (408) nm, with UV excitation at 280 (340) nm. In spite of its lower sensitivity, UV absorbance monitoring was necessary because several compounds showed no fluorescence (Table I, Figs. 2 and 3).

Compared with other proposed HPLC-based auxin determination systems [1,2,7–9,13], this combined chromatographic and spectral approach offers several advantages. Being isocratic, no time consuming column re-equilibration (necessary with gradient systems) was needed. Ethanol was used as the sample solvent and small amounts of 2-propanol as modifier of the mobile phase. They provided stability of the tested compounds and high selectivity and helped to minimize the organic wastes. No reduction reagents were needed. The use of ion-pair reagents and derivatization procedures could be avoided. For the determination, various chromatographic and spectral parameters were tested (Table I, Figs. 2 and 3). The simultaneous detection of fluorescence and UV absorbance at different wavelengths combined high sensitivity with high detection capacity. The highest recoveries were obtained with the described SPE system (using columns with prefilled Amberlite XAD-2). In addition, SPE was less time consuming than LLE procedures, and helped to reduce the production of toxic solvent wastes.

The reference compounds IPA and IAAld decomposed spontaneously in aqueous solvents. Only the decay products could be extracted. Therefore, IPA and IAAld probably cannot be detected in aerobic soil ecosystems and aqueous suspensions of microorganisms as free substances. Nevertheless, they can be important as intermediates in the auxin metabolism of living cells. If IPA, IAAld and IM are to be determined, special conditions (see Results) have to be chosen.

Standards of indole derivatives and TRP catabolites added to soil samples were bound by soil con-

stituents to individually different extents, and remained non-extractable (Table II). The losses seemed to depend mainly on the content of organic material in the soil and on the lipophilicity of the introduced compounds. The TRP catabolism in the soil samples was corrected for these losses.

TRP autoxidized to several substances including IAA in aqueous solvents. The peak areas of the decay products which were created during the incubation of soil samples with TRP were determined, and taken as the background for the microbial TRP catabolism. The main breakdown product of TRP could not be identified. It was very similar but not identical with ILA. ILA, however, is a critical compound if the pathways of IAA biosynthesis should be determined [1,2]. With the presented method, we were able to check with the second HPLC separation if detected substances (*e.g.*, ILA) were identical with the respective standard compounds.

As an application example, soil samples from different agricultural fields were tested for TRP-induced auxin biosynthesis and actual contents of indole derivatives. The fields lay fallow, so exudation of auxins by plants was excluded.

In the soils, stimulation of auxin biosynthesis by TRP addition was necessary because as actually occurring indole derivatives, only TRP could be detected in considerable amounts apart from traces of IAA. This may indicate that in non-rhizosphere soil, the major part of the microflora is inactivated or metabolizes at reduced physiological status. In contrast, we could detect endogenous and excreted auxins in non-TRP-supplemented cultures of *Azospirilla* and *Rhizobia* which colonize the rhizosphere of crop plants (data not presented). Therefore, higher auxin contents may be found in rhizosphere soils.

In the TRP-spiked soil samples (Table III), we identified IAA as the major TRP catabolite. TOL and ILA were detected as representatives of the IPA pathway of auxin biosynthesis [1–3], and IAld and ICA as IAA catabolites [2]. Traces of IAM, the characteristic IAA intermediate in the IAM pathway of auxin biosynthesis [1–3], could only be monitored in the soil from Neumarkt. The detection of AnthrA in both soils revealed the presence of the "aromatic pathway" [14] of microbial TRP catabolism, and might indicate that TRP was converted as a source of carbon and nitrogen.

The higher total contents of C and N in the Scheyern soil (see Experimental) suggest, that the higher auxin biosynthesis in this soil (Table III) might be due to a higher microbial biomass. Clear evidence for microbial TRP catabolism was given by axenically performed experiments. In both sterilized soils, no TRP conversion was observed apart from the autoxidative TRP decay. The conversion of TRP to IAA and TOL via IPA in both agricultural soils agrees with the findings for *Azospirilla* [8,20,21], several *Rhizobia* [7], *Enterobacter cloacae* [3], *Pseudomonas putida* [9] and *Pseudomonas fluorescens* [5]. These bacteria are reported to promote plant growth and can be isolated from the rhizosphere of crop plants. We assume that the production and excretion of the auxins IAA and TOL are important factors in microbial plant growth promotion [20–22].

In our experimental design, the IAA concentrations ranged from 2.9 to 8.0 $\mu g/g$ dry soil. Frankenberger and Brunner [1] reported IAA production of 200–800 $\mu g/g$ soil. However, they used 37°C as the incubation temperature, a higher TRP supply of 40 mg, plant root-influenced soil from grassland and a different extraction and HPLC system with an ion-pair reagent. Detection of UV absorbance was at 254 nm, where indole derivatives show very poor absorbance. We assume that TRP autoxidation was not taken in account.

Owing to the influence of plants, especially in the rhizosphere, and to modified soil conditions (*e.g.*, water content), TRP catabolism and the pattern of detected substances may be different. Especially the occurrence of TAM, TOL and IAM in soils and microorganisms [1,2] needs further investigation.

ACKNOWLEDGEMENTS

We thank the GSF, Neuherberg, for supplying instruments and Evangelisches Studienwerk Villigst, for financial support.

REFERENCES

1 W. T. Frankenberger, Jr., and W. Brunner, *Soil Sci. Soc. Am. J.*, 47 (1983) 237.
2 G. Sandberg, A. Crozier and A. Ernstsen, in L. Rivier and A. Crozier (Editors), *The Principle and Practice of Plant Hormone Analysis*, Vol. 2, Academic Press, London, 1987, p.169.
3 J. Koga, T. Adachi and H. Hidaka, *Agric. Biol. Chem.*, 55 (1991) 701.

4 M. Sekine, T. Ichikawa, N. Kuga, M. Kobayashi, A. Sakurai and K. Syono, *Plant Cell Physiol.*, 29 (1988) 867.
5 S. Narumiya, K. Takai, T. Tokuyama, Y. Noda, H. Ushiro and O. Hayaishi, *J. Biol. Chem.*, 254 (1979) 7007.
6 J. M. Barea and M. E. Brown, *J. Appl. Bacteriol.*, 37 (1974) 583.
7 A. Ernstsen, G. Sandberg, A. Crozier and C. T. Wheeler, *Planta*, 171 (1987) 422.
8 A. Crozier, P. Arruda, J. M. Jasmin, A. M. Monteiro and G. Sandberg, *Appl. Environ. Microbiol.*, 54 (1988) 2833.
9 M. Wurst, Z. Prikryl and J. Vokoun, *J. Chromatogr.*, 286 (1984) 237.
10 M. Smidt and T. Kosuge, *Physiol. Plant Pathol.*, 13 (1978) 204.
11 S. Hutcheson and T. Kosuge, *J. Biol. Chem.*, 260 (1985) 6281.
12 T. Yamada, C. J. Palm, B. Brooks and T. Kosuge, *Proc. Natl. Acad. Sci. U.S.A.*, 82 (1985) 6522.
13 G. Sandberg, A. Crozier, A. Ernstsen and B. Sundberg, in H. F. Linskens and J. F. Jackson (Editors), *High Performance Liquid Chromatography in Plant Sciences*, Vol. 5, Springer, Berlin, 1987, p.73.
14 R. Y. Stanier, O. Hayaishi and M. Tsuchida, *J. Bacteriol.*, 62 (1951) 355.
15 I. Wöhler, *Mitt. Dtsch. Bodenkd. Ges.*, 59/I (1989) 639.
16 A. Stoessl and M. A. Venis, *Anal. Biochem.* 34 (1970) 344.
17 M. Iino, R. S.-T. Yu and D. J. Carr, *Plant Physiol.*, 66 (1980) 1099.
18 B. Andersson and K. Andersson, *J. Chromatogr.*, 242 (1982) 353.
19 A. E. Stafford, J. A. Kuhnle, J. Corse and E. Hautala, *J. Chromatogr.*, 294 (1984) 485.
20 V. L. D. Baldani, J. I. Baldani and J. Döbereiner, *Biol. Fertil. Soils*, 4 (1987) 37.
21 Y. Kapulnik, Y. Okon and Y. Henis, *Biol. Fertil. Soils*, 4 (1987) 27.
22 P. Martin, A. Glatzle, W. Kolb, H. Omay and W. Schmidt, *Z. Pflanzenernähr. Bodenkd.*, 152 (1989) 237.

Journal of Chromatography, 629 (1993) 267–276
Elsevier Science Publishers B.V., Amsterdam

CHROM. 24 577

High-performance liquid chromatography–thermospray mass spectrometry of ten sulfonamide antibiotics

Analysis in milk at the ppb level

J. Abián, M. I. Churchwell and W. A. Korfmacher*

US Food and Drug Administration, National Center for Toxicological Research, Jefferson, AR 72079 (USA)

(First received January 13th, 1992; revised manuscript received August 5th, 1992)

ABSTRACT

Ten sulfonamide antibiotics including sulfanilamide (SNL), sulfamethazine (SMZ), sulfamethizole (SMTZ), sulfachloropyridazine and sulfaquinoxaline (SQX), were analyzed by thermospray (TSP) mass spectrometry on-line with a high-performance liquid chromatography–UV detection system. Except for the pairs SMZ–SMTZ and sulfadimethoxine–SQX, the standards were resolved in both the UV and TSP profiles. Co-eluting compounds could be differentiated in TSP by their different relative molecular masses. The $[M + H]^+$ ion was the base peak for all the standards except SNL, which showed an $[M + NH_4]^+$ ion. Collision-induced dissociation of the $[M + H]^+$ ions afforded daughter ion spectra characterized by common ions at *m/z* 92, 108 and 156, and ions derived from the amine substituent ($[MH - 155]^+$). TSP detection limits [signal-to-noise ratio (S/N) > 3] were below 20 ng (scan mode), 2 ng (selected reaction monitoring, daughter ions from $[M + H]^+$) and 400 pg (selected ion monitoring). UV detection limits were *ca.* 2 ng ($S/N > 5$). Results obtained from the multi-residue analysis of spiked cow milk samples at the low ng/ml level are presented.

INTRODUCTION

Sulfonamides are a group of antibacterial agents widely used in veterinary practice for the treatment of infections and to promote growth of food-producing animals. The presence of residues of these compounds can be detected in meat [1] and milk [2,3] from treated animals. Owing to the possible carcinogenic character of some members of this group [4,5], and the potential development of resistance through ingestion that could make sulfonamides ineffective as therapeutic drugs [6], analysis for these compounds has become necessary in food surveys. For some sulfonamides the US Food and Drug Administration has established limits that oscillate between 0 and 100 ppb (w/w) in edible animal tissues and between 0 and 10 ppb in milk [7].

Current analytical methods for sulfonamides are based on gas chromatographic (GC) or liquid chromatographic (LC) techniques. Various methods using GC with electron-capture detection [8] or high-performance LC (HPLC) with UV detection [9] that afford detection limits below the 100 ppb level have been published recently. In addition, mass spectrometry (MS) was suggested or used for confirmation of the target compounds by these workers.

HPLC methods offer the advantage over GC that they require no previous derivatization of the sample. Some techniques that use LC–MS interfaces such as HPLC–MS using direct liquid introduction (DLI) [10] and supercritical fluid chromatography coupled to TSP or moving-belt interfaces [11] have

Correspondence to: Dr. Joaquín Abián, Department of Neurochemistry, CID, CSIC, Jordi Girona 18–26, 08034 Barcelona, Spain (present address).

* Present address: Department of Drug Metabolism, Schering-Plough, 60 Orange Street, Bloomfield, NJ 07003, USA.

0021-9673/93/$06.00

been shown to be useful for analyses for sulfonamides in meat and some biological fluids such as plasma and urine. Recently, Pleasance *et al.* [12] showed the utility of HPLC–ionspray MS for the determination of 21 sulfonamides and described the application of parallel HPLC–diode-array UV detection and HPLC–ionspray tandem mass spectrometry (MS–MS) to the characterization of sulfadimethoxine in salmon flesh. Finally, LC–electrospray MS using capillary LC and capillary zone electrophoresis has also been applied by Perkins *et al.* [13] to the analysis of sulfonamide standards.

Among the LC–MS techniques, HPLC–thermospray (TSP) MS could be considered as one of the most suitable methods for the determination of medium- and high-polarity compounds. TSP has been applied previously with good results to the determination of sulfonamides in meat [14]. Although the eluent composition with TSP is restricted to a relatively narrow range of buffers and solvents, the spectrometric information obtained often easily compensates for the loss of chromatographic separation or resolution. Further, MS–MS techniques can be applied in order to enhance structural information. The inherent high selectivity of the MS–MS technique often allows the design of methods with minor sample clean-up requirements.

In this paper, we describe the use of HPLC–TSP-MS and HPLC–TSP-MS–MS for the determination of ten sulfonamides (Fig. 1). This list includes the more important ones in terms of the violation rates of the established maximum levels, *i.e.*, sulfamethazine, sulfadimethoxine, sulfathiazole and sulfachloropyridazine [8].

The application of TSP to the determination of these compounds in milk at the low ng/ml level is presented. Some approaches to the direct analysis of milk by TSP have been previously investigated in

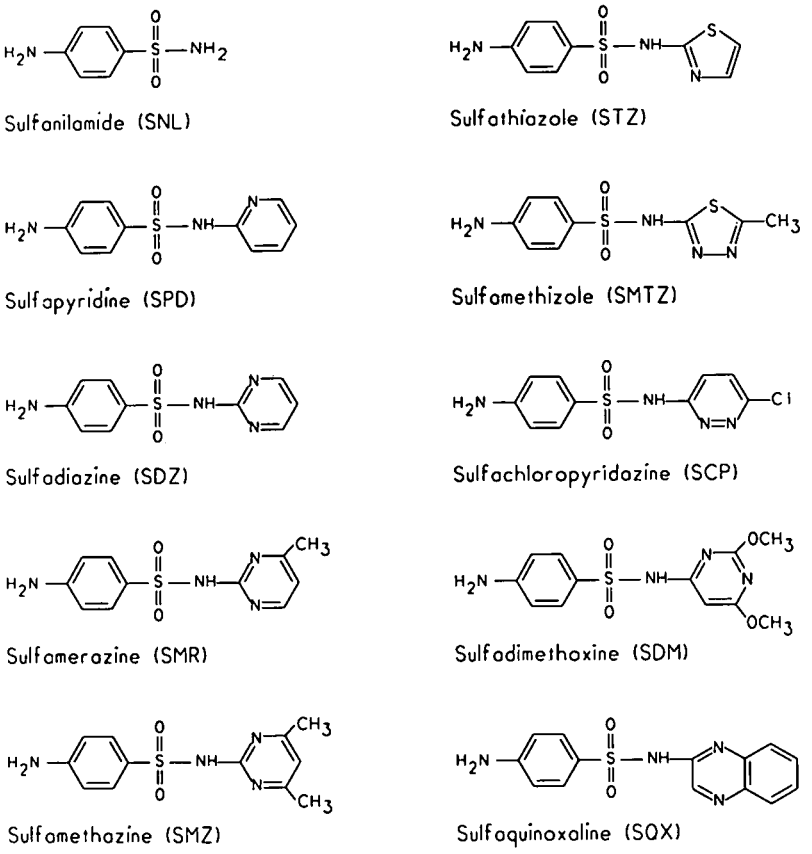

Fig. 1. Structures of the ten sulfonamides.

this laboratory for a group of three sulfonamides [15]. In this work, we also tested the use of on-line preconcentration and clean-up methods in order to obtain a rapid and specific procedure for multi-residue analysis.

EXPERIMENTAL

Standards and reagents

Sulfanilamide (SNL), sulfapyridine (SPD), sulfadiazine (SDZ), sulfamerazine (SMR), sulfamethazine (SMZ), sulfathiazole (STZ), sulfamethizole (SMTZ), sulfachloropyridazine (SCP), sulfadimethoxine (SDM) and sulfaquinoxaline (SQX) (see Fig. 1) were obtained from Sigma (St. Louis, MO, USA). Standard solutions at 1 mg/ml in methanol were prepared and stored below 0°C.

Ammonium acetate was obtained from Fluka (Ronkonkoma, NY, USA). Water was purified through a Milli-Q system (Millipore–Waters, Bedford, MA, USA). Other reagents and solvents were of analytical-reagent or chromatographic grade.

Preparation of milk extracts

A 5-ml volume of control and spiked (5–500 ng/ml) milk (commercially available whole cow milk) were acidified with concentrated hydrochloric acid (100 μl) and sonicated for 15 s. Proteins were removed by centrifugation at 3000 *g* for 10 min. The precipitate was washed with 2 ml of water and recentrifuged. Lipids in the aqueous phase were extracted twice with 5 ml of hexane. Phase separation was helped by centrifugation for *ca.* 1 min at 1500 *g*. The extracted aqueous sample was evaporated to dryness at low pressure, the residue was dissolved in methanol and the solution was centrifuged. The methanolic phase was evaporated to dryness and the residue was dissolved in 3 ml of water. Aliquots of 50–500 μl of this solution were injected.

Chromatography

A Spectra-Physics (San Jose, CA, USA) SP8700XR programmer and pumping system, a Rheodyne (Cotati, CA, USA) Model 7125 injector with a 20-μl sample loop and a 5-μm Spherisorb ODS-2 reserved-phase column (15 × 0.46 cm I.D.) (Phase Separations, Norwalk, CT, USA) were used. The column exit was connected to a Spectra 100 variable-wavelength detector (Spectra-Physics) equipped with a Model 9550-0150 high-pressure microbore cell (2 mm path length, 250 nl) capable of operating up to 7000 p.s.i. (1 p.s.i. = 6894.76 Pa) (Linear Instrument, Reno, NV, USA). A Shimadzu (Kyoto, Japan) C-R3A Chromatopac integrator was used as a recorder for the UV detector.

Two solutions were used for chromatography. Solvent A was a 0.1 *M* ammonium acetate buffer (1% formic acid) and solvent B was acetonitrile (ACN)–water (70:30) containing 0.1 *M* ammonium acetate (1% formic acid).

Sulfonamides were chromatographed at a flow-rate of 1 ml/min, with a gradient programme starting at 100% solvent A. After injection a linear gradient up to 20% solvent B in 30 s was used. After 1 min, solvent B was increased to 75% in 10 min.

A schematic diagram of the system used for the analysis of spiked milk extracts is shown in Fig. 2. The gradient programmer (PROG), HPLC pump (PUMP A), injector (INJ), analytical column (COL 2) and solvents are the same as described before, except for the use of a 500-μl sample loop. The analytical column (COL 2) was preceded by a precolumn unit (COL 1) from Brownlee Labs. (Santa Clara, CA, USA). The precolumn consisted of an MPLC holder and a disposable 3-cm cartridge filled with 10-μm RP-18 stationary phase, and was used as a preconcentration and clean-up system. The precolumn flow could be directed to either the analytical column or waste by means of a Rheodyne Model 7040 switching valve (V2). Another Model 7040 valve (V1) was used in order to backflush the precolumn system when needed. Continuous eluent flow through the analytical column to the mass spectrometer during the preconcentration and clean-up steps or during precolumn backflushing was assured by means of an independent HPLC unit (PUMP B) (Model 6000A, Waters, Milford, MA, USA). Samples were injected (100–500 μl) under the initial HPLC conditions and after a 3-min wash of the precolumn the flow was directed to the analytical column and the solvent gradient indicated before was started.

Thermospray mass spectrometry

A Finnigan (San Jose, CA, USA) TSQ 70 triple quadrupole mass spectrometer equipped with a Finnigan TSP source and interface was used. The exit of the UV detector was connected to the TSP

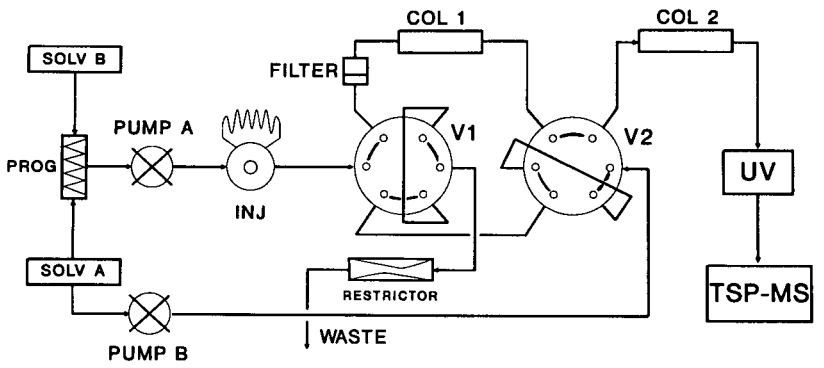

Fig. 2. Scheme of the HPLC system used for the analysis of milk samples. Valve position is depicted as it is during TSP analysis (COL 1 on-line with COL 2). The valve V1 allows backflushing of the precolum COL 1; valve V2 switches the exit of COL 1 between WASTE (during preconcentration and clean-up) and the entry of COL 2 (during TSP analysis). For details, see text.

interface through a 0.5-μm on-line HPLC filter.

The interface temperature was set at 80–85°C. The source and manifold temperatures were kept at 250 and 70°C, respectively. For the MS–MS experiments, argon at *ca.* 0.4 mTorr (1 Torr = 133.322 Pa) (manifold readout) was used as the collision gas. Collision energies of 40–50 eV were used for most of the work.

RESULTS AND DISCUSSION

The structures of the compounds assayed are depicted in Fig. 1. The on-line UV and TSP profiles obtained using our chromatographic conditions are shown in Fig. 3. As can be seen in the UV profile, except for the pairs SMZ–SMTZ (8.4 min) and SDM-SQX (12.1 min), complete chromatographic resolution was obtained. The chromatographic peaks in the TSP profile show some tailing that is not observed in the corresponding UV chromatogram. This loss of resolution on the TSP profile was not the result of the presence of dead volumes due to the on-line UV detection system and thus should be explained by band diffusion and adsorption–des-

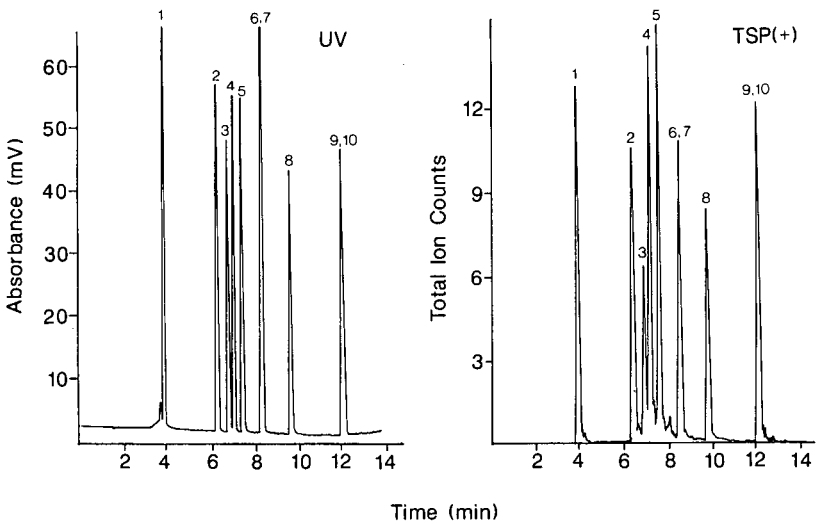

Fig. 3. On-line UV and TSP profiles obtained by injection of 400 ng of each sulfonamide (40 ng of SQX). HPLC conditions as indicated under Experimental. For these chromatograms COL 1 in Fig. 2 was bypassed and no preconcentration and clean-up steps were used. UV detection at 254 nm. Full-scan (100–300 u) MS detection of positive ions; filament off. 1 = SNL; 2 = SDZ; 3 = STZ; 4 = SPD;5 = SMR; 6 = SMTZ; 7 = SMZ; 8 = SCP; 9 = SDM; 10 = SQX.

orption processes in the TSP interface. These adsorption–desorption phenomena could also be responsible for some spurious TSP signals, such as that observed at 8 min in the profile.

Acetonitrile was shown to be a better organic modifier than methanol for this application (Fig. 4). Although in general methanol affords better ionization efficiencies than ACN when these solvents are used at medium or high concentrations in TSP, in this instance methanol-based eluents showed more background noise and instability during the gradient mixing process. In addition, TSP chromatographic peaks were sharper using ACN as the organic modifier.

The use of an interface temperature gradient was not necessary for good performance because the ACN concentration was kept low during the chromatography and most of the compounds eluted in a narrow range of ACN percentage (between *ca.* 15 and 35%).

The TSP mass spectra of these compounds were very simple (Table I). Except for SNL, all the spectra showed a base peak due to the $[M + H]^+$ ion and very little if any fragment ion signals. SNL showed an $[M + NH_4]^+$ adduct (base peak) in addition to the protonated molecule. Other low-abundance signals were observed in the spectra. SMZ, SCP, SDM and SQX showed signals at $[MH-155]^+$ that also were observed in the collision-induced dissociation (CID) spectra as shown below. Further, SPD showed a signal at *m/z* 186 that could arise from the loss of SO_2 from the $[M + H]^+$ ion at *m/z* 250.

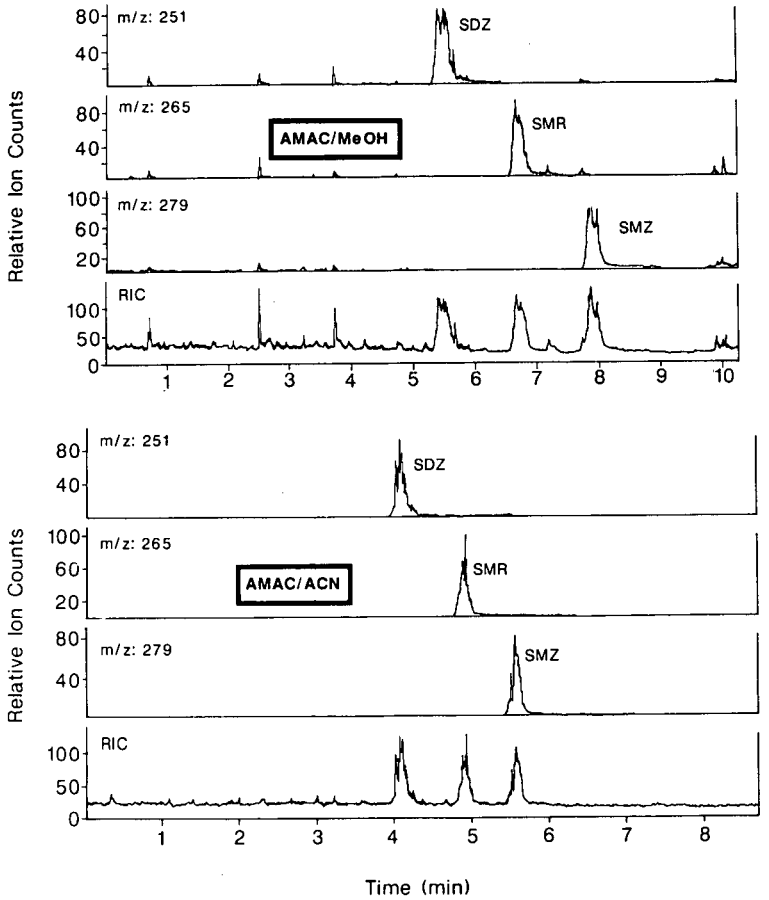

Fig. 4. HPLC–TSP-MS of SMZ, SMR and SPD using (a) MeOH- and (b) ACN-based eluents. The eluent gradient programs were (a) from 10 to 27% MeOH in 4 min and (b) from 12 to 25% MeCN in 4 min. Other conditions as decribed under Experimental.

TABLE I

TSP MASS SPECTRA AND RETENTION TIMES (t_R) OF THE TEN SULFONAMIDES

Compound	t_R (min)[a]	M_r	Base peak	Other ions[b]
SNL	3.9	172	$[M + NH_4]^+$	173[c] (25)
SPD	7.2	249	$[M + H]^+$	186 (2)
SDZ	6.4	250	$[M + H]^+$	–
SMR	7.6	264	$[M + H]^+$	–
SMZ	8.5	278	$[M + H]^+$	124[d] (2)
STZ	6.9	255	$[M + H]^+$	–
SMTZ	8.4	270	$[M + H]^+$	–
SCP	9.8	284	$[M + H]^+$	130[d] (3)
SDM	12.1	310	$[M + H]^+$	156[d] (2)
SQX	12.2	300	$[M + H]^+$	146[d] (7)

[a] HPLC–TSP-MS conditions as described under Experimental and in Fig. 3.

[b] The relative abundance (%) is given in parentheses after the m/z value of the ion.

[c] $[M + H]^+$ ion.

[d] $[MH - 155]^+$ signal ($m/z = M_r - 154$). See also Fig. 5 and Table II.

As the ten compounds have different relative molecular masses, co-eluting sulfonamides can easily be differentiated by their different $[M + H]^+$ base peaks. For this reason, chromatographic resolution and separation are not as critical parameters as in UV methods and therefore it is not neccesary to use time-consuming HPLC procedures or more than one injection per sample as described previously for the multi-residue analysis of these compounds [9].

Full-scan detection limits were in the range 5–20 ng of the compounds injected on-column (scan range 150–330 u, $S/N > 3$ for the ion trace at $[M + H]^+$). These values are slightly over the 2 ng detection limit ($S/N > 5$) estimated for the UV analysis using our chromatographic system. UV detection limits are determined by the high absorption of the eluent and the baseline drift at high detector sensitivities owing to the ammonium acetate buffer and the ACN gradient programming. Further, and for comparative purposes, it should be taken into account that the reduced path length of the microbore UV cell results in the loss of about two thirds of the sensitivity of a conventional cell.

Selected ion monitoring of the $[M + H]^+$ signals ($[M + NH_4]^+$ for SNL) afforded detection limits of *ca.* 400 pg on-column (multiple ion detection of the ten ions, 2 s per cycle, $S/N > 5$). These detection limits could be lowered to the 100 pg level by programming the ions to be monitored at the different elution zones (one to three ions monitored at the same time).

CID of the $[M + H]^+$ ion ($[M + NH_4]^+$ for SNL) gives tandem mass spectra characterized by four major signals at m/z 92, 108, 156 and $M_r - 154$ (Table II and Fig. 5). These signals are equivalent to those previously observed in DLI [10], chemical ionization [8,16,17] ionspray [12] and electrospray [13] MS–MS of these compounds. Brumley *et al.* [17] using high-resolution mass measurements and, more recently, Pleasance *et al.* [12] using the data obtained from granddaughter ion experiments suggested some possible structures and formation pathways for these ions. In addition to these major daughter ion peaks, signals corresponding to the $[MH - 93]^+$ and $[MH - 66]^+$ ions are observed in some of the spectra with low relative abundance and can be assigned to the $[O_2SNHR]^+$ and $[MH - H_2SO_2]^+$ ions [10,12,13,16,17].

Collision-induced ions at m/z 92, 108 and 156 are common to the sulfonamides when TSP is used as the ionizing technique. It is interesting that, for SNL, the signal at m/z 156, also present in its electrospray tandem mass spectra [13], is not observed in the CID spectra of the $[MH]^+$ ion when ionspray, a closely related ion evaporation-based technique, is used [12]. These common daughter ions can be used for group recognition in MS–MS. In this way, selected reaction monitoring in the parent ion mode (Q3 focuses on the fragment at m/z 156 and Q1 focuses alternatively on the different $[M + H]^+$ parent ions) affords additional specificity to the analysis. The fragment at m/z 156 was selected as the daughter ion to be monitored because of its high relative abundance in all ten of the sulfonamides.

Optimum collision gas pressure (determined as that which provides a maximum signal at 50 eV collision energy) was found between 0.3 and 0.5 mTorr (manifold readout) for this fragmentation. Lower or higher pressures afforded a low CID fragment intensity owing to a small number of collisions or to ion scattering, respectively. Characterization of the actual gas pressure was shown to be only approximate, and the average 0.4 mTorr gas pressure selected for the experiments oscillated as far as 0.05–0.07 mTorr around the central value during normal TSP operation.

TABLE II

DAUGHTER IONS OBSERVED ON THE CID MASS SPECTRA OF THE $[M + H]^+$ IONS FROM THE SULFONAMIDES

Collision energy, 50 eV; collision pressure, 0.5 mTorr. See references in text and Fig. 5 for the ion structures.

Compound	Parent $m/z = M_r + 1$[a]	$[H_2NPh]^+$ $m/z = 92$	$[H_2NPhO]^+$ $m/z = 108$	$[H_2NPhSO_2]^+$ $m/z = 156$	$[H_3NR]^+$ $m/z = M_r - 154$	$[O_2SNHR]^+$ $m/z = M_r - 92$	$[MH - H_2SO_2]^+$ $m/z = M_r - 65$
SNL[b]	100	6	3	21	–	–	–
SPD	100	11	5	32	4	–	5
SDZ	100	20	10	48	7	2	–
SMR	100	11	8	35	10	5	–
SMZ	100	9	5	30	14	9	1
STZ	100	21	9	69	2	–	–
SMTZ	75	17	9	100	2	–	–
SCP	100	13	6	48	3	–	–
SDM	100	8	5	70	[c]	–	5
SQX	100	11	9	82	6	–	–

[a] For SNL, $m/z = M_r + 18$.
[b] Also shows the $[M + NH_4 - NH_3]^+$ ion at $m/z = M_r + 1$ with 13% relative abundance.
[c] Indicates that this ions is isobaric with the CID ion $[H_3NPhSO_2]^+$.

The effect of the collision energy on the total peak area for each sulfonamide is shown in Fig. 6. All the compounds showed a maximum signal level between 30 and 60 eV. Below 30 eV, the response decreases rapidly, except for SNL (for which the selected parent is the $[M + NH_4]^+$ ion), which shows intense fragmentation ions at energies as low as 10 eV.

Owing to ion scattering in the collision cell and to the non-quantitative fragmentation processes, detection limits in the MS–MS mode are higher than those obtained in the MS mode (2 ng on-column when monitoring the ten $[M + H]^+$ parents).

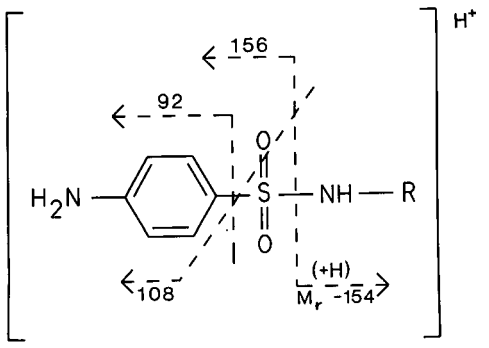

Fig. 5. Visualization of the possible fragment structures derived from the CID of the $[M + H]^+$ ions of the ten sulfonamides.

Analysis of milk

The detection limits are low enough to allow the multi-residue analysis of these compounds at the 10 ppb levels required for milk surveys. Although some work has been done on their determination in meat by TSP [14], no data have been reported for milk except for our preliminary report where diluted milk samples were injected into the HPLC–TSP-MS system without prior clean-up [15]. Current methods for the extraction of sulfonamides from milk utilize large volumes of organic solvents such as diethyl ether and ethyl acetate and are not suitable for automation of analysis. In order to overcome these problems, some workers have shown the utility of solid cartridge extraction columns for sample clean-up [18,19]. Extensive clean-up is required owing to the low levels to be measured and the presence of co-eluting compounds in the milk that also show a response using the UV detector.

In Fig. 7, the ion traces obtained in the analysis of a milk sample spiked at 20 ng/ml are shown. The extraction procedure described under Experimental uses minimum sample and organic solvent volumes and hence it should be possible to process in parallel a large number of samples rapidly. Although the clean-up is not good enough for HPLC–UV detection, the sensitivity and specificity of the HPLC–TSP-MS technique allowed the analysis of milk

samples using this simple procedure. Initially, the extraction procedure used included only protein precipitation and lipid extraction. An aliquot of the aqueous phase was injected directly into the HPLC system. Using this method, rapid degradation of the TSP response occurred owing to the deposition of solid materials in the interface tip. This residue, probably from milk carbohydrates and remaining proteins, was eliminated using the methanol extraction as described under Experimental.

The preconcentration and clean-up system shown in Fig. 2 was used with good results. The system could be easily automated and needs only two different solvent solutions. A continuous flow through COL 2 is assured by means of PUMP B when the exit of the precolumn is directed to waste. In this way, it is possible to maintain a more stable TSP performance and to stabilize COL 2 with the initial eluent composition during the injection and clean-up steps. The Spectra-Physics pump used for chromatography was very sensitive to pressure changes and some flow-rate problems affecting proper TSP interface performance were observed when the eluent of PUMP A was directed to COL 2 from the "waste" position. These problems were eliminated when a restrictor (an old 10-μm analyt-

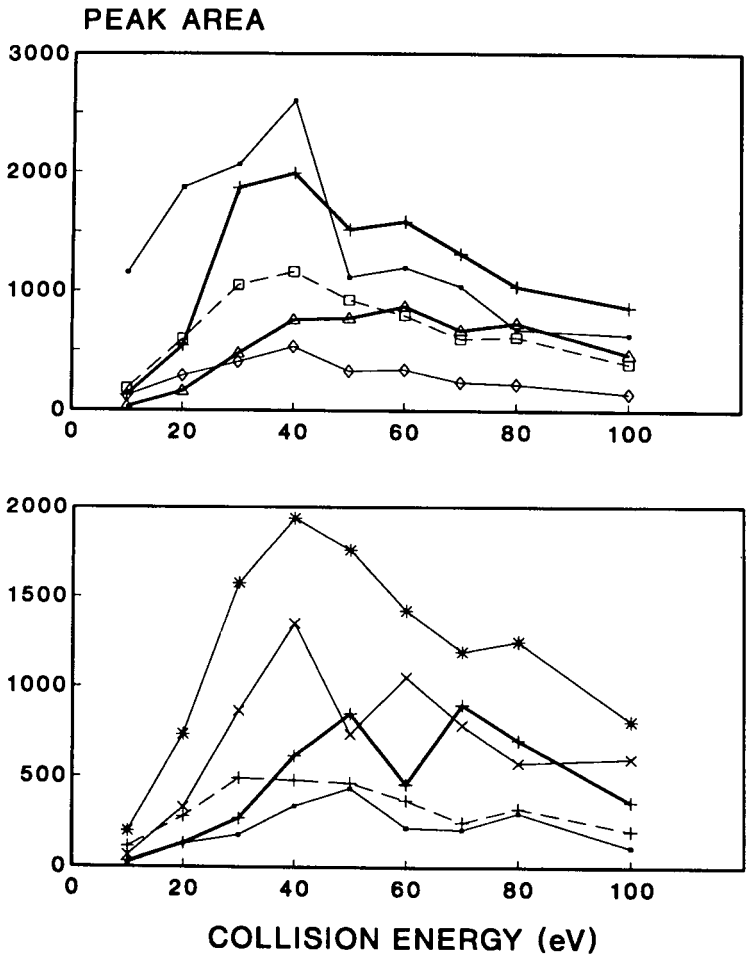

Fig. 6. Effect of collision energy on total peak area obtained in the SRM analysis (parent ion mode using the ion at m/z 156 as the common daughter ion) of the ten sulfonamides. Top: ■ = SNL; + = SPD; □ = STZ; ◇ = SMTZ; △ = SMZ. Bottom: ■ = SQX; + (solid line) = SDM; * = SDZ; × = SMR; + (dashed line) = SCP.

ical column), situated in the waste exit, was used to smooth the pressure difference between the two positions of valve V2. In some instances, the use of sample loops and injection volumes of up to 1 ml was tested without observing any detrimental effect in the TSP analysis. Precolumn concentration allows further sample clean-up by retaining lipid residues that can be washed out after each analysis.

Also, the method eliminates polar compounds from the sample that could plug the interface or interfere with the ionization processes. Hence, after precolumn washing, the common Na^+ (or Cl^- in the negative-ion mode)-derived adducts usually present in the spectra of compounds from salt-containing matrices were not observed. An unresolved problem of the on-line precolumn concentration method is that the washing step results in the loss of SNL. This compound, the most polar of the group assayed, showed low retention characteristics in the precolumn system and eluted (the UV detector was connected to the waste exit) as a broad peak in the first 5 min even when the eluent contained no ACN. In contrast, no losses of SDZ or STZ, the next eluting compounds, were detected under these conditions during a 10-min elution period.

As can be seen in Fig. 7, matrix-derived background noise and peak interferences are not important in determining the overall sensitivity of the TSP technique. Thus, HPLC–MS–MS procedures offer no advantage over HPLC–MS for trace detec-

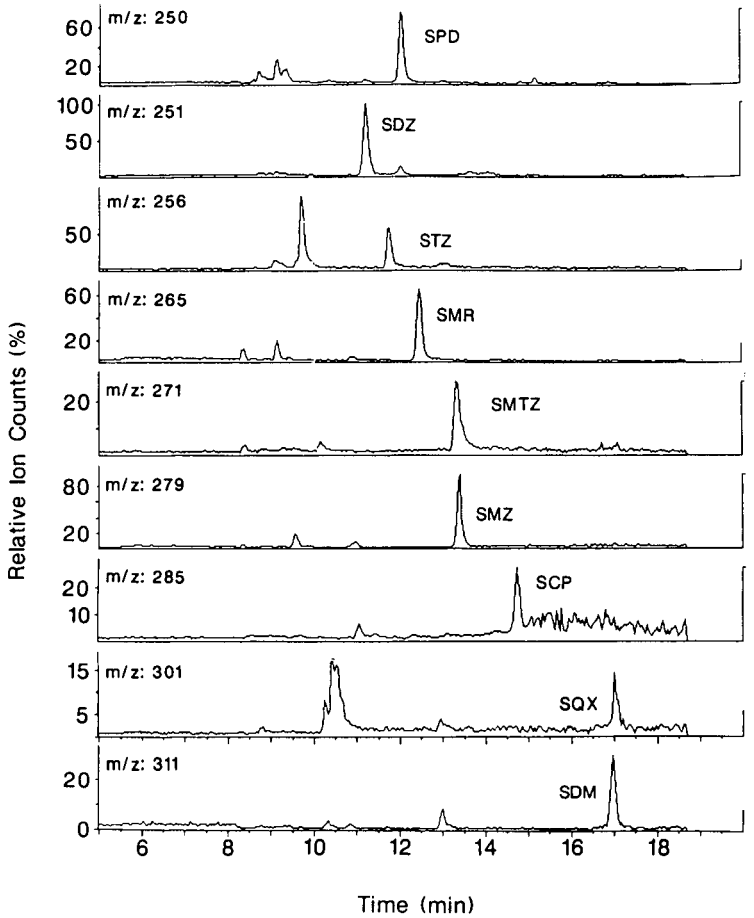

Fig. 7. HPLC–TSP-MS analysis (selected ion monitoring) of a cow milk sample spiked with 20 ng/ml of each sulfonamide (SNL is lost in the clean-up step).

tion in milk (actually, MS–MS shows higher detection limits than SIM analyses) but can be used when the amounts of the target compounds are at the high ppb level and a more specific characterization of the compounds is required.

CONCLUSIONS

The ten sulfonamide antibiotics tested in this work can be separated and characterized by HPLC–TSP-MS and HPLC–TSP-MS–MS. Co-eluting sulfonamides SMTZ and SMZ and SDM and SQX are readily resolved by their different relative molecular masses. The sensitivity of the technique allows its application to the multi-residue analysis of these compounds in biological matrices with minor sample preparation. The technique allows the detection of nine of these compounds in milk at the low ppb level using a simple and rapid clean-up procedure, and could be easily adapted to other HPLC–UV sample preparation methods for compound confirmation and/or characterization using HPLC–MS or HPLC–MS–MS.

ACKNOWLEDGEMENTS

J. A. was supported by an appointment to the Oak Ridge Associated Universities postgraduate research program at the National Center for Toxicological Research, which is administered by the Oak Ridge Associated Universities through an interagency agreement between the US Department of Energy and the US Food and Drug Administration.

REFERENCES

1 R. F. Bevill, R. M. Sharma, S. H. Meachum, S. C. Wozniak, D. W. A. Bourne and L. W. Dittert, *Am. J. Vet. Res.*, 38 (1977) 973.
2 D. L. Collins-Thompson, D. S. Wood and L. Q. Thomson, *J. Food Protect.*, 58 (1988) 632.
3 L. Larocque, C. Garignan and S. Sved, *J. Assoc. Off. Anal. Chem.*, 73 (1990) 365.
4 *NCTR Technical Report for Experiment Number 420*, National Center for Toxicological Research, Jefferson, AR, 1989.
5 P. B. Hansen and J. Bichel, *Acta Radiol.*, 37 (1952) 258.
6 N. Haagsma, G. J. M. Pluijmakers, M. M. L. Aerts and W. M. J. Beek, *Biomed. Chromatogr.*, 2 (1987) 41.
7 *US Code Fed. Reg.*, 1991, Title 21, Sections 556.620–556.690.
8 J. E. Matusik, R. S. Sternal, C. J. Barnes and J. A. Sphon, *J. Assoc. Off. Anal. Chem.*, 73 (1990) 529.
9 M. D. Smedley and J. D. Weber, *J. Assoc. Off. Anal. Chem.*, 73 (1990) 875.
10 J. D. Henion, B. A. Thomson and P. H. Dawson, *Anal. Chem.*, 54 (1982) 451.
11 J. R. Perkins, D. E. Games, J. R. Startin and J. Gilbert, *J. Chromatogr.*, 540 (1991) 239.
12 S. Pleasance, P. Blay, M. A. Quilliam and G. O'Hara, *J. Chromatogr.*, 558 (1991) 155.
13 J. R. Perkins, C. E. Parker and K. B. Tomer, *J. Am. Soc. Mass Spectrom.*, 3 (1992) 139.
14 M. Horie, K. Saito, Y. Hoshino, N. Nose, M. Tera, T. Kitsuwa, H. Nakazawa and Y. Yamane, *Eisei Kagaku*, 36 (1990) 283.
15 M. I. Churchwell, J. Bloom and W. A. Korfmacher, in *Proceedings of the 39th ASMS Conference on Mass Spectrometry and Allied Topics, Nashville, TN, May 19–24, 1991*, p. 1342.
16 E. M. H. Finlay, D. E. Games, J. R. Startin and J. Gilbert, *Biomed. Environ. Mass Spectrom.*, 13 (1986) 633.
17 W. C. Brunley, Z. Min, J. E. Matusik, J. A. G. Roach, C. J. Barnes, J. A. Sphon and T. Fazio, *Anal. Chem.*, 55 (1983) 1405.
18 Y. Ikay, H. Oka, N. Kawamura, J. Hayakawa, M. Yamada, K.-I. Harada, M. Suzuki and H. Nakazawa, *J. Chromatogr.*, 541 (1991) 393.
19 V. K. Agarwal, *J. Liq. Chromatogr.*, 14 (1991) 699.

Journal of Chromatography, 629 (1993) 277–281
Elsevier Science Publishers B.V., Amsterdam

CHROM. 24 661

Liquid chromatographic determination of amoxicillin preparations

Interlaboratory validation

Hsiou-Chuan Chung and Mei-Chich Hsu

National Laboratories of Foods and Drugs, Department of Health, Executive Yuan, 161-2 Kuen-Yang Street, Nankang, Taipei 11513 (Taiwan)

(First received July 16th, 1992; revised manuscript received October 6th, 1992)

ABSTRACT

A previously published column liquid chromatographic method proposed for the analysis of amoxicillin preparations was subjected to an interlaboratory validation. The method is rigorously defined in terms of performance requirements, yet allows a degree of flexibility to the individual analyst. Nine participating laboratories submitted results for the analysis of four samples in duplicate. Estimates for the repeatability and reproducibility of the method, expressed as relative standard deviations of the results of the analysis of amoxicillin preparations, were found to be less than 0.96% and 6.29%, respectively.

INTRODUCTION

A more specific and reliable method is needed for the assay of amoxicillin preparations because the current official procedures lack specificity [1–4]. This paper reports the results and evaluation of a collaborative study to validate a column liquid chromatographic (LC) method for the determination of the potency of bulk amoxicillin and amoxicillin capsule, injection and granule formulations. The protocol for analysis was basically that previously described [5], except that a degree of flexibility was allowed to the individual analyst, while rigorously defining the performance criteria of the method to maintain control.

Control of the method is maintained by specifically defining minimum performance criteria for a system suitability test. Flexibility of the method lies in the discretion given to the analyst to select the specific analytical system (*i.e.*, instrument, injector, detector and column, etc.). The analyst is encouraged to use individual judgement in adjusting the operating conditions to meet the performance criteria.

EXPERIMENTAL

Collaborative study

Each of nine collaborators received a reference standard of amoxicillin sodium, an internal standard of acetaminophen, duplicate samples of bulk material, commercial powdered capsule, injection and granule composites. The collaborators also received a set of instructions regarding the amount of sample to take for analysis, a copy of the method and a report form for recording results. They were also asked to describe specific operational parameters of the instrument system used and to submit their report forms along with their chromatograms. These samples were to be measured against a refer-

Correspondence to: Mei-Chich Hsu, National Laboratories of Foods and Drugs, Department of Health, Executive Yuan, 161-2 Kuen-Yang Street, Nankang, Taipei 11513, Taiwan.

0021-9673/93/$06.00

ence amoxicillin sodium sample with a potency of 847.1 μg/mg.

Instrumentation

Each laboratory was asked to use routine LC equipment. Instruments were to be equipped with a 254-nm UV detector and a recording device. In order to obtain a wide diversity of systems, analysts were encouraged to use their own columns. However, only microparticulate reversed-phase packing materials that exhibit some degree of polarity, such as hydrocarbon-bonded silicas, were allowed.

Reagents

Reference material amoxicillin sodium was an NLFD house standard (National Laboratories of Foods and Drugs, Taiwan). Acetaminophen was a gift from Winthrop Laboratories Taiwan Branch Office, Sterling Products International (Taipei, Taiwan). Methanol was of LC grade. Glacial acetic acid was of analytical-reagent grade. Triply distilled water with a resistivity greater than 15 MΩ was used.

Mobile phase

The mobile phase was methanol–1.25% acetic acid (20:80, v/v). The mobile phase was filtered (0.45-μm Millipore filter) and degassed prior to use. The mobile phase may be sparged with helium through a 2-μm metal filter for the duration of the analysis.

Internal standard solution

The internal standard, acetaminophen (40.0 mg), was dissolved in 10.0 ml of methanol and diluted to 1.0 l with water to give the internal standard solution.

Amoxicillin standard solution

To prepare amoxicillin standard solution, internal standard solution was added to an accurately weighed amount of amoxicillin sodium standard equivalent to a 50.0-mg potency of amoxicillin and the volume was adjusted to 50.0 ml.

Sample solution

All solutions of amoxicillin samples were prepared in the same manner as the reference material.

Conditions for determination

A constant operating temperature (15–30°C) was maintained. The eluent flow-rate, which was not to exceed 2.0 ml/min, was adjustedto give peaks of satisfactory retention and configuration. The detector sensitivity was adjusted to produce peak heights of 40–90% full-scale detection, with a chart speed of 0.5 mm/min.

System suitability

The column was equilibrated with mobile phase. A minimum of three injections of amoxicillin standard solution were chromatographed. The relative standard deviation for the ratio of peak responses should be $\leqslant 2.0\%$. Injections of 20 μl were suggested for all solutions to be analysed.

Assay and calculations

Identical volumes of carefully measured standard and sample solutions were injected sequentially into the chromatograph. The peak response was normalized to the internal standard and compared with that of the reference material to give the amoxicillin content as follows: $(P_u\ C_s\ I_s/P_s\ C_u\ I_u) \times 847.1 =$ amoxicillin potency (μg/mg), where P = peak response of amoxicillin, C = concentration of solution, I = peak response of internal standard, u = analyte sample and s = reference material. Calculations and data reduction may be performed manually or with a data processing system. Duplicate injections were run or each preparation.

RESULTS AND DISCUSSION

Table I shows the diversity of instrument systems used by the collaborators. The adoption of suitability tests can obviate many problems arising from deficiencies in most analytical instrument systems because they demonstrate whether a particular system can perform satisfactorily.

All of the collaborators were able to meet the system suitability requirements of the method. The times required for the collaborators to complete the analysis of the samples in the study varied from one to several days.

The Dixon test for outliers, when applied to laboratory means for each sample, showed only one outlier overall. The lowest result for bulk drug, that of laboratory 2, was flagged as an outlier. The data for bulk drug from laboratory 2 were omitted.

TABLE I

INSTRUMENT SYSTEMS USED IN THE COLLABORATIVE STUDY OF THE LIQUID CHROMATOGRAPHIC METHOD FOR AMOXICILLIN

Laboratory	Instrument	Detector	Injector	Mode[a]	Column	Length × I.D. (cm × mm)
1	Waters 600E	W-486	715 WISP	A	Nucleosil C_{18}	30 × 3.9
2	Shimadzu	SPD-6AV	SIL 1A	M	Inertsil 10-ODS	25 × 4.6
3	Waters 510	W-486	712 WISP	A	μBondapak C_{18}	30 × 3.9
4	Spectroflow 400	Spectroflow 757	Micromeritics 725	A	Partisil ODS-3[b]	25 × 4.6
5	Hitachi L-6200	L-4000	Rheodyne	M	Inertsil 10-ODS	30 × 3.9
6	Waters 510	W-481	Shimadzu	M	Inertsil 5-ODS	15 × 4.6
7	Jasco 880PU	L-200	740 WISP	A	LiChrosorb RP-18	25 × 4.5
8	Toyo Soda Ccpd	Spectromonitor II 1202	Rheodyne 7125	M	Chemosorb ODS C_{18}	25 × 4.0
9	Gasukuro 576	502U	–	A	μBondapak C_{18}	30 × 3.9

[a] M = manual; A = automatic.

[b] Bulk drug, capsule and injection samples were analysed with a Partisil ODS-3 column and granule sample with an Ultrasphere 5 ODS column.

The statistical terms used are those given by the Association of Official Analytical Chemists [6] and/or commonly used by statisticians. The analysis of variance with each sample is shown in Table II. Results of the analysis of the samples, together with means and relative standard deviations (R.S.D.), are given in Table III. In addition to the mean, a measure of the precision was also calculated for (a) the within-laboratory standard deviation or repeatability (S_r), (b) the between-laboratories standard deviation or reproducibility (S_R), (c) repeatability relative standard deviation (R.S.D.$_r$) and (d) reproducibility relative standard deviation (R.S.D.$_R$). The R.S.D.$_r$ values were 0.59% for bulk drug, 0.80% for capsule, 0.96% for injection and 0.52% for granule and the R.S.D.$_R$ values were 0.86% for bulk drug, 2.38% for capsule, 6.29% for injection and 2.59% for granule (Table III).

The results of standard addition recovery studies of amoxicillin from sample composites of commercial preparations are given in Table IV. The average recoveries were all close to 100.0%. These data fur-

TABLE II

ANALYSIS OF VARIANCE

Source of variation	Sum of squares (1)	Degree of freedom (2)	Mean square (1)/(2)
Between laboratories[a]			
Bulk drug	7.62	6	1.270
Capsule	65.69	7	9.384
Injection	407.46	7	58.208
Granule	97.87	7	13.981
Between replicates			
Bulk drug	2.71	7	0.387
Capsule	4.48	8	0.560
Injection	5.42	8	0.677
Granule	2.26	8	0.283

[a] Eight laboratories.

TABLE III

RESULTS FOR THE ANALYSIS OF AMOXICILLIN BULK DRUG AND DOSAGE FORMS

Collaborator	Bulk drug[a] (%)		Capsule[a] (%)		Injection[a] (%)		Granule[b](%)	
1	106.8	107.5	94.2	94.1	94.3	94.5	108.0	107.6
2	101.7[c]	102.6[c]	91.4	91.1	84.2	84.5	100.2	100.2
3	108.1	108.3	94.8	94.6	78.3	77.8	105.6	105.9
4	106.7	106.0	94.0	94.4	87.9	87.5	105.6	105.9
5	109.3	107.4	97.9	98.2	85.6	86.3	100.6	100.4
6	106.4	107.1	96.2	96.8	93.6	93.7	104.9	105.0
7	107.2	107.2	91.7	93.2	83.7	83.4	103.4	104.8
8	106.1	106.8	94.4	96.9	87.6	90.7	102.6	104.1
9[d]	104.7	105.5	92.5	93.2	79.8	80.8	103.8	103.5
Mean	107.21		94.62		87.08		104.06	
S_r	0.62		0.75		0.82		0.53	
S_R	0.91		2.23		5.43		2.67	
R.S.D.$_r$ (%)	0.59		0.80		0.96		0.52	
R.S.D.$_R$ (%)	0.86		2.38		6.29		2.59	

[a] Compared with reference substance.
[b] Determined as percentage of declared concentration for granule of 100 mg/g.
[c] Outlier by Dixon's test.
[d] Data from our laboratory; not included in statistical analysis.

TABLE IV

RECOVERY OF AMOXICILLIN FROM VARIOUS COMMERCIAL COMPOSITES

Product	Manufacturer	Added (mg)	Found (mg)	Average recovery (%)
Capsule, 250 mg	A	11.9	12.04	100.5
	B	12.5	12.86	
	C	12.4	12.62	
	D	11.1	11.17	
	E	13.1	13.00	
	F	11.9	11.82	
	G	10.8	10.83	
	H	11.0	10.96	
Capsule, 500 mg	D	12.4	12.60	100.3
	E	13.4	13.12	
	F	11.4	11.37	
	G	13.3	13.29	
	H	13.8	13.67	
	I	12.2	12.43	
	J	12.0	12.16	
Injection, 250 mg per vial	K	13.9	14.35	103.3
Injection, 500 mg per vial	D	13.4	13.72	102.5
Granule, 200 mg/g	H	12.8	12.57	99.2
	L	13.6	13.63	

ther indicate that the proposed LC method is relatively unaffected by the sample matrix.

Collaborators' comments

Most collaborators commented favourably on the method. They used a different brand of packing material than that specified (μBondapak C_{18}) in the method and obtained suitable chromatographic separations.

Collaborator 4 analysed bulk drug, capsule, injection samples with a Partisil ODS-3 column. In order to improve the separation of amoxicillin in granule and internal standard, an Ultrasphere 5 ODS column was used.

Collaborator 6 found that the peak for amoxicillin was sharper when the mobile phase contained phosphate buffer rather than acetic acid. However, the retention times were lengthened for both the amoxicillin and the internal standard. Collaborator 1 considered the method to be superior with respect to specificity to the official method using mercury nitrate titration [1], and to microbiological and iodimetric methods [2–4].

CONCLUSIONS

The collaborative study of the reversed-phase column LC method for the determination of amoxicillin in bulk, capsule, injection and granule preparations showed good reproducibility between laboratories. The method is now under consideration by the Chinese Pharmacopeia.

ACKNOWLEDGEMENTS

The authors are grateful to the following for their participation in this collaborative study: Dr. Kuang-Yang Hsu, Department of Pharmaceutics, School of Pharmacy, Taipei Medical College; Eli Lilly, Taiwan; Nang Kuang Pharmaceutical; Pfizer, Taiwan; Union Chemical Laboratories, Industrial Technology Research Institute; Upjohn Laboratories, Taiwan; Winthrop Laboratories Taiwan Branch Office, Sterling Products International, Taipei, Taiwan; and Yung Shin Pharmaceutical. The authors also thank Kingdom Pharmaceutical and Winthrop Laboratories Taiwan Branch Office, Sterling Products International, Taipei, Taiwan, for their generous gifts of samples and standards. This work was supported by grant 81-64 from the Department of Health, Executive Yuan, Taipei, Taiwan.

REFERENCES

1 *British Pharmacopoeia 1988*, HM Stationery Office, London, 1988.
2 *Minimum Requirements for Antibiotic Products of Japan*, English Version, Japan Antibiotics Research Association, Japan, 1986.
3 *Code of Federal Regulations, Title 21, Part 440*, US Government Printing Office, Washington, DC, 1990.
4 *United States Pharmacopeia XXII, National Formulary XVII*, United States Pharmacopeial Convention, Rockville, MD, 1990.
5 M.-C. Hsu and P.-W. Hsu, *Antimicrob. Agents. Chemother.*, 36 (1992) 1276.
6 W. J. Youden and E. W. Steiner, *Statistical Manual of the AOAC*, Association of Official Analytical Chemists, Arlington, VA, 1990.

Journal of Chromatography, 629 (1993) 283–290
Elsevier Science Publishers B.V., Amsterdam

CHROM. 24 683

Identification by particle-beam liquid chromatography–mass spectrometry of transformation products of the antioxidant Irganox 1330 in food-contact polymers subjected to electron-beam irradiation

David W. Allen, Malcolm R. Clench, Andrew Crowson and David A. Leathard

Division of Chemistry, School of Science, Sheffield City Polytechnic; Pond Street, Sheffield, S1 1WB (UK)

(First received July 9th, 1992; revised manuscript received October 12th, 1992)

ABSTRACT

Transformation products of Irganox 1330 [1,3,5-trimethyl-2,4,6-tris(3′,5′,di-*tert.*-butyl-4-hydroxybenzyl)benzene] in food contact polymers subjected to electron-beam irradiation have been analysed by particle-beam LC–MS. It has been shown that the principal degradation products arise *via* (1) oxidation of hindered phenol groups to give compounds having quinone methide structures or (2) cleavage of *tert.*-butyl groups or (3) cleavage of hindered phenol sub-units or (4) combinations of the above processes. Whilst quinone-methide-derived oxidation products are also observed in related thermally oxidised samples, products arising from the cleavage of *tert.*-butyl groups are only detected in irradiated samples.

INTRODUCTION

There is considerable interest in determining the effects of irradiation on food-contact polymers. Electron-beam irradiation treatment of pre-packaged foods offers an alternative approach to γ-irradiation, being more amenable to use as an on-line process. It has been shown that both electron-beam and γ-irradiation lead to the transformation of antioxidants present in these polymers [1–4]. The extent of transformation has been reported for the hindered phenol antioxidants Irganox 1076 and Irganox 1010 and the hindered phosphite stabiliser Irgafos 168. In these studies the extent of transformation was determined by extraction of irradiated polymers followed by high-performance liquid chromatography (HPLC).

Identification of transformation products is required in order to assist in the assessment of their potential toxicity and to examine the extent of their migration into food simulant media. In this paper data on the extent of transformation of Irganox 1330 (**1**), a hindered phenol antioxidant, and identification of some of its transformation products, are presented.

The transformation products have been analysed by liquid chromatography–mass spectrometry (LC–MS) using a particle-beam type interface [5]. This type of LC–MS interface is particularly suitable for the structural characterisation of unknowns since it can operate in conventional electron impact (EI) ionisation mode and hence yield spectra containing both molecular weight and structural information.

Correspondence to: D. W. Allen, Division of Chemistry, School of Science, Sheffield City Polytechnic, Pond Street, Sheffield, S1 1WB, UK.

EXPERIMENTAL

Irradiation

Samples of polypropylene homopolymer stabilised with 0.1% Irganox 1330 were prepared by sin-

tering to produce small pellets which were then subjected to progressive doses of irradiation from a 4.5-MeV Dynamitron continuous electron beam facility in air.

Extraction

The irradiated stabilised polypropylene (0.5 g) was extracted under reflux in chloroform (10 ml) for 4.5 hours to isolate the extractable transformation products. The extract was then microfiltered using a 0.45-μm pore size nylon 66 membrane filter and 1.0-cm Whatman GF/D pre-filter. The resulting extract was evaporated almost to dryness under oxygen free nitrogen in a screw cap vial. Ethyl acetate (3 ml) was then added to the extract to precipitate polymer oligomers. After re-microfiltration the extract was evaporated down to 0.5 ml. For quantitative analyses Irganox 1076 (0.6 mg) was added prior to the extraction as an internal standard.

High-performance liquid chromatography

HPLC analyses were performed using a mobile phase consisting of ethyl acetate–methanol–water (44:36:20) pumped at a flow-rate of 0.7 ml/min through a Spherisorb 10-cm S5 ODS1 analytical column fitted with a Spherisorb 5-cm S10 ODS1 guard column. Detection of the starting material and its transformation products was achieved using a Philips PU4021 multichannel UV–Vis detector. The resulting data were processed using a Dell 210 microcomputer equipped with the Philips analytical PU 6003 diode array detector system (V3.0).

TABLE I

EXTENT OF TRANSFORMATION OF IRGANOX 1330 (0.1%, w/w) IN POLYPROPYLENE HOMOPOLYMER WITH INCREASING IRRADIATION DOSE

Electron beam irradiation dose (kGy)	Intact Irganox 1330 remaining (%)
0	100
1	93
5	69
10	61
25	38
50	24

Liquid chromatography–mass spectrometry

LC–MS analyses were performed on a VG Trio 1 mass spectrometer fitted with a VG LINC particle-beam interface. The HPLC conditions used were identical to those described above.

The mass spectrometer was operated under the following conditions: ionisation mode: EI; electron energy: 70 eV; trap current: 150 μA; source temp.: 200°C; scan range: 50–850 u; scan rate: 3 s/scan. All data were recorded on a VG LAB-BASE data system.

RESULTS AND DISCUSSION

Table I shows the extent of transformation of Irganox 1330 for increasing doses of irradiation. The Irganox 1330 was present at an initial concentration of 0.1% (w/w) in a sample of polypropylene homopolymer.

The extent of transformation for this hindered phenolic antioxidant follows a similar trend to that found for other antioxidants of this type, previously reported by this group [1–4].

Fig. 1 shows a comparison between the single-wavelength UV chromatogram at 275 nm and the total ion count (TIC) for an LC–MS run on the same sample. The chromatograms are very similar with only small retention time differences. It is important to note that the TIC gives a more accurate indication of the relative amounts of the various transformation products than the UV chromatogram, which is dependent upon the molar absorption coefficients of the various products. Fig. 2A shows the mass spectrum obtained for the peak eluting at t_R = 19.38 min. This spectrum shows an intense molecular ion at m/z 774 and is readily identified as the parent compound **1**. The principal fragment ion **2**, observed at m/z 219, is believed to correspond to a sub-unit of the parent molecule.

An ion of lower abundance corresponding to cleavage of the same bond but with charge retention on the remaining three ring system can also be observed at m/z 555. There is also evidence for fragmentation in the same region but on the other side of the CH_2 group, leading to a loss of 205 mass units from the molecular ion. The rest of the spectrum is dominated by side chain losses of the tertiary butyl groups.

The peaks eluting after the parent compound

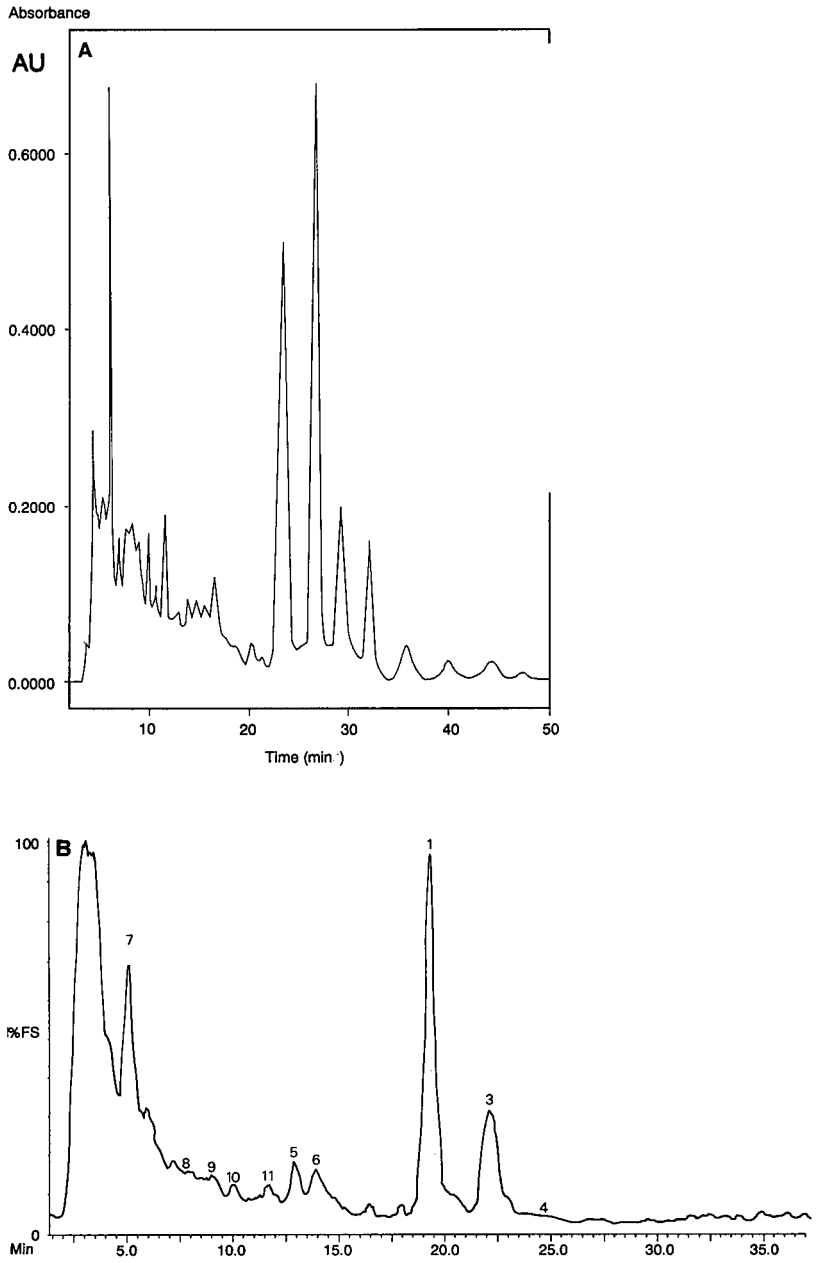

Fig. 1. (A) UV chromatogram at 275 nm. (B) Total ion chromatogram.

may be identified as decomposition products arising by oxidaton of the parent compound. The major component at t_R = 22.01 min gave the mass spectrum shown in Fig. 2B. This shows an intense molecular ion at m/z 772 and is believed to correspond to the substituted *para*-methylenebenzoquinone type structure **3**.

Oxidation of a second phenolic group is also observed to give a component of M_r 770 at t_R = 24.44 min, structure **4**. The conversion of Irganox 1330 to

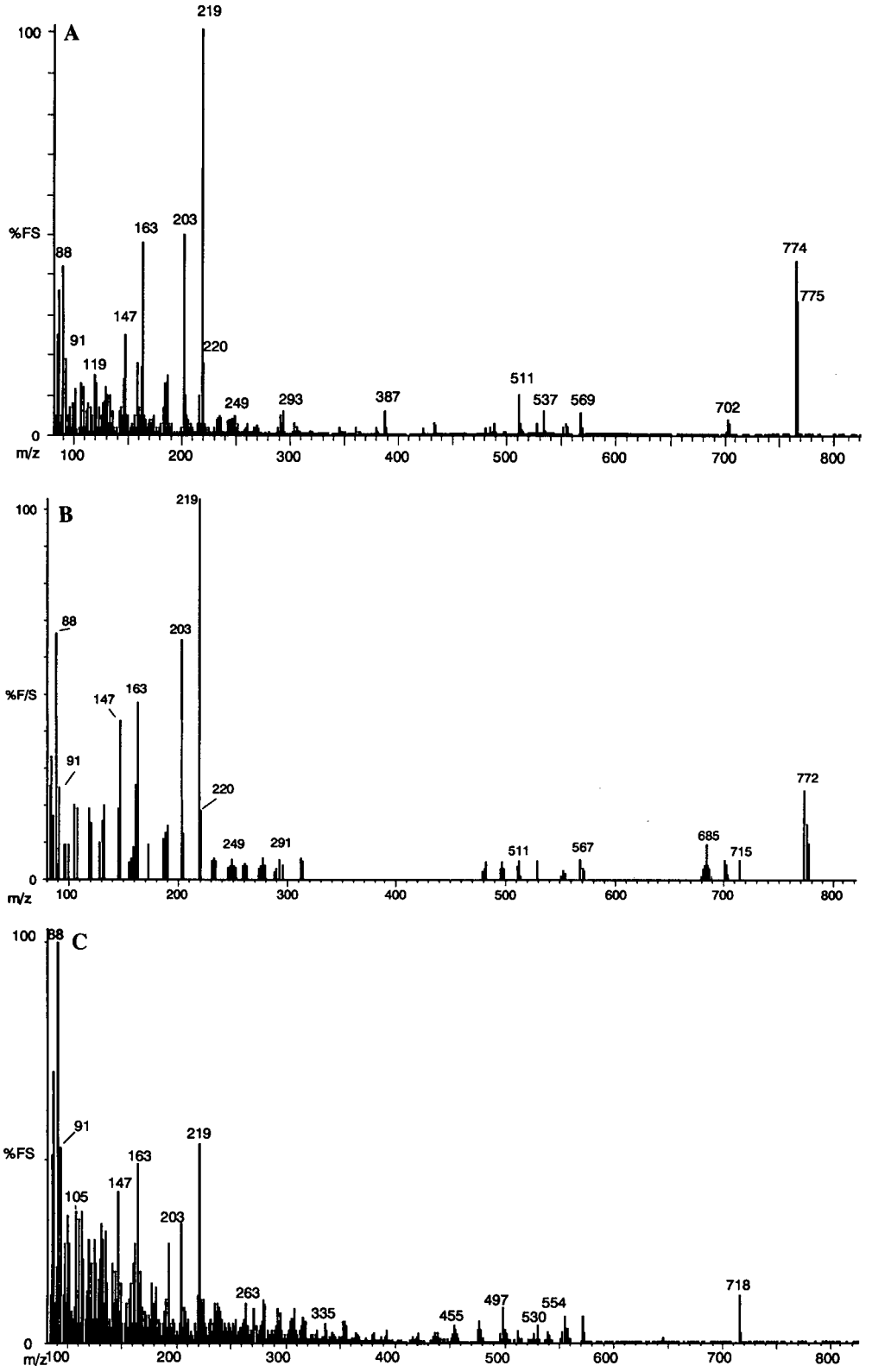
A
100
%FS
0
m/z
219
163
203
88
147
91
119
220
249
293
387
511
537
569
702
774
775
100
200
300
400
500
600
700
800
B
100
%F/S
0
m/z
219
88
203
147
163
91
220
249
291
511
567
685
715
772
100
200
300
400
500
600
700
800
C
100
%FS
0
m/z
88
91
219
163
147
105
203
263
335
455
497
530
554
718
100
200
300
400
500
600
700
800

Fig. 2.

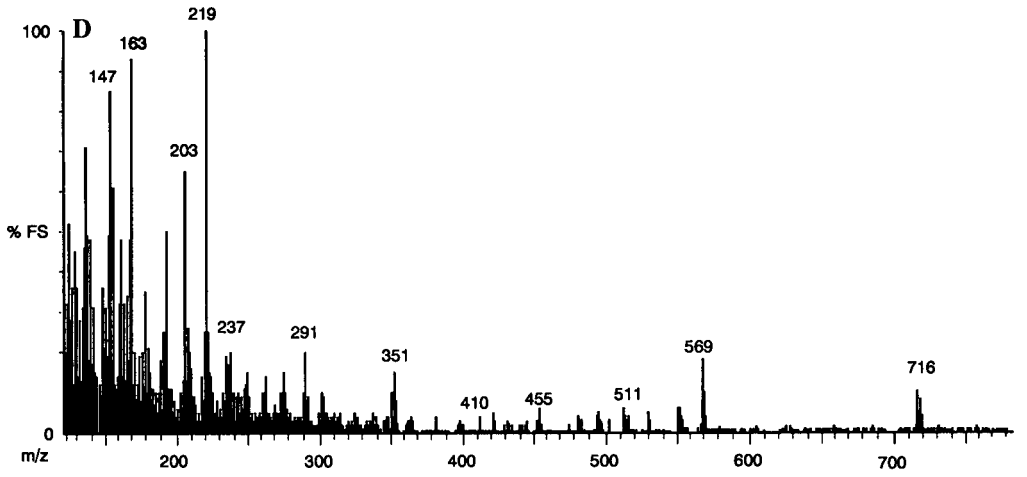

Fig. 2. Mass spectrum obtained for (A) Irganox 1330 (structure **1**) (M_r = 774); (B) structure **3** (M_r = 772); (C) structure **5** (M_r = 718); (D) structure **6** (M_r = 716).

these quinone methide structures *via* chemical oxidation has been reported by Koch [6]. The data presented here represents the first conclusive evidence of similar processes occurring under irradiation conditions.

Other transformation products have been detected and structures tentatively proposed. The structures correspond to combinations of oxidation of the *p*-methylenephenolic groups, loss of *tert.*-butyl groups, loss of one or more hindered phenol subunit groups, or combinations of the above. Fig. 2C is an example of the mass spectra obtained from these decomposition products. This product eluting at t_R = 12.87 min shows a clear molecular ion at *m/z* 718. The structure may be readily interpreted as arising from the loss of one C_4H_8 group from the parent molecule to give the structure **5**. [The loss of both *tert.*-butyl groups from one of the hindered phenol units present in Irganox 1330, leading to structure **7**, is supported by the relative intensities of key fragment ions in its mass spectrum. The relative intensity of the ion of *m/z* 219 (88%) to that of the ion of *m/z* 163 (35%) (the latter corresponding to a mono-*tert.*-butylated hydroxybenzyl unit) is significantly greater than in the mass spectrum of compound **5** (Fig. 2C) in which the above ions are of comparable intensity.] It is of interest that products arising from the loss of *tert.*-butyl groups are not observed among those formed under thermal oxidation conditions. The loss of *tert.*-butyl groups probably arises as a result of protodealkylation reactions due to the acidic conditions generated in the polymer during irradiation.

The corresponding quinone methide structure **6** (*m/z* 716) is observed eluting at t_R = 13.95 min and the mass spectrum is shown in Fig. 2D. Loss of one complete sub-unit from the parent molecule with or without oxidation leads to structures of RMM 584, 582 and 580. These were observed eluting at t_R = 7.91, 8.58 and 10.08, respectively. Table II summarises the transformation products identified from the LC–MS data.

TABLE II

SUMMARY OF THE TRANSFORMATION PRODUCTS IDENTIFIED FROM THE LC–MS DATA

Structure number	Relative molecular mass	LC–MS retention time (min)
1	774	19.38
3	772	22.01
4	770	24.44
5	718	12.87
6	716	13.95
7	662	4.96
8	584	7.91
9	582	8.58
10	580	10.08
11	556	11.63

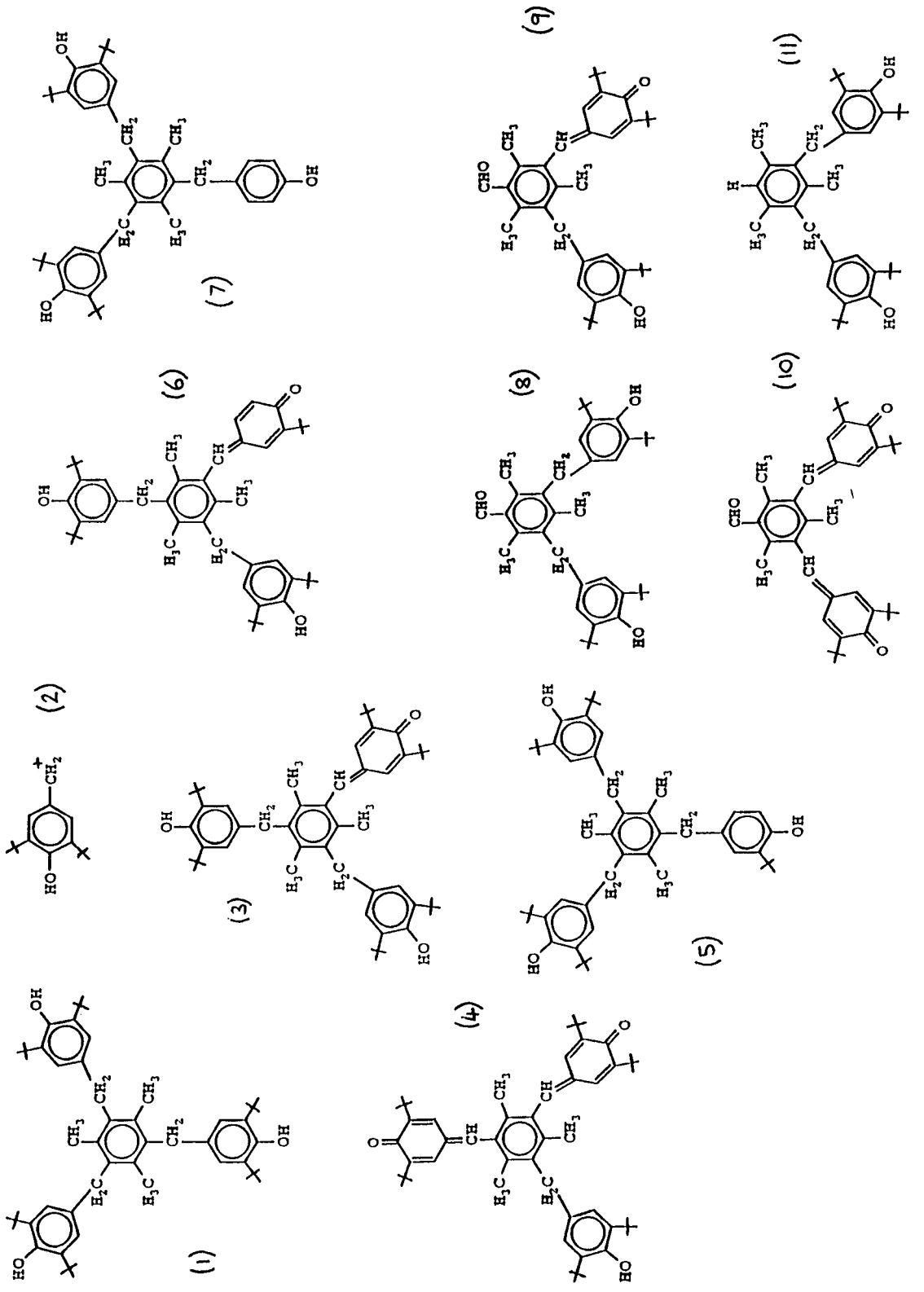
(1)
(2)
(3)
(4)
(5)
(6)
(7)
(8)
(9)
(10)
(11)

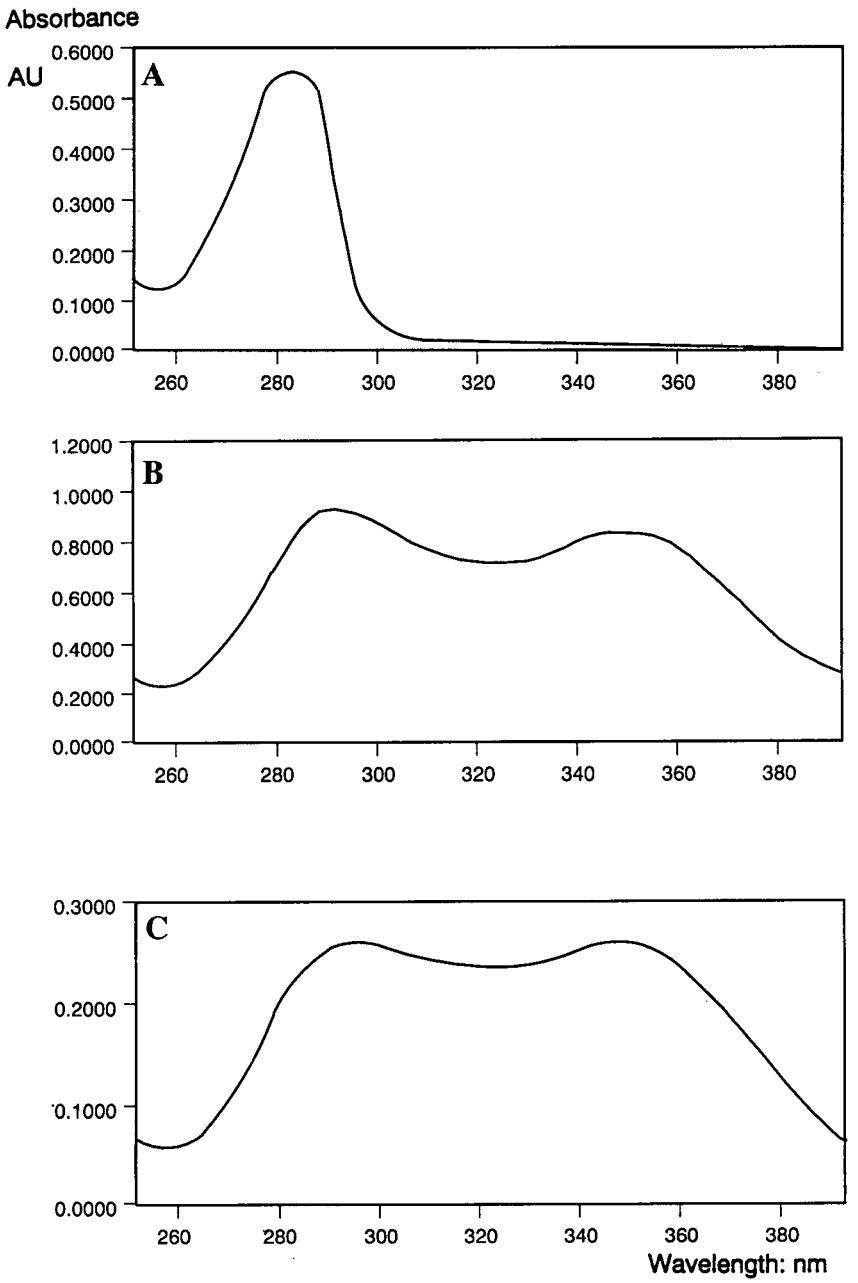

Fig. 3. UV spectrum obtained for (A) Irganox 1330 (structure **1**); (B) structure **3**; (C) structure **4**.

The use of the multichannel detector enabled UV spectra of many of the transformation products to be obtained. These spectra appear to support the types of structures we have proposed.

Fig. 3A–C shows the UV spectra for Irganox 1330 (**1**), structure (**2**) (RMM 772) and structure (**4**) (RMM 770), respectively. The spectra show that oxidation of one or more phenolic groups to pro-

duce quinone methide type units gives rise to intense absorption in the UV spectrum at longer wavelengths *i.e.* above 300 nm. Absorption of this type has also been observed in the UV spectra of other transformation products.

CONCLUSIONS

Transformation of Irganox 1330 in food contact polymers subjected to electron beam irradiation gives rise to a range of products similar to that observed in chemical oxidation, proceeding *via* the formation of quinone methide species derived from oxidation of the parent molecule, presumably as a result of reactions with alkylperoxyl radicals and related hydroperoxides. Also detected are a related series of oxidation products from which radiation-induced cleavage of *tert.*-butyl groups has occurred. These products have not been detected in related thermally oxidised samples.

Particle-beam LC–MS appears to offer a rapid method for the identification of such involatile, oxidative transformation products derived from high-molecular-weight hindered phenol antioxidants. We hope to improve our analytical conditions so as to identify the more polar products eluting near to the solvent front. The methodology described here will also be applied to the investigation of transformation products derived from other antioxidants.

ACKNOWLEDGEMENTS

This work was supported by the Ministry of Agriculture, Fisheries and Food, to whom thanks are due and is Crown Copyright. The authors thank VG Masslab for the gift of the LINC interface. The authors are indebted to ICI (Chemicals and Polymers Group) plc and Ciba-Geigy plc for the provision of information and materials, and to Viritech Ltd. (Swindon) for the use of their electron-beam irradiation facilities.

REFERENCES

1 D. W. Allen, D. A. Leathard, C. Smith and J. D. McGuinness, *Chem. Ind. (London)*, (1987) 198.
2 D. W. Allen, D. A. Leathard and C. Smith, *Chem. Ind. (London)*, (1987) 854.
3 D. W. Allen, A. Crowson and D. A. Leathard, *Chem. Ind. (London)*, (1990) 16.
4 D. W. Allen, D. A. Leathard and C. Smith, *Radiat. Phys. Chem., Int. J. Radiat. Appl. Instrum., Part C*, 38 (1991) 461.
5 F. Browner and R. Willoughby, *Anal. Chem.*, 56 (1984) 2626.
6 J. Koch, *Angew. Makromol. Chem.*, 20 (1971) 21.

Journal of Chromatography, 629 (1993) 291–296
Elsevier Science Publishers B.V., Amsterdam

CHROM. 24 656

Improvement of continuous counter-current gas–liquid chromatography for practical use

Katsuya Sato

Laboratory of Industrial Analytical Chemistry, Faculty of Technology, Tokyo Metropolitan University, 1-1 Minamiohsawa, Hachioji-shi, Tokyo 192-03 (Japan)

Katsunori Watabe

Central Research Laboratory, Shimadzu Corporation, Kyoto (Japan)

Toshihide Ihara and Toshiyuki Hobo

Laboratory of Industrial Analytical Chemistry, Faculty of Technology, Tokyo Metropolitan University, 1-1 Minamiohsawa, Hachioji-shi, Tokyo 192-03 (Japan)

(First received March 24th, 1992; revised manuscript received July 16th, 1992)

ABSTRACT

Counter-current gas–liquid chromatography, in which samples are processed continuously, is suitable for preparative separations. Following previous work, which made the fundamental aspects clear, a scaled-up instrument was constructed. Several factors that influence the sample separation, such as selection of the liquid phase, separation temperature, gas- and liquid-phase flow ratio, sample feed rate and the structure of separation tower, were evaluated in order to optimize separations on the scaled-up system. Under the optimum operating conditions, a mixture of *cis*- and *trans*-decahydronaphthalene (1:1, w/w) could be introduced at a rate of 7.2 ml/h into the system and a purity of each isomer of more than 95% was obtained continuously for more than 15 h.

INTRODUCTION

In continuous counter-current gas–liquid chromatography (CCGLC), the gas and liquid phases move in opposite directions, which makes continuous sample introduction possible for preparative-scale purification. In a previous paper, we reported a high-temperature continuous CCGLC system and demonstrated some applications [1]. However, the system was not suitable for practical use because the maximum sample feed rate was less than 1 ml/h and further investigations on the operating condition were required. In this work, we designed a larger scale CCGLC system and studied the influences of operating parameters such as liquid phase, separation temperature, gas and liquid flows, maximum sample feed rate and tower structure on a two-component separation. Decahydronaphthalene stereoisomers, the separation of which has been studied previously and found to be difficult [1], were chosen as the test sample in order to evaluate the new system.

Correspondence to: Professor Dr. Toshiyuki Hobo, Laboratory of Industrial Analytical Chemistry, Faculty of Technology, Tokyo Metropolitan University, 1-1 Minamiohsawa, Hachioji-shi, Tokyo 192-03, Japan.

EXPERIMENTAL

Instrumentation

The new CCGLC system is similar to the previ-

0021-9673/93/$06.00

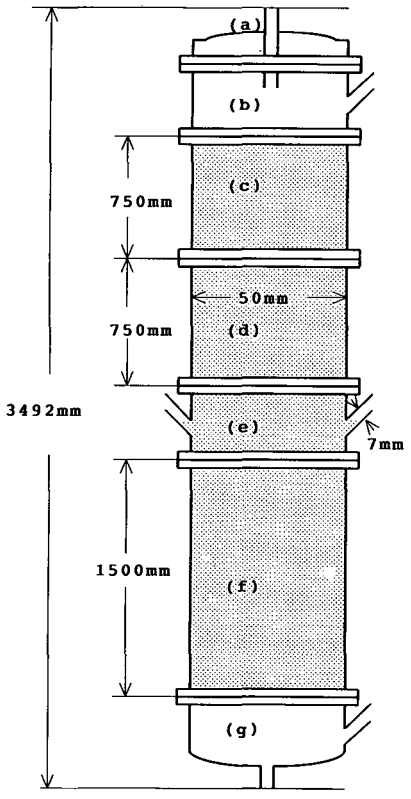

Fig. 1. Separation tower. (a) Liquid-phase inlet unit; (b) top gas-phase outlet unit; (c) upper separating section unit; (d) lower separating section unit; (e) bottom gas-phase outlet unit; (f) stripping section unit; (g) gas-phase inlet and liquid-phase outlet unit.

ous one [1], with the following differences. The tower diameter was enlarged from 17 mm to 50 mm. The tower consisted of seven Pyrex glass units, namely a liquid-phase inlet, a top gas-phase outlet, an upper separating section, a lower separating section and a gas-phase inlet. Stainless-steel nets were placed inside the liquid-phase inlet, gas-phase outlets and gas-phase inlet for fixing the stainless-steel helical-coil packing (Naniwapac). The packing was placed in the hatched area in Fig. 1. Silicone-rubber sheets were inserted between the glass-to-glass interfaces to prevent gas leaks.

The gas flow system is shown in Fig. 2. Two nitrogen cylinders (B grade, Nippon Sanso) were connected to the flow system and used alternately because the system consumed more nitrogen than the previous system. Trace amounts of oxygen in the nitrogen were removed by the heated purifiers (300 mm × 6 mm I.D. stainless-steel tubes) packed with reduced copper beads (1–2 mm diameter). Two purifiers were used alternately and reactivated by passage of hydrogen at 300°C when not being used. The nitrogen was fed after heating to the temperature of the tower using heaters inserted in the gas line.

The liquid phase was pumped into the top of the tower by a constant-flow pump (Shibata Model SPC-200 micro pump). The temperatures of the pump, liquid phase tank and flow line were kept at 60, 100 and 70°C, respectively. Samples were fed to the middle of the tower using a constant-flow pump (Senshu Kagaku Model 3100S) through a syringe needle. The whole sample flow line was heated to keep the viscosity of samples low.

One of the two components eluted from the tower was trapped in the collector (volume 25 ml) after cooling by a water-jacketed cooler, as shown in Fig. 3. Nine mantle heaters were placed around the tower and the temperatures were controlled independently. The temperature was monitored using thermister thermometers (Takara Kogyo A600 and D226) and a thermosensor (Takara Kogyo BXK-67).

Sample

A decahydronaphthalene stereoisomer mixture, which was not sufficiently separated with the previous system [1], was used as the test sample. *trans*-Decahydronaphthalene (b.p. 187.2°C) and *cis*-decahydronaphthalene (b.p. 195.7°C) were purchased from Tokyo Kasei Kogyo (Tokyo, Japan) and a 1:1 mixture was prepared.

Measurement of partition coefficients

The partition coefficients were calculated from the gas chromatographic retention times. A Shimadzu Model GC-8A gas chromatograph equipped with a flame ionization detector was used. Samples were injected onto a 2 m × 3.0 mm I.D. column packed with 20% Apiezon C on Chromosorb W AW DMCS (80–100 mesh).

Measurement of the purity of the eluates

The collected product was dissolved in 2–3 ml of dichloromethane and 1 μl was injected into a gas

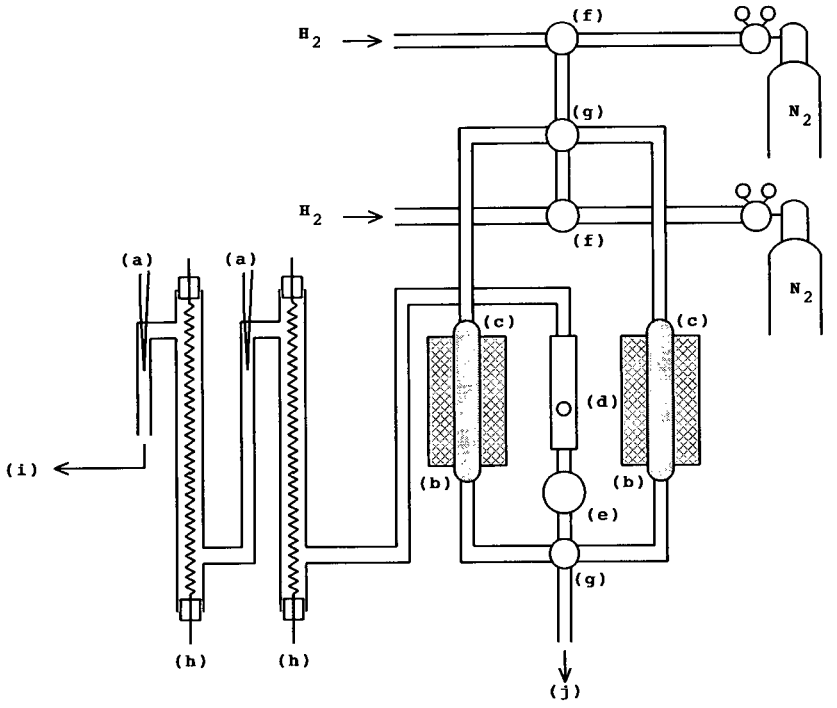

Fig. 2. Gas flow system. (a) Thermocouple; (b) electrical furnace; (c) reactor packed with reduced copper beads; (d) flow meter; (e) control valve; (f) three-way valve; (g) four-way valve; (h) heaters; (i) to separation tower; (j) to vent.

chromatograph. A 2 m × 3.0 mm I.D. column packed with 20% Apiezon C on Chromosorb W AW DMCS (80—100 mesh) was used at 130°C.

RESULTS AND DISCUSSION

Theoretical approach to the optimum separation

Liquid phase. For the liquid phase, silicone KF-54 (Shinetsu Kagaku) and Apiezon C were tested. Packed columns with both liquid phases were prepared and the partition coefficients were obtained. The values on KF-54 (162 for the *trans* and 208 for the *cis* form at 140°C) were smaller than those on Apiezon C (358 and 464, respectively, at 142°C). The ratios of the partition coefficients (separation factor), however, were almost the same (1.284 with KF-54 at 140°C and 1.296 with Apiezon C at 142°C). Although both liquid phases had similar separation properties, Apiezon C was chosen because its better stability in long-term operation.

Partition coefficients. The logarithm of the partition coefficient is linearly related to the reciprocal of the separation temperature. From the partition coefficient data at 121, 142, 162 and 183°C, the following empirical equations were derived by approximation:

$$\ln K_t = 4.72(1/T) \cdot 10^3 - 5.48$$

$$\ln K_c = 4.87(1/T) \cdot 10^3 - 5.60$$

where K_t and K_c are the partition coefficients of the *trans* and *cis* forms, respectively, and T (K) is the separation temperature. The correlation coefficient was 1.

Optimum flow ratios and separation temperature. The gas- and liquid-flow ratio (G/L) in the separation section should be between the two partition coefficients in CCGLC. When the separation is low, partition coefficient becomes large, then G/L also becomes large. This means that a high gas flow-rate should be used. As the trapping efficiency becomes low at high gas flow-rates, a high separation tem-

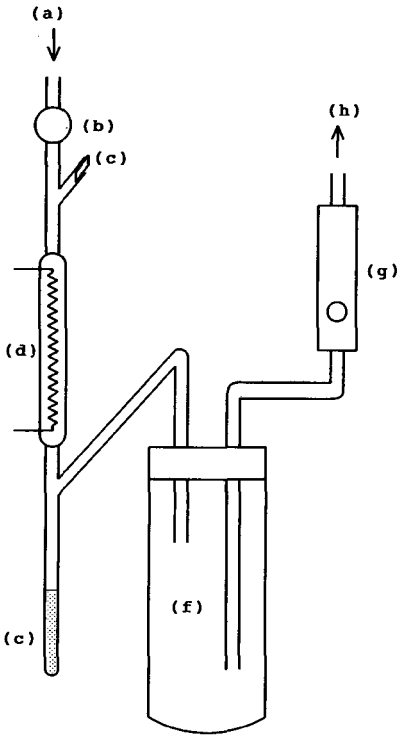

Fig. 3. Trap system. (a) From separation tower; (b) needle valve; (c) sampling port; (d) water jacket; (e) collector; (f) trap; (g) flow meter; (h) to vent.

perature is to be preferred. However, at low temperatures, the separation efficiency becomes high as the separation factor increases. Therefore, to determine the optimum separation temperature, those factors should be taken into consideration.

Maximum sample feed rate. The maximum sample feed rate, F_{max}, is calculated by the following equation:

$$F_{max} = \frac{tK_cP_t(G - LK_t) + cK_tP_c(LK_c - G)}{tK_c(760 - P_t) + cK_t(760 - P_c)} \cdot \frac{273}{273 + T'} \cdot \frac{1}{22400} \text{ (mol/min)}$$

where t and c are the contents of the *trans* and *cis* forms, respectively ($t + c = 100$), K_t and K_c are the partition coefficients of the *trans* and *cis* forms, P_t and P_c (mmHg) are the vapour pressures of the *trans* and *cis* forms, G and L (ml/h) are the flow-rates of the gas and liquid phases, respectively, and T' (°C) is the separation temperature.

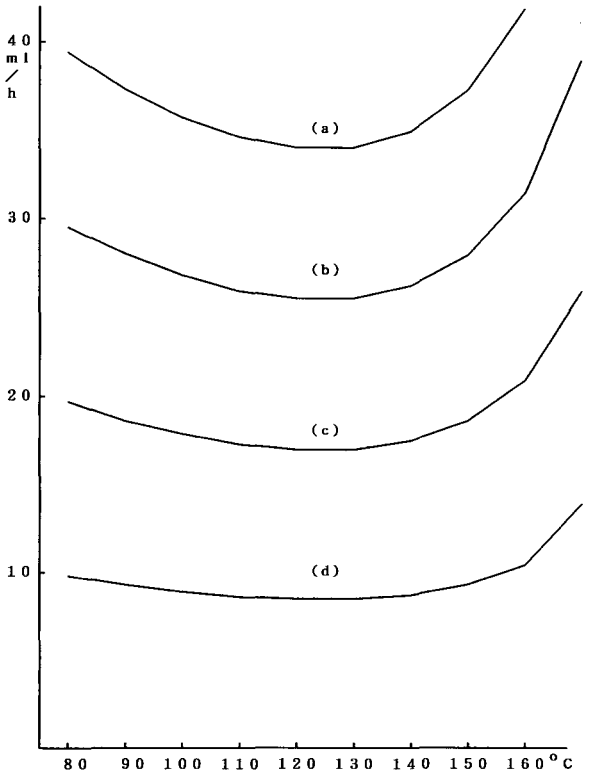

Fig. 4. Calculated maximum sample feed rate *vs.* separation temperature. Sample, decahydronaphthalene isomer mixture (1:1, w/w); liquid phase, Apiezon C; liquid phase flow-rate, (a) 0.4, (b) 0.3, (c) 0.2 and (d) 0.1 l/h.

The calculated maximum feed rates of the decahydronaphthalene sample are plotted against temperature in Fig. 4. The calculated maximum feed rates were lowest at *ca.* 125°C. The maximum sample feed rate is also proportional to the liquid flow-rate. Considering the limitation of the liquid flow-rate and the structure of the system, the sample feed rates were set from 7.2 to 14.7 ml/h. Better results were obtained at lower sample feed rates.

Tower structure

Tower construction. In the previous work [1], the separation tower was made from a single glass tube. However, the newly constructed tower was made from seven units, which made possible the insertion of the thermosensors in several locations. This structure was also convenient for fixing the stain-

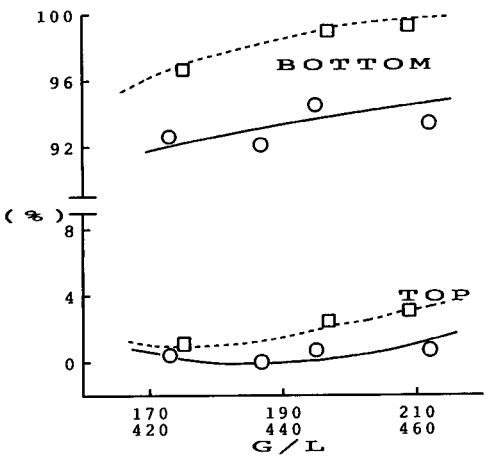

Fig. 5. Content of *cis*-decahydronaphthalene in the bottom and top recovered fractions: comparison of separation efficiency according to separation tower diameter. Tower diameter: ○ = 17 mm; □ = 50 mm.

less-steel net inside the tower. No influence on the separation efficiency was observed when these connected sections were used.

Diameter of the tower. It is generally considered that the separation efficiency decreases as the diameter increases. In this experiment, however, the data obtained with a diameter of 50 mm was better than that with 17 mm. The concentration of impurity at the top of the 17 mm diameter tower was lower than that with the 50 mm diameter tower, but at the bottom that of the 50 mm diameter tower was much higher than that of the 17 mm diameter tower, as shown in Fig. 5. Both towers had same length and were operated under optimum conditions and the sample feed rates were about half of the calculated values. Different liquid phases, namely silicone KF-54 and Apiezon C, were used in the 17 and 50 mm diameter towers, but the ratios between the partition coefficients and G/L values were similar. Hence the poor purity at the bottom of the 17 mm diameter tower might be due to the tower being overloaded and the excess component fell to the bottom of the tower, which suggests that the effective amount of liquid phase was small. It is assumed that thick-film flow might have occurred at the glass wall and the effective depth of the liquid film depth decreased.

Packing. Direct feeding of liquid phase into the new tower did not seem to make a uniform liquid film on the packing. It was considered that the viscosity of the liquid at room temperature was too low to disperse the liquid phase uniformly. Therefore, the liquid was diluted with chloroform (1:1, v/v) and an aliquot of the mixture was fed into the tower to coat the packing surface. The chloroform was then removed by raising the temperature of the tower. The condition of the helical wire packing and the standing angle of the tower were critical for obtaining a uniform coating.

Gas preheating

When the gas was introduced directly from the high-pressure cylinder through the purifier, fluctuation of the liquid flow at the bottom of the tower was observed. It was considered that the direct flow from the cylinder partially cooled the liquid phase, which made liquid phase viscous and caused turbulent flow. On preheating the gas to the temperature of the stripping section, no fluctuation in flow occurred.

The inner diameter of the gas outlet at the midpoint of the tower was so narrow (7 mm) compared with the diameter of the tower (50 mm) that the liquid phase flowed out with the gas steam and liquid phase flooding occurred. To prevent this flooding, an additional outlet was added on the opposite side to the first one.

Liquid-phase flow

To keep the liquid flow smooth, the viscosity of the liquid phase should be sufficiently low. From the test experiment, it was found necessary to heat the liquid phase to $>60°C$. Further, the liquid phase at the entrance of the tower should be heated to the temperature of the tower so as not to change the separating conditions, because a cold liquid phase lowered the temperature. The stainless-steel wire net at the top of the tower was confirmed to work as a distributor and a uniform flow of the liquid phase resulted.

Optimization of operating conditions

The gas-phase flow-rates were within the range 63.7–139.2 l/h. Above 100 l/h, poor trapping efficiency resulted. The liquid flow-rates were from 0.195 to 0.376 l/h, which were determined from the gas flow-rates and G/L values. The experiments

were carried out at tower temperatures of 140 and 150°C. Three sample feed rates were chosen for the different liquid flow-rates: 7.2 ml/h at a liquid flow-rate of 0.195 l/h, 12.0 ml/h at 0.294 l/h and 14.1 ml/h at 0.376 l/h. Each feed rate was determined by considering a safer running and was lower than the calculated maximum feed rate.

The optimum operating conditions at 150°C were studied by changing the gas flow-rates. At around $G/L = 383$, 93% *trans* form and 89% *cis* form were obtained. The difference between the actual and theoretical optimum G/L values was about 18%. It was assumed that the actual temperature was 3–4°C lower than the measured temperature. The optimum operating conditions at 140°C were also studied by changing the gas flow-rates. At $G/L = 460$, 97.5% *trans* form and 98.8% *cis* form were obtained. At 140°C, the difference between actual and theoretical optimum G/L was about 7.7%. The same reason for the difference was assumed, but it became smaller. The partition coefficient at 150°C was small and therefore the consumption of gas phase could be small. However, higher purities of products were obtained at 140°C than at 150°C. The separation factor seemed more effective.

Separation of decahydronaphthalene stereoisomers

The mixture of *trans*- and *cis*-decahydronaphthalene (1:1, w/w) was separated by long-term operation under the optimum conditions. For more than 15 h, steady results of >95% purity for both isomers were achieved.

CONCLUSIONS

For preparative purposes, a scaled-up CCGLC system was constructed and the optimum operating conditions were investigated. Separation of a decahydronaphthalene stereoisomer mixture was attempted and 97.5% pure *trans* form from the top and 98.8% pure *cis* form from the bottom of the separating tower at 140°C were achieved. The purity of the *cis* form in the eluate from the bottom of the tower (98.8%) was much improved compared with the result (92.1%) in the previous study [1].

REFERENCE

1 K. Watabe, H. Kanda, K. Sato and T. Hobo, *J. Chromatogr.*, 590 (1992) 289.

Journal of Chromatography, 629 (1993) 297–307
Elsevier Science Publishers B.V., Amsterdam

CHROM. 24 641

Gas chromatographic analysis of alkanolamine solutions using capillary and packed columns

Olukayode Fatai Dawodu and Axel Meisen

Department of Chemical Engineering, University of British Columbia, 2216 Main Mall, Vancouver, BC V6T 1Z4 (Canada)

(First received May 8th, 1992; revised manuscript received September 18th, 1992)

ABSTRACT

The detailed analysis of amine solutions used in natural gas treatment is usually based on gas chromatographic (GC) methods which utilize columns packed with Tenax GC or TA, a porous polymer based on 2,6-diphenyl-*p*-phenylene oxide. This technique has the advantages of the ability to separate the various compounds in solution, minimum sample preparation and short analysis times. Advances in chromatography have shown the general superiority of capillary columns for the analysis of complex solutions. Unfortunately, Tenax is available only in packed columns. This paper presents the results of GC analyses of fresh and partially degraded alkanolamine solutions in which the Tenax column was replaced with a polyethylene glycol-based fused-silica, wide-bore capillary column (15 m × 0.53 mm I.D., 1.0-μm film thickness). It was found that the capillary column provides better peak shape, requires significantly less sample size, maintains higher sensitivity and offers a faster and more efficient separation than the Tenax packed columns.

INTRODUCTION

Alkanolamines are commonly used to remove impurities such as CO_2, H_2S, COS and CS_2 from natural, refinery and other industrial gases in reversible absorption–desorption processes. However, irreversible or degradation reactions sometimes occur, resulting in the formation of undesirable degradation compounds. As the degradation compounds build up in solution, the concentration of the functional amines is reduced, thus limiting the absorption capacity of the process. The degradation compounds may also contribute to other problems such as corrosion [1–3], foaming [4–6] and fouling [7]. Therefore, routine analyses of plant solutions are conducted to determine the state of the plant solution and to take remedial actions for ensuring the desired plant efficiency.

Early attempts to analyse partially degraded amine solutions used methods such as potentiometric titration [8], acid titration and Kjedahl total nitrogen determination [4,9], fractional distillation and crystallization [10]. These methods were generally unsuccessful owing to a lack of reproducibility, inability to separate degradation compounds, decomposition of amines and degradation compounds at elevated temperatures and long analysis times. Derivatization has been tried as a means of making the amines more volatile, less polar and consequently more amenable to gas chromatographic (GC) analysis [11–13]. Although fairly successful, GC analysis of derivatized degraded amine solutions suffers some drawbacks which were outlined by Saha *et al.* [14]. As a result, the latter group developed a direct GC technique using a column packed with Tenax GC, a porous polymer based on 2,6-diphenyl-phenylene oxide developed by Van Wijk [15]. This column successfully separated a mixture of monoethanolamine (MEA), diethanolamine (DEA) and triethanolamine (TEA) in about 8 min. The use of the Tenax GC column was subsequently extended to the analysis of partially de-

Correspondence to: A. Meisen, Department of Chemical Engineering, University of British Columbia, 2216 Main Mall, Vancouver, BC V6T 1Z4, Canada.

0021-9673/93/$06.00

graded alkanolamine solutions and the detailed analytical conditions have been reported [16–18]. Other studies involving the analysis of fresh and partially degraded alkanolamine solutions using Tenax columns in combination with other columns [19,20] have also been reported. Recently, Tenax TA has replaced Tenax GC. The former is claimed to offer better tolerance to impurities, thereby limiting the number of minute peaks on the chromatogram.

Advances in GC have shown the general superiority of capillary columns for the analysis of complex solutions. Unfortunately, Tenax is available only in packed columns. This paper presents comparisons between polar capillary, semi-polar capillary and packed columns. The results show that the polar polyethylene glycol-based, wide-bore, fused-silica, bonded-phase capillary column performs better than the semi-polar capillary or the Tenax packed column in the analysis of fresh and partially degraded alkanolamine solutions.

EXPERIMENTAL

GC adaptation

A Hewlett-Packard HP 5830A gas chromatograph which is configured for packed columns was adapted for capillary columns by installing appropriate adaptors in the injection and detector ports. The adaptors consisted of a glass injection port liner and connectors which converted the 1/4- and 1/8-in. (1 in. = 2.54 cm) injection and detector ports respectively, to the dimensions of the capillary column. They also provided a means of adding make-up carrier gas.

Chromatographic columns

Analyses of fresh and degraded alkanolamine solutions were performed by using the following four columns under the conditions listed in Table I:

(1) Tenax TA packed column (9 ft. × 1/8 in. I.D.; 1 ft. = 30.48 cm); purchased from Supelco, Oakville, Canada);

(2) Supelcowax 10, a polyethylene glycol-based, fused-silica, cross-linked, bonded-phase capillary column (15 m × 0.53 mm I.D., 1.0-μm film thickness; purchased from Supelco);

(3) DB-Wax, a polyethylene glycol-based, fused-silica, cross-linked, bonded-phase capillary column (15 m × 0.53 mm I.D., 1.0 -μm film thickness; purchased from Chromatographic Specialities, Brockville, Canada).

(4) HP-17, a 50% phenyl–methyl-polysiloxane-based, cross-linked capillary column (10 m × 0.53 mm I.D., 2.0-μm film thickness; purchased from Hewlett-Packard, Avondale, PA, USA).

Detector sensitivity

Owing to their small diameters, capillary columns are characterized by low carrier gas flow-rates

TABLE I

OPERATING CONDITIONS FOR GC ANALYSIS

Parameter	Tenax TA	Supelcowax 10	DB-Wax	HP-17
Injection temperature (°C)	300	280	300	300
Detector (flame ionization) temperature (°C)	300	280	300	300
Oven temperature programme:				
Initial (°C)	150	125	125	125
Isothermal (min)	0.5	0.5	0.5	0.5
Rate (°C/min)	8.0	8.0	8.0	8.0
Final (°C)	300	275	230	280
Maximum (°C)[a]	350	280	230	280
Sample size (μl)	1.0	0.2	0.2	0.2
Nitrogen flow-rate:				
Column (ml/min)	23.0	8.0	8.0	8.0
Make-up (ml/min)	0.0	30.0	30.0	30.0

[a] Maximum temperature for column conditioning.

(< 10 ml/min), which increase the number of separation units per unit column length, and hence the separation efficiency, compared with packed columns. For flame ionization detectors at high sensitivity, the nitrogen, hydrogen and air flow-rate ratios are *ca.* 1:1:30. Thus, at typical air flow-rates of 300 ml/min, a nitrogen flow-rate of about 30 ml/min is required. To achieve this, it is necessary to add 25–30 ml/min of nitrogen (carrier gas) as make-up to the carrier flow leaving the capillary column.

Column conditioning

Prior to use, the capillary columns were conditioned by temperature-programmed heating at 2°C/min in the GC oven while maintaining a constant carrier gas flow-rate of *ca.* 10 ml/min, for about 16 h. For factory-preconditioned columns, only a short cure of 2–3 h was necessary. To avoid damage to the active material in the column, the highest temperature used during conditioning did not exceed the maximum temperature listed for the column (see Table I).

Amine solutions

Analyses were conducted on mixtures of alkanolamines and samples of partially degraded alkanolamine solutions obtained from the laboratory and a gas plant. The alkanolamines numbered 1–9 in Table II and those in Table III are commercially available, and were purchased from Aldrich (Milwaukee, WI, USA). Others such as hydroxyethyloxazolidone (HEOD), hydroxyethylimidazolidone (HEI), tris(hydroxyethyl)ethylenediamine (THEED) and bis(hydroxyethyl)imidazolidone (BHEI), were synthesized following previously described procedures [18]. Some of the mixtures used were prepared by adding known masses of alkanolamines to volumetric flasks and diluting to volume. When the primary objective was to demonstrate the abilities of the columns to separate the amines, the individual concentrations of the amines were not determined.

RESULTS AND DISCUSSION

The performances of the aforementioned columns can be compared in terms of retention time, peak shape, sensitivity limit, sample size, elution order, reproducibility, durability, calibration and cost.

Retention time

The retention times in Table II show that the capillary columns elute the compounds faster than the Tenax column. The differences in retention times range from 2.5 to over 10 min. Although the shorter

TABLE II

RETENTION TIMES OF ALKANOLAMINES IN VARIOUS COLUMNS USING THE OPERATING CONDITIONS IN TABLE I

Peak No.	Compound	Retention time (min)[a]			
		Tenax TA	Supelcowax 10	DB-Wax	HP-17
1	Monoethanolamine (MEA)	3.69	1.09	1.18	0.32
2	Aminomethylpropanol (AMP)	5.13	1.15	1.31	0.37
3	Diglycolamine (DGA)	8.78	3.09	3.73	0.98
4	Hydroxyethylpiperizine (HEP)	12.82	4.97	5.68	2.46
5	Methyldiethanolamine (MDEA)	10.53	5.02	5.76	1.56
6	Diisopropanolamine (DIPA)	11.27	5.24	5.97	2.00
7	Diethanolamine (DEA)	10.83	6.77	7.54	1.94
8	Bis(hydroxyethyl)piperazine (BHEP)	16.86	10.76	11.49	6.14
9	Bis(hydroxyethyl)ethylenediamine (BHEED)	16.04	11.71	12.63	5.65
10	Hydroxyethyloxazolidone (HEOD)	17.78	13.92	14.83	7.17
11	Hydroxyethylimidazolidone (HEI)	19.34	15.34	18.59	8.43
12	Tris(hydroxyethyl)ethylenediamine (THEED)	21.00	17.00	24.39	10.02
13	Bis(hydroxyethyl)imidazolidone (BHEI)	22.94	18.20	30.68	11.42

[a] Retention times may vary by up to 5%, depending on the age of the column and the concentrations of the compounds.

and less polar HP-17 column was able to elute the compounds faster than the polyethylene glycol columns, column bleeding commenced at about 200°C and was very significant above 240°C. This caused poor separation of the degradation compounds with high boiling points. The greater film thickness in the HP-17 column may have contributed to the significant bleeding observed. More generally, it appears that successful analysis of partially degraded alkanolamine solutions requires highly polar columns. It is also noted that for the non-volatile degradation compounds, the retention times in the DB-Wax column are greater than those in the Supelcowax 10 and Tenax TA columns. The reason for this is the lower temperature limit of the DB-Wax column (230°C) as opposed to 280°C and 350°C for the Supelcowax 10 and Tenax TA columns, respectively. The higher temperature limit of the Supelcowax 10 column may be due to a different bonding procedure used for the DB-Wax column. This property, plus the fact that both columns contain the same active material and cost approximately the same, make the former a more suitable choice for the analysis of partially degraded alkanolamine solutions. Further comparisons of column performances were therefore limited to the Tenax TA packed column and the Supelcowax 10 capillary column.

Peak shape

Figs. 1–6 show three sets of typical chromatograms of aqueous alkanolamine mixtures obtained using the Tenax TA and Supelcowax 10 columns. In both instances, the capillary column produced sharper peaks and better baseline separation. Lower temperature programming may eliminate the peak shouldering observed with the Tenax column, but will require longer analysis times. As will be shown later, the degree of shouldering observed does not seem to affect the reproducibility.

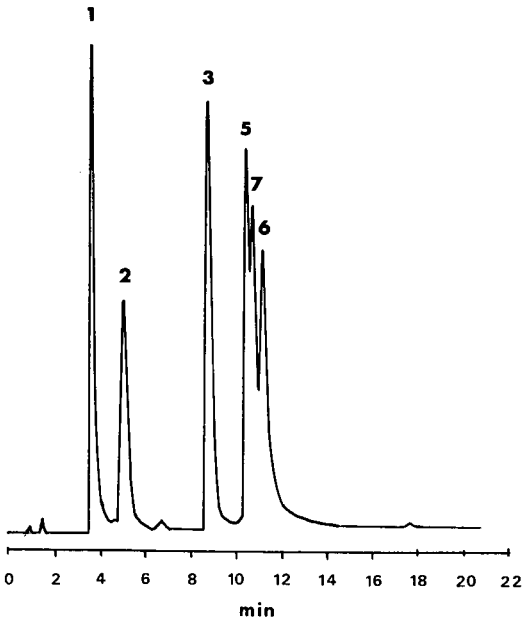

Fig. 1. Chromatogram showing the separation of a mixture of alkanolamines using the Tenax TA packed column. Peak numbers as in Table II.

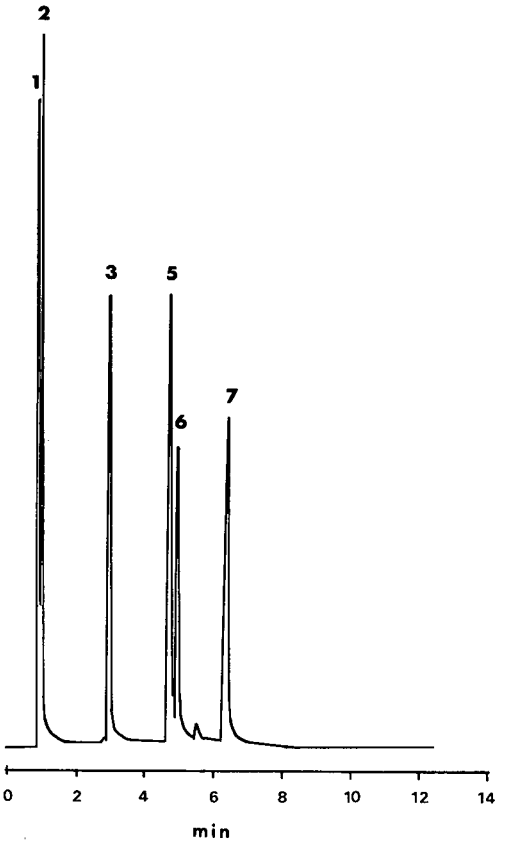

Fig. 2. Chromatogram showing the separation of a mixture of alkanolamines using the Supelcowax 10 capillary column. Peak numbers as in Table II.

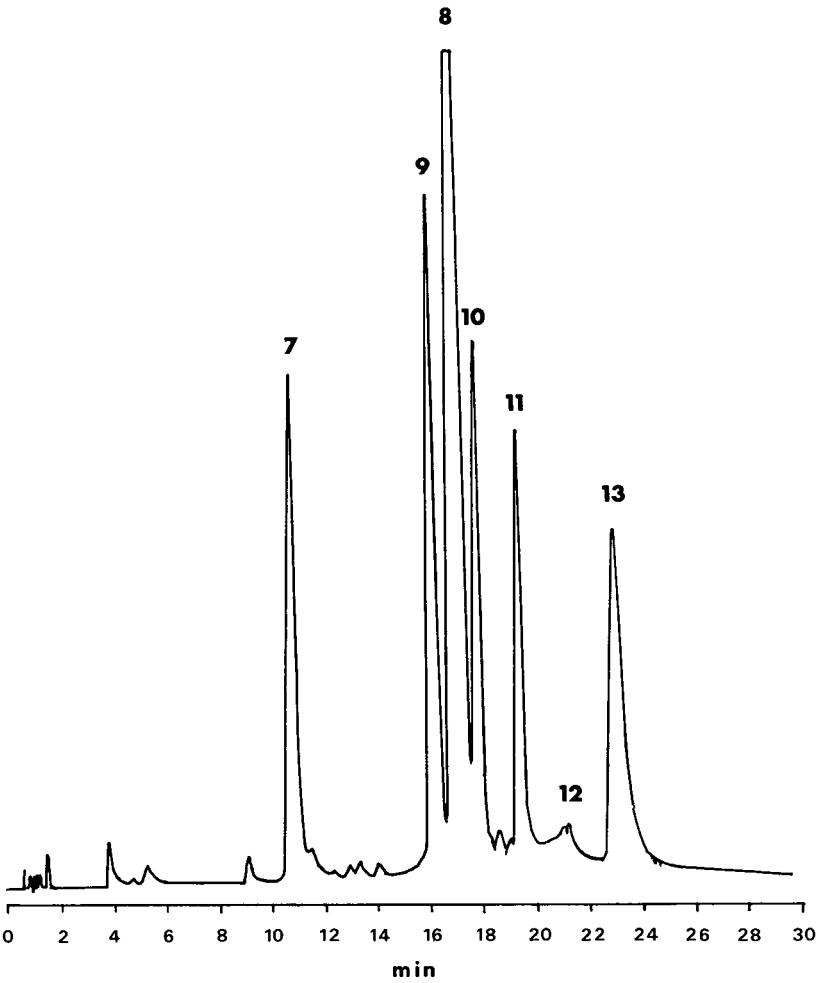

Fig. 3. Chromatogram showing the separation of a mixture of DEA and degradation compounds using the Tenax TA packed column. Peak numbers as in Table II.

Sample size

Capillary columns generally require smaller samples than packed columns. In the present instance, 0.2-μl samples were injected into the capillary columns as opposed to the 1 μl typically used for the Tenax TA column; no decrease in of sensitivity resulted. A further advantage of the Supelcowax 10 column is its ability to handle larger sample volumes typical of packed columns, while still maintaining the high separation efficiency of capillary columns (see Figs. 7 and 8). The syringe used for sample injection was fitted with a Chaney adapter that ensured reproducible sample volumes in all instances.

Sensitivity limits

To establish the sensitivity limits, and aqueous solution containing nine alkanolamines at concentrations ranging from 0.01 to 0.05 mol/l (see Table VI) was analysed with the Tenax TA and Supelcowax 10 columns. As shown in Figs. 7 and 8, the Tenax column did not produce peaks for MEA and BHEED whereas the Supelcowax 10 column only failed to separate the latter. Further, the Supelcowax 10 column separated the remaining eight compounds, unlike the Tenax TA column, which could not separate DEA from MDEA or BHEP from HEOD. As degradation compounds usually occur

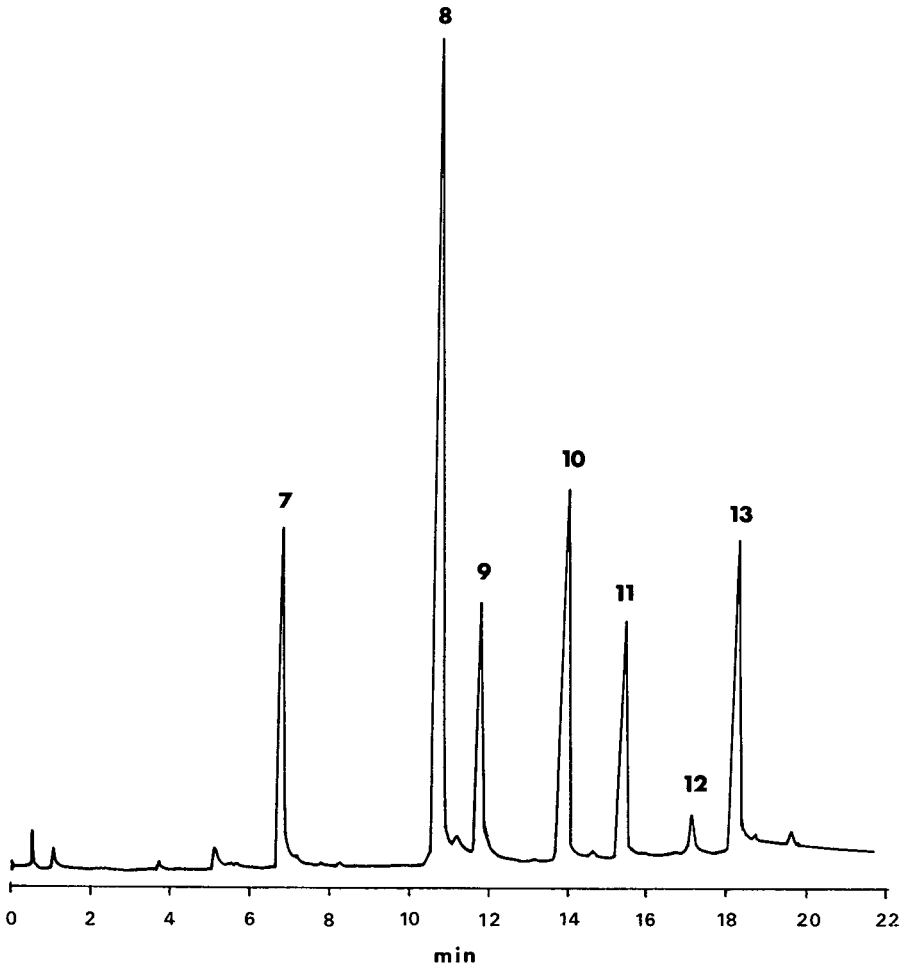

Fig. 4. Chromatogram showing the separation of a mixture of DEA and degradation compounds using the Supelcowax 10 capillary column. Peak numbers as in Table II.

in low concentrations, the higher sensitivity exhibited by the Supelcowax 10 column is a significant advantage over the Tenax TA column. The ability to separate DEA from MDEA also makes the Supelcowax 10 column better suited for detailed analyses of blended solutions of MDEA and DEA. The inability of the Tenax column to separate as efficiently as the Supelcowax 10 column may be due to a net loss of sample, which probably arises from column adsorption.

It is noteworthy that all the peaks eluted had corresponding integrated areas which indicated that these compounds can be determiend at the reported levels by using the appropriate calibration graphs. The regression equations for the present calibration graphs are not provided because they vary from one laboratory to another and depend on factors such as age of column and mode of sample injection. However, the calibration method used in this work is described later.

Elution order

The retention times listed in Table II indicate that the order of elution with the Tenax TA column differs from that with the capillary columns. To highlight this difference, the retention times of mono-

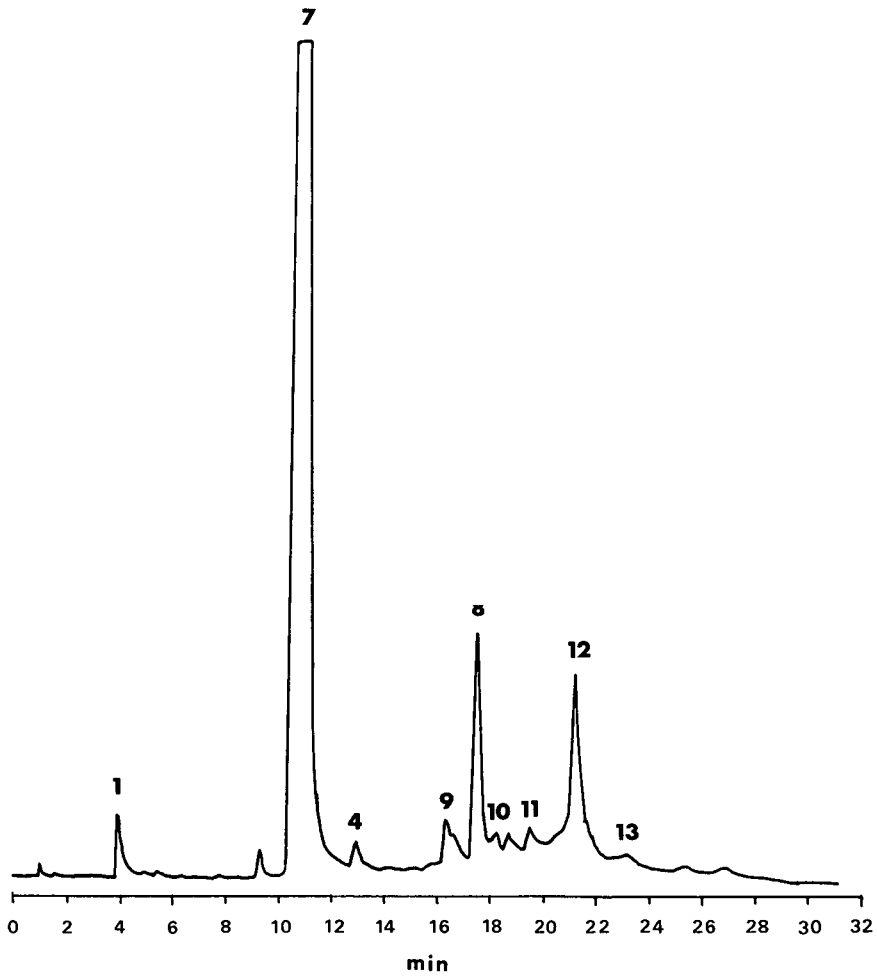

Fig. 5. Chromatogram showing the separation of an industrial DEA solution using the Tenax TA packed column. Peak numbers as in Table II.

ethanolamine, diethanolamine and their alkyl derivatives using Supelcowax 10 and Tenax columns were individually determined using the pure compounds, and are listed in Table III together with pertinent physical properties. For the Supelcowax 10 column the elution order appears to be based on boiling point, which, in turn, is influenced by the degree of hydrogen bonding of the compounds. Thus, the alkyl derivatives with higher relative molecular masses but lower boiling points are eluted before the base compounds. Conversely, the Tenax TA column shows an elution order based more on relative molecular mass than boiling point. The degree of column adsorption may also have influenced the elution order. As the capillary column contained a thin film of active material, few or no adsorption problems arose. In contrast, the mode of separation in the Tenax column is based on adsorption on the porous polymer followed by diffusion into the carrier stream. The rate of the latter determines the retention time and is influenced by molecular size, boiling point and the strength of the adsorption between the compound and the column material. The absence of significant adsorption in the Supelcowax 10 column may also be responsible for its higher sensitivity over the Tenax TA column.

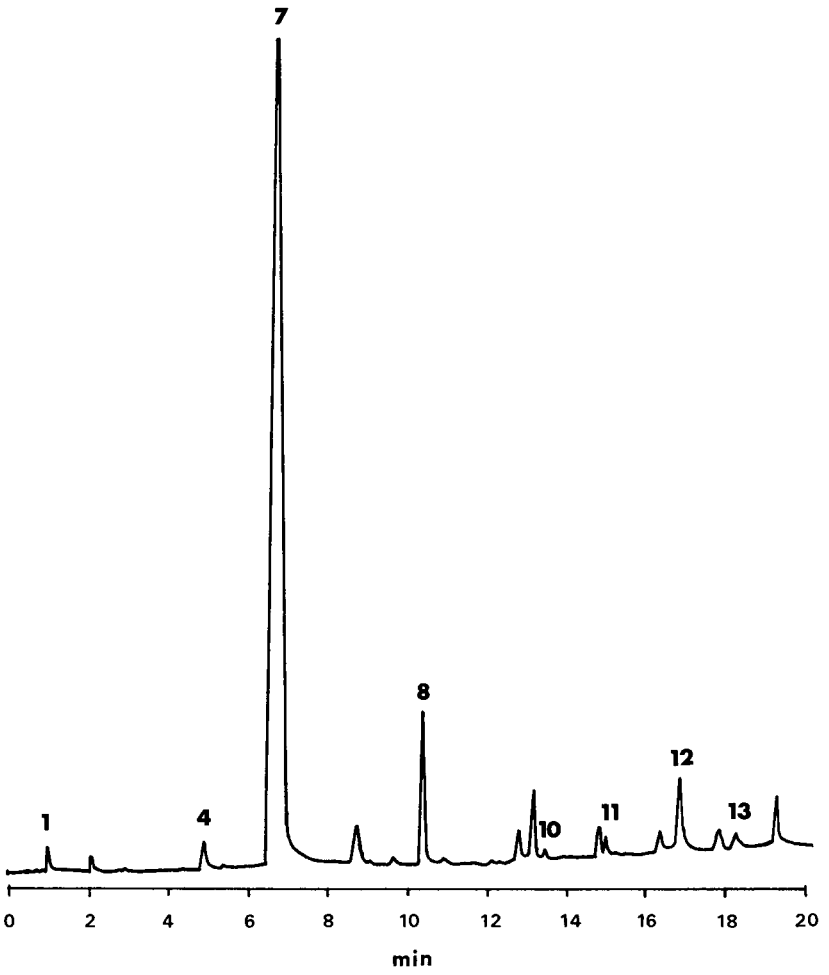

Fig. 6. Chromatogram showing the separation of an industrial DEA solution using the Supelcowax 10 capillary column. Peak numbers as in Table II.

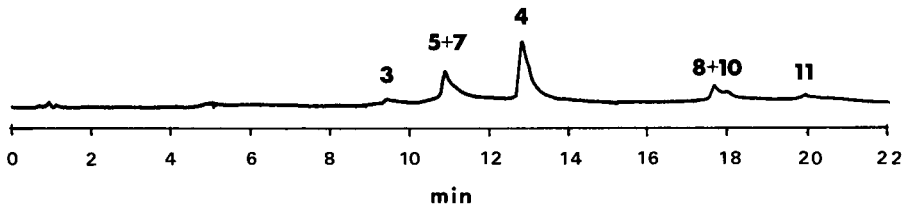

Fig. 7. Chromatogram showing the separation of 0.01–0.05 mol/l of alkanolamines using the Tenax TA column. Sample volume = 1 μl. Peak numbers as in Table II.

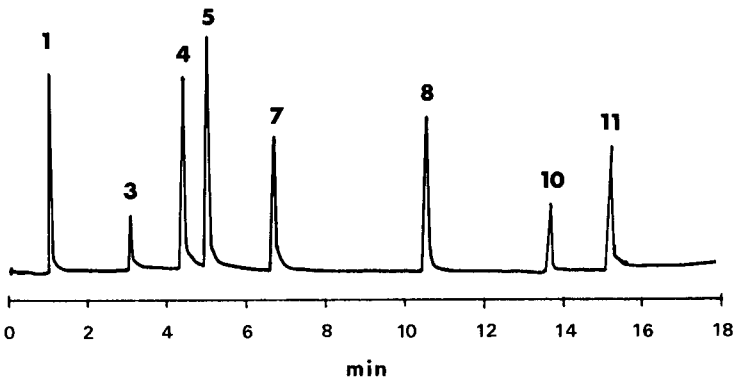

Fig. 8. Chromatogram showing the separation of 0.01–0.05 mol/l of alkanolamines using the Supelcowax 10 capillary column. Sample volume = 1 μl. Peak numbers as in Table II.

Reproducibility

In order to compare the reproducibility of analysis, three solutions were analysed using both columns. Solution 1 was arbitrarily mixed without particular attention to the concentrations of the alkanolamines. Solution 3 was a 1:4 dilution of solution 2. The standard deviation for each compound was determined from the concentration values obtained in four consecutive analyses performed on the same mixture. The only exception was solution 1, where the standard deviations were based on the integrated peak areas. Typical chromatograms for solutions 1 and 3 are shown in Figs. 3 and 4 and Figs. 7 and 8, respectively. The results in Tables IV–VI indicate that at high concentrations (Table IV) the reproducibilities of analyses with the Tenax and Supelcowax 10 columns are comparable, except for the ethylenediamines (BHEED and THEED), where the Supelcowax 10 column was superior. At lower concentrations (Tables V and VI), the degradation compounds (HEP, BHEED, BHEP, HEOD and HEI) showed better reprodubility with the Supelcowax 10 than the Tenax column. The Supelcowax 10 column is thus more reliable for the determination of low concentrations of degradation compounds.

Durability

Laboratory experience has shown that the Tenax column could be used for extended analyses over 4–6 months without any appreciable change in re-

TABLE III

ELUTION ORDER WITH SUPELCOWAX 10 AND TENAX TA COLUMNS USING THE OPERATING CONDITIONS IN TABLE I

Compound	M_r	Density (g/cm^3)	B.p. (°C)	Elution order	
				Supelcowax 10	Tenax TA
Monoethanolamine	61	1.012	70	4	1
Methylaminoethanol	75	0.935	159	2	2
Dimethylaminoethanol	89	0.887	139	1	3
Ethylaminoethanol	89	0.914	169–170	3	4
Diethanolamine	105	1.097	217/150 mmHg[a]	7	6
Methyldiethanolamine	119	1.038	246–248	5	5
Ethyldiethanolamine	133	1.014	246–252	6	7

[a] 1 mmHg = 133.322 Pa.

TABLE IV

REPRODUCIBILITY OF ANALYSIS BASED ON STANDARD DEVIATIONS (SOLUTION 1) (n = 4)

Compound	Deviation (%)[a]	
	Tenax TA	Supelcowax 10
DEA	5.19	6.25
BHEED	11.33	4.95
BHEP	1.09	2.78
HEOD	5.62	3.75
HEI	3.42	4.90
THEED	20.94	7.10
BHEI	6.83	5.10

[a] Deviation (%) = 100 (standard deviation/mean area).

tention times and separation efficiency [16–18]. Judging from the reproducibility of retention times and separation efficiency within the 2 months duration of its use, the Supelcowax 10 column appears to be as durable as the Tenax TA column. However, a more objective assessment of durability will require subjecting both columns to analyses of the same solutions over the same length of time and observing the changes in retention times and separation efficiency. It should be noted that the Supelcowax 10 column is fragile and can easily be inactivated through oxidation of the polyethylene glycol film. To prevent this occurrence, the column ends should be flame sealed when in storage or a constant flow of carrier gas must be maintained whenever the column is installed in the GC system.

TABLE V

REPRODUCIBILITY OF ANALYSIS BASED ON STANDARD DEVIATIONS (SOLUTION 2) (n = 4)

Compound	Concentration (mol/l)	Standard deviation (mol/l)	
		Tenax TA	Supelcowax 10
MEA	0.206	0.008	0.014
DGA	0.128	0.007	0.015
HEP	0.116	0.010	0.005
MDEA	0.111	0.015	0.005
DEA	0.148	0.009	0.009
BHEED	0.072	0.008	0.005
BHEP	0.057	0.003	0.002
HEOD	0.066	0.006	0.002
HEI	0.130	0.017	0.006

TABLE VI

REPRODUCIBILITY OF ANALYSIS BASED ON STANDARD DEVIATIONS (SOLUTION 3) (n = 4)

Compound	Concentration (mol/l)	Standard deviation (mol/l)	
		Tenax TA	Supelcowax 10
MEA	0.052	Not detected	0.013
DGA	0.032	0.016	0.013
HEP	0.029	0.002	0.003
MDEA	0.028	0.016[a]	0.001
DEA	0.037		0.004
BHEED	0.018	Not detected	Not detected
BHEP	0.014	0.007[b]	0.001
HEOD	0.017		0.002
HEI	0.033	0.011	0.004

[a] Value reported is for MDEA and DEA eluted as one peak.
[b] Value reported is for BHEP and HEOD eluted as one peak.

Calibration

The Supelcowax 10 column can be used for quantitative analysis just like the Tenax column. This involves the preparation of calibration graphs obtained from plots of peak area *versus* concentration for standard solutions. The calibration graphs are subsequently used to determine the concentrations corresponding to the peak areas resulting from the analysis of partially degraded alkanolamine solutions generated in the laboratory and industrially. Such graphs prepared with the Supelcowax 10 column for 0–3.2 M MEA, 0–5 M DEA and MDEA and 0–0.5 M degradation compounds such as HEOD, BHEP and HEI were linear.

Cost

The 15-m Supelcowax 10 capillary column is about 2.5 times more expensive than the 2.7-m Tenax TA column. The conversion kit necessary to use the capillary column in a GC system configured for packed columns is an additional cost. However, as the conversion kit makes it possible to carry out both capillary and packed column analyses, this advantage far outweighs the initial cost of the conversion kit. Further, the superior analyses offered by the capillary column should compensate for its higher cost.

The durability of the Supelcowax 10 column under extended analysis still needs to be firmly established. This may, in the long run, have a bearing on cost comparisons.

CONCLUSIONS

It has been shown that Supelcowax 10, a capillary column lined with polyethylene glycol, can be used in place of a Tenax packed column for the GC analysis of fresh and partially degraded alkanolamine solutions. The analytical conditions that permit good resolution of mixtures of amines have been established, although a lower initial temperature and/or temperature programme may suffice when analysing close-boiling amines. The capillary column provides better peak shape, maintains higher sensitivity, requires less samples and offers a faster and more efficient separation than the Tenax packed column. The higher sensitivity combined with the generally better reproducibility of analysis make the Supelcowax 10 capillary column more reliable than the Tenax column in the determination of low concentrations of degradation compounds. This work thus extends the use of capillary columns to the GC analysis of fresh and partially degraded alkanolamine solutions encountered in the clean-up of natural, refinery and other industrial gases.

ACKNOWLEDGEMENT

Financial assistance by the Natural Sciences and Engineering Research Council is gratefully acknowledged.

REFERENCES

1 K. L. Moore, *Corrosion*, 16 (1960) 111.
2 W. D. Hall and J. G. Barron, in *Proceedings of the 31st Annual Gas Conditioning Conference, Norman, OK, March 2–4, 1981*, p. c1.
3 A. Chakma and A. Meisen, *Ind. Eng. Chem., Prod. Res. Dev.*, 25 (1986) 627.
4 A. L. Kohl and F. C. Riesenfeld, *Gas Purification*, 4th edition, Gulf Publishing, Houston, TX, 4th ed., 1985.
5 R. C. Pauley and R. Hashema, in *Proceedings of the 39th Annual Gas Conditioning Conference, Norman, OK, March 6–8, 1989*, p. 219.
6 R. F. Smith, and A. H. Younger, *Hydrocarbon Process*, 51 (1972) 98.
7 A. Chakma and A. Meisen, *Can. J. Chem. Eng.*, 65 (1987) 264.
8 M. S. Henry and M. Grennert, *Pet. Refiner*, 34 (1955) 177.
9 *Gas Conditioning Fact Book*, Dow Chemical, Midland, MI, 1962.
10 L. D. Polderman and A. B. Steele, *Oil Gas J.*, 54 (1956) 206.
11 L. E. Brydia and H. E. Persinger, *Anal. Chem.*, 39 (1967) 1318.
12 R. Piekos, K. Kobyiczyk and J. Grzybowski, *Anal. Chem.*, 47 (1975) 1157.
13 E. T. Choy and A. Meisen, *J. Chromatogr.*, 187 (1980) 145.
14 N. C. Saha, S. K. Jan and R. K. Dua, *Chromatographia*, 10 (1977) 368.
15 R. van Wijk, *J. Chromatogr. Sci.*, 8 (1970) 418.
16 M. L. Kennard and A. Meisen, *J. Chromatogr.*, 267 (1983) 373.
17 A. Chakma and A. Meisen, *J. Chromatogr.*, 457 (1988) 287.
18 O. F. Dawodu and A. Meisen, *J. Chromatogr.*, 587 (1991) 237.
19 C. J. Kim and G. Sartori, *Int. J. Chem. Kinet.*, 16 (1984) 1257.
20 G. D. Robbins and J. A. Bullin, *Energy Prog.*, 4 (1984) 229.

Journal of Chromatography, 629 (1993) 309–320
Elsevier Science Publishers B.V., Amsterdam

CHROM. 24 633

Analysis of multi-component mixtures by high-resolution capillary gas chromatography and combined gas chromatography–mass spectrometry

II. Trace aromatics in an *n*-alkane matrix

E. Matisová

Department of Analytical Chemistry, Faculty of Chemical Technology, Slovak Technical University, Radlinského 9, 812 37 Bratislava (Czechoslovakia)

Š. Vodný

Department of Textile, Cellulose and Paper, Faculty of Chemical Technology, Slovak Technical University, Radlinského 9, 812 37 Bratislava (Czechoslovakia)

S. Škrabáková and M. Onderová

Department of Analytical Chemistry, Faculty of Chemical Technology, Slovak Technical University, Radlinského 9, 812 37 Bratislava (Czechoslovakia)

(First received May 6th, 1992; revised manuscript received July 30th, 1992)

ABSTRACT

The achievement of and problems with the trace analysis of multi-component mixtures are demonstrated on a complex organic mixture containing trace amounts of numerous aromatic substances in an *n*-alkane matrix with a boiling range of 151–270°C. Qualitative analysis of trace aromatics was performed, after a preseparation step, on a preconcentrated LC fraction by high-resolution capillary GC–MS with electron impact ionization from mass spectra, mass chromatograms using a single-column separation system (HP-PONA column) and splitless injection. With direct injection of the sample and selected-ion monitoring of aromatics there were problems with interferences from ions of the matrix. 185 aromatic compounds belonging to various aromatic groups (mainly alkylbenzenes, indanes, tetralins, naphthalenes and acenaphthenes) were identified at concentrations of individual aromatics in the range 10^{-3}–10^{-6}%.

INTRODUCTION

In a previous paper [1] we demonstrated the achievement of and problems with the qualitative analysis of multi-component mixtures for a complex hydrocarbon sample. We have shown the possibilities of using single-column capillary GC (with a commercially available, chemically bonded, non-polar silicone capillary column) for the detailed analysis of aromatic hydrocarbons in a petroleum fraction with a boiling range of 150–350°C, which is the raw material for the production of *n*-alkanes. The emphasis was placed on identification of aro-

Correspondence to: E. Matisová, NSERC–AES, Industrial Research, Chair in Atmospheric Chemistry, York University, 4700 Keele Street, North York, Ontario M3J 1P3, Canada (present address until September 1993).

0021-9673/93/$06.00

matics with a boiling range of 150–270°C. The concentration of the aromatics was approximately equal to that of the constituents of other hydrocarbon groups (alkanes, naphthenes). Single-column high-resolution capillary GC [2–4] and multi-dimensional GC systems fail in the separation aromatics from compounds of other hydrocarbon groups in complex mixtures with broad ranges of boiling points [5]. For highly complex samples, aromatics were analysed in the concentrate from a liquid chromatographic fraction. Capillary columns with non-polar silicone stationary phase were chosen for their good selectivity towards alkylbenzenes and good inter-laboratory reproducibility [6,7].

For better selectivity of non-polar silicones (compared with squalane), donor–acceptor interactions of the free electron pairs of oxygen and π-electrons of the aromatic ring [8] should be responsible. With squalane there are only dispersion forces. The characterization of individual aromatics (256) was based on a combination of isothermal retention data (on OV-101) and mass spectral data measured under optimized temperature-programmed (TPG) conditions using PONA fused-silica capillary columns, which are special-purpose cross-linked methylsilicone phase columns tailored for hydrocarbon analysis (alkanes, alkenes, naphthenes, aromatics). Mass spectral data for aromatic compounds can be unambiguously interpreted [9–11]. It was shown that a combination of GC–MS with electron impact (EI) ionization (mass chromatography, mass fragmentography) is a great help in distinguishing various groups of compounds eluting in one peak [1,12].

This part of the work was intended to show the possibilities and difficulties of the analysis of aromatics in multi-component mixtures at trace concentrations. During the preparation of *n*-alkanes from the raw material [1], small amounts of aromatics pass into the final product. As aromatics are potential carcinogens, the quality of *n*-alkanes, utilized as the raw materials in various other technologies, depends also on the composition and content of aromatics.

For trace analysis it was necessary to take into consideration the nature and concentration of the compounds being analysed and the nature of the sample matrix in deciding whether a preseparation and/or preconcentration step was needed and in choosing the correct system for sample introduction, separation and detection [13–17]. In this paper stress is laid on qualitative analysis. With respect to the appropriate sample amounts for GC (for identification purposes), coupling with mass spectrometry (GC–MS) is the best choice of coupled techniques.

EXPERIMENTAL

Gas chromatography was performed with a Model 5890A Series II gas chromatograph equipped with split–splitless injection, flame ionization detection (FID), a Model 3396A integrator and Vectra Model ES/12 personal computer (Hewlett-Packard, Avondale, PA, USA). The analysis was carried out on a PONA fused-silica capillary column (Hewlett-Packard) with 0.5-μm film thickness (50 m × 0.2 mm I.D.). Hydrogen was used as carrier gas at a linear velocity of 40 cm/s for TPG conditions adjusted to the initial temperature of the temperature programme. In the split injection mode (1:70) the TPG conditions were from 70 to 160°C at 1.5°C/min, then to 220°C at 15°C/min and held for 15 min. With splitless injection the septum purge flow-rate was 2 ml/min and a flow of 49 ml/min passed the split outlet; the split valve was closed for 1.0 min during injection. Splitless injections (liner, 7.8 cm × 2 mm I.D.) were performed with the column at 35°C; this temperature was held for 1 min, then increased at 10°C/min to 70°C, at 1.5°C/min to 160°C and finally at 15°C/min to 220°C, which was held for 15 min. The injector and detector temperatures were 270 and 300°C, respectively.

GC–MS measurements with EI ionization (70 eV ionization energy) were performed on an HP Model 5890A gas chromatograph equipped with a split–splitless injection system and a Model 5970B mass-selective detector (MSD) (Hewlett-Packard) with a direct interface. All experimental work was done on a PONA column under the given TPG conditions with helium as the carrier gas at a linear velocity of 38 cm/s at the initial temperature of the temperature programme. The other instrumental conditions were as follows: in the total ion current (TIC) and SIM modes, detector temperature 275°C, electron multiplier voltage 2200 V and treshold 1000; in the TIC mode, scan speed 1.4 scans/s; in the SIM mode, scan speed 2.8 scans/s and dwell time 100 ms.

Trace aromatics were analysed in a C_9–C_{14} *n*-

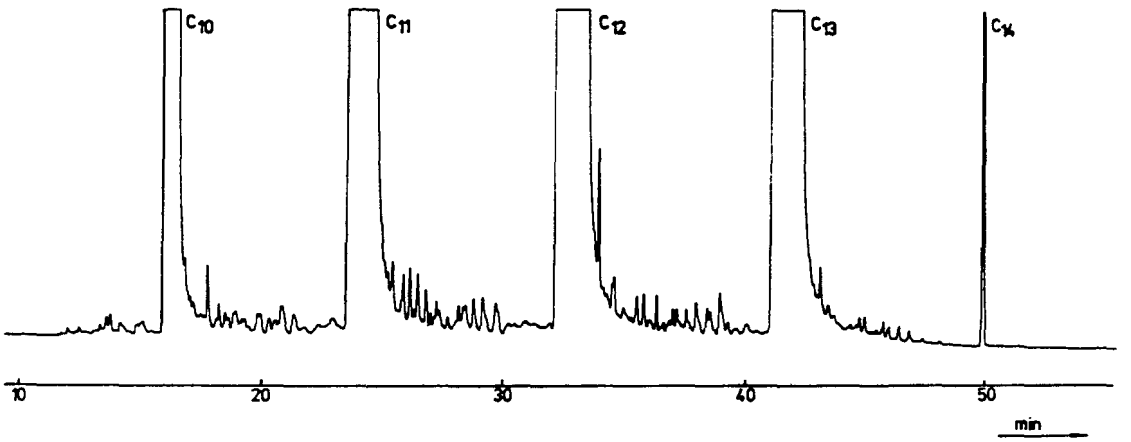

Fig. 1. Gas chromatogram of the light fraction of *n*-alkanes on an HP PONA column with temperature programming from 70°C at 1.5°C/min to 160°C; carrier gas, hydrogen at 40 cm/s; split injection (1:70); volume injected, 0.15 μl; detection FID.

alkane matrix with the following composition: C_9, 0.004%; C_{10}, 15.541%; C_{11}, 32.720%; C_{12}, 30.195%; C_{13}, 21.314%; and C_{14}, 0.031% (boiling range 151–270°C). Aromatics were isolated by column liquid chromatography on silica gel and preconcentrated in dichloromethane [18]. Isolated aromatic fractions in dichloromethane were injected (1 μl) with a 10-μl Hamilton syringe with a 0.8-μl plug of solvent using the hot needle injection technique. In direct injection of the final product of *n*-alkanes, 0.15–0.2 μl was injected with a 1-μl Hamilton syringe; the analytical column was connected with a retention gap (2 m × 0.53 mm I.D. fused-silica uncoated tubing) using a press-fit connector.

RESULTS

The study of the composition of trace aromatics in a complex *n*-alkane matrix by direct measurement of GC retention data is impossible. As an il-

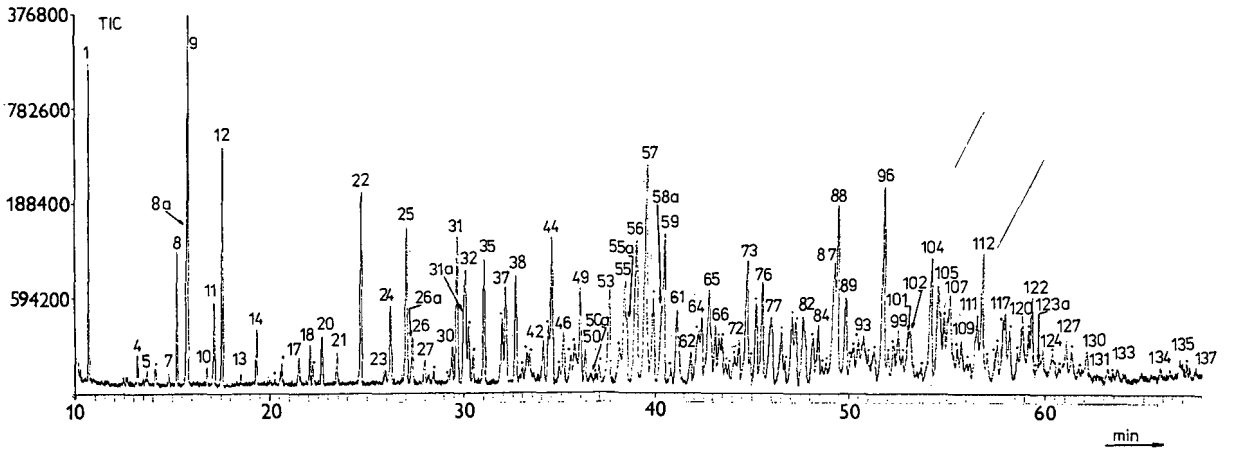

Fig. 2. TIC chromatogram of isolated trace aromatics in dichloromethane on an HP PONA fused-silica capillary column; carrier gas, helium at 38 cm/s; splitless injection; temperature programme, 35°C, held for 1 min, then increased at 10°C/min to 70°C, at 1.5°C/min to 160°C and at 15°C/min to 220°C, held for 15 min. Peak designation is given in Table I; peaks that are not included there come from the blind experiment on the isolation procedure [17].

lustration, the gas chromatogram of the light fraction of *n*-alkanes on a PONA column under TPG conditions with split injection is shown in Fig. 1.

To follow the qualitative distribution of aromatics from the raw material (a petroleum fraction) to the final product of *n*-alkanes, GC–EI-MS as a fundamental method was utilized. Qualitative analysis of trace aromatics was performed in two ways: after preseparation in the LC fraction, by GC–MS collecting mass spectra and mass chromatograms, and by the direct injection of the sample (without preseparation) by selected-ion monitoring (SIM). A single high-resolution column with immobilized polydimethylsilicone was used. The experimental conditions (splitless injection, TPG conditions) were optimized using FID.

Analysis of trace aromatics after preseparation from the matrix

For the detailed analysis of individual aromatics, it was necessary to collect mass spectra. From Fig. 1 it follows that owing to the overwhelming concentration of *n*-alkanes (a matrix consisting of 99.81% C_9–C_{14} *n*-alkanes plus a small amount of isoalkanes) there is co-elution with several aromatics, and with the use of splitless injection the co-elution

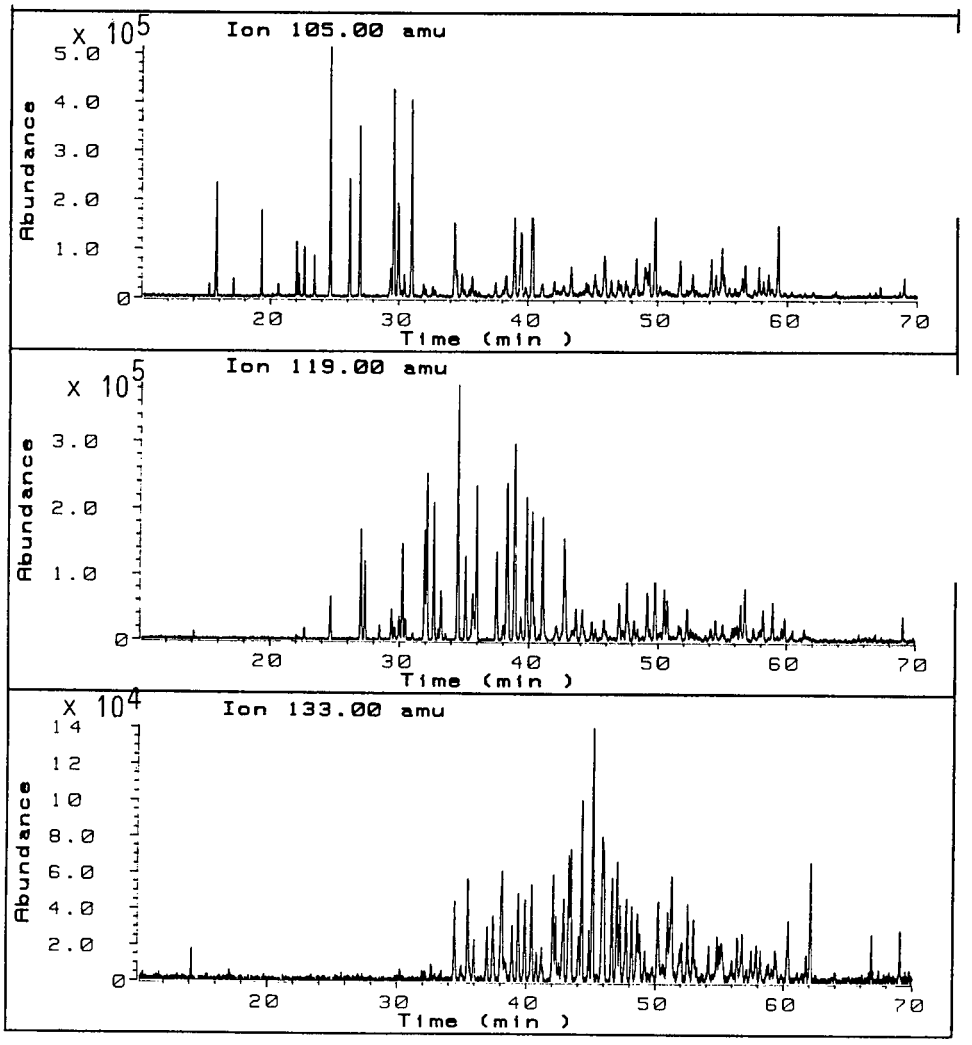

Fig. 3. Mass chromatograms of selected ions of alkylbenzenes of isolated trace aromatics. Experimental conditions as in Fig. 2.

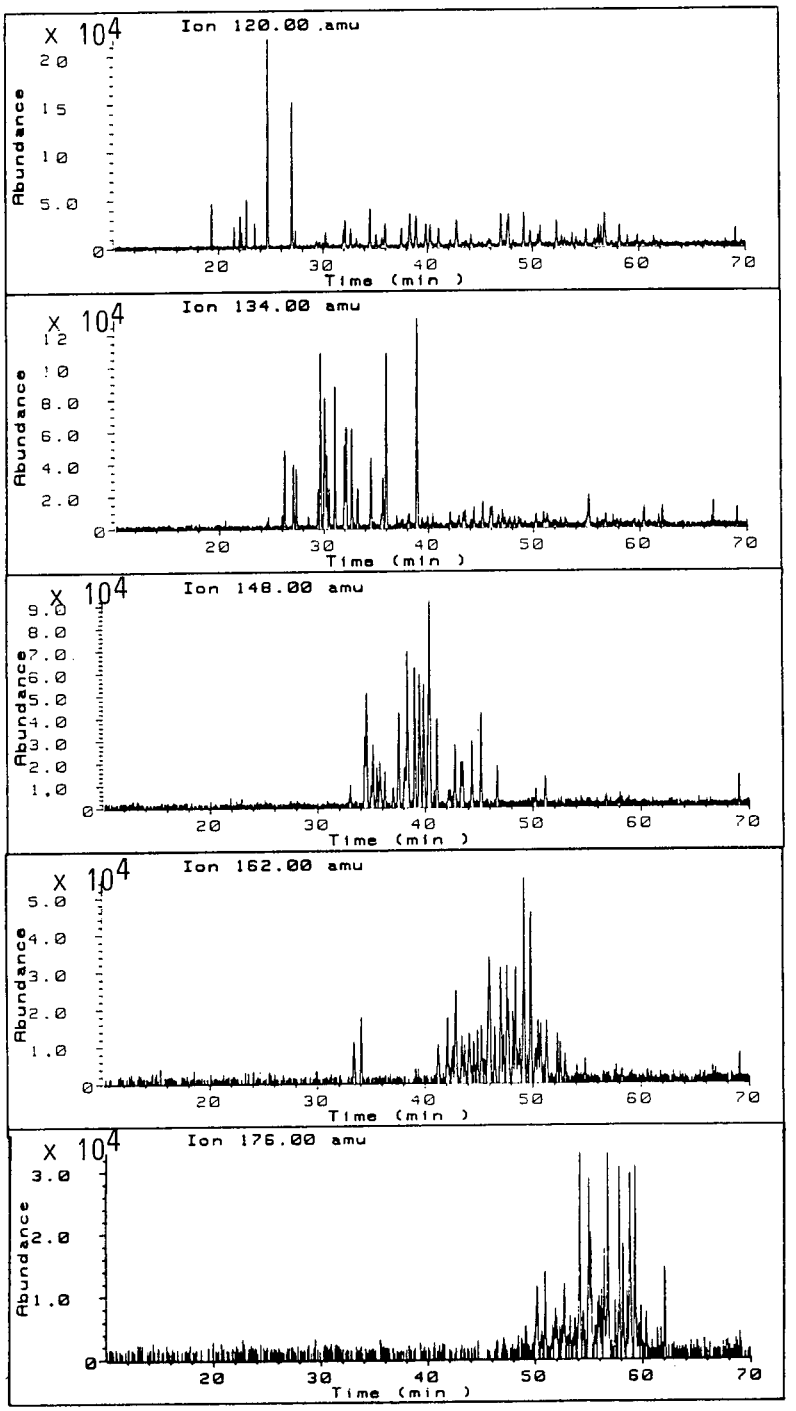

Fig. 4. Mass chromatograms of molecular ions of alkylbenzenes of isolated trace aromatics. Experimental conditions as in Fig. 2.

TABLE I

RESULTS OF ANALYSIS OF TRACE AROMATICS IN *n*-ALKANE MATRIX

Peak No.	Compound[a]	$\bar{X}$ (10^{-4}%)[b]	R.S.D. (%)
1	MeB	10.48	4.3
8	EtB	6.01	4.8
8a	1,3-DiMeB	5.34	5.1
9	1,4-DiMeB	16.61	4.8
10	C_8H_8 (styrene)	0.71	5.3
11	1,2-DiMeB	3.77	6.0
14	iPrB	4.28	6.7
17	nPrB	1.87	4.1
18	1-Et-3-MeB	3.29	4.9
19	1-Et-4-MeB	1.53	6.2
20	1,3,5-TriMeB	3.17	9.2
21	1-Et-2-MeB	1.82	5.7
22	1,2,4-TriMeB	17.00	10.0
23	tBuB	1.44	31.0[c]
24	sBuB	6.74	2.1
25	1,2,3-TriMeB + 1-Me-3-iPrB	15.04	5.5
26	1-Me-4-iPrB	3.50	4.9
27	Indane C_9	1.89	6.5
28	1-Me-2-iPrB	8.19	6.8
29	1-Me-3-nPrB	0.49	26.3[d]
30	1,3-DiEtB	2.89	6.4
31	1-Me-4-nPrB	11.11	5.4
31a	1,4-DiEtB	5.00	5.2
32	nBuB	10.02	6.6
33	1,3-DiMe-5-EtB	4.43	6.5
34	1,2-DiEtB	2.42	7.1
35	1-Me-2-nPrB	9.92	5.3
36	1,4-DiMe-2-EtB	4.91	5.4
37	1,3-DiMe-4-EtB	8.48	5.1
38	1,2-DiMe-4-EtB + indane C_{10}	9.47	7.4
39	1-Et-PrB	1.29	12.1[c]
40	1,3-DiMe-2-EtB	2.35	7.0
43	1-Et-3-iPrB	4.78	3.5
44	1-Me-3-sBuB + 1,2-DiMe-3-EtB	14.52	4.9
45	1-Et-2-iPrB	1.25	4.1
46	1-Me-4-sBuB	3.82	4.7
47	1,3-DiMe-5-iPrB	2.27	4.7
48	1,2,4,5-TetraMeB + AB C_{11}	3.92	5.4
49	1,2,3,5-TetraMeB	8.21	4.7
50	iPeB	2.79	4.5
52	1,4-DiMe-2-iPrB	1.21	6.1
53	1-Et-3-nPrB	9.91	5.8
54	1,2-DiMe-4-iPrB	2.56	7.5
55	1,3-DiMe-5-nPrB	16.77	5.2
55a	Me-indane		
56	1,2,3,4-TetraMeB + AB C_{11}	11.02	5.5
57	1,4-DiEt-2-MeB + tetralin C_{10}	16.98	5.1
58	1,4-DiMe-2-nPrB	10.06	10.9
59	1-Me-2-nBuB	13.65	4.4
60	1,3-DiEt-2-MeB	0.81	11.2[c]
61	DiMe-nPrB + Naph + AB C_{12}	8.06	4.3
62	DiMe-indane C_{11} + AB C_{12}	2.96	3.6

TABLE I *(continued)*

Peak No.	Compound[a]	$\bar{X}$ (10^{-4}%)[b]	R.S.D. (%)
63	DiMe-indane C_{11}	7.14	3.3
64	DiMe-indane C_{11}	7.06	3.0
65	1,2-DiMe-3-nPrB + DiMe-indane C_{11}	11.75	4.8
66	DiMe-indane C_{11}	9.13	4.6[d]
67	1,2,5-TriMe-3-EtB + indane C_{12}	9.63	18.8[d]
68	1,3,5-TriMe-2-EtB + AB C_{12}		
69	1-Et-4-sBuB	2.51	31.7[d]
70	Indane C_{12}		
71	DiMe-sBuB	3.26	6.3
72	1,2,3-TriMe-5-EtB	3.88	5.3
73	Me-tetralin C_{11}	12.13	5.0
74	1,3-DiMe-4-sBuB	4.49	10.4
75	1,2,4-TriMe-3-EtB	5.81	5.2
76	Indane C_{11}	10.79	4.9
77	1,3-Di-nPrB	9.14	6.4
78	AB C_{12} + indane C_{11}	4.77	6.4
79	1,2,3-TriMe-4-EtB	1.79	7.0
80	1,2,4-TriEtB	11.88	4.5
81	1-Me-3-nPeB + indane C_{11}		
82	1-Et-4-nBuB + indane C_{12}	6.97	4.5
83	1,2,3-TriEtB + indane C_{12}	2.48	4.9
84	1-Me-2-nPeB	4.84	5.0
85	AB C_{12}	1.53	5.1
86	AB C_{12} + AB C_{13}	1.95	3.8
87	AB C_{12}	27.83	5.6
88	Indane C_{11}		
89	AB C_{12}	9.57	5.5
90	AB C_{13} + indane C_{12}	1.36	9.9
91	AB C_{12} + AB C_{13}	3.64	8.2
92	AB C_{12} + indane C_{12}	4.93	7.0
93	AB C_{12} + indane C_{12}	5.73	6.0
94	AB C_{13}	3.53	9.4
95	AB C_{12}	3.61	7.6
96	Indane C_{11} + MeNaph	22.10	5.4
97	AB C_{13} + indane C_{12}	3.29	7.4
98	AB C_{12} + AB C_{13} + indane C_{12}	4.81	6.0
99	AB C_{13} + AB C_{12} + indane C_{12}	3.55	31.5[e]
100	AB C_{13} + indane C_{12}	2.72	8.0
101	AB C_{13} + indane C_{12}	9.01	5.6
102	Indane C_{12} + MeNaph		
103	AB C_{13} + indane C_{13}	0.83	9.4[c]
104	AB C_{13}	15.76	3.9
105	Indane C_{12}	9.81	6.6
106	Indane C_{12}	7.29	7.6
107	AB C_{13} + indane C_{12}	3.99	10.3
108	Indane C_{12}	1.22	15.0[d]
109	Indene C_{12}	2.03	9.6
110	AB C_{13}	1.23	13.4[e]
111	AB C_{13} + indane C_{12} + indane C_{13}	6.80	5.6
112	AB C_{13} + indane C_{12}	7.40	5.6[d]
113	Indane C_{12} + indane C_{13}	7.52	17.0[e]
114	AB C_{13} + indane C_{12} + indane C_{13}	4.10	11.4[e]
115	Indane C_{12}		

(Continued on p. 316)

TABLE I *(continued)*

Peak No.	Compound[a]	$\overline{X}$ (10^{-4}%)[b]	R.S.D. (%)
116	AB C_{13}	9.74	7.0
117	Indane C_{12}		
118	AB C_{13}	3.35	11.8[d]
119	AB C_{13} + indane C_{13}	3.11	15.4[d]
120	AB C_{13}	5.72	7.6
121	AB C_{14} + biphenyl	2.92	10.6[d]
122	AB C_{13} + indane C_{12}	4.80	10.1
123	AB C_{14} + indane C_{13}	0.99	17.9[d]
124	Indane C_{13} + AB C_{13} + AB C_{14}	1.42	20.6[c,d]
125	AB C_{13} + AB C_{14} + indane C_{13}	3.49	20.7[d]
126	AB C_{14} + indane C_{13}	1.00	23.8[d]
127	Indane C_{12} + Naph C_{12} + MeAcen	2.66	11.7[c]
128	Indane C_{12} + indane C_{13}	1.93	15.7[c]
129	AB C_{13} + AB C_{14}	0.69	30.0[d]
130	AB C_{13} + DiMeNaph	1.64	16.1[e]
131	Naph C_{12}	1.01	10.3[c]
132	AB C_{14} + Naph C_{12}	0.60	11.5[c]
133	Indane C_{12} + indane C_{13} + MeAcen	0.38	11.8[c]
134	AB C_{14} + indane C_{13}	0.23	12.6[c]
135	AB C_{14}	1.22	10.4[c]
136	AB C_{14}	0.32	11.8[c]
137	AB C_{15} + indane C_{13} + MeAcen	0.43	12.9[c]

[a] Abbreviations: Me = methyl; Et = ethyl; Pr = propyl; Bu = butyl; Pe = pentyl; B = benzene; AB = alkylbenzene; Naph = naphthalene; Acen = acenaphthene; n = normal; i = iso-; s = sec.-; t = *tert.*-.

[b] $\overline{X}$ (%) = mean value of aromatics content from four GC determinations (n = 4) in mass%.

[c] Small peaks.

[d] Poorly resolved peaks.

[e] Pair of compounds which in some analyses were integrated as individual peaks and in other analyses were integrated as one peak.

is much more apparent. Therefore, a preseparation step was used [18]. Aromatics were isolated from the matrix by column LC on silica gel. The recovery of components across the complete boiling point range was greater if preconcentration of the dichloromethane fraction was performed by distillation rather than vacuum evaporation. Recoveries for the whole procedure were thoroughly studied using a model mixture and were found to be 80.67% within the confidence interval $L_{1,2}$ (R) ± 8.26% at a significance level of 95% (α = 0.05).

The TIC chromatogram of aromatics in concentrated form (LC fraction) is given in Fig. 2. Identification using the combined technique was based on information obtained from interpretation of the acquired mass spectra and mass chromatograms of selected ions of characteristic aromatic groups found in the mixture (alkylbenzenes, indanes/tetralins, indenes, naphthalenes and acenaphthenes/biphenyls); examples for alkylbenzenes, the most frequently occurring compounds in the multi-component mixture studied, are given in Figs. 3 and 4.

The acquired mass spectra and mass chromatograms of the molecular ions of trace aromatics made possible the determination of the molecular mass and carbon numbers of the individual components and/or the type and number of substituents. In many instances mixed mass spectra were obtained and from the mass chromatograms of selected ions it was possible to confirm the number or the type of compounds eluted in one peak. The data obtained for trace aromatics in the *n*-alkane matrix (Table I) were compared with those published in Part I (aromatics in a petroleum fraction at percentage concentrations) [1]. The concentration of individual aromatics in the light fraction of *n*-alkanes is included in Table I and was found to be in the range 10^{-3}–10^{-6}%, which corresponds to 10–10^{-2} ppm.

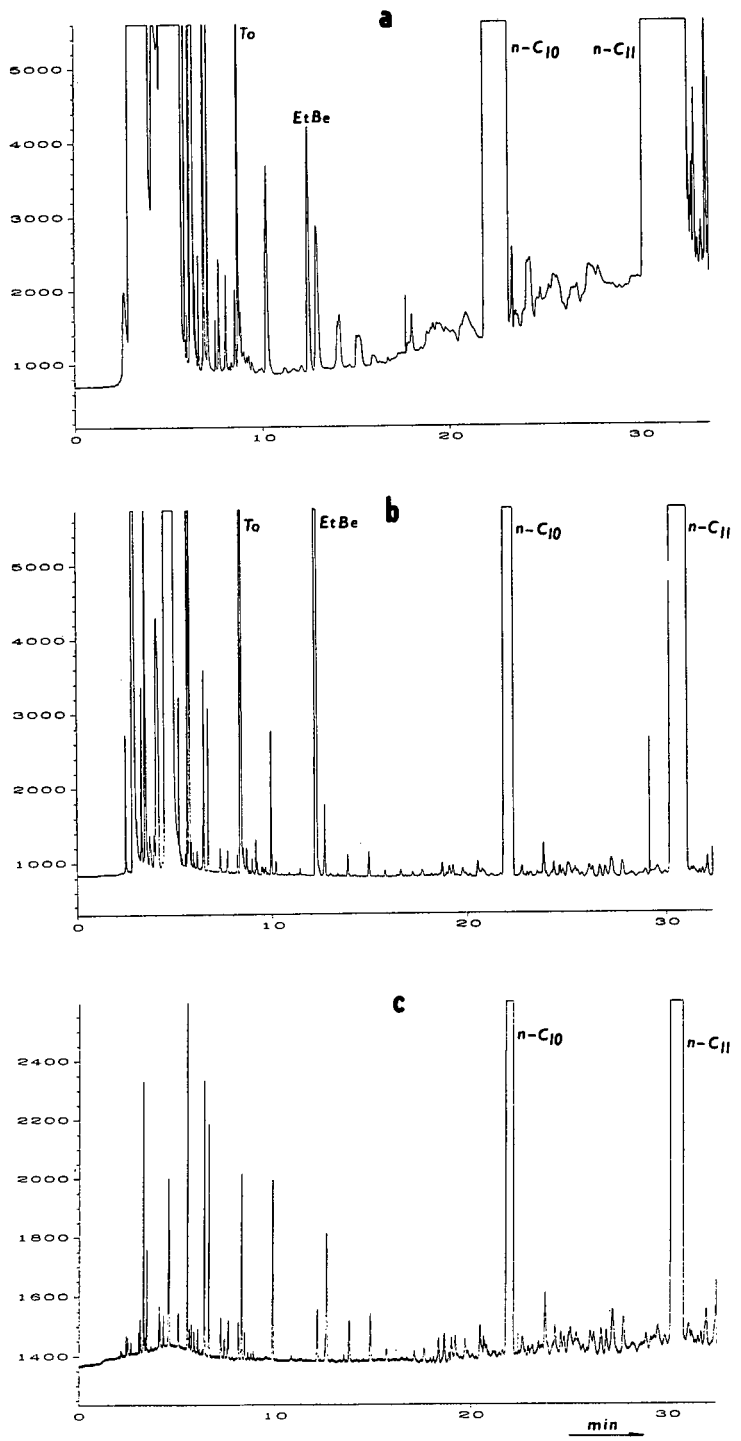

Fig. 5. Part of the chromatogram of the light fraction of *n*-alkanes on an HP PONA column under TGP conditions (as in Fig. 2) with hydrogen as carrier gas, splitless injection and FID. (a) Volume of sample injected 0.2 μl [with 10 ppm standard addition of toluene (To) and ethylbenzene (EtBe)] and $CHCl_3$ 0.8 μl; (b) same conditions as in (a) with a precolumn (2 m × 0.53 mm I.D. uncoated fused-silica tubing); and (c) same conditions as in (b) without standard additions in the sample and without any solvent.

We have discussed the reproducibility of the GC determination of individual trace aromatics and the overall aromatic content (including the isolation procedure) in a recent paper [18]. It can be concluded that most aromatics (within the given boiling point range) passed from the raw material into the *n*-alkane final product in about the same mutual relative abundance.

Direct analysis of trace aromatics in an n-alkane matrix by SIM

To establish the distribution of aromatics from the raw material to the final product of *n*-alkanes, we tried to apply SIM for two reasons: aromatics in the raw material were known [1] and to overcome the tedious preseparation step. The aim of SIM is not to obtain detailed data on the individual aromatics, but rather group-type information, carbon number. After the direct injection of the sample with splitless injection we encountered chromatographic problems (peak broadening; peak splitting) and problems with interferences from ions from the matrix.

The first question to be solved was peak broadening and peak splitting after direct sample injection. To improve the peak shape by utilizing the solvent effect we injected the sample (with standard addition of toluene and ethylbenzene to follow the effect) with a solvent. By trial and error we tested several solvents (dichloromethane, pentane, hexane, chloroform, benzene), various solvent combinations and optimized parameters of splitless injection [19], but without succes. On analysing aromatics in dichloromethane after the preseparation step there were no problems with peak shape when using splitless injection (Figs. 2–4). With direct injection the matrix of the sample (*n*-alkanes) gave problems in achieving good solvent effect for aromatic compounds. The best results were obtained with chloroform; a gas chromatogram obtained with FID is shown in Fig. 5a, although also in this instance the results were not sufficient for further GC–MS measurements. From the results obtained it can be concluded that it was difficult to find a solvent that fulfils the demands concerning its boiling point and

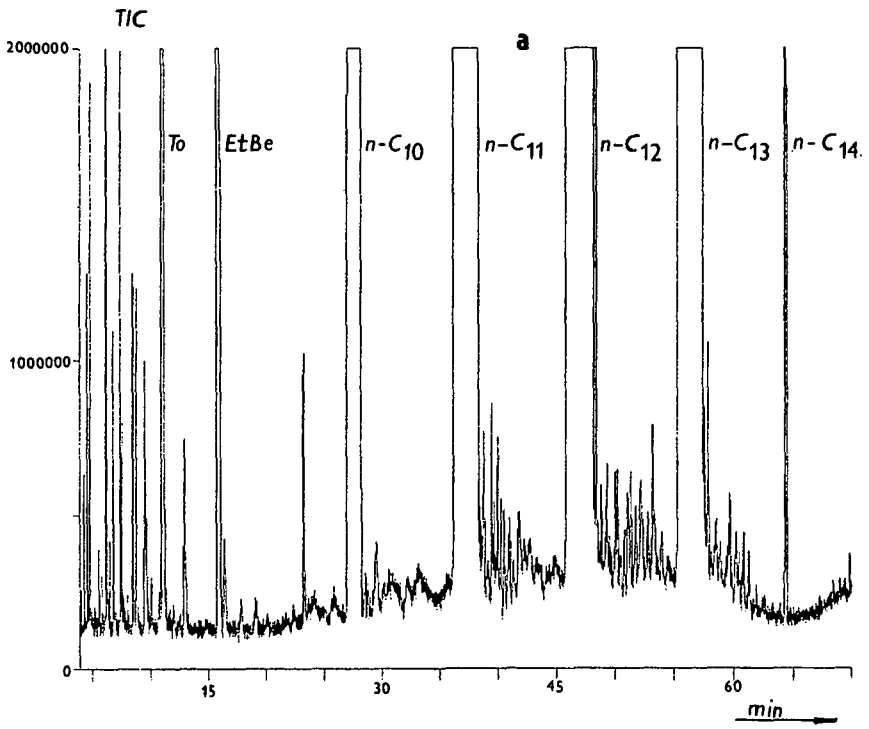

Fig. 6.

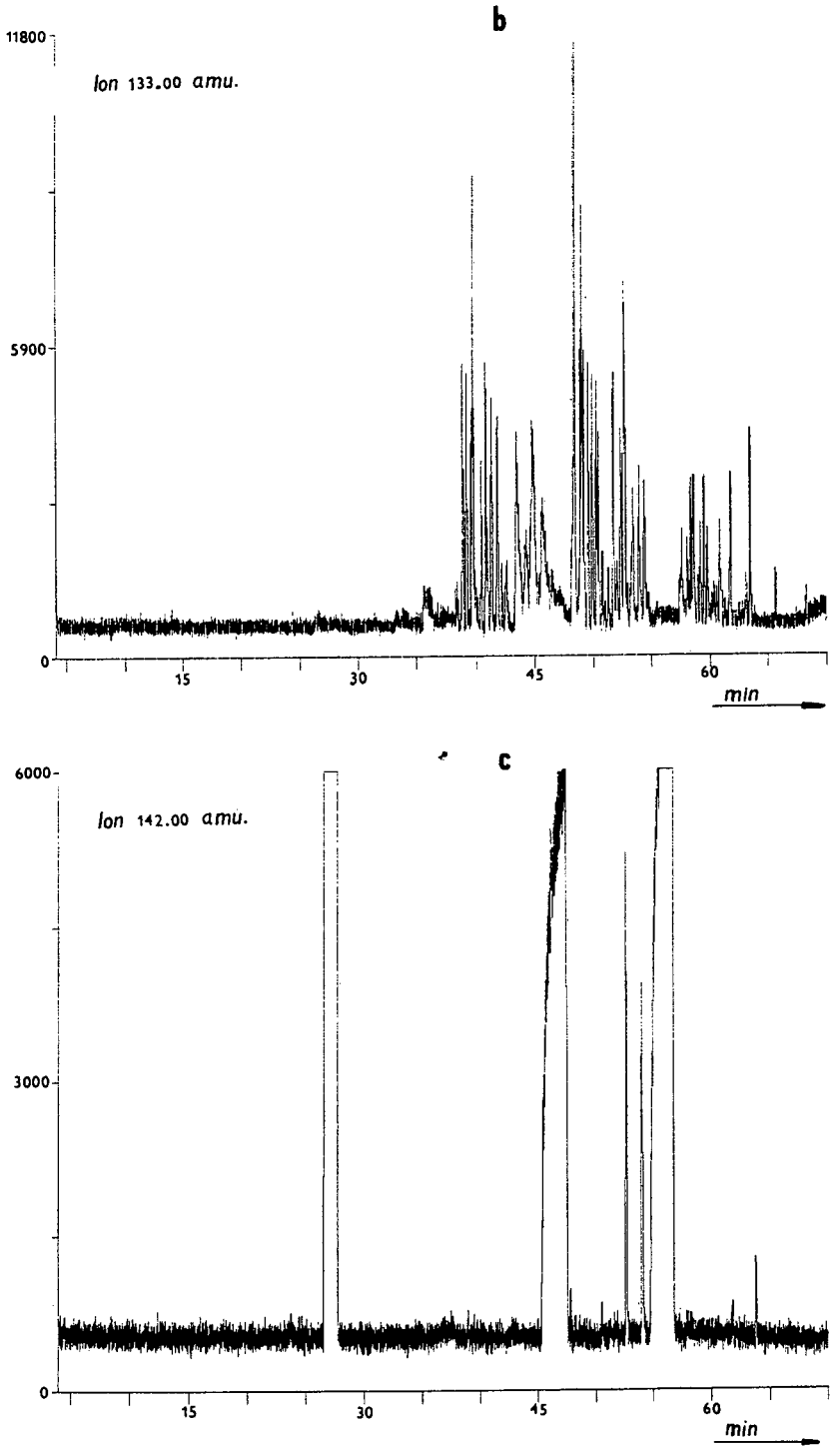

Fig. 6. GC–MS of the light fraction of *n*-alkanes by direct injection of the sample with the retention gap. Other experimental conditions as in Fig. 2. (a) TIC chromatogram with standard addition of toluene (To) and ethylbenzene (EtBe); (b) SIM of alkylbenzenes (ion of *m/z* 133); (c) SIM of naphthalenes (ion of *m/z* 142).

its polarity towards the analyte compounds, stationary phase and sample matrix. Band broadening in space can be suppressed by stationary phase focusing via a retention gap [20,21]. All the solutes that are spread over the flooded zone are carried on to the stationary phase where they are retained. In our case, after connection of the analytical column (using a press-fit connector) with a precolumn, all the problems were solved; good peaks shape were obtained with co-injection of the sample with any solvent (Fig. 5b) or without a solvent (Fig. 5c).

The second problem we encountered with SIM was interferences from ions from the matrix. Although *n*-alkanes show completely different characteristic ions to aromatics, a thorough study of the mass spectra of compounds of the matrix showed that there are small ions which at very high concentrations of matrix compounds are monitored in addition to specific ions of aromatic compounds at trace concentrations (*e.g.*, naphthalenes, indenes). Another problem was disturbances to the monitoring trace ions of aromatics during the elution of matrix compounds (alkylbenzenes, indanes/tetralins, acenaphthenes/biphenyls). Examples are given in Fig. 6.

CONCLUSIONS

In the analysis of multi-component organic mixtures with components present in trace concentrations in a complex sample matrix, the application of a single-column separation system with splitless injection of trace components by capillary GC and GC–EI-MS was useful. A preseparation step was found to be necessary.

For trace aromatics (in the range 10^{-3}–10^{-6}% by mass) in an *n*-alkane matrix (99.81% C_9–C_{14}) plus a small amount of isoalkanes, it was shown that the identification of individual aromatics is necessary after a preseparation step [18] for several reasons. Several aromatics are co-eluted with *n*-alkanes. Although we used a very efficient system (PONA columns under optimized conditions), it was insufficient to resolve complex mixtures. Group-type characterization according to classes of aromatic compounds (alkylbenzenes, indanes/tetralins, indenes, naphthalenes and acenaphthenes/biphenyls) by direct injection of the sample and SIM was not possible, although chromatographic problems (peak splitting, peak broadening) were solved, as there were serious problems with interferences from ions from the matrix. 185 individual C_7–C_{15} aromatics were characterized (from mass spectra and mass chromatogram) in the concentrate from the LC fraction.

REFERENCES

1 E. Matisová, E. Jurányiová, P. Kuráň, E. Brandšteterová, A. Kočan and Š. Holotík, *J. Chromatogr.*, 552 (1991) 301.
2 B. Kumar, R. K. Kuchhal, P. Kumar and P. L. Gupta, *J. Chromatogr. Sci.*, 24 (1986) 99.
3 C. L. Stuckey, *J. Chromatogr. Sci.*, 7 (1969) 177.
4 E. Matisová, J. Krupčík, P. Čellár and A. Kočan, *J. Chromatogr.*, 346 (1985) 17.
5 E. Matisová, *J. High Resolut. Chromatogr.*, 15 (1992) 213.
6 E. Matisová, *J. Chromatogr.*, 438 (1988) 131.
7 E. Matisová and P. Kuráň, *Chromatographia*, 30 (1990) 328.
8 J. Krupčík and P. Sandra, in preparation.
9 I. M. Whittemore, in K. H. Altgelt and T. H. Gouw (Editors), *Chromatography in Petroleum Analysis*, Marcel Dekker, New York, 1979, pp. 41–74.
10 F. W. McLafferty, *Interpretation of Mass Spectra*, University Science Books, Mill Valley, CA, 3rd ed., 1980, pp. 179–181.
11 M. E. Steward and E. W. Pitzer, *J. Chromatogr. Sci.*, 26 (1988) 218.
12 D. Rosenthal, *Anal. Chem.*, 54 (1982) 63.
13 D. H. McMahon, *J. Chromatogr. Sci.*, 23 (1985) 137.
14 R. P. Snell, J. W. Danielson and G. S. Oxborrow, *J. Chromatogr. Sci.*, 25 (1987) 225.
15 R. R. Freeman and M. A. Hayes, *J. Chromatogr. Sci.*, 26 (1988) 138.
16 J. V. Hinshaw, *J. Chromatogr. Sci.*, 26 (1988) 142.
17 J. Curvers, *Ph.D. Thesis*, Eindhoven Technical University, Eindhoven 1985.
18 E. Matisová, L. Kubuš and E. Jurányiová, *J. High Resolut. Chromatogr.*, 14 (1991) 713.
19 J. V. Hinshaw, *LC·GC*, 4 (1991) 18.
20 K. Grob, Jr., *J. Chromatogr.*, 213 (1981) 3.
21 K. Grob, Jr., *J. Chromatogr.*, 237 (1982) 15.

Journal of Chromatography, 629 (1993) 321–327
Elsevier Science Publishers B.V., Amsterdam

CHROM. 24 647

Determination of selected chlorinated benzenes in water by purging directly to a capillary column with whole column cryotrapping and electron-capture detection

Stewart A. Rounds* and James F. Pankow

Department of Environmental Science and Engineering, Oregon Graduate Institute, 19600 NW von Neumann Drive, Beaverton, OR 97006-1999 (USA)

(First received June 2nd, 1992; revised manuscript received September 24th, 1992)

ABSTRACT

The purge with whole column cryotrapping (P/WCC) method for the determination of volatile organic compounds (VOCs) in aqueous samples is adapted for use with an electron-capture detector. In this method, VOCs are stripped from an aqueous sample with an inert purge gas and transferred directly to the head of a capillary column for subsequent GC analysis. To prevent the column from plugging with ice during the purge step, and to reduce the chromatographic interference caused by the reaction of small amounts of water with thermal electrons in the detector, a glass-bead water trap is placed in-line between the purge vessel and the gas chromatograph. The water trap is constructed of a short length of 0.32 cm O.D. stainless-steel tubing filled with 0.5 mm diameter glass beads. By maintaining the trap at −10°C during the purge, most of the water can be removed from the purge gas. Transmission of the analytes to the column is then achieved with a subsequent, short purge of the trap at 25°C. The method was tested with the chlorinated benzenes. Despite their high molecular masses, the more chlorinated members of this group have large enough Henry's law constants that they *can* be determined with a purge technique. Experimental purging efficiencies were determined and compared to theoretical values. This method allows the simplicity and the high reliability of the P/WCC method to be combined with the exceptionally high sensitivity of an electron-capture detector.

INTRODUCTION

The EPA purge and trap (P&T) method [1,2] is the standard technique for the determination of volatile organic compounds (VOCs) in aqueous samples. In the P&T method, VOCs are stripped from the aqueous phase with an inert gas and transferred to a sorbent bed. Analytes trapped on the bed are then thermally desorbed to the column of a gas chromatograph for analysis. Recently, Pankow [3] and Pankow and Rosen [4] introduced the purge with whole column cryotrapping (P/WCC) method, in which analytes purged from the aqueous phase are transferred immediately to the head of a capillary GC column, eliminating the need for an intermediate sorbent trap. Due to its inherent simplicity, the P/WCC method offers a variety of advantages over conventional P&T [3,4], including improved detection of very volatile compounds, lower background contamination, shorter analysis times, and lower capital costs.

Due to the finite vapor pressure of water, a small amount of water is transferred to the GC column during the purge step of the P/WCC method. Applying the ideal gas law, 0.023 μl of water is expected to be removed from solution per ml of purge gas at 25°C. The presence of water in the purge

Correspondence to: J. F. Pankow, Department of Environmental Science and Engineering, Oregon Graduate Institute, 19600 NW von Neumann Drive, Beaverton, OR 97006-1999, USA.

* Present address: United States Geological Survey, Water Resources Division, 10615 S.E. Cherry Blossom Drive, Portland, OR 97216, USA.

0021-9673/93/$06.00

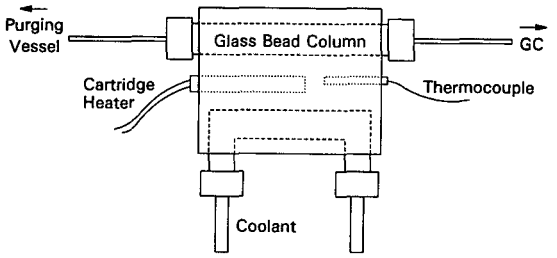

Fig. 1. The glass-bead water trap.

gas is a potential problem. Purging for long periods of time can transfer enough water that a small-bore capillary column held at cryotrapping temperature can become plugged with ice. Too much water on the column can cause chromatographic problems such as peak-splitting [4]. In addition, water can interfere with the response of some types of detectors. The electron-capture detector is particularly sensitive to trace amounts of water. Indeed, a few microliters of water passing through an electron-capture detector can produce a very large, asymmetrical peak that can completely obscure a portion of the chromatogram. In order to combine the simplicity and reliability of the P/WCC method with the selectivity and extreme sensitivity of the electron-capture detector, most of the water in the purge gas must be removed before it is allowed to reach the gas chromatograph.

Purge gas desiccation is commonly effected by forcing the gas to pass through a short length of polar tubing such as Nafion [5,6]. Transmission of analytes through Nafion tubing, however, has been found to be less than quantitative for some compounds, causing unacceptable memory effects [6,7]. Alternatively, a simple cold-zone, glass-bead water trap has been developed by Rosen [7] and Pankow [8]. A schematic of the glass-bead water trap is illustrated in Fig. 1. The water trap consists of a 6.5 cm length of 0.32 cm stainless-steel tubing packed with 0.5 mm diameter glass beads to provide a large, inert surface area. The trap is encased in an aluminum block whose temperature can be regulated with coolant or with a cartridge heater and thermocouple. In the first part of the purge (phase I), the water trap is held at a subambient temperature such as -10°C with a liquid coolant. Because the vapor pressure of ice at -10°C (260.4 Pa) is substantially lower than that of water at 25°C (3171.5 Pa), most of the water purged from solution will be retained in the cold trap. By rapidly raising the temperature of the trap to 25°C during the last minute or so of the purge (phase II), any analytes retained in the trap during phase I are quickly and efficiently removed and focussed on the GC column [8]. By minimizing the phase II purge time, the amount of water transferred to the column is minimized. The theoretical desiccation efficiency of the water trap has been discussed in detail by Pankow [8].

In this study, the P/WCC method is adapted for use with an electron-capture detector and tested with a set of chlorinated benzenes. Purge gas desiccation is effected with the glass-bead water trap. Theoretical purging efficiencies are calculated and compared to experimentally determined values.

THEORY

When a clean, inert gas is bubbled at a flow-rate F (ml/min) through a volume of water V_{s1} (ml) for a period of time t_1 (min), the removal of a volatile analyte from aqueous solution is given by [9]

$$\frac{c_1}{c_{1,0}} = \exp\left[-\left(\frac{H}{RT_1}\right)\frac{F}{V_{s1}}t_1\right] \quad (1)$$

where c_1 is the aqueous concentration of the analyte at time t_1, $c_{1,0}$ is the initial aqueous concentration, H (Pa · m^3/mol) is the Henry's law constant of the analyte at temperature T_1 (K), and R is the gas constant (8.314 Pa · m^3/mol · K). The derivation of eqn. 1 involves a number of assumptions. The temperature and aqueous volume are assumed to be constant during the purge. The liquid phase is considered to be well mixed, and the gas phase is assumed to behave ideally. The partial pressure of the analyte must be small compared to the total pressure, and Henry's law must apply over the concentration range of interest. In addition, the distribution of analyte between the gas and liquid phases is assumed to reach equilibrium by the time the bubbles leave the liquid phase.

Because the bubbles are in contact with the solution for a limited amount of time, full gas/liquid equilibrium will probably not be achieved before the bubbles exit the liquid phase [10]. Eqn. 1, therefore, may slightly overpredict the removal of analyte from

the aqueous phase. Despite this possibility, Pankow and Rosen [4] obtained excellent agreement with eqn. 1 for all of the purgeable priority pollutants. With $c_1/c_{1,0}$ given by eqn. 1, the maximum possible efficiency (fractional removal) of the purging process e_{p1} is defined as

$$e_{p1} = 1 - c_1/c_{1,0} \quad (2)$$

For a given compound, purging efficiency increases with t_1 and is largely a function of V_{g1}/V_{s1} ($= F \cdot t_1/V_{s1}$), where V_{g1} is the total volume of purge gas bubbled through the solution at time t_1.

The transfer efficiency of analytes through the water trap during phase II of the purge can also be modeled as a purging process. Some portion of each analyte will probably be transmitted to the GC column when the trap is cold (temperature T_2). In the worst case, the analytes purged from solution during phase I are fully retained in the water trap. The concentration of analyte in the water trap at the beginning of phase II, then, is given by

$$c_{2,0} = \frac{c_{1,0}V_{s1}}{V_{s2}}\left\{1 - \exp\left[-\left(\frac{H}{RT_1}\right)\frac{F}{V_{s1}}t_c\right]\right\} \quad (3)$$

where t_c is the time during which the trap is cold (phase I purge time, minutes), and V_{s2} is the volume of water retained in the trap during phase I. The magnitude of V_{s2} is easily calculated by considering the vapor pressures of ice and water at T_2 and T_1, respectively [8].

Taking into account the fact that the purge gas entering the water trap is not necessarily free of analyte, the concentration in the trap during phase II is given by

$$c_2 = \frac{c_{1,0}V_{s1}}{V_{s2}}\left[\lambda_{2,2} - \frac{\lambda_{1,c}}{V_{s1} - V_{s2}}(V_{s1}\lambda_{2,2} - V_{s2}\lambda_{1,2})\right] \quad (4)$$

$$\lambda_{i,j} = \exp\left[-\left(\frac{H}{RT_1}\right)\frac{F}{V_{si}}t_j\right] \quad (5)$$

where t_2 is the phase II purge time ($t_2 = t_1 - t_c$, min). Following Pankow [8], the purging efficiencies for the water trap e_{p2} and for the overall purge $E_{overall}$ are defined as

$$e_{p2} = 1 - c_2/c_{2,0} \quad (6)$$

$$E_{overall} = e_{p1}e_{p2} \cdot 100\% \quad (7)$$

Given sufficient time to strip analytes from the water trap, e_{p2} will approach 100% and e_{p1} will approximate $E_{overall}$. The correspondence between e_{p1} and $E_{overall}$ is illustrated in Fig. 2 as a function of t_2, using $V_{s1} = 5$ ml, $V_{s2} = 4.23$ μl, $F = 20$ ml/min, $t_c = 10$ min, $T_1 = 298$ K, and various values of H. Even for compounds with H values as low as 10 Pa · m^3/mol, theory predicts that a phase II purge time of 0.5 min is sufficient to efficiently transfer analytes from the warmed water trap to the GC column. Because the experimental application of this method will require *ca.* 0.5 min to warm the trap from T_2 to T_1, a phase II purge time of 1 to 2 min should be adequate to prevent significant retention of analytes in the trap.

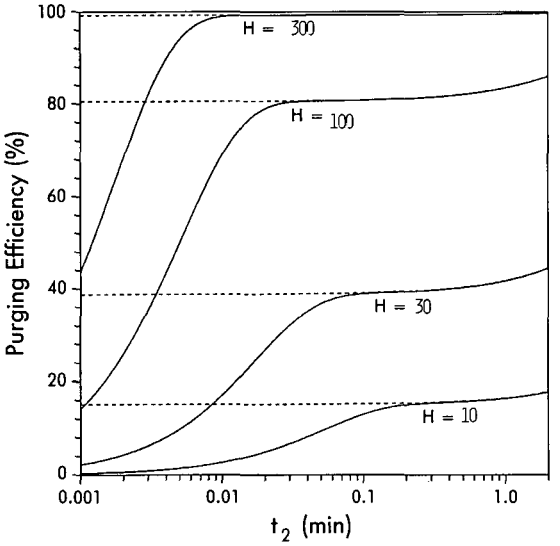

Fig. 2. Theoretical purging efficiencies as a function of t_2 for a range of H values. The dashed lines represent e_{p1}, the maximum possible purging efficiency, while the solid lines denote $E_{overall}$, the overall purging efficiency when all analytes are assumed to be retained completely in the water trap during phase I of the purge. Conditions: $V_{s1} = 5$ ml, $V_{s2} = 4.23$ μl, $F = 20$ ml/min, $t_c = 10$ min, $T_1 = 298$ K, $T_2 = 263$ K.

EXPERIMENTAL

A schematic of the P/WCC apparatus with incorporation of the water trap is illustrated in Fig. 3. Notable modifications to the setup discussed by Pankow [8] are the use of a 6-port Carle valve (Hach, Loveland, CO, USA) to control carrier gas pressure

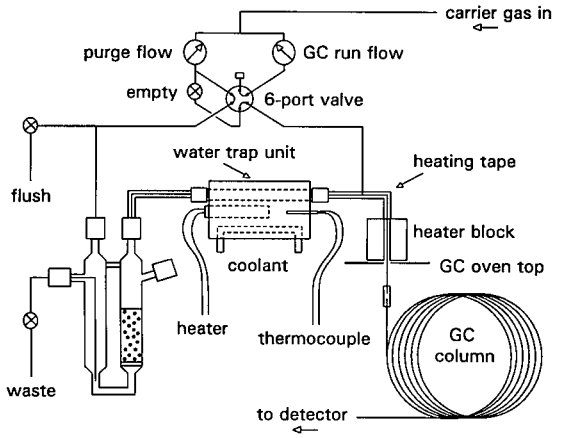

Fig. 3. Schematic of the P/WCC apparatus with the glass-bead water trap. Snap valves are denoted by cross-hatched circles.

and flow direction, and the use of heating tape on the transfer line between the purge vessel and the gas chromatograph. The Carle valve provides a simple method to start and stop the purge, while the heated transfer line eliminates cold spots near the water trap and increases the transmission efficiency of the less volatile analytes to the GC. The basic operating procedures of both the P/WCC method and the water trap have been described elsewhere [3,4,8].

The P/WCC apparatus was interfaced to a Varian 3400 gas chromatograph equipped with an electron-capture detector. The electron-capture detector temperature was set at 350°C, and the most sensitive range was used. Ultra-high-purity nitrogen was used as detector make-up gas at a flow-rate of 28.5 ml/min. The GC column was a 27 m × 0.32 mm I.D. DB-624 fused-silica capillary column with a 1.8 μm film thickness manufactured by J&W Scientific (Folsom, CA, USA). To further reduce the ability of ice to plug the column, a 0.5 m × 0.53 mm I.D. DB-624 column with a 3.0 μm film thickness was installed in front of the main column. The two columns were joined with a universal press-fit connector (Restek, Bellefonte, PA, USA). The head of the column was connected to the transfer line in a "non-ice-trap" configuration [4]; the column was extended through the transfer line union and into the heated zone above the GC oven. The temperatures of the transfer line and the GC interface heater block were both 220°C.

Ultra-high-purity helium was used as the purge and carrier gas. A purge gas flow-rate of 20 ml/min was maintained with a purge pressure of 269 kPa. The carrier gas pressure for the GC run was 90 kPa. To prevent overpurging and erratic flow-rates at both the start and end of the purge, precautions were taken to equalize the gas pressure across the purge vessel at those times. Such equalization was achieved before the start of the purge by selecting the purge position on the 6-port valve and opening the "empty" snap valve. The purge was then started by closing the "empty" valve. At the end of the purge, the 6-port valve was turned to the GC run position, and the excess pressure upstream of the purge vessel was vented by temporarily opening the "flush" snap valve.

The total purge time (t_1) for all analyses was 12 min. All were performed at ambient laboratory temperature ($T_1 \approx 298$ K). During phase I of the purge, the water trap was held at −10°C ($T_2 = 263$ K) with a liquid coolant composed of ethylene glycol–water (50:50, v/v). The phase I purge time (t_c) was 10 min. Phase II of the purge was 2 min (t_2) and was performed at 298 K. Whole column cryotrapping was performed at −30°C. The GC temperature program was ballistic from −30°C to 50°C, then at 5°C/min to 250°C. After the GC run was completed, the water trap was backflushed at 100°C to remove the trapped water, and the sample was drained from the purge vessel through the waste line. The three characteristic modes of the water trap are summarized in Table I.

RESULTS AND DISCUSSION

The glass-bead water trap effectively reduced the

TABLE I

CHARACTERISTICS OF THE THREE WATER TRAP MODES

	Phase I purge	Phase II purge	Backflush
Coolant	On	Off	Off
Heater	Off	On	On
Temperature	−10°C	25°C	100°C
Flow	to GC	to GC	to PV[a]
Duration	10 min	2 min	4 min

[a] PV = Purge vessel.

amount of water transmitted to the GC column. When the water trap was in use, the column never plugged with ice. Purge times of up to 17 min were tested (t_2 = 2 min, V_{g1} = 340 ml). Not only did the column never plug with ice under these conditions, but no measurable decrease in the purge flow-rate was observed. Without the water trap, purge volumes of approximately 100 ml were sufficient to plug the column, even when the column was installed in the "ice-trap" [4] configuration. Moreover, the water trap reduced the chromatographic interference of water to a manageable level. Unlike flame ionization detectors, electron-capture detectors are extremely sensitive to relatively small amounts of water. In the absence of a water trap, enough water was transmitted to the column to create a very large, asymmetric peak that obscured several minutes of the chromatogram. The use of the water trap, therefore, was key to the successful coupling of an electron-capture detector to P/WCC.

This method was tested with a standard containing several chlorinated benzenes. Electron-capture detector response is quite sensitive to the degree of chlorination; in general, the detection limit for a given compound class will decrease as the number of chlorines increases. Consequently, the chlorobenzenes in the aqueous standard were present at different concentrations: chlorobenzene (3.7 ng/ml), each dichlorobenzene (0.11 ng/ml), each trichlorobenzene (0.028 ng/ml), each tetrachlorobenzene (0.019 ng/ml), pentachlorobenzene (0.011 ng/ml), and hexachlorobenzene (0.011 ng/ml). Fig. 4a shows the chromatogram that results from purging 5.0 ml of the standard, while Fig. 4b is the result of repurging the same standard. Both chromatograms are plotted on identical scales. The electron-capture detector was not very sensitive to chlorobenzene, and hexachlorobenzene behaved erratically; neither is shown in Fig. 4. Good resolution was obtained for all but two of the remaining compounds. Fig. 5 illustrates the overlap of the 1,2,3,5- and 1,2,4,5-tetrachlorobenzene peaks. For a 5.0-ml sample, representative method detection limits are 0.01 ng/ml for 1,2-dichlorobenzene, 0.003 ng/ml for 1,2,4-trichlorobenzene, and 0.0006 ng/ml for 1,2,4,5-tetrachlorobenzene.

Experimentally purging efficiencies were calculated by [4]

$$E_{obs} = \frac{A_i - A_r}{A_i} \cdot 100\% \quad (8)$$

where A_i is the peak area resulting from the initial purge and A_r is the corresponding peak area from the repurge. Values of E_{obs} were obtained for both

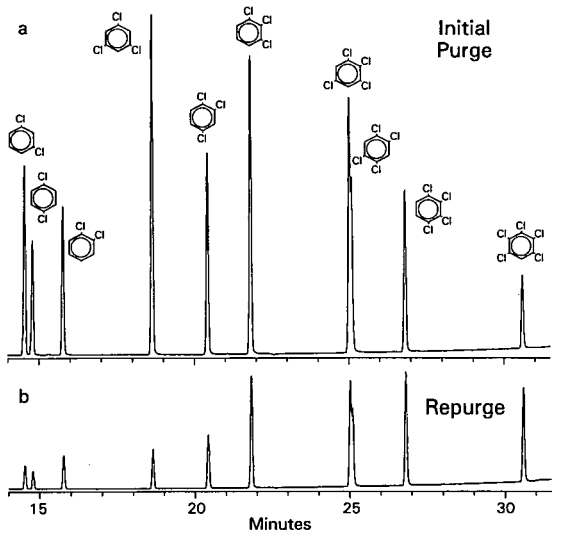

Fig. 4. Portions of (a) the initial and (b) repurge chromatograms of a 5-ml water sample containing each of the chlorinated benzenes. Temperature program: 50 to 250°C at 5°C/min.

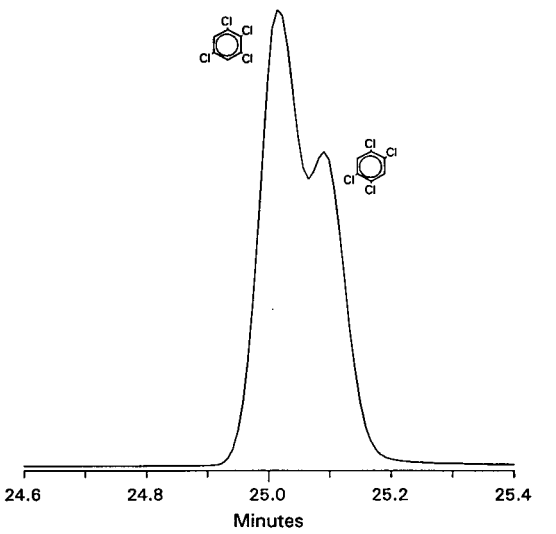

Fig. 5. Representative section of a chromatogram showing the overlap of peaks for 1,2,3,5- and 1,2,4,5-tetrachlorobenzene.

TABLE II

HENRY'S LAW CONSTANTS (H), PREDICTED PURGING EFFICIENCIES ($E_{overall}$), AND OBSERVED PURGING EFFICIENCIES (E_{obs}) FOR THE CHLORINATED BENZENES

Compound	H^a (Pa · m³/mol)	5-ml sample		1-ml sample	
		$E_{overall}{}^b$ (%)	$E_{obs}{}^c$ (%)	$E_{overall}{}^b$ (%)	$E_{obs}{}^c$ (%)
Chlorobenzene	364	99.9	ND[d]	100.0	ND
1,2-Dichlorobenzene	192	97.6	77.6	100.0	92.7
1,3-Dichlorobenzene	364	99.9	88.0	100.0	94.4
1,4-Dichlorobenzene	314	99.8	85.1	100.0	94.0
1,2,3-Trichlorobenzene	131[e]	92.2	62.8	100.0	82.8
1,2,4-Trichlorobenzene	233	98.9	73.4	100.0	88.6
1,3,5-Trichlorobenzene	233[e]	98.9	88.5	100.0	94.3
1,2,3,4-Tetrachlorobenzene	263[e]	99.4	30.7	100.0	30.4
1,2,3,5-Tetrachlorobenzene	162[e]	95.7	61.3	100.0	63.9
1,2,4,5-Tetrachlorobenzene	263[e]	99.4	52.7	100.0	54.8
Pentachlorobenzene	162[f]	95.7	NA[g]	100.0	NA
Hexachlorobenzene	83[h]	90.0	NA	100.0	NA

[a] H data from Mabey *et al.* [11] except as noted (T_1 = 298 K).
[b] $E_{overall}$ was calculated from eqns. 1–7, using T_1 = 298 K, R = 8.314 Pa · m³/mol · K, F = 20 ml/min, t_c = 10 min, t_2 = 2 min, and V_{s2} = 4.23 μl.
[c] E_{obs} was calculated using eqn. 8.
[d] ND = Not detected.
[e] H data from Mackay and Shiu [12].
[f] Vapor pressure estimated from a vapor pressure *versus* boiling point regression; H estimated using that vapor pressure and solubility data from Verschueren [13].
[g] NA = Not available. Results were inconsistent.
[h] H estimated using vapor pressure and solubility data from Verschueren [13].

1.0- and 5.0-ml samples. The results are compared to theoretical values of $E_{overall}$ in Table II. $E_{overall}$ represents the maximum possible purging efficiency because e_{p2} is approximately 100% and e_{p1} is known to be a theoretical maximum. All experimental values are lower than expected on the basis of theory. The differences between theoretical and observed values increase with decreasing compound volatility. Portions of the discrepancies might be due to errors in the values of H. Inefficient transmission of compounds through the water trap at T_1 also would result in E_{obs} values less than $E_{overall}$. Retention in the trap or the transfer line would be more problematic for the heavier compounds such as tetra- and pentachlorobenzene. In addition, if gas–liquid equilibrium was not fully achieved as each gas parcel contacted the liquid phase, then negative deviations in the values of E_{obs} would be expected.

If the degree to which gas–liquid equilibrium *is* achieved is constant throughout the purge, then better predictions of $E_{overall}$ might be obtained through the use of an *effective* Henry's law constant, where the effective value of H is given by

$$H_{eff} = \gamma H \tag{9}$$

and γ is the fraction of equilibrium attained. The value of γ is expected to be smaller for a 1.0-ml sample than for a 5.0-ml sample due to the shorter contact time with the liquid phase. Using this approach, the differences between E_{obs} and $E_{overall}$ in Table II for the di- and trichlorobenzenes can be reconciled using a single value of γ for each value of V_{s1}. Those γ values, however, are not small enough to explain the low E_{obs} values of the tetrachlorobenzenes or the inefficient transmission of pentachlorobenzene to the gas chromatograph. Given the need to heat the transfer line to 220°C to increase throughput of the heavier compounds, and the fact

that E_{obs} values for the tetrachlorobenzenes were found to be independent of V_{s1}, the lower than expected purging efficiencies might be due to hold-up in the transfer line or in the water trap. A higher phase II water trap temperature or a longer phase II purge time might increase these purging efficiencies.

CONCLUSIONS

The purge with whole column cryotrapping method of Pankow and Rosen [4] was adapted for use with an electron-capture detector and tested with a set of chlorinated benzenes. Purge gas desiccation with a simple glass-bead water trap allowed the use of large purge gas volumes, prevented the GC column from plugging with ice, and reduced the interference of water in the chromatogram. Good chromatographic resolution was obtained. Despite smaller than expected purging efficiencies, this simple P/WCC method shows promise for the quick and effective determination of volatile and semi-volatile compounds such as the di-, tri- and tetrachlorobenzenes. With further study, this method might also be extended to include pentachlorobenzene and the even less volatile hexachlorobenzene.

SYMBOLS

A_i	peak area from initial purge
A_r	peak area from repurge
c_1	concentration of analyte in aqueous sample (ng/ml)
$c_{1,0}$	initial concentration of analyte in sample (ng/ml)
c_2	concentration of analyte in water trap during phase II purge (ng/ml)
$c_{2,0}$	concentration of analyte in water trap at beginning of phase II (ng/ml)
e_{p1}	maximum possible purging efficiency from the sample
e_{p2}	purging efficiency of analytes from the water trap
E_{obs}	observed purging efficiency (%)
$E_{overall}$	overall efficiency (%) for purging of analytes from a sample to the GC column
F	flow-rate of purge gas through the purge vessel (ml/min)
H	Henry's law constant (Pa · m^3/mol) for the analyte at T_1
H_{eff}	effective Henry's law constant (Pa · m^3/mol)
R	gas constant (8.314 Pa · m^3/mol · K)
t_c	time during which the water trap is cold (min)
t_1	total purge time (min)
t_2	phase II purge time (min)
T_1	temperature in the purge vessel and in the warm trap (K)
T_2	temperature in the cold trap (K)
V_{g1}	volume of purge gas bubbled through the sample (ml)
V_{s1}	volume of sample (ml)
V_{s2}	volume of liquid water in the trap (ml)
γ	fraction of gas–liquid equilibrium attained

ACKNOWLEDGEMENT

The authors thank Lorne M. Isabelle for technical assistance.

REFERENCES

1 J. E. Longbottom and J. J. Lichtenberg (Editors), *Test Methods for Organic Chemical Analysis of Municipal and Industrial Wastewater, EPA-600/4-82-057*, US Environmental Protection Agency (EPA), Washington, DC, 1982.
2 US EPA, *Methods for the Determination of Organic Compounds in Finished Drinking Water and Raw Source Water*, Physical and Chemical Methods Branch, EMSL, Cincinnati, OH, 1986, Method 524.2.
3 J. F. Pankow, *J. High Resolut. Chromatogr. Chromatogr. Commun.*, 10 (1987) 409.
4 J. F. Pankow and M. E. Rosen, *Environ. Sci. Technol.*, 22 (1988) 398.
5 P. G. Simmonds, *J. Chromatogr.*, 289 (1984) 117.
6 J. W. Cochran, *J. High Resolut. Chromatogr. Chromatogr. Commun.*, 11 (1988) 663.
7 M. E. Rosen, *Ph. D. Thesis*, Oregon Graduate Institute, Beaverton, OR, 1988.
8 J. F. Pankow, *Environ. Sci. Technol.*, 25 (1991) 123.
9 J. F. Pankow, *Anal. Chem.*, 58 (1986) 1822.
10 D. Mackay, W. Y. Shiu and R. P. Sutherland, *Environ. Sci. Technol.*, 13 (1979) 333.
11 W. R. Mabey, J. H. Smith, R. T. Podoll, H. L. Johnson, T. Mill, T. Chou, J. Gates, I. W. Partridge, H. Jaber and D. Vandenberg, *Aquatic Fate Process Data for Organic Priority Pollutants, EPA-440/4-81-014*, US EPA, Washington, DC, 1982.
12 D. Mackay and W. Y. Shiu, *J. Phys. Chem. Ref. Data*, 10 (1981) 1175.
13 K. Verschueren, *Handbook of Environmental Data on Organic Chemicals*, Van Nostrand Reinhold, New York, NY, 2nd ed., 1983.

Journal of Chromatography, 629 (1993) 329–337
Elsevier Science Publishers B.V., Amsterdam

CHROM. 24 581

Determination of coplanar polychlorobiphenyl congeners in biota samples

M. D. Pastor, J. Sanchez, D. Barceló and J. Albaigés

Environmental Chemistry Department, CID–CSIC, c/Jordi Girona 18, 08034 Barcelona (Spain)

(First received April 3rd, 1992; revised manuscript received August 6th, 1992)

ABSTRACT

A method for the separation of coplanar congeners of polychlorobiphenyls (PCBs) (IUPAC Nos. 81, 77, 126 and 169) from other organic micropollutants such as hydrocarbons, organochlorinated pesticides and other PCBs is described. It involves a two-step clean-up procedure with sulphuric acid treatment and LC fractionation (Hypercarb column) and permits the isolation of the coplanar congeners of PCBs in biota samples. The separation of the coplanar PCBs in the Hypercarb column requires only 100 ml of *n*-hexane. Recoveries ranged from 84 to 97% for these and sixteen other PCB congeners. Gas chromatography (GC) with electron-capture detection of all the compounds was performed using capillary GC columns of different polarity, CP-Sil-8 CB or DB-5, DB-17 or DB-225, followed by confirmation by GC–mass spectrometry in the electron impact and selected ion monitoring mode. The whole analytical method permits the determination of individual PCBs in biota samples at a level of 1 ng/g wet tissue.

INTRODUCTION

Residue levels of polychlorobiphenyls (PCBs) have been found in aquatic biota, both continental and marine, as a result of their widespread distribution, environmental persistence and high lipophylicity [1–3]. Among the 209 possible PCB congeners, only *ca.* 150 have been reported in to the total environment. Seven of them (IUPAC Nos. 28, 52, 101, 118, 138, 153 and 180) were selected as the most relevant because of their distribution throughout the chromatogram and coverage of the chlorination range, use in technical mixtures, relative ease of determination and proved toxicity. Consequently, they are commonly mentioned in environmental regulations [4].

In the last few years, increasing attention has been paid to congeners having two *para*-chlorines and at least one *meta*-chlorine that show the same type of toxicity as 2,3,7,8-tetrachloridibenzo-*p*-dioxin (2,3,7,8-TCDD). These congeners are also called "coplanar" PCBs, as they lack *ortho*- and contain *meta*- and *para*-chlorine atoms, thus making a coplanar conformation more probable [3]. They show particularly high "dioxin-like" toxicity, *e.g.*, PCBs with IUPAC Nos. 81, 77, 126 and 169. Considerable toxicity is also attributed to some mono-*ortho*-chlorinated PCBs, especially IUPAC Nos. 105 and 156. Based on toxic and biochemical potencies, the relative toxicity of PCB congeners compared with 2,3,7,8-TCDD may be expressed as toxicity equivalence factors (TEFs). The total "dioxin-like" toxicity of a mixture of PCBs may be calculated as the summation of the concentration of individual toxic congeners times their TEF and it is used in environmental studies [5]. Therefore, to cope with the new requirements of monitoring programmes there is a need for the development of analytical methods for the isolation of the different groups of PCBs. In this sense, for the isolation of the previously mentioned seven PCB congeners there is an extensive literature of analytical methods mainly based on sulphuric acid clean-up, sorption

Correspondence to: D. Barceló, Environmental Chemistry Department, CID–CSIC, c/Jordi Girona 18, 08034 Barcelona, Spain.

0021-9673/93/$06.00

column chromatography with Florisil and silica–alumina [3], gel permeation chromatography [6] and normal-phase high-performance liquid chromatography (LC) [7]. However, for the isolation of the more toxic PCBs, only a few methods have been developed, basically using activated charcoal columns [8–11] and recently developed methods involving 2-(1-pyrenyl)ethyldimethylsilylated silica LC column [12] and Florisil column chromatography [13].

The separation techniques for isolating coplanar PCBs have been reviewed recently [3,8]. Initial methods of isolation used carbon or granular charcoal in various grades and particle sizes. More recently, silica has been coated with graphite as the basis of the commercially available LC Hypercarb column. The separation is based on the retention of planar or near planar molecules by the graphitic surface of the adsorbent. Non-planar molecules are either unretained or have a limited retention, whereas non-*ortho*-substituted PCBs can assume a coplanar configuration more readily than the *ortho*-substituted isomers, allowing a stronger interaction with the planar porous graphitic carbon structure. In general, the existing methods for the isolation of planar PCBs congeners from other PCB congeners have been criticized because large volumes of eluent, *e.g.*, over 1000 ml [14], per sample are needed. In other instances, the use of highly carcinogenic solvents is involved (*e.g.*, benzene) [9,15,16] or the need for multiple solvents, *e.g.*, methylene chlorine, cyclohexane and toluene [17] and light petroleum and toluene [18].

This paper report on the isolation of coplanar PCB congeners from environmental samples with the use of sulphuric acid treatment and a Hypercarb LC column. Further confirmation is achieved by using capillary GC columns of different polarity and/or GC–MS in the electron impact (EI) and selected ion monitoring (SIM) mode.

EXPERIMENTAL

Reagents and apparatus

All solvents (*n*-hexane, dichloromethane and diethyl ether) were of pesticide grade from Merck (Darmstadt, Germany). Alumina, Florisil and silica gel were also obtained from Merck. Analytical-reagent grade individual PCB components (Promochem, Wesel, Germany) with IUPAC numbers are shown in Table I. For substitution patterns of the different PCBs, see ref. 3.

An eluent flow-rate of 3 ml/min of *n*-hexane was delivered by a Model 64 high-pressure pump (Knauer, Bad-Homburg, Germany) coupled with a UV detector set at 254 nm (Knauer). Standard solutions and biota samples containing coplanar PCBs were injected via a 50- and 400-μl loop, respectively (Rheodyne, Cotati, CA, USA). A Hypercarb (Shandon Scientific, Warrington, UK) porous graphitic carbon (7-μm particle size) LC column (50 × 4.7 mm I.D.) was used. The material has a surface area of about 150 m^2/g, a mean pore volume of 2.0 cm^3/g and a particle porosity of 70%.

Samples of 2 μl were injected in the splitless mode (gas hold-up time = 35 s) with a Hewlett-Packard (Palo Alto, CA, USA) Model 7673A automatic sampler in a Hewlett-Packard Model 5890 capillary gas chromatograph equipped with a ^{63}Ni electron-capture detector at 310°C. The columns used were CP-Sil-8-CB (Chrompack, Middelburg, Netherlands) and DB-5, both containing 5% phenyl–95% methylpolysiloxane, DB-17 containing 50% phenyl–50% methylpolysiloxine and DB-225 containing 50% cyanopropyl–50% phenylpolysiloxane, all from J and W Scientific (Folsom, CA, USA). The chromatographic conditions for each column used are given in the figure legends.

A Hewlett-Packard Model 5995 GC–MS instrument interfaced to a Model 59970C data system was used. The DB-225 GC column was used for GC–MS confirmation of coplanar PCB congeners, with direct introduction into the ion source and with the temperature programmes indicated in the figure legend. Helium was used as the carrier gas (30 cm/s). The ion source and the analyser were maintained at 200 and 230°C, respectively. EI mass spectra were obtained at 70 eV.

Sample work-up

The protocols that can be used for the isolation of coplanar PCBs from other organic compounds are shown in Fig. 1. The general analytical scheme shown is much broader than the results indicated in this paper. A major point of this paper is that using a common method (method A) that permits the determination of a broad range of pollutants such as PCBs, DDTs, hydrocarbons and organochlorine

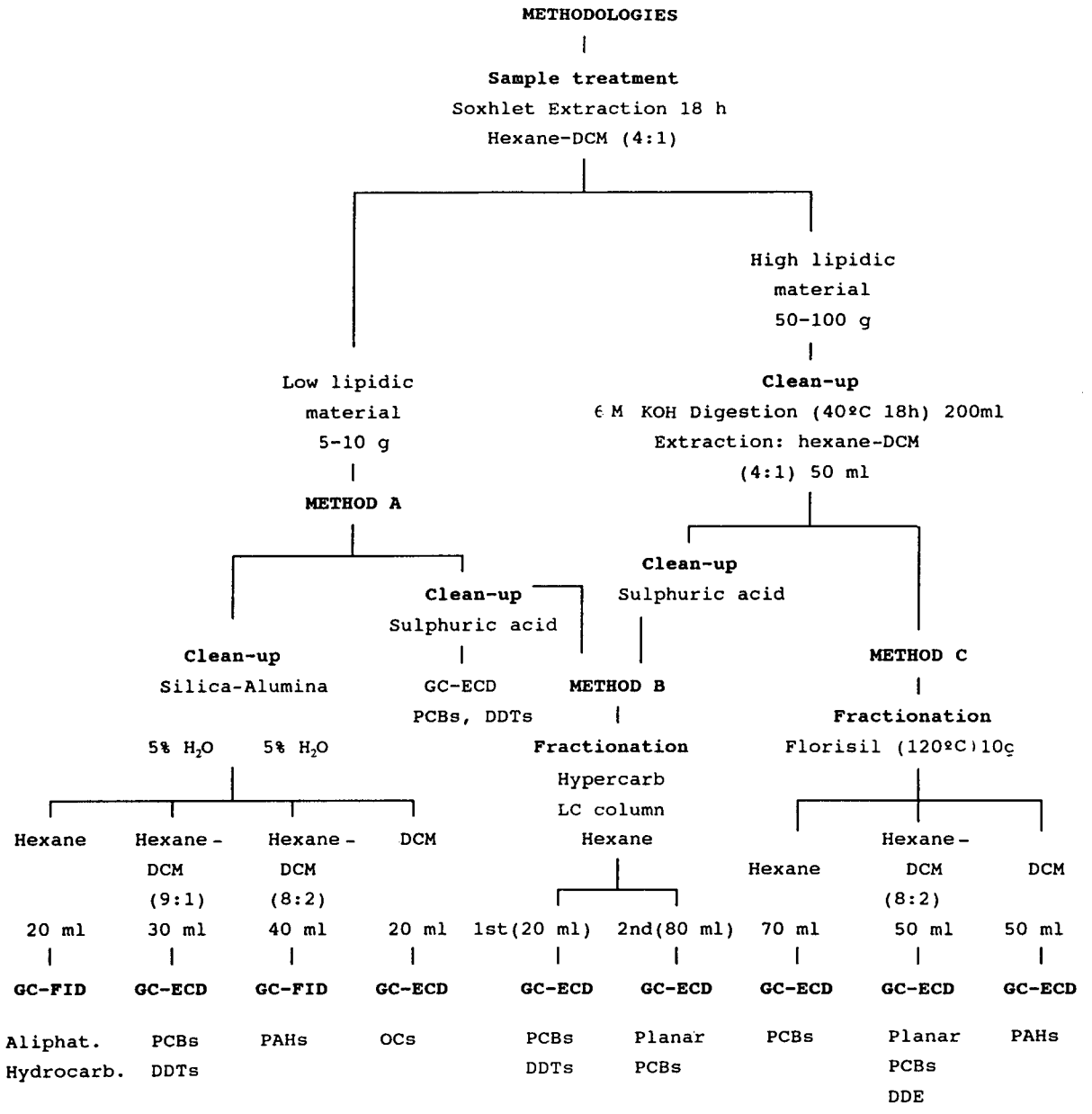

Fig. 1. Analytical methodology used for the isolation of coplanar PCBS from other PCBs and several organic micropollutants. PAH = polycyclic aromatic hydrocarbons; OC = organochlorine pesticides: DDTs = *pp'*-DDT + *pp'*-DDE + *pp'*-DDD; DCM = dichloromethane.

pesticides (OCs), we can easily include in the protocol method B, which is a "daughter" method from method A. Method B should permit the isolation of coplanar PCBs, and also of all the other pollutants. This indicates that although coplanar PCBs are relevant from the point of view of toxicity and can be found in biota samples, we should also not forget the other major organic pollutants that are currently determined in biota samples within the different monitoring programmes.

For the recovery studies, spiking of the samples was carried out prior to the extraction by careful mixing of the standard solution (10 ml of a solution of 50 or 200 ng/ml for coplanar or conventional PCBs) with the sample to be analysed in the Soxhlet apparatus, before extraction and fractionation.

After extraction was completed, the organic extract was dissolved in *n*-hexane (10 ml) and cleaned up by vigorous shaking with 3 ml of sulphuric acid for about 3 min. This extract obtained is injected into a Hypercarb LC column (*ca.* 200 μl) using *n*-hexane as eluent at 3 ml/min. In this way, the coplanars PCBs (IUPAC Nos. 81, 77, 126 and 169) are collected in the second LC fraction between 25 and 110 ml. Subsequently, the different solutions collected were evaporated just to dryness and the residues were dissolved in 250 μl of isooctane and were then ready to be injected into the GC–ECD and/or GC–MS systems for quantification.

Quantitative analysis

External calibration was used with the mixed PCB congeners containing 40–200 pg/μl in isooctane, injecting the samples and standards with the automatic sampler.

The linearity of the detector was determined by injecting a series of PCB congeners at ten different concentrations and plotting the ratio of the peak-height response to the mass of the determinand against the mass injected to determine the true linear range for the determinand. The system was linear between 80 to 400 pg injected.

RESULTS AND DISCUSSION

Studies on recoveries

The recoveries and relative standard deviations (R.S.D.s) obtained for a variety of PCBs obtained using the different methods are indicated in Table I. Most of the PCBs can be easily separated using DB-5 or CP-Sil-8 CB apolar capillary columns. However, the whole separation of all the group of PCBs is not possible even using these stationary phases in a 30- or 50-m column, which are the most widely used for monitoring PCBs in environmental samples. Concurrent analysis with a more polar column has been suggested [19,20]. This is certainly required for the complete separation of congeners 149–118 and 138–163 (IUPAC numbers). In addition, the polar DB-17 GC column also improves the separation between PCBs 153 and 105. Co-elution problems between certain congeners, such as PCBs 138 and 163, were found during a certification exercise, where most of the laboratories were using DB-5-type columns; the two congeners were not resolved, thus making it impossible to certify the PCB 138 congener. Consequently, certification of PCB 138 was indicated as the total amount of PCB 138 + 163 [4]. The separation of this particular mixture was until now only known to be possible either on a very polar SP-2330 (biscyanopropylsiloxane) column [19] and recently on a polar FFAP (polyethylene glycol terephthalate) column [20]. Here we recommend for the first time a DB-17 capillary column for a complete separation of PCB pairs that usually co-elute using DB-5-type columns.

Fig. 2 shows GC–ECD traces of a fish sample, *Sardina pilchardus*, using these two columns. When we compared the columns for a variety of PCBs, we found that the complete separation of PCBs 118 and 149 is only achieved by using the more polar DB-17 column. This result shows that in order to avoid the problems encountered and described above, monitoring programmes involving analysis for a variety of PCBs should include the use of two GC columns of different polarity.

A typical LC separation using the Hypercarb column corresponding to a mixture of PCBs and the coplanar PCBs Nos. 81, 77, 126 and 169 is shown in Fig. 3. In Fig. 4 the GC–ECD traces of (A) the total sulphuric acid extract obtained with method A, (B) the injection of the first fraction and (C) the injection of the second fraction are shown. The GC–ECD traces in Fig. 4A and B are almost identical, which makes it impossible to distinguish the coplanar PCBs. This indicates that (i) when using conventional clean-up procedures with sulphuric acid the toxic PCB congeners cannot be analysed directly, as their peaks are confused with the predominant peaks of other PCBs, and (ii) the amount of toxic coplanar PCB congeners is small compared with the total amount of PCBs and they can only be distinguished on injecting the second fraction (Fig. 4C). Good recoveries are obtained for the conventional PCBs and DDTs obtained in the first fraction, as pointed out by other workers when using carbon column fractionation [11].

Fig. 5 shows the GC–ECD traces of an extract of

TABLE I

AVERAGE RECOVERIES VALUES AND RELATIVE STANDARD DEVIATIONS OF PCB CONGENERS USING THE DIFFERENT METHODS REPORTED IN FIG. 1

Concentrations of PCB congeners varied between 50 and 200 ng/g (n = 5). n.d. = Not detected (below 1 ng/g).

PCB IUPAC No.	Method A				Method C			
	Silica–alumina		Hypercarb column, method B via method A		Hexane		Hexane–CH_2Cl_2	
	Recovery (%)	R.S.D. (%)	Recovery (%)	R.S.D. (%)	Recovery (%)	R.S.D. (%)	Recovery (%)	R.S.D. (%)
28	77	4	80	2	77	7	n.d.	–
44	87	4	86	2	83	5	n.d.	–
52	84	5	85	10	64	9	10	50
61	87	6	85	9	76	9	n.d.	–
77	n.d.	–	92	7	n.d.	–	97	2
81	n.d.	–	94	6	n.d.	–	102	10
101	80	5	97	6	61	9	2	50
105	90	7	93	6	66	8	13	50
118	87	8	89	4	102	5	n.d.	–
126	n.d.	–	90	8	n.d.	–	96	7
128	97	3	96	9	105	4	n.d.	–
138	85	5	90	6	72	7	4	25
149	90	5	96	5	92	4	n.d.	–
153	90	3	101	6	90	7	1	50
156	91	7	89	9	84	7	3	30
163	85	5	90	5	88	4	n.d.	–
169	n.d.	–	97	7	n.d.	–	95	7
170	93	4	97	9	94	6	n.d.	–
180	84	7	99	8	88	4	n.d.	–
187	90	5	104	6	88	4	n.d.	–

Scomber scombrus spiked at 50 ng/g with coplanar PCBs and 200 ng/g with PCBs obtained using method C. Fig. 5A and B show the profiles obtained after injecting (A) the *n*-hexane and (B) the *n*-hexane–dichloromethane fractions. Although the recoveries of the coplanar PCBs 77, 126 and 169 were very high, two problems were encountered: first, co-elution of PCB 81 with DDE, and second, the separation of all the PCB congeners is incomplete, so PCBs 105 and 156 are obtained in both the first and second fractions. In addition, other congeners, which are not coplanar, are also obtained in this second fraction, as can be seen in Table II. This indicates that this method does not offer a complete separation of coplanar PCBs from conventional PCBs as does the Hypercarb LC column. In any event, we can agree with a recent paper [13] that recommended the use of Florisil column chromatography for the isolation of coplanar PCBs 77, 126 and 169 without determining PCB 81, which is the one that causes co-elution problems with DDE using this method.

GC–MS confirmation

The use of GC–MS for confirmation purposes in PCB analysis has been pointed out by several workers [9,13,21], who indicated that there is a need to avoid problems related to cross-contamination. The determination of coplanar congeners of PCBs depends on the level of the other co-extractants and it will depend on the biota sample studied. Thus, confirmation by GC–MS is necessary, as there are always several interfering peaks in the GC–ECD traces [9]. Rigorous protocols such as for PCDDs have

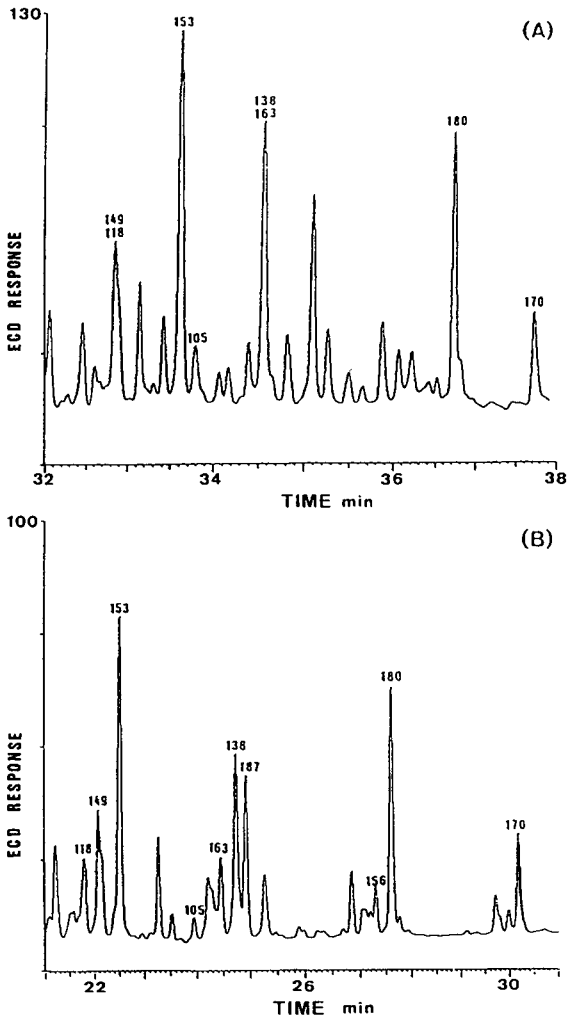

Fig. 2. GC–ECD traces of an extract of biota sample of *Sardina pilchardus* obtained using method A with only sulphuric acid clean-up and with (A) a 30 m × 0.25 mm I.D. 0.25-μm DB-5 capillary column, temperature programmed from 80 to 290°C at 6°C/min, the final temperature being maintained for 10 min, helium as carrier gas at a flow velocity of 30 cm/s, high-purity nitrogen as make-up gas at a flow-rate of 60 ml/min and an injector temperature of 270°C, and (B) a 0.25-μm DB-17 column (30 m × 0.25 mm I.D.) with a temperature programme identical with that for the DB-5 column. Concentrations IUPAC Nos. 118, 149, 153, 138, 187, 180 and 170 were 0.1, 0.2, 4.6, 3.7, 3.5, 1.8 and 0.1, ng/g wet tissue, respectively.

also recently been developed for more toxic PCBs involving isotope dilution GC with high-resolution MS [16].

The main ions used for confirmation purposes in GC–MS with SIM are indicated in Table II. $[M]^+$

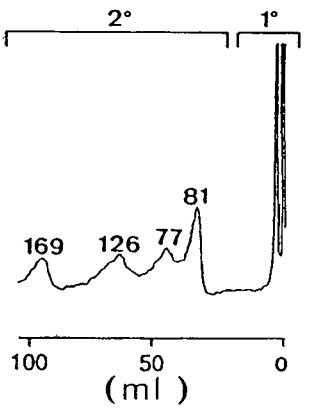

Fig. 3. LC–UV traces of a standard mixture containing 50 ng/ml of several PCBs in an LC Hypercarb column (volume injected, 400 μl). Fractions obtained: (1) corresponding to common PCBs and (2) coplanar congeners of PCBs. UV detection at 254 nm; eluent, *n*-hexane at a flow-rate of 3 ml/min.

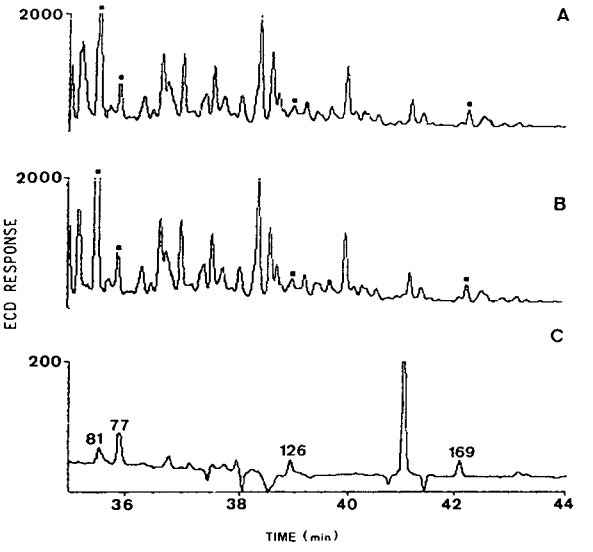

Fig. 4. GC–ECD traces of an extract of herring oil obtained after sulphuric acid clean-up treatment using method A, and before and after passing the sample extract through the Hypercarb column. A capillary column of 50 m × 0.12 mm I.D. coated with 0.25-μm chemically immobilized CP-Sil-8 CB was temperature programmed as for the DB-5 column in Fig. 2. The GC–ECD traces correspond to the injection of (A) the extract obtained after clean-up with sulphuric acid, (B) after collecting the first fraction and (C) after collecting the second fraction of Hypercarb column. Amount of co-planar PCBs congeners in the sample were 2, 3, 2 and 2 ng/g of PCBs No. 81, 77, 126 and 169, respectively.

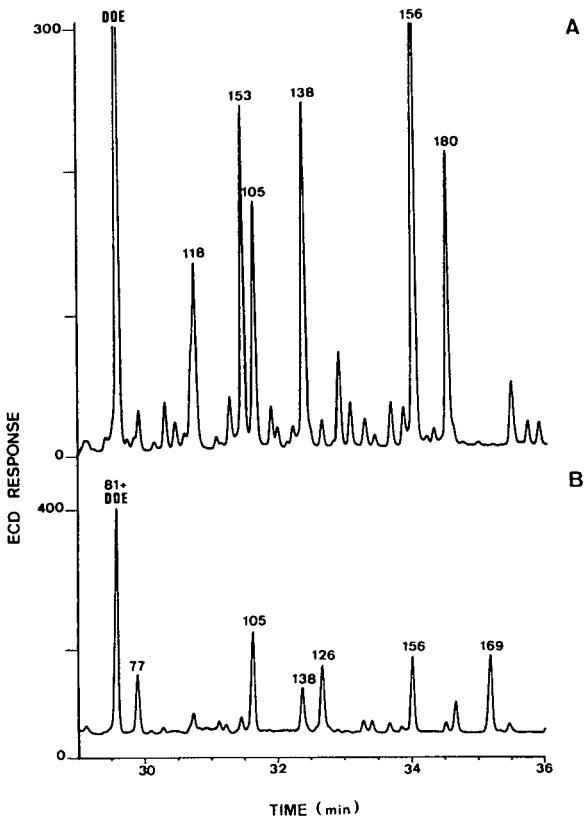

Fig. 5. GC–ECD traces of an extract of *Scomber scombrus* spiked at 50 ng/g with coplanar PCBs and at 200 ng/g with the other PCB congeners obtained using method C. (A) and (B) show the profiles obtained after injecting (A) the *n*-hexane and (B) the *n*-hexane–dichloromethane fractions. A DB-5 capillary column was used under the experimental conditions given in Fig. 2.

TABLE II

RETENTION TIMES AND MAIN IONS OF COPLANAR PCBs CONGENERS IN SEVERAL GC COLUMNS

IUPAC No.	Retention time (min)			Main ions (*m/z*)
	DB-5	DB-17	DB-225	
81	35.5	30.0	22.5	290, 292
77	35.9	30.4	24.4	290, 292
126	39.0	32.9	31.5	324, 326
169	42.1	35.1	39.2	360, 362

and $[M + 2]^+$ cluster ions were used as the identification criteria together with the retention times of the pure standards. Fig. 6 shows the GC–MS traces of the fractions obtained in the Hypercarb fractionation procedure (Fig. 4B and C) of a herring fish oil. The retention times of the suspected peaks of the four coplanar PCBs (Fig. 6B) match well with the peaks of an authentic mixture of these congeners (Fig. 6A). Moreover, their relative abundances parallel those of the original chromatogram (Fig. 4C). The higher noise level exhibited by this fraction in the GC–MS analyses is consistent with the very low concentrations of the coplanar PCBs with respect to other components. In fact, coplanar PCB congeners usually occur at concentration levels 10–50 times lower than those of the conventional PCBs. The use of GC–MS with SIM enabled a limit of detection of less than 1 ng/g in the sample analysed to be achieved.

The fraction corresponding to the other PCBs (Fig. 6C) also shows many more peaks in the GC–MS traces than the fraction of coplanar PCB congeners, although the GC–MS analysis was carried out using SIM. This is a common feature when analysing PCB mixtures as all the PCBs with an identical number of chlorines will exhibit similar diagnostic ions, so PCBs with four, five and six chlorines

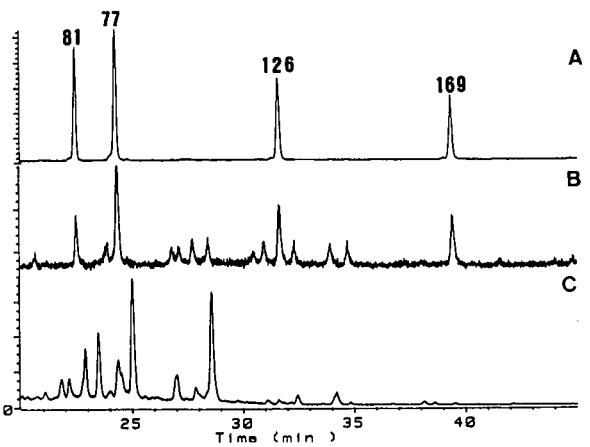

Fig. 6. GC–MS with SIM of (A) standard sample of PCBs 81, 77, 126 and 169, (B) the extract of the same herring oil corresponding to Fig. 4C and (C) that corresponding to Fig. 4B. A 0.25-μm DB-225 capillary column (15 m × 0.15 mm I.D.) was used. The injector temperature was kept at 240°C and the column temperature was programmed from 90 to 150°C at 10°C/min and from 150 to 240°C at 1.5°C/min.

in their structure will exhibit the same diagnostic ions as the coplanar PCB congeners monitored in the samples shown in Fig. 6.

The different coplanar PCB congeners shown in Figs. 4 and 6 were determined in concentrated fish oil. However, when their determination must be carried out in conventional biota tissues, some sample requirements must be considered. The most important is that the amount should be increased *ca.* tenfold to produce an ideal ECD response [22]. This is indicated in the analytical scheme in Fig. 1, with the recommendation of using a larger amount of sample for the isolation of coplanar PCBs.

The method reported involving Hypercarb fractionation provides good recoveries of coplanar congeners of PCBs 81, 77, 126 and 169 and offers a complete separation from the conventional PCBs and other micropollutants, such as organochlorine pesticides. This method can be easily coupled to existing clean-up procedures in most environmental laboratories currently analysing PCB congeners and other organic micropollutants in biota samples. A major criticism of the proposed method may be the re-use of the Hypercarb column in the analysis of large numbers of biota samples. The column used in this work has been used for *ca.* 100 analyses with no problems with its re-use. After each analysis, the column was washed with *n*-hexane and dichloromethane for the elimination of possible interferences. Such a washing step will help in removing possible dioxins, as the same column can be used for isolation of these compounds but eluting with more polar solvents. Although it is partly true that the present method is expensive, as the column contains 7-μm particles with a cost of *ca.* US $1000, *versus* the lower cost of using other particle sizes of 40–100 μm in disposable cartridges, so far we have been able to use the Hypercarb column for 100 analyses, with a column-cost per analysis of US $10, which is about 2–3 time more expensive than using cartridges.

CONCLUSIONS

A general analytical scheme (methods A and B in Fig. 1) that facilitates the isolation of coplanar PCB congeners Nos. 81, 77, 126 and 169 from sixteen other PCBs and several organic micropollutants such as organochlorine pesticides and hydrocarbons has been reported. Concerning the determination of conventional PCB congeners, it has been shown for the first time that a DB-17 capillary column offers a complete separation of PCB congeners 149–118 and 138–163, which cannot be achieved with the DB-5 common.

A two-step clean-up method with sulphuric acid and LC fractionation with Hypercarb has been proposed for the determination of coplanar PCB congeners (IUPAC Nos. 81, 77, 126 and 169). It uses *n*-hexane as the eluent in a small volume (100 ml) and it is safer, as confirmation by GC–MS with SIM is guaranteed. Their determination is feasible at low levels of 1 ng/g in wet tissue. The proposed method is superior to Florisil column chromatography, which showed interferences from other PCBs and organochlorine pesticides, such as DDE.

ACKNOWLEDGEMENT

Financial support from PLANICYT (Grant NAT 89-0927) is gratefully acknowledged.

REFERENCES

1 J. S. Waid (Editor), *PCBs and the Environment*, Vols. I, II and III, CRC Press, Boca Raton, FL, 1987.
2 R. D. Kimbourg and A. A. Jensen (Editors), *Halogenated Biphenyls, Terphenyls, Naphthalenes, Dibenzodioxins and Related Products*, Elsevier, Amsterdam, 2nd ed., 1989.
3 V. Lang, *J. Chromatogr.*, 595 (1992) 1.
4 B. Griepink, E. A. Maier, H. Muntau and D. E. Wells, *Fresenius' J. Anal. Chem.*, 339 (1991) 173.
5 B. Larsen, S. Bøwadt and S. Fachetti, *Int. J. Environ. Anal. Chem.*, 47 (1992) 147.
6 P. Fernandez, C. Porte, D. Barceló, J. M. Bayona and J. Albaigés, *J. Chromatogr.*, 456 (1988) 155.
7 G. Petrick, D. E. Schulz and J. C. Duinker, *J. Chromatogr.*, 435 (1987) 241.
8 P. de Voogt, D. E. Wells, L. Reutergardh and U. A. Th. Brinkman, *Int. J. Environ. Anal. Chem.*, 40 (1990) 1.
9 S. Tanabe, N. Kannan, T. Wakimoto and R. Tatsukawa, *Int. J. Environ. Anal. Chem.*, 29 (1987) 199.
10 C. S. Creaser and A. Al-Haddad, *Anal. Chem.*, 61 (1989) 1300.
11 L. M. Smith, T. R. Schwartz, K. Feltz, T. J. Kubiak, *Chemosphere*, 21 (1990) 1063.
12 P. Haglund, L. Asplund, U. Järnberg and B. Jansson, *J. Chromatogr.*, 507 (1990) 389.
13 S. J. Harrad, A. S. Sewart, R. Boumphrey, R. Duarte-Davidson and K. C. Jones, *Chemosphere*, 24 (1992) 1147.
14 J. N. Huckins, D. L. Stalling and J. D. Petty, *J. Assoc. Off. Anal. Chem.*, 63 (1980) 750.
15 C. S. Hong and B. Bush, *Chemosphere*, 21 (1990) 173.

16 D. W. Kuehl, B. C. Butterworth, J. Libal and P. Marquis, *Chemosphere*, 22 (1991) 849.
17 J. L. Sericano, A. M. El-Hussein and T. L. Wade, *Chemosphere*, 23 (1991) 915.
18 H. Steinwandter, *Fresenius' J. Anal. Chem.*, 342 (1992) 416.
19 B. Larsen and J. Riego, *Int. J. Environ. Anal. Chem.*, 40 (1990) 59.
20 J. de Boer, Q. T. Dao and R. Van Dortmund, *J. High Resolut. Chromatogr.*, 15 (1992) 249.
21 P. de Voogt, *Chemosphere*, 23 (1991) 901.
22 D. E. Wells and I. Echarri, *Int. J. Environ. Anal. Chem.*, 47 (1992) 75.

Journal of Chromatography, 629 (1993) 339–343
Elsevier Science Publishers B.V., Amsterdam

CHROM. 24 643

Gas chromatographic determination of trace nitrite after derivatization with ethyl 3-oxobutanoate

Takao Mitsuhashi

Hyogo Prefectural Institute of Public Health, Arata-cho, Hyogo-ku, Kobe 652 (Japan)

(First received June 16th, 1992; revised manuscript received September 22nd, 1992)

ABSTRACT

A gas chromatographic method was developed for the determination of nitrite using ethyl 3-oxobutanoate as a derivatization reagent. Nitrite was reacted with ethyl 3-oxobutanoate in the presence of hydrochloric acid to form ethyl 2-hydroxyimino-3-oxobutanoate (EHOB) quantitatively. The resulting EHOB was extracted with ethyl acetate and then determined sensitively by gas chromatography with electron-capture detection. This method has been applied successfully to the determination of nitrite in river water and human saliva, with a detection limit of 2 ng/ml and recoveries of 94–100%.

INTRODUCTION

Nitrite is widespread in nature and its level varies widely among foods and in the environment. Nitrite is generally regarded as a hazardous compound, because it may react with amines and amides to produce carcinogenic N-nitroso compounds [1]. Nitrite is also known to produce excess abnormal haemoglobin, causing methaemoglobinaemia [2]. The development of a method for the determination of nitrite in foods and the environments is, therefore, of great importance. Several techniques have been reported for the determination of nitrite, including spectrophotometry [3–5], polarography [6], fluorimetry [7], flow-injection analysis [8] and ion chromatography [9]. Gas chromatographic (GC) determinations of nitrite have also been reported using different derivatization reagents, *e.g.* hydralazine [10], *o*-phenylenediamine [11], aromatic primary amines [12–14] and pentafluorobenzyl bromide [15]. However, some of the GC methods have disadvantages such as instability of the reaction product, a high reaction temperature or a time-consuming reaction.

It is wel known that nitrite reacts readily with ethyl 3-oxobutanoate in acidic media to give ethyl 2-hydroxyimino-3-oxobutanoate (EHOB) [16,17]:

$$CH_3COCH_2CO_2C_2H_5 \xrightarrow[H^+]{NO_2^-} CH_3COCH(NO)CO_2C_2H_5 \longrightarrow \underset{\text{EHOB}}{CH_3COC(=NOH)CO_2C_2H_5}$$

Correspondence to: T. Mitsuhashi, Hyogo Prefectural Institute of Public Health, Arata-cho, Hyogo-ku, Kobe 652, Japan.

0021-9673/93/$06.00

We have developed a GC method, using the above reaction, in which trace amounts of nitrite are converted into EHOB. The derivatization is very fast and proceeds quantitatively without temperature control. Owing to the high sensitivity of EHOB to electron-capture detection (ECD), nitrite at ppb levels can be successfully determined by this method.

EXPERIMENTAL

Apparatus

Chromatographic analyses were performed on a Yanako (Kyoto, Japan) G-2800 gas chromatograph equipped with a ^{63}Ni-source electron-capture detector. A glass column (2 m × 3 mm I.D.) was packed with 5% diethylene glycol succinate + 1% H_3PO_4 on 60–80-mesh Chromosorb W DMCS (Gasukuro Kogyo, Tokyo, Japan). Nitrogen was used as the carrier gas at a constant flow-rate of 45 ml/min. The detector, injection port and column temperatures were maintained at 260, 220 and 200°C, respectively. The peak heights were measured with a digital integrator (Yanako S-1200).

For mass spectral identification of the nitrite derivative, a Hewlett-Packard Model 5890 gas chromatograph coupled with a Hewlett-Packard Model 5970B mass spectrometer was used. An HP-1 (100% dimethylpolysiloxane) (Hewlett Packard) capillary column (12 m × 0.2 mm I.D.) was directly interfaced to the electron-impact ion source. The injection port and interface temperatures were maintained at 250 and 280°C, respectively. The initial column oven temperature was 60°C and was increased at 20°C/min to 200°C. The ionizing voltage was 70 eV. Helium was used as the carrier gas at 4 psi (27.6 kPa).

Reagents

Ethyl 3-oxobutanoate was obtained from Tokyo Kasei Kogyo (Tokyo, Japan) and used as received. All other reagents were of analytical-reagent grade. Distilled, deionized water was used throughout. A stock standard nitrite solution (1 mg/ml) was prepared by dissolving 1.500 g of sodium nitrite (dried at 110°C for 3 h) in 1 l of water. Working standard solutions were prepared by appropriate dilution of this stock standard solution.

Samples

River water samples were collected from the city of Kobe. Human saliva samples (1 g) were weighed into a 100-ml volumetric flask and diluted to volume with water. The sample solutions were centrifuged at 3000 rpm (*ca.* 1000 *g*) for 5 min to remove insoluble matter and the supernatants were subjected to GC analysis.

Procedure

A 10-ml volume of sample solution was placed in a 20-ml test-tube fitted with a ground-glass stopper, then 0.02 ml of ethyl 3-oxobutanoate and 1 ml of concentrated hydrochloric acid (*ca.* 11 *M*) were added successively. The mixture was allowed to stand for 5 min at room temperature, then 5 ml of ethyl acetate were added. After shaking for 1 min, the ethyl acetate layer was transferred into a 10-ml test-tube and dehydrated with a small amount of anhydrous sodium sulphate. A 2-μl aliquot of the ethyl acetate extract was injected into the gas chromatograph and the derivative peak height was measured.

A 10-ml volume of each standard solution (0.01–0.1 μg/ml) was treated in the same manner to prepare a calibration graph. The nitrite content in the sample solution was calculated from the calibration graph.

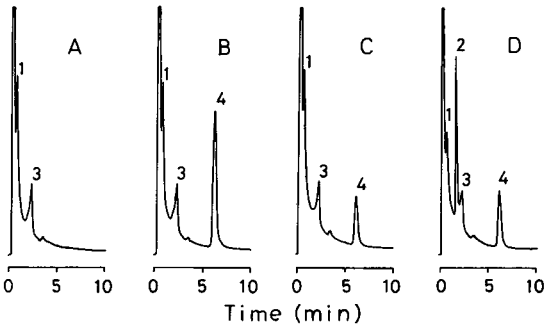

Fig. 1. Gas chromatograms obtained in the analyses of (A) reagent blank, (B) 0.1 μg/ml nitrite, (C) river water and (D) human saliva. Peaks: 1 = ethyl 3-oxobutanoate; 2 and 3 = unknowns; 4 = ethyl 2-hydroxyimino-3-oxobutanoate (EHOB). For GC conditions, see Experimental.

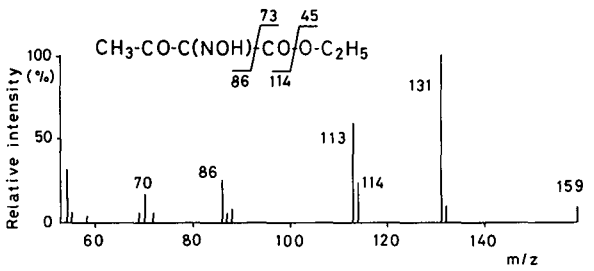

Fig. 2. Mass spectrum of nitrite derivative of ethyl 3-oxobutanoate.

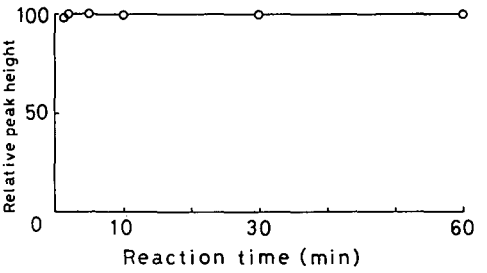

Fig. 4. Effect of reaction time on the formation of EHOB. For other conditions, see Experimental.

RESULTS AND DISCUSSION

Identification of the derivative

The application of the reaction of nitrite with ethyl 3-oxobutanoate to give EHOB [15,16] to the determination of nitrite has not been reported. Initially, we tried to confirm whether this reaction occurred even at low concentrations of nitrite; a 0.1 μg/ml nitrite standard solution was subjected to the derivatization. Fig. 1 shows gas chromatograms obtained for (A) reagent blank, (B) nitrite standard (0.1 μg/ml), (C) river water and (D) human saliva. Peaks 1 and 4 correspond to ethyl 3-oxobutanoate and its nitrite derivative, respectively. The identification of the derivative (peak 4) was carried out by GC–MS. The mass spectrum obtained (Fig. 2) exhibits the parent ion at *m/z* 159 and fragment ions at *m/z* 114 and 86. The mass spectrum shows the derivative to be EHOB. No change in the chromatograms was observed whether the chromatography was done immediately or after storage of the ethyl acetate extract at room temperature for a few days, indicating that EHOB is relatively stable.

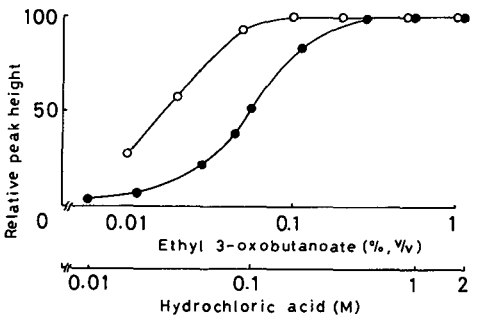

Fig. 3. Effects of (○) ethyl 3-oxobutanoate and (●) hydrochloric acid concentrations on the formation of EHOB. For other conditions, see Experimental.

Optimum derivatization conditions

The reaction of nitrite with ethyl 3-oxobutanoate proceeds in acidic media. We chose hydrochloric acid, which has been widely used in nitrite reactions [16]. In order to optimize the derivatization conditions, we examined the effects of the concentrations of ethyl 3-oxobutanoate and hydrochloric acid and the reaction time, using a 0.1 μg/ml nitrite standard solution. The derivatizations were carried out in almost the same manner as described under Experimental. The concentrations of ethyl 3-oxobutanoate and hydrochloric acid in the reaction mixture were varied separately and the peak heights of the resulting EHOB were measured.

Fig. 3 shows the effect of the concentration of ethyl 3-oxobutanoate on the formation of EHOB. When the ethyl 3-oxobutanoate concentration in the reaction mixture was higher than 0.1% (v/v), the peak height of the resulting EHOB reached a maximum. Fig. 3 also shows the effect of the concentration of hydrochloric acid. The EHOB peak height reached a maximum at hydrochloric acid concentrations above 0.5 *M*. From these results, final concentrations of *ca.* 0.2% (v/v) ethyl 3-oxobutanoate and *ca.* 1 *M* hydrochloric acid were adopted.

Fig. 4 shows the effect of reaction time on the formation of EHOB. The derivatization was completed rapidly. The peak height of EHOB became a maximum with reaction times longer than 2 min. Therefore, the reaction time was fixed at 5 min.

Several organic solvents were tested for extraction of the resulting EHOB. The distribution coeffi-

TABLE I

EFFECT OF FOREIGN ANIONS

The concentration of nitrite was 0.1 μg/ml.

Anion	Added as	Concentration (μg/ml)	Relative peak height[a]
None			100.0 ± 1.8
Cl^-	NaCl	100	101.4 ± 0.4
F^-	KF	100	99.5 ± 3.2
Br^-	KBr	100	99.4 ± 0.9
I^-	KI	100	69.5 ± 0.7
I^-	KI	10	93.8 ± 0.6
NO_3^-	KNO_3	100	100.9 ± 2.2
SO_4^{2-}	Na_2SO_4	100	98.9 ± 3.2
SO_3^{2-}	Na_2SO_3	100	69.0 ± 3.0
SO_3^{2-}	Na_2SO_3	10	96.1 ± 1.6
CO_3^{2-}	Na_2CO_3	100	98.4 ± 3.9
HCO_3^-	$NaHCO_3$	100	100.7 ± 3.4
HPO_4^{2-}	K_2HPO_4	100	96.8 ± 3.4
$H_2PO_4^-$	KH_2PO_4	100	99.9 ± 3.3
CH_3COO^-	CH_3COONa	100	101.3 ± 1.9
SCN^-	KSCN	100	87.9 ± 2.9
SCN^-	KSCN	10	94.3 ± 2.1

[a] Mean ± standard deviation for three determinations.

cient of EHOB, defined as the ratio of the concentration in the organic phase to that in the aqueous phase, were measured by a double extraction. The ratio of the concentration or peak response of the first to that of the second extract is equal to one plus the distribution coefficient (D) times the ratio of the volume of the organic phase (V_o) to that of the aqueous phase (V_a):

$$C_1/C_2 = 1 + DV_o/V_a$$

The distribution coefficients are 53 for ethyl acetate, 27 for diethyl ether, 0.27 for cyclohexane and 0.02 for *n*-hexane. When ethyl acetate was used as the extraction solvent, *ca.* 96% of the resulting EHOB in the aqueous phase was transferred into the ethyl acetate extract in this method.

Calibration

A calibration graph was constructed by plotting the peak height of EHOB (y) *versus* the concentration of nitrite (x). A good linear relationship, $y = 0.358x + 0.021$, with a correlation coefficient of 0.998, was obtained in the range 0.01–0.1 μg/ml. The relative standard deviations for five replicate derivatizations of nitrite were 3.4% at 0.01 μg/ml and 1.5% at 0.1 μg/ml. EHOB has a high ECD response, and the detection limit of the method was found to be 0.02 μg of nitrite in 10 ml of aqueous sample.

TABLE II

DETERMINATION OF NITRITE IN RIVER WATER AND HUMAN SALIVA WITH RECOVERY TEST

Sample	NO_2^- added[a]	NO_2^- found[a]		Recovery (%)
		Spectrophotometric method [4]	GC method (this work)[b]	
River water				
A	0	0.025	0.026 ± 0.001	
	0.05		0.073 ± 0.002	94
B	0	0.027	0.026 ± 0.001	
	0.05		0.076 ± 0.001	100
C	0	0.012	0.014 ± 0.001	
	0.05		0.063 ± 0.001	98
Human saliva				
A	0	4.67	4.56 ± 0.14	
	5		9.27 ± 0.42	94.2
B	0	5.41	5.20 ± 0.07	
	5		9.94 ± 0.36	94.8

[a] Units: river water, μg/ml; human saliva, μg/g.
[b] Mean ± standard deviation for three determinations.

Effect of foreign anions

The effect of foreign anions, which may co-exist in the sample, on the determination of nitrite was studied. Table I shows the results of interferences by Cl^-, F^-, Br^-, I^-, NO_3^-, SO_4^{2-}, SO_3^{2-}, CO_3^{2-}, HCO_3^-, HPO_4^{2-}, $H_2PO_4^-$, CH_3COO^- and SCN^-. Most of the anions examined, at a concentration of 100 μg/ml, did not interfere with the formation of EHOB. On the other hand, I^-, SO_3^{2-} and SCN^- interfered seriously. The interferences by I^- and SO_3^{2-} may be attributed to the reduction of nitrite by the anions. However, these three anions at a concentration of 10 μg/ml showed no significant interference. The levels of I^-, SO_3^{2-} and SCN^- in ordinary environmental samples are usually lower than the interfering concentrations shown in Table I. These results suggest that this method can be used for the determination of nitrite in environmental samples.

Applications

River water and human saliva samples were analysed by both this method and a spectrophotometric method [4]. Recovery tests with nitrite added to these samples were also carried out in order to assess the efficiency of the method. Fig. 1 shows typical gas chromatograms obtained for river water (C) and human saliva (D). Table II shows the results for the determination and recovery of nitrite in real samples. The nitrite concentrations for each sample determined by the two methods were in good agreement. The recoveries of the spiked nitrite were greater than 94%. The results in Table II indicate that there is no significant interference from the sample matrices in the derivatization step and in the GC determination.

CONCLUSION

A simple and sensitive GC method was developed for the determination of nitrite at trace levels. The reliability and selectively of the method are excellent, and it can be used to determine nitrite accurately at ppb levels in a variety of samples.

ACKNOWLEDGEMENT

The author is grateful to Professor K. Okamoto (Tokushima University) for assistance with the preparation of the manuscript.

REFERENCES

1 R. Fudge and R. W. Truman, *J. Assoc. Publ. Anal.*, 11 (1973) 19.
2 A. Knotek and P. Schmidt, *Pediatrics*, 34 (1964) 78.
3 P.Griess, *Chem. Ber.*, 12 (1879) 426.
4 *Standard Methods for the Examination of Water and Wastewater*, American Public Health Association, New York, 14th ed., 1976, p. 434.
5 H. P. S. Rathore and S. K. Tiwari, *Anal. Chim. Acta*, 242 (1991) 225.
6 S. K. Chang, R. Kozeniauskas and G. W. Harrington, *Anal. Chem.*, 49 (1977) 2272.
7 R. Montes and J. J. Laserna, *Anal. Sci.*, 7 (1991) 467.
8 T. Ohta, Y. Arai and S. Takitani, *Anal. Sci.*, 3 (1987) 549.
9 L. Eek and N. Ferrer, *J. Chromatogr.*, 322 (1985) 491.
10 A. Tanaka, N. Nose, F. Yamada, S. Saito and A. Watanabe, *J. Chromatogr.*, 206 (1981) 531.
11 M. Akiba, K. Toei and Y. Shimoishi., *Bunseki Kagaku*, 22 (1973) 924.
12 K. Funazo, M. Tanaka and T. Shono, *Anal. Chem.*, 52 (1980) 1222.
13 K. Funazo, K. Kusano, M. Tanaka and T. Shono, *Analyst (London)*, 107 (1982) 82.
14 T. Chikamoto and S. Nagata, *Chem. Lett.*, (1980) 737.
15 H.-L. Wu, S.-H. Chen, K. Funazo, M. Tanaka and T. Shono, *J. Chromatogr.*, 291 (1984) 409.
16 O. Touster, *Org. React.*, 7 (1953) 327.
17 H. Adkins and E. W. Reeve, *J. Am. Chem. Soc.*, 60 (1938) 1328.

Journal of Chromatography, 629 (1993) 345–359
Elsevier Science Publishers B.V., Amsterdam

CHROM. 24 634

Influence of linear velocity and multigradient programming in supercritical fluid chromatography

S. Küppers, M. Grosse-Ophoff and E. Klesper

Lehrstuhl für Makromolekulare Chemie, Aachen Technical University, Worringer Weg 1, W-5100 Aachen (Germany)

(First received July 17th, 1992; revised manuscript received September 21st, 1992)

ABSTRACT

The chromatographic plate height, resolution and time requirements in supercritical fluid chromatography depend on the physical properties of the mobile phase (pressure, mobile phase composition, temperature and linear velocity), on the chemical structure of the analyte, which determines vapour pressure and solubility, and on various properties of the stationary phase. If a given homologous series of compounds, or a test mixture simulating a homologous series, is used with a specific chromatographic column, the chromatographic properties for the compounds in these test mixtures will vary with pressure, mobile phase composition, temperature, velocity and the relative molecular mass of the individual compounds. If in addition to a suitable column a temperature is chosen which, for simplicity, is kept constant, and which is known to lead to good or even optimum resolution, the pressure, composition and relative molecular mass dependence of the Van Deemter plate height minimum, as determined experimentally at this temperature, can be used for predicting an optimum linear velocity programme. This velocity programme can be used either as a stand-alone programme or can be adapted to and superimposed on pressure or composition programmes, or even on combined pressure–composition programmes. The linear velocity dependence of plate height and resolution for a mobile phase composed of a mixture of carbon dioxide and methanol on a column packed with unbonded silica gel is presented. This dependence was measured at different pressures and compositions, employing four condensed aromatics as a test analyte. Each chromatogram of the analyte was therefore measured at constant temperature, velocity, pressure and composition, varying the last three physical properties between chromatograms. The data are presented as Van Deemter plots and as three-dimensional plots showing the dependence of resolution and capacity factor on velocity and either pressure or composition. Based on these data, the change in the linear velocity suitable for pressure programmes, mobile phase composition programmes and for increase in the relative molecular mass of the analyte is discussed. The conclusion is that a pressure (density) programme needs a superimposed negative linear velocity programme for the purpose of decreasing the plate height and increasing the resolution, whereas such a programme is not necessary to a comparable extent for composition programming. If compounds with a wide range of relative molecular masses are separated, the superimposing of a negative linear velocity programme on to a composition programme is also advantageous. For programming the physical properties of a mobile phase, *i.e.*, pressure, density, composition, temperature and velocity, a number of closely related equations are proposed and some corresponding programme curves are shown. Hardware needs for programming are also briefly discussed.

INTRODUCTION

Supercritical fluid chromatography (SFC) has been established as a routine method in some areas of analytical chemistry. For the further development of SFC, a general knowledge of the possibilities for the optimization of efficiency and resolution by gradient programming is important. The first generation of commercially available capillary SFC instruments were designed to achieve pressure (density) programmes by controlling and programming the pressure at the column inlet, thereby usually increasing the flow-rate through a capillary column whenever a "fixed" restrictor was employed at the column outlet. As is well recognized, the problem with this pressure programming technique is an increase in the linear velocity in the column, which may strongly decrease plate numbers, *i.e.*, efficiency.

Correspondence to: E. Klesper, Lehrstuhl für Makromolekulare Chemie, Aachen Technical University, Worringer Weg 1, W-5100 Aachen, Germany.

0021-9673/93/$06.00

A second problem with the first generation of capillary SFC instrumentation was that the change in the nature of the mobile phase via programming of a composition gradient was not possible. A means of solving these problems was shown independently by different groups using pressurized gases or liquids as programmable counter pressure media at the outlet of open-tubular and other microcolumns [1–3]. These difficulties were not inherent in the use and commercialization of SFC instruments employing larger diameter packed columns because regulating valves at the column outlet could be used from the beginning of the development of SFC apparatus. Recently, self-controlling regulating valves as part of feedback loops have been introduced for larger diameter packed columns [4–7]. The regulation devices allow pressure and composition gradients independently of each other and of the feed rate of the pumps, which means that these devices allow also independent linear velocity programming for a continuous optimization of efficiency. Instruments using such valves have already become commercially available and more are expected to follow.

An SFC instrument that is capable of all these gradient programming techniques, including temperature programming, offers both the capability and the problem of finding the optimum single or combination gradient method. For instance, the optimum velocity programme to be superimposed on a composition programme, a pressure programme or a temperature programme is not entirely obvious and few relevant data are available in the literature. It can be expected, however, that the combination of a velocity programme with a temperature programme, or *vice versa*, should be applied, considering that a negative temperature programme reduces diffusion and diffusion coefficients, which is to be counteracted by a negative velocity programme, whereas a positive temperature programme increases diffusion and the velocity probably needs increasing. It might be expected also that in combination with other positive gradients, *i.e.*, pressure and composition, a usually negative velocity programme is useful if optimized efficiency and resolution are required throughout a separation.

This paper reports first the influence of linear velocity on plate height at different pressures and compositions, choosing a constant temperature of 150°C. The chromatographic system consisted of a column packed with unbonded silica which had been modified with methanol (see Experimental). The mobile phases were composed of mixtures of carbon dioxide (CO_2) and methanol and the test analyte consisted of a mixture of four condensed aromatic hydrocarbons. All individual chromatograms were obtained keeping the linear velocity, pressure, composition and temperature constant. Analogous work on the same system at constant pressure, composition and temperature at the more simply attainable constant flow-rates instead of constant linear velocities will be presented elsewhere [8]. The present results are expressed as the usual Van Deemter plots [9] of plate height *versus* linear velocity at constant pressure, composition and temperature. Because these Van Deemter plots were obtained at different pressures and compositions, it can be seen how a change in pressure or in composition affects the plots. This is equivalent to obtaining a first answer about how a pressure or a composition programme is to be combined with a velocity programme. Some information can even be obtained about suitable ternary combinations of programmes for velocity, pressure and composition. Previous studies of Van Deemter plots with different unbonded, bonded or coated silica phases in packed columns have shown significant differences in the HETP for different stationary phases and for the same stationary phase applied with different analytes [10–13]. Both results are to be expected on account of the different interdiffusion coefficients and capacity factors of the analytes. The mobile phases in these previous studies were pure CO_2 and CO_2–methanol mixtures.

This paper also reports on the influence of linear velocity on the capacity factors and resolution at different pressures and compositions at a constant temperature of 150°C. The results are presented in three-dimensional graphs, in which capacity factor and resolution are plotted against velocity and either pressure or composition. Again, information is obtained from this type of plot about suitable combinations of velocity, pressure and composition for binary gradient programmes.

Because gradient programmes having a good separation effect may follow relatively simple mathematical equations, a self-consistent set of simple equations appears desirable for programming the different parameters of the mobile phase. Therefore, a basic equation was developed that is applicable to

velocity, flow, pressure, density, composition or temperature programmes, singly or in combination as simultaneous or consecutive programmes. Emphasis was placed on employing a minimum of freely choosable constants in the equations, yet retaining maximum flexibility. Some hardware requirements for using the programmes are discussed with a view to combining GC with SFC by pressure or density programmes in the same chromatogram.

EXPERIMENTAL

The chromatographic equipment used was a modified Hewlett-Packard (Waldbronn, Germany) HP 1084B with a Model LC-75 UV detector (Perkin-Elmer, Düsseldorf, Germany) modified to be equipped with a high-pressure UV detector cell for pressures up to 350 bar as described previously [7,14]. The pressure-regulating system was composed of an electronically controlled Hitec valve (Bronkhorst Hitec, Ruurlo, Netherlands) [7], followed in series downstream by a Tescom (Elk River, MN, USA) back-pressure regulator analogous to published arrangements [4]. The complete pressure programming system consisted of these valves, an IBM AT PC and an ADDA converter as described previously [7].

The carbon dioxide eluent (99.995% purity) (Linde, Cologne, Germany) was prepressurized with helium in the storage cylinder and delivered as a liquid to the pump, the cylinder being turned upside down. The methanol (Merck, Darmstadt, Germany) was delivered from liquid storage bottles which were part of the original equipment of the HP 1084B chromatograph. A laboratory-made analytical column (250 mm × 4.6 mm I.D.), packed with LiChrospher Si 100 (5 μm particle diameter) (Merck) by a slurry packing procedure [15], was used. The column was conditioned with methanol at 300°C and 300 bar before use according to an earlier procedure employing 1,4-dioxane [16] instead of methanol. It is found that this conditioning leads to reaction of methanol with the silica, as is shown by the C content of the silica after conditioning. As the analyte a polyaromatic hydrocarbon mixture composed of naphthalene, anthracene, pyrene and chrysene was used at concentrations between $1 \cdot 10^{-2}$ and $1 \cdot 10^{-3}$ mol/l of each component in heptane. The sample was injected by means of a Rheodyne Model 7125 valve (ICT Handelsgesellschaft, Frankfurt, Germany) equipped with a 20-μl sample loop. The temperature of the column was kept constant at 150°C by use of a Hereaus (Hanau, Germany) forced circulation air oven.

The elution time of the solvent heptane was taken as the dead time, t_0, whereby the pulse of heptane led to a negative peak in the UV detector. The linear velocity, u, determined from t_0 and $u = L/t_0$ (L = column length), was varied by changing the mobile phase pump flow-rate, and ranged from 0.07 to a maximum of 1.05 cm/s at 150 bar and 150°C. Both of these values arise because of hardware limitations of the instrument used. Thereby, the maximum linear velocity attainable was lower at higher than at lower pressures. The optimum linear velocity, u_{opt}, was obtained from the Van Deemter plots by both splines and best estimates. Similar results were obtained in both instances.

The plate height (HETP) was calculated from the column length, L, the retention time of the eluted peak, t_r, and its peak width at half-height, $w_{0.5}$, by means of the equation

$$\mathrm{HETP} = \frac{L}{5.54}\left(\frac{w_{0.5}}{t_r}\right)^2 \tag{1}$$

The capacity factor, k', and the resolution between peaks i and j, R^*_{ij}, were calculated according to $k' = (t_r - t_0)/t_0$ and [17]

$$R^*_{ij} = \frac{f_{ij}}{g_{ij}} + \frac{d_{ij}}{w'_i + w'_j}\sqrt{\ln 4} \tag{2}$$

with $d_{ij} > 0$, where f_{ij} is the depth of the valley between the two peaks i and j, g_{ij} is the average height of the two peaks, w' is the peak width at half-height and k_{ij} is the distance between the baseline intercepts of the tangents to the peaks. For determining d_{ij}, on each peak a tangent is drawn on that side of the peak which is adjacent to the other peak. The average resolution R^*_m is the arithmetric mean of the R^*_{ij}.

$$R^*_m = \sum_1^n R^*_{ij}/n \tag{3}$$

where n is the number of peak pairs in the analyte mixture, *i.e.*, $n = 3$ in the present case. For the plotting of the three-dimensional graphs, in which k' is plotted on one of the axes and R^*_m is represented by

shading the three-dimensional surface, a computer programme (Unimap; Uniras European Software Contractors, Lyngby, Denmark, and Düsseldorf, Germany) was used as described in detail previously [18].

RESULTS AND DISCUSSION

The HETP in SFC, as opposed to gas chromatography (GC), depends on physical properties of the mobile phase other than temperature and linear velocity. The HETP in SFC is in addition a function of pressure or density and mobile phase composition, besides also being dependent, as in GC, on the physical properties of the sample components, *i.e.*, vapour pressure and chemical structure, and on the stationary phase.

If in SFC a given stationary phase and a given homologous series of components, or a test mixture simulating a homologous series, is used, the HETP values for the compounds in these mixtures then vary only with pressure, mobile phase composition, temperature and velocity. At a given pressure, composition and temperature the experimentally determined Van Deemter curves show a plate height minimum at an optimum linear velocity, u_{opt}, for each compound in the analyte mixture. Provided that the dependence of the Van Deemter plate height minimum and of the corresponding u_{opt} on pressure, composition and temperature is known for a given analyte mixture, a suitable velocity programme can be derived for the separation either as a stand-alone programme or for superimposition of the velocity programme on a pressure, composition or temperature programme.

First, the linear velocity dependence of the HETP for a binary mobile phase composed of different relative amounts of CO_2 and methanol will be presented. All experiments were performed with a test mixture of naphthalene, anthracene, pyrene and chrysene on an unbonded, normal-phase LiChrospher 100 (5 μm) silica gel stationary phase. The experiments were carried out at a range of pressures and compositions but always at a constant temperature of 150°C. The reasons for choosing a constant temperature of 150°C were to reduce the number of chromatograms needed for the study and because it was found that the optimum resolution was obtained at *ca.* 150°C with, however, significant changes in the optimum temperature with pressure and composition.

In the Van Deemter plots in Figs. 1–5 increasing amounts of methanol (2.5, 5, 10, 20 and 30%, v/v) were employed for the CO_2–methanol binary mobile phase. In Fig. 1a–c the mobile phase is CO_2 with 2.5% of methanol. An increase in pressure from 150 (Fig. 1a) via 200 (Fig. 1b) and 250 bar (Fig. 1c) to 300 bar (Fig. 1d) leads generally to a decreased, and in part unchanged or even increased, plate height at u_{opt}. This decrease in HETP conflicts with the usual notion that increasing pressure tends always to increase the plate height. Chrysene shows increasing HETP with increase in pressure. The behaviour of chrysene may be explained by a larger decrease in the interdiffusion coefficient with pressure than occurs for the smaller molecules.

Turning to Figs. 2–5, with 5, 10, 20 and 30% of methanol in the mobile phase, the results with respect to the pressure dependence of HETP at u_{opt} are similar to those in Fig. 1. For Figs. 2–5 the HETP again decreases or remains about the same with increase in pressure as far as naphthalene, anthracene and pyrene are concerned, but tends to increase for chrysene. It should be noted, however, that the scatter of the data for the HETP in Figs. 1–5 is considerable. Nevertheless, the behaviour of the three lower relative molecular mass compounds is clear and that of chrysene stands out.

The second effect of pressure, which is also of significance, is the shift of the HETP minimum in the Van Deemter curves to lower values of the optimum velocity, u_{opt}, when the pressure increases. At the same time, there is a tendency for narrowing the range of the low HETP around the location of u_{opt}, steepening the slopes of the low- and the high-velocity branches of the Van Deemter curves. Nevertheless, there is still a reasonably wide range of velocity that can be used even for the highest pressure (300 bar). The curves indicate also that, generally, a lower linear velocity for the minimum is found when the relative molecular mass or the size of the sample molecule increases. Considering that naphthalene is eluted first and chrysene last during the separation and taking the Van Deemter plots for 10% methanol as an example (Fig. 3), the velocity might be reduced during the separation by pressure programming from about $u = 0.4$ cm/s for the elution of naphthalene to 0.15 cm/s for the elution of chrysene to

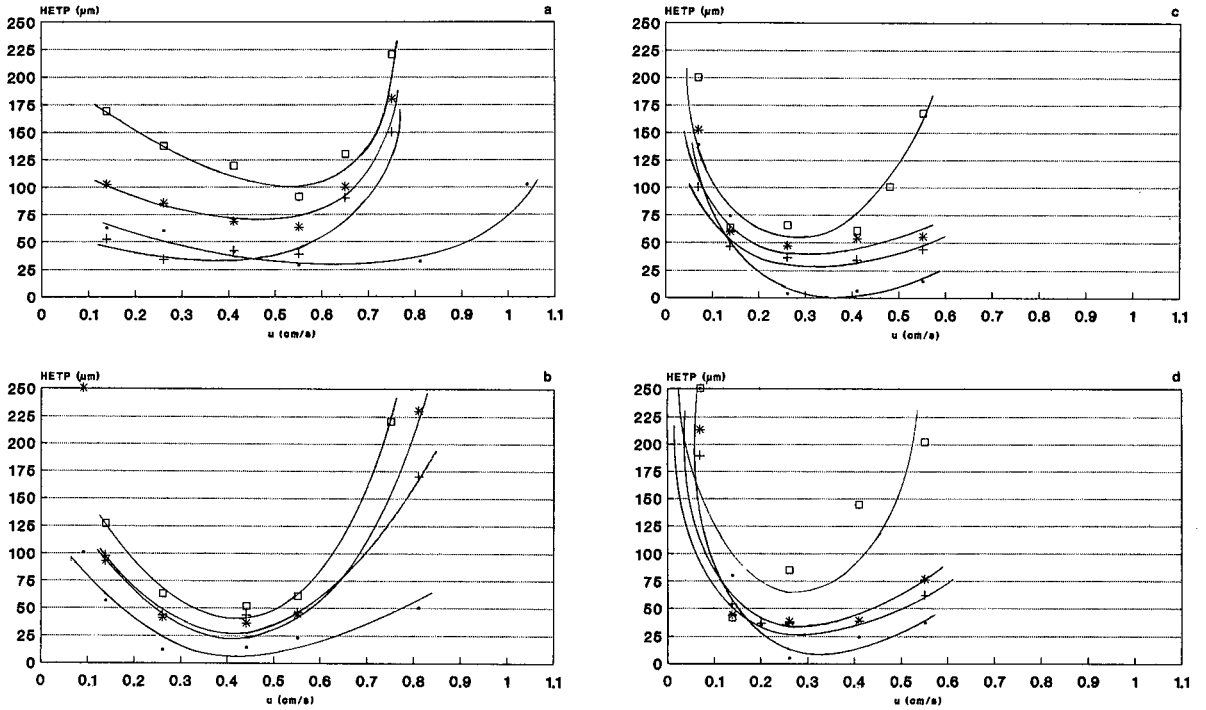

Fig. 1. Van Deemter plots for a mobile phase of carbon dioxide–2.5% (v/v) methanol for (a) 150, (b) 200, (c) 250 and (d) 300 bar and 150°C. Column, 250 mm × 4.6 mm I.D., packed with unbonded silica gel (5 µm). Test mixture: ■ = naphthalene; + = anthracene; ✳ = pyrene; □ = chrysene. Additional conditions as given in the text.

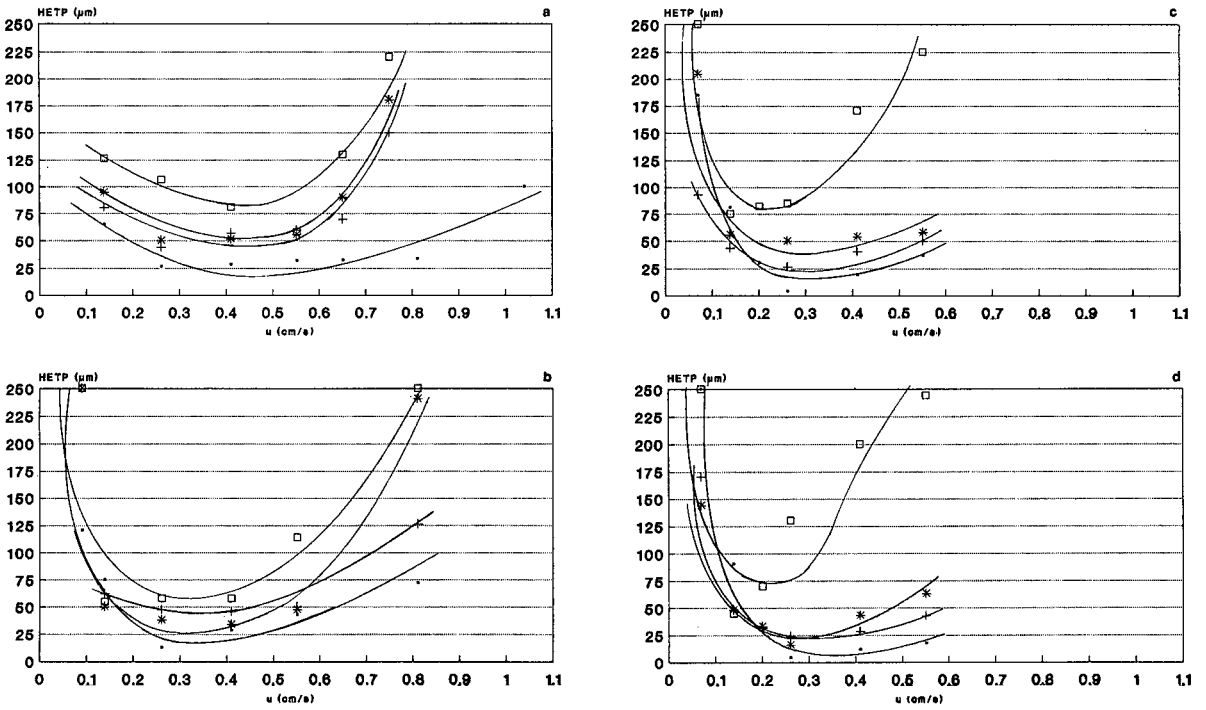

Fig. 2. Van Deemter plots for a mobile phase of carbon dioxide–5% (v/v) methanol for (a) 150, (b) 200, (c) 250 and (d) 300 bar. Other conditions and symbols as in Fig. 1.

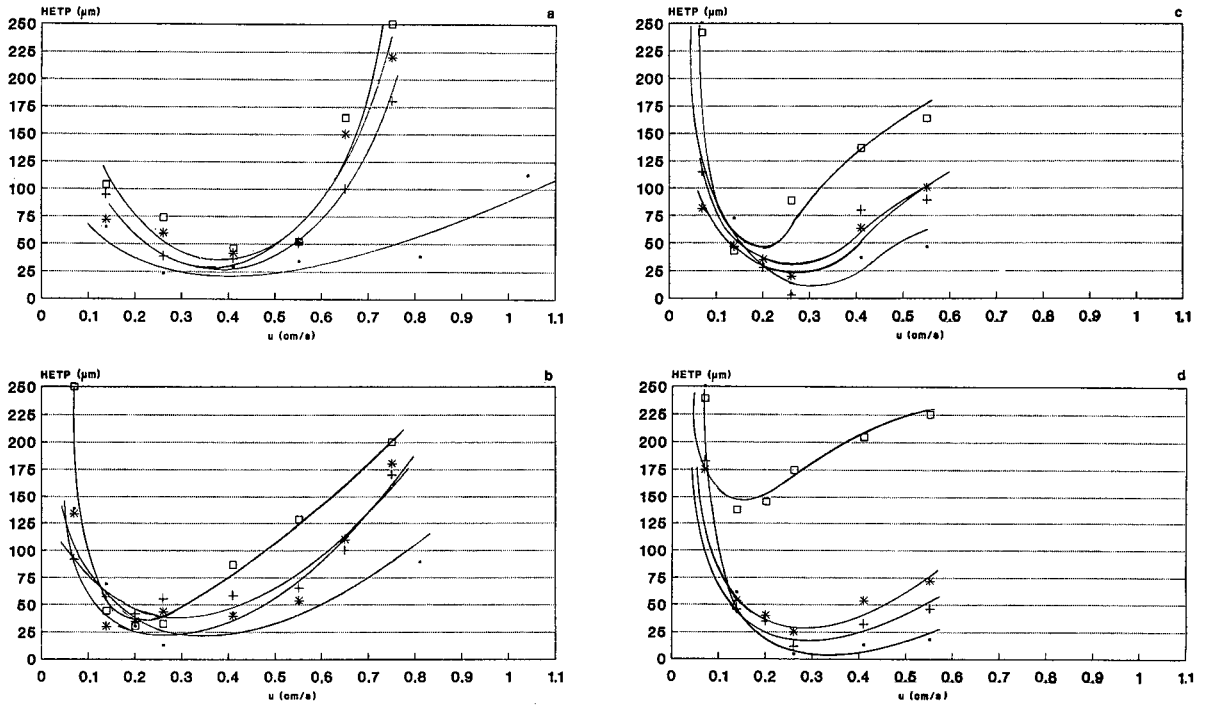

Fig. 3. Van Deemter plots for a mobile phase of carbon dioxide–10% (v/v) methanol for (a) 150, (b) 200, (c) 250 and (d) 300 bar. Other conditions and symbols as in Fig. 1.

obtain low HETPs for all compounds in the mixture. Even if the pressure is kept constant, a decrease in the linear velocity during the separation appears to be advisable.

Turning now explicitly to the influence of the composition of the mobile phase on the Van Deemter curves, one might compare different compositions at the same pressure, that is, 2.5, 5.0, 10.0, 20.0 or 30.0% (v/v) methanol at, for instance, 200 bar (Figs. 1b, 2b, 3b, 4b and 5a). If one compares the different compositions at 150 bar, a trend for the HETP minimum to move to lower linear velocities is observed when the proportion of methanol increases. This trend is smaller, however, than that observed when at a constant composition the pressure is increased from 150 to 300 bar. Moreover, comparing the movement of the HETP minima to lower u_{opt} when the methanol content is increased, it is seen that at lower pressures the shift of u_{opt} is more pronounced than at higher pressures. The first observation, *i.e.*, the smaller influence of composition on u_{opt}, can possibly be explained by smaller decrease in the free volume and the diffusion coefficient of the mobile phase when the more powerful solvent, here methanol, is added at concentrations up to 30% at constant pressure, as compared with a larger decrease in the free volume when the pressure is raised from 150 to 300 bar at constant composition. To give an example of the decrease in linear velocity when employing a composition programme at constant pressure: if a composition programme is run from 2.5 to 30% methanol at 200 bar, the velocity might be decreased from about 0.4 to 0.2 cm/s. Thereby, the starting velocity (0.4 cm/s) is derived from the Van Deemter curve of the first-eluting compound, naphthalene, and the final velocity (0.2 cm/s) is obtained from the last-eluting compound, chrysene.

The effect of the composition, *i.e.*, of an increasing concentration of methanol, on the magnitude of the HETP at u_{opt} is not clear from the present data. On the whole, there is no increase in HETP with an increasing content of methanol. In detail, at 150 bar an increase in methanol content from 2.5 to 30%

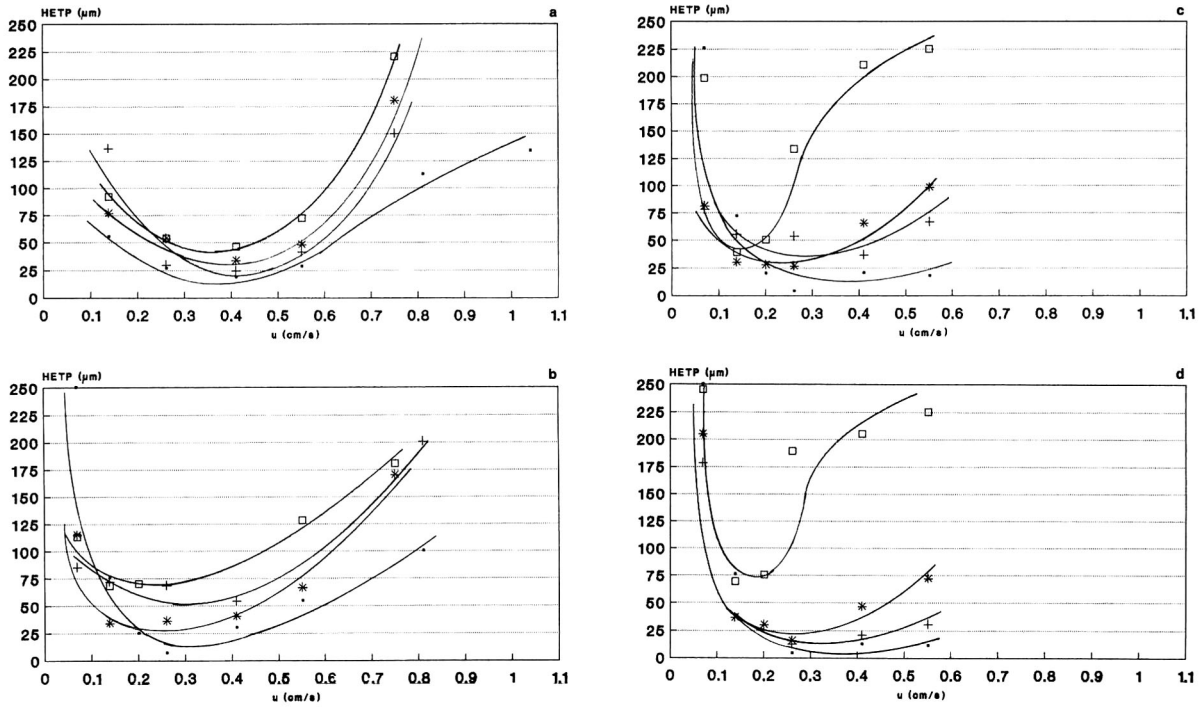

Fig. 4. Van Deemter plots for a mobile phase of carbon dioxide–20% (v/v) methanol for (a) 150, (b) 200, (c) 250 and (d) 300 bar. Other conditions and symbols as in Fig. 1.

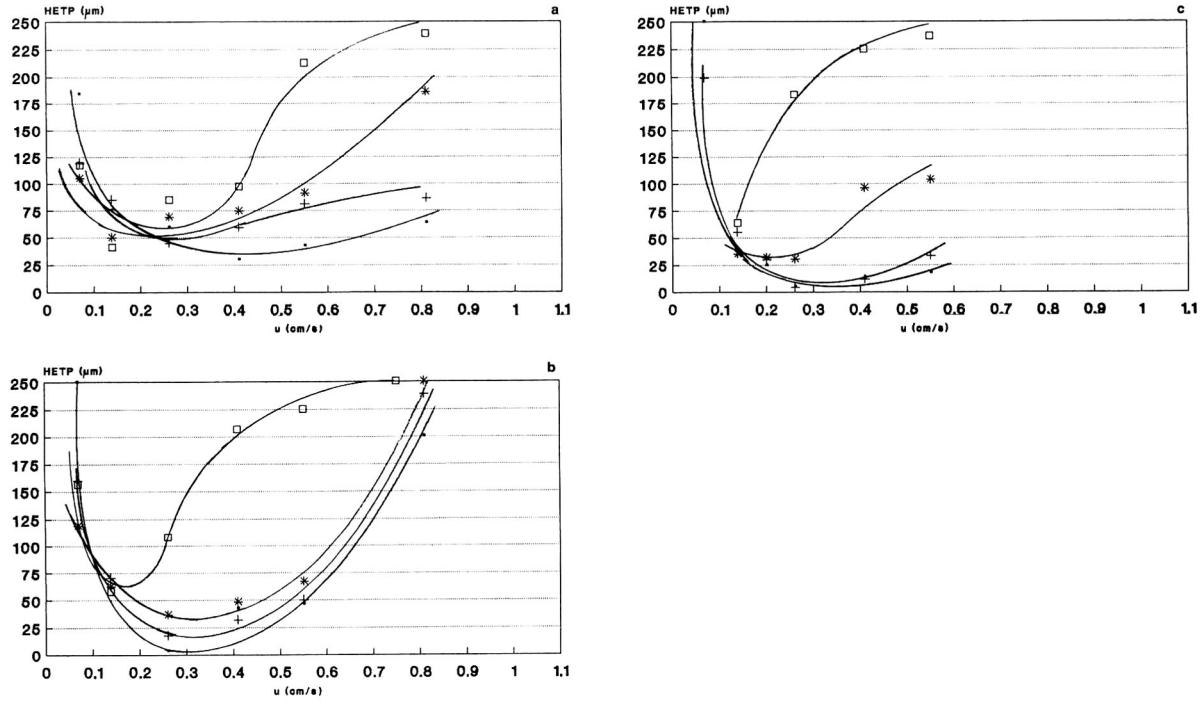

Fig. 5. Van Deemter plots for a mobile phase of carbon dioxide–30% (v/v) methanol for (a) 200, (b) 250 and (c) 300 bar. Other conditions and symbols as in Fig. 1. Data for 150 bar are not presented because at 150°C and 30% (v/v) methanol the area of phase separation was close according to experimental observations, calculation of the critical temperature, T_c, following Chueh and Prausnitz in Reid *et al.* [24] and to the literature data [25].

leads to a smaller HETP at u_{opt}. At 200, 250 and 300 bar no clear trend to either higher or smaller HETP can be discerned.

It is of interest, of course, to establish what influence a change in temperature has on the Van Deemter curves. It can be expected, for instance, that at higher temperatures higher velocities appear to be tolerable. Not many Van Deemter plots in which the temperature has been varied have been published so far. Therefore, the possibilities for comparison with respect to temperature are limited. Two published Van Deemter plots for different methanol contents in CO_2 (3000 psi and 80°C), employing Deltabond CN as the stationary phase and carbazole and naphthalene as analytes, show that increasing the content of methanol does not significantly increase the HETP at u_{opt} but raises the slope of the high-velocity branch [10]. Another Van Deemter plot with pure CO_2 at 50°C, employing octadecyl-bonded silica as the stationary phase and phenanthrene as the analyte, shows a decrease in HETP on increasing the pressure from 170 to 240 bar both for u_{opt} and the high-velocity branch [11]. The results of both studies appear to be compatible with the present results.

At the same pressure, composition and temperature, *i.e.*, for a given Van Deemter plot, the order of the HETP for the different analytes is as expected from their interdiffusion coefficients. Naphthalene has the lowest and chrysene the highest plate height, with anthracene and pyrene being intermediate, as seen in Figs. 1–5. In the literature an opposite order is found in several instances, *i.e.*, an analyte of a lower molar volume has a larger plate height than that with a higher molar volume [11,19–21]. One may possibly explain this opposite order by the type

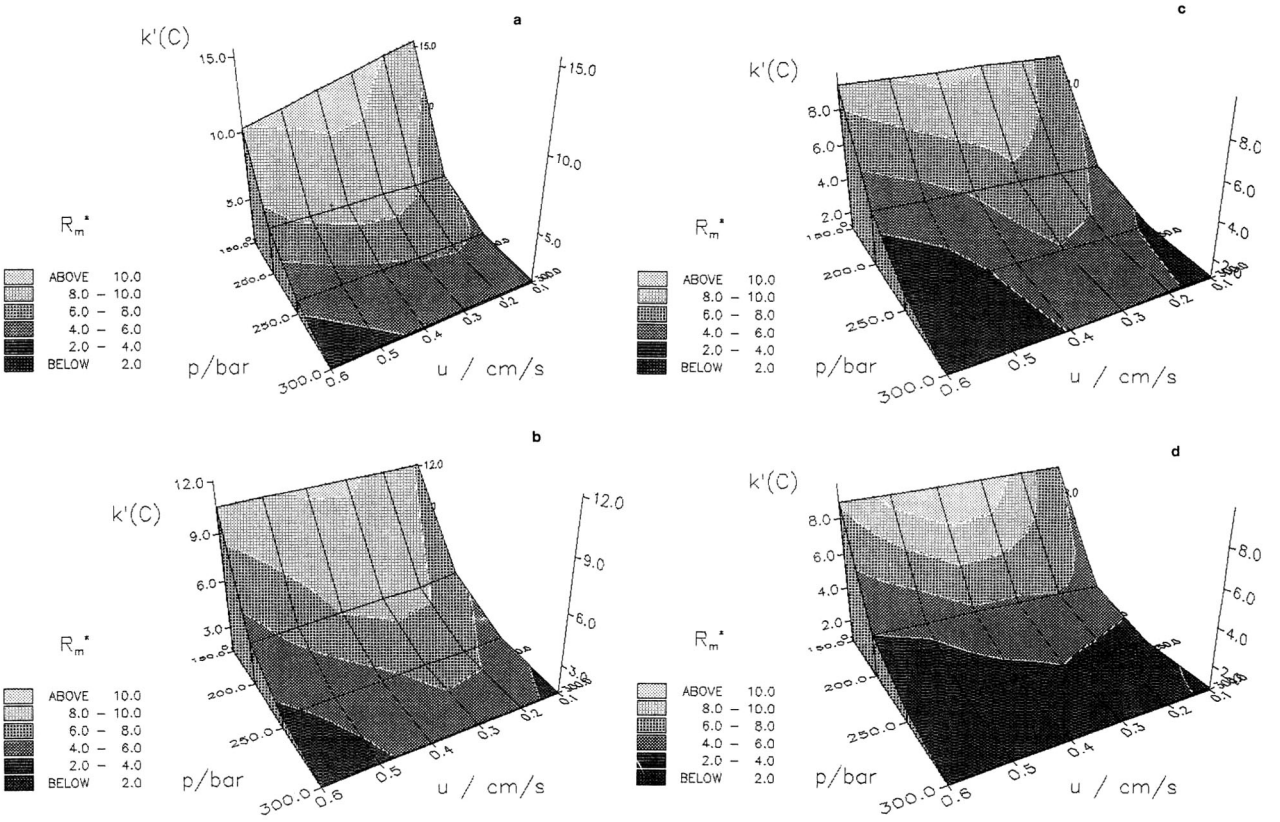

Fig. 6. Graphs of the capacity factor of chrysene, k'(C), *versus* column end pressure, p, and average linear velocity, u. Arithmetic average of resolution between naphthalene, anthracene, pyrene and chrysene, R_m^*, represented as shading of surface. Mobile phase composition: (a) 2.5%; (b) 5%; (c) 10%; (d) 20% methanol in CO_2. Other conditions as in Fig. 1.

of pores, the pore size and the pore size distribution. With on average narrow pores, a narrow pore size distribution and restrictions on cross-section down the length of the pores, it is conceivable that the larger analytes are ad- or absorbed mainly near the entrance of the pores, whereas the smaller analytes may penetrate more deeply into the pores. This may lead to an apparently higher interdiffusion coefficient for the larger analytes and an apparently smaller interdiffusion coefficient for the smaller analytes. The stationary phase used in this work does apparently not fulfil these conditions as the normal order of HETP for analytes of different molecular sizes is observed.

Although the HETP is the preferred measure for judging the quality of a column, the retention time and the resolution are the final criteria for judging the time requirement and quality of a separation for a given analyte mixture on a specific column. The capacity factor is to a first approximation independent of linear velocity and column length, not only in GC and HPLC but also, to a lesser extent, even in SFC, and is given by the ratio of the retention times in the stationary and mobile phases. Therefore, one may consider the capacity factor as a dimensionless retention time measure. In Fig. 6, three-dimensional plots are shown with the capacity factor of chrysene, k'(C), plotted on the z-axis and the pressure at the column end, p, and the linear velocity, u, on the x- and y-axes, respectively. The average resolution, R_m^*, is shown as shading on the three-dimensional surface of the graph. The average resolution, R_m^*, shows a definite maximum at low pressures and at intermediate linear velocities. If the pressure is increased, the maximum tends to move toward lower velocities. This is connected with the decrease in the interdiffusion coefficient at higher density. The capacity factor k'(C) tends to decrease at higher velocities, which may be due to the higher pressure drop over the column arising at higher velocities. An increase in methanol content from 2.5% (Fig. 6a) to 20% (Fig. 6d) leads to considerable decreases in both k'(C) and R_m^*. The same is seen in Fig. 7 with similar three-dimensional graphs in which, however, the p axis is replaced by a %B axis and p = constant in Fig. 7a (200 bar), Fig. 7b (250 bar) and Fig. 7c (300 bar). The R_m^* values show, as in Fig. 6, a maximum which in this instance is located at low %B and again at a medium linear velocity. Also, the

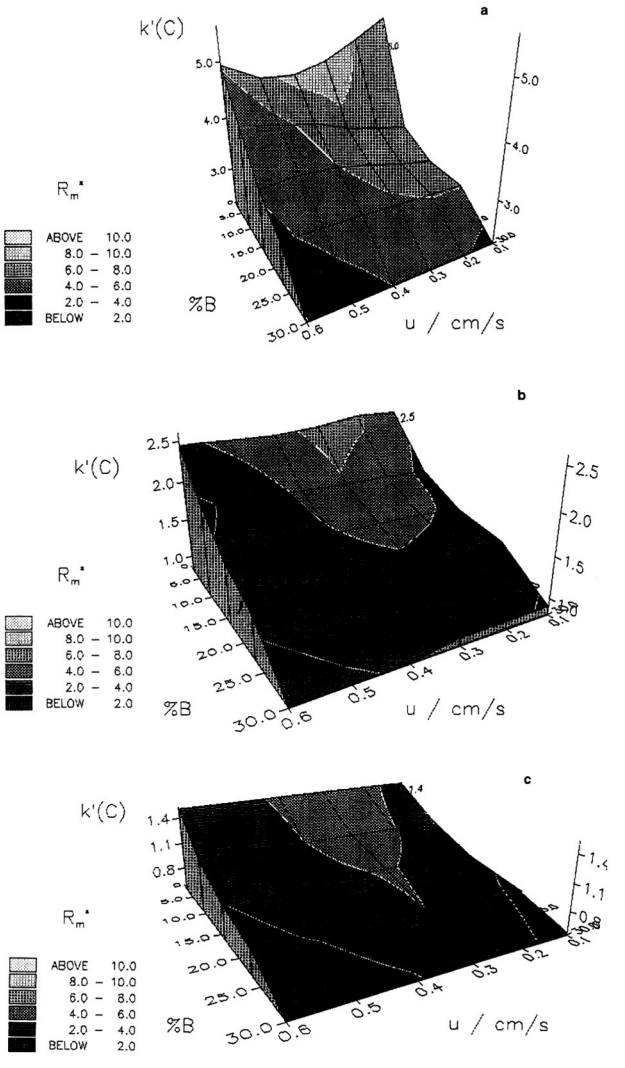

Fig. 7. Graphs of k'(C) *versus* concentration of methanol in CO_2 (%B) and linear velocity (u). R_m^* is shown as shading of surface. Column end pressure: (a) 200; (b) 250; (c) 300 bar. Other conditions as in Fig. 1.

k'(C) values tend to decrease at higher velocities. Inspection of both Figs. 6 and 7 points to a larger change in k'(C) and R_m^* with p than with %B over the ranges investigated. In general, however, the question of p or %B having a larger influence on k' and R_m^* will depend not only on the size of the range, but also on the nature of the two components making up the mobile phase. For instance, it is seen in other cases that the %B of a component with a higher

dissolution power for a specific analyte than methanol will decrease k'(C) more than the pressure p over the chromatographically useful range of %B and p.

Fig. 6 shows that for positive pressure gradient programming at a constant %B and at 150°C, a negative velocity programme is advisable in order to remain at optimum resolution throughout the pressure programme. This appears to be less the case with a positive composition programme as is indicated by Fig. 7, because the optima of k'(C) and R_m^* remain essentially at the same velocity during a %B programme.

Three-dimensional diagrams of the type in Figs. 6 and 7, wherein chromatographic parameters such as capacity factor k', selectivity α, plate number N, plate height H and resolution R are plotted *versus* two physical properties, selected from pressure/density, composition, temperature and linear velocity, contain much useful information for SFC. The information exceeds that available from Van Deemter two-dimensional diagrams, not exhibiting different p, %B or T as parameters. Nevertheless, important information is not contained in the three-dimensional plots, even if by a sufficient number of plots the influence of all four of the physical properties on the chromatographic parameters is shown. The missing information is the time, or time increment, during which a specific set of physical properties of the mobile phase holds during programming. For instance, for pressure programming no information is contained in the three-dimensional plots about the time which is allotted by a programme to a specific pressure level, or pressure increment at a given pressure level. This information can only be supplied by a pressure–time function, that is, by a pressure programme curve. On the other hand, a favourable pressure–time function may be selected from the three-dimensional plots and then both resolution and time requirement for the chromatogram may be estimated. It is thereby understood that the reading of quantitative values cannot be made from three-dimensional plots but that the two-dimensional plots which are the precursors of the three-dimensional diagrams must be utilized. Obviously, it is of major importance to choose a suitable programme curve.

The question of whether a pure mobile phase consisting of component A or a mixed mobile phase consisting of a constant ratio of components A and B is to be preferred for pressure programming with the present or any other system depends to an approximation on the dissolution ability and the diffusion coefficient of component B relative to component A at the same pressure and temperature. If, for instance, by adding B to A there is a significantly higher dissolution ability to be gained with not too great a decrease in diffusion coefficient, then pressure programming with a mixture of A and B should be of advantage. The question of whether a constant mixture of A and B or a composition programme in A and B is to be preferred is related to the difference in the diffusion coefficients between A and B, *i.e.*, as a rule on how much smaller the diffusion coefficient of B is. If there is a large difference, it is of advantage to elute as many compounds in the analyte mixture as possible with zero or low contents of B in the mobile phase. The remaining compounds in the analyte mixture may require steadily increasing contents of B for elution. In such a case a composition programme may yield better resolution in a shorter time than a pressure programme with a constant mixture of A and B.

For the chromatographic system used here, Figs. 6 and 7 can be utilized for a comparison of pressure and composition gradient programmes. Pressure programmes going from 200 to 300 bar with a mobile phase of constant composition of A (CO_2) and B (methanol), *i.e.*, 2.5, 5, 10 or 20% B (Fig. 6) are available for comparison with composition programmes going from 2.5 to 30% B at constant 200, 250 or 300 bar (Fig. 7). For a suitable comparison, it may be considered that both the pressure and the composition programmes should start at the same pressure and composition, *e.g.*, at 200 bar–2.5% B, or at 200 bar–5% B; or at 250 bar–2.5% B or at 250 bar–5% B; etc. Starting a pressure programme at 300 bar is not possible for this comparison because no experiments above 300 bar were conducted. The temperature is comparable, as it is 150°C for all data. As a result of the indicated identical conditions, the compared pressure and composition programmes start at the same k' for the analytes. As the end point for the pressure and composition programmes to be compared one should probably use the same retention time, t_r. Because in the three-dimensional diagrams not t_r but k' is plotted, we are led to use k'. Because both the

starting and the ending k' cannot be read with sufficient accuracy from the three-dimensional plots, the two-dimensional plots of k'(C) *versus* u and of R_m^* *versus* u, which provided the precursors of the three-dimensional diagrams, were considered. At optimum velocities, the composition programmes in Fig. 7 lead on average to about same resolutions as the pressure programmes in Fig. 6, but exhibited higher capacity factors. This is probably connected with the relatively small increase in dissolution power for the analytes used here when methanol is added to CO_2 in the supercritical mobile phase.

Equations useful for gradient programming have rarely been proposed. One equation has been employed for composition [22] and one for density [23] programmes. It would be of interest, however, for practical use, for the comparison of the results of different workers and for clarity, if simple equations could be found that can be employed for all types of gradient programming, *i.e.*, for the programming of pressure, density, composition of binary mobile phases, temperature, volume flow-rate or average linear velocity. Thus, one or a few equations should be adaptable by appropriate changes of definitions to the programming of all gradients. A composition programme that has frequently been used previously is [22]

$$Q'_B = \frac{P_B}{1 - P_B} = \frac{P_B}{P_A} \tag{4}$$

with

$$P_A + P_B = 1 \tag{5}$$

where Q'_B is an arbitrary, but proportional, measure of real time whose proportionality constant may be freely chosen for each chromatographic run. The real time may be expressed in hours, minutes, seconds or other units, as convenient. The P are fractions of volume flow, the volume flow usually taken as the feed rates of the pumps. The definitions of P are

$$P_B = \frac{F_B}{F_A + F_B} \tag{6a}$$

$$P_A = \frac{F_A}{F_A + F_B} \tag{6b}$$

where F_A and F_B are the volume flow-rates of components A and B, respectively, of the binary mobile phase. Whenever it holds that $F_A + F_B = F_t$ = constant, where t = total and F_t is the total volume flow-rate, during a chromatographic run, this programming equation fulfils the condition for an asymptotic increase in the content of component B in the mobile phase during the programme. Component B usually is chosen to possess the higher migrating (solubility) power for the analyte as compared with the base component A. An asymptotic increase is desirable because with increasing relative molecular mass or increasing polarity of the compounds in the analyte mixture, the differences in physical properties between compounds in the analyte mixture often become smaller and smaller as the molecular size and/or the polarity of the compounds increase. This is immediately obvious, for instance, for homologues and oligomers. However, not all SFC hardware allows the additional condition needed for running a composition programme of eqn. 4, *i.e.*, $F_A + F_B$ = constant. In this event another programme equation is needed. Moreover, eqn. 4 is not applicable to the other gradients because a pressure gradient, for instance, starts at a constant pressure level which does not change during a run like P_A does. Also, the desirability of an asymptotic, or at least progressively slower, increase in a programme applies not only to composition programmes but probably also to programmes of pressure, density, temperature, volume flow-rate or linear velocity.

For example, an equation for a volume flow-rate programme may tentatively be written in the same general form as eqns. 4 and 5 for the composition programme, *i.e.*,

$$Q'_F = \frac{P_F}{1 - P_F} = \frac{P_F}{P'_F} \tag{7}$$

with

$$P_F + P'_F = 1 \tag{8}$$

Here Q_F is again the arbitrary time scale and P_F and P'_F are fractions of flow-rate as defined by

$$P_F = \frac{F_a}{F_0 + F_a} \tag{9a}$$

$$P'_F = \frac{F_0}{F_0 + F_a} \tag{9b}$$

where F_0 is the volume flow-rate at which the programme starts and F_a is the additional flow-rate which increases during the programme. F_0 is a constant and $F_0 + F_a = F_t$; F_t is the total flow-rate, which changes as F_a changes. However, $F_0 + F_a = F_t$ leads to a programme curve that is not asymptotic but linear. In order to introduce a curvature again, the equation must be raised to powers different from 1, *i.e.*,

$$Q'_F = \left(\frac{P_F}{1 - P_F}\right)^a = \left(\frac{P_F}{P'_F}\right)^a \quad (10)$$

With exponents $a > 1$ the curvature is downward (towards the Q axis) and with $a < 1$ it is upward, the curvature becoming more pronounced the more the exponent a differs from 1.

Instead of writing eqns. 4 and 10 in terms of the reduced quantities P, they may also be written in the corresponding absolute quantities. Starting from eqn. 7, substituting eqn. 9a and b, raising to the power of a and introducing an arbitrary constant factor k yields for eqn. 10

$$Q_F = k\left(\frac{F_a}{F_0}\right)^a = k\left(\frac{F_t - F_0}{F_0}\right)^a = k\left(\frac{F_t}{F_0} - 1\right)^a \quad (11)$$

One might be of the opinion that the introduction of a constant factor such as k is superfluous because Q_F is connected with time by any arbitrary factor. However, if more than one programme is applied to the same chromatographic run it is convenient to have at hand an additional means for expanding or compressing each programme curve individually, and by this means being able to retain a single, overall time scale applicable to all programmes of the chromatographic run.

When wishing to programme the other physical parameters, *i.e.*, pressure, density, temperature or linear velocity, one has only to redefine the terms in eqn. 11. In turn, F_0 then becomes the starting pressure, p_0, or the starting density, ρ_0, or the starting temperature, T_0, or the starting average linear velocity, u_0, all of which are constants for a given programme. F_a becomes then, respectively, the additional pressure, p_a, the additional density, ρ_a, the additional temperature, T_a, or the additional linear velocity, u_a, all of which are the parameters that change during a given programme. Finally, F_t becomes the total pressure, p_t, the total density, ρ_t, the total temperature, T_t, or the total linear velocity, u_t. Otherwise, eqn. 11 remains the same, considering, however, that the factor k and the exponent a may be chosen differently for each programme and might therefore also be renamed as, for instance, l, m, n, ..., and b, c, d, ..., respectively.

The flexibility of the hardware is of concern not only for composition programming but also for pressure programming. When one is able to start pressure programmes at a few bars, say at $p_0 = 3$ or 10 bar, and then increases the pressure above the critical pressure p_c ($p_0 + p_a = p_t > p_c$, with $T > T_c$), one is in the position to combine GC and SFC without needing to change the mobile phase. One could start, for instance, with CO_2, ethane, or trifluoromethane at 3 bar and proceed by means of a pressure programme to leave the GC and enter the SFC region. However, liquified gases such as CO_2 possess a considerable vapour pressure at ambient temperature which must be exceeded in the pumping device if one desires to pump the mobile phase in its liquid state. With the pumps currently used, the mobile phase is metered as a liquid and not as a gas as by a compressor or from a pressure cylinder. This vapour pressure prevents a chromatogram being started at a pressure lower than the vapour pressure of the liquid mobile phase at the temperature of the pumping device. Therefore, a back-pressure controller immediately downstream of the pumping device, which keeps the pressure in the pump well above the vapour pressure and constant, is necessary. Keeping the pressure constant has the added advantage that no changes in the compressibility of the pumped liquid occur when the pressure is changing in the column, *e.g.*, during a pressure programme. This lack of compressibility change is even more convenient when two or more liquids need to be pumped separately, as is the case for composition programmes. In Fig. 8 a schematic diagram of an SFC apparatus is shown which possesses a pressure-controlling device downstream of two pumps. The apparatus is capable of independent programming of all physical variable which affects the mobile phase and the column.

Taking the gradient programme of the average linear velocity, u, as a further example and to demonstrate the effect which exponent c and factor m have on the shape of the programme curve of Q_u *versus* u_t, we can write

$$Q_u = m\left(\frac{u_a}{u_0}\right)^c = m\left(\frac{u_t - u_0}{u_0}\right)^c = m\left(\frac{u_t}{u_0} - 1\right)^c \quad (12)$$

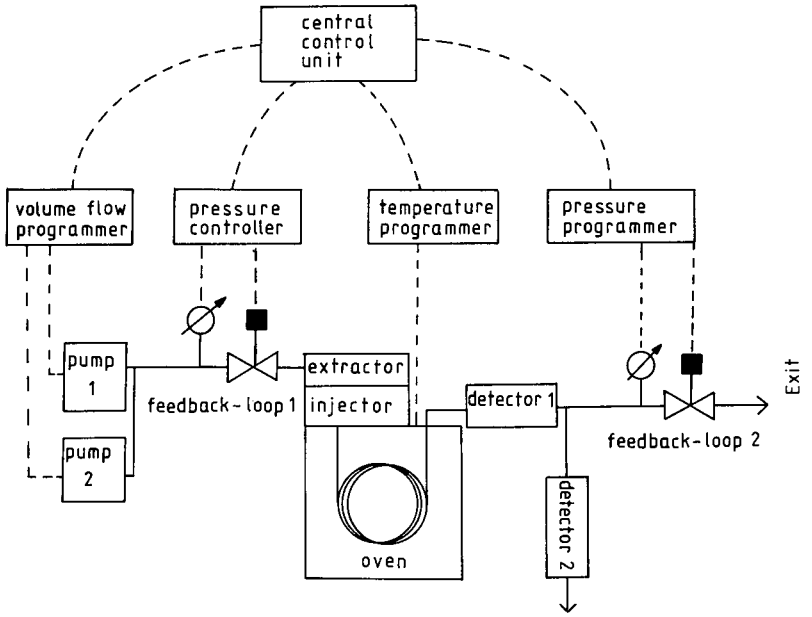

Fig. 8. Schematic diagram of SFC apparatus capable of combining GC and SFC during the same chromatographic run, without changing the pumping (delivery) arrangement and with or without changing the mobile phase during a given run, as made possible by a pressure-controlling feedback loop downstream of the pumps. The apparatus is capable of independently controlling and programming pressure, density, composition, temperature and volume flow-rate (linear velocity).

In Fig. 9a, the effect of the exponent c on the shape of the programme curve is shown, assuming the values $c = 3.0$, 2.0, 1.5, 1.0 and 0.5 with $m = 1$ and $u_0 = 0.1$ cm/s. As is obvious from eqn. 12, an exponent $c = 1.0$ must produce a linear programme, *i.e.*, a straight line, exponents $c > 1.0$ lead to curvatures towards the Q_u axis and $c < 1.0$ produce curvatures towards the u_t axis. There is a common intersection of all curves at $Q_u = 1$ and $u_t = 0.2$ cm/s. Such a common intersection of all curves occurs whenever $(u_t - u_0)/u_0 = 1$. A common intersection can be utilized as a common end-point for different programmes. Together with a common starting point, this will simplify comparison of different programmes because they may then differ only by their curvature. Also, any section of any curve may

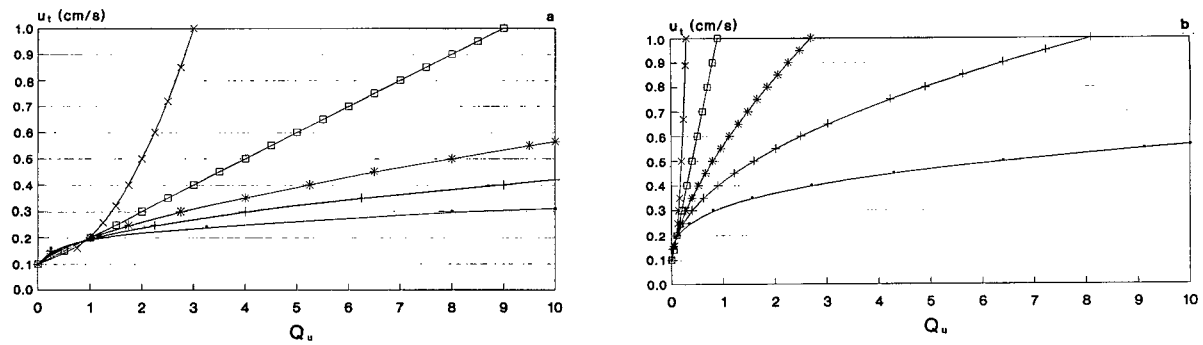

Fig. 9. Curves for gradient programming as examples of programming the average linear velocity u_t *versus* Q_u units, the latter units being proportional to time. Curves in Fig. 9a and b calculated by eqn. 12. (a) Factor $m = 1$, velocity $u_0 = 0.1$; (b) $m = 0.1$, $u_0 = 0.1$. The exponent c in eqn. 12 was varied as follows: ■ = 3.0; + = 2.0; ✱ = 1.5; □ = 1.0; × = 0.5.

be used as a full programme, for instance the section between $Q_u = 0$ and 1, or between $Q_u = 1$ and 10. Moreover, the factor m may be utilized to compress the curves by choosing factors $m < 1$ or to expand the curves with $m > 1$. The compression is seen in Fig. 9b, where $m = 0.1$ instead of $m = 1$ in Fig. 9a, leading to a compression by factor 10 in comparison with Fig. 9a.

Variability in choosing different shapes of the programme curve arises not only from the exponent and factor and by selecting a desirable section of the curve, within or beyond their common point of intersection, but also by using curves in their reverse direction. In the latter instance a positive programme turns into a negative programme and *vice versa*, whereby the shape of the programme in the reverse direction is different from the shape of that in the forward direction, because the greatest change of slope is not at the beginning but at the end of the programme. This type of programme curve may be of interest whenever the solubility differences between the compounds of an analyte mixture become larger the later the compounds elute. This behaviour of an analyte mixture is opposite to that found in homologous series.

CONCLUSIONS

The results of this study can be divided into three parts, *i.e.*, those concerning plate height, resolution and equations for gradient programming. With respect to plate height, it can be concluded that for a positive pressure programme at constant mobile phase composition and constant temperature, a negative linear velocity programme should be superimposed, *i.e.*, run simultaneously, in order to stay within the area of the optimum plate height in the Van Deemter diagrams. The higher the relative molecular mass and molecular size, the stronger this effect might become and, therefore, when separating higher relative molecular mass compounds by pressure or density programming in SFC, improvement is possible by superimposing an appropriate linear velocity programme. The second basic gradient besides pressure which was explicitly considered in this study is that of composition programming. A positive composition gradient at constant pressure does not need to the same extent as a pressure gradient an additional negative linear velocity programme to improve plate height. Nevertheless, and even without a composition or a pressure programme, the influence of the relative molecular mass of the sample itself on the plate height makes it desirable to have the capability of applying a negative linear velocity programme, especially if an analyte mixture with a wide relative molecular mass range of the individual compounds is to be separated.

Second, with respect to resolution and capacity factor, three-dimensional graphs show that for positive pressure programmes negative linear velocity programmes improve the resolution. For positive composition programmes a negative velocity programme is not needed, or only to a lesser extent. If the temperature stability of the analytes allows, it is speculated that a negative linear velocity programme may be wholly or in part substituted by a positive temperature programme to keep the resolution at a high level. This applies not only to a positive composition programme but also to a positive pressure programme, or to an analyte mixture of wide relative molecular mass range without a pressure or composition programme. The reason is that the negative velocity programme is to compensate for a decrease in interdiffusion coefficient with increasing pressure, composition and relative molecular mass range. This decrease in the interdiffusion coefficient may be counteracted also by increasing the temperature.

Third, the results obtained by pressure and composition programmes, or by velocity and temperature programmes, depend to a considerable extent on the shape and the total time of the programme, even for an otherwise similar programme. "Similar" means in this case identical start and end-point for, *e.g.*, the pressure programmes to be compared among each other. A set of related equations (essentially only one equation) has been presented that allows programme curves of different shapes for the programming of pressure, density, composition, temperature, flow-rate and average linear velocity. Because the equations are of simple form and easy to use, they might be of help in practical method development.

ACKNOWLEDGEMENTS

Financial support by the Deutsche Forschungs-

gemeinschaft is gratefully acknowledged. We also thank A. Hütz for drawing the three-dimensional graphs on a PC.

REFERENCES

1 D. E. Raynie, K. E. Markides, M. L. Lee and S. R. Goates, *Anal. Chem.*, 61 (1989) 1178.
2 T. A. Berger and C. Toney, *J. Chromatogr.*, 465 (1989) 157.
3 H. G. Janssen, J. A. Rijks and C. A. Cramers, *J. Microcol. Sep.*, 2 (1990) 26.
4 A. Giorgetti, N. Pericles, H. Widmer, K. Anton and P. Dätwyler, *J. Chromatogr. Sci.*, 27 (1989) 318.
5 T. Berger and J. Deye, *J. Chromatogr. Sci.*, 29 (1988) 390.
6 M. Saito, Y. Yamauchi and H. Kashiwazki, *Chromatographia*, 25 (1988) 801.
7 S. Küppers, B. Lorenschat, F. P. Schmitz and E. Klesper, *J. Chromatogr.*, 475 (1989) 85.
8 S. Küppers, M. Grosse-Ophoff and E. Klesper, in preparation.
9 J. J. van Deemter, F. J. Zuiderweg and A. Klinkenberg, *Chem. Eng. Sci.*, 5 (1956) 271.
10 M. Ashraf-Khorassani, L. T. Taylor and S. Shah, *Anal. Chem.*, 62 (1990) 1173.
11 P. A. Mourier, M. H. Caude and R. H. Rosset, *Chromatographia*, 23 (1987) 21.
12 D. R. Gere, R. Board and D. McManigill, *Anal. Chem.*, 54 (1982) 736.
13 D. Leyendecker, F. P. Schmitz and E. Klesper, *J. Chromatogr.*, 315 (1984) 19.
14 D. Leyendecker, D. Leyendecker, F. P. Schmitz and E. Klesper, *J. High Resolut. Chromatogr. Chromatogr. Commun.*, 9 (1986) 566.
15 F. P. Schmitz, H. Hilgers, B. Lorenschat and E. Klesper, *J. Chromatogr.*, 346 (1985) 69.
16 F. P. Schmitz, D. Leyendecker and D. Leyendecker, *J. Chromatogr.*, 389 (1987) 245.
17 F. P. Schmitz, *J. Chromatogr.*, 356 (1986) 261.
18 A. Hütz, D. Leyendecker, F. P. Schmitz and E. Klesper, *J. Chromatogr.*, 505 (1990) 99.
19 D. Leyendecker, F. P. Schmitz, D. Leyendecker and E. Klesper, *J. Chromatogr.*, 321 (1985) 273.
20 R. W. Stout, J. J. de Stefano and L. R. Snyder, *J. Chromatogr.*, 181 (1983) 263.
21 D. Leyendecker, F. P. Schmitz and E. Klesper, *J. Chromatogr.*, 315 (1984) 19.
22 F. P. Schmitz, H. Hilgers, B. Lorenschat and E. Klesper, *J. Chromatogr.*, 346 (1985) 69.
23 J. C. Fjeldsted, W. P. Jackson, P. A. Paeden and M. L. Lee, *J. Chromatogr. Sci.*, 21 (1983) 222.
24 R. Reid, J. Prausnitz and T. Sherwood, *The Properties of Gases and Liquids*, McGraw-Hill, New York, 3rd ed., 1977.
25 E. Brunner, *J. Chem. Thermodyn.*, 17 (1985) 671.

Journal of Chromatography, 629 (1993) 361–370
Elsevier Science Publishers B.V., Amsterdam

CHROM. 24 658

Calibration of spectrophotometric detectors for supercritical fluid chromatography

U. Meier and Ch. Trepp

Institute of Process Engineering and Cryogenics, Swiss Federal Institute of Technology, ETH Zentrum, CH-8092 Zurich (Switzerland)

(First received July 23rd, 1992; revised manuscript received October 2nd, 1992)

ABSTRACT

A simple peak-area calibration method for supercritical fluid chromatography (SFC) with spectrophotometric detectors is presented. The method was developed originally for high-performance liquid chromatography and is based on the molar absorptivity of the analytes. It allows calibration independent of detector specifications, flow cell geometry and operating parameters. The adaptation of this method to SFC and the particular influence of the density variations of the highly compressible SFC eluent on calibration and reproducibility of results are discussed. SFC hardware requirements and operational and calibration procedures that are prerequisites for accurate quantitative SFC results were considered. The method was tested with samples of fatty acid glycerol esters, α-tocopherol (vitamin E) and its acetate in carbon dioxide–ethanol eluents with two different UV detectors. Errors and shortcomings of the method that narrow the scope of its applications are discussed.

INTRODUCTION

In the literature published on supercritical fluid chromatography (SFC), only a few papers have dealt with quantification other than by internal standard methods. The latter, however, require the addition of a known amount of a standard substance to the sample solution. The chosen standard substance should behave in a way similar to that of the sample constituents as far as retention and detection properties are concerned. It is not always possible, however, to find such a standard substance or to mix it with the sample in a reproducible way. This applies in the particular situation where SFC is directly coupled to the source of the sample, *e.g.*, in systems with on-line supercritical fluid extraction (SFE) of the sample [1] or, as in our case, where SFC is directly coupled with a high-pressure equilibrium cell for phase composition measurements [2]. In these situations it is highly desirable to have a method that links the integrated peak areas with the total number of sample molecules, irrespective of detector type, flow cell geometry and operating parameters of the SFC equipment.

Such a method was presented by Torsi *et al.* [3] for applications in high-performance liquid chromatography (HPLC) and tested experimentally with different UV–Vis detectors [4]. They found that their method worked well for some commercial UV detectors (three out of five), whereas others showed deviations of up to 20%. These were explained by deflections of the light beam at the flow cell caused by either wedged flow cell windows or non-ideal flow causing density gradients across the flow cell diameter. Peck and Morris [5] investigated such effects. They found window wedge angles of up to 2° for commercial flow cells and made photographs of tracer flow patterns in the cell, which exhibit considerable deviation from a constant distribution of sample substance across the width of the light beam. These effects are held responsible for baseline drifts and excess noise of the detector signal.

Correspondence to: U. Meier, Institute of Process Engineering and Cryogenics, Swiss Federal Institute of Technology, ETH Zentrum, CN-8092 Zurich, Switzerland.

0021-9673/93/$06.00

SFC exhibits some particular features that distinguish it from HPLC: the dense gas eluents are much more compressible than the liquid solvents used in HPLC. Spectroscopic detectors (UV–Vis, IR, fluorescence) for SFC operate at pressures up to 350 bar, which may affect the optical properties of the flow cells. As a further complication, SFC requires back-pressure control devices for releasing the system pressure after the detector. The use of passive restrictors [6] results in pressure-dependent flow, which is unacceptable in many instances, especially if absolute quantification is required. Active control valves are difficult to find or to build for the small flow-rates of the dense gas eluent, particularly if packed microbore or capillary columns are used. The method presented here requires the determination of the volume flow-rate of the eluent in the detector flow cell, which is simple in HPLC but more complex in SFC, because the SFC eluent density inside the flow cell depends on pressure, temperature and composition (if mixed eluents or modifiers are used).

Some aspects of the following theory have been presented before (in relation to HPLC). However, to the authors' knowledge, these have never been integrated into an applicable calibration method for SFC, and the effects of major changes in eluent density have not been treated.

In this paper we discuss the following theoretical aspects: Lambert–Beer law, the effect of SFC eluent density changes on peak shapes and integrated peak areas and non-plug flow in the detector flow cells. The validity of the theory is checked against standard calibration procedures, the measurement and control facilities required for application of the method are described and the problems arising are discussed.

THEORY

The Lambert–Beer law relates light absorbance, A, to the concentration of the absorbing molecules in the light path, c (mol/l), their molar absorptivity, ε ($\times 1000$ cm^2/mol) and the length of the light path, l_0 (cm). Considering that in chromatography A and c are time dependent, we can write

$$A_\lambda(t) \equiv \log (I_0/I)_\lambda = \varepsilon_\lambda \, l_0 \, c(t) \quad (1)$$

The deduction of this law assumes that sample concentrations are small [6] and that solvent effects on sample spectra are unimportant.

Chromatographic detectors determine the light intensity I_0 at the start of a run, thus taking the initial absorbance of the eluent without any sample present as the datum value. Problems may arise if short wavelengths are chosen (< 210 nm), where end absorption of SFC eluents increases, particularly if they contain modifiers. In such cases there may not be enough energy available for proper measurements; artefacts result, as will be shown in the results for the calibration of oleic acid glycerides.

An ideal detector requires either an exactly parallel light beam passing through its flow cell, or a constant refractive index inside the cell, at least during one chromatographic run [4,5]. Parallelism of light beams depends on the optical set-up and is hardly ever fully accomplished, whereas constancy of refractive index depends on constant density and constant composition of the eluent. If density is to be constant, no temperature, pressure or modifier concentration programming is allowed in SFC. Changing the density would create detector baseline drifts and/or disturb quantitation. Temperature constancy of the flow cell is very important, but badly neglected in the design of many commercial HPLC and SFC detectors. Refractive index fluctuations due to sample peak concentration variations cannot be avoided. According to Peck and Morris [5], no ideal mixing takes place in conventional flow cells, such that peaks will always cause a certain increase in signal noise.

There are several effects of changing the SFC eluent density. First, it determines the solubility and miscibility of modifiers and samples. Increasing density normally enhances solubilities. As high-pressure phase equilibria are complex, care has to be taken not to operate in the two-phase region. Failure to do so would result in unexpected and irreproducible behaviour of the chromatographic system. Phase behaviour of the binary system carbon dioxide–ethanol was reported by Panagiotopoulos and Reid [7]. It exhibits a marked influence of temperature on the immiscibility gap, particularly at low ethanol concentrations (up to 10% ethanol). At 50°C at least 120 bar are required to keep clear of the two-phase region.

The second effect of density is in changing the shape of sample peaks. With a density decrease due

to eluent temperature rising along the flow path (*e.g.*, in the detector), the volume of a peak carrying the sample expands accordingly, and the maximum of the local peak concentration function $c(x)$ falls while the peak width increases.

The third effect of density is in changing the flow velocity of the eluent. A rise in temperature will increase the velocity, in proportion to the decrease in density, decreasing the residence time of sample molecules in the detector flow cell. Consequently, peak widths of the time-dependent concentration function $c(t)$ "seen" by the detector [when a given peak $c(x)$ passes through] decrease.

The point of interest is in knowning the resulting composite effect of density on the peak area determined by integrating the detector signal $A(t)$. Expansion of the peak width is compensated for by the increase in the flow velocity, so that the peak width in terms of time remains unaffected by an increase in density. The decrease in the local concentration maximum, however, is not compensated for. We therefore expect that integrated peak areas, a_i, will change proportionally with eluent density in the detector flow cell, ρ_{fc}:

$$a_i = \int_{\text{peak}} A(t)\mathrm{d}t \approx \rho_{fc} \quad \text{(s)} \tag{2}$$

The third element of the method is the concept of residence time distribution in the flow cell and its effect on the measured optical absorbance. If the flow cell is considered as a closed vessel of any geometry and any flow pattern, being swept by a steady-state flow of eluent of constant density, then the concentration profile of any peak measured at the inlet, $c(t)$, can be related to its profile at the outlet, $c_{out}(t)$, by any normalized exit age distribution functon $E(t)$ [8] by the following equation:

$$c_{out}(t) = \int_0^t c(t')\ E(t-t')\mathrm{d}t' \quad \text{(mol/l)} \tag{3}$$

where t' is a dummy variable running from 0 to t. $E(t'')$ has the following properties:

$$\int_0^\infty E(t'')\mathrm{d}t'' = 1; \quad \int_0^t E(t'')\mathrm{d}t'' \equiv F(t); \quad \int_t^\infty E(t'')\mathrm{d}t'' = 1 - F(t) \tag{4}$$

$F(t)$ is the fraction of fluid that remains in the vessel for a time shorter than t. Levenspiel [8] showed that $F(t)$ is the normalized outlet response of a step function at the vessel inlet. Further, we define a function $R(t'')$:

$$R(t'') \equiv 1 - F(t'')$$

with

$$\int_0^\infty R(t'')\mathrm{d}t'' = \tau = \frac{V}{\dot{V}} \quad \text{(s)} \tag{5}$$

This is the same R function as used, but not explained, by Torsi and co-workers [3,4]. The integral under the R function curve is equal to the mean residence time τ of fluid flowing through the vessel (volume V) at a given flow-rate.

With these tools we can now determine the number of sample molecules n_{fc} present in the flow cell volume V_{fc} from the peak concentration profile at the inlet, $c(t)$, and the residence time distribution function $E(t'')$. With $c_{fc}(t)$ being the average concentration in the flow cell at any time t, we obtain

$$n_{fc}(t) = V_{fc}\ c_{fc}(t) = \dot{V}\int_0^t c(t')\left(\int_{(t-t')}^\infty E(t'')\mathrm{d}t''\right)\mathrm{d}t' \quad \text{(mol)} \tag{6}$$

The inner integral represents that fraction of the sample which entered the flow cell at any time $t' < t$ and remains in the flow cell longer than $t - t'$. With eqns. 4 and 5, eqn. 6 is rewritten as

$$n_{fc}(t) = \dot{V}\int_0^t c(t')[1 - F(t-t')]\mathrm{d}t' = \dot{V}\int_0^t c(t')\ R(t-t')\mathrm{d}t' \quad \text{(mol)} \tag{7}$$

With the rules for Laplace transformations, this so-called "convolution integral" can be integrated to yield a product of separate and simple integrals:

$$\int_0^\infty n_{fc}(t) = V_{fc}\int_0^\infty c_{fc}(t)\mathrm{d}t = \dot{V}\int_0^\infty c(t)\mathrm{d}t\int_0^\infty R(t)\mathrm{d}t = n_{peak}\tau \quad \text{(mol s)} \tag{8}$$

where n_{peak} is the total number of moles injected with the sample and conveyed in the peak.

It is important to note that the deduction of this equation did not require any assumption concerning ideal flow patterns in the flow cell. It is therefore generally valid for constant density, steady-state flow through a closed flow cell. Assuming that all of the sample molecules present in the cell are illumi-

nated by the detector light beam, and that the assumptions of the Lambert–Beer law (eqn. 1) are fulfilled, we find a simple relationship between integrated peak areas and the amount of sample:

$$a_i = \int_0^\infty A_\lambda(t)\mathrm{d}t = \frac{\varepsilon_\lambda\, l_0\, n_{peak}}{\dot{V}} = \frac{\varepsilon_\lambda\, l_0\, n_{peak}\, \rho_{fc}}{\dot{m}} \quad \text{(s)} \quad (9)$$

We find that in addition to the amount of sample and its molar absorptivity, the length of the light path, the mass flow-rate and the density of the eluent in the flow cell determine the integrated peak area, which corresponds to the qualitative considerations leading to the proportionality eqn. 2.

Eqn. 9 is rearranged in order to define a calibration factor that ideally is equal to the molar absorptivity of the sample:

$$e_\lambda \equiv \left(\frac{a_i\, \dot{m}}{l_0\, n_{peak}\, \rho_{fc}}\right)_{meas.} \approx \varepsilon_\lambda \quad (10)$$

It follows that the parameters in eqns. 9 and 10 must be known accurately and be controlled reproducibly in order to be able to use the molar absorptivity for detector calibration in SFC. We explain below how we achieved this goal experimentally.

EXPERIMENTAL

The SFC system developed during this work is shown in Fig. 1. It was built for the purpose of direct measurement of high-pressure equilibrium phase compositions.

The first aim is to achieve constant, reproducible and pulse-free flow. For that purpose, an Isco 260D syringe pump is used to deliver liquid carbon dioxide (99.99%, recondensed from vapour) at constant pressure. A second, similar pump (Isco μLC500, constant volume flow-rate mode) delivers ethanol (puriss., 99.8%) as the polar modifier. Mixing occurs in a simple tee-fitting, followed by a piece of coiled capillary tubing. For the purpose of temperature adjustment these are immersed in the same water-bath that contains the two high-pressure sample injection valves.

The valves used are motor-driven Valco C6W (2 μl, for light equilibrium phase) and Valco C14W (0.06 μl, for heavy equilibrium phase), followed by a third valve for injection of calibration solutions (Valco C6W, 20 μl, with automatic filling system).

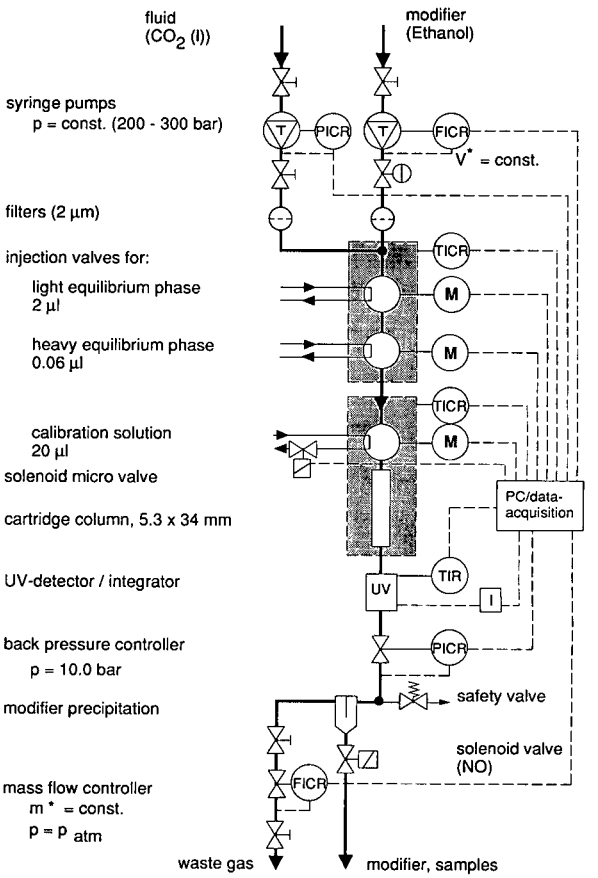

Fig. 1. Flow diagram of supercritical fluid chromatograph (shaded: temperature-controlled areas).

This last valve is kept at the column temperature (typically 30°C) by a metal block thermostat.

A short cartridge column with Nucleosil 100-3 packing (unmodified spherical silica, 3 μm particle diameter, 100 Å pore diameter, packing dimensions 34 mm × 5.3 mm diameter) separates the sample components. It allows for typical run times as short as 1–5 min.

The UV detectors used are a Perkin-Elmer LC235 (35 diode-array) and an Isco V4 (variable-wavelength). A Perkin-Elmer LC1100 integrator is used to integrate peak areas.

The second important element for achieving constant flow is the pressure release valve. A Brooks 5835P high-pressure control valve (k_{vs} value $2 \cdot 10^{-5}$, orifice diameter 0.051 mm) with electronic

back-pressure controller and pressure transducer reduces the pressure to 10 bar, thus avoiding the formation of solid carbon dioxide. The modifier is precipitated at this pressure and a Brooks 5850E mass-flow controller releases the carbon dioxide (with small amounts of modifier vapour) to atmospheric pressure.

The system is remote controlled by a personal computer (Olivetti M24) with data acquisition hardware (Burr-Brown PCI 20000). The software is written in Turbo Pascal and allows the measurement, storage and statistical evaluation of all the important SFC parameters (pressures, temperatures, flow-rates), on-line calculation and display of non-measurable system parameters (such as eluent density in the detector flow cell) and time-controlled chromatographic runs at constant intervals.

The parameters in eqn. 9 were determined in the following ways.

The length of the flow cell optical light path, l_0, was taken from the manufacturer's specifications, as we were not in a position to measure it at the operating pressures. According to Torsi *et al.* [4], however, deviations from nominal values of several percent may occur.

The sample amount, n_{peak}, was determined with calibration substances from Sigma, dissolved in UV-grade heptane. Impurities in the calibration substances used, inaccuracies of the weighing balance and evaporation of the solvent contribute to composite errors. The volumes of the injection valve sample loops may deviate widely from nominal values. It was therefore determined by filling the loop with mercury, switching the valve, flushing the loop with compressed air and consequently weighing the ejected mercury. For small volumes several consecutive fill–eject cycles were combined into one weighing to increase accuracy (results are given in Table I).

The density of the eluent in the flow cell, ρ_{fc}, was initially measured at different pressures, temperatures and ethanol concentrations by means of a Paar DMA 512 high-pressure/high-temperature oscillating tube densitometer cell. Later it was calculated on-line from measured values of flow cell temperature, pressure and eluent flow-rate. Flow cell temperature was measured by means of a thermocouple and pressure was determined from the value measured at the pump (which was checked regularly by a dead-weight gauge), diminished by the system pressure drop calculated from eluent flow-rates by means of an empirical correlation. This pressure drop was always smaller than 30 bar.

The mass flow-rate of the eluent was determined from the signals of the mass-flow controller (carbon dioxide mass flow-rate, calibrated regularly by means of a laboratory wet test meter) and of the ethanol pump (ethanol volume flow-rate).

TABLE I

NOMINAL AND MEASURED SAMPLE LOOP VOLUMES OF SOME HPLC INJECTION VALVES USED IN THIS WORK

Loop No.	Type[a]	Nominal volume (μl)	Volume measured (μl)	S.D.[b] (μl)	R.S.D.[b] (%)	Deviation from nominal value (%)
1	E	20	20.484	0.053	0.26	+2.4
2	E	10	10.713	0.071	0.67	+7.1
3	E	5	6.117	0.031	0.50	+22.3
4	E	2	1.995	0.027	1.38	−0.3
5	I	1	0.606	0.0154	2.54	−39.4
6	I	0.5	0.540	0.0115	2.14	+8.0
7	I	0.2	0.180	0.0082	4.56	−10.0
8	I	0.06	0.06281	0.00095	1.52	+4.7

[a] E = External loop; I = internal loop.
[b] $n = 10$.

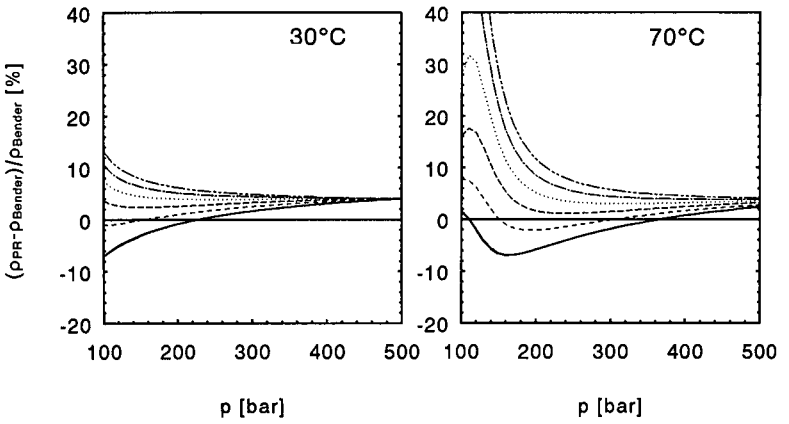

Fig. 2. CO_2–ethanol density: deviation of values calculated with Peng–Robinson EOS from values determined with Bender EOS (pure CO_2). Ethanol content (%): ——— = 0; --- = 2; – – – = 4; · · · · · = 6; — · — = 8; — · · — = 10.

RESULTS

Sample volume

Eight different loop volumes (internal and external types) were measured. We obtained the values given in Table I. The actual volumes deviate by up to 39% from the nominal values.

Eluent density

Many SFC controllers offer density programming, based on measurement of pressure and temperature and calculation of densities by means of simple cubic equations of state (EOS), requiring only a few, fluid-specific parameters. We calculated density values for pure carbon dioxide with the Peng–Robinson (PR) EOS model. In the ranges 30–90°C and 100–500 bar the resulting values deviate by up to 9% from reference values (Fig. 2, solid lines). Such a performance is insufficient if eqns. 9 and 10 are to be used for calibration.

For the determination of pure SFC eluent densities, the Bender EOS is much more suitable [9]. This is a 20-parameter modified Benedict–Webb–Rubin EOS. It was adjusted for carbon dioxide by Sievers [10] and deviates by less than 0.5% from reference measurements, except in the vicinity of the critical point.

As we wanted to determine the densities of carbon dioxide with small amounts (up to 10 mol%) of a polar modifier (ethanol), we were seeking EOS models that perform well for this system. We tried a PR EOS model with mixing rules proposed and optimized for carbon dioxide–ethanol by Panagiotopoulos and Reid [7], which performs well in predicting phase boundaries. We calculated densities for various amounts of ethanol (Fig. 2, broken lines; 2–10 mol%) and compared them with densitometric measurements at around 26°C and between 100 and 300 bar. While the PR EOS model predicts increasing densities with increasing ethanol content, measurements (errors $\pm 0.7\%$) indicate that the eluent densities, in this range, remain virtually unaffected by small contents of ethanol. Hence values calculated with the PR EOS model are generally too high (Fig. 3, closed symbols; deviation *ca.* +7% for 10 mol% ethanol).

As a consequence, we applied the Bender EOS for pure carbon dioxide to calculate eluent densities with less than 8 mol% ethanol. The resulting errors are smaller than 1% in the range 150–300 bar (Fig. 3, open symbols).

UV absorbance of carbon dioxide–ethanol SFC eluents

In order to ascertain the absorbance of the eluents, we measured diode signals and absorption values of carbon dioxide eluents with various contents of ethanol with the LC 235 diode-array detector. Fig. 4 shows that diode signals at different wavelengths above 220 nm do not vary significantly with ethanol contents. At wavelengths below 210 nm however, the carbon dioxide absorbance increases and the ethanol absorbance becomes significant.

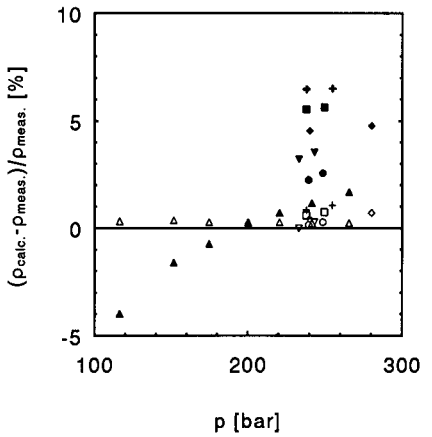

Fig. 3. CO_2–ethanol density: deviation of values calculated with Peng–Robinson EOS (closed symbols) and with Bender EOS (pure CO_2, open symbols) from densitometer measurements at various pressures and compositions ($24.5 < T < 26.7$°C). Ethanol content (%): △, ▲ = 0; ○, ● = 2; ▽, ▼ = 4; ◇, ◆ = 6; □, ■ = 8; +, + = 10.

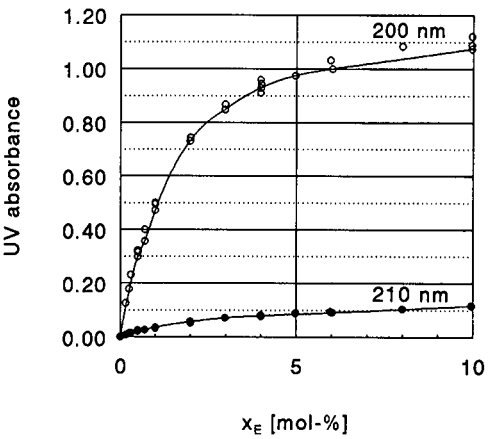

Fig. 5. UV absorbance of CO_2–ethanol eluent (ethanol contents between 0 and 10 mol%) at 200 and 210 nm (33°C, 245 bar).

lowering the diode signals by two decades at 195 nm. At this wavelength, the signal is too weak to distinguish varying ethanol contents. In the normal operating mode, however, the LC235 detector does not give any warning that signals are too weak and erroneous measurements occur.

Fig. 5 shows the absorbances of eluents containing ethanol compared with a pure carbon dioxide eluent. Whereas according to the Lambert–Beer law the dependence of absorbance on ethanol concentration ought to be linear, we find that at low wavelengths (weak detector signals) this is no longer true; at 200 nm the detector response is strongly non-linear.

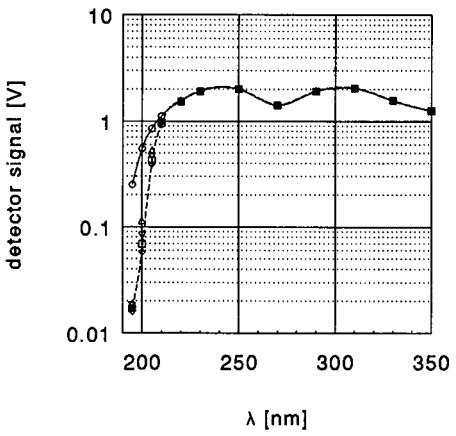

Fig. 4. UV detector diode-array signals at wavelengths between 195 and 350 nm and various ethanol contents of the CO_2 eluent (33°C, 245 bar). Ethanol content (mol%): ○ = 0; △ = 1.986; ▽ = 3.029; □ = 3.976; ◇ = 5.189; + = 5.972.

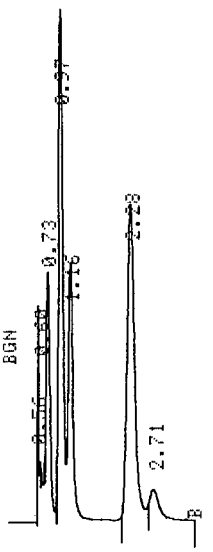

Fig. 6. Separation of underivatized technical grade monoolein (mixture of mono-, di- and triglycerides). Numbers on peaks indicate retention times in minutes. Eluent: CO_2–5.0 mol% ethanol. Column: 34 × 5.3 mm I.D. Nucleosil 100, 3 μm (silica spheres, unmodified); 27°C; eluent density: 929 g/l; 0.84 g/min CO_2. Detector: Perkin-Elmer LC235, 210 nm.

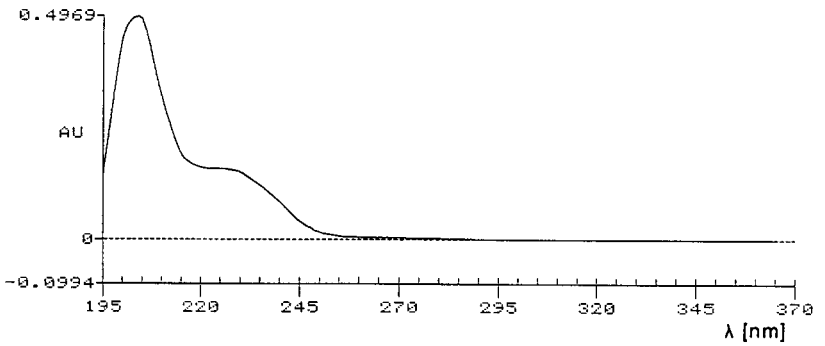

Fig. 7. UV spectrum of 2-monoolein ($t = 2.29$ min). SFC parameters as in Fig. 6. The "maximum" at 205 nm is an artefact.

Separation and calibration of glycerides

The short columns used in this work performed very well in the separation of underivatized technical-grade monoolein (oleic acid glycerol ester), which is a mixture of about 40% monoglyceride, 40% diglyceride and 16% triglyceride, with small amounts of free glycerol, fatty acids and non-oleic acid esters. Fig. 6 shows a typical chromatogram recorded at 210 nm. According to the spectrum output of the LC235 diode-array detector (Fig. 7), this wavelength ought to be close to the maximum absorbance of oleic acid glycerol esters. Only later did we find that the "maximum" is an artefact due to the above-mentioned weakness of the signals below 210 nm, where the real absorbance continues to increase.

We tried to quantify the results with runs on pure calibration substances. Fig. 8 shows the marked non-linearity of glyceride calibration factors (eqn. 10) at this wavelength. It is not clear whether this is due to the weakness of the signal (non-linear range of the detector) or to measurement too distant from the absorption maximum, where solvent effects and/or eluent absorbance might interfere.

Separation and calibration of tocopherols

Owing to the difficulties with glycerides, we chose substances with a distinct absorbance maximum at longer wavelengths in the UV region. Fig. 9 shows the separation of a solution of α-tocopherol and α-tocopherol acetate at 279 nm with the same short silica cartridge columns utilized throughout this work. A very clear separation of solvent (UV-grade

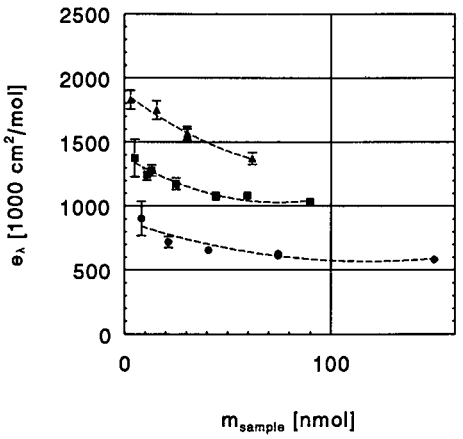

Fig. 8. Calibration factors for (●) mono-, (■) di- and (▲) triglycerides *vs.* sample size.

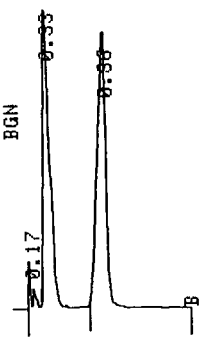

Fig. 9. Separation of α-tocopherol (vitamin E) and α-tocopherol acetate (solution in heptane). Numbers at peaks indicate retention times in minutes. Eluent: CO_2–0.5 mol% ethanol. Column: 34 × 5.3 mm I.D. Nucleosil 100, 3 μm (silica spheres, unmodified); 30°C; eluent density: 925 g/l; 2.6 g/min CO_2. Detector: Isco V4, 279 nm.

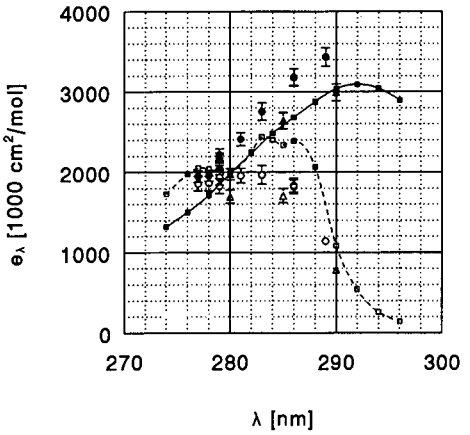

Fig. 10. Comparison between calibration factors of α-tocopherol (vitamin E) (closed symbols) and α-tocopherol acetate (open symbols) determined from (□, ■) literature spectra, (△, ▲) measurements with LC235 detector and (○, ●) measurements with V4 detector.

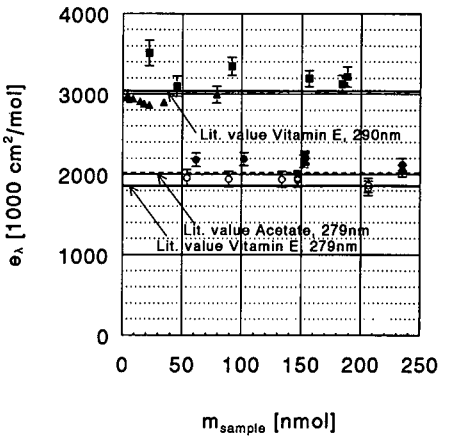

Fig. 11. Calibration factors of α-tocopherol (closed symbols) and α-tocopherol acetate (open symbols) *vs.* sample size. ○, ● = V4 detector (279 nm); ■ = V4 detector, 290 nm; ▲ = LC235 detector, 290 nm.

heptane), the acetate and tocopherol is achieved with low contents of modifier and a high average column velocity. The detector used initially was the Isco V4.

The values for e_λ calculated from eqn. 10 at first did not match the literature values. Measurements with various wavelengths showed that the V4 detector wavelength selector was maladjusted by 6 nm. Additional measurements with the LC235 detector and comparison with literature data [11] yielded the results presented in Fig. 10.

Whereas the LC235 measurements for α-tocopherol fit the literature curves exactly, the values for acetate are 20–30% below the literature values, although the shape of the spectrum is approximately preserved. After correction of the wavelength readings by −6 nm, the values obtained with the V4 were *ca.* 15% higher than those with the LC235. Its values for tocopherol were higher and those for acetate were lower than the literature values.

As both substances were injected in the same sample solution, and as the absorption maxima match with literature data and the tocopherol values measured by the LC235 always coincided with the literature values, it is assumed that the lower acetate absorbance values are caused by interaction of the SFC eluent.

As the V4 values are consistently higher than the LC235 values for both substances (by 10–15%), the most probable explanation is that the length of the optical path in the V4 detector flow cell is greater than the nominal length by that percentage. This is easily plausible considering the very small path length of only 1 mm. We could not verify this explanation or check whether the deviation is pressure dependent.

Fig. 11 shows a number of measurements made to check the linearity of the detector response with various amounts of sample. Both detectors were used and measurements were taken at two different wavelengths (readings for the V4 detector corrected by −6 nm) and with different SFC operating parameters.

The linearity is satisfactory in the range of measurement error. The deviations below 50 nmol (V4, 290 nm, large error bars) are caused by integration problems due to the very small peaks.

CONCLUSIONS

The method introduced in this paper is well suited for rough calibration of spectrometric detectors in SFC and for approximate comparison of peak values obtained on different detectors at different operating parameters of the SFC. It cuts short the otherwise extensive and time consuming calibration procedure required for relating integrated peak areas to amount of sample if no internal standard method can be used.

It requires a knowledge of molar absorptivity values for the analyte substances and an SFC system with stable, reproducible flow and equipment for the determination of mass flow-rate and density in the detector flow cell, in addition to its optical path length.

These prerequisites are met neither easily nor cheaply (hardware requirements). Deviations from literature values and among the values measured with the two detectors (Fig. 11) show that it is not straightforward to apply the method and obtain accurate quantitative results. Under normal laboratory conditions it is difficult to measure the optical path length of the detector cell and to judge solvent effects of SFC eluents on the UV spectra of samples. For these reasons, the time-consuming calibration procedures described here will still be required if accurate quantitation is to be achieved.

SYMBOLS

A	Optical absorbance
a_i	Peak area (integrated)
c	Concentration
E	Exit age distribution
e	Calibration factor
F	Normalized outlet (response) function of an inlet step function
I	Light intensity
l_0	Optical path length
$\dot{m}$	Mass flow-rate
n	Number of moles of sample
R	Residence time distribution
t	Time
V	Volume
$\dot{V}$	Volume flow-rate

Greek letters

ε	Molar absorptivity
λ	Wavelength
ρ	Density
τ	Mean residence time

Subscripts

fc	Flow cell
i	Integrated
meas.	Measured

ACKNOWLEDGEMENTS

We thank the Swiss Federal Institute of Technology (ETH), Zurich, the Basle Chemical Industry Fonds and the Emil Barell Foundation for sponsoring this research project.

REFERENCES

1 W. Pipkin, *LC · GC Int.*, 5 (1992) 8–10.
2 U. Meier, *Dissertation*, No. 9756, ETH, Zurich, 1992.
3 G. Torsi, G. Chiavari, C. Laghi, A. M. Asmundsdottir, F. Fagioli and R. Vecchietti, *J. Chromatogr.*, 482 (1989) 207–214.
4 G. Torsi, G. Chiavari and M. T. Lippolis, *LC · GC Int.*, 5 (1992) 37–39.
5 K. Peck and M. D. Morris, *J. Chromatogr.*, 448 (1988) 193–201.
6 R. D. Smith, in M. Yoshioka (Editor), *SFC and Micro-HPLC*, VSP, Utrecht, 1989, Ch. 2.1.
7 A. Z. Panagiotopoulos and R. C. Reid, in Th. G. Squires and M. E. Pauliatis, *High-pressure phase equilibria in ternary fluid mixtures with a supercritical component (ACS Symposium Series*, No. 329), American Chemical Society, Washington, DC, 1987, pp. 115–121.
8 O. Levenspiel, *Chemical Reaction Engineering*, Wiley, New York, 2nd ed., 1972, Ch. 9.
9 U. Sievers, *Chem.-Ing.-Tech.*, 58 (1986) 220.
10 U. Sievers, *Fortschr. Ber. VDI Z., Reihe 6*, 155 (1984) 8.
11 *Sadtler's Atlas of UV Spectra*, Sadtler Research Laboratories, Philadelphia, PA, No. 20771 UV, 1973, and 2780 UV, 1975.

Journal of Chromatography, 629 (1993) 371–378
Elsevier Science Publishers B.V., Amsterdam

CHROM. 24 663

Effect of sample stacking on resolution, calibration graphs and pH in capillary zone electrophoresis

J. L. Beckers and M. T. Ackermans

Laboratory of Instrumental Analysis, Eindhoven University of Technology, P.O. Box 513, 5600 MB Eindhoven (Netherlands)

(First received September 2nd, 1992; revised manuscript received October 6th, 1992)

ABSTRACT

For the determination of components present in samples at very low concentrations, large injection volumes have to be applied in order to introduce a detectable amount of the analytes in capillary zone electrophoresis (CZE). To obtain a good resolution, the sample analytes have to be concentrated in narrow bands and therefore sample stacking is often applied. Sample stacking can lead to an increase in the electroosmotic flow and extra peak broadening during the analysis, through which the gain in resolution will be lost. Further, the presence of different electrolytes in the capillary can cause pH shifts. In this paper a model is given for the calculation of migration times of components applying sample stacking, and the effects of sample stacking in CZE on resolution, calibration graphs and pH are discussed.

INTRODUCTION

For the determination of components by capillary zone electrophoresis (CZE) [1,2], the components must be separated from their matrix and reliable linear calibration graphs with low detection limits must be obtained. For low detection limits, especially for components present in samples at low concentrations, large sample volumes have to be injected. In such a case, sample components must be concentrated, however, in order to obtain a high resolution and adequate detection. For this reason, sample stacking is often applied, *i.e.*, the sample is introduced at low ionic strength compared with that of the background electrolyte. Through the high local electric field strength, sample components migrate very quickly from the sampling zone, stack down in the background electrolyte owing to the much lower electric field strength and concentrate in very short sample zones. During the sample stacking procedure several interesting phenomena occur. Huang and Ohms [3] discussed the effect of a non-uniform electrical field on the migration behaviour of different sample ions and the effect on sample injection in electrokinetic injection. Chien and Helmer [4] reported on electroosmotic properties and peak broadening in field-amplified capillary electrophoresis owing to a mismatch between the electroosmotic flow (EOF) in the sampling zone and background electrolyte in the capillary and concluded that the broadening mechanism will be a limiting factor for sample stacking in CZE. Burgi and Chien [5–7] found the preparation of a sample dissolved in a tenfold diluted background electrolyte to be an optimum condition for sample stacking and discussed field-amplified sample injection in CZE. No attention was paid to possible pH shifts due to the presence of different electrolytes in the capillary.

As a high electroosmotic flow leads to short analysis times, a low resolution can be the result and the linear character of the calibration graphs vanishes. In this paper the effect of sample stacking on resolution, calibration graphs and pH shifts with the injection of long sampling zones at low concentrations is considered.

Correspondence to: J. L. Beckers, Laboratory of Instrumental Analysis, Eindhoven University of Technology, P.O. Box 513, 5600 MB Eindhoven, Netherlands.

0021-9673/93/$06.00

EXPERIMENTAL

For all CZE experiments a P/ACE System 2000 HPCE instrument (Beckman, Palo Alto, CA, USA) was used. All experiments were carried out applying a Beckman eCAP capillary tubing (75 μm I.D.) with a total length of 46.7 cm and a distance between injection and detection of 40.0 cm. The wavelength of the UV detector was set at 214 nm. All experiments were carried out with application of a constant voltage of 10 kV and the operating temperature was 25°C. Sample introduction was performed by applying pressure injection where a 1-s pressure injection equals an injected amount of *ca.* 6 nl and an injected length of 0.136 cm. Data analysis was performed using the laboratory-written data analysis program CAESAR. These conditions were also used in all calculations.

RESULTS AND DISCUSSION

Effect of sample stacking on resolution

In sample stacking a long sampling zone at low ionic strength compared with that of the background electrolyte is introduced in a zone electrophoretic system, through which the local electric field strength will be very high compared with that of the background electrolyte. In Fig. 1a the capillary is filled to a length l with a sample dissolved in diluted background electrolyte S. The capillary length is L_C and the length to the detector is L_D. If E_S, ρ_S, $m_{EOF,S}$, E_B, ρ_B and $m_{EOF,B}$ are the electric field strengths (V/m), the resistivities (Ω^{-1} m^{-1}) and mobilities of the EOF (m^2/V · s) of the diluted background electrolyte in the sampling zone S and of the background electrolyte B in the capillary, respectively, and if the capillary is filled to a fraction x ($= l/L_C$) during the sampling procedure, for the overall velocity of the EOF, $v_{EOF,tot}$, can be derived [3,4,6]:

$$v_{EOF,tot} = xv_{EOF,S} + (1 - x)v_{EOF,B} = xm_{EOF,S}E_S + (1 - x)m_{EOF,B}E_B \quad (1)$$

and for the electric field strengths in the zones S and B, respectively:

$$E_S = \frac{\rho_S V_{tot}}{[x\rho_S + (1 - x)\rho_B]L_C}; \quad E_B = \frac{\rho_B V_{tot}}{[x\rho_S + (1 - x)\rho_B]L_C} \quad (0 < x < 1) \quad (2)$$

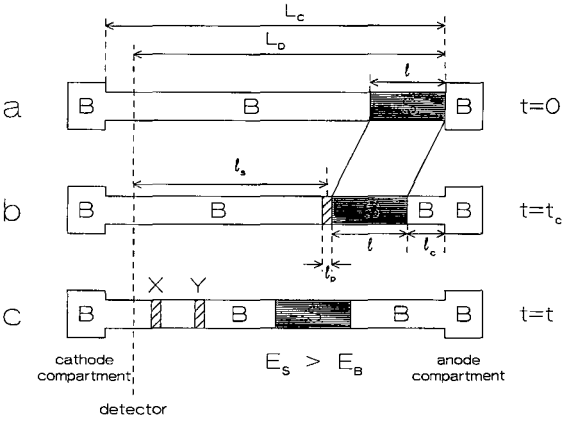

Fig. 1. Effect of sample stacking. (a) Original situation with sampling zone S (sample components dissolved in dilute background electrolyte) behind background electrolyte B. (b) After a short concentration time t_c, the cationic sample components are concentrated in narrow zones with a length l_p between background electrolyte B and the sampling zone S. The electric field strength E_S is larger than E_B. The boundary between sampling zone S and background electrolyte B moves at the velocity of the EOF. (c) The separation of the components X and Y occurs in background B. L_C = capillary length; L_D = distance between injection and detection; l = length of injected sampling zone S; l_c = displacement of sampling zone during stacking procedure; l_p = peak width of sample component after stacking procedure; l_s = separation length after stacking procedure; B = background electrolyte; S = diluted background electrolyte in sampling zone.

whereby V_{tot} is the total applied voltage (V) over the capillary with length L_C. For all calculations and experiments the composition of the background electrolyte B and the dilution factor K are given, where K is the ratio of the concentrations of the background electrolyte B and diluted background electrolyte S, which is approximately equal to the ratios E_S/E_B and ρ_S/ρ_B.

From eqns. 1 and 2 it can be concluded that for increasing values of x and ρ_S, $v_{EOF,tot}$ will be determined to an increasing extent by the properties of the diluted background electrolyte in the sampling zone S. The migration times t_1 of the front and t_2 of the backside of the sampling zone S to reach the detector can be calculated according to

$$t_1 = \frac{L_D - l}{v_{EOF,tot}}; \quad t_2 = \frac{L_D}{v_{EOF,tot}} \quad (3)$$

Sample components (the equations given are valid for cationic species, where the EOF is in the direc-

tion of the cathode) will migrate quickly out of the sampling zone and stack down between sampling zone S and background electrolyte B (see Fig. 1b). After a short concentration time $t_{c,i}$ sample component i will be concentrated to a very short zone, with length $l_{p,i}$ (see Fig. 1b) according to

$$t_{c,i} = \frac{l}{m_i E_S}; \; l_{p,i} = t_{c,i} m_i E_B = l \cdot \frac{E_B}{E_S} = l \cdot \frac{\rho_B}{\rho_S} \quad (4)$$

Eqn. 4 shows that the concentration factor $l/l_{p,i}$ in sample stacking is equal to the K value.

The sampling zone S moves in time $t_{c,i}$ over a distance of

$$l_{c,i} = t_{c,i} v_{EOF,tot} = \frac{l}{m_i E_S} \cdot v_{EOF,tot} \quad (5)$$

After this stacking procedure the components will migrate and be separated according to the zone electrophoretic principle (see Fig. 1c). The separation process takes place for the largest part in the background electrolyte B, at an electric field strength of E_B, with an effective separation length l_S. The total migration time of a component i will therefore be

$$t_{tot,i} = t_{c,i} + \frac{l_S}{v_i} = t_{c,i} + \frac{L_D - l - l_{c,i} - \frac{1}{2} \cdot l_{p,i}}{m_i E_B + v_{EOF,tot}} \quad (6)$$

To check the given model, for several dilutions of different background electrolytes the mobilities of the EOF were measured and with eqns. 1–3 the corresponding t_1 and t_2 values were calculated as a function of the injected length. The experimental values can easily be obtained from the dip in the UV signal in the electropherograms. As an example, in Fig. 2 the calculated relationships between migration times t_1 and t_2 and the injected length and measured values are given for background electrolytes of 0.02 M tris(hydroxymethyl)aminomethane (Tris) adjusted to pH 4.5 by adding acetic acid with $K = 4$ (dashed lines) and 0.02 M histidine–0.02 M 2-(N-morpholino)ethanesulphonic acid (MES) with $K = 5$ (solid lines). The experimental values agree with calculated values although for small injected lengths the experimental values are higher than the calculated values, *i.e.*, the effect of the low concentration in the sampling zone will be partially cancelled by diffusion.

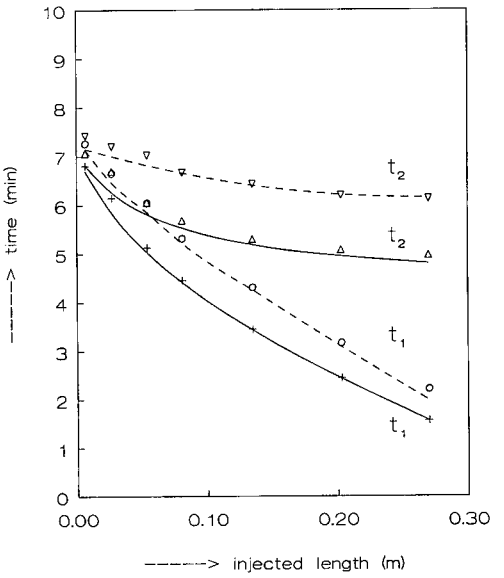

Fig. 2. Calculated relationships between migration times t_1 of the front and t_2 of the rear sides of the sampling zone and injected length for a background electrolyte of 0.02 M Tris acetate at pH 4.5 with $K = 4$ (dashed lines) and 0.02 M histidine–0.02 M MES with $K = 5$ (solid lines) and measured (▽) t_2 and (○) t_1 values in Tris acetate and (△) t_2 and (+) t_1 values in 0.02 M histidine–0.02 M MES.

In Fig. 3 the calculated relationships between t_1 and t_2 values and the total migration times of histidine and imidazole (lines) and measured values are given, applying the background electrolyte 0.02 M

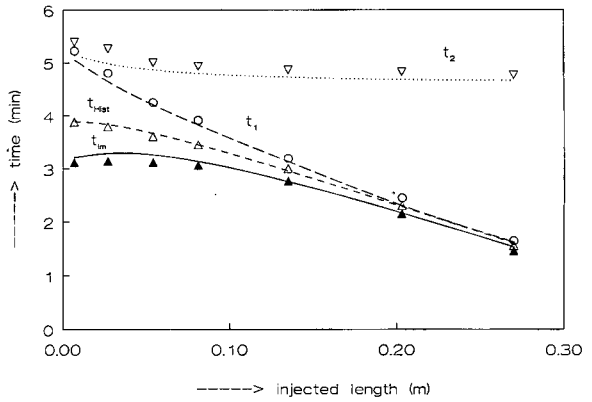

Fig. 3. Relationships between calculated (lines) and measured values of (▽) t_2, (○) t_1 and migration times of (△) histidine and (▲) imidazole *versus* injected length applying a background electrolyte of 0.02 M β-alanine–0.01 M MES ($K = 10$).

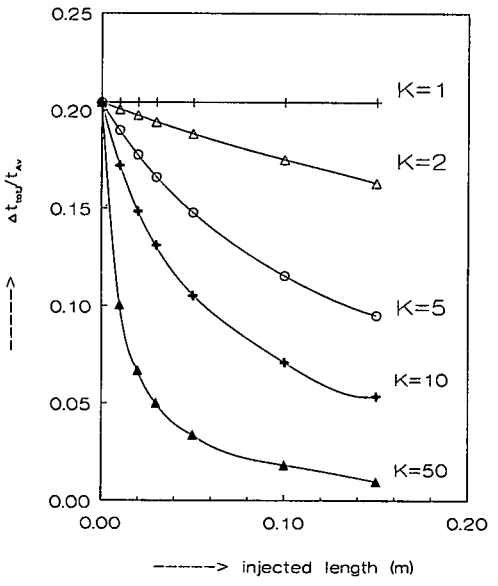

Fig. 4. Calculated relationships between $\Delta_{tot,i}/t_{Av}$ and injected length for two components with mobilities of $50 \cdot 10^{-9}$ and $30 \cdot 10^{-9}$ m^2/V · s in a background electrolyte of 0.02 *M* Tris–0.02 *M* MES for K = 1–50.

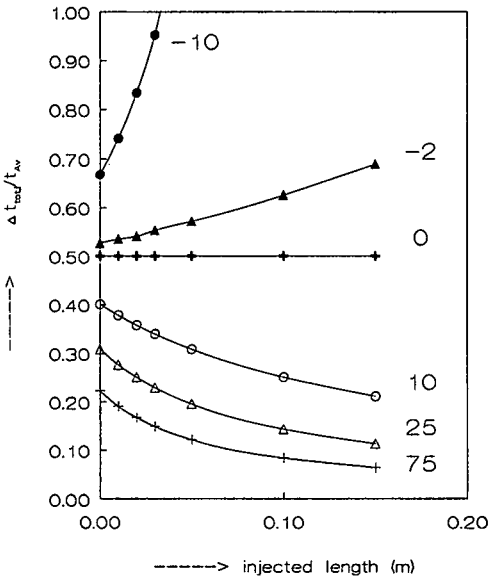

Fig. 5. Calculated relationships between $\Delta t_{tot,i}/t_{Av}$ and injected length for two components with mobilities of $50 \cdot 10^{-9}$ and $30 \cdot 10^{-9}$ m^2/V · s assuming several different mobilities of the EOF. For all calculations K was 10 and $m_{EOF,S}$ was assumed to be $1.5m_{EOF,B}$. The numbers on the right refer to $m_{EOF,B}$ (10^{-9} m^2/V · s).

β-alanine–0.01 *M* MES (K = 10). As can be seen, the calculated and measured values show good agreement. It is notable, however, that the migration times of imidazole and histidine, with a large difference in ionic mobility ($52.0 \cdot 10^{-9}$ and $29.6 \cdot 10^{-9}$ m^2/V · s, respectively) hardly differ and they cannot be separated by injecting large sample volumes. They migrate just before the front of the sampling zone S (t_1).

Although with the foregoing model no resolution factors can be calculated, because peak broadening effects due to injection and the mismatch between the velocities of the EOF in sampling zone and background electrolyte are unknown, the ratio $\Delta t_{tot,i}/t_{Av}$ can be calculated and handled as parameter for the separation efficiency of two components with an average migration time t_{Av}. As an example, in Fig. 4 the calculated relationships, using the foregoing eqn. 6, between $\Delta t_{tot,i}/t_{Av}$ and injected length are given using measured values of the mobilities of the EOF for several dilutions of a background electrolyte of 0.02 *M* Tris–0.02 *M* MES for two components with ionic mobilities of $50 \cdot 10^{-9}$ and $30 \cdot 10^{-9}$ m^2/V · s, showing a dramatic decrease in separation efficiency on injecting large amounts of very dilute samples. The reason for this effect is easy to understand. The injection of a large sample volume reduces the effective separation length and the effective electric field strength over the background electrolyte B diminishes because the largest part of the applied voltage stands over the sampling zone, whereas the velocity of the EOF generally increases because the mobility of the EOF over the sampling zone is high. For K = 1 these effects seem to be negligible, but no concentration effect occurs. Note that in practice the resolution will be even more decreased than indicated in Fig. 4 owing to extra peak broadening effects. To show the effect of decreasing values of the mobility of the EOF, in Fig. 5 the calculated relationships between $\Delta t_{tot,i}/t_{Av}$ and injected length are given for two components with mobilities of $50 \cdot 10^{-9}$ and $30 \cdot 10^{-9}$ m^2/V · s for several values of m_{EOF}. The numbers on the right in Fig. 5 are the $m_{EOF,B}$ values of the background electrolyte B, whereas the values of $m_{EOF,S}$ (K = 10) are always taken arbitrarily as $1.5m_{EOF,B}$. As can be seen from Fig. 5, the decrease in separation power is smaller for lower m_{EOF} values and the separation power even increases for reversed EOF, although in

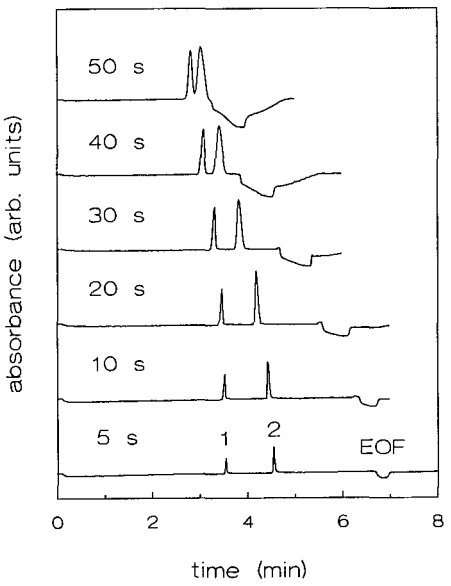

Fig. 6. Electropherograms for the separation of (1) imidazole and (2) histidine in water (0.0001 *M*) for different injection times applying as the background electrolyte 0.01 *M* Tris acetate at pH 4.8. Decreasing resolution is obtained for longer injection times.

that event the migration times will be much higher. From Figs. 4 and 5 it can be concluded that injection of large sample volumes has a disastrous effect on the separation efficiency. This can be seen in Fig. 6, where the measured electropherograms are given for the separation of imidazole and histidine (both 0.0001 *M* in water) applying a background electrolyte of 0.01 *M* Tris adjusted to pH 4.8 by adding acetic acid using several different pressure injection times (a 10-s injection equals an injected length of 1.36 cm), showing the strong decrease in separation power.

Effect of sample stacking on calibration graphs

Strong variations in migration times due to variations in the velocity of the EOF can considerably affect the linear character of the calibration graphs of measured temporal peak area *versus* injected amount. To study the effect of introducing large sample volumes, experiments were performed with 0.01 *M* Tris adjusted to pH 4.8 by adding acetic acid as background electrolyte and a sample consisting of imidazole and histidine both dissolved in background electrolyte and water (0.0001 *M*) for injection times varying from 5 to 60 s, corresponding to sample lengths from 0.68 to about 8.13 cm. In these experiments the migration times of the zones for the

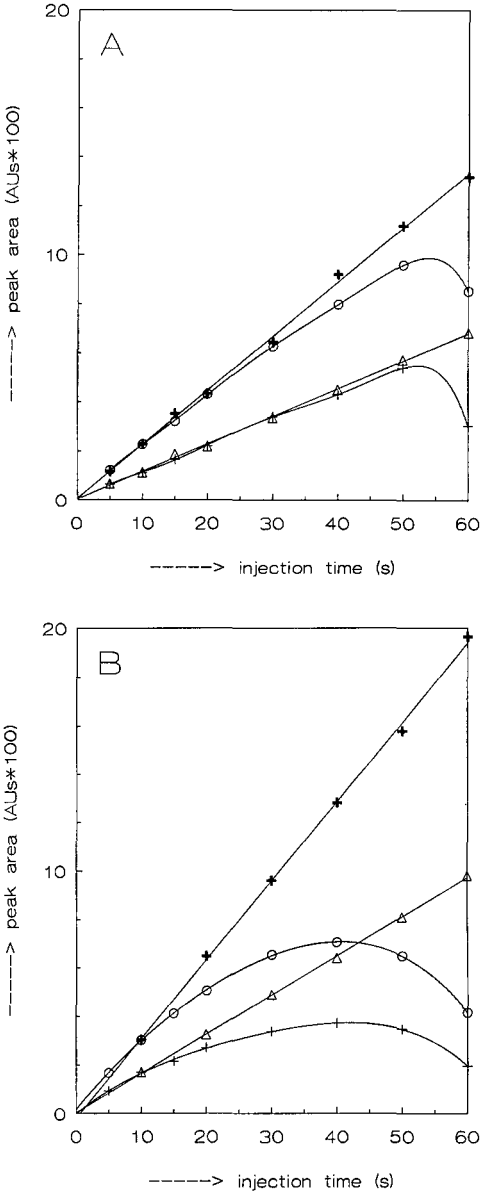

Fig. 7. Measured relationships between peak area and pressure injection time for (+) imidazole and (○) histidine dissolved in water (0.0001 *M*) and (△) imidazole and (+) histidine dissolved in background electrolyte (0.0001 *M*) applying a background electrolyte of 0.01 *M* Tris acetate at pH 4.8 and applying (A) a constant voltage of 10 kV and (B) a constant direct current of 5 μA.

sample dissolved in background electrolyte (measured from the rear side of the zones) were fairly constant, indicating constant migration velocities, through which temporal peak area can be handled in the calibration graphs. All peaks were rectangular owing to the absence of any concentrating effect and both temporal peak area and zone lengths show a linear relationship with injection times. In Fig. 7A the relationships between measured temporal peak area and injection time are given for histidine and imidazole dissolved in water and in background electrolyte and applying a constant voltage of 10 kV. For the samples dissolved in background electrolyte linear relationships are obtained, whereas the aqueous solutions deviate from linearity, especially for large injection times. To study the effect of working at a constant voltage compared with a constant direct current, we repeated the experiments in Fig. 7A but applying a constant current of 5 μA. The calibration graphs are shown in Fig. 7B. The non-linearity for the aqueous sample solutions was much stronger because at a constant current the electric field strengths increase, resulting in much higher velocities of the EOF.

Effect of sample stacking on pH

If a capillary is partially filled with a buffer solution 2 with a different composition to that of the background electrolyte 1 (see Fig. 8), the mass balance of the hydrogen ions over solution 2 will be in imbalance, resulting in pH shifts. Roughly, four different cases can be distinguished, *viz.*, the E gradients in both electrolytes are equal but the pH in electrolyte 2 is (A) higher or (B) lower than those in electrolyte 1, and the cases where the pH values are equal but the E gradient in electrolyte 2 is (C) higher or (D) lower than those of electrolyte 1.

The amount of hydrogen ions (across unit area per unit time) entering the electrolyte 2 (from the rear side) is $[H^+]_1 m_H E_1$ when the amount leaving this zone on the front is $[H^+]_2 m_H E_2$ (the subscripts 1 and 2 refer to the composition of the electrolytes 1 and 2, respectively). The extent of the flow of the hydrogen ions is indicated with an arrow in Fig. 8. If the entering and leaving amounts of hydrogen ions are not equal, pH shifts can be expected with time. If the entering flow of hydrogen ions is larger then the leaving flow, a pH decrease at the rear side and a higher pH in front of the concentration boundaries between electrolytes 1 and 2 can be expected, as indicated in Fig. 8 by dotted lines. The size of the pH shift is difficult to define and depends on several factors, such as the length over which the capillary is filled with electrolyte 2, time of analysis, pH of the system and buffer capacity. At, *e.g.*, a pH of 6 or higher the buffer capacity will be sufficient to compensate for the small differences in the entering and leaving flows of the hydrogen ions, but at low pH problems can be expected because the differences will be much larger.

In sample stacking, we will have generally case C, whereby electrolyte 1 is a background electrolyte at high concentration and the sample is introduced in a large zone at low concentration. If a long sampling zone is introduced, the concentration time of the components will be long and if during that time the pH at the rear side of the sampling zone increases, through which weak cationic species ac-

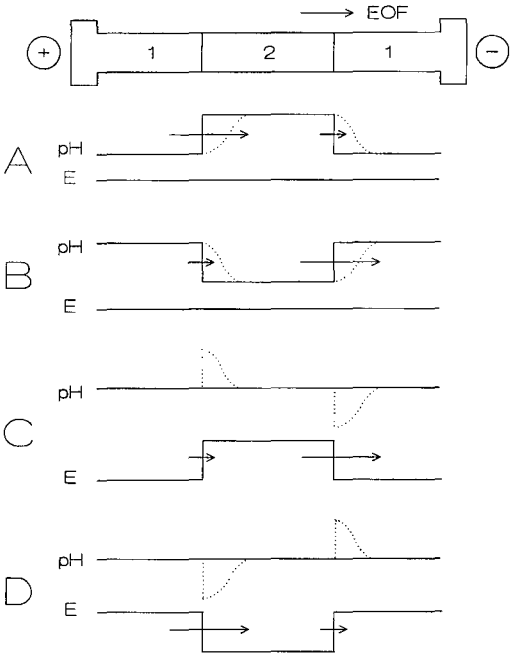

Fig. 8. Introducing two different electrolytes 1 and 2 into a capillary can result in pH shifts. Four different cases can be distinghuished, *viz.*, the E gradients in both electrolytes are equal but the pH in electrolyte 2 is (A) higher or (B) lower than those in electrolyte 1 and the pH values are equal but the E gradient in electrolyte 2 is (C) higher or (D) lower than those of electrolyte 1. Expected pH shifts are indicated by dotted lines. The arrows represent the entering and leaving flows of the hydrogen ions in zone 2.

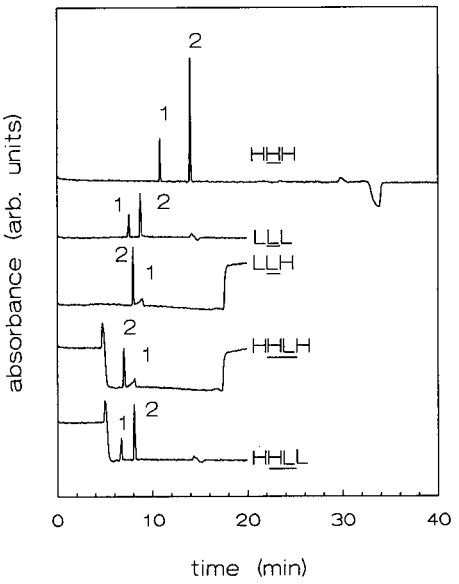

Fig. 9. Electropherograms for the separation of (1) creatinine and (2) clenbuterol (0.0005 *M* in water) with different electrolytes in the cathode and anode compartments and separation capillary. The electrolytes applied are 0.02 *M* Tris (electrolyte H) and 0.002 *M* Tris (electrolyte L) adjusted to pH 4.0 by adding formic acid. The electropherograms are labelled with letters, where the first and last letters indicate the applied electrolyte in the cathode and anode compartments respectively, and the underlined letters indicate the capillary content. Hence, the label HHLH means that the cathode compartment is filled with electrolyte H, the capillary is partially filled with electrolyte H on the cathode side and with electrolyte L on the anode side and the anode compartment is filled with electrolyte H. Applying a normal CZE system (HHH and LLL), creatinine migrates in front of clenbuterol. Application of solution H at the rearside of an L zone (LLH and HHLH) results in reversed migration. The concentration boundaries between H and L electrolytes are indicated by a strong UV shift, owing to differences in UV absorbances of the electrolytes.

quire a lower mobility, the concentration effect will be lost. In such instances bad peak shapes can be the result. Even double peaks were obtained on the electropherograms.

Applying field-amplified CZE, the sample components are introduced behind an electrolyte at low concentration (electrolyte 2). To indicate that pH shifts can occur and can lead to a different migration behaviour and bad peak shapes, several electropherograms are given for the separation of a solution of 0.0005 *M* in water of (1) creatinine and (2) clenbuterol applying different electrolyte systems. At pH 4 clenbuterol can be considered to be completely protonated whereas creatinine is partially protonated and small pH changes will change its effective mobility considerably (its p*K* value is 4.83). The electrolytes applied are always solutions of 0.02 and 0.002 *M* Tris, both adjusted to a pH of 4.0 by adding formic acid. The electrolyte at a concentration 0.02 *M* Tris formate will be indicated by H and that a concentration of 0.002 *M* Tris formate by L. The electropherograms in Fig. 9 are labelled with a letter system, in which the first and last letters indicate the applied electrolyte in the cathode and anode compartments, respectively, and the underlined letters indicate the capillary content. Hence, the label HHLH means that the cathode compartment is filled with electrolyte H, the capillary is partially filled with electrolyte H on the cathode side and with electrolyte L on the anode side and the anode compartment is filled with electrolyte H.

In Fig. 9, the electropherograms HHH and LLL are given for application of normal CZE systems with the electrolyte H and L, respectively, and in both electrolytes creatinine shows a higher effective mobility than clenbuterol. If the cathode compartment and separation capillary are filled with electrolyte L and the anode compartment with electrolyte H (electropherogram LLH), the *E* gradient at the rear side is much lower, through which the hydrogen flow entering at the rear side is too small to maintain a pH of 4 and the pH in the separation capillary will increase. In the electropherogram the migration order of clenbuterol and creatinine is reversed, confirming the pH shift. In the electropherogram HHLH, field-amplified CZE was applied. The separation capillary was partially filled with electrolyte L and the sample was introduced between electrolyte L and H (anode compartment). In zone L a pH increase can be expected, through which clenbuterol and creatinine migrate in the reverse order again. If, however, the anode compartment is also filled with electrolyte L (electropherogram HHLL), the pH of electrolyte L will be constant and clenbuterol and creatinine again migrate in the normal order. From Fig. 9 it can be concluded that the presence of different electrolytes in the capillary and electrode compartments, *e.g.*, in sample stacking or field-amplified CZE, can lead to pH shifts resulting in a different migration order, bad peak shapes and loss of separation power.

CONCLUSIONS

Applying sample stacking, migration times of sample components can be calculated with the given model. Although the given model is fairly simple, *e.g.*, diffusion effects are neglected, the calculated and measured values agree fairly well. Calculations with this model indicate a dramatic decrease in separation power owing to an increasing contribution of the electroosmotic flow to the net migration of sample components, whereas the electric field strength in the separation compartment strongly decreases, in contrast with electrokinetic injection [6]. Also, calibration graphs can be far from linear, by introducing large volumes of very dilute samples and undesirable pH shifts can cause a different migration behaviour if the capillary is filled with different electrolytes.

Although by the application of sample stacking and field-amplified CZE the separation efficiency can be increased owing to the concentration effect, it may only be applicable for the injection of small sampling zones. Another approach for handling extremely large injection volumes in CZE was given by Chien and Burgi [8], whereby the whole separation capillary is filled with sample. By applying a high voltage with reversed polarity, the sample buffer is removed, whereafter the ZE separation can be carried out. A better resolution can also be obtained by suppressing the EOF or applying closed systems. Although the separation length will be decreased on injecting a long sampling plug, this length is then fully used for the separation of the analytes, as the system does not migrate through the capillary owing to the EOF.

REFERENCES

1 F. E. P. Mikkers, F. M. Everaerts and Th. P. E. M. Verheggen, *J. Chromatogr.*, 169 (1979) 1.
2 J. W. Jorgenson and K. D. Luckacs, *Anal. Chem.*, 53 (1981) 1298.
3 X. Huang and J. I. Ohms, *J. Chromatogr.*, 516 (1990) 233.
4 R. L. Chien and J. C. Helmer, *Anal. Chem.*, 63 (1991) 1354.
5 D. S. Burgi and R. L. Chien, *Anal. Chem.*, 63 (1991) 2042.
6 R. L. Chien and D. S. Burgi, *J. Chromatogr.*, 559 (1991) 141.
7 R. L. Chien and D. S. Burgi, *J. Chromatogr.*, 559 (1991) 153.
8 R. L. Chien and D. S. Burgi, *Anal. Chem.*, 64 (1992) 1046.

Journal of Chromatography, 629 (1993) 379–384
Elsevier Science Publishers B.V., Amsterdam

CHROM. 24 666

Analysis of anthraquinone sulphonates

Comparison of capillary electrophoresis with high-performance liquid chromatography

Stephen J. Williams and David M. Goodall

Chemistry Department, University of York, York YO1 5DD (UK)

Kenneth P. Evans

ICI Specialties, P.O. Box 42, Blackley, Manchester M9 3DA (UK)

(First received June 17th, 1992; revised manuscript received September 29th, 1992)

ABSTRACT

Capillary electrophoresis (CE) and high-performance liquid chromatography (HPLC) are compared for the analytical separation of anthraquinone-1-sulphonate and its related impurities anthraquinone-2-sulphonate, anthraquinone-1,8-disulphonate and anthraquinone-1,5-disulphonate. Optimum conditions for CE use a borate solution (50 m*M* NaH_2BO_3 and 8 m*M* H_3BO_3) as background electrolyte at pH 10.0, and for HPLC acetonitrile–water (60:40) containing 0.8% (w/v) cetyltrimethylammonium bromide as eluent. Analysis times are comparable by both techniques. Quantitative aspects including CE and HPLC efficiency, linearity, precision and limits of detection (LOD) are compared. For anthraquinone-1-sulphonate the CE concentration LOD is 0.7 $\mu g\ ml^{-1}$ and the HPLC LOD is 6 ng ml^{-1}: mass LODs are 3 and 60 pg, respectively. Assay precision is 2% R.S.D. in peak area by CE using instruments from several manufacturers. This is improved to better than 0.5% R.S.D. in relative peak areas when a co-injected analyte is used as an internal standard, showing that injection is the factor limiting precision in CE. Integration errors give a significant contribution to the observed error in relative peak areas.

INTRODUCTION

Of increasing interest in capillary electrophoresis (CE) [1,2] are quantitative aspects of the technique [3,4] and its performance relative to established separation methods. For small molecules CE can provide robust assays, but for large molecules which are particularly subject to sample matrix effects and capillary wall interactions the full potential of CE has yet to be established. Reproducibility of sample injection is a key determinant of accuracy and precision in absolute quantitation whilst detector sensitivity constrains dynamic range, accuracy and limit of detection [5,6]. Other factors which must be carefully controlled are background electrolyte composition [5,7] and pH [8], capillary surface condition [7,9], and capillary temperature [10].

In this paper we report a systematic study of the analysis of anthraquinone-1-sulphonate and related impurities, and compare CE results with those achievable by HPLC.

Correspondence to: D. M. Goodall, Chemistry Department, University of York, York YO1 5DD, UK.

EXPERIMENTAL

Instrumentation

Four commercial CE instruments were used in this study: (I) Applied Biosystems (ABI) 270A; (II)

0021-9673/93/$06.00

Beckman P/ACE 2000; (III) Spectra-Physics Spectrophoresis; (IV) Waters Quanta 4000. II and IV were fitted with 75 μm internal diameter (I.D.) fused-silica capillaries, whilst I and III had 50 μm I.D. capillaries. In all cases samples were introduced by hydrodynamic injection at the anodic end of the capillary and detected by UV absorbance in the range 254–260 nm. Electrophoresis was carried out at applied voltages of 20 kV for I, II, IV and 15 kV for III. Corresponding field strengths were: I, 280; II, 350; III, 360; IV, 330 V cm^{-1}. Temperatures set were 30°C for I and II and 25°C for III, whilst IV operated at ambient temperature.

HPLC linearity data were obtained using a system comprising a pump (Altex 110A), autosampler (Perkin-Elmer 420), UV detector (Perkin-Elmer 75T) and integrator (Hewlett-Packard 3354). All other HPLC analyses were carried out using a chromatograph (Hewlett-Packard HP 1090L) fitted with a diode array detector (HP 1040). The detection wavelength was 254 nm and bandwidth 4 nm. A 10-μl injection volume and a 25 cm × 4.5 mm ODS Hypersil column at 40°C were used for all HPLC experiments.

Materials

The anthraquinone sulphonates used were obtained from various sites within the ICI Fine Chemicals Manufacturing Organisation. Compounds and their purities were: sodium anthraquinone-1-sulphonate (96%), sodium anthraquinone-2-sulphonate (97%), sodium anthraquinone-1,5-disulphonate (82%), and potassium anthraquinone-1,8-disulphonate (75%). The CE background electrolyte found to give optimum separation was a borate buffer at pH 10.0 (50 m*M* Na_2HBO_3 and 8 m*M* H_3BO_3) prepared from sodium tetraborate and sodium hydroxide solutions. The HPLC eluent found to give optimum separation was acetonitrile–water (60:40) containing 0.8% (w/v) cetyltrimethylammonium bromide (CTAB). The acetonitrile was of HPLC grade (Rathburn) with CTAB obtained from ICI Pharmaceuticals.

RESULTS AND DISCUSSION

Separations

CE separations of the four anthraquinone sulphonates (Fig. 1) were carried out over a range of pH

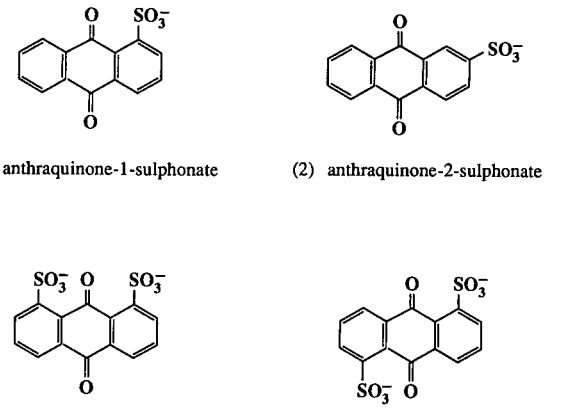

Fig. 1. Structures of (1) anthraquinone-1-sulphonate, (2) anthraquinone-2-sulphonate, (3) anthraquinone-1,8-disulphonate, (4) anthraquinone-1,5-disulphonate.

values. Fig. 2 shows the optimised separation using borate as background electrolyte at pH 10. The low pK_a of the sulphonic acid group ensured that the analytes were negatively charged at all pH values investigated and migrated against the electroosmotic flow. The electroosmotic flow has greater magnitude than the electrophoretic mobilities of the analytes, and their migration times to the detector are in reverse order to the magnitude of their electrophoretic mobilities. The electrophoretic mobility order is 4 > 3 > 2 > 1, with the dianions having higher values than the monoanions as expected, and baseline resolution was obtained for all peaks. Reversal of the polarity coupled with operation at low pH (20 m*M* sodium citrate, pH 2.5) resulted in all sulphonates eluting in under 6 min. However, resolution was found to be much worse than in the high pH case and unsuitable for quantitative studies.

Fig. 3 shows the optimised HPLC separation. The order of elution can be explained in part by considering the effect of ion pairing with CTAB. The greater the interaction the molecules have with the cationic surfactant the more hydrophobic they become, and the greater their retention on the C_{18} stationary phase. The disulphonates form stronger ion pairs than the monosulphonates, and the greater local charge density on the 1,8-dianion than on the 1,5-dianion explains why anthraquinone-1,8-disulphonate forms the strongest ion pair and elutes last.

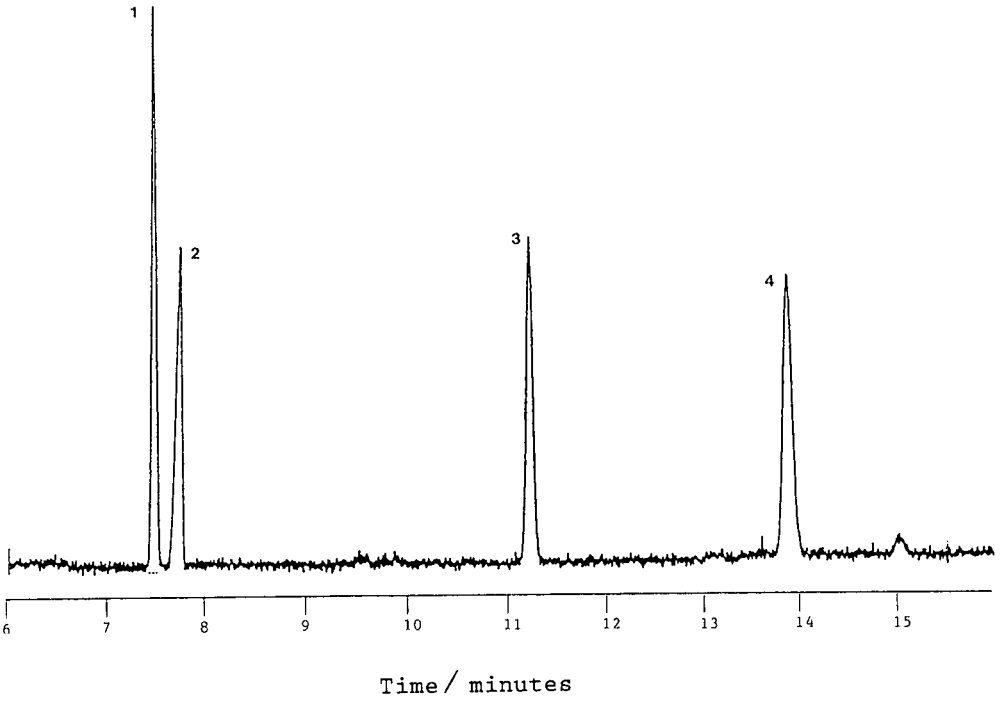

Fig. 2. Electropherogram of anthraquinone sulphonates. Conditions: buffer, 50 m*M* NaH_2BO_3 and 8 m*M* H_3BO_3 pH 10.0; capillary, 72 cm (50 cm to detector) × 50 μm I.D.; applied voltage, 20 kV; temperature, 30°C; detection, UV absorbance at 254 nm; injection, 1 s vacuum. Sample concentration 0.1 mg ml^{-1}.

Efficiency

In comparing the CE and HPLC separations in Figs. 2 and 3, it should be noted that the analysis times are comparable (14–17 min), although HPLC has better resolution for peaks 1 and 2 and could be made at least twice as fast whilst still retaining good resolution between these two peaks. CE has better peak shape and efficiency. With efficiency defined in terms of number of theoretical plates, *N*,

$$N = 5.54\ l^2/w^2 \quad (1)$$

where *l* is the length to the detector and *w* the peak width at half height, CE efficiencies are in the range $1.2 \cdot 10^5$–$6.7 \cdot 10^4$ theoretical plates compared to HPLC efficiencies of $1.8 \cdot 10^4$–$2.6 \cdot 10^3$ theoretical plates.

Linearity

For anthraquinone-1-sulphonate, plots of peak area *versus* concentration over the range 0–350 μg ml^{-1} were made to determine linearity for both HPLC and CE. Correlation coefficients were found to be 0.99995 and 0.99999, respectively. Excellent correlation coefficients were obtained on all CE systems when using peak area. In all cases plots of peak height *versus* concentration showed curvature indicative of peak broadening above an anthraquinone-1-sulphonate concentration of 50 μg ml^{-1}. This value is in the lower part of the linear range for the analyte, and emphasises, as has been noted elsewhere [6], the importance of using peak area rather than peak height in quantitative studies using CE.

Limit of detection

Table I compares limits of detection (LOD) for CE and HPLC, with concentration LOD values taken with the ratio of signal to peak-to-peak noise level equal to 2:1. The primary data for the CE analysis are given in Fig. 4; the peak-to-peak noise is $1 \cdot 10^{-4}$ AU at 254 nm, using a risetime of 1 s, and the LOD for anthraquinone-1-sulphonate is 0.7 μg

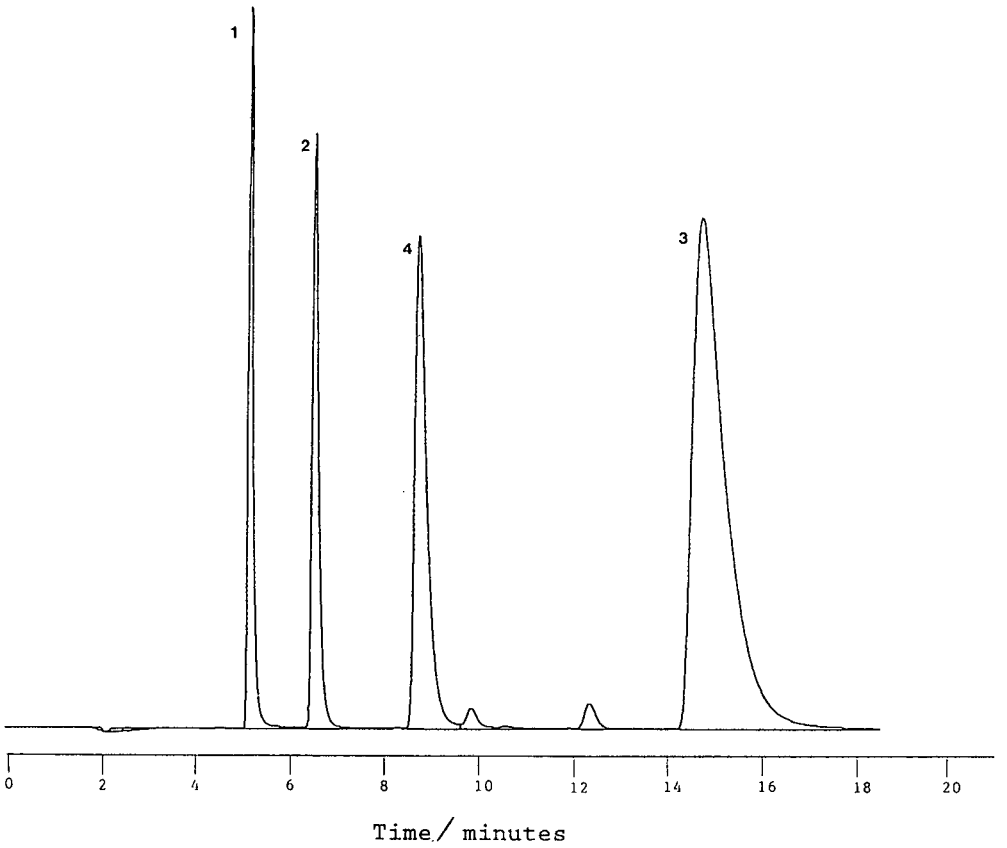

Fig. 3. Chromatogram of anthraquinone sulphonates. Conditions: eluent, acetonitrile–water (60:40) containing 0.8% (w/v) CTAB; column, 25 cm × 4.5 mm ODS Hypersil; flow-rate, 1 ml min^{-1}; temperature, 40°C; detection, UV absorbance at 254 nm; injection, 10 μl. Sample concentration 0.1 mg ml^{-1}.

ml^{-1} ($2 \cdot 10^{-6}$ *M*). To derive accurate mass LOD values in CE it is vital to know accurately the injection volume. For the ABI instrument used this has been determined by microscopic measurement of water displacement by air with correction for surface tension, and measured values were found to agree well with those calculated using the Poiseuille equation [6].

A criticism frequently levelled at CE is that whilst its mass detection limits are good due to the small injection volume, compared with HPLC its concentration limits of detection are poor. This is born out by the data in Table I, where it can be seen that the mass LOD is 20 times better for CE than for HPLC, but that HPLC can detect a 100 times less concentrated sample. Concentration LOD differences using absorbance detection are essentially a function of the difference in optical path lengths between the HPLC detector flow cell (1 cm) and the CE capillary ($5 \cdot 10^{-3}$ cm).

TABLE I

CONCENTRATION AND MASS DETECTION LIMITS FOR ANTHRAQUINONE-1-SULPHONATE

Method	Injection volume (μl)	Concentration detection limit (μg ml^{-1})	Mass detection limit (pg)
CE	0.004	0.7	2.8
HPLC	10	0.006	56

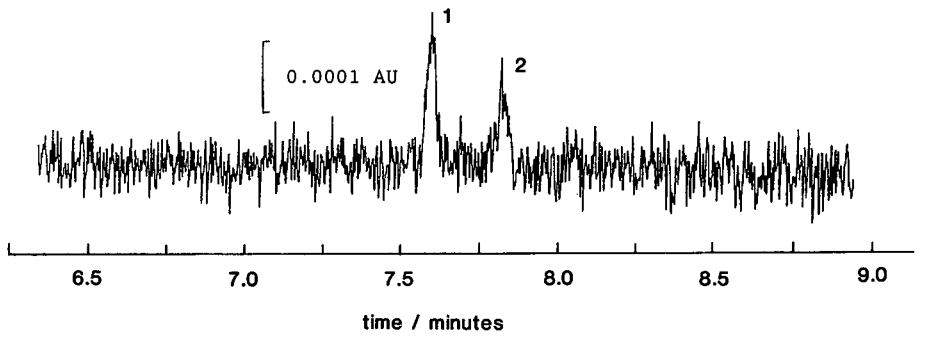

Fig. 4. Electropherogram of (1) anthraquinone-1-sulphonate and (2) anthraquinone-2-sulphonate used to determine LOD. Conditions as in Fig. 2, except sample concentration 1.6 μg ml^{-1}.

Precision

For studies of precision in the HPLC method 15 injections of sample were made at a concentration of 0.1 mg ml^{-1}. The relative standard deviation (R.S.D.) in peak area was found to be 0.5%.

Representative results of studies of reproducibility of migration time and peak areas in CE are given in Table II. Since the area of a peak is proportional to its migration time [11], improved peak area R.S.D.s are expected to result after normalising peak areas for migration times. R.S.D.s obtained from data based on 33 replicate injections on one instrument do indeed improve on normalisation (bracketted values), consistent with errors in peak area and migration time being correlated. In contrast to this, with another instrument the area R.S.D.s are not improved by normalisation and the errors appear to be uncorrelated. Correlated errors may be evident in a series where there is drift in retention time (*e.g.*, using a new capillary [9]).

After normalisation, peak area R.S.D.s are 2% for all anthraquinone sulphonates on both instruments. The last column in Table II shows the effect of ratioing the peak area of the anthraquinone-1-sulphonate to that of a second component in the mixture of analytes injected. R.S.D.s in relative peak areas are up to a factor 7 better than R.S.D.s in absolute peak areas, and the removal of all correlated errors as shown in Table II yields very good R.S.D. values, less than 0.5%. This proves that injection is the dominant source of error, limiting peak area reproducibility to 2% in the present generation of automated CE instruments. If it is desired to quantitate analytes to a higher degree of

TABLE II

REPRODUCIBILITY OF MIGRATION TIMES AND PEAK AREAS

Instrument	Analyte	R.S.D. (%)		
		Migration time	Peak area[c]	Peak area (1) / Peak area (4)
II[a]	(1) Anthraquinone-1-sulphonate	0.5	1.9(1.9)	0.4
	(4) Anthraquinone-1,5-disulphonate	0.7	2.1 (2.6)	
III[b]	(1) Anthraquinone-1-sulphonate	0.9	2.2 (2.0)	0.9 (0.3)
	(4) Anthraquinone-1,5-disulphonate	1.7	3.1 (2.2)	

[a] Data based on 17 replicate injections.
[b] Data based on 33 replicate injections.
[c] Normalized peak areas in brackets.

precision, either multiple injections (to decrease the standard error on the mean) or the use of an internal standard is required.

One factor often overlooked in quantitative studies in CE is the effect of integration on area determination. Grushka and Zamir [12] have shown that for a Gaussian peak the relative error in the area, $\delta A/A$, is given by

$$\frac{\delta A}{A} = \frac{4}{\sqrt{2\pi}} \left(\frac{S}{N}\right)^{-1} \frac{w^{3/2}}{n} \quad (2)$$

where S/N is the ratio of signal to root-mean-square noise, w is the width of the peak at half height, and n is the number of data samplings across this width [12]. Inserting values obtained using an integration rise time of 1 s (3.3 data points per second) and analyte concentration 0.1 mg ml^{-1} gives a calculated contribution to the relative peak area R.S.D. using the 1,5-disulphonate as internal standard for anthraquinone-1-sulphonate of *ca.* 0.2%, *i.e.*, a significant contribution to the observed values of 0.3–0.4% given on the last column of Table II.

CONCLUSIONS

The comparison of CE with HPLC for the analysis of anthraquinone-1-sulphonate and three related impurities shows that both techniques give baseline-resolved separations within 17 min. CE gives better peak shape and efficiency, but HPLC has the better resolution for anthraquinone-1-sulphonate and its -2- isomer. Whereas CE is superior in its mass limit of detection, HPLC has an advantage of two orders of magnitude in concentration limit of detection. Excellent correlation coefficients are obtained for peak area as a function of concentration for both techniques. Assay precision is 0.5% R.S.D. in peak area by HPLC and 2% by CE, though the latter is improved to better than 0.5% R.S.D. using an internal standard. Closely comparable figures were obtained on CE instruments from four different manufacturers, showing that injection is the factor limiting precision in every case. The use of an internal standard is therefore recommended for high-precision CE analyses. An analysis of errors in integration in CE shows that these are significant at the 0.2% R.S.D. level, and it will be advisable to work at the highest practicable analyte concentration and at a high digitisation rate when seeking the highest precision in CE.

ACKNOWLEDGEMENTS

We wish to acknowledge support from the SERC for an SERC CASE studentship to S.J.W., and assistance from Applied Biosystems, Beckman, Spectra Physics and Waters for the use of CE instrumentation.

REFERENCES

1 R. A. Wallingford and A. G. Ewing, *Adv. Chromatogr.*, 29 (1989) 1.
2 W. G. Kuhr, *Anal. Chem.*, 62 (1990) 403R.
3 D. M. Goodall, S. J. Williams and D. K. Lloyd, *Trends Anal. Chem.*, 10 (1991) 272.
4 E. B. Dose and G. A. Guiochon, *Anal. Chem.*, 63 (1991) 1154.
5 D. J. Rose and J. W. Jorgenson, *Anal. Chem.*, 60 (1988) 642.
6 S. E. Moring, J. C. Colburn, P. D. Grossman and H. H. Lauer, *LC · GC*, 8 (1) (1990) 34.
7 M. Zhu, R. Rodriguez, D. Hansen and T. Wehr, *J. Chromatogr.*, 516 (1990) 123.
8 K. Salomon, D. Burgi and J. C. Helmer, *J. Chromatogr.*, 549 (1991) 375.
9 D. K. Lloyd, *Anal. Proc.*, 29 (1992) 169.
10 J. H. Knox and I. H. Grant, *Chromatographia*, 61 (1987) 24.
11 X. Huang, W. F. Coleman and R. N. Zare, *J. Chromatogr.*, 480 (1989) 95.
12 E. Grushka and I. Zamir *Chem. Anal. (N.Y.)*, 98 (1989) 529.

Journal of Chromatography, 629 (1993) 385–388
Elsevier Science Publishers B.V., Amsterdam

CHROM. 24 710

Short Communication

Enantiomer separations of secondary alkanols with little asymmetry by high-performance liquid chromatography on chiral columns

Toru Takagi, Naoki Aoyanagi, Kazuhiko Nishimura, Yasuhiro Ando and Toru Ota

Department of Chemistry, Faculty of Fisheries, Hokkaido University, Hakodate 041 (Japan)

(First received August 5th, 1992; revised manuscript received October 23rd, 1992)

ABSTRACT

Enantiomer separations of secondary alkanols with little asymmetry, $CH_3(CH_2)_nCHOH(CH_2)_{n+1}CH_3$, as their 3,5-dinitrophenylurethane (3,5-DNPU) derivatives were carried out by high-performance liquid chromatography (HPLC) using a chiral column Sumichiral OA-4100 containing N-(*R*)-1-(α-naphthyl)ethylaminocarbonyl-(*S*)-valine chemically bonded to silanized silica. Enantiomer separations (α = 1.06–1.07, R_s = 1.31–1.43) of 2-butanol, 3-hexanol and 4-octanol were obtained by HPLC at low temperature (−20 to −40°C). Enantiomer separation of 5-decanol (α = 1.02, R_s = 0.88) was obtained by HPLC at −20°C after four recyclings. Enantiomer separations (α = 1.07–1.10, R_s = 1.05–1.28) of 2-butanol and 3-hexanol were obtained as 3,5-DNPU derivatives by HPLC using a YMC A-K03 chiral column containing (*R*)-1-(1-naphthyl)ethylamine polymer chemically bonded to spherical silica at ambient temperature.

INTRODUCTION

Enantiomer separations of secondary alcohols are important in analyses of physiologically active materials such as aromas, insect pheromones and products from some enzyme reactions, as described in a review [1].

Diastereomeric (*S*)-(+)-2-phenylpropionate derivatives of secondary alcohols have been separated by gas–liquid chromatography with 5% QF-1 on Gas-Chrom Q. There was no separation of 2-butanol and 4-octanol, and only a very slight separation for the 3-hexanol derivative [2]. As these alcohols of even carbon number have carbinol substituents that differ by only one carbon, they are referred to as secondary alkanols with little asymmetry (**I**) in this paper. The general structure of **I** is

$$\underset{\displaystyle\mathrm{OH}}{CH_3(CH_2)_nCH(CH_2)_{n+1}CH_3}$$

I

This paper presents an HPLC method on a chiral stationary phase for complete separations of **I** with carbon numbers 4, 6 and 8, and a fair separation of **I** of carbon number 10.

EXPERIMENTAL

Samples and reagents

Racemic 2-butanol, 3-hexanol, 4-octanol, 5-decanol and (*S*)-(+)-2-butanol (purities > 99%), 2-

Correspondence to: Toru Takagi, Department of Chemistry, Faculty of Fisheries, Hokkaido University, Hakodate 041, Japan.

0021-9673/93/$06.00

and 4-decanol (purities > 98%) and 3-decanol (purity > 95%) were obtained from Tokyo Kasei (Tokyo, Japan). 3,5-Dinitrophenyl isocyanate reagent and a Sumichiral OA-4100 chiral column were obtained from Sumika Chemical Analysis (Osaka, Japan). Dehydration of pyridine was carried out with calcium hydride (Tokyo Kasei). Pyridine (500 ml) was preliminarily dehydrated over molecular sieve 4A (50 g) overnight. Pyridine separated by decantation was refluxed with calcium hydride (2 g) for 5 h and then distilled. Toluene was dehydrated on sodium wire.

HPLC

The 3,5-dinitrophenylurethane (3,5-DNPU) derivatives of the secondary alkanols were prepared on the basis of the procedures described for the derivatization of several aromatic and aliphatic chiral alcohols [3]. About 2 mg of 3,5-dinitrophenyl isocyanate was reacted with about 1 mg of the alkanol in dry toluene (4 ml) in the presence of dry pyridine (40 μl) for 1 h.

HPLC separations were carried out with a Shimadzu (Kyoto, Japan) LC-6A instrument equipped with a chiral column. Two columns, Sumichiral OA-4100 (stainless steel, 50 cm × 4 mm I.D.) packed with 5-μm particles of N-(*R*)-1-(α-naphthyl) ethylaminocarbonyl-(*S*)-valine chemically bonded to γ-aminopropylsilanized silica, and YMC A-K03 (stainless steel, 25 cm × 4.6 mm I.D.) packed with 5-μm particles of (*R*)-1-(1-naphthyl)ethylamine polymer phase covalently bonded to 300 Å wide-pore spherical silica, were used as chiral stationary phase columns. *n*-Hexane–1,2-dichloroethane–ethanol (80:20:1, v/v/v) was used as the mobile phase at a constant flow-rate (0.5 ml/min). Peaks were monitored with a Shimadzu SPD-1 UV detector at 254 nm. A Hitachi (Tokyo, Japan) 638-0805 recycle valve was used for recycling. The column was dipped into an ethanol bath, which was kept at a specified low temperature to within about 1.0°C by an immersion cooler with an exclusive controller.

RESULTS AND DISCUSSION

Enantiomer separations of racemates of 2-butanol, 3-hexanol, 4-octanol and 5-decanol were carries out as their 3,5-DNPUs by HPLC on Sumichiral OA-4100. At room temperature, each racemate of 3-hexanol and 4-octanol was partially resolved into enantiomers, but 2-butanol and 5-decanol did not show any separation. In previous studies [4,5], we observed that mono- and diacylglycerols were better resolved into enantiomers at low temperature. The chiral phase HPLC of the alkanols was also carried out at low temperature. The results are shown in Fig. 1 and Table I (A).

At −20 to −40°C, clear enantiomer separations were obtained for 2-butanol, 3-hexanol and 4-octanol, but the separation of 5-decanol enantiomers was poor. The separation of 5-decanol enantiomers was much improved by recycling, as shown in Fig. 2 and Table I (B). Enantiomer separations of second-

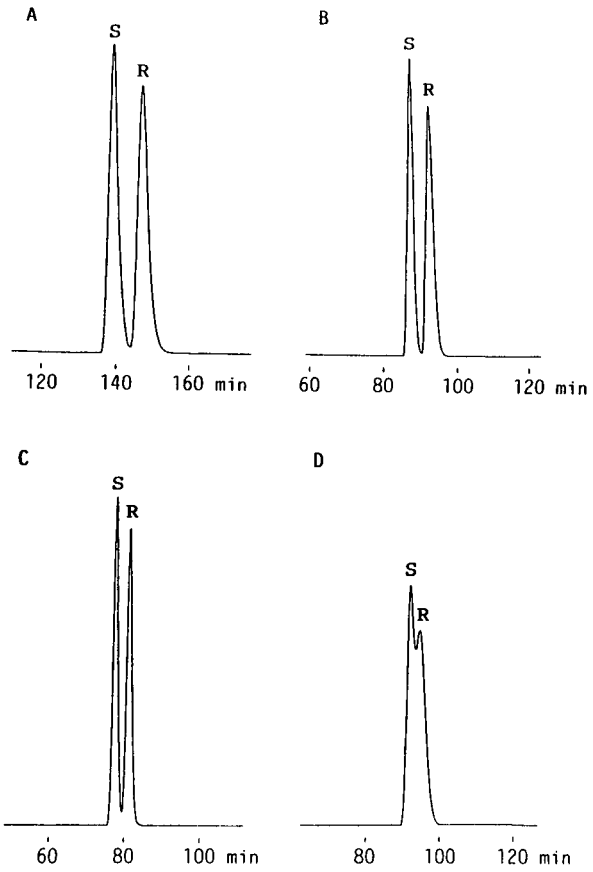

Fig. 1. Enantiomer separation of racemic secondary alkanols as 3,5-DNPU derivatives on an OA-4100 chiral column at low temperature. Mobile phase, *n*-hexane–1,2-dichloroethane–ethanol (80:20:1, v/v/v); flow-rate, 0.5 ml/min; detection at 254 nm. Samples and column temperature: (A) 2-butanol, −40°C; (B) 3-hexanol, −30°C; (C) 4-octanol, − 20°C; (D) 5-decanol, −20°C.

TABLE I

ENANTIOMER SEPARATIONS OF CHIRAL SECONDARY ALKANOLS BY HPLC ON CHIRAL COLUMNS

Column	Alcohol	Configuration	Column temperature (°C)	V_r^b (ml)	α^c	R_s^d
(A) OA-4100	2-Butanol	*S*	−40	63.47	1.06	1.43
		R		67.53		
	3-Hexanol	*S*	−30	37.87	1.07	1.39
		R		39.85		
	4-Octanol	*S*	−20	32.82	1.06	1.31
		R		34.66		
	5-Decanol	*S*	−20	38.40	1.02	0.34
		R		39.35		
(B) OA-4100	5-Decanol[a]	*S*	−20	218.88	1.02	0.88
		R		223.71		
(C) A-K03	2-Butanol	*S*	26	41.52	1.07	1.05
		R		44.37		
	3-Hexanol	*S*	26	25.43	1.10	1.28
		R		27.86		
	4-Octanol	*S*	26	18.25	1.04	0.48
		R		19.02		
	5-Decanol	*R,S*	26	14.74	Not separated	

[a] At fourth recycle.
[b] Retention volume.
[c] Separation factor.
[d] Peak resolution.

ary decanol isomers as 3,5-DNPUs on OA-4100 at room temperature are shown in Table II (A). The separation of 5-decanol was very difficult in comparison with those of 2-, 3- and 4-decanols. In general, enantiomer separations of the secondary decanols decreased in the order of 2-, 3-, 4- and 5-isomers, *i.e.*, with decreasing asymmetry of the molecule. Enantiomer separaration of 5-decanol was first achieved using an OA-4100 column after several recycles at low temperature. This difficulty is attributable to the low asymmetry of 5-decanol.

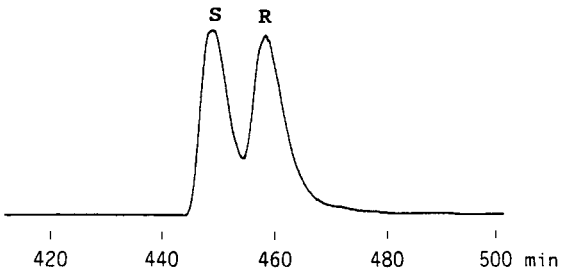

Fig. 2. Enantiomer separation of racemic 5-decanol as 3,5-DNPU derivatives on an OA-4100 column. Peaks were monitored at the fourth recycle. Column temperature, −20°C; other conditions as in Fig. 1.

The configurations of peak components were assigned on the basis of the results obtained with coinjection of (*S*)-2-butanol and racemic 2-butanol. The (*S*)-2-butanol peak emerged earlier than the (*R*)-2-butanol peak. This indicates that the retention time of the *S* enantiomer is shorter than that of the *R* isomer in the HPLC of the secondary alkanols with little asymmetry on the chiral phase under the conditions used in this study.

The secondary alkanols were also separated as 3,5-DNPUs by HPLC on a YMC A-K03 chiral column at ambient temperature [Tables I (C) and II (B)]. In this instance, the enantiomers of 2-butanol, 3-hexanol and 2-, 3- and 4-decanol were resolved even at room temperature, whereas 4-octanol enantiomers were partially resolved, and 5-decanol was not resolved at all. As individual peaks obtained on the YMC A-K03 column were broad with peak tailing, recycling and low-temperature tech-

TABLE II

ENANTIOMER SEPARATION OF SECONDARY DECANOLS BY HPLC ON CHIRAL COLUMNS AT ROOM TEMPERATURE[a]

Column	Alcohol	Configuration	V_r^b (ml)	α^c	R_s^d
(A) OA-4100	2-Decanol	*S*	19.73	1.09	2.23
		R	21.40		
	3-Decanol	*S*	17.73	1.09	2.32
		R	19.39		
	4-Decanol	*S*	17.64	1.06	1.31
		R	18.58		
	5-Decanol	*R,S*	21.82	Not separated	
(B) A-K03	2-Decanol	*S*	17.40	1.24	3.37
		R	21.61		
	3-Decanol	*S*	16.46	1.15	2.17
		R	18.96		
	4-Decanol	*S*	15.48	1.05	0.72
		R	16.31		
	5-Decanol	*R,S*	14.74	Not separated	

[a] Room temperature = 26°C.
[b] Retention volume.
[c] Separation factor.
[d] Peak resolution.

niques could not be applied for separation on the A-K03 column. The YMC A-K03 column is useful for enantiomer separations of 2-butanol and 3-hexanol at room temperature.

In Fig. 1A–C, the peak-area ratios of the *S* to the *R* enantiomer are 0.98–0.99. This shows that the methods in this paper can be applied to the determination of enantiomer ratios and examination of the optical purity of secundary alkanols. The peak-area ratios of the *S* to the *R* enantiomers in Fig. 2 are 0.86–0.90. The smaller peak area for the *S* enantiomer seems to be caused by counting the tailing part of the *S* enantiomer peak as part of the *R* enantiomer peak. In this case, the enantiomer ratios are approximately determined by the HPLC method.

To achieve the separation of 5-decanol enantiomers on OA-4100, as shown in this study, an extremely long elution time was required in comparison with the enantiomer separations of the other secondary alkanols. The method presented here must be improved for complete separation of 5-decanol in a shorter time, and for separations of higher homologues of the secondary alkanols with little asymmetry.

REFERENCES

1 T. Takagi, *Prog. Lipid Res.*, 29 (1990) 277–298.
2 S. Hammarström and M. Hamberg, *Anal. Biochem.*, 52 (1973) 169–179.
3 N. Oi and H. Kitahara, *J. Chromatogr.*, 265 (1983) 117–120.
4 T. Takagi and Y. Ando, *Lipids*, 26 (1991) 542–547.
5 T. Suzuki, T. Ota and T. Takagi, *J. Chromatogr. Sci.*, 30 (1992) 315–318.

Journal of Chromatography, 629 (1993) 389–393
Elsevier Science Publishers B.V., Amsterdam

CHROM. 24 735

Short Communication

Characterization of flavonoids by liquid chromatography–tandem mass spectrometry

Yong Y. Lin

NYS Institute for Basic Research in Developmental Disabilities, 1050 Forest Hill Road, Staten Island, NY 10314 (USA)

Kwokei J. Ng

Department of Drug Metabolism, Schering-Plough Research Institute, Bloomfield, NJ (USA)

Shenjiang Yang

Zejiang Agricultural University, Hangzhou (China)

(First received August 10th, 1992; revised manuscript received October 28th, 1992)

ABSTRACT

Thermospray LC–MS–MS was used to study a catechin mixture extracted from the tea plant *Camellia sinensis*. Four major catechins, (−)-epicatechin, (−)-epigallocatechin, (−)-epicatechin 3-O-gallate, and (−)-epigallocatechin 3-O-gallate were quickly recognized in the mixture by their $[M + H]^+$ ions. Collission-induced dissociation (CID) spectra of the $[M + H]^+$ ions gave simple fragmentation patterns, which permitted characterization of the substituents and the ring structures of the molecules. Several representative flavonoids and their glycosides were also studied by thermospray LC–MS–MS. Their CID spectra showed three types of ring cleavages in the pyran ring of the flavonoids, and differentiation among flavanone, flavone, and flavonol was made. LC–MS–MS appears to be the method of choice for the analysis of plant flavonoids including their glycosides.

INTRODUCTION

The history of tea in China started as early as 5000 years ago, when it was discovered as a herbal medicine, and some significant pharmacological and health effects of the tea plant, *Camellia sinensis*, have gained support from scientific research in recent years. Catechins, the main flavonoid constituents of *Camellia sinensis*, have been shown to be inhibitory against mutagenic and tumorigenic activities [1-5]. (−)-Epigallocatechin 3-O-gallate, the most abundant catechin in the plant, was shown to have a radioprotective effect when it was administered to mice [6]. Catechins have also been known to have broad antibacterial and antiviral activities against herpes simplex, leukemia, influenza and cytomegaloviruses. Two catechins, (−)-epigallocatechin 3-O-gallate and (−)-epicatechin 3-O-gallate, were found to inhibit HIV reverse transcriptase and cellular DNA and RNA polymerases [7]. Although

Correspondence to: Yong Y. Lin, NYS Institute for Basic Research in Developmental Disabilities, 1050 Forest Hill Road, Staten Island, NY 10314, USA.

0021-9673/93/$06.00

the mechanism of the pharmacological effects of catechins remains unclear, the strong antioxidant activity of catechins as radical scavengers might play some role [8]. Several polyphenols from plants, such as methylgallate [9], 5,6,7-trihydroxyflavone [10], oxidized polymeric compounds of caffeic acid [11], and tannic acid [12], have also been reported to have antiviral activities.

In connection with our interest in the study of structure and biological activity relationship of flavonoids [13], we have explored an effective means of mass spectrometric identification of plant flavonoids by LC–MS–MS. Catechin mixtures extracted from *Camellia sinensis* and several other plant flavonoids (Fig. 1) were studied by thermospray LC–MS–MS, and we found that this technique can be used effectively for the identification of catechins and other flavonoids in complex mixtures.

EXPERIMENTAL

Materials

A catechin mixture was supplied by Zejiang Agricultural University, Hangzhou, China. The mixture was obtained by extraction of green tea leaves of *Camellia sinensis* briefly as follows [14]: the dried tea leaves were extracted three times with approximately 10 volumes of hot water. Catechins were precipitated with $CaCO_3$ solution to separate them from the caffeine, redissolved in acid medium, and re-extracted into ethyl acetate. Evaporation of the ethyl acetate gave light brown powders, which consisted mostly of catechins. Pure flavonoids were obtained from Aldrich (Milwaukee, WI, USA).

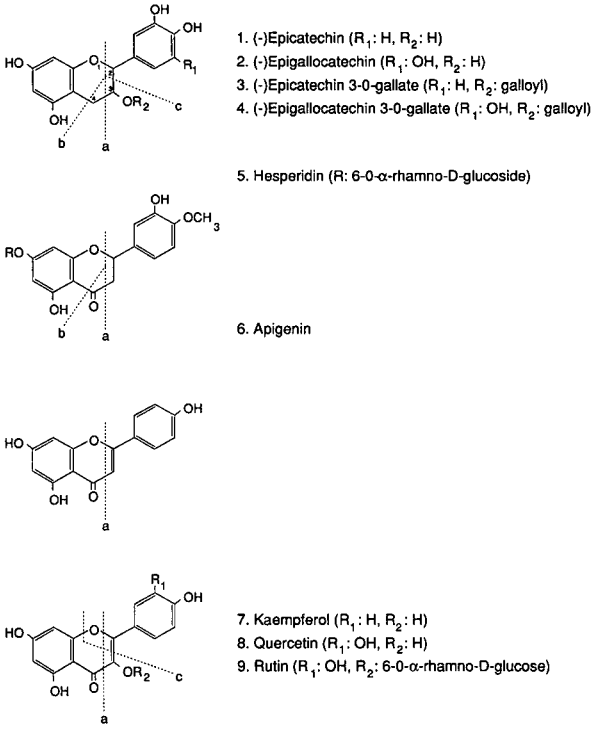

Fig. 1. Structures of catechins and flavonoids.

LC–MS–MS

Mass spectra were obtained with a Finnigan MAT TSQ 70 mass spectrometer interfaced to a Waters 600-MS HPLC system. For HPLC a methanol–water (30:70) mixture containing 0.05% trifluoroacetic acid was used at a flow-rate of 1 ml min^{-1}. A Waters reversed-phase C_{18} column, 25 cm × 2.0 mm I.D. packed with 5-μm particles, was used. The effluent from the column was passed into the Finnigan MAT thermospray LC–MS interface. Collision-induced dissociation (CID) spectra were obtained at 20–70 eV collision energy using argon at 2–4 mTorr (1 Torr = 133.322 Pa) in the non-linear collision cell.

RESULTS

Thermospray LC–MS and CID spectra of tea catechin mixture

The mass chromatogram of the thermospray LC–MS obtained with a 30-μl injection of 1 mg/ml of the catechin mixture is shown in Fig. 2. The reconstructed total ion chromatogram, bottom trace of Fig. 2, showed only four distinct peaks. The mass spectra of the peaks (Table I) all gave abundant $[M + H]^+$ ions consistent with the expected four major tea catechins [15], (−)-epicatechin (*m/z* 291), (−)-epigallocatechin (*m/z* 307), (−)-epicatechin 3-O-gallate (*m/z* 443), and (−)-epigallocatechin 3-O-gallate (*m/z* 459). As clearly demonstrated by the mass chromatograms in Fig. 2, the thermospray LC–MS provides mass spectrometric identification of the four major catechins in the plant. In addition to the $[M + H]^+$ ions, the presence of gallic esters in (−)-epicatechin 3-O-gallate (**3**) and (−)-epigallocatechin 3-O-gallate (**4**) are indicated in the LC–MS spectra by the ions *m/z* 275 and 291 derived from the loss of 168 u from the corresponding $[M + H]^+$

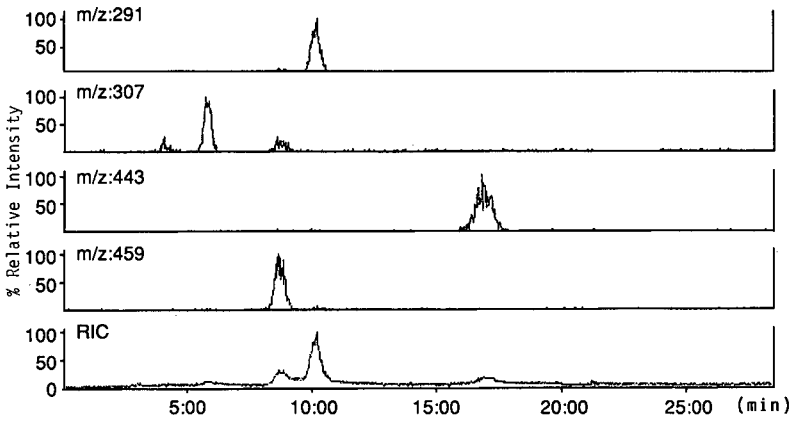

Fig. 2. Mass chromatograms of a catechin mixture from *Camellia sinensis* analyzed by thermospray LC–MS. RIC = reconstructed total ion chromatogram.

ions. Furthermore, in the CID spectra ions of *m/z* 153 and 151 derived from galloyl moiety as well as the ions *m/z* 273, 289 ([M + H − 170]) derived, respectively, from the loss of gallic acid (170 u) from the corresponding $[M + H]^+$ ions (Table I) also indicated the presence of gallic esters. We have also analyzed the mixture with particle-beam LC–MS, but the results were less informative, because two of the catechins, (−)-epicatechin 3-O-gallate (**3**) and (−)-epigallocatechin 3-O-gallate (**4**), failed to give molecular ions, only fragmentation ions (results not shown).

In order to obtain additional structural information from fragmentation ions, CID spectra of the above $[M + H]^+$ ions were studied. The CID spectra of catechins consist of three types of cleavages, *a*, *b* and *c*, at the dihydropyran rings of catechins, and elimination ions of the substituent at the 3-position of the ring. Fig. 3 is an example of the CID spectrum for the $[M + H]^+$ (*m/z* 443) ion of (−)-

TABLE I

THERMOSPRAY MS AND CID SPECTRA OF CATECHINS AND FLAVONOIDS

Compound	Thermospray MS *m/z* (rel.%)[a]		CID spectra *m/z* (rel.%)[a]			
	$[M + H]^+$	[others]	[A]	[B]	[C]	[others]
1	*291*(100)	275(6)	139(100)	165(10)	123(58)	207(18), 147(13)
2	*307*(100)		139(100)	181(10)	139(100)	223(4), 163(7)
3	*443*(100)	291(40), 275(100), 273(24)	139(24)	165(5)	123(100)	291(47), 273(18), 153(14), 151(22)
4	*459*(40)	307(13), 291(100), 285(25)	139(100)	181(5)	139(100)	307(17), 289(34), 153(14), 151(18)
5	611(10)	465(8)				
		303(100)	153(100) 149(19)	177(68)	–	
6	*271*(100)		153(89) 119(100)	–	–	
7	*287*(100)		153(100)	–	121(70)	
8	*303*(100)		153(100)	–	137(60)	
9	*611*(8)	465(3)	–	–	–	465(27), 303(100), 165(7), 147(24), 129(45)
		303(100)	153(100)	–	137(70)	

[a] CID spectra were obtained with the italicized MS ions.

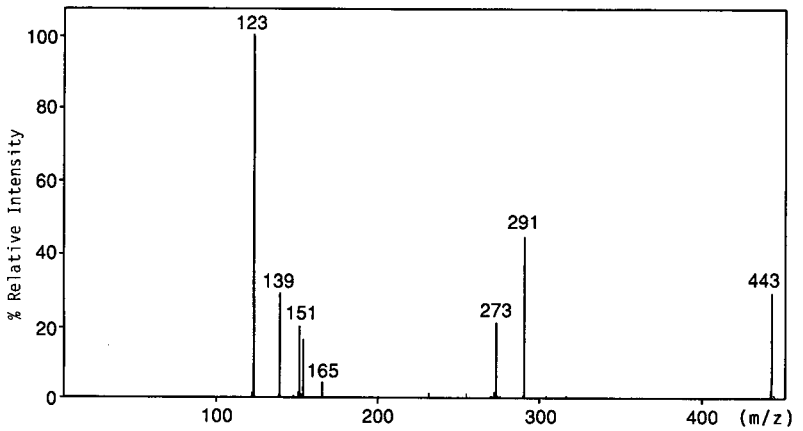

Fig. 3. CID spectrum of $[M + H]^+$ (*m/z* 443) of (−)-epicatechin 3-O-gallate (**3**). The CID spectrum was obtained using a collision energy of 21 eV.

epicatechin 3-O-gallate **3**. The spectrum is simple yet informative for the structure, and the assignment of the ions can be made as follows: *m/z* 443 ($[MH^+]$), 291 ($[MH^+ - R_2 + H]$), 273 ($[MH^+ - R_2OH]$), 165 (cleavage *b* − R_2 + H), 153 ($[R_2^+]$), 151 ($[R_2^+ - H_2]$), 139 (cleavage *a*), and 123 (cleavage *c*). The CID spectra of other catechins are included in Table I.

Thermospray MS and CID spectra of some representative flavonoids

In addition to catechins, we also studied thermospray MS and CID spectra of some representative flavonoids: flavanone, hesperidin **5**; flavone, apigenin **6**; and flavonols, kaempferol **7**, quercetin **8**, and rutin **9** (Fig. 1). The thermospray MS of non-glycosylated flavonoids **6**, **7**, and **8** all gave single $[M + H]^+$ peaks with no fragmentation. The thermospray MS of two flavonoid O-glycosides, hesperidin **5** and rutin **9** gave simple three ion spectra of *m/z* 611, 465, and 303, which clearly represent the ions of $[M + H]^+$, [M − rhamnosyl], and [M − rhamnoglucosyl moieties]; thus, both aglycone and glycosyl substituents in the molecules can be recognized. However, further characterization of the aglycone and glycosyl components was achieved by the study of their CID spectra. As shown by the spectra in Table I and the structures in Fig. 1, all catechin and flavonoid molecules undergo facile cleavages *a* and produce *m/z* 139 with catechins **1–4** and *m/z* 153 for flavonoids **5–9**. The facile cleavage *a* in catechins or flavonoids can be attributed to the formation of stable arylcarbonium and or arylcarbonyl ions, respectively. The cleavage *a* ions, such as *m/z* 139 or 153, in the CID spectrum generate the diagnostic ions for the identification of catechin or flavonoid molecules in complex mixtures. Cleavages *b* were observed with catechins **1–4** and flavanone **5**, but not with flavone **6** or flavonols **7–9**. The absence of cleavage *b* in flavone or flavonol may due to the presence of the α,β-unsaturated ketone in the pyran ring resulting in stabilization of the ring bond between C-4 and C-5 by the extension of arylic conjugation between the two aromatic rings. Cleavage *c*, the cleavage of the bond between C-2 and C-3 of the pyran ring, is only observed with catechins **1–4** and flavonol **7–9**, which have O-substitutions at the C-3 position. Therefore, differentiation among catechin, flavanone, flavone, and flavonol can be made by CID spectra. For a glycosyl flavonoid, rutin **9** for example, CID spectra can be obtained with either the $[M + H]^+$ *m/z* 611 or the ion of aglycone *m/z* 303. From the CID spectrum of *m/z* 303, the aglycone of the flavonoid can be characterized as a flavonol by the cleavage *a* (*m/z* 153) and cleavage *c* (*m/z* 137), and additional fragmentation ions indicative of the disaccharide moieties are obtained by the CID spectrum of *m/z* 611 (Table I).

DISCUSSION

Comprehensive information on electron impact (EI) MS fragmentation patterns is available for the major classes of aglycone flavonoids; only when the

individual flavonoids are subjected to EI-MS analysis, can their fragmentation be assigned and distinguished [16–20]. However, flavonoids are usually present as non-volatile mixtures in plants, and their analysis usually must be carried out by GC–MS with their trimethylsilyl or permethyl derivatives [21–24]. LC–MS with moving belt has been used to study flavonoids under both EI and chemical ionization (CI) conditions. Under the CI conditions, the spectra provide only $[M + H]^+$ ions for molecular mass information with little fragmentation; on the other hand, EI–MS has been hampered by difficulties with high background contribution and notable diminution of the molecular ion, especially with highly polar and non-volatile compounds [25]. Fast atom bombardment MS has been used to study the glycosidic linkages in glycosyl flavonoids, but it has provided little information on the aglycone structures [26]. Therefore, the thermospray LC–MS–MS we have shown appears to be the method of choice for the study of flavonoids, including their glycosides, as complex mixtures that exist in the plant kingdom.

ACKNOWLEDGEMENTS

This work was supported by the New York State Office of Mental Retardation and Developmental Disabilities. We thank Bob White of Finnigan MAT for examining catechin samples under particle beam LC–MS.

REFERENCES

1 T. Okuda, K. Mori and H. Hayatsu, *Chem. Pharm. Bull.*, 32 (1984) 3755.
2 T. Kada, K. Kaneco, S. Matsuzaki, T. Matsuzaki and Y. Hara, *Mutat. Res.*, 50 (1985) 127.
3 S. Yoshizawa, T. Horiguchi, H. Fujiki, T. Yoshida and T. Sugimura, *Phytother. Res.*, 1 (1987) 44.
4 H. Mukhtar, M. Das, W. A. Kahn, Z. Y. Wang, D. P. Bik and D. R. Bickers, *Cancer Res.*, 48 (1988) 2361.
5 Y. Fujita, T. Yamane, M. Tanaka, K. Kuwata, J. Okuzumi, T. Takahashi, H. Fujiki and T. Okuda, *Jpn. Cancer Res.*, 80 (1989) 503.
6 S. Uchida, M. Ozaki, K. Suzuki and M. Shikita, *Life Sci.*, 50 (1911) 147.
7 H. Nakane and K. Ono, *Biochemistry*, 29 (1990) 2841.
8 S. Uchida, R. Edamatsu, M. Hiramatsu, A. Mori, G. Nonaka, I. Nishioka, M. Niwa and M. Ozaki, *Med. Sci. Res.*, 15 (1987) 831.
9 C. J. M. Kane, J. H. Menna, C. C. Sung and Y. C. Yeh, *Biosci. Rep.*, 8 (1988) 95.
10 K. Ono, H. Nakane, M. Fukushima, J. C. Chermann and F. Barre-simoussi, *Biochem. Biophys. Res. Commun.*, 160 (1989) 982.
11 C. Schewe, R. Klocking, B. Helbig and T. Schewe, *Biomed. Biochim. Acta*, 3 (1991) 299.
12 M. Nishikawa, T. Yamagishi, G. E. Dutschman, W. B. Parker, A. J. Bodner, R. E. Kilkuski, Y. C. Chen and K. H. Lee, *J. Nat. Prod.*, 52 (1989) 762.
13 Y. Y. Lin, C. M. J. Chen, Y. S. Kim and X. Yang, in Proceedings of *Biological Mass Spectrometry*, Kyoto '92, Sanei Publications, Kyoto, 1992, in press.
14 X. Yang, L. Ye and Z. Jia, *Acta Agric. Univ. Zhejian*, 18 (1992) 19.
15 E. A. H. Roberts, in T. A. Geisman (Editor), *The Chemistry of Flavonoid Compounds*, Oxford, London, 1962, p. 468.
16 T. J. Mabry and K. R. Markham, in J. B. Harborne, T. J. Mabry and H. Mabry (Editors), *The Flavonoids*, Academic Press, New York, 1975, p. 78.
17 T. J. Mabry and A. Ulubelen, in G. R. Walker and O. Dermer (Editors), *Biomedical Application of Mass Spectrometry*, Wiley, New York, 1980, p. 1131.
18 K. R. Markham, in J. B. Harborne (Editor), *The flavonoids – Advances in Research*, Vol. 2, Chapman & Hall, London, 1989, p. 427.
19 J. J. Grayer, in J. B. Harborne (Editor), *Methods in plant biochemistry*, Vol. 1, Academic Press, San Diego, 1989, p. 607.
20 P. A. Hedin and V. A. Phillips, *J. Agric. Food Chem.*, 40 (1992) 607.
21 Y. Yinon, D. Issachar and H. G. Boettger, *Org. Mass Spectrom.*, 13 (1978) 167.
22 M. Stobieki and P. Wojtaszek, *J. Chromatogr.*, 508 (1990) 391.
23 W. Greenaway and R. Whatley, *J. Chromatogr.*, 519 (1990) 145.
24 A. Sakushima and S. Nishibe, *Biomed. Environ. Mass. Spectrom.*, 19 (1990) 319.
25 D. E. Games and F. Martinez, *J. Chromatogr.*, 474 (1989) 372.
26 M. Becchi and D. Fraisse, *Biomed. Environ. Mass Spectrom.*, 18 (1989) 122.

Journal of Chromatography, 629 (1993) 394–397
Elsevier Science Publishers B.V., Amsterdam

CHROM. 24 713

Short Communication

Determination of volatile fatty acids in landfill leachates by high-performance liquid chromatography

Jen-Fon Jen, Ching-Wen Lin and Chi-Jung Lin

Department of Chemistry, National Chung-Hsing University, Taichung 40217 (Taiwan)

Chieng-Tong Yan

Department of Industrial Safety and Hygiene, Hung-Kuang Junior College of Nursing and Medical Technology, Sha-Luh, Taichung (Taiwan)

(First received August 11th, 1992; revised manuscript received October 23rd, 1992)

ABSTRACT

HPLC with UV detection was used to determine the volatile fatty acids in landfill leachates. It successfully determined formic acid, which could not be detected by GC with flame ionization detection. Calibration graphs were linear with very good correlation coefficients ($r > 0.999$). The application of the method is illustrated by the analysis of leachate samples collected from the Taichung sanitary landfill.

INTRODUCTION

In order to find the best conditions for wastewater treatment, a distillation–GC method with flame ionization detection (FID) has been described to determine the volatile fatty acids in landfill leachates [1]. However, FID cannot detect formic acid owing to its combustion products, CO_2 and H_2O [2]. Moreover, problems alway exist because of the high polarity of the acids, which lead to asymmetric peaks or ghosting [3,4]. High-temperature conditioning is often needed to overcome these effects [1]. In general, HPLC appears to be superior to GC for determining organic compounds with high polarity and low volatility. Both reversed-phase and cation-exchange columns have succeeded in separating organic acids, followed by mass spectrometric detection [5,6].

In this paper, the determination of volatile fatty acids in landfill leachates by HPLC–UV detection after distillation is described. From previous studies, a 75% distillate collection after discarding the first 7.5% of light-end distillate was judged to be the best pretreatment of the leachate sample for chromatographic analysis [1]. The performance of the HPLC–UV method was compared with that of the GC–FID method. The samples analysed were leachates from the Taichung sanitary landfill.

Correspondence to: J.-F. Jen, Department of Chemistry, National Chung-Hsing University, Taichung 40217, Taiwan.

0021-9673/93/$06.00

EXPERIMENTAL

Apparatus

A Shimadzu (Kyoto, Japan) LC-9A system equipped with a Rheodyne Model 7125 injection valve (20-μl sample loop) was used. A Spherisorb 5 ODS column (250 mm × 4.6 mm I.D.) (Supelco, Bellefonte, PA, USA) was used to separate the fatty acids. A Soma Model S-3702 UV detector and a Shimadzu C-R6A Chromatopac integrator were used to detect and record the chromatograms. A Radiometer PHM 82 pH meter with a glass electrode was used for pH measurements.

Reagents

Distilled, deionized water was used to prepare all solutions. Stock standard solutions (1000 μg/ml) of formic, acetic, propionic, *n*-butyric and isobutyric acids were prepared from ACS reagent-grade chemicals (Riedel-de Häen, Germany). Working standard solutions of these acids were prepared fresh daily by appropriate dilution of the stock standard solutions with water. The sulphuric acid used in the distillation process and to adjust the pH of eluent was of ultrapure grade from Aldrich (Milwaukee, WI, USA). The chromatographic eluent was prepared from HPLC-grade methanol (Mallinckrodt, St. Louis, MO, USA) and water, the pH being adjusted with 0.05 *M* sulphuric acid. All eluents were filtered through a 0.45-μm PVDF membrane filter and degassed by sonication before use.

Sample pretreatment

Pretreatment of leachate samples was performed by distillation. Sulphuric acid was added to increase the recovery of volatile fatty acids. The assembly of the distillation apparatus and the operating procedures were as described previously [1]. An aliquot of 75 ml of distillate was collected for HPLC–UV analysis after the first 7.5 ml of distillate had been discarded.

HPLC–UV procedure

Elution was performed with a flow-rate gradient to shorten the running time. The eluent was methanol–water (3:97, v/v) of pH 4.0, adjusted with 0.05 *M* sulphuric acid. The flow-rate gradient was initially 1.0 ml/min for 5 min, increased to 2.0 ml/min in 3 min, held for 7 min, and finally decreased to 1.0 ml/min in 3 min.

RESULTS AND DISCUSSION

In the determination of volatile fatty acids by GC, asymmetric peaks and ghosting phenomena often appear because of the high polarity of the fatty acids. These may create difficulties in peak identification and lead to quantitative errors. Unfortunately, GC–FID cannot determine formic acid. In a previous study [1], no formic acid was detected by GC–FID even when the concentration was raised to 2000 μg/ml. In order to overcome the shortcomings of GC–FID in the determination of volatile fatty acids, the HPLC–UV method was examined for this application.

HPLC is a useful technique for separating organic compounds of high polarity and low volatility. For the determination of fatty acids with UV detection, the wavelength should be set at 210 nm, which is the maximum absorption wavelength for fatty acids. However, the baseline was not stable at this wavelength, so 230 nm was selected. Owing to their high polarity, short-chain fatty acids are only briefly retained on the ODS column. However, the separation of formic acid from acetic acid is very difficult with an eluent of relatively high polarity. Based on the pK_a difference between formic acid (3.75 at 20°C) and acetic acid (4.75 at 20°C), an ion-suppression technique was employed to improve the separation. The eluent pH was adjusted to 4.0 (based on calibration of the pH meter in water). Fig. 1 shows the chromatograms of volatile fatty acids obtained for (a) a standard solution and (b) a real sample. Formic acid was separated from acetic acid and was detected by the UV detector, and the isomers of isobutyric and *n*-butyric acid were also separated.

Because the volatile fatty acids do not contain strong UV-absorbing groups, their detection would be poor. However, the concentrations of volatile fatty acids in landfill leachates are generally high. Therefore, the applicability of the HPLC–UV method to the determination of volatile fatty acids in leachates is not affected.

To test the applicability of the method to analysis of real samples for volatile fatty acids, the standard addition method was used. A series of 5-ml volumes of standard acid solutions with different concentrations were added individually to 95-ml landfill leachate samples. After distillation pretreatment and

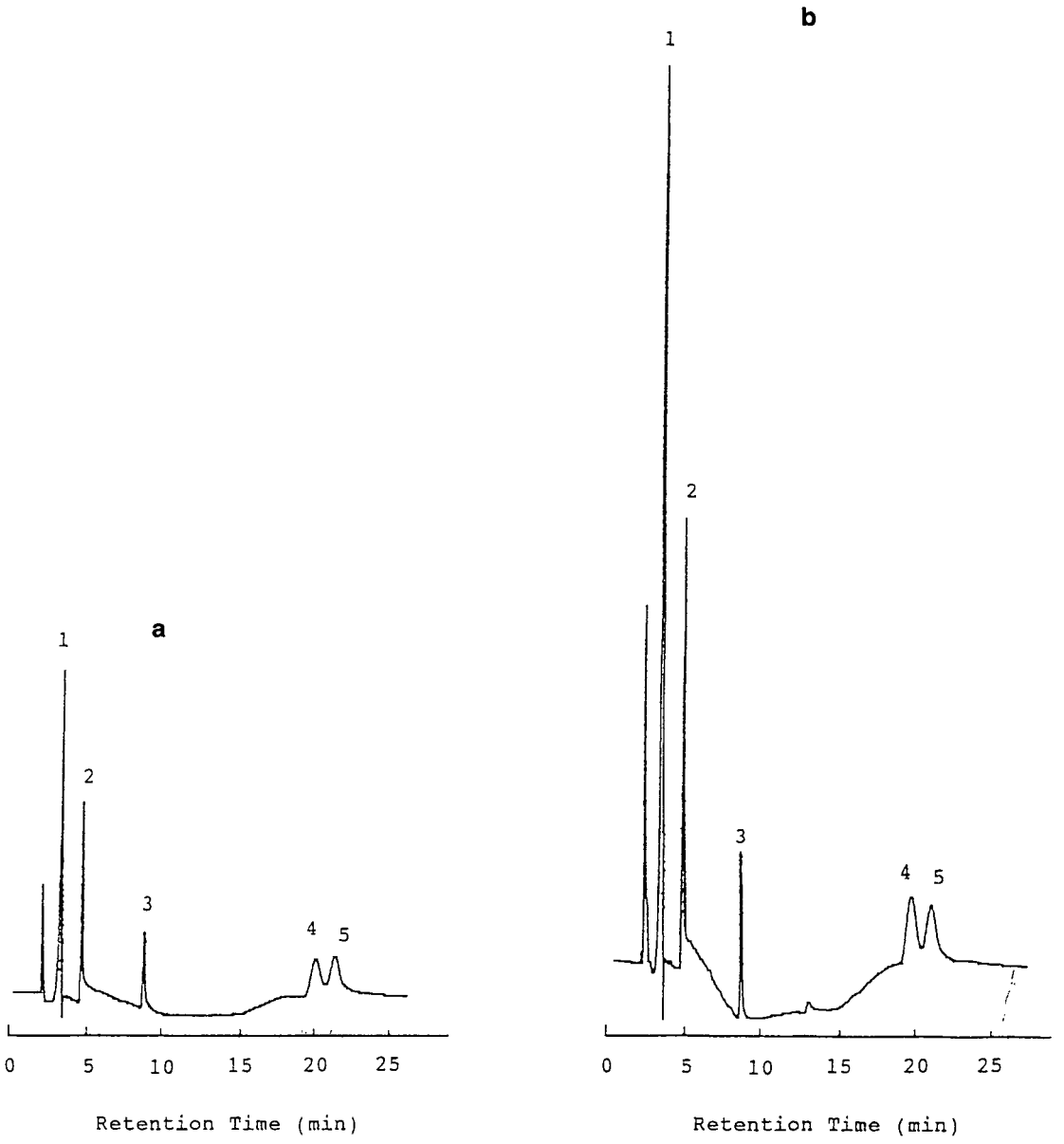

Fig. 1. HPLC of volatile fatty acids under the optimum conditions. (a) Standard solution (500 μg/ml for each acid); (b) landfill leachate sample. Peaks: 1 = formic acid; 2 = acetic acid; 3 = propionic acid; 4 = isobutyric acid; 5 = *n*-butyric acid.

HPLC–UV determination, calibration graphs were constructed for the five volatile acids. They all showed good linearity with correlation coefficients >0.999. These results imply that the HPLC–UV method with an appropriate sample pretreatment can be useful for the determination of volatile fatty acids in landfill leachate.

Results of replicate measurements on leachate samples from the Taichung sanitary landfill are given in Table I. The values obtained and their standard deviations are comparable to those obtained by GC–FID except that the detection of formic acid was impossible by GC–FID. The results confirm

TABLE I

COMPARISON OF THE RESULTS OBTAINED BY GC–FID AND HPLC–UV METHODS

Volatile fatty acid	HPLC–UV		GC–FID	
	Concentration (μg/ml)	R.S.D. (%)[a]	Concentration (μg/ml)	R.S.D. (%)[a]
Formic	680	2.32	–	–
Acetic	728	1.73	713	1.95
Propionic	531	2.14	523	2.44
Isobutyric	548	3.38	560	2.72
n-Butyric	479	1.60	485	2.29

[a] Relative standard deviation for five determinations.

the applicability of the distillation–HPLC–UV procedure to the determination of volatile fatty acids in landfill leachates if a 23-min separation time is acceptable.

CONCLUSIONS

In contrast to the GC–FID method, the HPLC–UV procedure is able to determine formic acid and is free from ghosting, although it is more time-consuming and has poorer detection limits than GC–FID. The method is suitable for the determination of volatile fatty acids in landfill leachates.

ACKNOWLEDGEMENT

The authors thank the National Science Council of Taiwan for financial support under grant NSC 79-0208-M-005-25.

REFERENCES

1 J.-F. Jen and C.-T Yan, *Anal. Chim. Acta*, 264 (1992) 259–264.
2 D. M. Ottenstein and D. A. Bartley, *J. Chromatogr. Sci.*, 9 (1971) 673–681.
3 J. C. Dupreez and P. M. Lategan, *J. Chromatogr.*, 150 (1978) 259–262.
4 D. A. M. Geddes and M. N. Gilmaur, *J. Chromatogr. Sci.*, 8 (1970) 394–397.
5 C. P. Tsai, *Anal. Chem.*, 58 (1986) 2–6.
6 F. Pacholec, D. R. Eaton and D. T. Rossi, *Anal. Chem.*, 58 (1986) 2581–2583.

Journal of Chromatography, 629 (1993) 398–400
Elsevier Science Publishers B.V., Amsterdam

CHROM. 24 744

Short Communication

Determination of N-hydroxysuccinimidyl-activated polyethylene glycol esters by gel permeation chromatography with post-column alkaline hydrolysis

Bhavana Shah and Eric Watson

Amgen Inc., Amgen Center, 1900 Oak Terrace Lane, Thousand Oaks, CA 91320-1789 (USA)

(First received September 4th, 1992; revised manuscript received November 9th, 1992)

ABSTRACT

An HPLC method is reported for the determination of N-hydroxysuccinimidyl-activated polyethylene glycol ester. The activated polyethylene glycol sample is first separated by size-exclusion chromatography on a polymeric column with tetrahydrofuran as the eluent, and after elution is subjected to post-column on-line hydrolysis with 0.1 *M* sodium hydroxide. Liberation of N-hydroxysuccinimide occurs rapidly and is monitored by UV detection at 266 nm. The amount released is determined from a standard curve generated from free N-hydroxysuccinimide and used to calculated the concentration of active ester initially present.

INTRODUCTION

Administration of proteins for therapeutic treatment is severely hampered by short half-lives in the circulatory system. It has been shown that the covalent attachment of polyethylene glycols, most often of M_r 5000, to enzymes and proteins has a major affect on their activity and physical properties. In particular, several reports have demonstrated the effect of increased circulating lives from the use of such polyethylene glycol (PEG) conjugates without any complications arising from immunogenicity [1,2].

Correspondence to: E. Watson, Amgen Inc., Amgen Center, 1900 Oak Terrace Lane, Thousand Oaks, CA 91320-1789, USA.

The protein–PEG adducts are typically prepared by reaction of the proteins with N-hydroxysuccinimidyl-activated PEG esters. These active esters are very unstable under aqueous conditions. There are few analytical methods available for determining the purity of these activated esters. The only previously reported method involved liberation of N-hydroxysuccinimide under alkaline conditions and following the increase in absorption at 266 nm [3]. This method provides only an estimate of the activated PEG ester since it will also determine any free N-hydroxysuccinimide and related degradation products present which may have been derived from the activated ester or reaction products. This report describes an on-line HPLC method with post-column hydrolysis for the determination of intact activated PEG ester.

0021-9673/93/$06.00

METHODS AND MATERIALS

Materials

N-Hydroxysuccinimide (NHS) and methoxypolyethylene glycolsuccinimidyl succinate (SS-MPEG) were obtained from Sigma (St. Louis, MO, USA). HPLC-grade tetrahydrofuran (stabilized with 0.029% butylated hydroxytoluene) was purchased from Fisher Scientific (Santa Clara, CA, USA).

Chromatographic separation

The chromatographic system consisted of a Kratos Spectroflow 400 system equipped with a Kratos URS 051 post column delivery pump. A single mixing coil, 2 ml, was found to be sufficient for complete hydrolysis and was used at room temperature. The liberation of NHS was monitored with a Shimadzu SPD-6A UV detector set at 266 nm.

Samples for analysis (0.25%) are prepared by weighing an amount of SS-MPEG into tetrahydrofuran. An aliquot, 100 μl, is injected into a gel permeation column (G2500HXL, 30.0 cm × 7.8 mm) obtained from Supelco (Bellefonte, PA, USA). The eluent is tetrahydrofuran at a flow-rate of 0.5 ml/min and the separated activated ester passes directly into the post-column system where it is hydrolyzed by 0.1 *M* sodium hydroxide delivered at 0.5 ml/min.

RESULTS

Hydrolysis of activated ester

Under base conditions, hydrolysis of the activated ester proceeds rapidly with the liberation of NHS, the λ_{max} of which is 266 nm. The effect of post-column mixing time and temperature on the liberation of NHS from SS-MPEG was evaluated. Comparison of the amount of NHS liberated from one and two 2-ml reaction coils showed no difference. Raising the temperature of the post-column reaction coil to 70°C had no effect on the amount of NHS liberated. Based on these results, a single 2-ml reaction coil at room temperature was used for all subsequent determinations. In a separate series of experiments, a comparison was made between 0.1 *M* sodium hydroxide and 0.1 *M* ammonium hydroxide for hydrolysing the activated ester. No difference in the amount of activated ester released occurred.

Analysis of active ester in SS-MPEG

Chromatography of PEG 5000 standard gave no response when analyzed in the current system. Fig. 1 shows the chromatogram obtained from 2 μg free NHS. The calibration plot curved toward the *y*-axis and was best fit with a non-linear model, $y = a_1x + a_2x^2$. For the standard curve shown in Fig. 2, the best fit for the standard curve was obtained from the binomial equation

$$y = 1.1391 \cdot 10^{-2} + 0.52097x + 1.9164 \cdot 10^{-2},$$
$$R^2 = 0.999.$$

Fig. 3 shows the chromatogram obtained from SS-MPEG when separated by size-exclusion chromatography and hydrolyzed by sodium hydroxide in the post-column reaction system. The major peak represents the M_r 5000 PEG ester while the peak that elutes ahead of it is considered to be a higher-molecular-mass PEG ester. The free NHS present was determined to be 0.2%. Determination of the amount of activated ester present in the original sample was based on the assumption that a single mol of NHS/mol activated ester was present in the original sample. The content of activated ester, SS-MPEG, M_r 5000 was found to be 63% (R.S.D. 2%, $n = 10$). The reported content by the supplier is >75%, which agrees with the results here when the higher-molecular-mass material is included.

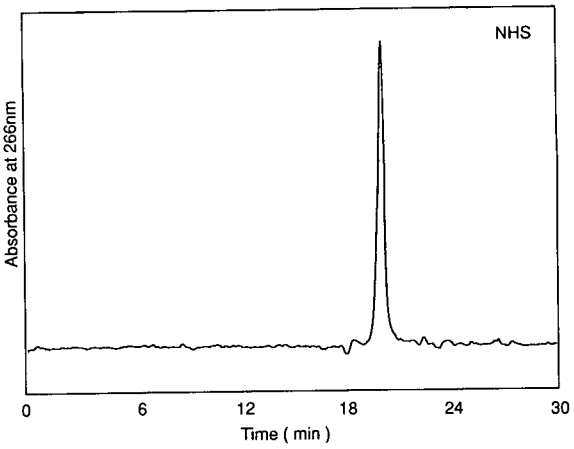

Fig. 1. Chromatogram from 2 μg free NHS.

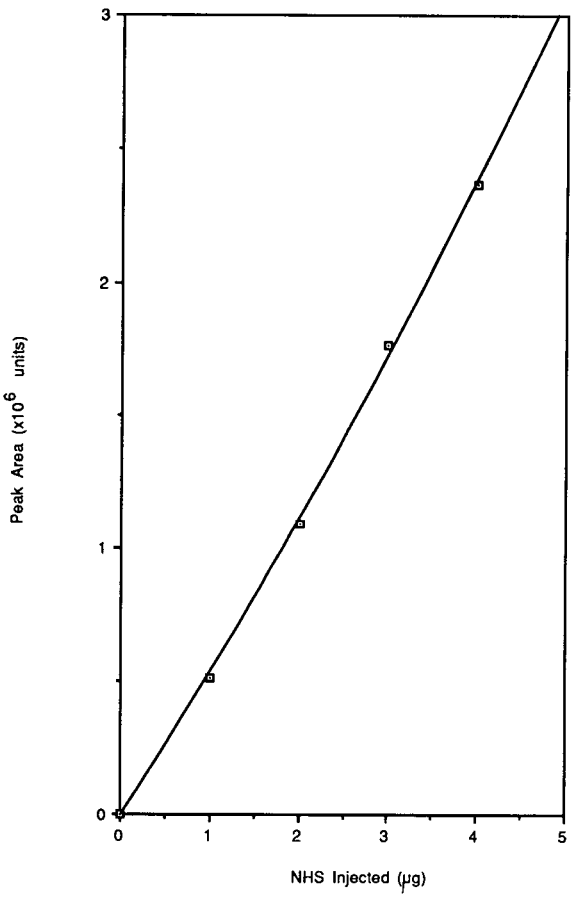

Fig. 2. Calibration plot obtained from NHS fitted to a binomial equation.

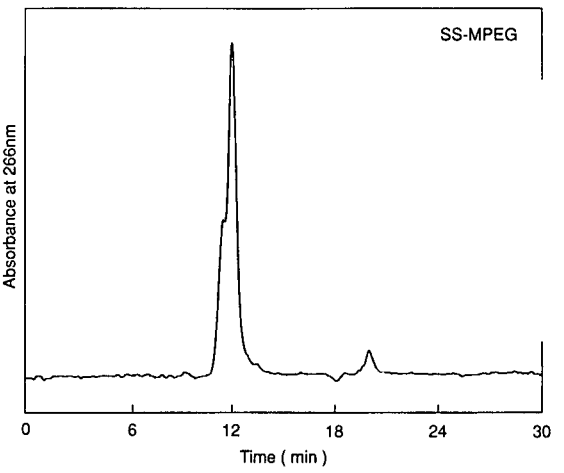

Fig. 3. Chromatogram obtained from SS-MPEG.

CONCLUSIONS

(1) Size-exclusion chromatography followed by post-column hydrolysis under basic conditions is a fast and relatively simple method for determining the purity of active succinimidyl esters.

(2) The technique provides a method that can be used to determine the stability, and monitor the purity of the ester produced by different processing steps.

(3) The overall method can also be applied without modification to determine the purity of other activated esters, *e.g.*, succinimidyl glutarate, succinimidyl carbonate and succinimidyl carboxymethyl.

(4) One potential drawback with the described procedure is that quantitation is carried out using free NHS as the standard. If experimental factors adversely affect the chromatography of NHS, *e.g.*, such as column adsorption, without a corresponding effect on the activated ester, then it is possible that variability would be introduced into the assay. To date, we have not observed this occurring, but it is a valid concern worth noting. This problem could be overcome by using a highly pure, characterized activated ester as the standard for quantitation.

REFERENCES

1 N. V. Katre, M. J. Knauf, D. P. Bell, P. Hirtzer, Z. Luo and J. D. Young, *J. Biol. Chem.*, 263 (1988) 15064–15070.
2 N. V. Katre, *J. Immunology*, 144 (1990) 209–213.
3 T. Miron and M. Wilchek, *Anal. Biochem.*, 126 (1982) 433–435.

Journal of Chromatography, 629 (1993) 401
Elsevier Science Publishers B.V., Amsterdam

CHROM. 24 725

Book Review

Advances in electrophoresis, Vol. 5, edited by A. Chrambach, M. J. Dunn and B. J. Radola, VCH, Weinheim, 1992, XII + 414 pp., price DM 268.00, £ 100.00, ISBN 3-527-28404-4

Electrophoresis is a venerable old lady, but she still manages to find enthusiastic young lovers. Nowadays these are mostly molecular biologists and geneticists, working on DNA separation, fingerprinting, sequencing etc. This volume of the *Advances in Electrophoresis* series serves well the stated purpose of the editors and provides an authoritative platform to some of the leading experts in the field, who contributed the first four articles.

In many ways, the most interesting is the first article by Joan Noolandi, on the theory of DNA gel electrophoresis. As is well known, migration of large DNA segments in gels does not follow conventional theory, this giving rise to fanciful new concepts, such as biased reptation and elastic bag models. It has also given rise to a variety of experimental variations of electrodes and pulsed fields. Dr. Noolandi's presentation is clear and comprehensive.

DNA fingerprinting, described in some details by Jorg T. Epplen, has acquired important applications in animal and plant sciences, as well as in forensic sciences. The technique is largely based on the availability of synthetic probes searching for the naturally occurring simple repetitive oligonucleotide sequences. Dr. Epplen provides brief specifications for the experimental methodology for multilocus fingerprinting using digoxigenated or radioactively labelled probes.

More limited in its popularity is the footprinting analysis for the detection of drug–DNA interactions, as described by James C. Dabrowiak and co-authors from Syracuse University. It illustrates the usefulness of the method with binding studies of the anti-cancer drug Chromomycin A3. Similar in intent, though differing in methodology, is the electrophoretic study of DNA–protein interactions, described by Mark M. Garner.

The remaining five articles are of equally good calibre, though they address more conventional methodologies. Pier Giorgio Righetti, a perennial and ardent lover of electrophoresis, and his co-authors present a somewhat cursory review of various preparative techniques. Dominique Charron describes the use of two-dimensional gel electrophoresis to the human leucocyte antigen class II system, while Felix Wiederkehr applied the same and other techniques to cerebrospinal fluid proteins. Unfortunately, two-dimensional electrophoresis has not yet gained much clinical relevance.

Finally, Otto von Deimling and Thomas F. Wienker describe the use of electrophoresis for genetic studies of allelic variations of esterase isozymes in the house mouse. Menelaos Costas recommends the use of one-dimensional protein patterns for the classification, identification and typing of bacteria.

As a whole, this volume is an important contribution to the literature and belongs to the library of serious researchers in the field. Most of the articles are too advanced and specialized for the novice.

Tucson, AZ (USA) Milan Bier

Author Index

Abián, J., Churchwell, M. I. and Korfmacher, W. A.
High-performance liquid chromatography–thermospray mass spectrometry of ten sulfonamide antibiotics. Analysis in milk at the ppb level 629(1993)267

Ackermans, M. T., see Beckers, J. L. 629(1993)371

Albaigés, J., see Pastor, M. D. 629(1993)329

Allen, D. W., Clench, M. R., Crowson, A. and Leathard, D. A.
Identification by particle-beam liquid chromatography–mass spectrometry of transformation products of the antioxidant Irganox 1330 in food-contact polymers subjected to electron-beam irradiation 629(1993)283

Ando, Y., see Takagi, T. 629(1993)385

Aoyanagi, N., see Takagi, T. 629(1993)385

Armstrong, D. W., see Zukowski, J. 629(1993)169

Baker, S., see Durhan, E. 629(1993)67

Barceló, D., see Pastor, M. D. 629(1993)329

Barker, S. A., Long, A. R. and Hines II, M. E.
Disruption and fractionation of biological materials by matrix solid-phase dispersion 629(1993)23

Beckers, J. L. and Ackermans, M. T.
Effect of sample stacking on resolution, calibration graphs and pH in capillary zone electrophoresis 629(1993)371

Belsner, K., Pfeifer, M. and Wilffert, B.
Reversed-phase high-performance liquid chromatography for evaluating the lipophilicity of pharmaceutical substances with ionization up to log P_{app} = 8 629(1993)123

Berry, M. J. and Pierce, J. J.
Stability of immunoadsorbents comprising antibody fragments. Comparison of Fv fragments and single-chain Fv fragments 629(1993)161

Bier, M.
Advances in electrophoresis, Vol. 5 (edited by A. Chrambach, M. J. Dunn and B. J. Radola, Editors) (Book Review) 629(1993)401

Carr, P.W., see Helfferich, F.G. 629(1993)97

Chase, H. A., see McCreath, G. E. 629(1993)201

Chollet, D., Künstner, P. and Wermeille, M.
High-performance liquid chromatographic method for the determination of dimethindene in urine 629(1993)89

Chung, H.-C. and Hsu, M.-C.
Liquid chromatographic determination of amoxicillin preparations. Interlaboratory validation 629(1993)277

Churchwell, M. I., see Abián, J. 629(1993)267

Clench, M. R., see Allen, D. W. 629(1993)283

Coenegracht, P. M. J., see Wieling, J. 629(1993)181

Cooper, D. A., see Lurie, I. S. 629(1993)143

Crowson, A., see Allen, D. W. 629(1993)283

Daisey, J. M., see Gundel, L. A. 629(1993)75

Dawodu, O. F. and Meisen, A.
Gas chromatographic analysis of alkanolamine solutions using capillary and packed columns 629(1993)297

Desai, D. M. and Gal, J.
Enantiospecific drug analysis via the *ortho*-phthalaldehyde/homochiral thiol derivatization method 629(1993)215

Dijkstra, H., see Wieling, J. 629(1993)181

Djordjevic, N. M., Stegehuis, D., Liu, G. and Erni, F.
Improved ultraviolet detection in high-temperature open-tubular liquid chromatography 629(1993)135

Doornbos, D. A., see Wieling, J. 629(1993)181

Duineveld, C. A. A., see Wieling, J. 629(1993)181

Dunne, C., Meaney, M., Smyth, M. and Tuinstra, L. G. M. T.
Multimycotoxin detection and clean-up method for aflatoxins, ochratoxin and zearalenone in animal feed ingredients using high-performance liquid chromatography and gel permeation chromatography 629(1993)229

Durhan, E., Lukasewycz, M. and Baker, S.
Alternatives to methanol–water elution of solid-phase extraction columns for the fractionation of high log K_{ow} organic compounds in aqueous environmental samples 629(1993)67

Erni, F., see Djordjevic, N. M. 629(1993)135

Evans, K. P., see Williams, S. J. 629(1993)379

Floyd, T. R.
Chemical characterization of cellulose acetate by non-exclusion liquid chromatography 629(1993)243

Furton, K. G., Jolly, E. and Rein, J.
Variables affecting the supercritical fluid extraction of analytes from octadecylsilane solid-phase sorbents 629(1993)3

Gal, J., see Desai, D. M. 629(1993)215

Giese, R. W., see Saha, M. 629(1993)35

Goodall, D. M., see Williams, S. J. 629(1993)379

Grosse-Ophoff, M., see Küppers, S. 629(1993)345

Gundel, L. A., Mahanama, K. R. R. and Daisey, J. M.
Fractionation of polar organic extracts of airborne particulate matter using cyanopropyl-bonded silica in solid-phase extraction 629(1993)75

Hartmann, A., see Lebuhn, M. 629(1993)255

Helfferich, F. G.
Introduction to the series "Non-linear waves in chromatography" 629(1993)95

Helfferich, F. G. and Carr, P. W.
Non-linear waves in chromatography. I. Waves, shocks, and shapes 629(1993)97

Hines II, M. E., see Barker, S. A. 629(1993)23

Hobo, T., see Sato, K. 629(1993)291

Hsu, C.-Y. L. and Walters, R. R.
Optimization of sample application conditions for solid-phase extraction columns 629(1993)61

Hsu, M.-C., see Chung, H.-C. 629(1993)277

Ihara, T., see Sato, K. 629(1993)291

Jen, J.-F., Lin, C.-W., Lin, C.-J. and Yan, C.-T.
Determination of volatile fatty acids in landfill leachates by high-performance liquid chromatography 629(1993)394

Jolly, E., see Furton, K. G. 629(1993)3
Jonkman, J. H. G., see Wieling, J. 629(1993)181
Klesper, E., see Küppers, S. 629(1993)345
Konishi, H., Neff, W. E. and Mounts, T. L.
Correlation of reversed-phase high-performance liquid chromatography and gas–liquid chromatography for fatty acid compositions of some vegetable oils 629(1993)237
Korfmacher, W. A., see Abián, J. 629(1993)267
Krull, I. S., see Lurie, I. S. 629(1993)143
Künstner, P., see Chollet, D. 629(1993)89
Küppers, S., Grosse-Ophoff, M. and Klesper, E.
Influence of linear velocity and multigradient programming in supercritical fluid chromatography 629(1993)345
Leathard, D. A., see Allen, D. W. 629(1993)283
Lebuhn, M. and Hartmann, A.
Method for the determination of indole-3-acetic acid and related compounds of L-tryptophan catabolism in soils 629(1993)255
Lin, C.-J., see Jen, J.-F. 629(1993)394
Lin, C.-W., see Jen, J.-F. 629(1993)394
Lin, Y. Y., Ng, K. J. and Yang, S.
Characterization of flavonoids by liquid chromatography–tandem mass spectrometry 629(1993)389
Liu, G., see Djordjevic, N. M. 629(1993)135
Long, A. R., see Barker, S. A. 629(1993)23
Lowe, C. R., see McCreath, G. E. 629(1993)201
Lukasewycz, M., see Durhan, E. 629(1993)67
Lurie, I. S., Cooper, D. A. and Krull, I. S.
High-performance liquid chromatography using continuous on-line post-elution photoirradiation with subsequent diode-array UV or thermospray mass spectrometry detection 629(1993)143
Mahanama, K. R. R., see Gundel, L. A. 629(1993)75
Matisová, E., Vodný, Š., Škrabáková, S. and Onderová, M.
Analysis of multi-component mixtures by high-resolution capillary gas chromatography and combined gas chromatography–mass spectrometry. II. Trace aromatics in an *n*-alkane matrix 629(1993)309
McCreath, G. E., Chase, H. A., Purvis, D. R. and Lowe, C. R.
Novel affinity separations based on perfluorocarbon emulsions. Development of a perfluorocarbon emulsion reactor for continuous affinity separations and its application in the purification of human serum albumin from blood plasma 629(1993)201
McDonnell, T., Rosenfeld, J. and Rais-Firouz, A.
Solid-phase sample preparation of natural waters with reversed-phase disks 629(1993)41
Meaney, M., see Dunne, C. 629(1993)229
Meier, U. and Trepp, C.
Calibration of spectrophotometric detectors for supercritical fluid chromatography 629(1993)361
Meisen, A., see Dawodu, O. F. 629(1993)297
Mensink, C. K., see Wieling, J. 629(1993)181
Meyer, M. T., Mills, M. S. and Thurman, E. M.
Automated solid-phase extraction of herbicides from water for gas chromatographic–mass spectrometric analysis 629(1993)55
Mills, M. S., see Meyer, M. T. 629(1993)55
Mills, M. S. and Thurman, E. M.
Foreword 629(1993)1
Mills, M. S., Thurman, E. M. and Pedersen, M. J.
Application of mixed-mode, solid-phase extraction in environmental and clinical chemistry. Combining hydrogen-bonding, cation-exchange and Van der Waals interactions 629(1993)11
Mitsuhashi, T.
Gas chromatographic determination of trace nitrite after derivatization with ethyl 3-oxobutanoate 629(1993)339
Mounts, T. L., see Konishi, H. 629(1993)237
Nagatkina, M., see Zukowski, J. 629(1993)169
Neff, W. E., see Konishi, H. 629(1993)237
Ng, K. J., see Lin, Y. Y. 629(1993)389
Nishimura, K., see Takagi, T. 629(1993)385
Onderová, M., see Matisová, E. 629(1993)309
Ota, T., see Takagi, T. 629(1993)385
Pankow, J. F., see Rounds, S. A. 629(1993)321
Pastor, M. D., Sanchez, J., Barceló, D. and Albaigés, J.
Determination of coplanar polychlorobiphenyl congeners in biota samples 629(1993)329
Pawlowska, M., see Zukowski, J. 629(1993)169
Pedersen, M. J., see Mills, M. S. 629(1993)11
Pfeifer, M., see Belsner, K. 629(1993)123
Pierce, J. J., see Berry, M. J. 629(1993)161
Purvis, D. R., see McCreath, G. E. 629(1993)201
Rais-Firouz, A., see McDonnell, T. 629(1993)41
Rein, J., see Furton, K. G. 629(1993)3
Rosenfeld, J., see McDonnell, T. 629(1993)41
Rounds, S. A. and Pankow, J. F.
Determination of selected chlorinated benzenes in water by purging directly to a capillary column with whole column cryotrapping and electron-capture detection 629(1993)321
Saha, M. and Giese, R. W.
High-performance liquid chromatography *versus* solid-phase extraction for post-derivatization cleanup prior to gas chromatography–electron-capture negative-ion mass spectrometry of N1,N3-bis-(pentafluorobenzyl)-N7-(2-[pentafluorobenzyloxy]ethyl)xanthine, a product derived from an ethylene oxide DNA adduct 629(1993)35
Sanchez, J., see Pastor, M. D. 629(1993)329
Sato, K., Watabe, K., Ihara, T. and Hobo, T.
Improvement of continuous counter-current gas–liquid chromatography for practical use 629(1993)291
Shah, B. and Watson, E.
Determination of N-hydroxysuccinimidyl-activated polyethylene glycol esters by gel permeation chromatography with post-column alkaline hydrolysis 629(1993)398
Šimek, Z. and Vespalec, R.
Chromatographic properties of chemically bonded bovine serum albumin working as a chiral selector in alkaline mobile phases 629(1993)153
Škrabáková, S., see Matisová, E. 629(1993)309
Smyth, M., see Dunne, C. 629(1993)229
Stegehuis, D., see Djordjevic, N. M. 629(1993)135

Takagi, T., Aoyanagi, N., Nishimura, K., Ando, Y. and Ota, T.
Enantiomer separations of secondary alkanols with little asymmetry by high-performance liquid chromatography on chiral columns 629(1993)385
Thurman, E. M., see Meyer, M. T. 629(1993)55
Thurman, E. M., see Mills, M. S. 629(1993)1
Thurman, E. M., see Mills, M. S. 629(1993)11
Trepp, C., see Meier, U. 629(1993)361
Tuinstra, L. G. M. T., see Dunne, C. 629(1993)229
Vespalec, R., see Šimek, Z. 629(1993)153
Vodný, Š., see Matisová, E. 629(1993)309
Walters, R. R., see Hsu, C.-Y. L. 629(1993)61
Watabe, K., see Sato, K. 629(1993)291
Watson, E., see Shah, B. 629(1993)398
Wermeille, M., see Chollet, D. 629(1993)89
Wieling, J., Dijkstra, H., Mensink, C. K., Jonkman, J. H. G., Coenegracht, P. M. J., Duineveld, C. A. A. and Doornbos, D. A.
Chemometrics in bioanalytical sample preparation. A fractionated combined mixture and factorial design for the modelling of the recovery of five tricyclic amines from plasma after liquid–liquid extraction prior to high-performance liquid chromatography 629(1993)181
Wilffert, B., see Belsner, K. 629(1993)123
Williams, S. J., Goodall, D. M. and Evans, K. P.
Analysis of anthraquinone sulphonates. Comparison of capillary electrophoresis with high-performance liquid chromatography 629(1993)379
Yan, C.-T., see Jen, J.-F. 629(1993)394
Yang, S., see Lin, Y. Y. 629(1993)389
Zhong, W. Z.
Application of solid-phase extraction in the determination of U-82217 in rat serum, urine and brain 629(1993)83
Zukowski, J., Pawlowska, M., Nagatkina, M. and Armstrong, D. W.
High-performance liquid chromatographic enantioseparation of glycyl di- and tripeptides on native cyclodextrin bonded phases. Mechanistic considerations 629(1993)169

Vol. 629, No.2

Journal of Chromatography

NEWS SECTION

ANNOUNCEMENTS

INTERNATIONAL SYMPOSIUM "90 YEARS OF CHROMATOGRAPHY", ST. PETERSBURG, RUSSIA, APRIL 25–29, 1993

Celebrating the 90th anniversary of the invention of chromatography, the Scientific Council on Chromatography of the Russian Academy of Sciences is organizing this symposium to highlight the history and all advances in the field of chromatography.

Alongside the scientific program, an exhibition of equipment, accessories, chemical and chromatographic literature will be organized. The exhibition will promote a stronger interaction between instrumentation manufacturers and scientific communities.

For further information contact: Dr. L. Kolomiets, Institute of Physical Chemistry, 31 Leninsky prospect, 117915 Moscow, Russia. Fax: (+7-95) 952-7514.

FULLERENES '93, 1st INTERNATIONAL INTERDISCIPLINARY COLLOQUIUM ON THE SCIENCE AND TECHNOLOGY OF THE FULLERENES, SANTA BARBARA, CA, USA, JUNE 27 – JULY 1, 1993

The discovery of Buckminsterfullerene (C_{60}) and subsequently the other fullerenes (C_{28}, C_{76} etc.) has created considerable interest among physicists, chemists and materials scientists. Fullerenes '93 is an ideal opportunity for researchers from these disciplines to communicate with each other and discuss the impressive developments in the field and the opportunities offered by this new form of carbon. It is also intended that an informal agenda will emerge from this meeting for future research into the theory, processing and applications of the fullerenes.

Unlike the usual scientific meeting Fullerenes '93 will take the form of eight discussion sessions and eight poster sessions over four days. Each discussion session will commence with surveys presented by session leaders who will highlight selected themes. The session will then be opened up to delegates for debate. Relevant posters will be presented after each discussion.

Topics to be covered will include: clusters, the physics of fullerenes, the chemistry of fullerenes, the nanotechnology of fullerenes, the production of fullerenes, and applications.

Those wishing to present posters at Fullerenes '93 should submit two copies of abstracts appropriate to the subject area covered by the meeting.

All those interested in attending as a delegate or presenting a poster should write either to: (for North America) Kim Cavellero, Pergamon Seminars, 660 White Plains Rd, Tarrytown, NY 10591-5153, USA, or: (for UK and all other countries), Gill Spear, Pergamon Seminars, c/o Elsevier Advanced Technology, Mayfield House, 256 Banbury Road, Oxford OX2 7DH, UK. Tel.: (+44 865) 512242; Fax: (+44 865) 310981.

6th INTERNATIONAL SYMPOSIUM ON POLYMER ANALYSIS AND CHARACTERIZATION, CRETE, GREECE, JULY 11–14, 1993

This three-day symposium will consist of poster sessions, invited lectures, and round-table discussions and information exchange on recent advances in polymer characterization approaches, techniques, and applications.

Topics will include chromatography, infrared, NMR, mass spectrometry, chemical characterization, light scattering, rheology, microscopy, viscometry, surface analysis, thermal analysis, thermodynamics and solution properties of polymers, as well as general contributions on polymer analysis and characterization.

For further information contact: Judith A. Sjoberg, Professional Association Management, 815 Don Gaspar, Santa Fe, NM 87501, USA. Tel.: (+1-505) 989-4735; Fax: (+1-505) 989-1073.

9th INTERNATIONAL SYMPOSIUM ON ADVANCES AND APPLICATION OF CHROMATOGRAPHY IN INDUSTRY, BRATISLAVA, CZECHOSLOVAKIA, AUGUST 29–SEPTEMBER 3, 1993

This symposium will comprise of lectures, poster presentations and discussion sessions dealing with all aspects of chromatography and related techniques.

An exhibition of chromatographic equipment and literature will be held adjacent to the meeting.

The deadline for submission of Abstracts is February 25, 1993.

For further information contact: Department of Analytical Chemistry, Slovak Technica University, Radinského 9, 812 37 Bratislava, Czechoslovakia. Tel.: (+42-7) 560-43; Fax: (+42-7) 493-198.

EUROANALYSIS VIII, EUROPEAN CONFERENCE ON ANALYTICAL CHEMISTRY, EDINBURGH, UK, SEPTEMBER 5–11, 1993

Euroanalysis VIII, organized by the Analytical Division of The Royal Society of Chemistry on behalf of the Working Party on Analytical Chemistry of the Federation of European Chemical Societies, will cover developments in instrumentation and methodology in all areas of analytical chemistry, with emphasis on industrial, biomedical and environmental analysis. The programme will be designed to appeal both to practising analytical chemists in industry and to those in academia.

The programme will consist of invited keynote lectures, and contributed oral and poster papers. In order to ensure high quality, all contributed papers will be refereed. Some of the topics expected to be covered are:

Industrial analysis: validation of analytical measurements, process control analysis, materials analysis (including surface analysis), energy related analysis.

Pharmaceutical and biomedical analysis: pharmaceutical methods and drug metabolism, forensic science, bioselective methods, trace elements in medicine.

Environmental analysis: atmosphere, soils/sediments, food/drink, water.

Instrumental techniques: separation science, molecular spectrometry, atomic spectrometry, electroanalytical techniques, expert systems and chemometrics, coupled techniques, sensors, laser-based techniques, flow analysis

All invited lectures will be published in a collected volume as the proceedings of the conference. Authors of contributed papers will be invited to submit manuscripts for publication in the RSC journals. Abstracts of all papers will be available to registered scientific participants.

For further details, contact: Miss P.E. Hutchinson, Analytical Division, The Royal Society of Chemistry, Burlington House, Piccadilly, London W1V 0BN, UK. Tel.: (+44 71) 437 8656 Fax (+44 71) 734 1227;

2nd NATIONAL SYMPOSIUM ON PLANAR CHROMATOGRAPHY: MODERN THIN-LAYER CHROMATOGRAPHY, RESEARCH TRIANGLE PARK, NC, USA, SEPTEMBER 19–22, 1993

This symposium will explore in-depth the full potential of TLC as an analytical method, its eco-

nomical advantages, and its future in the modern lab. It will provide a forum for the exchange of ideas on all aspects of modern TLC, and will explore the practical aspects of TLC through lectures, posters, discussions, tutorial workshops, and exhibits.

A practical workshop on modern TLC will be presented.

All are invited to submit abstracts describing original research in the following areas:

- TLC in biomedical, environmental, forensic and toxicological analysis;
- Hyphenated techniques;
- Instrumentation;
- Quantitation;
- Radio-chromatography.

The deadline for submission of abstracts is March 1, 1993.

Advance registration (by August 16, 1993) is US$ 275; after August 16 US$ 325, and student registration is US$ 100.

For further information contact: Mrs. Janet Cunningham, Barr Enterprises, P.O. Box 279, Walkersville, MD 21793, USA. Tel.: (+1-301) 898-3772; Fax: (+1-301) 898-5596.

HTC 3 – 3rd INTERNATIONAL SYMPOSIUM ON HYPHENATED TECHNIQUES IN CHROMATOGRAPHY, ANTWERP, BELGIUM, FEBRUARY 22–25, 1994

The purpose of this symposium will again be to highlight and treat in-depth recent developments and progress in the field of hyphenations. It will cover all fundamental aspects, instrumental developments and applications of the various hyphenated chromatographic techniques such as GC–GC, GC–MS, PTV–GC–MS, GC–MS–MS, GC–FTIR, GC–AED, on-line air traps–GC, purge-and-trap–GC, extractors–GC (or LC), LC–MS, LC–NMR, LC–LC, LC–GC–MS, LC–LC–GC, LC–FIA–DAD, LC–SFC, SFC–LC, SFC–MS, SFC–FTIR, SFE–GC, SFE–LC, CZE–MS, and ITP–MS.

As HTC 2 clearly showed that hyphenated chromatographic methods have already evolved from a scientific research topic to a generally applied analytical technique, opening the way to further automation, therefore, during HTC 3, emphasis will also be placed on the design of hyphenated, on-line and at-line, "chromatographic analyzers".

Oral presentations in plenary and parallel sessions as well as poster presentations will be included in the scientific program. All are invited to submit papers in the above and related areas. The deadline for submission of abstracts is June 30, 1993. Papers presented at the symposium will be reviewed for publication in a special volume of the *Journal of Chromatography*.

A major portion of the symposium will be devoted to discussion sessions. Workshop type seminars will be organized in which scientists of the instrument manufacturers will present and discuss latest developments in instrumentation. A technical exhibition (instruments, books and accessories) will be organized during the meeting.

In connection with HTC 3, a number of short courses and hands-on workshops will be organized.

The official language of the symposium will be English.

For further information contact: Dr. R. Smits, p/a BASF Antwerpen N.V., Central Laboratory, Scheldelaan, B-2040 Antwerp, Belgium. Tel.: (+32-3) 568-2831: Fax: (+32-3) 568-3250.

20th INTERNATIONAL SYMPOSIUM ON CHROMATOGRAPHY, BOURNEMOUTH, UK, JUNE 19–24, 1994

This symposium will present a range of topical issues in plenary sessions, supported by detailed discussion of recent advances in each topic, together with strongly focused groups of poster presentations.

Recent advances to be highlighted in fundamental aspects of separations science and their applications will include:

- Planar chromatography;
- Capillary gas chromatography;
- Liquid chromatography;
- Supercritical fluid chromatography;
- Chiral separations;
- Capillary electrophoresis;
- Hyphenated techniques, including LC–GC, GC–MS, CE–MS, GC–FTIR, LC–MS, SFC–FTIR, SFC–MS, SFE–SFC–MS;
- Chemometrics in separation science;

- Computer-aided methods in the design and validation of separations systems;
- On-line sample preparation systems for chromatography preparative techniques in chromatography.

All scientists involved in any aspect of separation science, fundamental or applied, are invited to contribute to the 20th International Symposium on Chromatography.

A book of Abstracts of all scientific contributions will be distributed to each participant at the 20th ISC. All papers submitted will be considered for publication in a special issue of the *Journal of Chromatography* after refereeing. Each delegate will receive a copy of the special issue free of charge.

For further details contact: The Executive Secretary, The Chromatographic Society, Suite 4, Clarendon Chambers, 32 Clarendon Street, Nottingham NG1 5JD, UK. Tel.: (+44-602) 500-596; Fax: (+44-602) 500-614.

Announcements are included free of charge. Information on planned events should be sent well in advance (6 months) to: Journal of Chromatography, News Section, P.O. Box 330, 1000 AH Amsterdam, Netherlands, or by Fax: (+31 20) 5862304.

CALENDAR OF FORTHCOMING EVENTS

March 8–12, 1993
Atlanta, GA, USA
PITTCON '93, 44th Pittsburgh Conference and Exposition on Analytical Chemistry and Applied Spectroscopy

Contact: Mrs. Alma Johnson, Program Secretary, Pittsburgh Conference, 300 Penn Center Blvd., Suite 332, Pittsburgh, PA 15235-5503, USA. Tel.: (+1-412) 825-3220.

March 19, 1993
Antwerp, Belgium
Symposium on Possibilities and Limitations of Chiral Separation Techniques

Contact: Royal Flemish Chemical Society (KVCV), Working Party on Chromatography, c/o Dr. R. Smits, BASF Antwerpen NV, Central Laboratory, Scheldelaan, B-2040 Antwerp, Belgium. Tel.: (+32-3) 568-2831; Fax: (+32-3) 568-3250; Telex: 31047 basant b.

March 23–26, 1993
Brighton, UK
7th International Meeting on Instrumental Planar Chromatography

Contact: Executive Secretary, The Chromatographic Society, Suite 4, Clarendon Chambers, 32 Clarendon Street, Nottingham NG1 5JD, UK.

April 4–7, 1993
Wrexham, UK
Ion-Ex '93

Contact: Ion-Ex '93, Conference Secretariat, Faculty of Science, The North East Wales Institute, Connah's Quay, Deeside, Clwyd, CH5 4BR, UK. Tel.: (+44-244) 831-531 ext. 245 or 276; Fax: (+44-244) 814-305.

April 18–21, 1993
Baltimore, MD, USA
4th International Symposium on Pharmaceutical and Biomedical Analysis

Contact: Shirley Schlessinger, Symposium Manager, Suite 1015, 400 E. Randoph Drive, Chicago, IL 60601, USA. Tel.: (+1-312) 527-2011.

■ **April 25–29, 1993**
St. Petersburg, Russia
International Symposium "90 Years of Chromatography"

Contact: Dr. L. Kolomiets, Institute of Physical Chemistry, 31 Leninsky prospect, 117915 Moscow, Russia. Fax: (+7-95) 952-7514.

April 26–29, 1993
Clearwater, FL, USA
18th International Technical

Conference on Coal Utilization and Fuel Systems

Contact: Coal Utilization and Fuel Systems, Conference Organizing Committe, 1156 Fifteenth Street, NW, Suite 525, Washington, DC 20005, USA. Tel.: (+1-202) 296-1133; Fax: (+1-202) 223-3504.

May 3–5, 1993
Veldhoven, Netherlands
EURORESIDUE II – International Conference on Residues of Veterinary Drugs in Food

Contact: Dr. N. Haagsma, Section of Food Chemistry, Department of Food of Animal Origin, Faculty of Veterinary Medicine, University of Utrecht, P.O. Box 80.175, 3508 TD Utrecht, Netherlands. Tel.: (+31-30) 535-365/535-367; Fax: (+31-30) 532-365.

■ **May 3–5, 1993**
Szombathely, Hungary
5th Symposium on the Analysis of Steroids

Contact: Professor S. Görög, c/o Chemical Works of Gedeon Richter Ltd., P.O. Box 27, H-1475 Budapest, Hungary. Tel.: (+36-1) 1574-566; Fax: (+36-1) 1571-578; Telex: 22-5067 richt h.

May 9–14, 1993
Hamburg, Germany
17th International Symposium on Column Liquid Chromatography

Contact: Gesellschaft Deutscher Chemiker, Abteilung Tagungen, P.O. Box 900440, Varrentrappstrasse 40-42, W-6000 Frankfurt am Main 90, Germany. Tel: (+49-69) 7917-360; Fax: (+49-69) 7917-475.

May 24–28, 1993
Riva del Garda, Italy
15th International Sympsium on Capillary Chromatography

Contact: Professor Dr. P. Sandra, I.O.P.M.S., Kennedypark 20, B-8500 Kortrijk, Belgium. Tel.: (+32-56) 204-960; Fax: (+32-56) 204-859.

May 25–27, 1993
Ghent, Belgium
5th International Symposium on Quantitative Luminescence Spectrometry in Biomedical Sciences

Contact: Dr. Willy R.G. Baeyens, Symposium Chairman, University of Ghent, Pharmaceutical Institute, Harelbekestraat 72, B-9000 Ghent, Belgium. Tel.: (+32-91) 218-951, ext. 246; Fax: (+32-91) 217-902.

June 2–4, 1993
Stockholm, Sweden
International Symposium on Analysis of Peptides

Contact: Swedish Academy of Pharmaceutical Sciences, Symposium on "Analysis of Peptides", P.O. Box 1136, S-111 81 Stockholm, Sweden. Tel.: (+46-8) 245-085; Fax: (+46-8) 205-511.

June 2–4, 1993
Sandefjord, Norway
ICES-ELPHO '93, Meeting of the International Council of Electrophoresis Societies

Contact: Professor Nils Olav Solum, Research Institute for Internal Medicine, Rikshopitalet, Pilestredet 32, N-0027 Oslo, Norway. Tel.: (+47-2) 868-226; Fax: (+47-2) 868-303.

June 14–16, 1993
Arlington, VA, USA
Prep '93, 10th International Symposium on Preparative Chromatography

Contact: Washington Chromatography Discussion Group, c/o Barr Enterprises, P.O. Box 279, Walkersville, MD 21793, USA. Tel.: (+1-301) 898-3772; Fax: (+1-301) 898-5596.

■ **June 27–July 1, 1993**
Santa Barbara, CA, USA
Fullerenes '93, 1st International Interdisciplinary Colloquium on the Science and Technology of the Fullerenes

Contact: (for North America) Kim Cavellero, Pergamon Seminars, 660 White Plains Rd, Tarrytown, NY 10591-5153, USA, or: (for UK and all other countries), Gill Spear, Pergamon Seminars, c/o Elsevier Advanced Technology, Mayfield House, 256 Banbury Road, Oxford OX2 7DH, UK. Tel.: (+44 865) 512242; Fax: (+44 865) 310981

June 29–July 4, 1993
York, UK
XXVIII Colloquium Spectroscopicum Internationale

Contact: XXVIII Colloquium Spectroscopicum Internationale, Department of Chemistry (CSI Secretariat), Loughborough University of Technology, Loughborough, Leicestershire LE11 3TU, UK. Tel.: (+44-509) 222-575; Fax: (+44-509) 233-163; Telex: 34319.

■ **July 11–14, 1993**
Crete, Greece
6th International Symposium on Polymer Analysis and Characterization

Contact: Judith A. Sjoberg, Professional Association Management, 815 Don Gaspar, Santa Fe, NM 87501, USA. Tel.: (+1-505) 989-4735; Fax: (+1-505) 989-1073.

■ **July 11–15, 1993**
Brno, Czechoslovakia
Chemometrics III, 3rd Czechoslovak Chemometric Conference

Contact: Dr. Josef Havel, Department of Analytical Chemistry, Masaryk University, Kotlarska 2, CS-61137 Brno, Czechoslovakia. Tel.: (+42-5) 7129-284; Fax: (+42-5) 740-108.

July 26–29, 1993
Washington, DC, USA
107th Annual International Meeting and Exposition of the AOAC

Contact: Margaret Ridgell, AOAC, 2200 Wilson Blvd., Suite 400, Arlington, VA 22201-3301, USA. Tel.: (+1-703) 522-3032; Fax: (+1-703) 522-5468.

Aug. 23–27, 1993
Budapest, Hungary
9th Danube Symposium on Chromatography

Contact: Symposium Secretariat, Professor László Szepesy, Department of Chemical Technology, Technical University of Budapest, Budafoki út 8., H-1521 Budapest, Hungary. Tel.: (+36-1) 186-9000; Fax: (+36-1) 181-2755; Telex: 225931 muegy h.

Aug. 23–27, 1993
Calgary, Canada
9th International Conference on Fourier Transform Spectroscopy

Contact: Conference Office, The University of Calgary, 2500 University Drive NW, Calgary, Alberta T2N 1N4, Canada. Tel.: (+1-403) 220-5051; Fax: (+1-403) 289-7287.

■ **Aug. 24–27, 1993**
Boston, MA, USA
EPRI/EPA/DOE 1993 SO_2 Control Symposium

Contact: Electric Power Research Institute, Attn: Pam Turner, Conference Coordinator P.O. Box 10412, Palo Alto, CA 94303-9743, USA.

■ **Aug. 29–Sept. 3, 1993**
Bratislava, Czechoslovakia
9th International Symposium on Advances and Application of Chromatography in Industry

Contact: Department of Analytical Chemistry, Slovak Technica University, Radinského 9, 812 37 Bratislava, Czechoslovakia. Tel.: (+42-7) 560-43; Fax: (+42-7) 493-198.

Sept. 5–11, 1993
Edinburgh, UK
EUROANALYSIS VIII, 8th European Conference on Analytical Chemistry

Contact: Miss P.E. Hutchinson, Analytical Division, The Royal Society of Chemistry, Burlington House, Piccadilly, London W1V 0BN, UK. Tel.: (071) 4378656; Fax: (071) 734-1227; Telex: 268001.

Sept. 7–10, 1993
Verona, Italy
12th Internation Symposium on Biomedical Applications of Chromatography and Electrophoresis and 2nd International Symposium on the Applications of HPLC in Enzyme Chemistry

Contact: Dr. Franco Tagliaro, Istituto di Medicina Legale, Università di Verona, Policlinico, I-37134 Verona, Italy. Tel.: (+39-45) 807-4618/807-4246; Fax: (+39-45) 505-259.

Sept. 8–10, 1993
Prague, Czechoslovakia
4th Workshop on Chemistry and Fate of Modern Pesticides and Related Pollutants

Contact (for Eastern European countries): Dra. J. Hajslova, Department of Food Chemistry and Analysis, Institute of Chemical Technology, Suchbátarova 5, 166 28 Prague 6-Dejvice, Czechoslovakia. Fax: (+42-2) 311-4769. For all other countries, contact: IAEAC, M. Frei-Häusler, P.O. Box 46, CH-4123 Allschwil 2, Switzerland. Fax: (+41-61) 482-0805.

■ **Sept. 12–15, 1993**
Baltimore, MD, USA
1993 International Ion Chromatography Symposium

Contact: J.R. Strimaitis, Century International, P.O. Box 493, Medfield, MA 02052, USA. Tel.: (+1-508) 359-8777; Fax: (+1-508) 359-8778.

Sept. 19–22, 1993
Montreal, Canada
4th International Symposium on Chiral Discrimination

Contact: Chiral Secretariat, Conference Office, McGill University, West Tower, Suite 490, Montreal, Quebec H3A 1B9, Canada. Tel.: (+1-514) 398-3770; Fax: (+1-514) 398-4854.

■ **Sept. 19–22, 1993**
Research Triangle Park, NC, USA
2nd National Symposium on Planar Chromatography: Modern Thin-Layer Chromatography

Contact: Mrs. Janet Cunningham, Barr Enterprises, P.O. Box 279, Walkersville, MD 21793, USA. Tel.: (+1-301) 898-3772; Fax: (+1-301) 898-5596.

■ **Sept. 29–Oct. 1, 1993**
Lausanne, Switzerland
International Symposium on Phytochemistry of Plants used in Traditional Medicine

Contact: Professor K. Hostettmann, Institut de Pharmacognosie et Phytochimie, Ecole de Pharmacie, Université de Lausanne, BEP, CH-1015 Lausanne, Switzerland. Tel.: (+41-21) 692-2861; Fax: (+41-21) 692-2880.

■ **Feb. 22–25, 1994**
Antwerp, Belgium
HTC 3 – 3rd International Symposium on Hyphenated Techniques in Chromatography

Contact: Congress Secretariat, Dr. R. Smits, p/a BASF Antwerpen N.V., Central Laboratory, Scheldelaan, B-2040 Antwerp, Belgium. Tel.: (+32-3) 568-2831; Fax: (+32-3) 568-3250.

May 8–13, 1994
Minneapolis, MN, USA
HPLC '94: 18th International Symposium on Column Liquid Chromatography

Contact: Janet E. Cunningham, Barr Enterprises, P.O. Box 279, Walkersville, MD 21793, USA. Tel.: (+1-301) 898-3772; Fax: (+1-301) 898-5596.

■ **June 19–24, 1994**
Bournemouth, UK
20th International Symposium on Chromatography

Contact: The Executive Secretary, The Chromatographic Society, Suite 4, Clarendon Chambers, 32 Clarendon Street, Nottingham NG1 5JD, UK. Tel.: (+44-602) 500-596; Fax: (+44-602) 500-614.

June 20–24, 1994
Bournemouth, UK
20th International Symposium on Chromatography

Contact: Executive Secretary, The Chromatographic Society, Nottingham Polytechnic, Burton Street, Nottingham, NG1 4BU, UK. Tel.: (+44-602) 500-596; Fax: (+44-602) 500-614.

■ **October, 1994**
Budapest, Hungary
ITP '94: 9th International Symposium on Capillary Electrophoresis and Isotachophoresis

Contact: Dr. Ferenc Kilár, Central Research laboratory, University of Pécs, Medical School, Szigeti út 12, H-7643 Pécs, Hungary. Tel.: (+36-72) 24122; Fax: (+35-72) 15864 or 26244

■ Indicates new or amended entry.

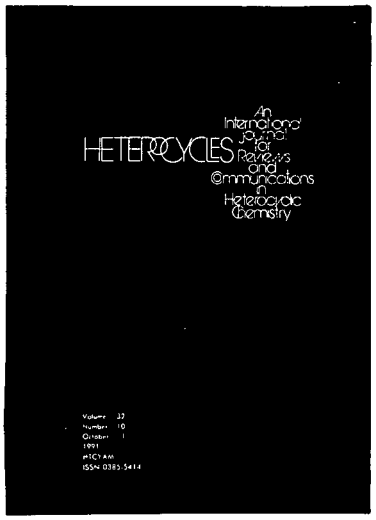

Audience

Organic and physical organic chemists, biochemists, pharmacologists and scientists studying heterocyclic compounds.

HETEROCYCLES

An international journal for reviews and communications in heterocyclic chemistry

AIMS AND SCOPE

Since its inception in 1973, *Heterocycles* has provided a platform for the rapid exchange of research in the areas of organic, pharmaceutical, analytical, and medicinal chemistry of heterocyclic compounds. The journal publishes reviews, communications, reports and original papers. There are two special sections. One lists new natural products with a heterocyclic ring system collected from current literature. The other lists such compounds whose total synthesis has been reported.

Due to the fact that the journal is able to publish articles within two months of receipt of the manuscripts, researchers in this field can obtain up-to-date information on heterocyclic research by reading *Heterocycles* regularly.

ABSTRACTED/INDEXED IN: Chemical Abstracts, Current Contents: Physical, Chemical & Earth Sciences, PASCAL/CNRS.

1993 SUBSCRIPTION INFORMATION

Volumes 35-36 in 14 issues
Dfl. 2280.00 / US $ 1373.50 (including postage)
ISSN 0385-5414

I would like ☐ a free sample copy of HETEROCYCLES.
☐ Instructions to Authors.
☐ to enter a subscription for 1993.
Please send me a Proforma Invoice.

Name _____
Address _____

The Dutch Guilder price (Dfl.) is definitive. US$ prices are for your convenience only and are subject to exchange fluctuations. Customers in the European Community should add the appropriate VAT rate applicable in their country to the price(s).

Elsevier Science Publishers
Attn. Eugene P.M. Wijnhoven
P.O. Box 330, 1000 AH Amsterdam
The Netherlands
Fax: (+31-20) 5862 845
In the USA & Canada
Attn. Judy Weislogel
P.O. Box 945, Madison Square Station
New York, NY 10160-0757, USA
Fax: (+1-212) 633 3880

CHROM 711\414\142\0068

Chromatography, 5th edition

Fundamentals and Applications of Chromatography and Related Differential Migration Methods

edited by **E. Heftmann**, *Orinda, CA, USA*

These are completely new books, organized according to the successful plan of the previous four editions. While avoiding repetition of material covered in the previous editions, the authors have succeeded in presenting a coherent and comprehensive picture of the state of each topic. The books provide beginners as well as experienced researchers with a key to understanding current activities in various separation methods. They will also serve as textbooks for graduate courses in technical, medical and engineering schools as well as all universities offering science courses.

Part A: Fundamentals and Techniques

Journal of Chromatography Library Volume 51A

Part A covers the theory and fundamentals of such methods as column and planar chromatography, countercurrent chromatography, field-flow fractionation, and electrophoresis. Affinity chromatography and supercritical-fluid chromatography are covered for the first time. Each topic is treated by one of the most eminent authorities in the field.

Contents Part A: 1. Theory of chromatography *(L.R. Snyder)*. 2. Countercurrent chromatography *(Y. Ito)*. 3. Planar chromatography *(S. Nyiredy)*. 4. Column liquid chromatography *(H. Poppe)*. 5. Ion-exchange chromatography *(H.F. Walton)*. 6. Size-exclusion chromatography *(L. Hagel and J.-C. Janson)*. 7. Affinity chromatography *(T.M. Phillips)*. 8. Supercritical-fluid chromatography *(P.J. Schoenmakers and L.G.M. Uunk)*. 9. Gas chromatography *(C.F. Poole and S.K. Poole)*. 10. Field-flow fractionation *(J. Janca)*. 11. Electrophoresis *(P.G. Righetti)*. Manufacturers and dealers of chromatography and electrophoresis supplies. Subject Index.

1992 xxxvi + 552 pages
Price: US $ 179.50 / Dfl. 350.00
ISBN 0-444-88236-7

Part B: Applications

Journal of Chromatography Library Volume 51B

Part B presents various applications of these methods. New developments are reviewed and summarized. Important topics such as environmental analysis and the determination of synthetic polymers and fossil fuels, are covered for the first time.

Contents Part B: 12. Inorganic species *(P.R. Haddad and E. Patsalides)*. 13. Amino acids and peptides *(C.T. Mant, N.E. Zhou and R.S. Hodges)*. 14. Proteins *(F.E. Regnier and K.M. Gooding)*. 15. Lipids *(A. Kuksis)*. 16. Carbohydrates *(S.C. Churms)*. 17. Nucleic acids, their constituents and analogs *(N-I Jang and P.R. Brown)*. 18. Porphyrins *(K. Jacob)*. 19. Phenolic compounds *(J.B. Harborne)*. 20. Drugs *(K. Macek and J. Macek)*. 21. Fossil fuels *(R.P. Philp and F.X. de las Heras)*. 22. Synthetic polymers *(T.H. Moury and T.C. Schunk)*. 23. Pesticides *(J. Sherma)*. 24. Environmental analysis *(K.P. Naikwadi and F.W. Karasek)*. 25. Amines from environmental sources *(H.A.H. Billiet)*. Manufacturers and dealers of chromatography and electrophoresis supplies. Subject Index.

1992 xxxii + 630 pages
Price: US $ 189.50 / Dfl. 370.00
ISBN 0-444-88237-5

Parts A & B Set
Set price: US $ 333.50 / Dfl. 650.00
ISBN 0-444-88404-1

Elsevier Science Publishers

P.O. Box 211, 1000 AE Amsterdam, The Netherlands
P.O. Box 882, Madison Square Station, New York, NY 10159, USA

PUBLICATION SCHEDULE FOR THE 1993 SUBSCRIPTION

Journal of Chromatography and *Journal of Chromatography, Biomedical Applications*

MONTH	O 1992	N 1992	D 1992	J	F	
Journal of Chromatography	623/1 623/2 624/1 + 2	625/1 625/2	626/1 626/2 627/1 + 2	628/1 628/2 629/1 629/2	630/1 + 2 631/1 + 2 632/1 + 2 633/1 + 2	The publication schedule for further issues will be published later.
Cumulative Indexes, Vols. 601–650						
Bibliography Section						
Biomedical Applications				612/1	612/2	

INFORMATION FOR AUTHORS

(Detailed *Instructions to Authors* were published in Vol. 609, pp. 439–445. A free reprint can be obtained by application to the publisher, Elsevier Science Publishers B.V., P.O. Box 330, 1000 AH Amsterdam, The Netherlands.)

Types of Contributions. The following types of papers are published in the *Journal of Chromatography* and the section on *Biomedical Applications:* Regular research papers (Full-length papers), Review articles, Short Communications and Discussions. Short Communications are usually descriptions of short investigations, or they can report minor technical improvements of previously published procedures; they reflect the same quality of research as Full-length papers, but should preferably not exceed five printed pages. Discussions (one or two pages) should explain, amplify, correct or otherwise comment substantively upon an article recently published in the journal. For Review articles, see inside front cover under Submission of Papers.

Submission. Every paper must be accompanied by a letter from the senior author, stating that he/she is submitting the paper for publication in the *Journal of Chromatography*.

Manuscripts. Manuscripts should be typed in **double spacing** on consecutively numbered pages of uniform size. The manuscript should be preceded by a sheet of manuscript paper carrying the title of the paper and the name and full postal address of the person to whom the proofs are to be sent. As a rule, papers should be divided into sections, headed by a caption (*e.g.*, Abstract, Introduction, Experimental, Results, Discussion, etc.). All illustrations, photographs, tables, etc., should be on separate sheets.

Abstract. All articles should have an abstract of 50–100 words which clearly and briefly indicates what is new, different and significant. No references should be given.

Introduction. Every paper must have a concise introduction mentioning what has been done before on the topic described, and stating clearly what is new in the paper now submitted.

Illustrations. The figures should be submitted in a form suitable for reproduction, drawn in Indian ink on drawing or tracing paper. Each illustration should have a legend, all the *legends* being typed (with double spacing) together on a *separate sheet*. If structures are given in the text, the original drawings should be supplied. Coloured illustrations are reproduced at the author's expense, the cost being determined by the number of pages and by the number of colours needed. The written permission of the author and publisher must be obtained for the use of any figure already published. Its source must be indicated in the legend.

References. References should be numbered in the order in which they are cited in the text, and listed in numerical sequence on a separate sheet at the end of the article. Please check a recent issue for the layout of the reference list. Abbreviations for the titles of journals should follow the system used by *Chemical Abstracts*. Articles not yet published should be given as "in press" (journal should be specified), "submitted for publication" (journal should be specified), "in preparation" or "personal communication".

Dispatch. Before sending the manuscript to the Editor please check that the envelope contains four copies of the paper complete with references, legends and figures. One of the sets of figures must be the originals suitable for direct reproduction. Please also ensure that permission to publish has been obtained from your institute.

Proofs. One set of proofs will be sent to the author to be carefully checked for printer's errors. Corrections must be restricted to instances in which the proof is at variance with the manuscript. "Extra corrections" will be inserted at the author's expense.

Reprints. Fifty reprints will be supplied free of charge. Additional reprints can be ordered by the authors. An order form containing price quotations will be sent to the authors together with the proofs of their article.